Metal Ion Sensing, Coordination Chemistry of Some N-,O-Donor Ligands and Synthesis of Substituted Benzenes and Cyclohexanols

A Dissertation Submitted to the
Indian Institute of Technology Guwahati as
Partial Fulfillment for the Degree of Doctor of Philosophy
in Chemistry

by

SANDEEP KUMAR
Roll No. 186122034

Department of Chemistry
Indian Institute of Technology Guwahati
Guwahati – 781039

MARCH 2025

DEDICATED

TO

MY PARENTS AND FAMILY

DEPARTMENT OF CHEMISTRY
INDIAN INSTITUTE OF TECHNOLOGY GUWAHATI
GUWAHATI–781039

DECLARATION

I do hereby declare that the research work embodied in this thesis entitled "**Metal Ion Sensing, Coordination Chemistry of Some N-,O-Donor Ligands and Synthesis of Substituted Benzenes and Cyclohexanols**" is the outcome of research work carried out by me under the supervision of Prof. V. Manivannan, at the Department of Chemistry, Indian Institute of Technology Guwahati, Assam, India.

In keeping with the general practice of reporting scientific observations, due acknowledgments have been made wherever the work described is based on the findings of other investigators.

Sandeep Kumar

IIT Guwahati — Sandeep Kumar

March, 2025 — (Roll.No.-186122034)

Dr. V. Manivannan
Professor
Department of Chemistry
Indian Institute of Technology
Guwahati-781039
Assam, INDIA

Ph: +91 361 258 2306 (O)
E-mail: mani@iitg.ac.in

CERTIFICATE

This is to certify that the research work presented in this thesis entitled "**Metal Ion Sensing, Coordination Chemistry of Some N-,O-Donor Ligands and Synthesis of Substituted Benzenes and Cyclohexanols**" is an authentic record of the results obtained from the research work carried out by **Sandeep Kumar** under my supervision in the Department of Chemistry, Indian Institute of Technology Guwahati, India. This work is original and has not been submitted elsewhere for a degree.

IIT Guwahati
March, 2025

Prof. V. Manivannan
(Thesis Supervisor)

ACKNOWLEDGMENTS

At the verge of completing my thesis work, I would like to acknowledge each and every person who helped directly or indirectly to my entire PhD journey.

I express my profound gratitude to my supervisor Prof. V. Manivannan for his constant guidance and encouragement throughout my PhD. During this time, his valuable ideas, suggestions and patience helped me a lot to carry out the research work for successful completion. He has given freedom to apply my ideas and corrected wherever needed which helped me to learn many things. I find myself privileged to have worked under his guidance.

I am very thankful to the doctoral committee members Prof. Anil Kumar Saikia, Prof. Shyam Prosad Biswas and Prof. Seenipandian Ravi for their valuable suggestions. I am also thankful to the entire faculty and staff members in the Department of Chemistry, Indian Institute of Technology Guwahati for providing the working environment throughout this period.

A special thanks to the Central Instruments Facility, Department of Chemistry and North East Centre for Biological Science and Healthcare engineering of Indian Institute of Technology Guwahati, for providing various instrumental facilities.

I am delighted to have friends like Vineet, Gangeshwar, Viksit, Radhakrishna, Harmesh, Chinmoy, Vinay, Sabina, Bittu, Rinki, Debjyoti, Sagnik, Tanumoy, Priyanka, Pran, Tirupati and Samir. I am also thankful to Arnab da, Ahmad, Anjela, Ujjwal, Gyani, Simra, Anil, Satyajit, Nisha and Halida for their support.

My heartiest gratefulness goes towards my senior lab mates Dr. Nibedita Behera, Dr. Satyajit Mahata, Dr. Jugal Bori and Dr. Araghni Bhattacharya for their sharing of experimental knowledge, Instrumental handling and data analysis. I am also grateful to present labmates Amlan Ranjan Rayasingh, Anisha Mondal, Alok Kumar and Rituraj Hazra for their cooperation during this period.

A special thanks to Dr. Prathapa S. Jagannatha who trained initially in Solving and refinement of single crystal XRD data.

The financial support from Indian Institute of Technology Guwahati is duly acknowledged.

Finally, I would like to thank my parents and family for their blessings, patience, faith and encouragement during this long period which helped me to stay positive in every conditions.

Sandeep Kumar

Preface

This Thesis contains six chapters. Chapter 1 is about Introduction, Materials and Methods. In this chapter introduction about fluorescence and various sensing mechanisms are discussed briefly. Some recent literature reports on detection of Zn^{2+}, Cu^{2+} and Pd^{2+} ions using different fluorescent probes have been discussed. Recent reports on benzannulation reactions for the synthesis of substituted benzenes have also been described. Along with this, materials, methods and instrumentation related to this thesis are described in details. In Chapter 2, a probe 3,3'-((-(5-(*tert*-butyl)-2-hydroxy-1,3-phenylene)bis(methaneylylidene))bis(hydrazin-1-yl-2-ylidene))bis(quinoxalin-2(1H)-one) (**LH**) showed very weak fluorescence (λ_{em} = 597 nm) in EtOH/HEPES buffer system (5 mM, pH = 7.4, 8:2, *v/v*) upon excitation with 419 nm light. Upon adding Zn^{2+} ion to the probe solution, a huge enhancement in fluorescence (λ_{em} = 537 nm) was observed with appearance of yellow green colour when seen in long UV light. Job′s plot and single crystal XRD method suggested a 2:1 binding ratio between Zn^{2+} and **LH**. A very low detection limit of 95 nM was calculated using **LH** for detection of Zn^{2+} ion. In Chapter 3, a heterocyclic probe 1-(imidazo[5,1-*a*]isoquinolin-3-yl)naphthalen-2-ol (**L2H**) has exhibited very high fluorescence in MeOH/HEPES buffer system (5 mM, pH = 7.4, 2:8, *v/v*) at λ_{em} = 437 nm when excited with λ_{ex} = 336 nm. But after addition of Cu^{2+} and Pd^{2+} ions the fluorescence got quenched. Job′s plot and mass spectral analysis suggested a 1:2 binding ratio between M^{2+} (M = Cu, Pd) and **L2H**. DFT/TDDFT calculation supported the experimentally observed red shifts in absorption spectra due to addition of Cu^{2+} and Pd^{2+} ion to probe solution. In Chapter 4, a polypyridine ligand (**L3**) containing two terpyridine arms was synthesized and utilized in synthesis of two new metal complexes of Co(II) and Mn(II) with compositions $[M_2(\mathbf{L3})Cl_4]\cdot 2H_2O$. Molecular structures of these three were established using single crystal XRD method. Taking inspiration from synthesis of terpyridine, Chapter 5 deals with synthesis of 1,2,4,6-tetrasubstituted benzenes from the reaction of aryl methyl ketones and aromatic aldehydes in 3:1 ratio in the presence of 3 equivalents of NaH in one pot condition. The reaction was regioselective in nature. In Chapter 6, changing the ratio of aryl methyl ketone and aromatic aldehyde from 3:1 to 3:2 in the presence of catalytic amount of NaH yielded 1,2,3,4,5-pentasubstituted cyclohexanol. Using this methodology some new and reported substituted cyclohexanols were synthesized.

Abbreviations

a	Unit cell dimension *a*
b	Unit cell dimension *b*
c	Unit cell dimension *c*
α	Interfacial angle in a unit cell
β	Interfacial angle in a unit cell
γ	Interfacial angle in a unit cell
Z	Unit cell formula unit
μ	Absorption coefficient
δ	Chemical shift in NMR
ppm	Parts per million
NMR	Nuclear magnetic resonance
HOMO	Highest occupied molecular orbital
LUMO	Lowest unoccupied molecular orbital
ORTEP	Oak Ridge Thermal Ellipsoid Plot
CHEF	Chelation enhanced fluorescence
CHEQ	Chelation enhanced quenching
ESIPT	Excited state intramolecular proton transfer
PET	Photoinduced electron transfer
DCM	Dichloromethane
THF	Tetrahydrofuran
DMSO	Dimethyl sulfoxide
DMF	N,N-Dimethylformamide

Table of Contents

Chapter 1

Introduction, Materials and Methods

Abstract

A brief discussion of metal ion sensing, fluorescent detection and its mechanism such as excited state intramolecular proton transfer (ESIPT), photoinduced electron transfer (PET), chelation enhanced fluorescence (CHEF), C=N isomerization, and chelation enhanced quenching (CHEQ) have been discussed with examples. A brief introduction about features and disadvantages of Zn^{2+}, Cu^{2+} and Pd^{2+} have been discussed. Accordingly, some recent developments on fluorescent detection of Zn^{2+}, Cu^{2+} and Pd^{2+} have also been discussed. In the next section of this thesis, synthesis of tetrasubstituted benzene has been described, a brief review on various reactions involved in synthesis of substituted benzenes have also been discussed.

1. Introduction

Metal ions are present in all living beings and play a pivotal role in biology as they regulate fundamental processes like metabolism, biomineralization, osmotic regulation, catalysis, signaling.[1] There is a high abundance of group 1 and 2 metals (Na, K, Ca and Mg) in many of the bio-organisms. However, transition metal ions (Fe, Cu, Zn, Mn, Ni, Co, W, Mo, Cr and V) also play a crucial role in biology. These transition metals are present in much lower levels with respect to group 1 and 2 metals and are frequently referred as trace metals. Metals like zinc, copper and iron are crucial component in many biological processes and enzymatic reactions.[2] The balanced concentration (homeostasis) of biological metal ions is necessary to regulate the fundamental processes; however, if the metal homeostasis is disturbed, it can lead to many diseases that include cancer,[3] and diabetes[4] neurodegenerative diseases.[5] Homeostasis disruption can be caused by lack of excretion of potential toxic metal ions,[6] excessive accumulation of zinc, iron and copper ions.[7,8] Increase in copper ion levels have been identified in tumor and cancer.[9] Imbalance in concentration of Zn^{2+} ion has also been linked to cancers and diabetes. As we have discussed, various metal ions have crucial role in biological processes having appropriate concentration; however, if there is disruption in their concentration can lead to fatal diseases. Hence it is essential to detect and quantify metal ions using various techniques. There are many conventional electroanalytical and spectrophotometric detection techniques available for the detection of small amounts of metal ions which include atomic absorption spectroscopy (AAS), inductive coupled plasma mass spectrometry (ICP-MS), voltammetry, chromatography.[10] However, they have limitations of

high cost, complex sample preparation, sensitivity, selectivity, time consuming, require skilled persons. On the other hand, the fluorescent detection technique is most advantageous over other available techniques as it provides quick response, high selectivity, low cost and low detection limit.[11]

Fluorescence is a phenomenon of emission of visible light upon irradiation of light of particular wavelength. The fluorescence property occurs for very short time of few nanoseconds after an absorption event, *i.e.*, as soon as light source is removed, the fluorescent materials stop to glow immediately. This phenomenon is highly useful in the field of analytical chemistry. The fluorescence property plays crucial role in the recognition of atoms, molecules or ions. The species which is going to be detected is known as analyte and the molecule with the help of which this species is detected is known as probe or sensor. Fluorescent sensors generally contain two parts one is metal chelating or binding unit (receptor) and other is signaling unit (fluorophore) capable of absorbing and emitting light; sometimes, these two parts are separated with spacer. When a particular analyte interacts or binds with binding unit of probe, there is alteration of signal observed because of electronic or molecular structure change, which helps in detection of that particular species. Typically, there is enhancement or decrease in fluorescence intensity observed upon interaction with analyte, if there is enhancement in fluorescence upon binding, it is termed as turn-on detection and if there is decrease in fluorescence intensity upon binding, the term turn-off detection is referred. Polydentate ligands containing O, N or S donor atoms are widely used in artificial fluorescent sensor for detection of metal ions as they provide strong complexing ability. Several factors should be accounted for design and development of fluorescent chemosensor, selective for specific metal ion which include donor atom preference, preferential coordination geometry, preorganization of polydentate ligand and HSAB principle.[12,13]

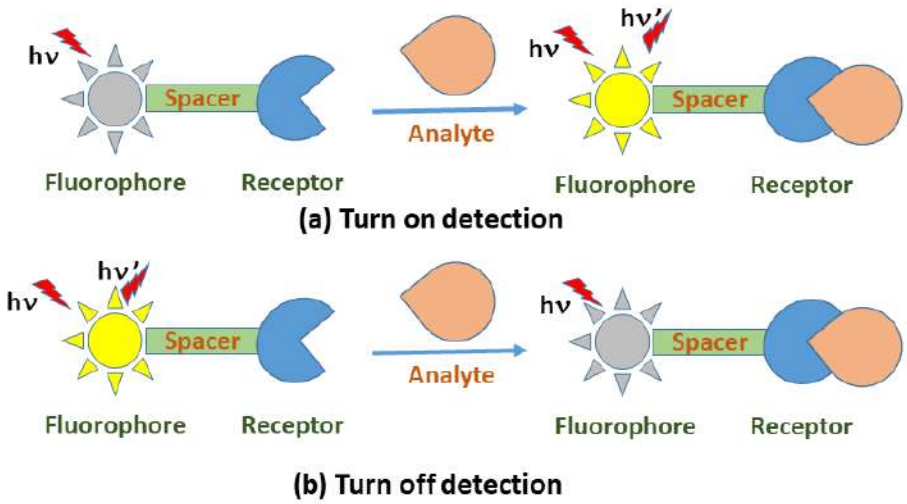

Figure 1. Schematic presentation of (a) turn on and (b) turn off fluorescent detection.

According to design of probe, their selectivity for particular analyte can be modified. Here in this chapter, a brief introduction of metal ion sensors and their mechanism of sensing has been discussed. Along with these, the metal ions which are used here in this thesis for detection are Zn^{2+}, Cu^{2+} and Pd^{2+} and hence a brief introduction about features and disadvantages of these metal ions and some recent reports for the recognition of these analytes using fluorescent probes have also been described.

1.1 Fluorescent sensing mechanism

Scientists have utilized practical approach to design and develop new and efficient chemosensor using several fluorescence mechanisms and with the help of concepts of supramolecular chemistry. These conventional mechanisms include photoinduced electron transfer (PET),[14,15] excited state intramolecular proton transfer (ESIPT),[16,17] intramolecular charge transfer (ICT),[18] ligand metal charge transfer (LMCT), metal ligand charge transfer (MLCT), fluorescence resonance energy transfer (FRET),[19] C=N isomerization,[20] chelation enhanced fluorescence (CHEF) and chelation enhanced quenching (CHEQ). Some of important mechanisms have been discussed here.

1.1.1 PET mechanism

Photoinduced electron transfer mechanism is generally used in explaining turn on fluorescent detection. The probe generally contains fluorophore and receptor (containing N, O or S donor atom) which are separated with spacer. In the unbound state, upon excitation with light having definite wavelength, there might be electron transfer taking place from free receptor to

fluorophore which in result decrease the fluorescence, however when analyte interacts with receptor, the electron transfer is no longer taking place and hence upon excitation, there is huge enhancement in fluorescence intensity was observed.[15]

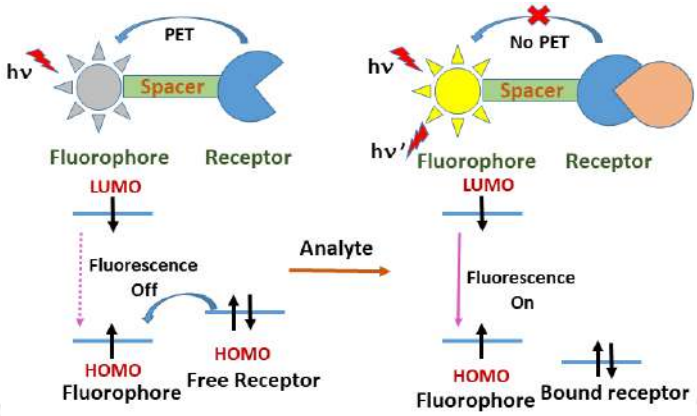

Figure 2. Schematic presentation of PET mechanism in turn on chemosensor.

Probe **1** was synthesized from benzothiazolyl-salicylaldehyde and 2-hydrazinoquinoline, and found to have ability to detect Zn^{2+} ion selectively accompanied by appearance of green fluorescence. The proposed sensing mechanism for the **1** towards Zn^{2+} was suggested to be restriction of PET upon coordination with Zn^{2+} ion. In free probe **1**, the lone pair at imine nitrogen participated in photoinduced electron transfer process, due to which it remained weakly fluorescent, however upon coordination with Zn^{2+} the PET process got inhibited and high enhancement in fluorescent intensity was observed.[21]

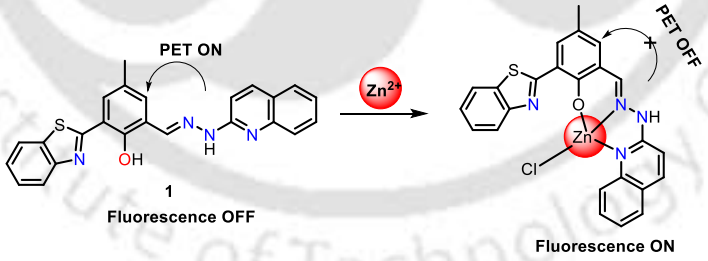

Figure 3. Proposed binding mechanism of **1**.

PET mechanism has also been useful in explaining turn off fluorescent detection of metal ions. The chemosensor itself remains highly fluorescent upon excitation with light of particular wavelength, however as soon as it interacts with metal ion, the photo excited electron of chemosensor can be transferred to vacant orbital of metal ion, consequently, quenching of fluorescence occurs.[22]

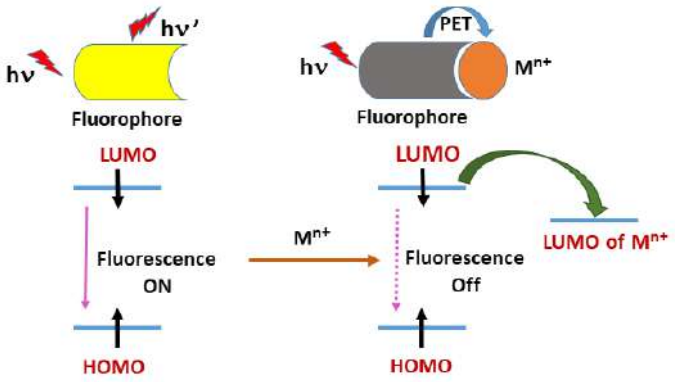

Figure 4. Schematic presentation of PET mechanism in turn off chemosensor.

A BODIPY based probe **2** having 2,2′-bipyridyl group was utilized in selective detection of Cu^{2+} ion. The probe **2** was highly fluorescent initially but when it interacted with Cu^{2+} and became non fluorescent due to operation of PET from excited state of fluorophore to bound Cu^{2+} via bipyridyl unit.[23]

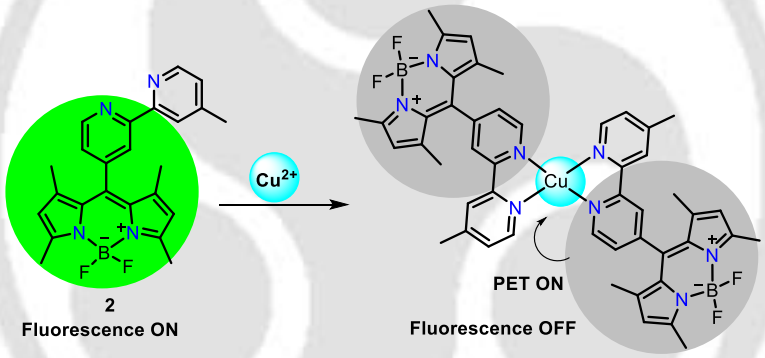

Figure 5. Sensing mechanism for turn off fluorescent recognition of Cu^{2+}.

1.1.2 ESIPT mechanism

Typically, the ESIPT process includes the shifting of a –OH (or –NHR) proton to the C=O (or C=N) upon excitation via a six or five membered ring. It is faster process (ranges in time scale of few picoseconds) as compared to electron transfer process.[24][25] ESIPT is four level photochemical process in which (i) fluorophore generally exists in enol form which upon photoexcitation goes to S_1 state, (ii) in this state acidity and basicity of hydrogen bond donor and hydrogen bond acceptor increases (iii) it favours the enol keto phototautomerization and as a result enol form is rapidly converting into keto form in its excited state S_1' (iv) after radiative decay, it comes to ground state S_0' which revert back to its original enol form at S_0 after reverse proton transfer (RPT). The ESIPT based fluorophores generally have high stokes

shift values. The process of ESIPT can be inhibited upon deprotonation and coordination with metal ions.

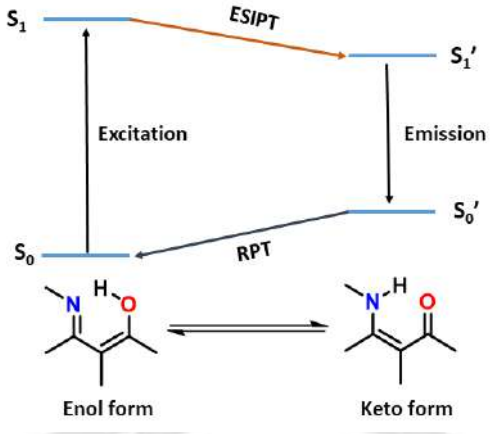

Figure 6. Schematic presentation of ESIPT mechanism in fluorescent probes.

The probe **3** was synthesized from 2-hydrazinobenzothiazole and 2,6-diformyl-4-methylphenol and acted as turn on fluorescent sensor for Zn^{2+}. A huge enhancement in fluorescence was observed when probe **3** coordinated with Zn^{2+} ion due to ESIPT process got inhibited.[26]

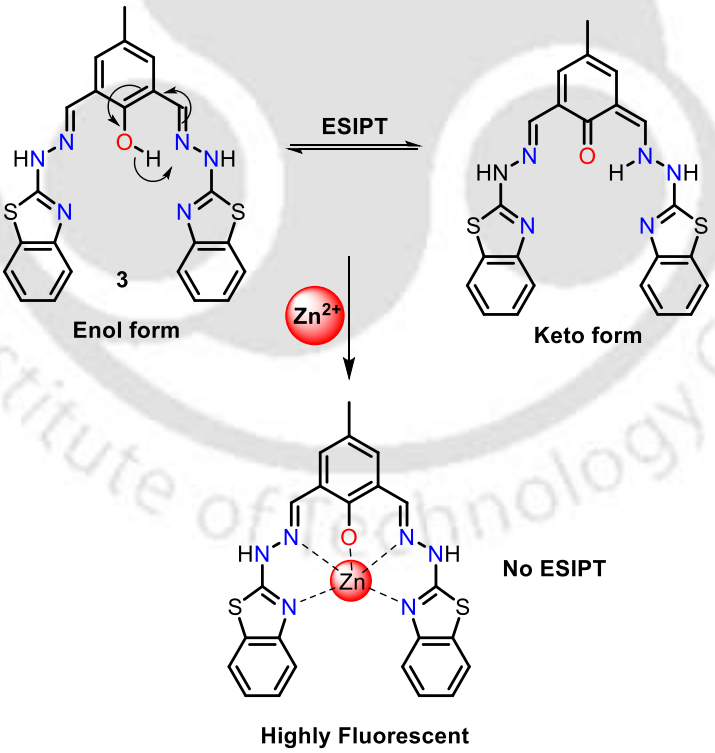

Figure 7. Mechanism of sensing of Zn^{2+} by probe **3**.

1.1.3 C=N isomerization mechanism

The C=N isomerization mechanism can also explain the phenomenon of fluorescence turn on upon complexation with metal ion. From various reports, it has been observed that the molecule containing unbridged C=N group may undergo isomerization upon excitation, and because of this isomerization molecule becomes non-fluorescent. However a dramatic enhancement in fluorescence intensity was observed when this C=N isomerization was restricted with the help of bridging on C=N group or complexation/chelation with a metal ion.[27] Typically, due to C=N isomerization, the probe remains non fluorescent whereas, upon coordination with metal ion, the complex shows high fluorescent intensity.

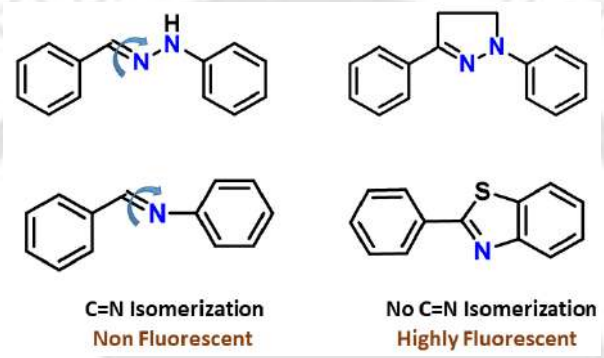

Figure 8. Bridged and un-bridged C=N containing compounds sowing weak and high fluorescence.

A fluorescent probe **4** having coumarin as signaling unit (fluorophore) and antipyrine as chelating moiety (receptor) linked together by C=N bond was reported. Free probe was almost non fluorescent due to C=N isomerization, however a remarkable enhancement in fluorescence was attained upon coordination with Zn^{2+} because of inhibition of C=N isomerization.[20]

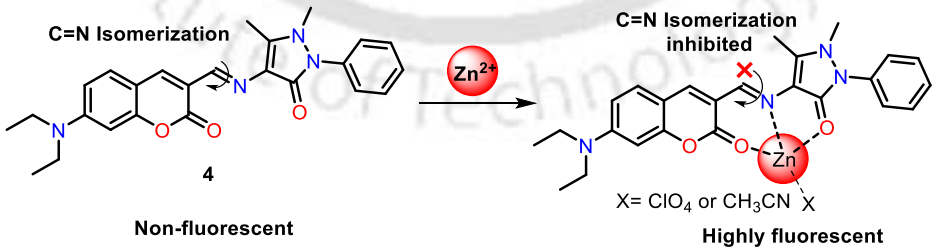

Figure 9. Proposed sensing mechanism for detection of Zn^{2+} by **4**.

1.1.4 CHEF and CHEQ mechanisms

Chelation enhanced fluorescence is another mechanism for explanation of turn on fluorescent detection. Chemosensor upon excitation remains non fluorescent initially because of non-

radiative decay due to viberation, rotation or interaction with solvent, however upon chelation with analyte, rigidity in chemosensor has been attained and favours radiative decay and hence there is huge enhancement in fluorescence is obtained. A terpyridine based ligand **5** was reported to have conformational flexibility in free state remained weakly fluorescent however upon coordination with Zn^{2+} ion, flexibility got decreased which in turns facilitates fluorescence emission due to occurrence of CHEF.[28]

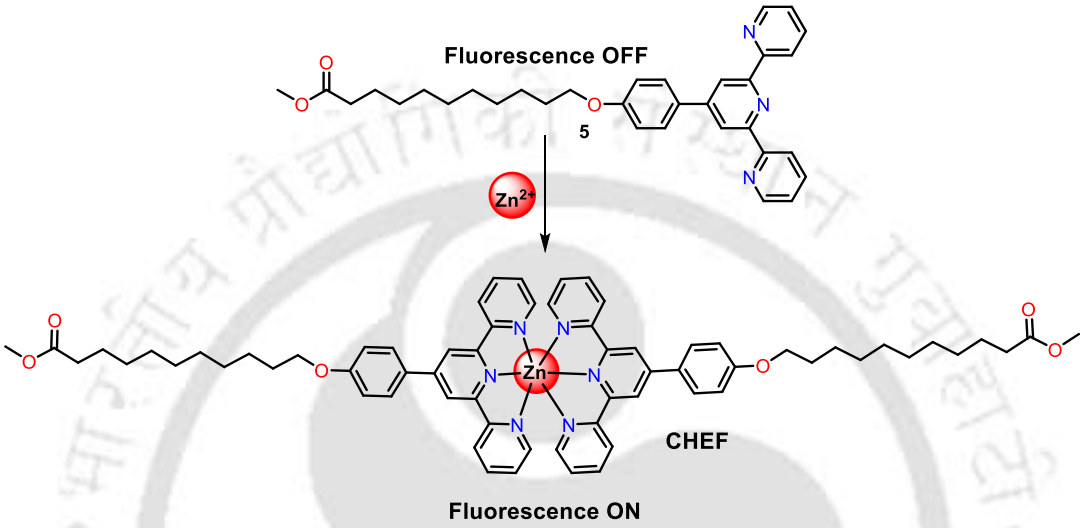

Figure 10. Binding mechanism **5** with Zn^{2+} ion

Conversely, in CHEQ mechanism, the sensor itself has high fluorescence upon excitation, but as soon as it chelates with analyte, this fluorescence phenomenon of sensor is disrupted because of formation of non-fluorescent complex which favours deactivation of photons in non-radiative pathway. This mechanism generally utilized in explaining turn off fluorescent detection. A schiff base probe **6** containing vanillin was reported that detects Cu^{2+} ion in turn off fashion because of occurrence of CHEQ.[29]

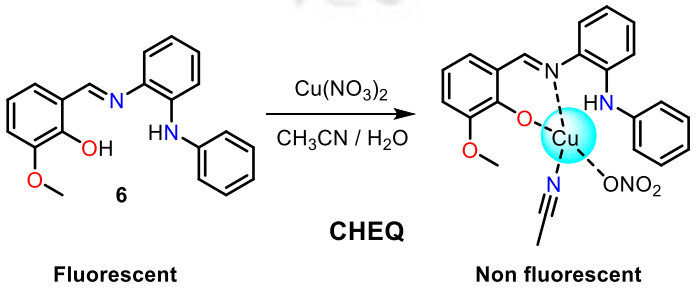

Figure 11. Fluorescent recognition of Cu^{2+} ion by **6**.

1.2 Recent development in fluorescent detection of Zn^{2+}, Cu^{2+} and Pd^{2+} ions

Some selected probes having selectivity for Zn^{2+}, Cu^{2+} and Pd^{2+} ions, utilizing aforementioned mechanisms have been illustrated here, as in Chapters 2 and 3 fluorescent detection of Zn^{2+}, Cu^{2+} and Pd^{2+} have been reported.

Zinc exists as Zn^{2+} ion in the human body and it is second most abundant trace metal ion after iron. It has great importance in physiological response. Zn^{2+} ion is found in active site of many enzymes like carbonic anhydrase and carboxypeptidase. In the human body, labile Zn^{2+} ion controls many events such as neuronal transmission, apoptosis, epilepsy and ischemia.[30] Its balanced concentration in our body regulates various processes like immunity growth and endocrine function.[31][32] However, its imbalance in concentration may lead to various fatal diseases like Alzheimer's and Parkinson's diseases.[33][34] Zn^{2+} has d^{10} electronic configuration in its valence shell, Cd^{2+} and Hg^{2+} also belong to same group having same fulfilled d^{10} electronic configuration. Due to their fulfilled d orbitals they are spectroscopically inaccessible and it becomes very hard to distinguish Zn^{2+} ion over Cd^{2+} and Hg^{2+} ions. Hence detection of zinc(II) is crucial. Fluorescence detection technique enables an easy way to distinguish these metal ions using appropriate fluorescent probes.

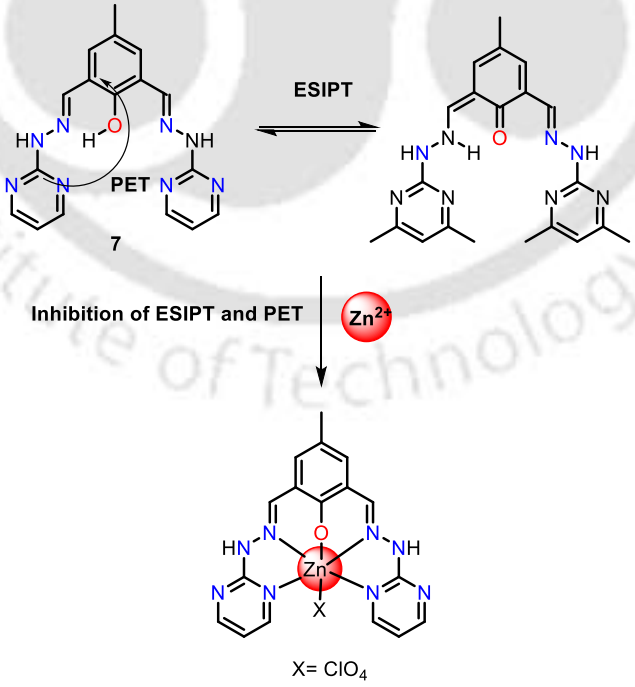

Figure 12. Sensing pathway of **7** for the detection of Zn^{2+} ion.

A probe **7** was synthesized using 2-hydrazinyl-4,6-dimethylpyrimidine and 2,6-diformyl-4-methylphenol. It was found to be a selective chemosensor for Zn^{2+} ion in fluorescent turn on fashion. The sensing mechanism for detection of zinc(II) ion was due to restriction of ESIPT and PET processes and onset of CHEF.[35] Another similar probe **8** was reported which can also detect Zn^{2+} in fluorescent turn on fashion. The probable sensing mechanism for the detection of Zn^{2+} was due to inhibition of PET and occurrence of CHEF, however, the role of ESIPT and C=N isomerization cannot be neglected.[36] There are various reports on detection of Zn^{2+} published based on quinoline (**9**),[37] 1,8-naphthalimide (**10**),[38] pyrene (**11**),[39] coumarin (**12**),[40] benzoxazole (**13**)[41] and fluorescein (**14**).[42]

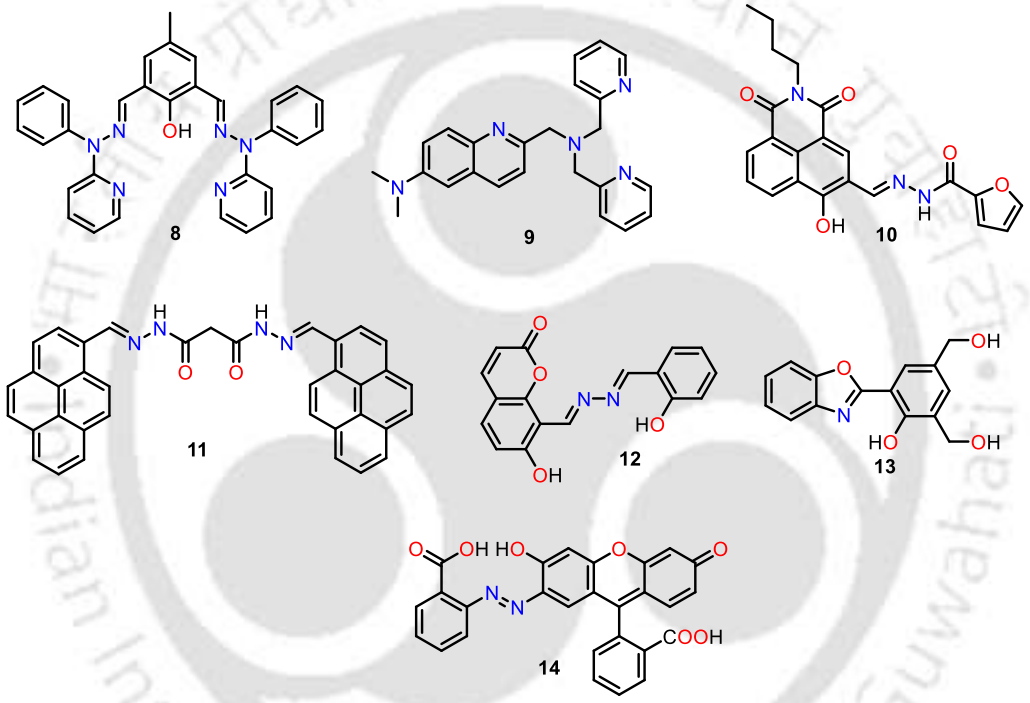

Figure 13. Some recent probes utilized for fluorescent detection of Zn^{2+} ion.

Copper (II) ion is third most abundant trace metal ion after iron and zinc. It has an important role in many physiological processes like brain function, cellular respiration and bone formation.[43][44][45] The permissible limit of Cu^{2+} in drinking water prescribed by WHO is 31.5 µM. Imbalance in concentration of Cu^{2+} in the human body may lead to fatal diseases like Parkinson′s, Menkes, Alzheimer′s and heart diseases.[46][47] Excess content of Cu^{2+} in environment reduces chlorophyll quantity and accordingly hinders photosynthesis and plant growth.[48][49] Wastewater containing excess amount of copper poses risk to surrounding organism.[50]

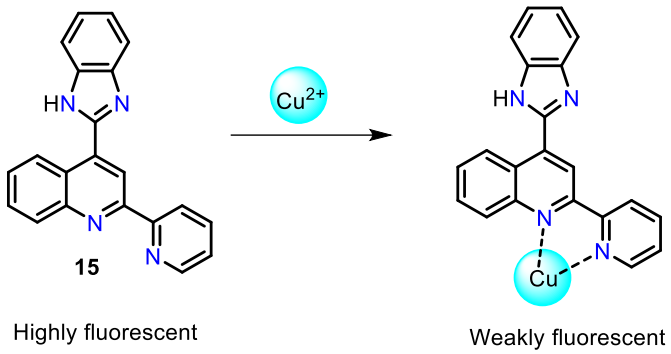

Figure 14. Proposed binding mode of **15** with Cu^{2+}.

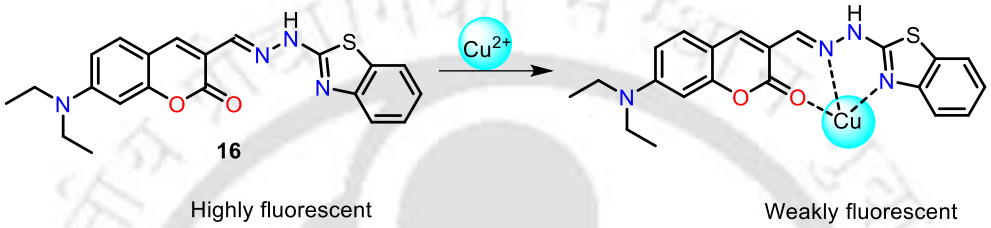

Figure 15. Proposed binding of **16** with Cu^{2+}.

On the other hand, palladium has applications in the various fields such as electronic devices,[51] fuel cells,[52] jewelry,[53] and catalyst in organic synthesis[54]. However, it has adverse effects in environment as well as human health, can bind with various proteins (silk fibroin, casein), DNA, thiol containing amino acids, can cause eye and skin irritation.[55] The permissible Pd^{2+} content in drugs was prescribed by WHO is 5-10 ppm.[56] A 2-pyridylquinoline based fluorescent chemosensor **15** was synthesized which acted turn off chemosensor for Cu^{2+} ion, the fluorescence intensity was quenched by 18 folds upon introduction of Cu^{2+} to probe solution.[57] Another coumarin based chemosensor **16** was synthesized and used as chemosensor for selective recognition of Cu^{2+} ion in the coexistence of various metal ions. The limit of detection was calculated to be 4.0 ppb.[58] A probe **17** for selective recognition of Pd^{2+} ion in aqueous medium via turn off fluorescence was reported which has pyridine-2,6-dicarboxamide and naphthyl groups, upon introduction of Pd^{2+} ion to the probe resulted in quenching of fluorescence.[59] Another quinoline-containing chemosensor **18** for selective fluorescent detection of Pd^{2+} was designed. It was used for detection of Pd^{2+} in various water samples.[60] Selective and sensitive turn on fluorescent detection of Pd^{2+} ion was achieved with a perylene diimide based fluorescent probe **19** in mixed aqueous media.[61] A very low detection limit of 7.32 nM was obtained by this probe for Pd^{2+} ion.

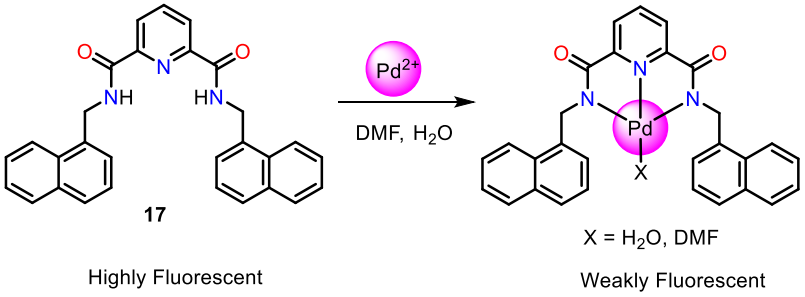

Figure 16. Proposed binding mode of **17** with Pd^{2+}.

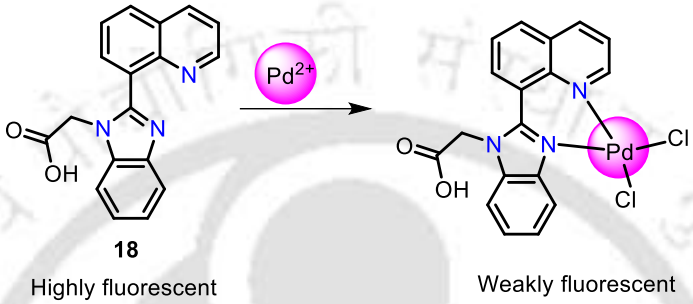

Figure 17. Proposed binding mode of **18** with Pd^{2+}.

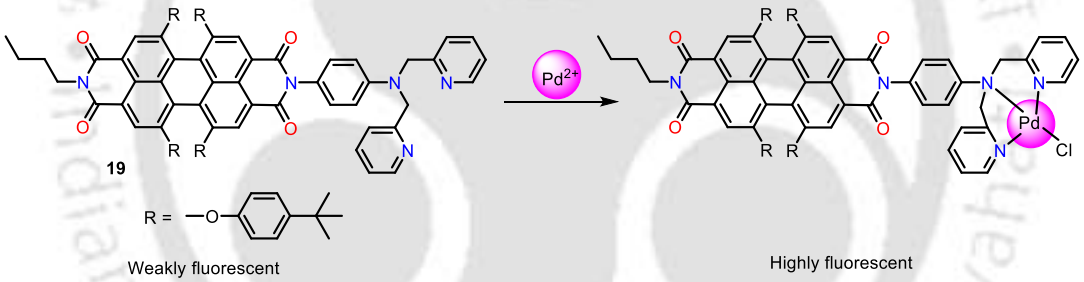

Figure 18. proposed binding mode of **19** with Pd^{2+}.

Sometimes copper and palladium may exist together such as heterogeneous catalysis which utilizes palladium /copper cocatalyst.[62] Therefore, their simultaneous detection is important. Some of the probes which detects both the Cu^{2+} and Pd^{2+} ions have been shown here. A probe bis-tetraphenylimidazole Schiff base **20** showed red fluorescence (at 550-650 nm) in aqueous solution but upon introduction of Cu^{2+} and Pd^{2+} ions, the fluorescence intensity was quenched tremendously.[63]

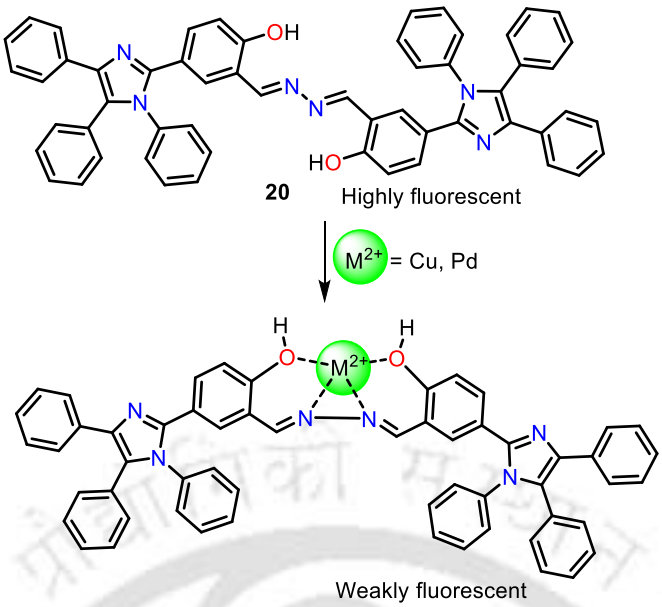

Figure 19. The sensing mechanism of **20** for Cu^{2+} and Pd^{2+}.

A probe **21** having purine derivative was synthesized and showed quenching of fluorescence upon inclusion of Cu^{2+} and Pd^{2+} into the HEPES buffer solution of probe. Using this probe, a very low detection limit 0.63 µM for Pd^{2+} and 1.19 µM for Cu^{2+} were achieved.[64]

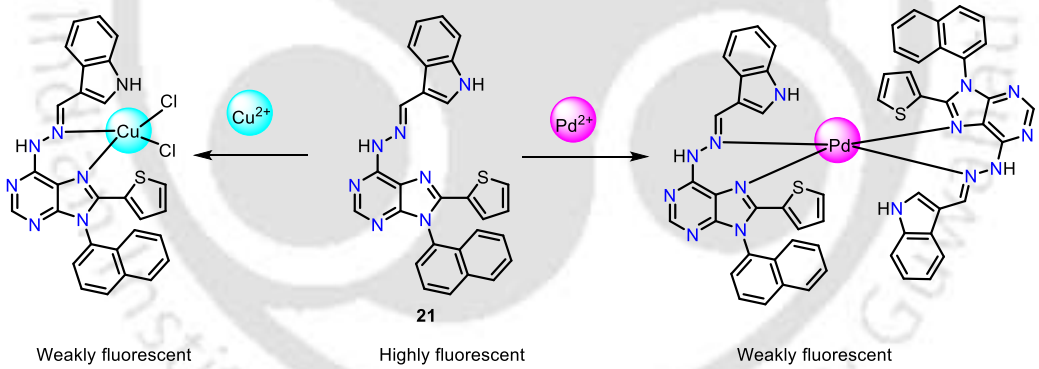

Figure 20. The probable binding mode of **21** with Cu^{2+} and Pd^{2+}.

1.3 Synthesis of substituted benzene

Substituted benzene are found in many natural products, agrochemicals and pharmaceuticals. They are also act as building blocks for the synthesis of today′s industrial chemicals and functional materials.[65] The function of these compounds generally depend upon the substituents attached to benzene ring and therefore synthesis of polysubstituted benzenes remained the center of attraction among the organic chemists. Conventionally, these substitution patterns were achieved by electrophilic and nucleophilic aromatic substitution reactions of pre-existing arenes as well as transition metal catalyzed cross coupling

reactions.[66] However, it has limitation of sequential manipulations of reactants and it involves many steps. On the other hand, these reactions involve expensive transition metal catalyst, multistep, harsh condition and also have limited substitution pattern. Therefore, the reaction which involves one pot synthesis for attainment of substituted benzenes having specific substitution patterns are most widely used. Benzannulation reactions are the reactions which involve the formation of benzene ring with definite substitution pattern from acyclic building blocks.[67] These reactions enable formation of desired substituted benzene in less number of steps, usually regioselective in nature with flexible substitution pattern. There are various benzannulation reactions reported and some of the recent ones have been discussed below.

A series of polysubstituted benzenes were synthesized utilizing a [3+3] benzannulation reaction of trifluoromethylalkenes and β,γ-alkynyl-α-ketoesters. This methodology has enabled access to wide range of polysubstituted benzenes.[68]

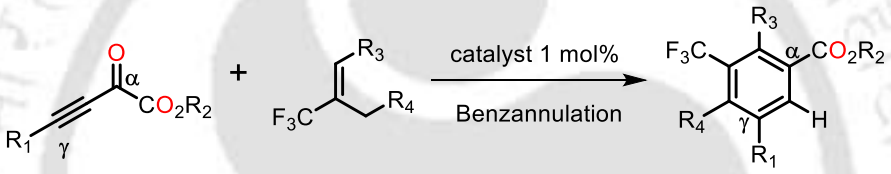

Mehta and co-workers reported synthesis of diversely functionalized carbazoles utilizing one-pot, transition metal free benzannulation reaction of 2-(2-oxo-2-arylethyl)-indole-3-carbaldehydes and ynones/alkynoate. Various natural products were also reported utilizing this methodology.[69]

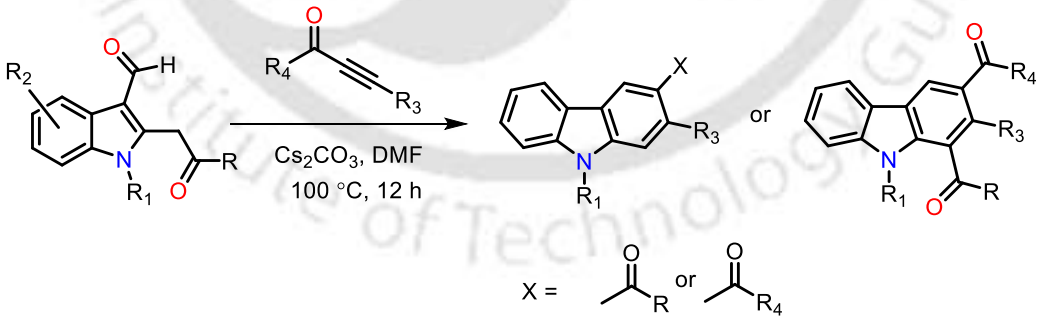

Another report on synthesis of substituted benzene (2-nitrobiaryls) using metal free, organocatalyzed [4 + 2] benzannulation reaction of nitroolefins and 1,4-dithiane-tethered enals.[70]

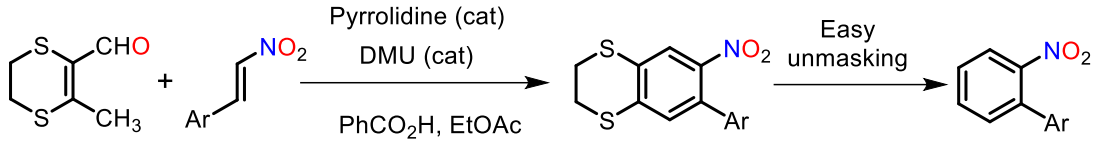

Varieties of polycyclic indeno[1,2 *a*]fluorenes were synthesized using domino benzannulation reaction of 2,3-dibromoindenone and acyclic 1,3-dicarbonylsin presence of base. This methodology described synthesis of pentacyclic molecules using 2,3-dibromoindenone.[71]

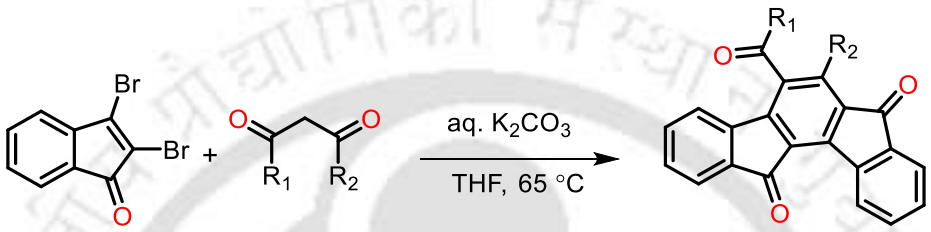

Another Ru(II) catalyzed regioselective [3+1+2] benzannulation reaction was adopted for synthesis of polysubstituted benzenes from allyl alcohol and acetylenedicarboxylate esters.[72]

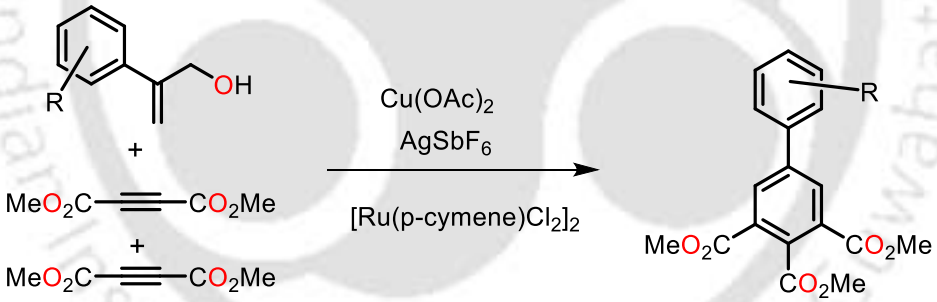

A [3+2+1] benzannulation reaction was adopted to synthesize polysubstituted arylnitriles via Tf_2O-mediated reaction of enaminones and acylacetonitriles. The reaction went in mild condition with high functional groups tolerance.[73]

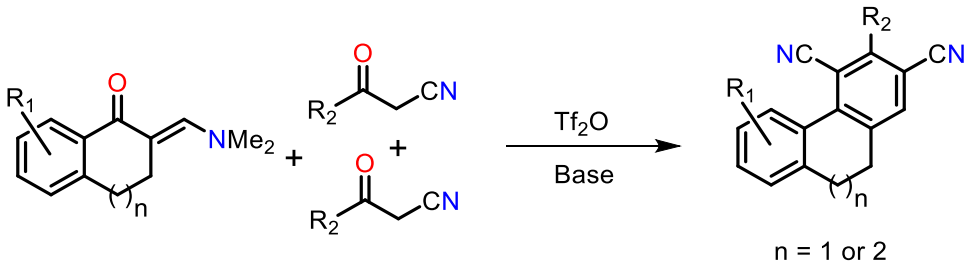

A phosphine catalyzed domino benzannulation reaction between allenoates and enamines has been published for the synthesis of substituted terephthalates.[74]

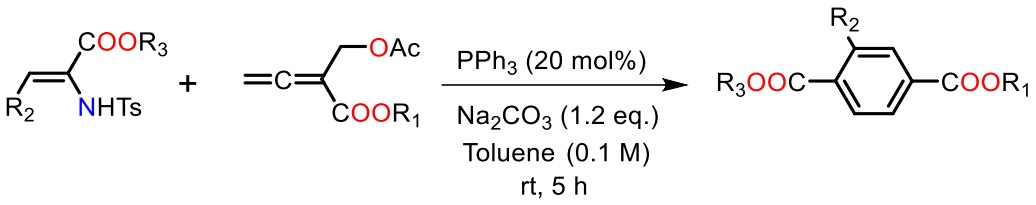

A tertiary amine catalyzed, [3+3] benzannulation reaction was carried out to synthesize a series of CF_3 substituted fully functionalized benzenes.[75] The methodology had features of high atom economy, exclusive chemoselectivity and require less number of steps for the synthesis.

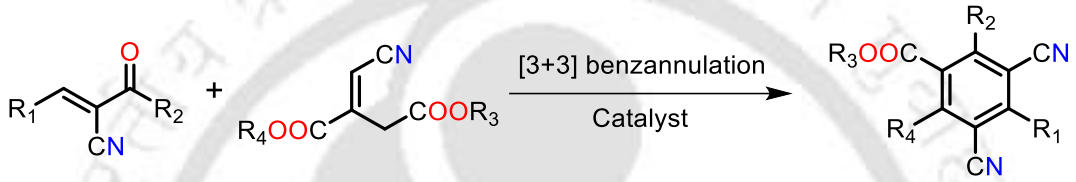

A Cs_2CO_3 mediated [4+2] benzannulation reaction was adopted for synthesis of fully substituted aryl α-keto esters from α-cyano-β-methylenones and ynediones.[76] This methodology features metal free condition, high functional groups tolerance, high atom economy.

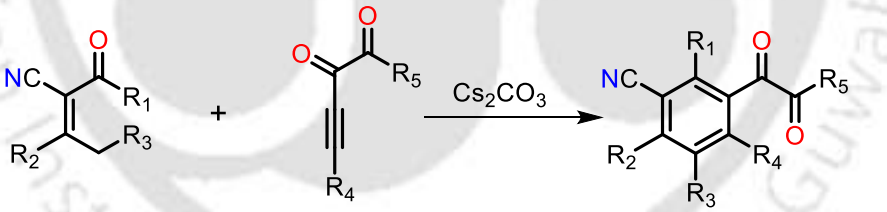

The cascade reaction of vinyloxirane and coumarin using catalytic amount of $BF_3{\cdot}OEt_2$ was adopted to synthesize benzocoumarin derivatives.[77] This reaction methodology has high functional groups tolerance and has potential development of drug.

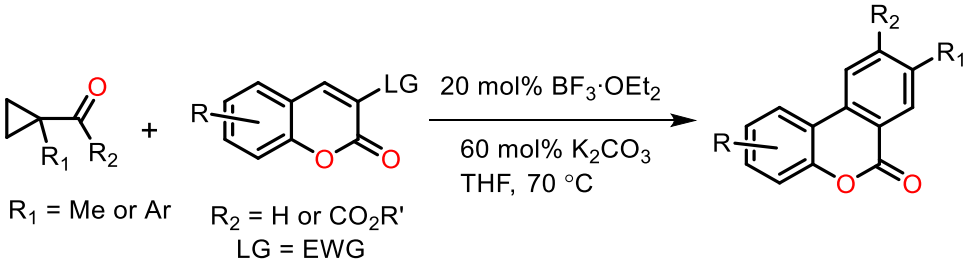

A series of highly substituted naphthalenes were synthesized from Ni(II)- catalyzed [2+2+2] benzannulation reaction of novel directing groups with alkynes.[78]

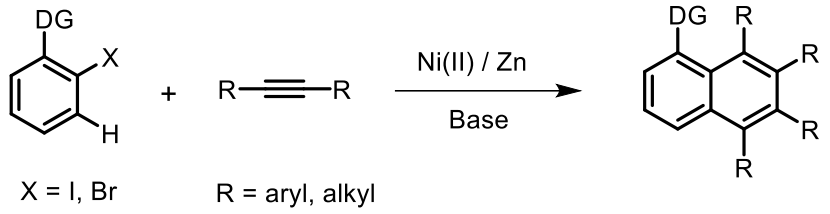

A series of polycyclic (hetero)aromatic organic compounds were synthesized by utilizing green and electrochemical methodology via [4+2] benzannulation reaction of biaryldiazonium salts and alkynes.[79] This methodology features a wide substrate scope.

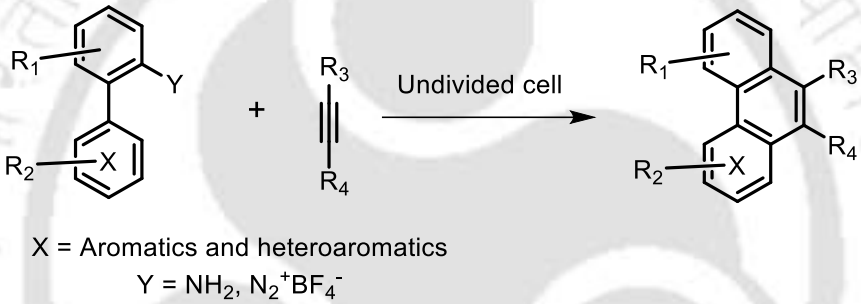

1.4 Objective of thesis

Inspired from survey on various reported literature of metal ion sensing, an effort has been made to evaluate metal ion sensing ability of 3,3′-((-(5-(tert-butyl)-2-hydroxy-1,3-phenylene)bis(methaneylylidene))bis(hydrazin-1-yl-2-ylidene))bis(quinoxalin-2(1H)-one) (**LH**) in Chapter 2. Similarly, in Chapter 3, metal ion sensing ability of bidentate ligand 1-(imidazo[5,1-*a*]isoquinolin-3-yl)naphthalen-2-ol (**L2H**) has been described. In Chapter 4, synthesis and coordination ability of a bis-terpyridine ligand has been discussed. Taking cue from the synthesis of terpyridine, a series of tetrasubstituted benzenes synthesis has been explored in Chapter 5 and a series of pentasubstituted cyclohexanols in Chapter 6.

1.5 Materials and methods

1.5.1 Materials

LiCl, KCl, NaCl, $CaCl_2$, $MgCl_2$, $AlCl_3$, $CrCl_3$, $MnCl_2$, $ZnCl_2$, $NiCl_2{\cdot}6H_2O$, $FeSO_4{\cdot}7H_2O$, $FeCl_3{\cdot}6H_2O$, $CoCl_2{\cdot}6H_2O$, $CuCl_2{\cdot}2H_2O$, $CdCl_2$, $HgCl_2$, $Pb(NO_3)_2$, $PdCl_2$, $PtCl_2$, $AgNO_3$, $AuCl_3$, oxalic acid, *o*-phenylenediamine, SeO_2, $NH_2NH_2{\cdot}H_2O$, aldehydes, aryl methyl ketones,

spectroscopic grade MeOH, DMSO, and CH_3CN solvents were supplied by Merck India. Isoquinoline, 2-hydroxynaphthaldehyde, 4-tert-butyl-2,6-diformylphenol, DMSO–d_6, $CDCl_3$, and HEPES buffer were purchased from Sigma Aldrich. The purchased sodium hydride was of 55-60% in mineral oil and molar ratio was calculated using this strength. No purification processes were performed in supplied chemicals and solvents used here for synthesis, characterization and experimental work.

1.5.2 Instrumentation and methods

An Agilent Cary 100 spectrophotometer and a Perkin Elmer Lambda-35 instruments were used for recording the UV-visible spectra with the help of quartz cuvettes (path length = 1 cm) in 200-800 nm range. For recording fluorescence spectra, a Horiba Fluoromax-4 spectrofluorometer instrument was used with the help of quartz cuvettes (path length = 1 cm). An Agilent QTOF6520 and Agilent 6546A series High Resolution Mass Spectrometers were used for recording mass spectra. Lifetime measurements (TRPL study) of probes and probes containing metal ions were determined by using Pico Second Time Resolved Fluorimeter Lifespec II by Edinburgh Instruments. Melting points of organic compounds were determined using Buchi melting point B-540 apparatus and are uncorrected. NMR studies were performed using a Bruker Advance 600 MHz NMR instrument. TMS was used as an internal reference in deuterated solvents; chemical shifts (δ scale) were reported in parts per million (ppm) unit. ^1H NMR spectra were reported in the sequence of multiplicity, coupling constant (Hz), and number of protons. A PerkinElmer FTIR Spectrum Two instrument was used for recording IR spectra.

1.5.3 UV–Vis and fluorescence spectroscopic studies

The EtOH/aqueous HEPES buffer (5 mM, pH = 7.4, 8:2, *v/v*) was used for solution studies in case of **LH** and unless otherwise stated, solution refers to this buffered solution. The stock metal salts (10 mM) were prepared in MeOH and diluted to 1 mM. For a UV-visible and fluorescence experiments, a 1 mM solution of **LH** was prepared in DMSO and diluted to 1.0×10^{-5} M in cuvette with EtOH/aqueous HEPES buffer. In the typical experiments, a quartz optical cell (path length = 1 cm) was filled with 3.0 mL of the **LH** solution (1.0×10^{-5} M) and then appropriate amounts of the corresponding metal ions (1mM) were added and spectra were recorded sequentially. The excitation wavelength employed here for the fluorescence experiment was 419 nm, and the emission spectra were recorded in the range 440-820 nm using an emission slit of 5 nm. all spectra were taken right away just after mixing **LH** with the metal

chloride solutions for one minute. Similarly, in case of **L2H**, the MeOH/aqueous HEPES buffer (5 mM, pH = 7.4, 2:8, *v/v*) was used for solution studies. **L2H** solution (2.0×10^{-5} M) was titrated with appropriate amounts of metal salt solutions (2 mM). The excitation wavelength used to record fluorescence spectra of **L2H** was 336 nm and the emission range 356-652 nm with slit length 5 nm were used.

1.5.4 Calculation of Detection Limit

The well accepted procedure employing equation (1) was used to calculate the detection limit of probes **LH** and **L2H** towards M^{2+} ion. Firstly, 15 times, with 2 minutes' gap between each fluorescence spectral recordings, the standard deviation (σ) of emission maxima of blank (the probes **LH** and **L2H**) were calculated. Fluorescence titration experiment was then performed with addition of appropriate amounts of MCl_2 solution. Emission maxima *vs* concentration of M^{2+} gave slope (k) of the fitted straight line and finally detection limit was calculated using following equation.[80]

$$Detection\ limit = \frac{3\sigma}{k} \qquad (1)$$

1.5.5 Binding ratio between analyte and probes

For the determination of binding stoichiometry between probes (**LH** and **L2H**) and M^{2+}, a method of continuous mole-fraction variation was used, and Job's plot was obtained. In the typical experiment, with consecutive change in mole fraction of M^{2+} ion (M = Zn, Cu, Pd) ranging from 0 to 1, emission maxima were recorded and plotted. After linear fitting, point of intersection obtained in the graph gives the mole fraction of M^{2+} ion which is exactly binding with **LH** or **L2H** and accordingly binding ratio between M^{2+} and **LH** / **L2H** were determined.

1.5.6 Evaluation of binding constant

The probe solutions were titrated with increasing concentrations of the M^{2+} ion. The binding constant for the formation of the respective host–guest complex was evaluated using the Benesi–Hildebrand (B–H) plot.[81,82]

$$\frac{1}{(I - I_0)} = \frac{1}{\{K(I_{max} - I_0)C^n\}} + \frac{1}{I_{max} - I_0} \qquad (2)$$

Where, I_0 is the emission intensity of probes, I_{max} is maximum emission intensity value and I is the observed emission intensity at that particular wavelength in the presence of a certain

concentration of the analyte of concentration (C). The binding constant K was determined from the slop of linear plot.

1.5.7 Determination of Fluorescence quantum yield

Fluorecsence quantum yield (Φ) were determined with the help of equation (3).[83,84]

$$\Phi_{sample} = \frac{OD_{standard} \times A_{sample}}{OD_{sample} \times A_{standard}} \times \Phi_{standard} \qquad (3)$$

Where "A" is the area under the emission spectral curve and OD refers to optical density at the excitation wavelength. Rhodamine 6G (Φ = 0.95 in ethanol) was used as reference to measure quantum yield.

1.5.8 Time-resolved fluorescence spectroscopy

As a source, a laser diode with 405 nm excitation wavelength was employed in case **LH** and **LH** + Zn^{2+} solutions. Using the DAS6 programme, the fluorescence decays were fitted.[85] The laser diode having 340 nm excitation wavelength was used as a source in case of **L2H** and **L2H** + M^{2+} (M = Cu, Pd) solutions.

1.5.9 X-ray crystallography

The structure of some organic compounds and metal complexes were also determined using a single XRD diffractometer. A Bruker Nonius Smart Apex III single-crystal X-ray diffractometer was used for crystallographic data collection. The cell reduction and data refinements were done with the help of Bruker Apex III program. SHELXS-14 was used Structure solution and refined by full matrix least-squares method.[86]

1.5.10 Theoretical study

The structure of probes and metal complexes were optimized using the density functional theory (DFT/TDDFT) method at the B3LYP level. In Chapter 2, 6311-G (d) basis set was used for all elements in **LH** and LanL2DZ basis set for its zinc complex. In Chapter 3, the structure of **L2H** was optimized using the basis set B3LYP/631-G (d, p) and LanL2DZ basis set for its complexes with Cu^{2+} and Pd^{2+} ions. All calculations were performed with Gaussian09 program[87] and molecular orbitals were visualized with the aid of Gauss View program.

1.6 Appendices

Each Chapter contains an appendix at the end of references.

References

[1] K. P. Carter, A. M. Young, A. E. Palmer, *Chem. Rev.* **2014**, *114*, 4564–4601.

[2] S. Chowdhury, B. Rooj, A. Dutta, U. Mandal, *J. Fluoresc.* **2018**, *28*, 999–1021.

[3] D. R. Williams, *Chem. Rev.* **1972**, *72*, 203–213.

[4] Y. W. Chen, C. Y. Yang, C. F. Huang, D. Z. Hung, Y. M. Leung, S. H. Liu, *Islets* **2009**, *1*, 169–176.

[5] S. Bolognin, L. Messori, P. Zatta, *NeuroMolecular Med.* **2009**, *11*, 223–238.

[6] Z. Ma, F. E. Jacobsen, D. P. Giedroc, *Chem. Rev.* **2009**, *109*, 4644–4681.

[7] K. J. Barnham, A. I. Bush, *Curr. Opin. Chem. Biol.* **2008**, *12*, 222–228.

[8] L. Zecca, M. B. H. Youdim, P. Riederer, J. R. Connor, R. R. Crichton, *Nat. Rev. Neurosci.* **2004**, *5*, 863–873.

[9] A. Gupte, R. J. Mumper, *Cancer Treat. Rev.* **2009**, *35*, 32–46.

[10] G. Sivaraman, M. Iniya, T. Anand, N. G. Kotla, O. Sunnapu, S. Singaravadivel, A. Gulyani, D. Chellappa, *Coord. Chem. Rev.* **2018**, *357*, 50–104.

[11] J. Li, C. Yin, F. Huo, *Dyes Pigm.* **2016**, *131*, 100–133.

[12] A. E. Martell, R. D. Hancock, R. J. Motekaitis, *Coord. Chem. Rev.* **1994**, *133*, 39–65.

[13] X. Qian, Z. Xu, *Chem. Soc. Rev.* **2015**, *44*, 4487–4493.

[14] B. Valeur, I. Leray, *Coord. Chem. Rev.* **2000**, *205*, 3–40.

[15] A. P. De Silva, T. S. Moody, G. D. Wright, *Analyst* **2009**, *134*, 2385–2393.

[16] A. C. Sedgwick, L. Wu, H. H. Han, S. D. Bull, X. P. He, T. D. James, J. L. Sessler, B. Z. Tang, H. Tian, J. Yoon, *Chem. Soc. Rev.* **2018**, *47*, 8842–8880.

[17] S. Sinha, B. Chowdhury, P. Ghosh, *Inorg. Chem.* **2016**, *55*, 9212–9220.

[18] P. Jiang, Z. Guo, *Coord. Chem. Rev.* **2004**, *248*, 205–229.

[19] E. Deplazes, D. Jayatilaka, B. Corry, *Phys. Chem. Chem. Phys.* **2011**, *13*, 11045–11054.

[20] J. S. Wu, W. M. Liu, X. Q. Zhuang, F. Wang, P. F. Wang, S. L. Tao, X. H. Zhang, S.

K. Wu, S. T. Lee, *Org. Lett.* **2007**, *9*, 33–36.

[21] Y. Chen, Y. Ma, L. Li, W. Sang, S. Feng, Y. Wang, C. Zhang, S. Yang, L. Xu, W. Lu, *New J. Chem.* **2025**, 2192–2200.

[22] A. Kumar, W. Hur, G. H. Seong, S. Kumar, P. S. Chae, *Dyes Pigm.* **2022**, *198*, 110025.

[23] L. Quan, T. Sun, W. Lin, X. Guan, M. Zheng, Z. Xie, X. Jing, *J. Fluoresc.* **2014**, *24*, 841–846.

[24] M. Y. Berezin, S. Achilefu, *Chem. Rev.* **2010**, *110*, 2641–2684.

[25] C. C. Hsieh, Y. M. Cheng, C. J. Hsu, K. Y. Chen, P. T. Chou, *J. Phys. Chem. A* **2008**, *112*, 8323–8332.

[26] L. Chen, H. Jiang, N. Li, Q. Meng, Z. Li, Q. Han, X. Liu, *Spectrochim. Acta A Mol. Biomol. Spectrosc.* **2022**, *268*, 120704–120720.

[27] J. Wu, W. Liu, J. Ge, H. Zhang, P. Wang, *Chem. Soc. Rev.* **2011**, *40*, 3483–3495.

[28] R. R. Panicker, S. Joseph, S. Dharani, M. L. John, A. T. Kuriappan, J. T. Abraham, S. Abdul Majeed, B. B. Pavankumar, S. K. Ashok Kumar, A. Sivaramakrishna, *Anal. Methods* **2024**, 232–245.

[29] S. Gurusamy, R. Nandini Asha, M. Sankarganesh, T. Christopher Jeyakumar, A. Mathavan, *Inorg. Chem. Commun.* **2022**, *143*, 109716.

[30] A. Q. Truong-Tran, L. H. Ho, F. Chai, P. D. Zalewski, *J. Nutr.* **2000**, *130*, 1459–1466.

[31] K. M. Wyss, E. E. Hardy, A. E. V. V Gorden, *Inorg. Chim. Acta* **2019**, *492*, 156–160.

[32] T. Hara, T. Takeda, T. Takagishi, K. Fukue, T. Kambe, T. Fukada, *J. Physiol. Sci.* **2017**, *67*, 283–301.

[33] D. Noy, I. Solomonov, O. Sinkevich, T. Arad, K. Kjaer, I. Sagi, *J. Am. Chem. Soc.* **2008**, *130*, 1376–1383.

[34] A. S. Prasad, *J. Trace Elem. Med. Biol.* **2012**, *26*, 66–69.

[35] A. Jana, B. Das, S. K. Mandal, S. Mabhai, A. R. Khuda-Bukhsh, S. Dey, *New J. Chem.* **2016**, *40*, 5976–5984.

[36] K. Mawai, S. Nathani, P. Roy, U. P. Singh, K. Ghosh, *Dalt. Trans.* **2018**, *47*, 6421–6434.

[37] B. You, L. Li, Z. Li, W. Wang, Y. Yang, W. Cheng, X. Luo, Y. Qian, *Talanta* **2025**, *284*, 127267.

[38] D. Xiang, S. Zhang, Y. Wang, K. Sun, H. Xu, *Tetrahedron* **2022**, *106–107*, 132648.

[39] B. K. Rani, S. A. John, *J. Photochem. Photobiol. A Chem.* **2021**, *418*, 113372.

[40] J. Fu, K. Yao, B. Li, H. Mei, Y. Chang, K. Xu, *Spectrochim. Acta A Mol. Biomol. Spectrosc.* **2020**, *228*, 117790.

[41] Y. Shang, S. Zheng, M. Tsakama, M. Wang, W. Chen, *Tetrahedron Lett.* **2018**, *59*, 4003–4007.

[42] K. Chantalakana, N. Choengchan, P. Yingyuad, P. Thongyoo, *Tetrahedron Lett.* **2016**, *57*, 1146–1149.

[43] J. Han, X. Tang, Y. Wang, R. Liu, L. Wang, L. Ni, *Spectrochim. Acta A Mol. Biomol. Spectrosc.* **2018**, *205*, 597–602.

[44] Y. L. Liu, L. Yang, P. Li, S. J. Li, L. Li, X. X. Pang, F. Ye, Y. Fu, *Spectrochim. Acta A Mol. Biomol. Spectrosc.* **2020**, *227*, 2–9.

[45] B. Dolai, S. I. Hazarika, S. Giri, A. K. Atta, *Inorg. Chim. Acta* **2018**, *483*, 496–503.

[46] Y. Yang, F. Huo, C. Yin, Y. Chu, J. Chao, Y. Zhang, J. Zhang, S. Li, H. Lv, A. Zheng, D. Liu, *Sensors Actuators B Chem.* **2013**, *177*, 1189–1197.

[47] L. Qu, C. Yin, F. Huo, Y. Zhang, Y. Li, *Sensors Actuators, B Chem.* **2013**, *183*, 636–640.

[48] C. Jonak, H. Nakagami, H. Hirt, *Plant Physiol.* **2004**, *136*, 3276–3283.

[49] L. Yan, K. Bao, X. Xu, L. Li, X. Wu, *J. Mol. Struct.* **2024**, *1316*, 139100.

[50] G. Cui, Y. Liu, Y. Chen, T. Song, S. Tong, *J. Contam. Hydrol.* **2021**, *242*, 103857.

[51] Z. Wu, L. Lu, L. Lu, X. Liang, C. Dun, S. Yan, E. Mu, Y. Liu, Z. Hu, *J. Phys. Chem. C* **2020**, *124*, 10935–10940.

[52] D. Y. Jang, J. Koo, H. R. Choi, J. W. Kim, H. J. Jeong, F. B. Prinz, J. H. Shim, *ACS*

Sustain. Chem. Eng. **2020**, *8*, 10529–10535.

[53] I. Ortega-Feliu, B. Gómez-Tubío, S. Scrivano, F. J. Ager, M. L. de la Bandera, M. A. Respaldiza, *Radiat. Phys. Chem.* **2020**, *167*, 108239.

[54] Y. Zhang, X. Zhang, J. Gao, C. Du, M. Xie, C. Au, J. Chen, L. Wan, *Macromol. Chem. Phys.* **2020**, *221*, 1–9.

[55] J. Kielhorn, C. Melber, D. Keller, I. Mangelsdorf, *Int. J. Hyg. Environ. Health* **2002**, *205*, 417–432.

[56] X. Jie, M. Liu, A. Peng, J. Huang, Y. Zhang, X. Wang, Z. Tian, *Talanta* **2018**, *183*, 164–171.

[57] P. A. More, G. S. Shankarling, *Sensors Actuators, B Chem.* **2017**, *241*, 552–559.

[58] N. K. Hien, M. Van Bay, N. C. Bao, Q. V Vo, N. D. Cuong, T. V. Thien, N. T. A. Nhung, D. U. Van, P. C. Nam, D. T. Quang, *ACS omega* **2020**, *5*, 21241–21249.

[59] P. Kumar, V. Kumar, R. Gupta, *RSC Adv.* **2017**, *7*, 7734–7741.

[60] L. Wang, X. Y. Zheng, X. Zhang, Z. J. Zhu, *Spectrochim. Acta A Mol. Biomol. Spectrosc.* **2021**, *249*, 119283.

[61] H. X. Wang, Y. H. Lang, H. X. Wang, J. J. Lou, H. M. Guo, X. Y. Li, *Tetrahedron* **2014**, *70*, 1997–2002.

[62] J. Huang, J. Chan, Y. Chen, C. J. Borths, K. D. Baucom, R. D. Larsen, M. M. Faul, *J. Am. Chem. Soc.* **2010**, *132*, 3674–3675.

[63] H. Wu, L. Lin, L. Zheng, H. Guo, F. Yang, *J. Photochem. Photobiol. A Chem.* **2022**, *432*, 114076.

[64] Z. Dong, W. Chen, H. Li, Y. Dai, T. Zheng, H. Zhang, H. Xu, H. Lu, *Inorg. Chem. Commun.* **2020**, *116*, 107915.

[65] (a) Y. Izawa, D. Pun, S. S. Stahl, *Science* **2011**, *333*, 209–213; (b) Z. Xi, *J. Am. Chem. Soc.* **1998**, *120*, 1672–1680; (c) M. Shanmugasundaram, M. S. Wu, M. Jeganmohan, C. W. Huang, C. H. Cheng, *J. Org. Chem.* **2002**, *67*, 7724–7729; (d) W. A. L. Van Otterlo, C. B. De Koning, *Chem. Rev.* **2009**, *109*, 3743–3782.

[66] (a) G. Illuminati, H. Gilman, *J. Am. Chem. Soc.* **1952**, *74*, 2896–2899; (b) W. J. Coates, A. McKillop, *J. Org. Chem.* **1990**, *55*, 5418–5420. (c) S. M. Bonesi, M. Fagnoni, A. Albini, *Angew. Chemie - Int. Ed.* **2008**, *47*, 10022–10025; (d) D. G. Yu, M. Yu, B. T. Guan, B. J. Li, Y. Zheng, Z. H. Wu, Z. J. Shi, *Org. Lett.* **2009**, *11*, 3374–3377; (e) J. L. Gustafson, D. Lim, K. T. Barrett, S. J. Miller, *Angew. Chemie - Int. Ed.* **2011**, *50*, 5125–5129.

[67] (a) P. Finkbeiner, K. Murai, M. Röpke, R. Sarpong, *J. Am. Chem. Soc.* **2017**, *139*, 11349–11352; (b) N. Asao, H. Aikawa, Y. Yamamoto, *J. Am. Chem. Soc.* **2004**, *126*, 7458–7459; (c) S. J. Hein, D. Lehnherr, W. R. Dichtel, *Chem. Sci.* **2017**, *8*, 5675–5681; (d) H. Arslan, F. J. Uribe-Romo, B. J. Smith, W. R. Dichtel, *Chem. Sci.* **2013**, *4*, 3973–3978.

[68] Q. He, Y. Q. Xiang, R. Zhou, B. Liu, R. H. Wang, X. K. Kong, S. Bai, M. Li, G. J. Yang, G. F. Zhu, *Org. Chem. Front.* **2025**, *12*, 2670–2675.

[69] S. Singh, R. B. Dadhe, S. Pabbaraja, G. Mehta, *J. Org. Chem.* **2025**, *90*, 2510–2520.

[70] I. Kumar, I. A. Shah, Y. K. Nagare, K. Rangan, E. Iype, R. Sharma, R. Kant, *Chem. Asian J.* **2025**, e202401408.

[71] V. Naik, F. A. Khan, *Synthesis* **2025**, *57*, 397–406.

[72] D. H. Dethe, A. Uike, N. C. Beeralingappa, *Org. Lett.* **2024**, *26*, 2013–2017.

[73] X. Zhang, F. Li, Y. Zhou, J. Zhang, B. Zhou, L. Chen, J. Lin, C. Zhang, *Org. Lett.* **2025**.

[74] D. Wang, J. Lin, Y. Zhu, Y. Huang, *Adv. Synth. Catal.* **2021**, *363*, 1873–1877.

[75] Q. Mao, Q. Zhao, M. Z. Li, R. Qin, M. L. Luo, J. Xue, B. H. Chen, H. J. Leng, C. Peng, G. Zhan, B. Han, *J. Org. Chem.* **2021**, *86*, 14844–14854.

[76] Q. Jia, G. Yin, Y. Lan, Y. Lin, Q. Ren, *Asian J. Org. Chem.* **2021**, *10*, 2161–2164.

[77] Y. Wang, Y. Wang, J. Qu, T. Yang, Y. Zhang, C. Yuan, H. Guo, C. Wang, *J. Org. Chem.* **2024**, *89*, 9462–9472.

[78] S. Thavaselvan, K. Parthasarathy, *Org. Biomol. Chem.* **2022**, *20*, 4309–4313.

[79] Y. Liu, P. Zhou, Y. Xu, Z. Yang, D. Wang, *Chem. Commun.* **2023**, *59*, 1681–1684.

[80] A. B. Bon, A. M. Costero, S. Gil, M. Parra, J. Soto, R.M. Manez and F. Sancenon, *Chem. Commun.*, **2012**, *48*, 3000–3002.

[81] H.A. Benesi, J.H. Hildebrand, *J. Am. Chem. Soc.* **1949**, *71*, 2703–2707.

[82] I.D. Kuntz, F.P. Gasparro, M.D. Johnston, R.P. Taylor, *J. Am. Chem. Soc.* **1968**, *90*, 4778–4781.

[83] A. Jana, B. Das, S.K. Mandal, S. Mabhai, A.R. Khuda-Bukhsh, S. Dey, *New J. Chem.* **2016**, *40*, 5976–5984.

[84] S. Majumder, A. Pramanik, S. Mandal, S. Mohanta, *J. Photochem. Photobiol. A Chem.* **2019**, *383*, 111987.

[85] H. S. Jung, P. S. Kwon, J. W. Lee, J. I. Kim, C. S. Hong, J. W. Kim, S. Yan, J. Y. Lee, J. H. Lee, T. Joo and J. S. Kim, *J. Am. Chem. Soc.*, **2009**, *131*, 2008–2012.

[86] G.M. Sheldrick, SHELXT–Integrated space-group and crystal-structure determination, *Acta Crystallogr. Sect. A* **2015**, *71*, 3–8.

[87] M. J. Frisch, G. W. Trucks, H. B. Schlegel, G. E. Scuseria, M. A. Robb, J. R. Cheeseman, G. Scalmani, V. Barone, B. Mennucci, G. A. Petersson, H. Nakatsuji, M. Caricato, X. Li, H. P. Hratchian, A. F. Izmaylov, J. Bloino, G. Zheng, J. L. Sonnenberg, M. Hada, M. Ehara, K. Toyota, R. Fukuda, J. Hasegawa, M. Ishida, T. Nakajima, Y. Honda, O. Kitao, H. Nakai, T. Vreven, J. A. Montgomery, Jr., J. E. Peralta, F. Ogliaro, M. Bearpark, J. J. Heyd, E. Brothers, K. N. Kudin, V. N. Staroverov, R. Kobayashi, J. Normand, K. Raghavachari, A. Rendell, J. C. Burant, S. S. Iyengar, J. Tomasi, M. Cossi, N. Rega, J. M. Millam, M. Klene, J. E. Knox, J. B. Cross, V. Bakken, C. Adamo, J. Jaramillo, R. Gomperts, R. E. Stratmann, O. Yazyev, A. J. Austin, R. Cammi, C. Pomelli, J. W. Ochterski, R. L. Martin, K. Morokuma, V. G. Zakrzewski, G. A. Voth, P. Salvador, J. J. Dannenberg, S. Dapprich, A. D. Daniels, Ö. Farkas, J.B. Foresman, J.V. O rtiz, J. Cioslowski and D.J. Fox, Gaussian 09, Revision D.01, Gaussian Inc, Wallingford CT, 2009.

Chapter 2

Fluorescent *Turn On* Detection of Zinc(II) Ion Using a Hydrazone Derived from 4-Tert-butyl-2,6-diformylphenol and 3-Hydrazineylquinoxalin-2(1*H*)-one*

Abstract

A polydentate chelating ligand (**LH**) was synthesized from 4-*tert*-butyl-2,6-diformylphenol and 3-hydrazineylquinoxalin-2(1H)-one and characterized by mass spectrometry, IR and NMR spectroscopy. **LH** is weakly fluorescent in EtOH – HEPES buffer (5 mM, pH = 7.4, 8:2, *v/v*) but exhibited a *turn on* response with Zn^{2+} ion having a workable pH range of 6 – 12 and thus is compatible with biological pH. This sensor is selective for Zn^{2+} ion, over various metal ions and anions as evident from competition experiments. The probable mechanism of sensing by **LH** is restriction of ESIPT, PET and C=N isomerization processes and on-set of CHEF process upon coordination to Zn(II) ion. Reversibility was established using EDTA test and applicability in various real samples were evaluated. The calculated limit of detection for Zn^{2+} ion was 95 nM and Job's plot as well as ^{1}H NMR titration suggested a 2:1 binding ratio between Zn^{2+} ion and **LH**. From the reaction (in ethanol) of $ZnCl_2$ with **LH**, in 2:1 ratio, crystalline solids of composition $[Zn_2(\mathbf{L})Cl_3]\cdot 2H_2O\cdot 2.5DMF$ was isolated and its molecular structure was established by single crystal XRD studies. DFT/TDDFT calculation supported the experimental electronic absorption spectrum.

*This work has been published in

S. Kumar, S. Mahata and V. Manivannan, *J. Photochem. Photobiol. A: Chem.* **2024**, *450*, 115436.

1. Introduction

The design and syntheses of chemosensors for molecules and ions (including proton) have remained center of attraction owing to their potential applications in chemical, biological and environmental sciences.[1] Fluorescence detection is the most advantageous among all available detection techniques owing to its high selectivity, quick response, low cost, and low detection limit.[2–4] When fluorescent sensors interact with analytes, their typical emission intensity may be increased (*turn on*) or quenched (*turn off*),[5] of which *turn on* chemosensors are supposed to be more efficient than that of *turn off* chemosensors.[6–9] Particularly this technique is more pertinent to spectroscopically and magnetically insensitive metal ions such as Zn^{2+}, Cd^{2+} and Hg^{2+} as they have d^{10} electronic configuration.[10] Among these three, Zn^{2+} ion has biological significance due to its critical role in growth, immunity, and endocrine function,[11,12] while other two are detrimental to the health. Zinc(II) is second most abundant trace metal ion in human body[13] and can be found in the active sites of numerous enzymes, including carboxy peptidase and carbonic anhydrase.[14] Human blood plasma typically contains Zn^{2+} ion in amounts between 12 and 6 μM.[15] An adequate amount of Zn^{2+} ion in our body regulates a number of processes, including neuronal transmission,[12] apoptosis,[16] epilepsy,[17] ischemia,[18] and so forth. However, an imbalance in its concentration can result in a number of diseases like Alzheimer's, prostate cancer and other neurodegenerative diseases being of particular concern.[19–23] Approximately, 1.1 billion people of global population are suffering from zinc deficiency all over the world.[11,24]

Due to their d^{10} electronic configuration and similar chemical characteristics, it is difficult to detect Zn^{2+} ion above Cd^{2+} and Hg^{2+} ions.[25,26] Therefore, it is essential to design *turn on* fluorescent chemosensors that can sensitively and selectively detect Zn^{2+} ion. There have been some studies available on the detection of Zn^{2+} ion based on coumarin,[27] rhodamine,[9] quinoline,[28] 1,8-naphthalimide,[29] benzothiazole,[30] pyrene[31] and other fluorophores. However, development of chemosensors that sensitively as well as selectively detect Zn^{2+} over Cd^{2+} and Hg^{2+} ions is still a demand.

In coordination chemistry, ligands derived from 4-substituted-2,6-diformylphenol are extremely important because their phenolic oxygen has a propensity to connect to two metal centers in a bridging fashion.[32] According to reports, these compounds possess an extensive role in catalysis, chemosensors, and have several biological activities.[33–37] On the other hand, quinoxalines are

significant heterocycles that have a variety of biological properties, including antibacterial, antifungal, and anticancer action.[38] Numerous earlier studies suggest that changing the substituents in the quinoxaline moiety could enhance its biological activity.[39] The quinoxaline moiety is an intriguing template for the development of ion sensors due to its well-known medicinal properties and significant involvement as a pharmacophore in numerous drugs.[40]

Considering these facts, a hydrazone chemosensor **LH**, synthesized from 4-*tert*-butyl-2,6-diformylphenol and 3-hydrazineylquinoxalin-2(1H)-one has the potential to detect Zn^{2+} ion in fluorescent *turn on* fashion, in biological pH range reversibly and with low detection limit.

2. Results and discussion

2.1 Syntheses

Compounds **P** and **Q** were synthesized according to literature procedure.[41,42] Ligand **LH** was synthesized in good yield by reacting 4-*tert*-butyl-2,6-diformylphenol with 3-hydrazineylquinoxalin-2(1H)-one (**Q**) in acetonitrile (Scheme 1). One equivalent of **LH** reacted readily with two equivalents of $ZnCl_2$ in ethanol (conditions similar to that used in spectroscopic studies) yielding solids of composition $[Zn_2(\mathbf{L})Cl_3]$ (**1**), which in DMF-CH_3CN mixture crystallized as **1**·$2H_2O$·2.5DMF at room temperature. Molecular structure of **1**·$2H_2O$·2.5DMF was determined using single crystal X-ray diffraction technique.

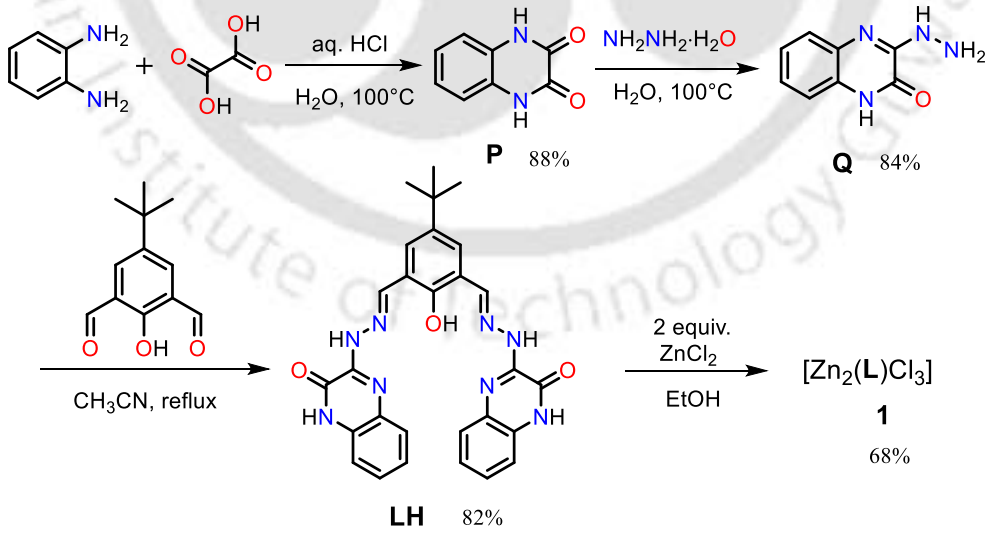

Scheme 1. Syntheses of **LH** and **1**.

2.2 Electronic absorption and emission spectra

The absorption spectra of **LH** in presence of different metal ions like Cr^{3+}, Mn^{2+}, Fe^{3+}, Fe^{2+}, Co^{2+}, Ni^{2+}, Cu^{2+}, Zn^{2+} Cd^{2+}, Hg^{2+}, Pb^{2+}, Pd^{2+}, Ag^{+}, Na^{+}, K^{+}, Li^{+}, Ca^{2+}, Mg^{2+}, Au^{3+} and Al^{3+} ions were investigated in EtOH–HEPES buffer solution (8:2, *v/v*, 5 mM, pH = 7.4). The probe **LH** showed absorption bands at 270, 367 and 393 nm along with shoulder at 347 and 409 nm and they may be attributed to $\pi \rightarrow \pi^*$ and $n \rightarrow \pi^*$ transitions (Figure 1). Upon the gradual addition of $ZnCl_2$ solution into **LH** solution, the intensity of peaks at 367 nm and 393 nm got gradually diminished and four bands were observed at 270 nm, 364 nm, 405 nm and 470 nm along with an isosbestic point at 419 nm (Figure 2). Presence of isosbestic point indicated that there are only two species present during the titration *viz*., ligand **LH** and its zinc complex **1**. A perceptible change from colorless to light yellow was observed upon addition of Zn^{2+} ion to **LH** is consistent with the observed red shift in the absorption band due to the formation of **1**. Whereas upon addition of Cd^{2+} ion and rest of the other metal ions, the pattern of the spectra remained same but with small reduction in absorbance values.

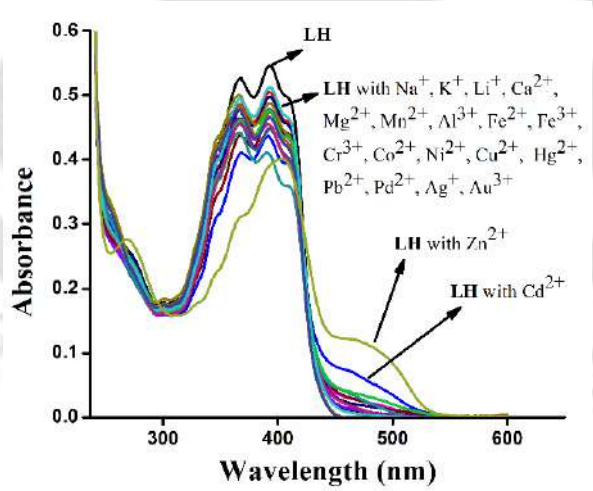

Figure 1. The absorption spectra of **LH** (10 µM) with various metal chloride solution (20 µM) in EtOH - aqueous HEPES buffer (5 mM, pH = 7.4, 8:2 *v/v*)

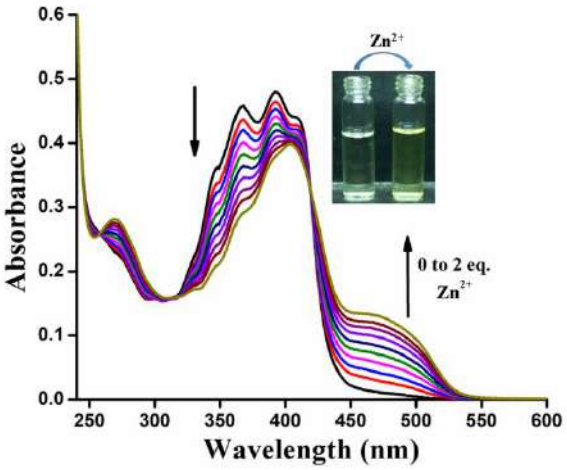

Figure 2. Changes in absorption spectra of **LH** upon gradual addition of $ZnCl_2$ Solution.

In EtOH – HEPES buffer (8:2, *v/v*, 5 mM, pH = 7.4) solution, **LH** was weakly fluorescent (λ_{em} = 597 nm) upon irradiation of with λ_{ex} = 419 nm. For the purpose of checking the emission behavior of **LH** with various metal ions, a fluorescence titration study was carried out. Upon titrating with soluble salts of Na^+, K^+, Li^+, Ca^{2+}, Mg^{2+}, Mn^{2+}, Fe^{2+}, Co^{2+}, Ni^{2+}, Cu^{2+}, Hg^{2+}, Pb^{2+}, Pd^{2+}, Cd^{2+}, Ag^+, Au^{3+}, Al^{3+}, Fe^{3+} and Cr^{3+} ions, the solution of **LH** remained weakly fluorescent (Figure 3). Whereas in case of Cd^{2+} ion, the weak emission peak got shifted to 533 nm but with no enhancement in emission intensity even upon further addition of $CdCl_2$ solution. However, solution of **LH** became fluorescent upon adding $ZnCl_2$ with the emission peak being observed at λ_{em} = 537 nm. The emission peak intensity increased with increasing amounts of $ZnCl_2$ which reached the maximum at 2 equivalents (Figure 4). So it can be concluded that **LH** can selectively recognize Zn^{2+} ion in fluorometric *turn on* fashion. This can also be comprehended by an appearance of yellowish-green colored fluorescence which can be seen through naked eye when kept under long UV. To ensure applicability of **LH** for the detection of Zn^{2+} ion, emission spectra of **LH** with some common zinc salts (zinc acetate, zinc nitrate, zinc triflate and zinc chloride) were recorded (Figure A5 (a)) and found that **LH** can detect Zn^{2+} ion with the same efficiency, irrespective of anions.

In order to assess the ability of **LH** as selective fluorescence receptor for Zn^{2+} ion, competitive experiment was carried out. In this experiment, to the solution obtained after the addition of various competing metal ions like Ag^+, Al^{3+}, Au^{3+}, Cd^{2+}, Co^{2+}, Cr^{3+}, Cu^{2+}, Hg^{2+}, Li^+, Na^+, Ni^{2+}, Pb^{2+}, Pd^{2+},

Pt^{2+} and Fe^{3+} to **LH**, $ZnCl_2$ solution was then added and fluorescence spectra of resultant solutions were recorded. The weakly fluorescent solution containing **LH** plus competing metals exhibited a *turn on* fluorescence response after adding $ZnCl_2$ (Figure A5 (b)) into it. Thus, **LH** has the potential to detect Zn^{2+} ion with coexistence of other metal ions listed above. In order to assess the utility of **LH** bound to zinc(II) ion as an anion sensor, the fluorescence responses of solutions obtained after titrating **LH** with $ZnCl_2$, common anions such as F^-, Br^-, CN^-, SCN^-, PO_4^{3-}, $S_2O_3^{2-}$, NO_3^-, SO_4^{2-}, $P_2O_7^{4-}$, HSO_4^-, CO_3^{2-}, HCO_3^-, AcO^-, ClO_4^- and $C_2O_4^{2-}$ were added and no perceptible changes in emission intensity (Figure A6) were observed. Thus, these anions did not have interfering effect on the sensing ability.

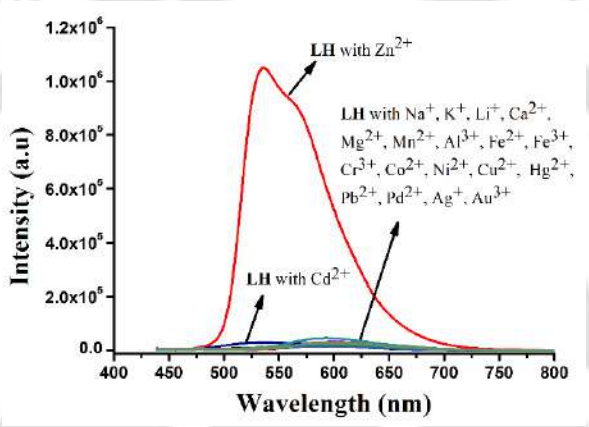

Figure 3. Emission spectra of **LH** (10 μM) in the presence of various metal ions (20 μM) in EtOH - aqueous HEPES buffer (5 mM, pH = 7.4, 8:2 *v*/*v*).

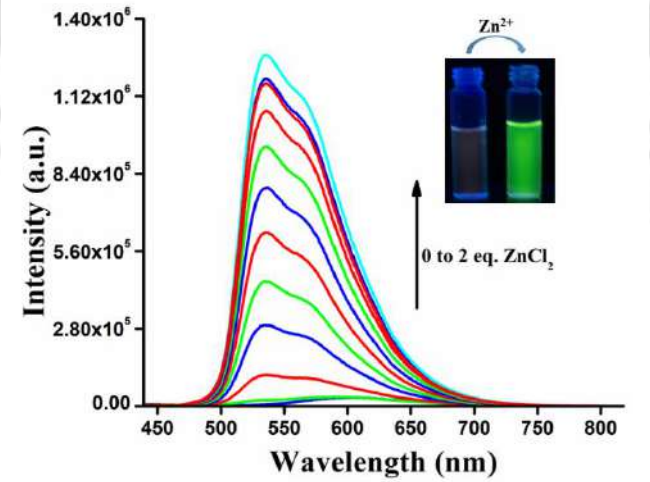

Figure 4. Changes in fluorescence spectra of **LH** upon gradual addition of $ZnCl_2$ solution.

2.3 pH effect and reversibility

Based on the results obtained from X-ray diffraction studies (*vide infra*) and Job's plot, the composition $[Zn_2(\mathbf{L})Cl_3]$ (**1**) has been assigned for the species present in the mixture containing **LH** and $ZnCl_2$. To know the potential applicability of **LH** as a chemosensor, the optimal pH range has been determined by recording the fluorescence intensity of **LH** in absence and presence of Zn^{2+} ion in EtOH-HEPES buffer solution (pH was adjusted by adding aqueous HCl and NaOH solutions) in the pH range 2 – 12. It has been found that free **LH** remained weakly fluorescent in range 2 – 12 with λ_{em} = 597 nm. In acidic medium (pH = 1 to 5) the emission intensity of solution of **LH** and $ZnCl_2$ was low but in the pH = 6 – 12 it exhibited appreciable fluorescence intensity. Thus the optimum pH window has been found to be 6 – 12 (Figure 5).

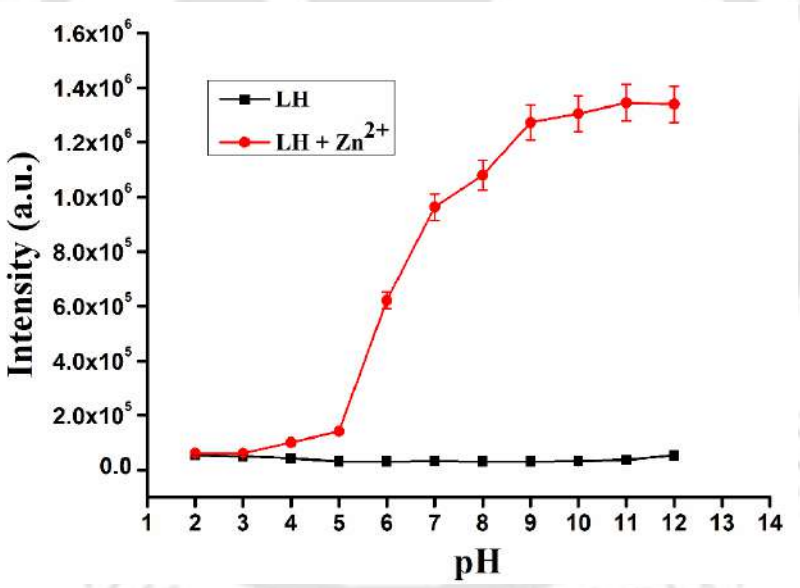

Figure 5. pH dependence of **LH** and its complex with Zn^{2+} ion.

The fluorescent solution of $[Zn_2(\mathbf{L})Cl_3]$ became weakly fluorescent upon adding two equivalents of Na_2EDTA solution due the formation of $[Zn(EDTA)]^{2-}$ ion and free **LH**. Upon further addition of $ZnCl_2$ to the resultant solution fluorescence was reestablished, and this cycle was repeated three times and found to be consistent (Figure A7 (a)).

The probe **LH** is equally efficient in detecting Zn^{2+} ion in real water samples collected from potable sources. They were filtered through 0.22 µm filter paper and after that **LH** (1×10^{-5} M) was titrated with various concentrations of Zn^{2+} ion (ranging from 0 to 2×10^{-5} M) and emission spectra were

recorded. The plot of emission maxima versus concentration of Zn^{2+} ion (Figure A7 (b)) is consistent with the observed results in EtOH-HEPES buffer.

2.4 Binding stoichiometry and fluorescence quantum yield

Job's plot was employed for finding the stoichiometry of binding between **LH** and Zn^{2+} ion. In this typical experiment, by varying mole fractions of Zn^{2+} ion against **LH** from 0 to 1, emission spectra were recorded. Emission maxima obtained were plotted against mole fraction of Zn^{2+} ion. Point of intersection (around 0.66) on linear fitting of this plot implied a 2:1 binding stoichiometry between Zn^{2+} and **LH** (Figure A8). In other words, for one equivalent of **LH**, 2 equivalents of Zn^{2+} ion is needed and this is consistent with the results of molecular structure determined using X-ray diffraction method. Fluorescence quantum yields (Φ) for **LH** and **LH** bound Zn^{2+} ion in ethanol were calculated from equation (3) in SI and were found be 0.011 and 0.193, respectively. These values are consistent with the *turn on* fluorescence response upon binding of **LH** to Zn^{2+} ion.

2.5 TRPL measurement and sensing mechanism

The time resolved photoluminescence (TRPL) measurements were performed to comprehend the mechanism of the *turn on* fluorescence detection of **LH** towards Zn^{2+} ion. The decay profiles are shown in (Figure A9 (a)). The lifetime (τ) for free LH was calculated to be 0.47 ns in EtOH-HEPES buffer solution. On the other hand, the lifetime for Zn^{2+} bound probe (**LH**) has been found to have greater lifetime of 0.98 ns (Table S1). This suggests that binding of Zn^{2+} ion to **LH** allowed CHEF to come into effect and hence lifetime of emissive species become greater than free probe **LH**. Operation of ESIPT mechanism in **LH** (involving intramolecular hydrogen bond between imine-N and phenolic O-H) has been established by recording the fluorescence spectra of **LH** in different solvents (Figure A9 (b)). Upon irradiation with λ_{ex} = 375 nm, **LH** exhibited a well separated dual bands. Bands at shorter wavelength (432 nm) may be for emission of enol form of **LH**, and bands at longer wavelengths (538-580 nm) are may be due to emission of keto form. The longer wavelength emissions exhibited a solvent dependency (hexane, 579 nm; dioxane, 553 nm; acetone, 550 nm; THF, 551 nm and acetonitrile, 549 nm). However, this longer emission wavelength was observed at 540 nm in protic solvents like EtOH/MeOH (about 40 nm difference with non-polar hexane and 10-13 nm with aprotic solvents). These observations were quite consistent the ESIPT phenomenon exhibited by sensors having similar structural features, reported previously.[43–51] Because of operation of ESIPT phenomenon in **LH**, a weak fluorescence was observed. Whereas

upon coordination with Zn^{2+} ions were accompanied by deprotonation of phenolic O-H which inhibited operation of ESIPT and hence very high fluorescence was observed. Other possible mechanism for weak fluorescence of **LH** may also be due to PET-ON process involving lone pair of electrons on imine–N and quinoxaline–N which no longer participate in electron transfer (PET-OFF) upon coordination with Zn^{2+} ion and fluorescence got enhanced tremendously. This process has been found to operate in similar chemosensors reported earlier by other authors.[52–55] Weak fluorescence may also be feasible because of C=N isomerization in **LH** whereas this isomerization gets inhibited upon coordination of **LH** with Zn^{2+} ion, hence fluorescence intensity getting enhanced [56]. Thus in free **LH**, ESIPT/PET/C=N isomerization rendered weak fluorescence while in **1**, inhibition of all these three process and on-set of CHEF rendered strong fluorescence (Figure 6).

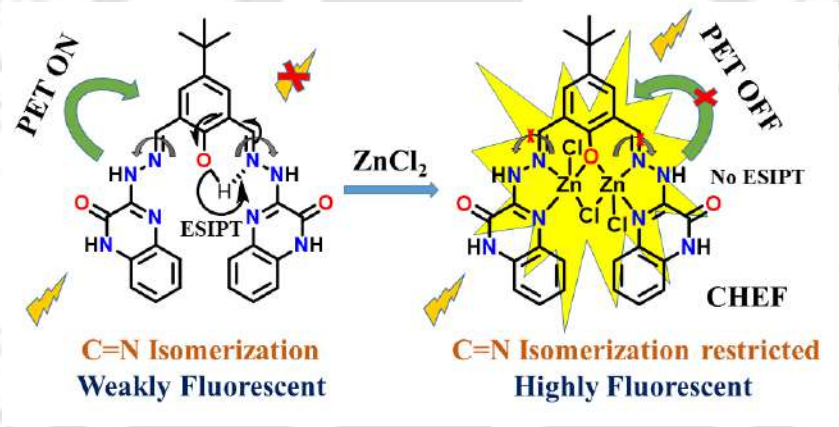

Figure 6. Probable sensing mechanism of Zn^{2+} ion by **LH**.

2.6 Limit of detection and binding constant

The minimum concentration of Zn^{2+} ion that can be detected using **LH** has been calculated using equation (1). From titration graph of $ZnCl_2$ with **LH** and applying detection limit formula (detection limit = $3\sigma/k$), the limit of detection was calculated to be 95 nM (Figure 7) which is quite less than the range of intracellular concentration (6-12 µM) of Zn^{2+} ion.[11] For ready reference, a comparison between various probes reported for Zn^{2+} ion detection and probe **LH** has been listed in Table S2. The probe **LH** has a very high binding affinity towards Zn(II) ion as evident from the binding constant of 1.345×10^{10} M^{-2} that was calculated from Benesi-Hildebrand plot (Figure A10).

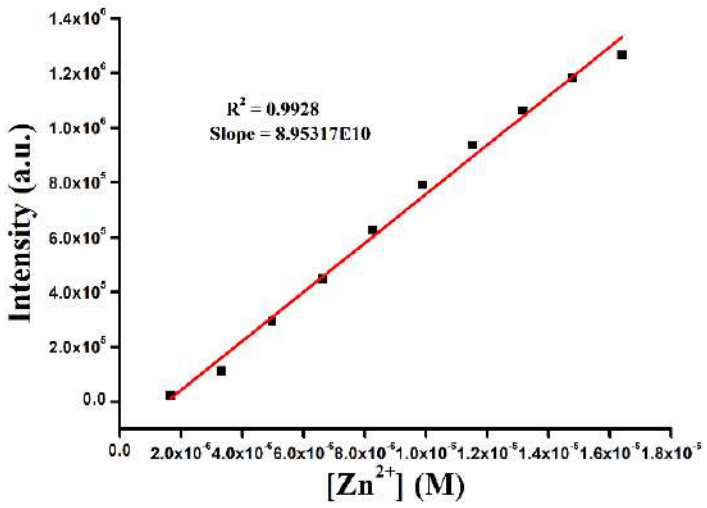

Figure 7. Plot of intensities at 537 nm *vs* concentration of $ZnCl_2$.

2.7 ^{1}H NMR titration

The interaction between **LH** with Zn^{2+} ion was also examined by ^{1}H-NMR titration experiment in DMSO-d_6 (Figure 8). With gradual addition of zinc chloride solution (two equivalents) to **LH** solution, two hydrazineyl NH protons (denoted by *) at 11.59 ppm got gradually shifted to 13.25 ppm. Other two NH protons (denoted by ●) of quinoxaline ring at 12.53 ppm shifted to 12.84 ppm. Whereas the peak at 12.63 ppm due to OH proton disappeared gradually suggesting coordination of **LH** as $\mathbf{L}^-$. The peak at 8.88 ppm due to imine protons (CH=N) shifted slightly to 8.81 ppm suggesting involvement of imine–N in coordination to Zn^{2+} ion. The peak in aromatic region ~7.24 ppm exhibited splitting due to coordination to Zn^{2+} ion. This is consistent with the formula $[Zn_2(\mathbf{L})Cl_3]$.

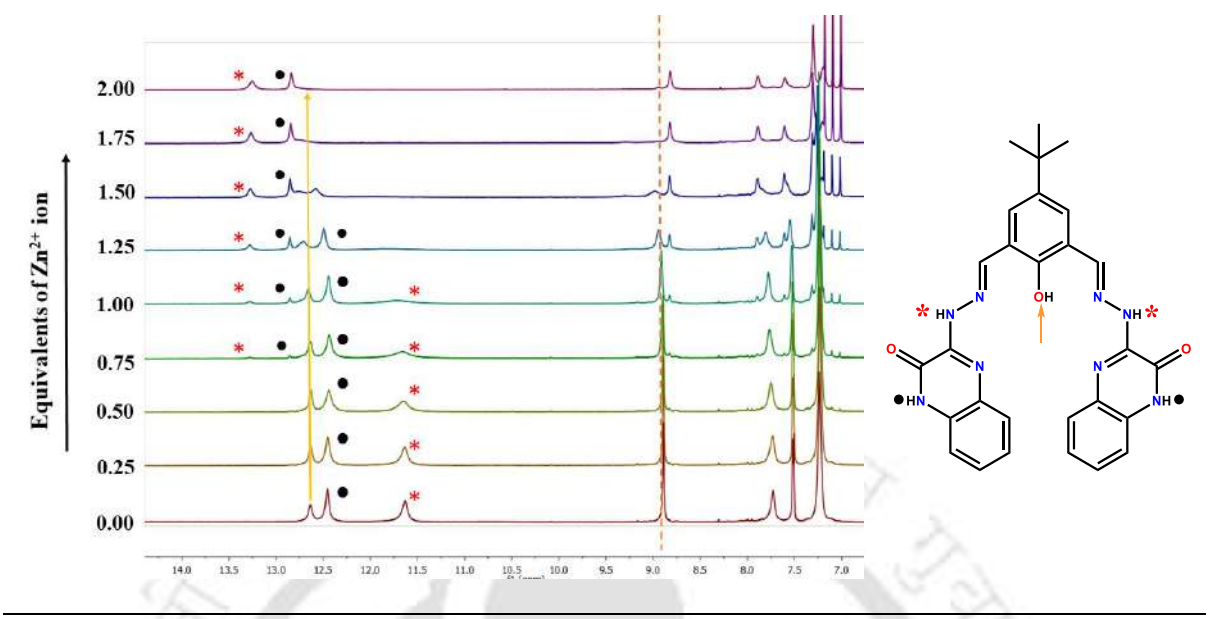

Figure 8. ^{1}H NMR Titration spectra obtained after gradual addition $ZnCl_2$ to **LH**.

2.8 Molecular structure

Molecular structure of **1**·2H_2O·2.5DMF was determined using single crystal X-ray diffraction method and crystallized in $P\bar{1}$ space group. Crystallographic data and refinement parameters are listed in Table S3. In **1**, the ligand binds in a pentadentate fashion and bridges two zinc(II) ions through the phenolate oxygen atom along with a bridging chloride ion. Each zinc atom is coordinated individually by the imine-N, quinoxaline-N and a chloride ion. These two zinc centers are penta coordinated having distorted square pyramidal geometries and are bound by five- and a six-membered chelate ring. Thus **LH** binds in the monoanionic form (**L**$^{-}$) in **1** and the ORTEP (50% probability) diagrams of **1** has been shown in Figure 9. In **1**, **L**$^{-}$ bridges Zn1 and Zn2 *via* phenolate oxygen O2 which results in formation of $Zn_2Cl_2O_2$ core having distances Zn1–Cl2 = 2.366(3); Zn2–Cl2 = 2.352(2); Zn1–O2 = 2.087(4) and Zn2–O2 = 2.101(5)Å with the non-bonded distance being Zn1···Zn2 = 3.319(2) Å. Selected bond parameters encompassing zinc centers in **1** are listed in Table S4. In the course of coordination with two zinc centers, the plane containing quinoxaline ring were tilted. The formulation of **1** with a 2:1 binding ratio between Zn^{2+} and **LH** in EtOH-HEPES buffer solution was also been obtained using Job's plot. Significant inter-molecular hydrogen bonding interactions present among **1**, water and DMF are N7···O6, 2.713(7); O3···N2, 2.844(9); O7···N8, 2.78(1); O7···O5, 2.80(1); O7···Cl3, 3.18(1); O1···O6, 2.73(1);

N3···O4, 2.77(1); Cl1···O6, 3.170(7).

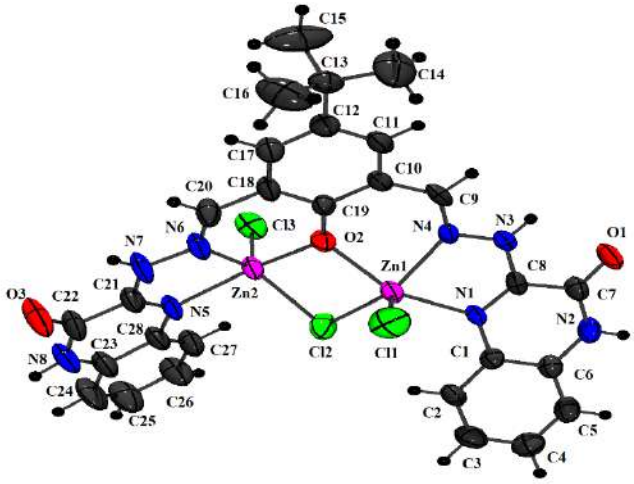

Figure 9. POV-Ray rendered ORTEP plot (50% probability) of **1**.

2.9 Computational study

The DFT/TDDFT calculations were carried out on **LH** with 6-311 G(d) basis sets the structural optimization was done at the B3LYP level whereas for [Zn_2(**L**)Cl_3] the lanl2dz basis set was assigned for all elements using a conductor-like polarizable continuum model (CPCM) applying ethanol as solvent.[2,57,58] The optimised structures for the ground state are depicted in Figure A11 and the frontier molecular orbitals are displayed in Figure A12 and A13. The electronic excitation energies of low-lying singlet states for ligand and **1** are shown in Table S5 and S6. Energies and contour diagram of HOMO and LUMO of **LH** and **1** were included in Figure 10. In HOMO of **LH**, π electron density resides on one half of the molecule (phenolate ring and one of the two quinoxaline moieties) whereas in LUMO on the other half of the molecule (phenolate ring and the other quinoxaline moiety), suggesting the occurrence of an intra-ligand charge transfer transition. On the other-hand in **1**, HOMO electron density resides on probe as well as on metal centres but in LUMO electron density is delocalized over whole ligand molecule. The net effect of complexation on the frontier orbitals is that the energies of HOMO and LUMO are stabilized to the extent of 0.44 eV and 0.65 eV respectively. This resulted in a net decrease the HOMO-LUMO energy gap from 3.492 eV (in **LH**) to 3.282 eV (in **1**), which has been observed experimentally as a slight red shift in the absorption maximum of **LH** upon binding to Zn^{2+} ion (Figure A14).

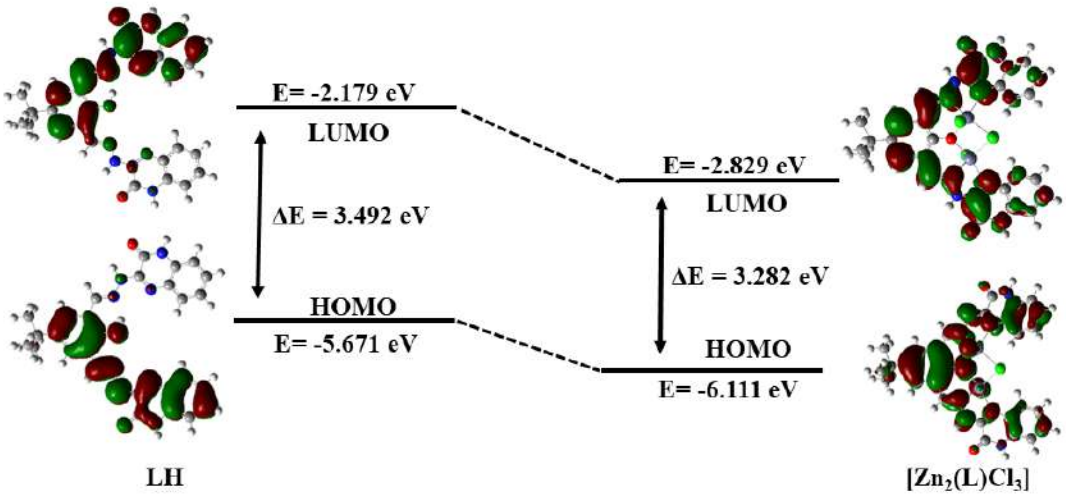

Figure 10. HOMO and LUMO of **LH** and **1** and their energies.

3. Conclusion

The hydrazone **LH** has been synthesized and is weakly fluorescent in nature, but act as a *turn on* chemosensor for selective fluorescent detection of Zn^{2+} ion in the biological pH. The probable modes fluorescence selectivity is due to restriction of ESIPT, C=N isomerization and PET processes and onset of chelation enhanced fluorescence (CHEF) process. Reversibility of sensing was established using EDTA test and Job's plot indicated a 2:1 binding ratio between Zn^{2+} ion and **LH**. A very low detection limit of 95 nM falls within the limit that is required for natural samples. Crystalline solids of composition $[Zn_2(\mathbf{L})Cl_3]\cdot 2H_2O\cdot 2.5DMF$ was obtained from ethanol medium in which the probe exists in its mono-anionic form, a condition similar to that used for fluorescence studies. Determination of the molecular structure revealed that in **1** the bivalent zinc centers are penta-coordinated. DFT/TDDFT calculations supported the experimentally observed results.

4. Experimental section

4.1 Syntheses

*4.1.1 3,3'-((-(5-(tert-butyl)-2-hydroxy-1,3-phenylene)bis(methaneylylidene))bis(hydrazin-1-yl-2-ylidene))bis(quinoxalin-2(1H)-one) (**LH**)*

Compounds **P** and **Q** were synthesized according to literature procedure.[41,42] To **Q** (353 mg, 2 mmol) in acetonitrile (15 mL), 4-*tert*-butyl-2,6-diformylphenol (210 mg, 1 mmol) was added with stirring and heated at reflux for 6 h. Precipitates of **LH** obtained was filtered and washed with ice-

cold acetonitrile and dried in desiccator over $CaCl_2$. (Yield: 427 mg, 82 %). ESI-MS (+): *m*/*z* calcd. for $[C_{28}H_{27}N_8O_3]^+$ ($M^+ + H$) 523.2201 found 523.2147. ^1H NMR (600 MHz, DMSO-d_6) δ 12.63 (s, 1H), 12.43 (s, 2H), 11.59 (s, 2H), 8.88 (s, 2H), 7.71 (s, 2H), 7.51 (d, *J* = 7.2 Hz, 2H), 7.24 (m, 6H), 1.35 (s, 9H). ^{13}C NMR (150 MHz, DMSO-d_6) δ 154.93, 151.22, 146.50, 146.08, 141.93, 133.11, 129.28, 126.68, 126.00, 125.35, 124.05, 120.54, 115.59, 34.44, 31.73 (Figure A1-A3). FTIR (ATR mode, cm^{-1}): 3345(w), 3228(m), 3048(w), 2970(w), 2907 (w), 1680(s), 1641 (m), 1620(m), 1570(s), 1419(m), 1217(s), 1137(w), 1090(m), 934(m), 899(w), 755(s), 649(m), 634(m), 587(s), 528(w), 480(s) (Figure A4).

*4.1.2 [Zn_2(**L**)Cl_3] ·2H_2O·2.5DMF (**1**·2H_2O·2.5DMF)*

To **LH** (53 mg, 0.1 mmol) in ethanol (15 mL) solid $ZnCl_2$ (30 mg, 0.22 mmol) was added and heated at reflux for 3 h. The mixture was cooled to room temperature, yellow colored precipitates of **1** obtained was filtered and washed with 20 ml of cold ethanol and dried in vaccuo over P_4O_{10}. Yield of **1**: (51 mg, 68%). Anal. calcd for $C_{28}H_{25}N_8O_3Cl_3Zn_2$, C, 44.33; H, 3.32; N, 14.77; found: C, 44.18; H, 3.34; N, 14.70% IR (cm^{-1}) ATR mode: 3238(m), 2970(w), 1702(s), 1628(m), 1615(m), 1575(s), 1560(s), 1532(w), 1474(w), 1420(m), 1348(m), 1249(m), 1222(m), 1092(m), 785(m), 766(s), 725(m), 704(w), 638(m), 597(m), 521(w), 475(s), 426(s) (Figure A4). Single crystals of **1**·2H_2O·2.5DMF suitable for X-ray diffraction studies were grown by slow evaporation in DMF-CH_3CN solvent mixture.

References:

[1] M.C. Nunes, F. dos Santos Carlos, O. Fuganti, D.D.M. Galindo, L. De Boni, G. Abate, F.S. Nunes, *Inorg. Chim. Acta.* **2020**, *499*, 119191.

[2] G. Sivaraman, M. Iniya, T. Anand, N.G. Kotla, O. Sunnapu, S. Singaravadivel, A. Gulyani, D. Chellappa, *Coord. Chem. Rev.* **2018**, *357*, 50–104.

[3] J. Li, C. Yin, F. Huo, *Dyes Pigm.* **2016**, *131*, 100–133.

[4] A. Bhattacharya, V. Manivannan, *J. Photochem. Photobiol. A Chem.* **2023**, *444*, 114913.

[5] S. Chowdhury, B. Rooj, A. Dutta, U. Mandal, *J. Fluoresc.* **2018**, *28*, 999–1021.

[6] S. Mahata, G. Janani, B.B. Mandal, V. Manivannan, *J. Photochem. Photobiol. A Chem.* **2021**, *417*, 113340.

[7] H. Zhu, J. Fan, B. Wang, X. Peng, *Chem. Soc. Rev.* **2015**, *44*, 4337–4366.

[8] B. Shirinfar, N. Ahmed, Y.S. Park, G. S. Cho, I.S. Youn, J. K. Han, H.G. Nam, K.S. Kim, *J. Am. Chem. Soc.* **2013**, *135*, 90–93.

[9] A. J. Weerasinghe, C. Schmiesing, S. Varaganti, G. Ramakrishna, E. Sinn, *J. Phys. Chem. B.* **2010**, *114*, 9413–9419.

[10] V. Venkatesan, S. Kumar R, S.K.A. Kumar, S.K. Sahoo, *Inorg. Chem. Commun.* **2019**, *102*, 171–179.

[11] K.M. Wyss, E.E. Hardy, A.E. V Gorden, *Inorg. Chim. Acta.* **2019**, *492*, 156–160.

[12] C.J. Frederickson, J. Y. Koh, A.I. Bush, *Nat. Rev. Neurosci.* **2005**, *6*, 449–462.

[13] Y. Li, K. Li, J. He, Talanta **2016**, *153*, 381–385.

[14] D. Maity, S. Kumar Mandal, B. Guha, P. Roy, *Inorg. Chim. Acta.* **2021**, *519*, 120258.

[15] Y. Li, Q. Niu, T. Wei, T. Li, *Anal. Chim. Acta.* **2019**, *1049*, 196–212.

[16] A.Q. Truong-Tran, L.H. Ho, F. Chai, P.D. Zalewski, *J. Nutr.* **2000**, *130*, 1459S-1466S.

[17] N. Tønder, F.F. Johansen, C.J. Frederickson, J. Zimmer, N.H. Diemer, *Neurosci. Lett.* **1990**, *109*, 247–252.

[18] D.W. Choi, J.Y. Koh, *Annu. Rev. Neurosci.* **1998**, *21*, 347–375.

[19] M.-C. Lee, W. C. Yu, Y. H. Shih, C. Y. Chen, Z. H. Guo, S. J. Huang, J.C.C. Chan, Y. R. Chen, *Sci*. *Rep*. **2018**, *8*, 1–16.

[20] D. Noy, I. Solomonov, O. Sinkevich, T. Arad, K. Kjaer, I. Sagi, *J*. *Am*. *Chem*. *Soc*. **2008**, *130*, 1376–1383.

[21] A.S. Prasad, *J*. *Trace Elem*. *Med*. *Biol*. **2012**, *26*, 66–69.

[22] L.C. Costellot, Y. Liu, J. Zou, R.B. Franklin, *J*. *Biol*. *Chem*. **1999**, *274*, 17499–17504.

[23] S.M. Henshall, D.E.H. Afar, K.K. Rasiah, L.G. Horvath, K. Gish, I. Caras, V. Ramakrishnan, M. Wong, U. Jeffry, J.G. Kench, **2003**, *22*, 6005–6012.

[24] K.M. Hambidge, N.F. Krebs, *J*. *Nutr*. **2007**, *137*, 1101–1105.

[25] X. Liu, P. Wang, J. Fu, K. Yao, K. Xue, K. Xu, *J*. *Lumin*. **2017**, *186*, 16–22.

[26] N. Behera, V. Manivannan, *J*. *Photochem*. *Photobiol*. *A Chem*. **2018**, *353*, 77–85.

[27] V. Kumar, U. Diwan, N. Tyagi, R.K. Mishra, M.K. Singh, K.K. Upadhyay, *J*. *Photochem*. *Photobiol*. *A Chem*. **2022**, *425*, 113692.

[28] J. Hojitsiriyanont, P. Chaibuth, K. Boonkitpatarakul, V. Ruangpornvisuti, T. Palaga, K. Chainok, M. Sukwattanasinitt, *J*. *Photochem*. *Photobiol*. *A Chem*. **2021**, *415*, 113307.

[29] D. Xiang, S. Zhang, Y. Wang, K. Sun, H. Xu, *Tetrahedron* **2022**, *106*, 132648.

[30] C.A.S. Pothulapadu, A. Jayaraj, N. Swathi, R.N. Priyanka, G. Sivaraman, *ACS Omega* **2021**, *6*, 24473–24483.

[31] M. Shellaiah, Y.T. Chen, N. Thirumalaivasan, B. Aazaad, K. Awasthi, K.W. Sun, S.P. Wu, M.C. Lin, N. Ohta, *ACS Appl*. *Mater*. *Interfaces*. **2021**, *13*, 28610–28626.

[32] E. moradinia, M. Mansournia, B. Notash, *J*. *Photochem*. *Photobiol*. *A Chem*. **2019**, *382*, 111963

[33] D.G. Kokare, V. Kamat, K. Naik, A. Nevrekar, A. Kotian, V.K. Revankar, *J*. *Mol*. *Struct*. **2017**, *1127*, 289–295.

[34] A. Kamath, V.K. Revankar, *J*. *Incl*. *Phenom*. *Macrocycl*. *Chem*. **2012**, *72*, 149–155.

[35] N.E. Borisova, A. Kostin, T. V Magdesieva, M.D. Reshetova, O. Nikitin, V. Paredes-García, M.T. Garland, P. Hermosilla-Ibáñez, W. Canon-Mancisidor, A. Rodionov, *New J*.

Chem. **2014**, *38*, 709–716.

[36] S. Anbu, R. Ravishankaran, M.F.C. Guedes Da Silva, A.A. Karande, A.J.L. Pombeiro, *Inorg*. *Chem*. **2014**, *53*, 6655–6664.

[37] S. Anbu, S. Kamalraj, C. Jayabaskaran, P.S. Mukherjee, *Inorg*. *Chem*. **2013**, *52*, 8294–8296.

[38] Y. Deepika, P. Surendra, N.K. Sachin, S. Shewta, *Int*. *J*. *Curr*. *Pharm*. *Rev*. *Res*. **2011**, *1*, 33–46.

[39] J.A. Pereira, A.M. Pessoa, M.N.D.S. Cordeiro, R. Fernandes, C. Prudêncio, J.P. Noronha, M. Vieira, *Eur*. *J*. *Med*. *Chem*. **2015**, *97*, 664–672.

[40] L.C. da Silva, V.G. Machado, F.G. Menezes, *Chem*. *Pap*. **2021**, *75*, 1775–1793.

[41] S.M. Annigeri, M.P. Sathisha, V.K. Revankar, *Transit*. *Met*. *Chem*. **2007**, *32*, 81–87.

[42] F.A.S. Alasmary, F.S. Alnahdi, A. Ben Bacha, A.M. El-Araby, N. Moubayed, A.M. Alafeefy, M.E. El-Araby, *J*. *Enzyme Inhib*. *Med*. *Chem*. **2017**, *32*, 1143–1151.

[43] L. Tang, M. Cai, P. Zhou, J. Zhao, Z. Huang, K. Zhong, S. Hou, Y. Bian, *J*. *Lumin*. **2014**, *147*, 179–183.

[44] S. Dutta, N. Basu, D. Mandal, *J*. *Photochem*. *Photobiol*. *A Chem*. **2023**, *435*, 114240.

[45] R. Arabahmadi, *J*. *Photochem*. *Photobiol*. *A Chem*. **2022**, *427*, 113797.

[46] C.J. Fahrni, M.M. Henary, D.G. VanDerveer, *J*. *Phys*. *Chem*. *A*. **2002**, *106*, 7655–7663.

[47] A. Aouina, H.O. Oloyede, R.A. Akong, J. Abdelhak, H. Görls, W. Plass, A.O. Eseola, *J*. *Photochem*. *Photobiol*. *A Chem*. **2021**, 406, 113006.

[48] A.O. Eseola, H. Görls, M. Bangesh, W. Plass, *New J*. *Chem*. **2018**, *42*, 7884–7900.

[49] J. Jayabharathi, V. Thanikachalam, M. Vennila, K. Jayamoorthy, *Spectrochim*. *Acta - Part A Mol*. *Biomol*. *Spectrosc*. **2012**, *95*, 446–451.

[50] X. li Yue, Z. qing Wang, C. rui Li, Z. yin Yang, *Tetrahedron Lett*. **2017**, *58*, 4532–4537.

[51] R. Alam, T. Mistri, R. Bhowmick, A. Katarkar, K. Chaudhuri, M. Ali, *RSC Adv*. **2016**, *6*, 1268–1278.

[52] A. Jana, B. Das, S.K. Mandal, S. Mabhai, A.R. Khuda-Bukhsh, S. Dey, *New J. Chem.* **2016**, *40*, 5976–5984.

[53] K. Mawai, S. Nathani, P. Roy, U.P. Singh, K. Ghosh, *Dalton Trans*. **2018**, *47*, 6421–6434.

[54] M. Khatun, P. Ghorai, J. Mandal, S. Ghosh Chowdhury, P. Karmakar, A. Saha, *J. Photochem. Photobiol. A Chem*. **2024**, *446*, 115145.

[55] Y. Hu, L.C. Du, J. Yang, *Inorg. Chim. Acta*. **2020**, *509*, 119675.

[56] B.K. Datta, D. Thiyagarajan, S. Samanta, A. Ramesh, G. Das, *Org. Biomol. Chem*. **2014**, *12*, 4975–4982.

[57] R. Bauernschmitt, R. Ahlrichs, *Chem. Phys. Lett*. **1996**, *256*, 454–464.

[58] R.E. Stratmann, G.E. Scuseria, M.J. Frisch, *J. Chem. Phys*. **1998**, *109*, 8218–8224.

Appendix:

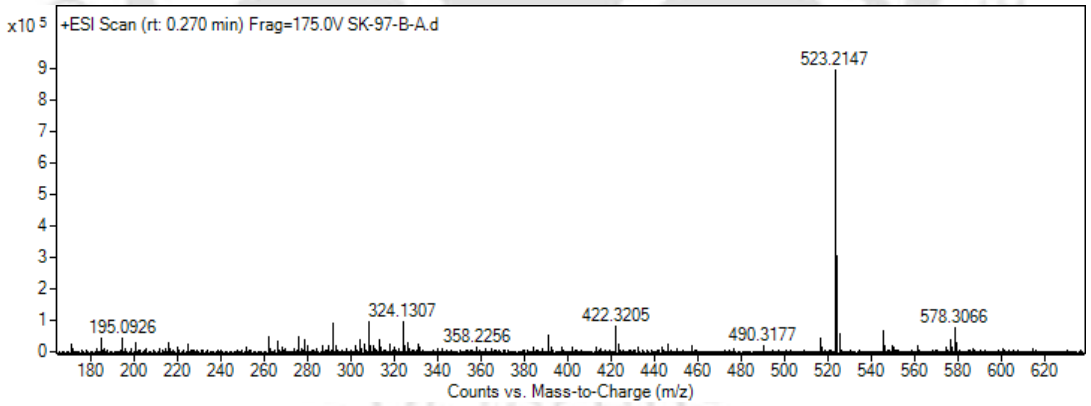

Figure A1. Mass spectrum of **LH**.

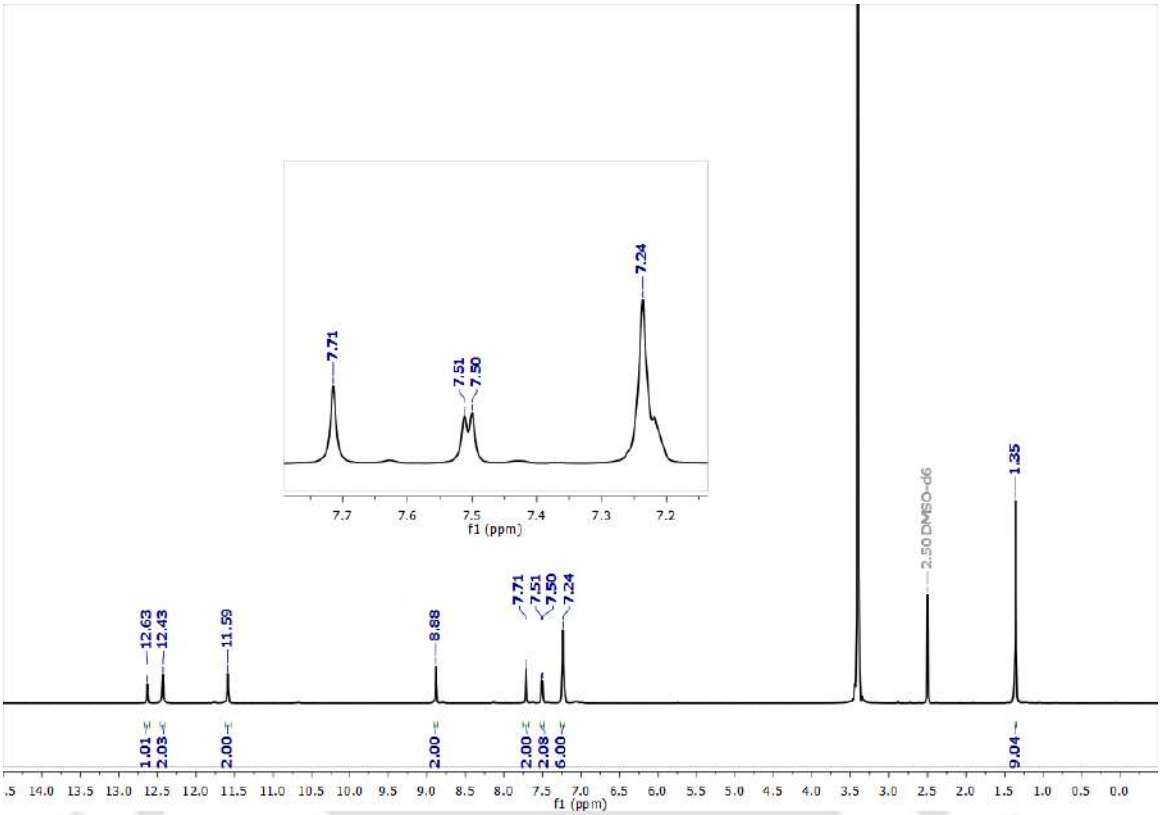

Figure A2. ^{1}H NMR spectrum of **LH**.

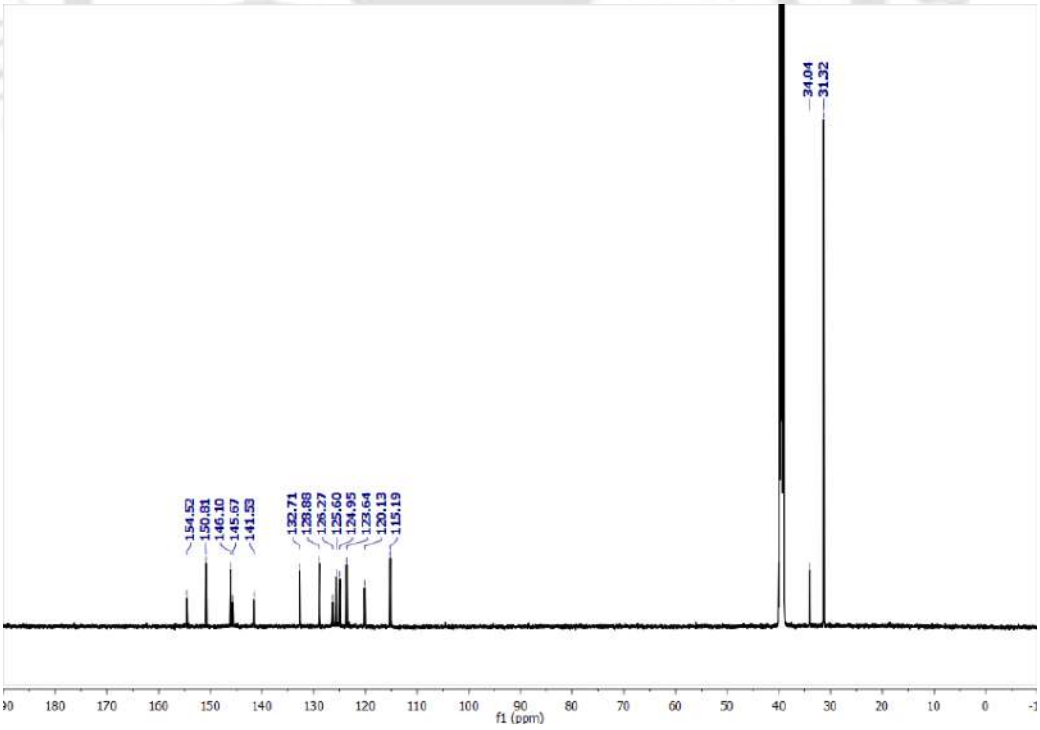

Figure A3. ^{13}C NMR spectrum of **LH**.

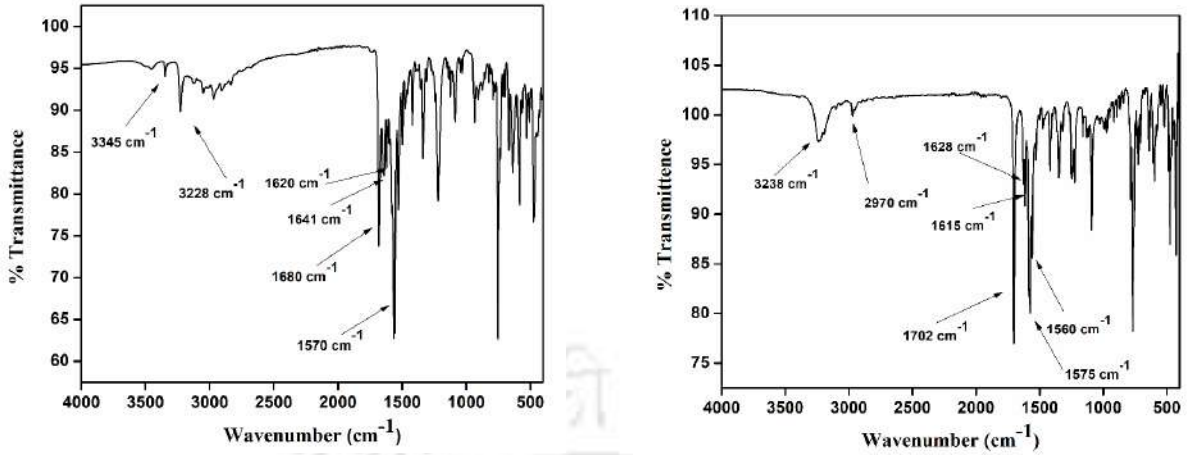

Figure A4. IR spectrum of **LH** and **1**.

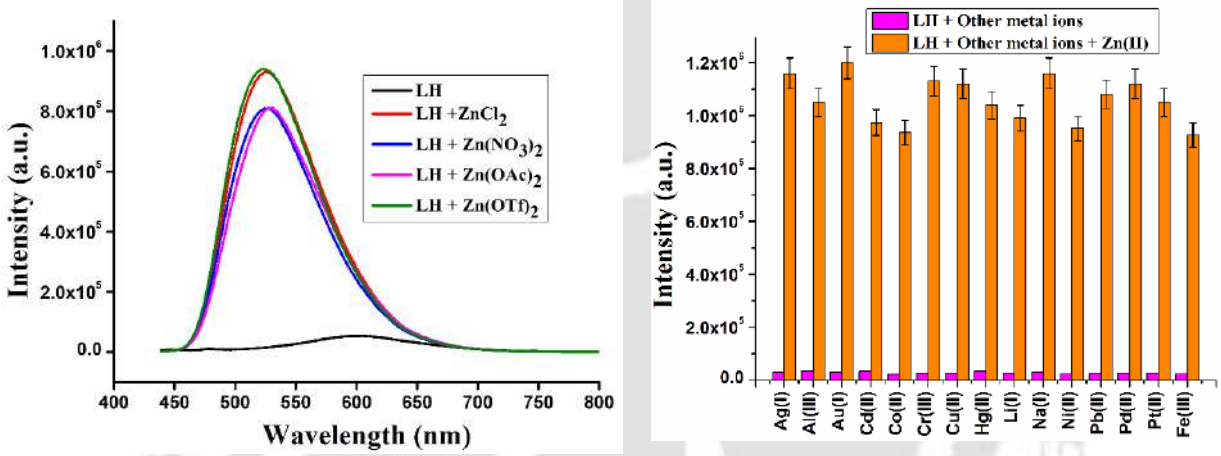

Figure A5. (a) Fluorescence spectra of **LH** with various zinc salts. (b) Bar diagram of fluorescence spectra of **LH** with other metal ions followed by addition of Zn^{2+} ion.

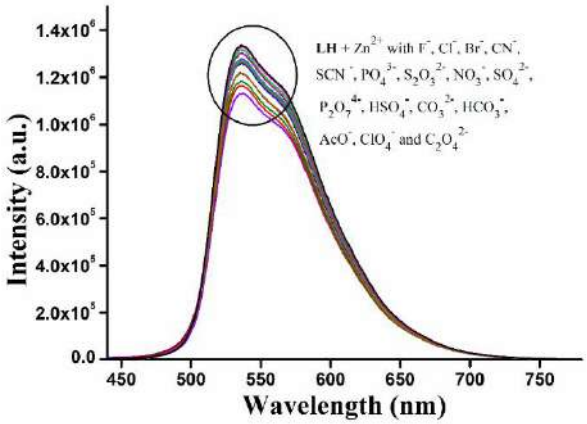

Figure A6. Anions interference effect on emission spectra of **1**.

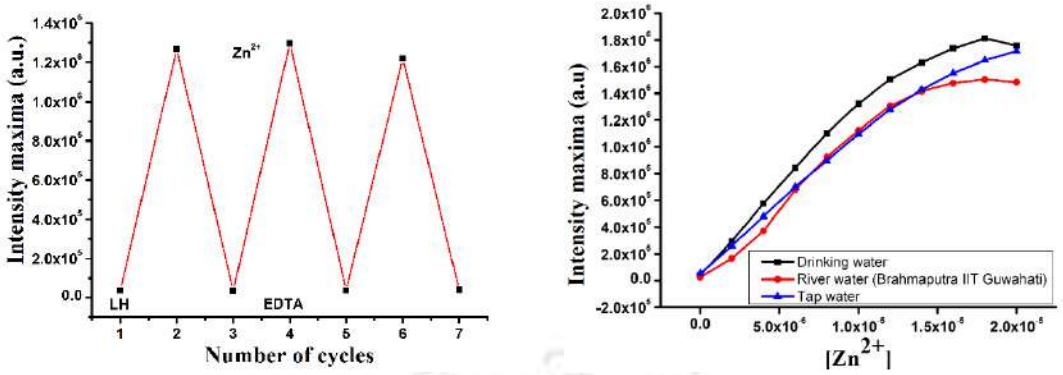

Figure A7. (a) Reversibility test of **LH** bound Zn^{2+} ion using Na_2EDTA. (b) Emission spectra observed in real water samples.

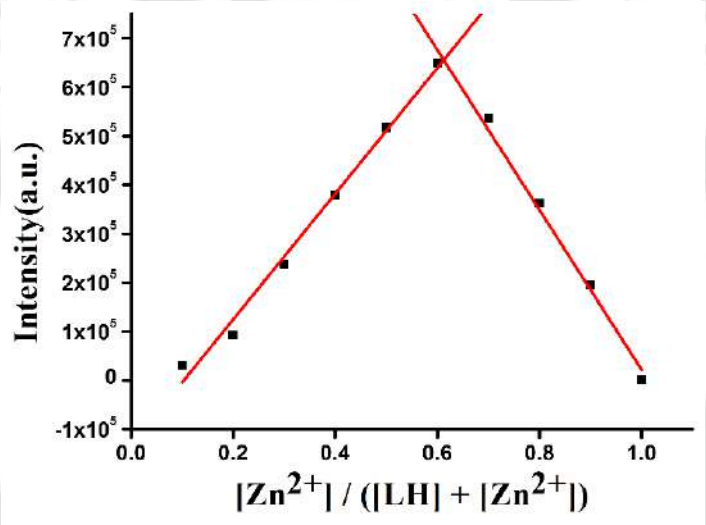

Figure A8. Job's plot of **LH** with varying mole fraction of Zn^{2+} ion.

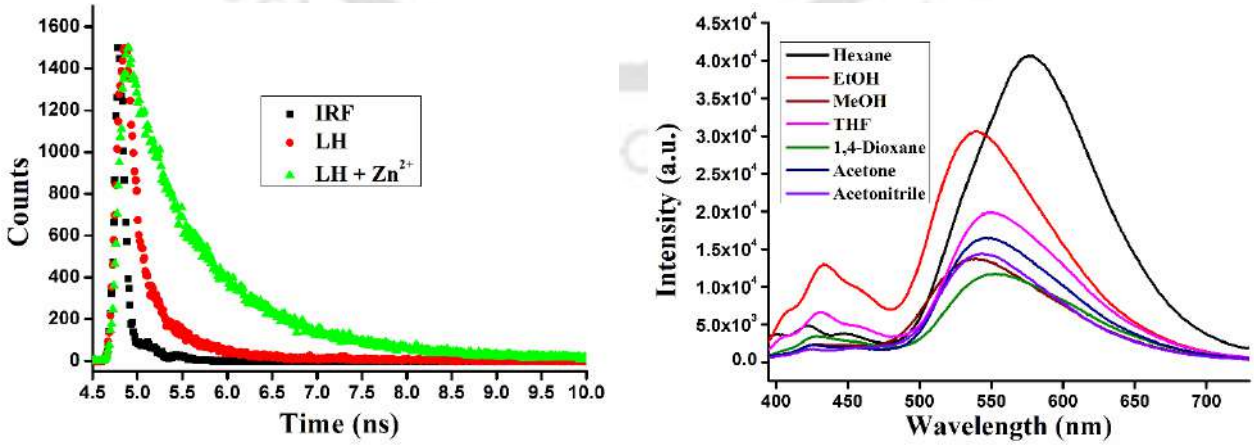

Figure A9. (a) Time resolved fluorescence decay profile of **LH** in absence and presence of $ZnCl_2$. (b) Fluorescence spectra of **LH** in different solvents.

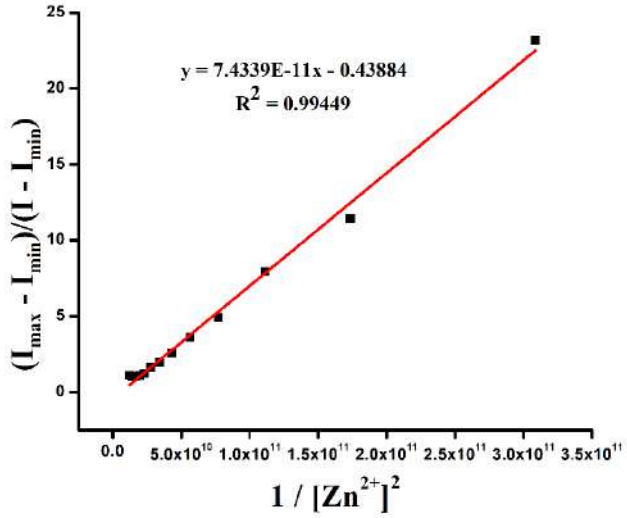

Figure A10. B-H plot for the determination of binding constant of **1**.

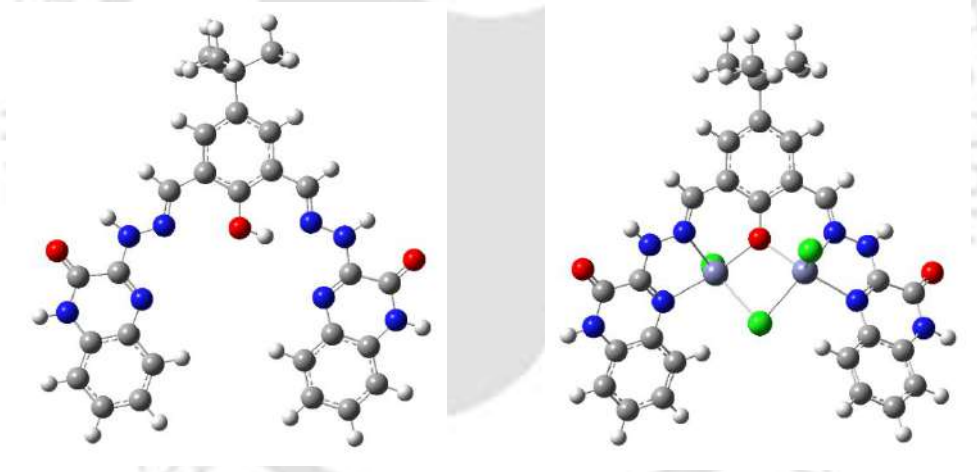

Figure A11. DFT optimized structure of (a) **LH** and (b) **1**.

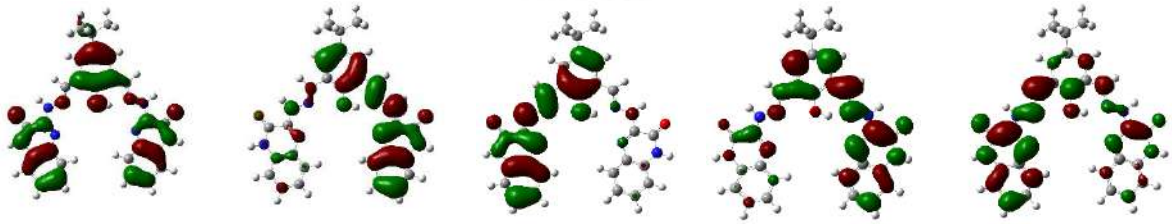

HOMO-2 HOMO-1 HOMO LUMO LUMO+1

Figure A12. Frontier molecular orbitals of **LH** involved in absorption.

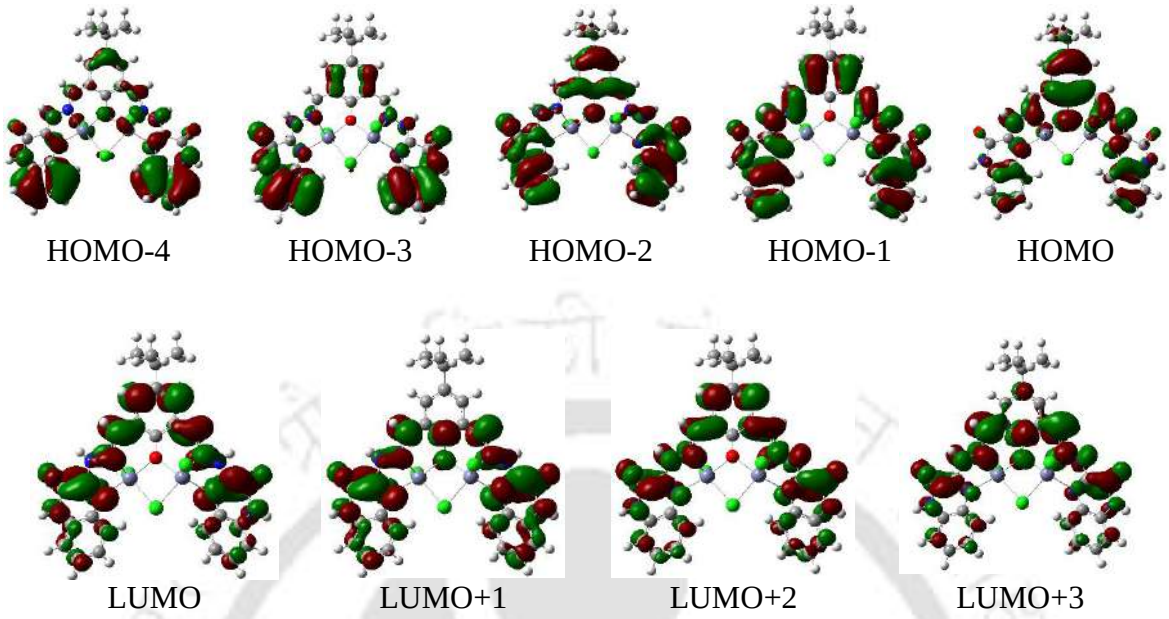

Figure A13. Frontier molecular orbitals of [Zn_2(**L**)Cl_3].

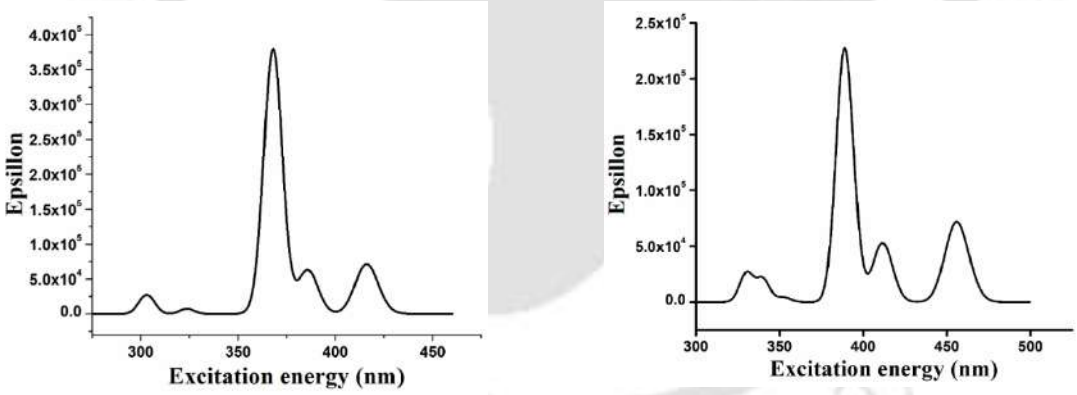

Figure A14. Simulated absorption spectrum of (a) **LH**. and (b) [Zn_2(**L**)Cl_3].

Table A1. Fluorescence decay parameter.

Sample	τ(ns)	χ^2
LH	0.47	1.084
LH + $ZnCl_2$	0.98	1.026

Table A2. Comparison table of some reported probes for detection of Zn^{2+} ion.

Probes	Selectivity for	Solvents	Detection limit
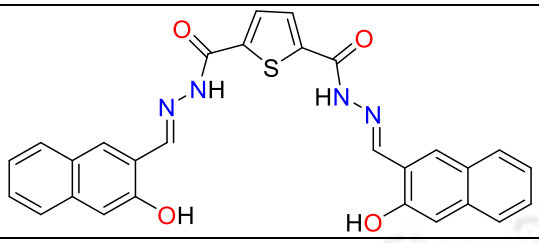	Zn^{2+} (turn-off)	DMSO/Water (6:4)	151 nM
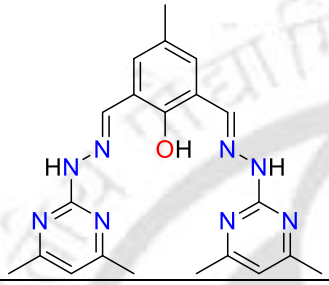	Zn^{2+} (turn-on)	DMSO/Water (1:9)	972 nM
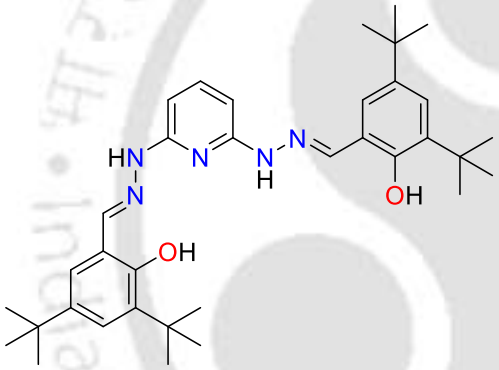	Zn^{2+} (turn-on)		7200 nM
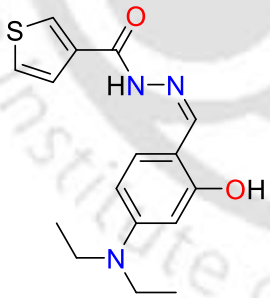	Zn^{2+} (turn-on)	DMSO/Water (1:1)	3.7 nM
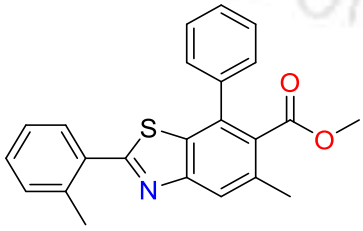	Zn^{2+} (turn-on)	$CH_3CN/H2O$ (9:1)	348 nM

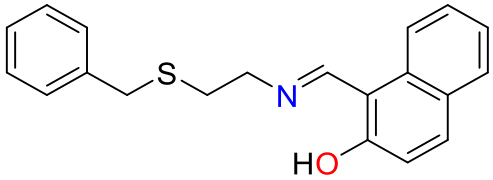	Zn^{2+} (turn-on)	EtOH/Water (9:1)	503 nM
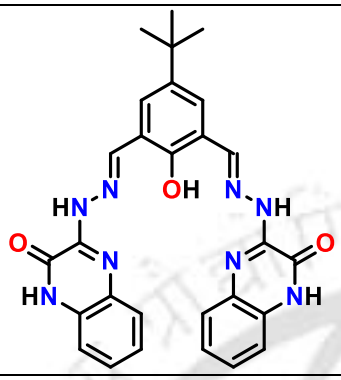	Zn^{2+} (turn-on)	EtOH/Water (8:2)	95 nM

Table A3. Crystallographic data and refinement parameters of **1**·2H_2O·2.5DMF.

Formula	$C_{71}H_{93}Cl_6N_{21}O_{15}Zn_4$
CCDC No.	2302879
Mol. wt.	1954.84
Cryst.color, habit	Red, needle
T, K	296.15
Cryst. syst.	Triclinic
Space group	*P*-1
a, Å	11.788(6)
b, Å	15.092(7)
c, Å	15.112(9)
α ,deg	103.109(18)
β, deg	111.214(18)
γ ,deg	102.342(19)
V, Å^3	2308(2)
Z	1
*D*calcd, g cm^{-3}	1.407
μ, mm^{-1}	1.269

GOF[a] on F^2	1.008
F(000)	1008.0
Reflection collected	51966
Unique reflections	8108
R_1[b], wR_2[c] ($I \geq 2\sigma(I)$)	0.0777, 0.1953
R_1[b], wR_2[c] (all data)	0.1500, 0.2217

[a]GOF (Goodness-of-fit) = $[\sum[w(F_0^2 - F_c^2)^2] / M - N]^{1/2}$ (M =number of reflections, N = number of parameters refined). [b] $R_1 = \sum \| F_0 | - | Fc \| / \sum | F_0 |$. [c]$wR_2 = [\sum[w(F_0^2 - F_c^2)^2] / \sum[w(F_0^2)^2]]$.

Table A4. Selected bond parameters in **1**.

Bond	Length (Å)	Bond	Angle (º)
Zn1–Cl1	2.244(3)	N1–Zn1–Cl1	103.44(18)
Zn1–Cl2	2.366(2)	N1–Zn1–Cl2	98.10(16)
Zn2–Cl2	2.352(2)	N4–Zn1–Cl1	117.5(2)
Zn2–Cl3	2.237(3)	N4–Zn1–Cl2	134.2(2)
Zn1–N1	2.154(5)	N4–Zn1–N1	76.6(2)
N3–N4	1.368(7)	O2–Zn1–Cl1	104.89(14)
Zn1–N4	2.100(6)	O2–Zn1–Cl2	82.63(13)
Zn2–N5	2.145(5)	O2–Zn1–N1	149.9(2)
N6–N7	1.360(7)	O2–Zn1–N4	81.54(19)
Zn2–N6	2.088(5)	Cl3–Zn2–Cl2	113.03(10)
Zn1–O2	2.087(4)	N5–Zn2–Cl2	100.22(15)
Zn2–O2	2.101(4)	N5–Zn2–Cl3	104.86(16)
		N6–Zn2–Cl2	138.32(17)
		N6–Zn2–Cl3	107.90(17)
		N6–Zn2–N5	76.04(19)
		N6–Zn2–O2	81.24(18)
		O2–Zn2–Cl2	82.70(13)
		O2–Zn2–Cl3	102.48(14)
		O2–Zn2–N5	148.67(19)

Table A5. Calculated energy levels of the low-lying transition in **LH**.

state	assignment		coefficient	energy (eV)	wave length (nm)	oscillator strength
	from	to				
S0→S1	HOMO-1	LUMO	14.4%	2.9804	416	0.2639

	HOMO	LUMO	80.3%			
	HOMO	LUMO+1	3.3%			
S0→S2	HOMO-1	LUMO	47.6%	3.2132	385.85	0.2312
	HOMO-1	LUMO+1	8%			
	HOMO	LUMO	16.4			
	HOMO	LUMO+1	26.7%			
S0→S3	HOMO-1	LUMO	36.5%	3.3683	367.10	1.3713
	HOMO-1	LUMO+1	5.7%			
	HOMO	LUMO+1	55.5%			
S0→S4	HOMO-1	LUMO+1	82.9%	3.4185	362.68	0.0722
	HOMO	LUMO+1	13.6%			
S0→S5	HOMO-2	LUMO	91%	3.683	336.7	0.1548

Table A6. Calculated energy levels of the low-lying transition in **1**.

state	**assignment**		**coefficient**	**energy (eV)**	**wave length (nm)**	**oscillator strength**
	from	**to**				
S0→S1	HOMO	LUMO	97.0%	2.7195	455.91	0.2656
S0→S2	HOMO	LUMO+1	98.5%	3.0123	411.59	0.1954
S0→S3	HOMO-1	LUMO+1	93.5%	3.1701	391.10	0.1434
S0→S4	HOMO-1	LUMO	97.3%	3.1908	388.57	0.7135
S0→S5	HOMO-2	LUMO	94.5%	3.5184	352.38	0.0159
S0→S6	HOMO-3	LUMO	14%	3.6456	340.09	0.0759
	HOMO-2	LUMO+1	81.2%			
S0→S7	HOMO-4	LUMO+2	12.7%	3.7427	331.27	0.0762
	HOMO-3	LUMO	69%			
	HOMO-2	LUMO+1	14.1%			

Chapter 3

Fluorometric *Turn Off* Detection of Cu^{2+} and Pd^{2+} Ions Using 1-(Imidazo[5,1-*a*]isoquinolin-3-yl)naphthalen-2-ol*

Abstract

The fused heterocycle 1-(imidazo[5,1-*a*]isoquinolin-3-yl)naphthalen-2-ol (**L2H**) has been synthesized and characterized by spectroscopic methods. Probe **L2H** upon irradiation with λ_{ex} = 336 nm, exhibited strong fluorescence with λ_{em} = 437 nm in MeOH/HEPES buffer (5 mM, pH = 7.4, 2:8, *v*/*v*). Upon adding several metal ions, the fluorescence intensity was quenched only by Cu^{2+} and Pd^{2+} ions. This fluorescence *turn-off* response by Cu^{2+} and Pd^{2+} ions was observed even in the coexistence of other metal ions and anions. From the Job's plot and mass spectra analysis, a 1:2 ratio of M^{2+}: **L2H** was obtained and the composition [Cu(**L2**)$_2$H$_2$O] and [Pd(**L2**)$_2$] has been assigned. The detection limit for Cu^{2+} and Pd^{2+} ions was determined to be 0.24 and 0.35 μM respectively and workable pH window to be 4-10. The binding of **L2H** to Cu^{2+} and Pd^{2+} resulted in red-shift in the UV-visible spectrum which was supported by DFT/TDDFT calculations.

*This work has been published in

S. Kumar, H. Phogat and V. Manivannan, *Luminescence* **2025**, *40*, e70104.

1. Introduction

In the fields of biochemistry and biotechnology, scientists rely heavily on fluorescent probes to detect various metal ions such as aluminium, chromium, cadmium, copper, arsenic, iron, palladium, mercury, zinc and so forth.[1–7] Palladium (Pd) complexes are particularly important in various coupling reactions like the Heck, Kumada, Suzuki, Stille, Sonagashira, and Negishi.[8–12] They are also used widely in the pharmaceutical industry and jewellery making.[13–15] Additionally, Pd-based Lindlar catalyst is crucial in hydrogenation reactions. Despite its importance, Pd can however be harmful if consumed above the permissible limit of 15 μg/day per person.[16] Since it readily binds with thymidine base, it can cause DNA damage[17] and can also inhibit enzymes like aldolase, carbonic anhydrase, trypsin, and creatine kinase.[18,19] Overexposure to Pd can also damage kidneys, liver, and bone marrow. Toxic waste containing palladium poses a threat to aquatic life. Therefore, detecting Pd is crucial for safeguarding human health and the environment.

Copper is an essential transition metal ion, the third most abundant trace metal ion in the human body and plays a crucial role in maintaining many vital physiological functions within the body. It is a key component in various metalloenzymes such as *cyt-c* oxidase and superoxide dismutase.[20,21] Additionally, copper-containing proteins like plastocyanin and azurin, are essential for electron transfer processes. Maintaining the right balance of copper is vital for ensuring proper cellular metabolism and enzyme function.[22–24] However, excessive accumulation of copper can be hazardous, concentration prescribed by WHO stands at 31.5 μM in drinking water.[25] Conditions like Menkes syndrome, Alzheimer's and Wilson's diseases can result from excess accumulation of copper.[26–28] Hence, it is essential to monitor copper level in water to avoid health problems.

Techniques based on fluorescent sensors offer a simpler, faster, and cost-effective approach for detecting these ions over other techniques.[29–31] Many colorimetric and fluorometric sensor systems based on BODIPY, coumarin, acridine, fluorescein, rhodamine, and naphthalimide have been developed for detecting Cu^{2+} or Pd^{2+} ions.[32–35] However, there is limited documentation on the use of single probes for detecting both metal ions simultaneously.[36,37] As Cu^{2+} and Pd^{2+} ions can be present together in samples,[38] there is a requirement for probes capable of detecting both ions simultaneously. As a result, many small molecular sensors have been designed for the fluorometric detection of Cu and Pd, offering a promising avenue for the

simultaneous detection of these ions. Some of probes for the selective and simultaneous detection of copper and palladium ions include 2-hydroxynaphthaldehyde, purine, bis-tetraphenylimidazole and so forth in the structural moiety (see Table A3).[31,37,39] In this Chapter, the development of 1-(imidazo[5,1-a]isoquinolin-3-yl)naphthalen-2-ol (**L2H**) as a probe that has demonstrated remarkable selectivity and sensitivity in detecting both Cu^{2+} and Pd^{2+} ions at very low concentrations has been described.

2. Results and discussion

The probe 1-(imidazo[5,1-*a*]isoquinolin-3-yl)naphthalen-2-ol (**L2H**) by virtue of having imidazo[5,1-*a*]isoquinoline and naphthol rings could be a potential fluorophore. Close analogues, 3-(1-isoquinolinyl)imidazo[5,1-*a*]isoquinoline was an effective fluorescent sensor for detecting palladium(II) ions[12] and 2-(imidazo[5,1-*a*]isoquinolin-3-yl)phenol was found to be selective for detection of Cu(II) ion in which *in situ* generated copper complex also served as cyanide ion sensor.[28] Hence this study to evaluate utility of **L2H** as a metal ion sensor was undertaken, which was synthesized using one equivalent each of 1-isoquinolinemethylamine, 2-hydroxynaphthaldehyde and selenium dioxide in EtOH (Scheme1).[40] The mass, ^{1}H and ^{13}C -NMR spectra were shown in Figure A1 - A3. The molecular structure of **L2H** has also been determined by single crystal XRD method and the ORTEP diagram has been shown in Figure 1. Presence of intermolecular hydrogen bonding interaction between N1 and O1 (2.678 (3) Å) in **L2H** has been shown in Figure A4. The crystallographic data and refinement parameters has been shown in Table A1. The solution studies were conducted using a mixture of methanol and aqueous HEPES buffer (5 mM, pH 7.4, in a 2:8 ratio). Unless otherwise stated, the MeOH/aqueous HEPES buffer (5 mM, pH = 7.4, 2:8, *v/v*) solvent system was used for the spectroscopic detection of metal ions.

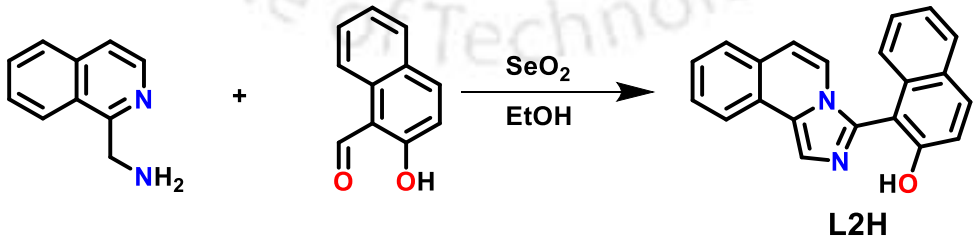

Scheme 1. Synthesis of probe **L2H**

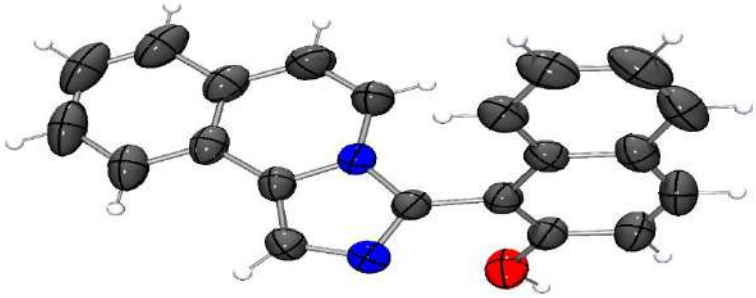

Figure 1. ORTEP diagram (50% probability) of **L2H**.

Due to the acidity of naphthyl-OH, **L2H** can readily form the conjugate base $\mathbf{L}^-$ which can be a potential bidentate chelating ligand coordinating through imidazo-N and naptholate-O atoms, by forming a six-membered chelate ring with metal ions. With this background, the ability of **L2H** as fluorescent metal ion sensor was undertaken in MeOH/HEPES buffer (5 mM, pH 7.4, 2:8, *v/v*) by employing chlorides of K^+, Fe^{3+}, Cd^{2+}, Pt^{2+}, Na^+, Fe^{2+}, Cu^{2+}, Li^+, Pb^{2+}, Zn^{2+}, Ni^{2+}, Mg^{2+}, Ca^{2+}, Mn^{2+}, Au^{3+}, Cr^{3+}, Pd^{2+}, Al^{3+} and Hg^{2+}. Stoichiometry studies (*vide infra*) suggested a $[Cu(\mathbf{L2})_2(H_2O)]$ and $[Pd(\mathbf{L2})_2]$ formula for the reactions of $CuCl_2$ and $PdCl_2$ with **L2H**, respectively.

Solvatochromism of probe **L2H** has been evaluated in MeOH, THF, DMF, DMSO, ACN, DCM, H_2O and 1,4-dioxane by both absorption and emission studies. In case of MeOH, THF, DMF, DMSO, ACN, H_2O and 1,4-dioxane (Figure A5) very little change in λ_{max} (335-340 nm) was observed ranging whereas in DCM, λ_{max} value shifted to 350 nm. On irradiation with λ_{ex} = 336 nm, λ_{em} showed a solvent dependent nature (Figure A6), namely, MeOH (428 nm), ACN (448 nm), 1,4-dioxane (435, 502 nm), THF (431, 509 nm), H_2O (459 nm), DMSO (432 nm), DCM (499 nm) and DMF (434 nm).

2.1 UV-Visible spectra

The UV-visible spectrum of **L2H** exhibited distinct absorption band with λ_{max} = 336 nm, which may be due to the n→π* transition. To **L2H**, when one equivalent of K^+, Fe^{3+}, Cd^{2+}, Pt^{2+}, Na^+, Fe^{2+}, Li^+, Pb^{2+}, Zn^{2+}, Ni^{2+}, Mg^{2+}, Ca^{2+}, Mn^{2+}, Au^{3+}, Cr^{3+}, Al^{3+}, and Hg^{2+} chloride was added, absorption band showed negligible change (Figure 2). However, upon gradual addition of half equivalent of Pd^{2+} and Cu^{2+} chloride, the intensity of the peak at 336 nm got diminished accompanied by appearance (Figure 3) of new band at λ_{max} = 389 nm (for Cu^{2+}) and 363 nm (for Pd^{2+}). This red shift in absorption spectrum of **L2H** upon adding Cu^{2+} and Pd^{2+} metal ions has been shown in Figure A7.

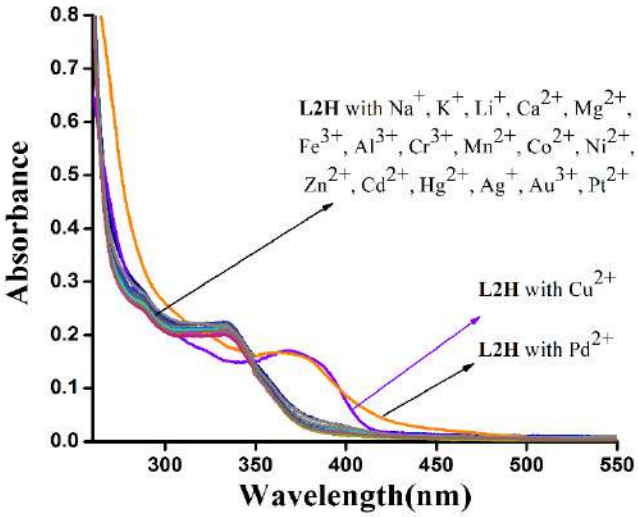

Figure 2. Electronic absorption spectra of **L2H** (20 μM) with various metal ions (20 μM).

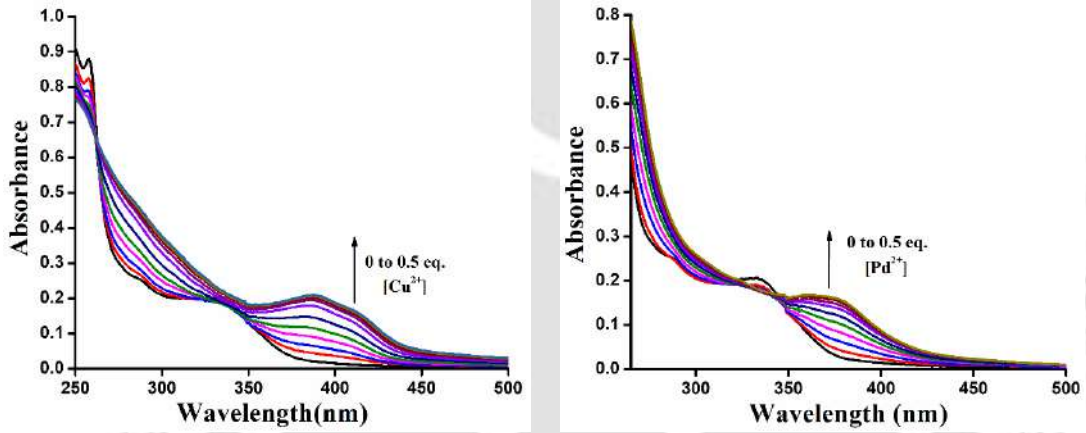

Figure 3. Variations in the UV-Visible spectra of **L2H** (20 μM) during gradual addition (0-10 μM) of $CuCl_2$ (left) and $PdCl_2$ (right).

2.2 Fluorescence spectra

The emission spectra of **L2H** was recorded in THF-H_2O and ACN-H_2O mixture (0-100% with 10% increments of H_2O). The intensity at λ_{em} = 437 nm increased with increase in H_2O content (2 times with 10-80% water in THF and 1.7 times with 10-80% water in ACN), then decreased with further increase in water percentage (Figure A8).

The solution of **L2H** was fluorescent with λ_{em} = 437 nm when excited with 336 nm light. No significant change in fluorescence intensity was noted after addition of two equivalents of soluble salts of K^+, Fe^{3+}, Cd^{2+}, Pt^{2+}, Na^+, Fe^{2+}, Li^+, Pb^{2+}, Zn^{2+}, Ni^{2+}, Mg^{2+}, Ca^{2+}, Mn^{2+}, Au^{3+}, Cr^{3+}, Al^{3+}, and Hg^{2+} ions to the **L2H** solution (Figure 4). However, during gradual addition of $CuCl_2$ and $PdCl_2$, shift in peak (432 nm for Cu^{2+}, 424 nm for Pd^{2+}) (Figure 5) accompanied by

decrease in fluorescence intensity was observed. Finally, after the addition of half-equivalent, quenching followed by a change in colour from light blue to colourless (under long-wave ultraviolet light) was observed (Figure A9). The quenching effect of $CuCl_2$ and $PdCl_2$ can be ascribed to the coordination of **L2H** with Cu^{2+} and Pd^{2+} ions. A study on metal ion competition further confirmed the selectivity of **L2H** for Cu^{2+} and Pd^{2+} ions. Treating **L2H** first with competing metal salts of same molarity and then introducing equimolar quantities of $CuCl_2$ or $PdCl_2$ showed that fluorescence intensity of **L2H** was effectively quenched only in the presence of Cu^{2+} and Pd^{2+} ions (Figure 6) despite the presence of various other metal ions. This competition study underscores the ability of **L2H** to selectively detect Cu^{2+} and Pd^{2+} ions even when other competing metal ions are present. The λ_{ex} values of 336 (**L2H**), 350 (**L2H** + Cu(II)) and 360 (**L2H** + Pd(II)) nm were obtained from the excitation spectra (Figure A10).

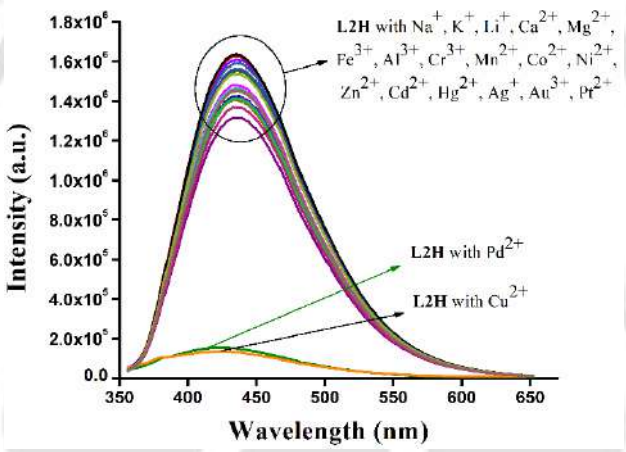

Figure 4. Fluorescence spectral behaviour of **L2H** (20 μM) with various metal ions (40 μM).

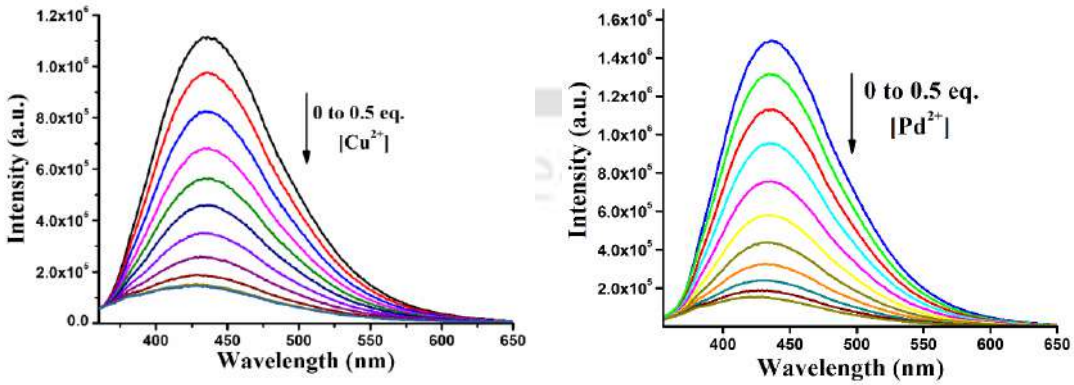

Figure 5. Variations in the emission intensity of **L2H** (20 μM) during gradual addition (0-10 μM) of $CuCl_2$ (left) and $PdCl_2$ (right).

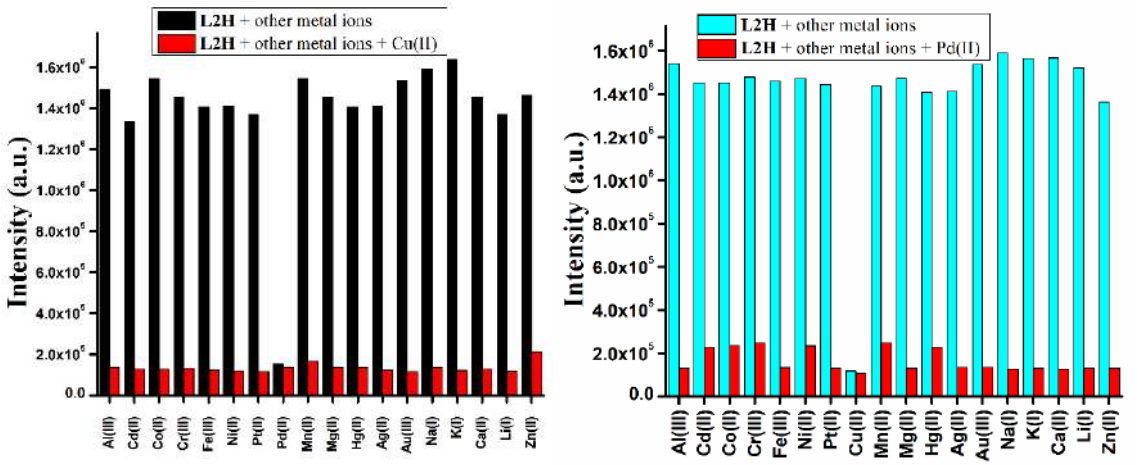

Figure 6. Bar diagrams of fluorescence intensity maxima of **L2H** with competing metal ions followed by the addition of Cu^{2+} (left) and Pd^{2+} (right) ions.

The selectivity of **L2H** towards Cu^{2+} and Pd^{2+} ions in presence of different anions, namely, I^-, SO_3^{2-}, SO_4^{2-}, SCN^-, F^-, Cl^-, Br^-, S^{2-}, $S_2O_3^{2-}$, NO_3^-, NO_2^-, HSO_4^-, CO_3^{2-}, $H_2PO_4^-$, ClO_4^-, PO_4^{3-}, N_3^-, HSO_3^-, AcO^- and AsO_2^- were also examined. Upon the addition of these anions to the *in situ* generated complex species, no discernible change in the emission spectral properties was observed. Thus, none of the anions restored the emission intensity, which meant that free **L2H** was not released at all from the complexed species (Figure A11).

2.3 Binding stoichiometry

The Job's method of continuous variation was employed to obtain the binding stoichiometry and the intersection point was around 0.33 for both metal ions (Figure A12), indicating a binding ratio of 1:2 between the metal ions and **L2H**. The binding constant from the fluorescence titration data was calculated to be 2.82×10^5 M^{-1} (for Cu^{2+}) and 9.46×10^4 M^{-1} (for Pd^{2+}) by using Benesi–Hildebrand plot (Figure A13). These findings underscore the strong affinity and specific interaction between **L2H** and the respective metal ions. The ESI mass spectrum of 1:2 mixture of $CuCl_2$/$PdCl_2$ and **L2H** contained peak at *m*/*z* = 699.1448 (calculated for $C_{42}H_{28}CuN_4O_3^+$, 699.1457; corresponding to the formula $[Cu(\mathbf{L2})_2(H_2O)]^+$ ion) and at *m*/*z* = 725.1187 (calculated *m/z* for $C_{42}H_{27}PdN_4O_2^+$, 725.1164; corresponding to the formula $[Pd(\mathbf{L2})_2+H]^+$ ion). Isotopic pattern calculated using m-Mass software matched correctly with those observed in the experimental mass spectrum (Figure A14 and A15). Thus, the compositions $[Cu(\mathbf{L2})_2H_2O]$ and $[Pd(\mathbf{L2})_2]$ consistent with 1:2 ratio were assigned. The binding of **L2H** with Cu^{2+} and Pd^{2+} was also examined through ^1H NMR titration of **L2H** with metal salts ($CuCl_2$ and $PdCl_2$) in DMSO-d_6. Upon gradual addition of $CuCl_2$ (0 to 0.5 eq.) to

L2H, the intensity of broad peak due to –OH (at 10.33 ppm) gradually decreased and disappeared after completion of adding 0.5 equivalent suggesting deprotonation of hydroxyl proton, accompanied by broadening of all aromatic peak because of paramagnetic nature of Cu^{2+} ion (Figure 7). [41–44] Such disappearance of –OH peak at 10.33 ppm was observed when $PdCl_2$ was added to **L2H**. However, aromatic peaks remained sharp because of diamagnetic nature of Pd^{2+} ion (Figure A16).

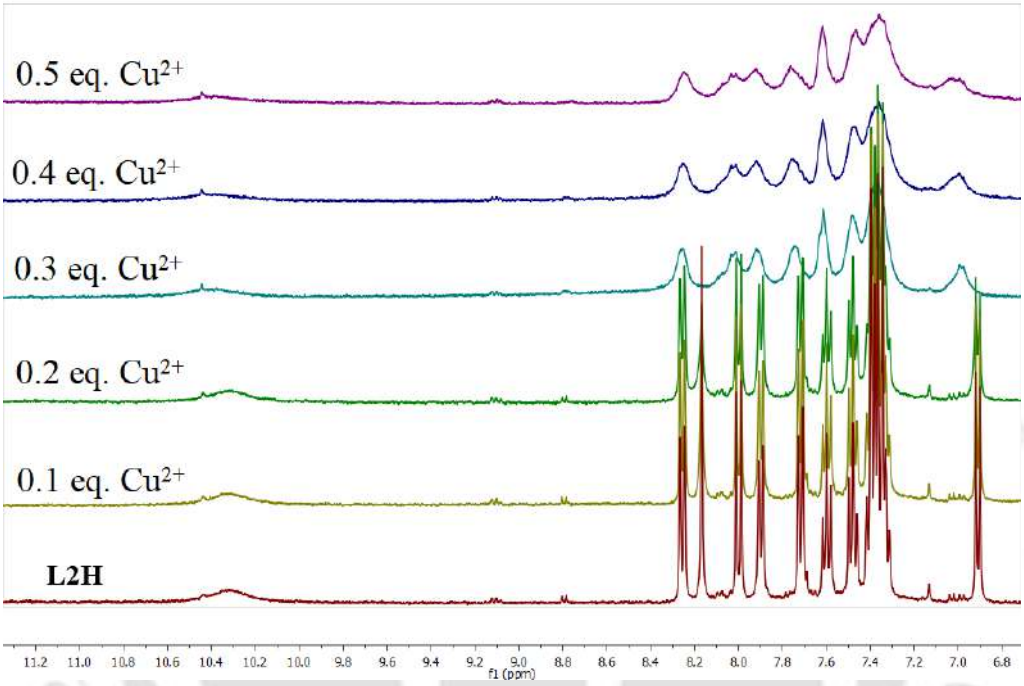

Figure 7. ^{1}H NMR titration of **L2H** with $CuCl_2$ in DMSO-d_6.

2.4 pH Effect and reversibility

The optimum pH range for fluorescence detection of Cu^{2+} and Pd^{2+} ions was determined by measuring the intensity (λ_{em} = 437 nm) at different pH adjusted using aqueous HCl and NaOH solutions. The emission intensity of **L2H** was quenched by both ions within a pH range of 4–10 (Figure 8). At pH < 4, **L2H** itself was weakly fluorescent, which was not affected by the addition of $CuCl_2$ and $PdCl_2$ due to protonation of the nitrogen atom and suppression of deprotonation of –OH group. Above pH = 10, due to formation of metal hydroxides the intensity remained unaffected.

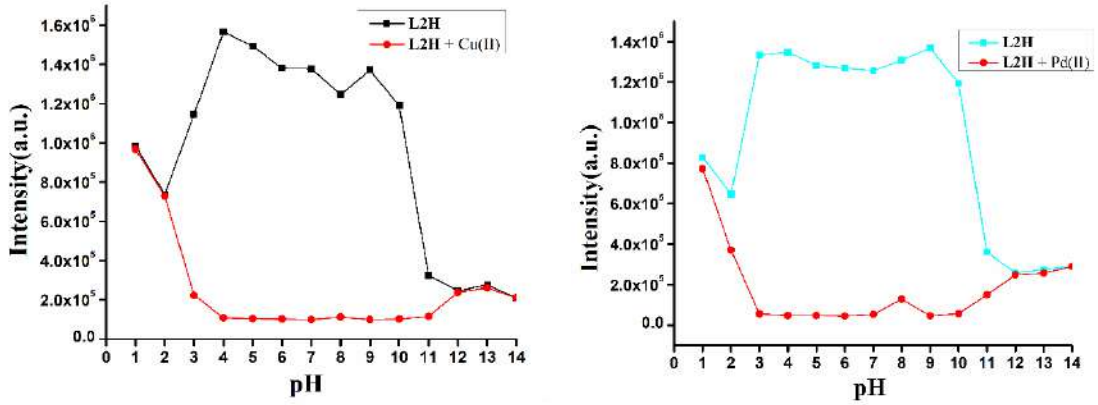

Figure 8. Fluorescence intensity *versus* pH plot.

The reversibility of binding of **L2H** with M (M = Cu^{2+} and Pd^{2+}) was tested by repeating addition of Na_2EDTA and MCl_2 (M = Cu, and Pd) solution. Initially, the solution containing only **L2H** showed high intensity which got quenched upon addition of half equivalent of metal ions. The intensity of same solution was restored upon addition of equimolar quantity (with respect to metal ion) of Na_2EDTA due to release of free **L2H** and sequestering of metal ions as soluble $[M(EDTA)]^{2-}$ (Figure A17). Fluorescence response time was observed to be 35 sec in case of Cu^{2+} ion while it was 75 sec with Pd^{2+} ion (Figure A18).

2.5 Detection in real water samples

Fluorescence titration experiments were conducted to evaluate the practical effectiveness of **L2H** in detecting Cu^{2+} and Pd^{2+} ions in environment water samples. Water samples collected Tap, potable sources, and river were collected, filtered through a 0.22 μM membrane and pH was adjusted to 7.4. A preliminary blank experiment was performed to verify the presence of these metal ions in the samples, which was found to be negative. These water samples were used for titration experiments and results were consistent with those obtained earlier (Figure A19), thus can be employed for environmental monitoring and water quality assessment.

2.6 Life time measurements

The quenching of fluorescence caused by complexation with Cu^{2+} and Pd^{2+} was confirmed by lifetime measurements through time-resolved fluorescence spectroscopy (TRPL). The fluorescence decay profiles of free **L2H** and in the presence of Cu^{2+} and Pd^{2+} ions (Figure A20 and Table A2) indicated that the average fluorescence lifetime (τ) for free **L2H** is 1.37 ns, while in the presence of Cu^{2+} and Pd^{2+} ions, got decreased to 0.93 and 0.98 ns respectively. This

reduction in lifetime suggested the formation of a non-fluorescent complex due to operation of chelation enhanced quenching (CHEQ) (Figure 9) and photoinduced electron transfer (PET) mechanisms. Probe **L2H** is highly fluorescent but fluorescence quenching upon coordination with Cu^{2+} and Pd^{2+} ions occurred may be due to photoinduced electron or energy transfer between fluorophore and M^{2+} ions.[45–49] Fluorescence quantum yield of free **L2H** was found to be 0.1233 and which decreased to 0.0035 {for [Cu(**L2**)$_2$(H_2O)]} and 0.0019 {for [Pd(**L2**)$_2$]}. Using the formula 3σ/k, the limit of detection for Cu^{2+} and Pd^{2+} was calculated to be 0.24 and 0.35 μM respectively (Figure A21).

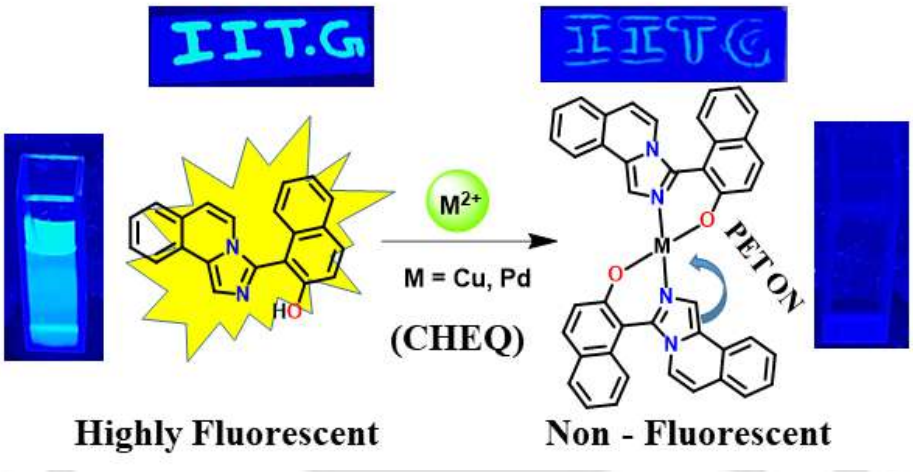

Figure 9. Probable mechanism of sensing.

2.7 Computational studies

Based on ^{1}H NMR titration, mass spectra, and Job's plot, the formulae [Cu(**L2**)$_2$$H_2O$] (**1**) and [Pd(**L2**)$_2$] (**2**) were assigned for performing DFT/TDDFT calculations (including **L2H**) utilizing the Gaussian09 software.[50] The geometries were optimized using 6-31G(d,p) basis set at the B3LYP level for **L2H**, while the lanl2dz basis set was applied to all elements in complexes and energy-optimized structures were shown in Figure A22. In both **1** and **2**, the central metal ion is coordinated by two $\mathbf{L}^-$ ions in a bidentate manner. The coordination involves the oxygen from the naphtholate group and the nitrogen atom from the imidazo group of the imidazo[5,1-*a*]isoquinoline moiety and this arrangement leads to a square planar geometry around the central metal ion in **2** and a square pyramidal geometry in **1**, with the water molecule occupying the axial position. Even though geometrical isomers can exist in both cases, the results were quite similar and the results for trans isomer is described here.

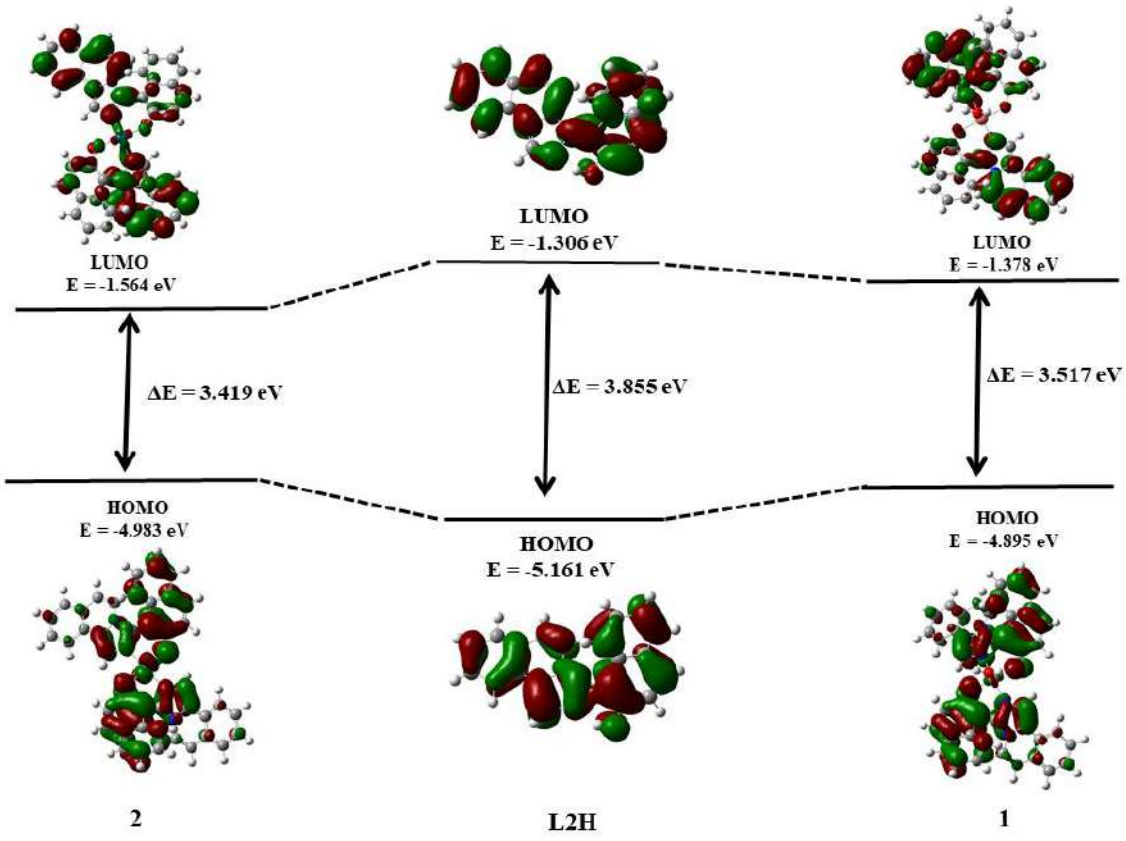

Figure 10. Energy level diagram.

In both HOMO and LUMO of **L2H**, the electron density is spread throughout the entire molecule. Electron density in the HOMO of **1** is concentrated mainly in naphthol and fused imidazo ring while that of LUMO in isoquinoline of imidazo[5,1-*a*]isoquinoline moiety. Upon complexation energy of the HOMO increased while that of LUMO decreased in both **1** and **2** (Figure 10). This resulted in reduction of the HOMO-LUMO energy gap by 0.338 eV (in **1**) and 0.436 eV (in **2**), which supported the experimentally observed red shift in the absorption peak of **L2H** in both complexes.

3. Conclusion

The probe **L2H** was synthesized and characterized using mass spectrometry, ^{1}H and ^{13}C NMR spectroscopy. This probe has been found to detect Cu^{2+} and Pd^{2+} ions selectively over various metal ions and anions through fluorescent *turn-off* fashion. Job's plot, mass spectra and ^{1}H NMR titration suggested a 1:2 binding ratio between M^{2+} ions (M = Cu, Pd) and **L2H**. The optimum pH window was determined to be 4-10 and EDTA test suggested that binding of the probe was reversible. A very low detection limit of 0.24 μM (for Cu^{2+}) and 0.35 μM (for Pd^{2+})

was determined which were very less in comparison with the permissible concentration suggested in WHO guidelines. The decreased fluorescence lifetime of **L2H** upon coordination with both ions indicated the quenching phenomena occurred through CHEQ and PET mechanisms. DFT/TDDFT studies were also in close agreement with experimental results. Thus, **L2H** can be a potential candidate for practical utility for the selective and sensitive detection of Cu^{2+} and Pd^{2+} ions.

4. Experimental section

4.1 Synthesis

*4.1.1 Synthesis of 1-(imidazo[5,1-a]isoquinolin-3-yl)naphthalen-2-ol (**L2H**)*

The probe **L2H** was synthesized following a previously reported literature procedure.[40] A mixture containing 1-isoquinolinylmethanamine (0.175 g, 1.106 mmol) and 2-hydroxynaphthalaldehyde (0.190 g, 1.106 mmol) was stirred in ethanol for 30 minutes. Solid selenium dioxide (0.122 g, 1.106 mmol) was introduced and stirred at room temperature. After 5 hours, saturated aqueous sodium thiosulfate solution (20 ml) was added, mixed thoroughly and then left undisturbed for 20 min. The turbid solution was filtered, washed 3 to 4 times with ethyl acetate and the solvent was evaporated from the combined filtrate and washings. The crude mixture was subjected to column chromatography over silica gel, **L2H** was eluted with 8% ethyl acetate in hexane. After evaporation of the volatiles, the yield of light yellow solid was 0.150 g (44%). ESI-MS (+): *m/z* calcd. for $C_{21}H_{15}N_2O^+$ $[M+H^+]$ 311.1179, found 311.1198. ^{1}H NMR (600 MHz, DMSO-d_6) δ 10.33 (s, 1H), 8.26 (d, *J* = 7.9 Hz, 1H), 8.17 (s, 1H), 8.00 (d, *J* = 9.0 Hz, 1H), 7.90 (dd, *J* = 7.9, 1.5 Hz, 1H), 7.72 (d, *J* = 7.7 Hz, 1H), 7.60 (t, *J* = 7.6 Hz, 1H), 7.48 (t, *J* = 7.5 Hz, 1H), 7.42 – 7.31 (m, 5H), 6.91 (d, *J* = 7.5 Hz, 1H). ^{13}C NMR (150 MHz, DMSO-*d6*) δ 154.6, 136.5, 134.3, 131.5, 128.4, 128.2, 128.1, 128.0, 127.2, 127.1, 127.1, 126.9, 124.5, 124.0, 123.3, 122.4, 122.0, 120.7, 118.3, 112.8, 108.7.

References

[1] Y. Yang, R. Shen, Y. Z. Wang, F. Z. Qiu, Y. Feng, X. L. Tang, D. cheng Bai, G. L. Zhang, W. S. Liu, *Sensors Actuators, B Chem.* **2018**, *255*, 3479–3487.

[2] X. Shi, H. Wang, T. Han, X. Feng, B. Tong, J. Shi, J. Zhi, Y. Dong, *J. Mater. Chem.* **2012**, *22*, 19296–19302.

[3] P. S. Nayab, M. Shkir, *Sensors Actuators, B Chem.* **2017**, *251*, 951–957.

[4] T. Gunnlaugsson, T. C. Lee, R. Parkesh, *Org. Lett.* **2003**, *5*, 4065–4068.

[5] S. Vishnu, A. Nag, A. K. Das, *Anal. Methods* **2024**, *16*, 5263–5271.

[6] C. Immanuel David, J. Lee, K. Ramanagul, V. Gothandapani, B. J. Kim, H. il Lee, *Anal. Chim. Acta* **2024**, *1305*, 342582.

[7] S. Kumar, S. Mahata, V. Manivannan, *J. Photochem. Photobiol. A Chem.* **2024**, *450*, 115436.

[8] S. Dhoun, I. Kaur, P. Kaur, K. Singh, *Dye. Pigment.* **2017**, *143*, 361–367.

[9] K. C. Nicolaou, P. G. Bulger, D. Sarlah, *Angew. Chem. Int. Ed.* **2005**, *44*, 4442–4489.

[10] R. Chinchilla, C. Nájera, *Chem. Soc. Rev.* **2011**, *40*, 5084–5121.

[11] C. Torborg, M. Beller, *Adv. Synth. Catal.* **2009**, *351*, 3027–3043.

[12] S. Mahata, A. Bhattacharya, J. P. Kumar, B. B. Mandal, V. Manivannan, *J. Photochem. Photobiol. A Chem.* **2020**, *394*, 112441.

[13] Q. Huang, Y. Zhou, Q. Zhang, E. Wang, Y. Min, H. Qiao, J. Zhang, T. Ma, *Sensors Actuators B Chem.* **2015**, *208*, 22–29.

[14] B. Zhu, C. Gao, Y. Zhao, C. Liu, Y. Li, Q. Wei, Z. Ma, B. Du, X. Zhang, *Chem. Commun.* **2011**, *47*, 8656–8658.

[15] M. Z. K. Baig, S. Pawar, R. N. P. Tulichala, A. Nag, M. Chakravarty, *Sensors Actuators B Chem.* **2017**, *243*, 226–233.

[16] C. E. Garrett, K. Prasad, *Adv. Synth. Catal.* **2004**, *346*, 889–900.

[17] C. K. S. Pillai, U. S. Nandi, *Biochim. Biophys. Acta (BBA)-Nucleic Acids Protein Synth.* **1977**, *474*, 11–16.

[18] J. D. Spikes, C. F. Hodgson, *Biochem. Biophys. Res. Commun.* **1969**, *35*, 420–422.

[19] M. D. Shultz, J. P. Lassig, M. G. Gooch, B. R. Evans, J. Woodward, *Biochem. Biophys. Res. Commun.* **1995**, *209*, 1046–1052.

[20] R. McRae, P. Bagchi, S. Sumalekshmy, C. J. Fahrni, *Chem. Rev.* **2009**, *109*, 4780–4827.

[21] K. J. Barnham, C. L. Masters, A. I. Bush, *Nat. Rev. Drug Discov.* **2004**, *3*, 205–214.

[22] S. J. Lippard, J. M. Berg, *Principles of Bioinorganic Chemistry*, Mill Valley, CA: University Science Books, **1994**.

[23] I. Bertini, *Biological Inorganic Chemistry: Structure and Reactivity*, Mill Valley, CA: University Science Books, **2007**.

[24] A. V Davis, T. V O'Halloran, *Nat. Chem. Biol.* **2008**, *4*, 148–151.

[25] WHO, WHO Guidelines Values for Chemicals that are of Health Significance in Drinking Water. Guidelines for Drinking Water Quality, Geneva, 3rd ed. **2008**.

[26] E. Gaggelli, H. Kozlowski, D. Valensin, G. Valensin, *Chem. Rev.* **2006**, *106*, 1995–2044.

[27] Y. H. Hung, A. I. Bush, R. A. Cherny, *JBIC J. Biol. Inorg. Chem.* **2010**, *15*, 61–76.

[28] S. Mahata, S. Dey, B. B. Mandal, V. Manivannan, *J. Photochem. Photobiol. A Chem.* **2022**, *427*, 113795.

[29] T. S. Neri, D. P. Rocha, R. A. A. Munoz, N. M. M. Coelho, A. D. Batista, *Microchem. J.* **2019**, *147*, 894–898.

[30] R. Cai, C. A. Shoukat, C. Zhang, X. Gao, H. Li, J. Chen, Y. Ji, X. Wu, *Analyst* **2023**, *148*, 3306–3311.

[31] H. Wu, L. Lin, L. Zheng, H. Guo, F. Yang, *J. Photochem. Photobiol. A Chem.* **2022**, *432*, 114076.

[32] N. K. Hien, M. Van Bay, N. C. Bao, Q. V Vo, N. D. Cuong, T. V. Thien, N. T. A. Nhung, D. U. Van, P. C. Nam, D. T. Quang, *ACS omega* **2020**, *5*, 21241–21249.

[33] X. Lu, Y. Zhan, W. He, *J. Photochem. Photobiol. B Biol.* **2022**, *234*, 112528.

[34] A. C. Gonçalves, J. L. Capelo, C. Lodeiro, A. A. Dos Santos, *Photochem. Photobiol. Sci.* **2017**, *16*, 1174–1181.

[35] S. Mahata, S. Kumar, S. Dey, B. B. Mandal, V. Manivannan, *Inorganica Chim. Acta* **2022**, *535*, 120876.

[36] W. Zhou, Q. Gao, D. Liu, C. Li, S. Liu, K. Xia, B. Han, C. Zhou, *Spectrochim. Acta Part A Mol. Biomol. Spectrosc.* **2020**, *237*, 118365.

[37] A. Kumar, Virender, B. Mohan, A. A. Solovev, M. Saini, H. Kumar Sharma, H. K. Sharma, *Microchem. J.* **2022**, *180*, 107561.

[38] J. Huang, J. Chan, Y. Chen, C. J. Borths, K. D. Baucom, R. D. Larsen, M. M. Faul, *J. Am. Chem. Soc.* **2010**, *132*, 3674–3675.

[39] Z. Dong, W. Chen, H. Li, Y. Dai, T. Zheng, H. Zhang, H. Xu, H. Lu, *Inorg. Chem. Commun.* **2020**, *116*, 107915.

[40] J. Bori, N. Behera, S. Mahata, V. Manivannan, *ChemistrySelect* **2017**, *2*, 11727–11731.

[41] R. S. Drago, *Physical Methods for Chemists* 2nd ed, Gainesville, FL: Surfside Scientific Publishers, **1977**, 500-552.

[42] S. Odisitse, G. E. Jackson, *Inorganica Chim. Acta* **2009**, *362*, 125–135.

[43] A. Paul, S. Anbu, G. Sharma, M. L. Kuznetsov, M. F. C. Guedes Da Silva, B. Koch, A. J. L. Pombeiro, *Dalt. Trans.* **2015**, *44*, 16953–16964.

[44] J. C. Ott, E. A. Suturina, I. Kuprov, J. Nehrkorn, A. Schnegg, M. Enders, L. H. Gade, *Angew. Chem. Int. Ed.* **2021**, *60*, 22856–22864.

[45] S. Liu, Y. M. Wang, J. Han, *J. Photochem. Photobiol. C Photochem. Rev.* **2017**, *32*, 78–103.

[46] D. T. Shi, B. Zhang, Y. X. Yang, C. C. Guan, X. P. He, Y. C. Li, G. R. Chen, K. Chen, *Analyst* **2013**, *138*, 2808–2811.

[47] L. Quan, T. Sun, W. Lin, X. Guan, M. Zheng, Z. Xie, X. Jing, *J. Fluoresc.* **2014**, *24*, 841–846.

[48] H. Li, J. Fan, X. Peng, *Chem. Soc. Rev.* **2013**, *42*, 7943–7962.

[49] L. Fabbrizzi, M. Licchelli, P. Pallavicini, A. Perotti, A. Taglietti, D. Sacchi, *Chem. - A Eur. J.* **1996**, *2*, 75–82.

[50] M. J. Frisch, Gaussian 09, Revision D. 01/Gaussian, **2009**.

Appendix

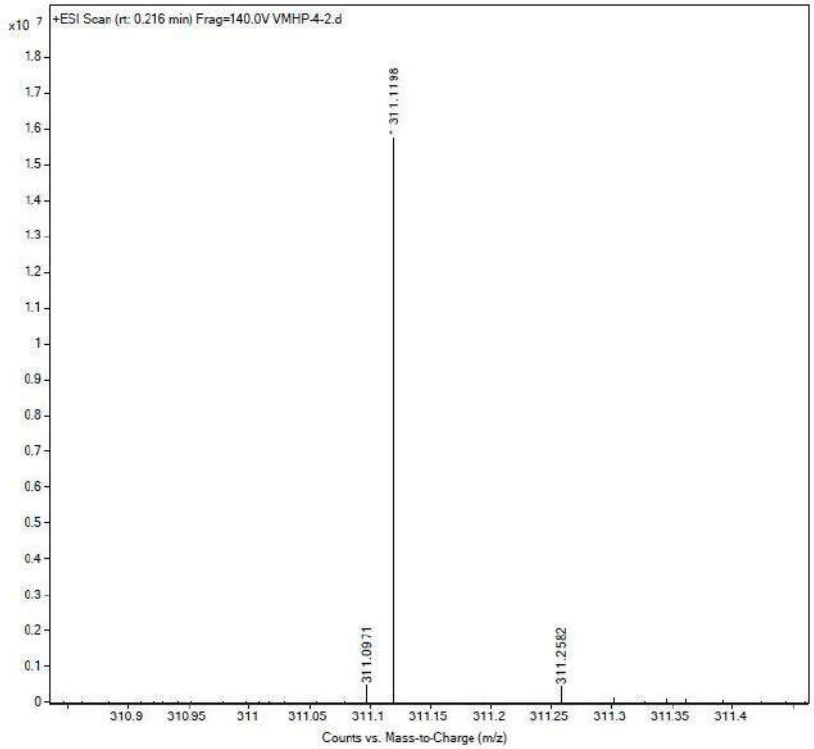

Figure A1. Mass Spectrum of **L2H**.

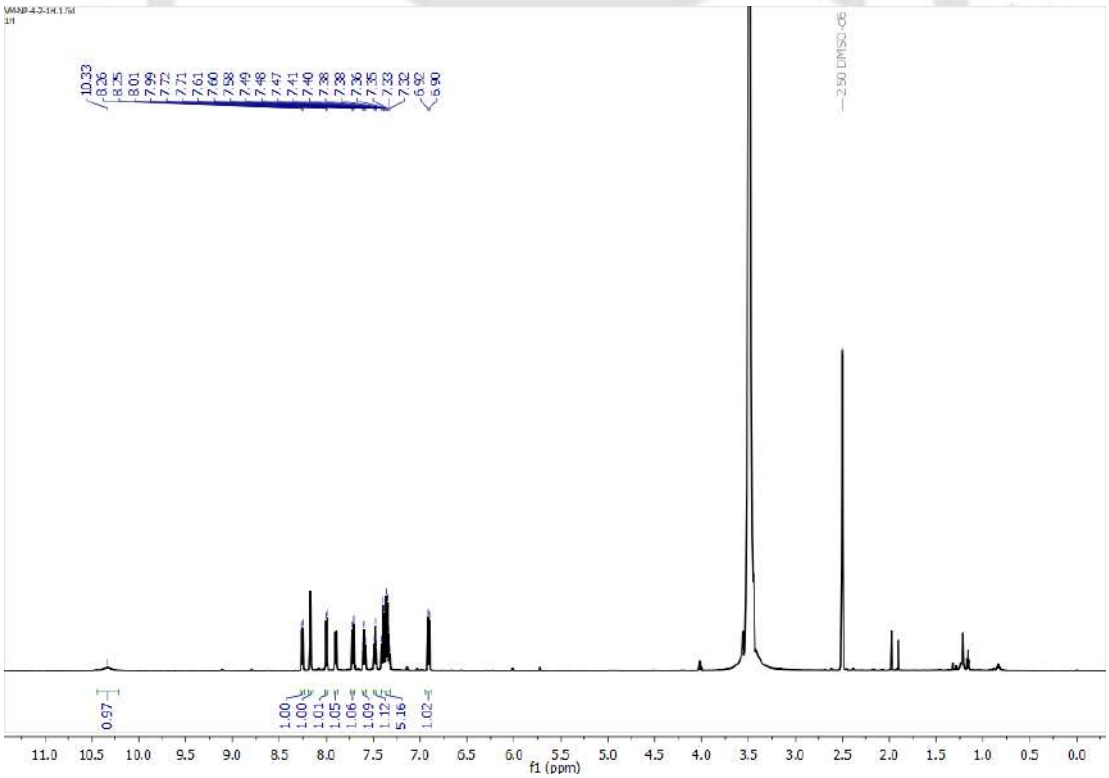

Figure A2. ^{1}H-NMR spectrum of **L2H**.

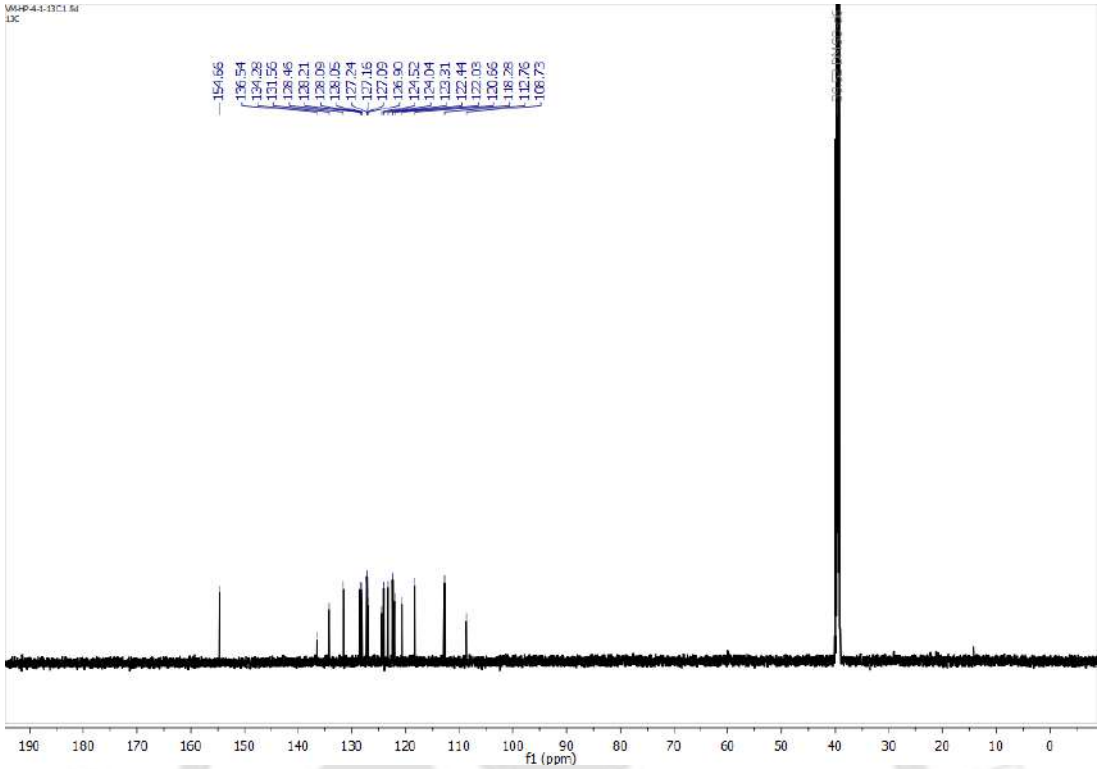

Figure A3. ^{13}C-NMRspectrum of **L2H**.

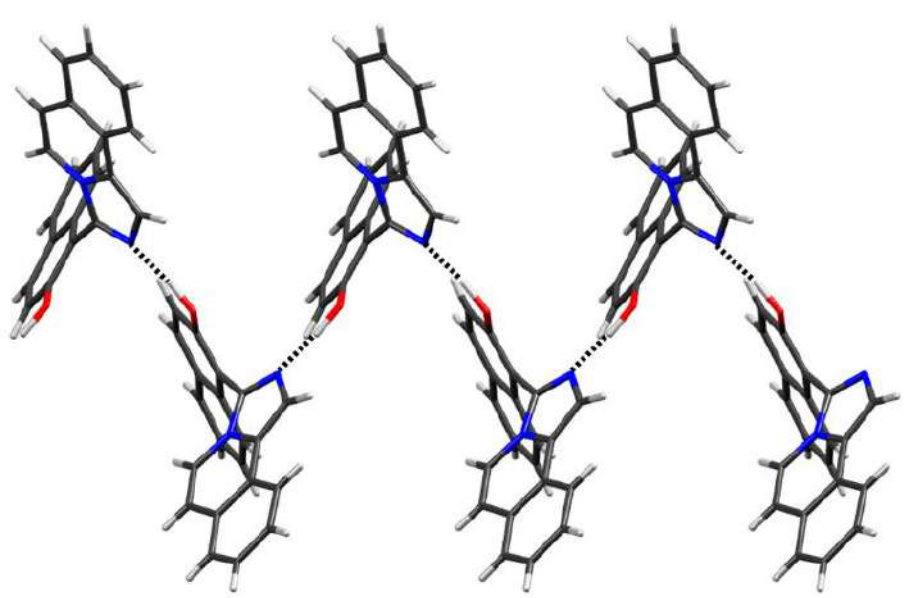

Figure A4. Packing diagram of **L2H** on viewing down the b-axis. Intermolecular hydrogen bond N1···O1, 2.678 (3) Å and the dihedral angle N1-C11-C12-C13, 62.2(4)°.

Table A1: Crystallographic data and refinement parameters of **L2H**.

Entry	**L2H**
Formula	$C_{21}H_{14}N_2O$
CCDC No.	2413598
Mol. wt.	310.34
Cryst.color, habit	yellow, block
T, K	295.00
Cryst. syst.	orthorhombic
Space group	*Pca2₁*
a, Å	15.3666(14)
b, Å	12.6613(12)
c, Å	8.3011(8)
α ,deg	90
β, deg	90
γ ,deg	90
V, Å^3	1615.1(3)
Z	4
*D*calcd, g cm^{-3}	1.276
μ, mm^{-1}	0.080
GOF[a] on F^2	1.119
F(000)	648.0
Reflection collected	36225
Unique reflections	2826
R_1[b], wR_2[c] $(I \geq 2\sigma(I))$	0.0342, 0.0777
R_1[b], wR_2[c] (all data)	0.0438, 0.0865

[a]GOF (Goodness-of-fit) = $[\sum[w(F_0^2 - F_c^2)^2] / M - N]^{1/2}$ (M =number of reflections, N = number of parameters refined). [b] $R_1 = \sum \| F_0 | - | Fc \| / \sum | F_0 |$. [c]$wR_2 = [\sum[w(F_0^2 - F_c^2)^2] / \sum[w(F_0^2)^2]]$

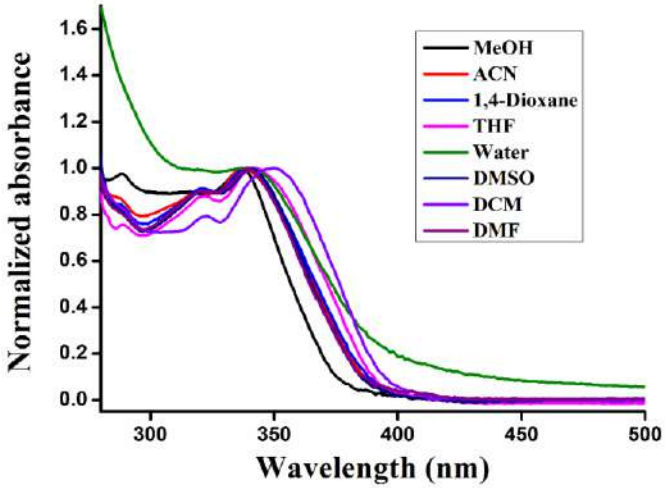

Figure A5. Normalized absorption spectra of **L2H** (20 μM) in presence of various solvents.

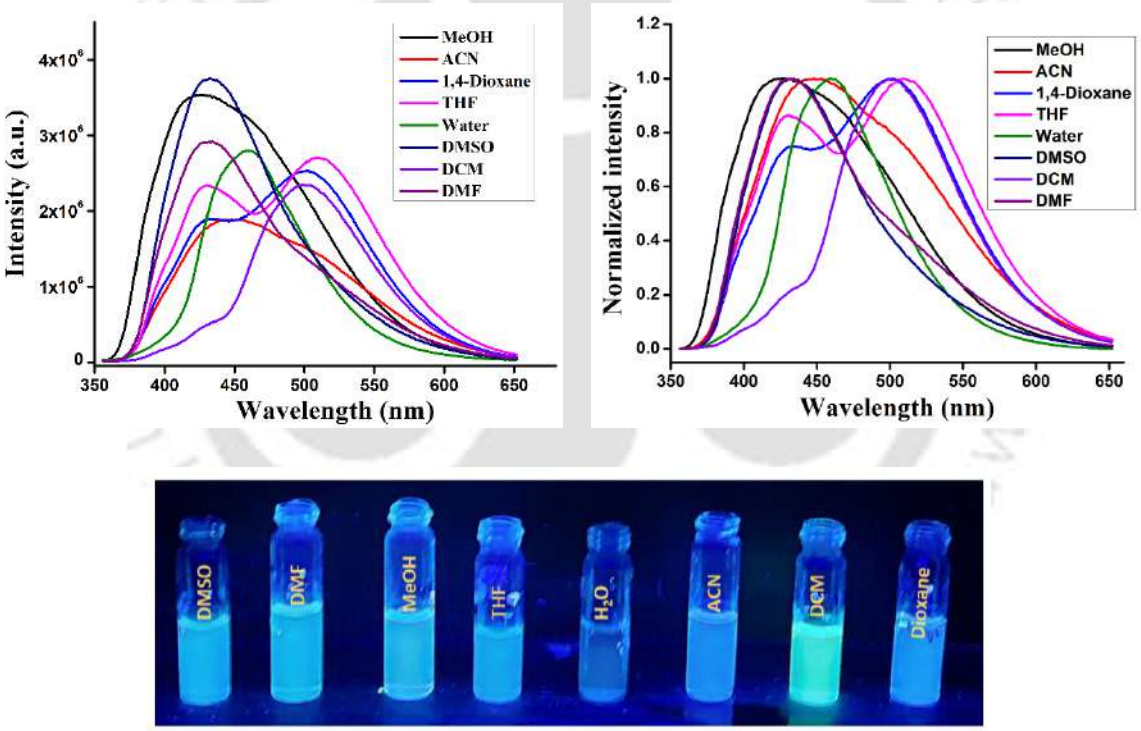

Figure A6. Un-normalized, normalized emission spectra of **L2H** (20 μM) in presence of various solvents and photograph of **L2H** solutions in different solvents observed under long UV light.

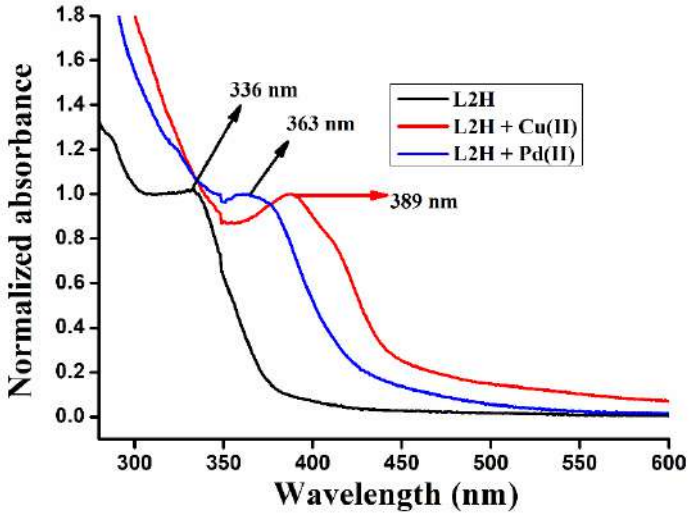

Figure A7. Normalized UV-Visible spectrum of **L2H** and **L2H** containing Cu(II) and Pd(II) ions.

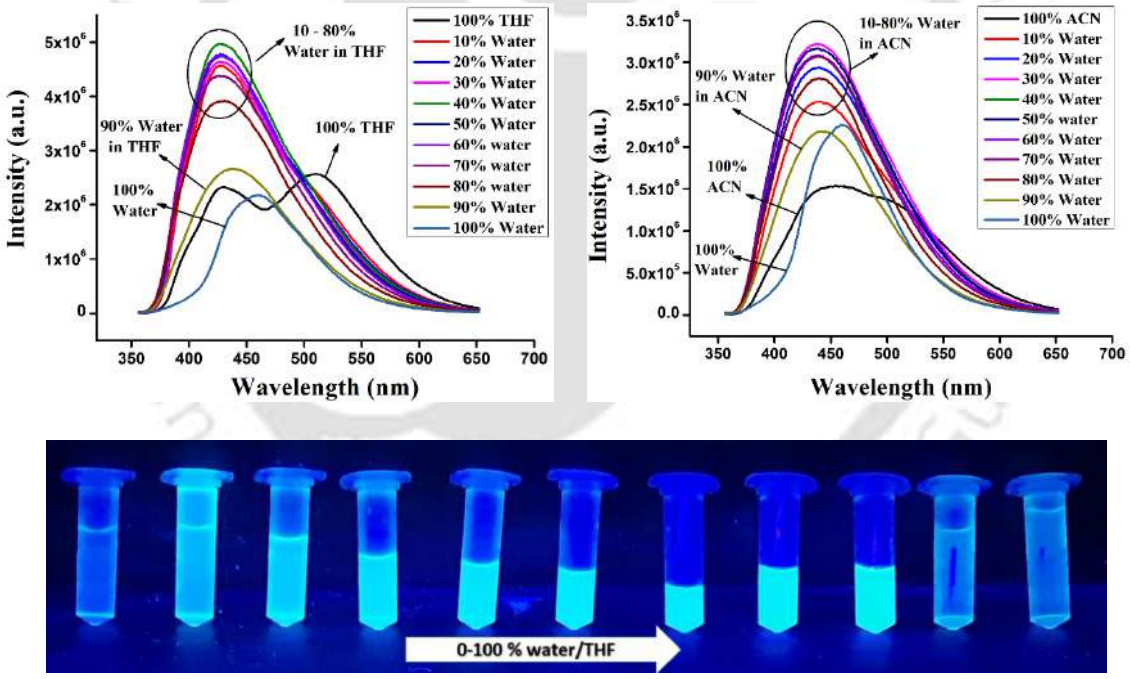

Figure A8. Emission spectra of **L2H** (20 μM) in THF/Water and ACN/Water (0-100% with the 10% increments of water) and photograph of solutions obtained in THF/water combination.

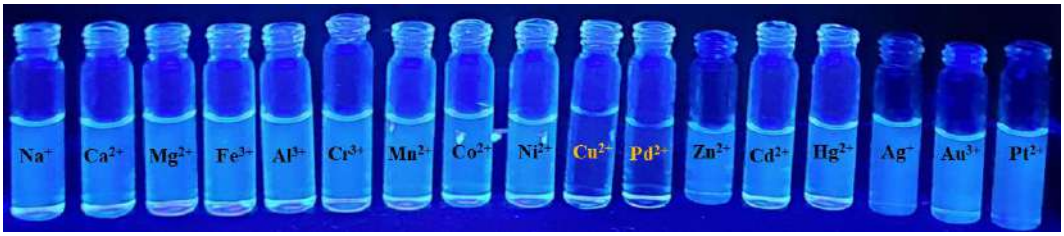

Figure A9. Fluorescence intensity examined under long ultraviolet (UV) light.

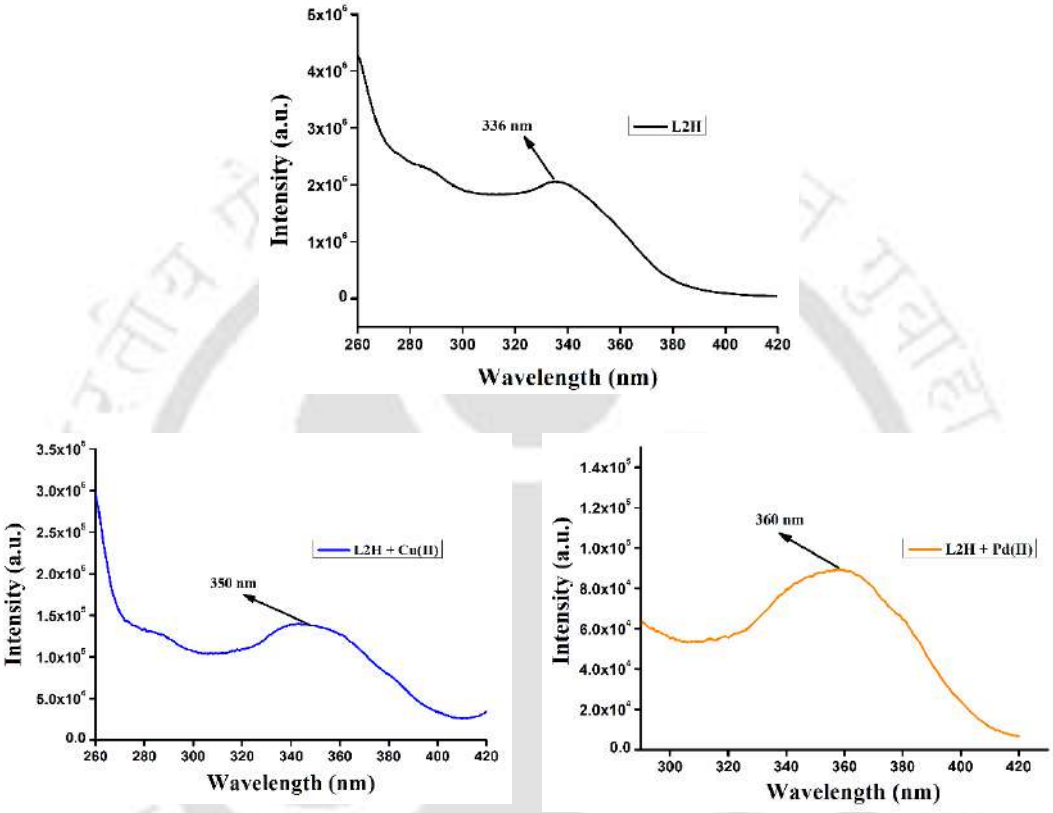

Figure A10. Excitation spectra of **L2H** and **L2H** with Cu^{2+} and Pd^{2+} ions.

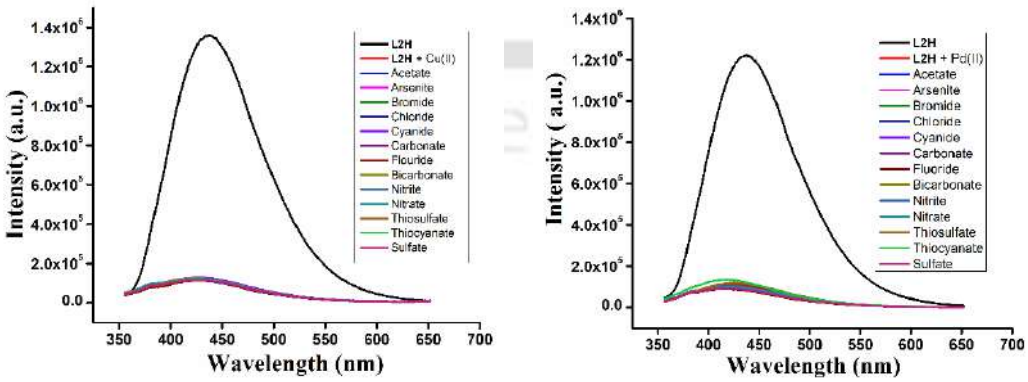

Figure A11. Variations in Fluorescence intensity of (a) [Cu(**L2**)$_2$H$_2$O] and (b) [Pd(**L2**)$_2$] with different anions.

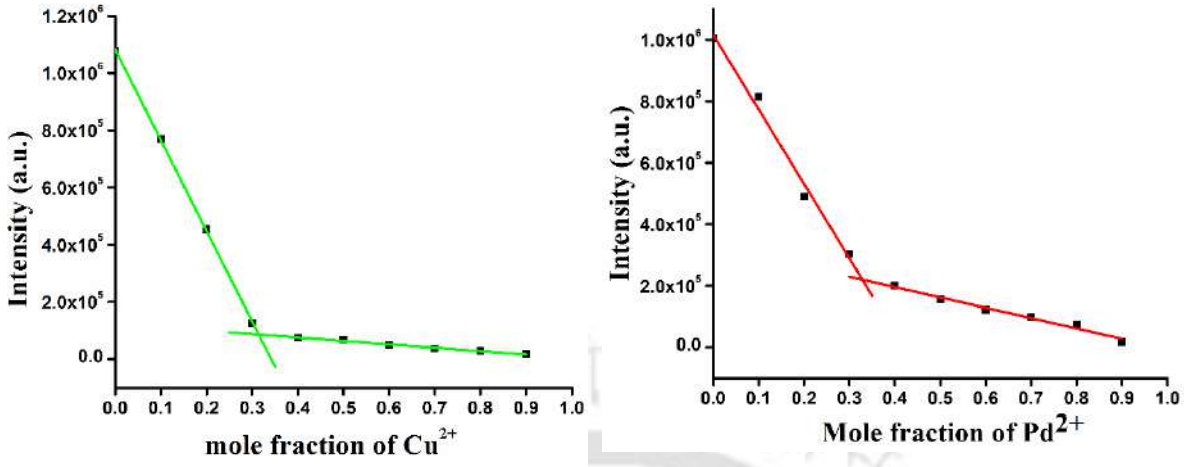

Figure A12. Job's plot of **L2H** with changing mole fraction of (a) Cu^{2+} and (b) Pd^{2+}ion.

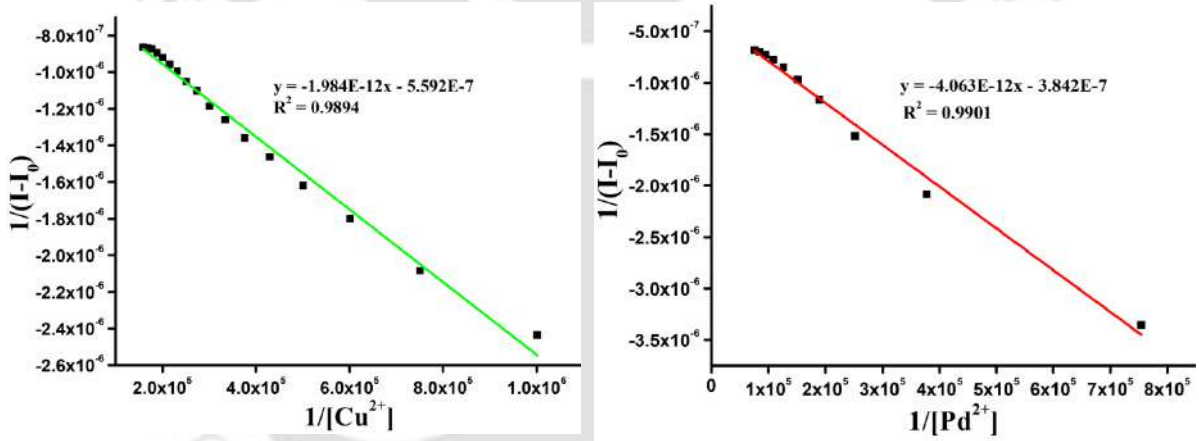

Figure A13. Benesi–Hildebrand plot for Binding constant (a) Cu^{2+} and (b) Pd^{2+}ion.

For Copper Complex

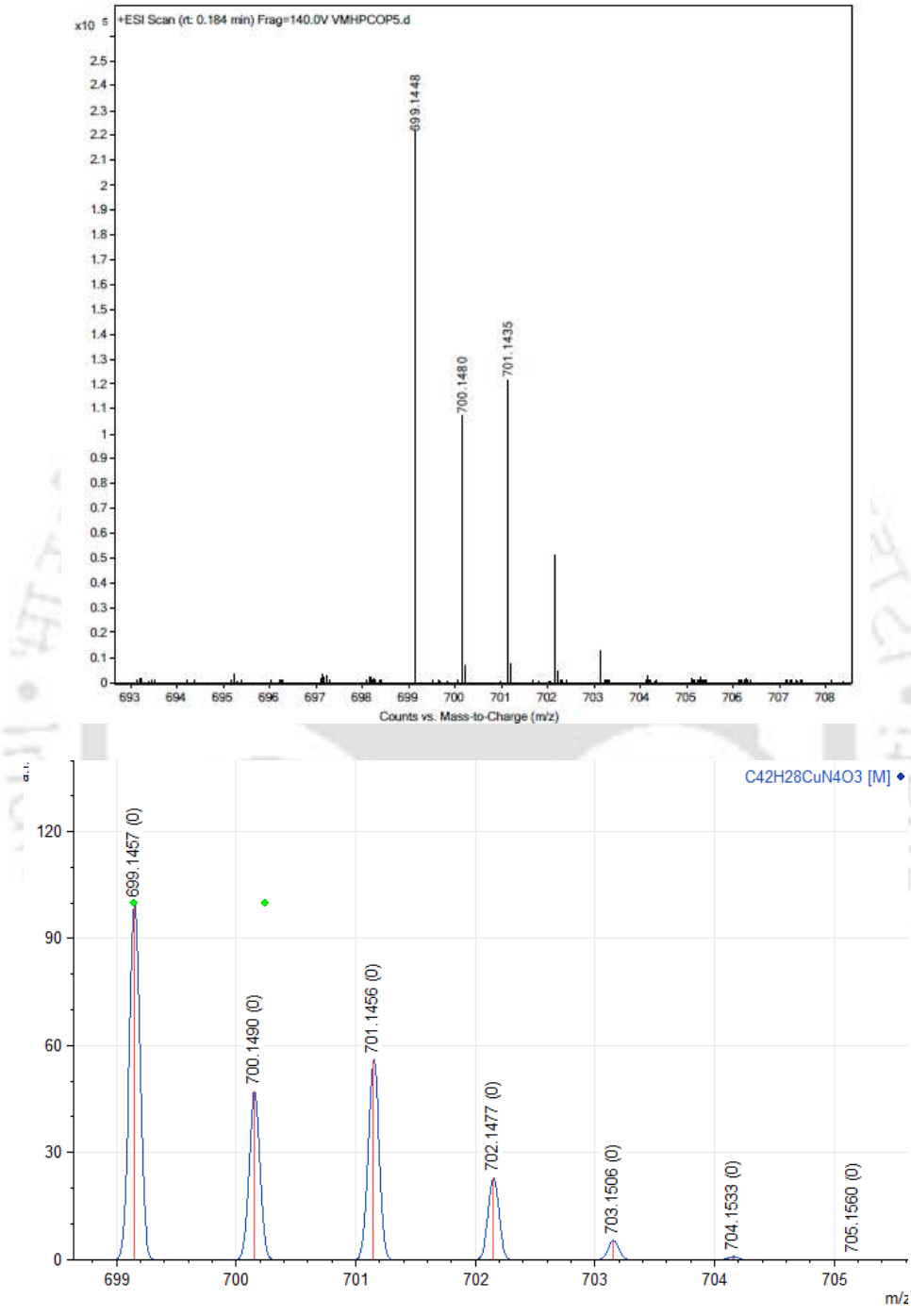

Figure A14. (a) Experimental and (b) calculated (mMass) mass spectrum for $[Cu(\mathbf{L2})_2(H_2O)]^+$ ion.

For Palladium Complex

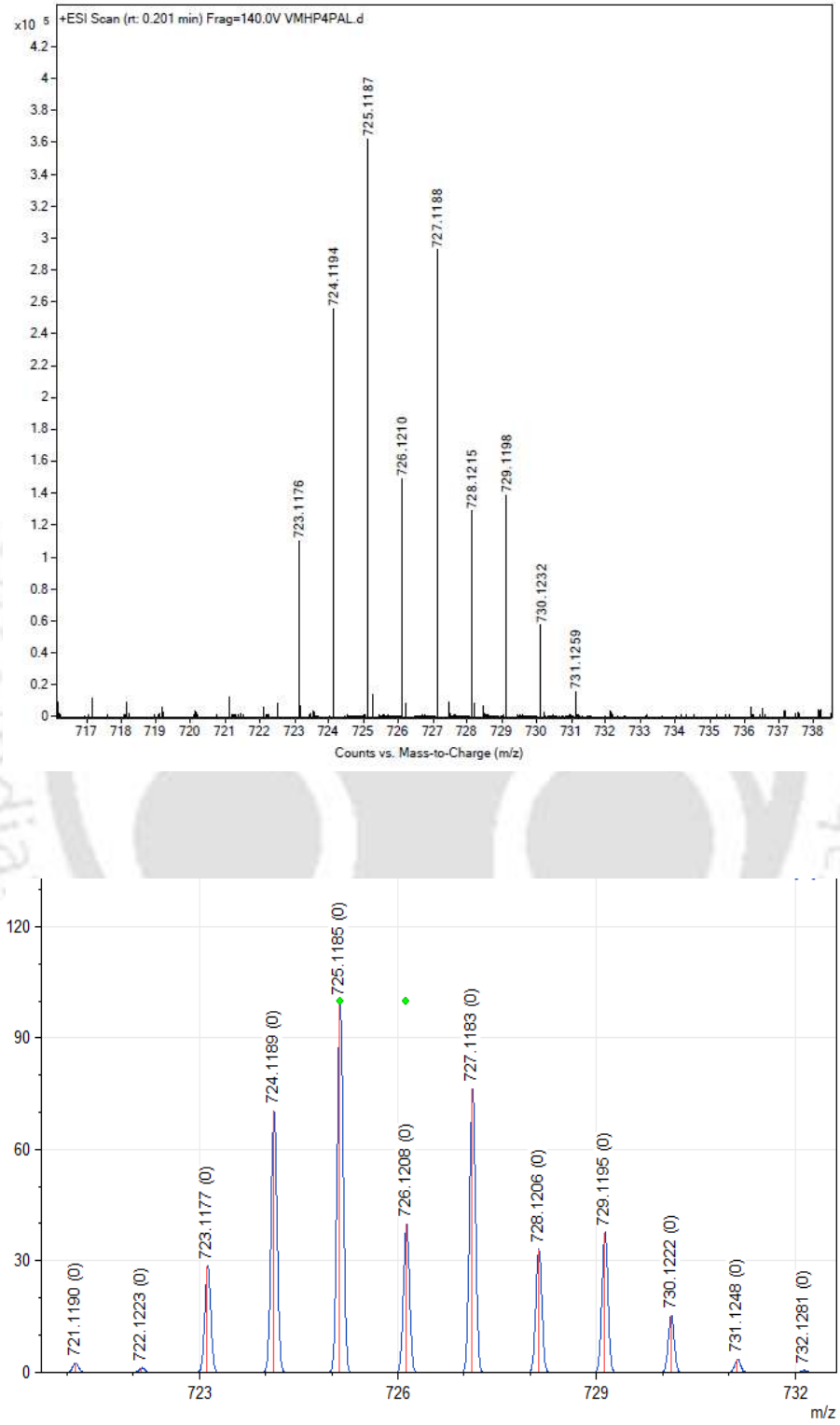

Figure A15. (a) Experimental and (b) calculated (mMass) mass spectrum for $[Pd(\mathbf{L2})_2 + H]^+$ ion.

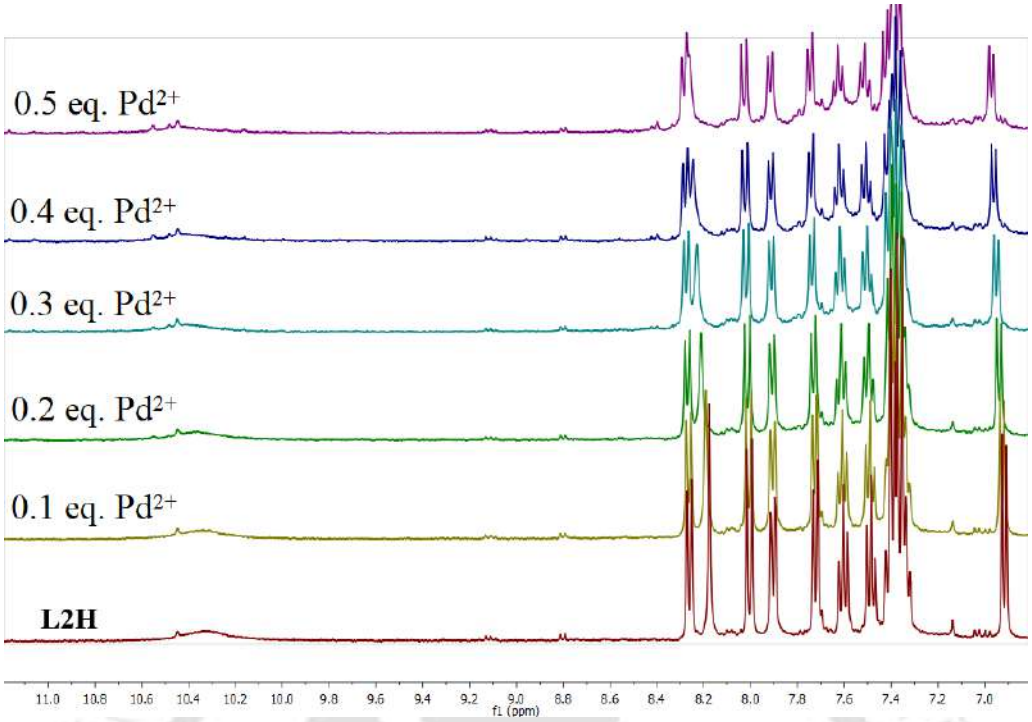

Figure A16. ^{1}H NMR titration of **L2H** with $PdCl_2$ in DMSO-*d6*.

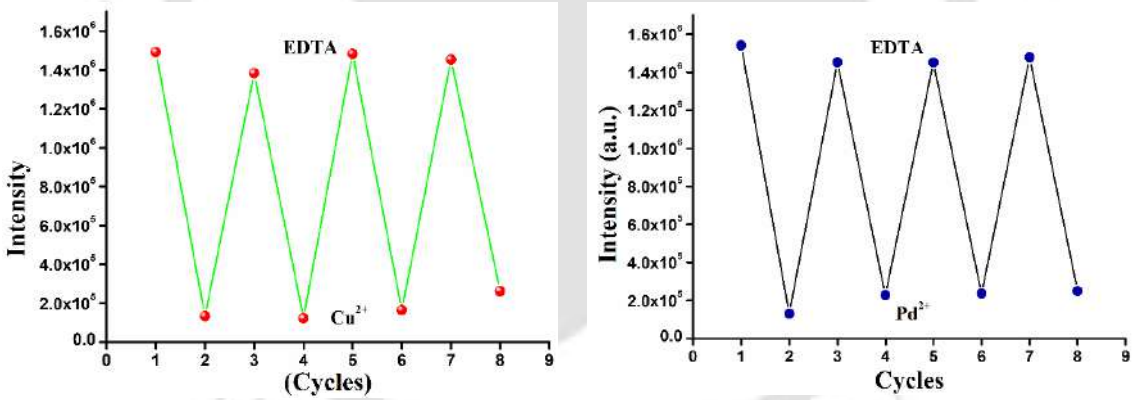

(a) (b)

Figure A17. Reversiblity test of probe **L2H** towards (a) Cu^{2+} and (b) Pd^{2+} ions.

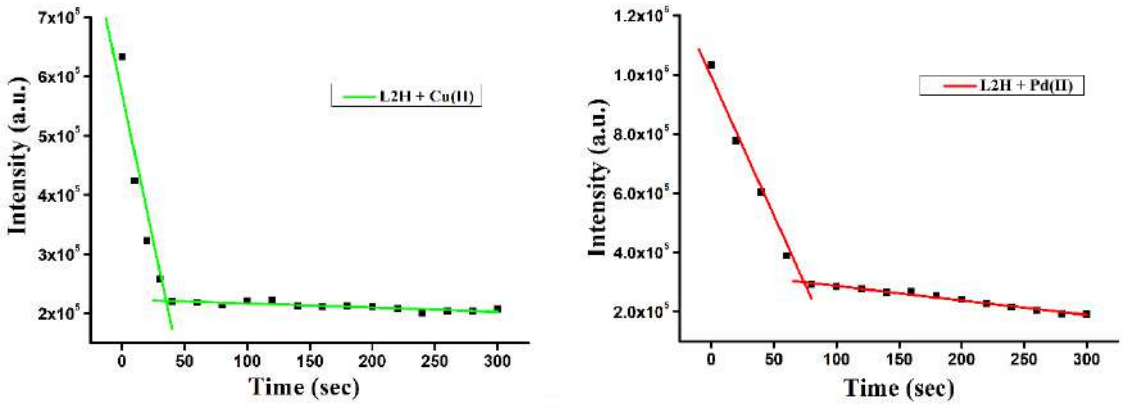

Figure A18. Fluorescence response time of **L2H** for Cu^{2+} (left) and Pd^{2+} (right).

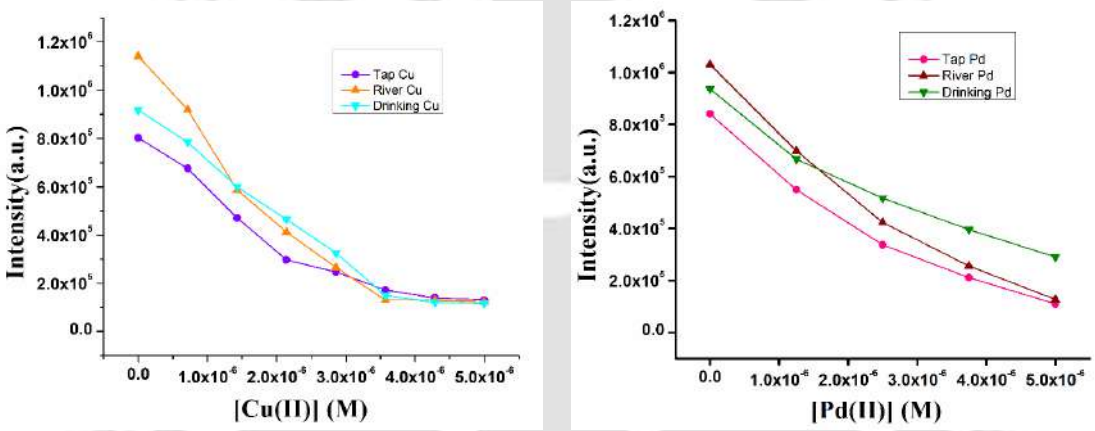

Figure A19. Variation in emission intensity of **L2H** along with (a) Cu(II) and (b) Pd(II) ions obtained in real water samples.

Table A2. Fluorescence decay parameters for life time measurements.

Sample	τ (ns)	χ^2
L2H	1.37	1.08
L2H+ Cu^{2+}	0.93	1.09
L2H+ Pd^{2+}	0.98	1.09

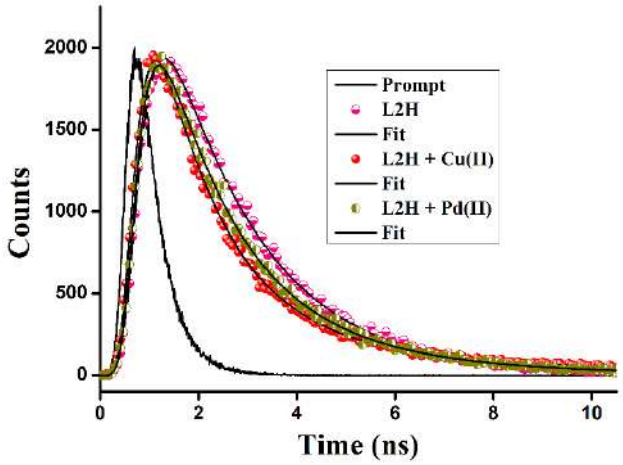

Figure A20. Life time Decay profile of **L2H**, **L2H** + Cu^{2+} and **L2H** + Pd^{2+}.

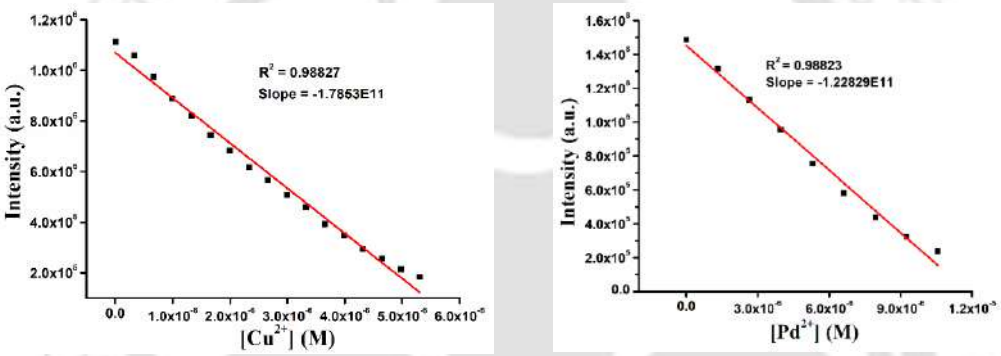

Figure A21. Limit of detection plots of **L2H** with (a) Cu^{2+} and (b) Pd^{2+} ions.

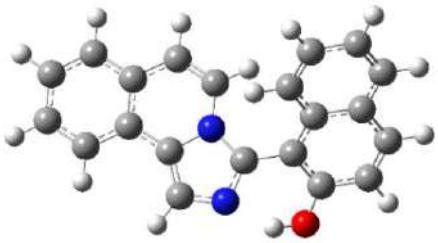

(a)

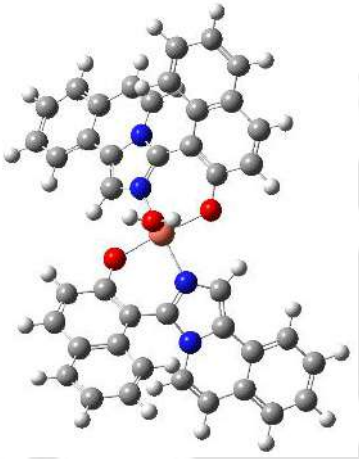

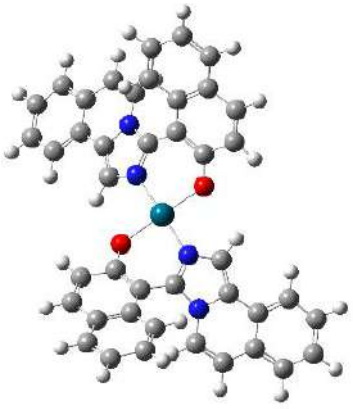

(b) (c)

Figure A22. DFT energy optimised structures for (a) **L2H** (b) **1** (c) **2**.

Table A3. Comparison of **L2H** with some reported probes.

Probe	Solvent	LOD
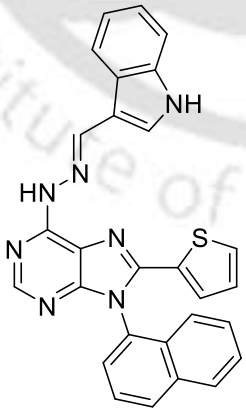	DMSO/aqueous HEPES Buffer (3:2, *v/v*)	1.19 μM (Cu^{2+}) 0.63 μM (Pd^{2+})

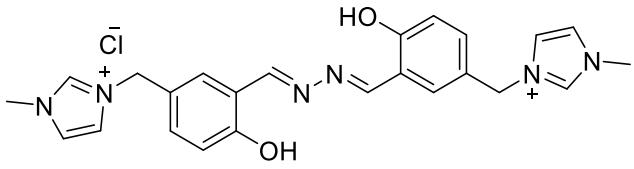	H_2O	0.08 µM (Cu^{2+}) 0.076 µM (Pd^{2+})
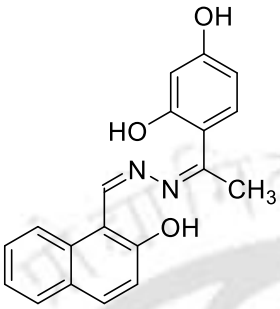	MeOH:H_2O (1:1, *v/v*)	0.49 µM (Cu^{2+}) 0.98µM (Pd^{2+})
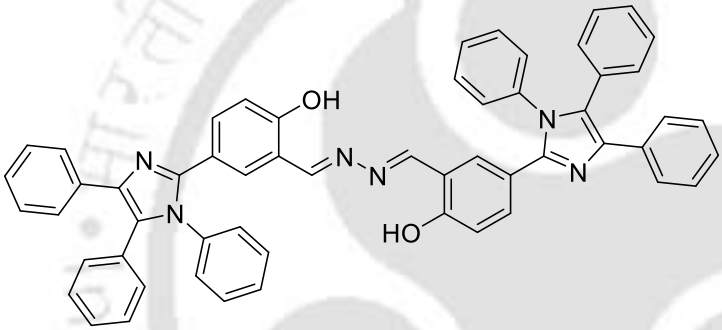	THF/H_2O (5/95, *v/v*)	0.83 µM (Cu^{2+}) 0.92µM (Pd^{2+})
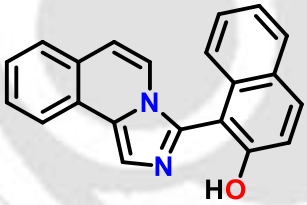	MeOH : HEPES buffer (5 mM, pH = 7.4, 2:8, *v/v*)	0.24 µM (Cu^{2+}) 0.35µM (Pd^{2+})

Chapter 4

Synthesis, Structural Characterization of Co(II) and Mn(II) complexes of a Polypyridine Ligand and Supramolecular Interactions

Abstract

A polypyridine ligand **L3**, was synthesized and characterized using mass spectrometry, ^{1}H-, ^{13}C- NMR, IR spectroscopy. Its 3D structure has been established using single crystal X ray diffraction method. The intermolecular interactions involved in **L3** has been discussed. Using **L3**, two new metal complexes of compositions $[M_2(\mathbf{L3})Cl_4]\cdot 2H_2O$ {M = Co(II) (**1**) and Mn(II) (**2**)} have been synthesized. Their molecular structures have been established using single crystal X ray diffraction method and intermolecular interactions involved in these complexes have also been illustrated.

1. Introduction

The multidentate chelating ligands containing polypyridine rings exhibit strong affinity with metal ions and form thermally stable coordination complexes. Terpyridine is one of the most versatile ligands which contain NNN chelating donor sites generally form square planar,[1] distorted square pyramidal,[2] trigonal bipyramidal,[3] and octahedral complexes[4] with various metal ions. Terpyridine ligands are considered as thermally and oxidatively robust,[5] and hence, these are widely used in diverse area of research like material sciences, medicines and supramolecular chemistry.[6,7] Because of their potential to form stable metal complexes with transition metal ions and rare earth metal ions, these metal complexes have wider applications in material science, optoelectronics,[8] photovoltaics,[9] medicines[10] and catalytic applications such as organometallic catalysis as well as biomimetic oxidation and reduction reactions.[11,12] In the field of therapeutic applications, these metal complexes possess ability to intercalate with DNA and may serve as anticancer agents.[13,14] Their unique photophysical properties, make them valuable components for enhancing the efficiency of energy conversion processes. Furthermore, terpyridines and their metal complexes have diverse applications in supramolecular chemistry.[15] The supramolecular assemblies possess enchanting photophysical and redox properties and hence utilized in development of advanced materials and exploring new frontiers in molecular engineering.[16] The Co(II) complexes of terpyridines was utilized in electrocatalytic reduction of CO_2.[17] A wide variety of cobalt-catalyzed coupling reactions, hydro-formylation,[18] cycloaddition,[19] cyclopropanation of alkenes[20] and radical polymerization were reported.[21] While Mn(II)-terpyridine complexes have applications in a variety of reactions including C–C cross coupling, radical mediated oxidative cyclization, hydrosilylation, epoxidation of alkene and C–H activation reactions.[22] Mn(II)-

terpyridine mono-complexes were particularly employed as water-oxidation catalysts (WOCs), mimicking green plants' natural photosystem-II (PS-II).[11,23] Furthermore, the Co(II) and Mn(II) metal complexes were also utilized in various catalytic reactions such as dehydrogenative coupling of alcohols and amines.[24]

On these backgrounds, a polypyridine ligand **L3** containing two terpyridine (NNN) arms was synthesized and characterized using mass spectrometry, ^{1}H ^{13}C, IR spectroscopy. The 3D structure of **L3** has been established using single crystal XRD measurement. Using **L3**, two metal complexes of Co(II) and Mn(II) ions have been synthesized and their 3D structures were established using single crystal XRD studies. Furthermore, the supramolecular interactions involved in ligand and these metal complexes have also been discussed.

2. Results and discussions

2.1 Synthesis of L3

The polypyridine ligand (**L3)** containing seven pyridine rings was synthesized (Scheme 1) from the reaction of 4:4:1 mixture of 2-acetylpyridine, NaOH and 2,6-pyridinedicarboxaldehyde in PEG-300 solvent.[25]It was characterized by mass spectrometry, ^{1}H, ^{13}C NMR and IR spectroscopy (Figure A1-A3) as well as single-crystal XRD. In ^{1}H NMR spectrum (Figure A2), protons present in the Ring-I appeared as characteristic singlet peak at 9.28 ppm. In ^{13}C NMR spectrum (Figure A3), 11 signals were observed which indicated the presence 11 unique carbon atoms in **L3**.

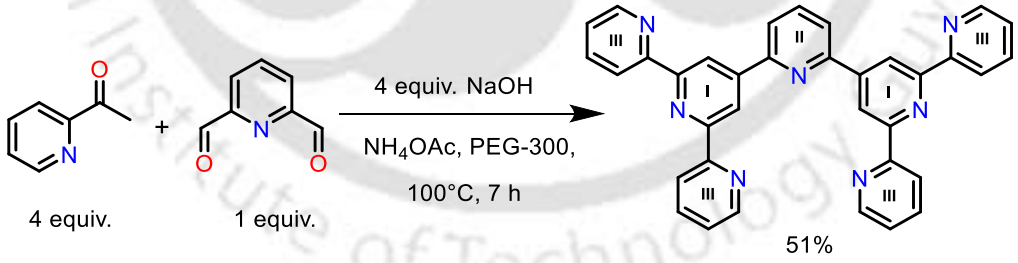

Scheme 1. Synthesis of ligand **L3**.

2.2 Molecular structure of L3

Single crystals of **L3** suitable for X-ray diffraction studies were grown by slow evaporation of **L3** solution in DCM-toluene solvent mixture. It crystallized in *I4₁/a* space group and ORTEP diagram (50% probability) has been shown (Figure 1). The nitrogen atoms of the adjacent pyridine rings stayed in trans-trans geometry to each other to avoid repulsion caused by lone pair electrons and each aromatic ring deviate slightly from planarity with torsional angles lying

in the range 1.0(4) – 12.1(4)°. In the packing diagram, inter-molecular interaction present are (i) π···π having the calculated inter-planar distance between two central Ring-II (N4, C16-C20) of 3.44 Å and (ii) C–H···N interaction about C29–H29···N1 with a C29···N1 distance of 3.289(5) Å (Figure 2). Due to this C29–H29···N1 interaction, a cyclic tetrameric packing generated by a four-fold axis has been observed. Because of these two interactions, a beautiful 3D architecture has been observed on viewing down the *b*-axis (Figure 3). The **L3** can be a potential ligand by virtue of having seven N-donor sites, synthesis of its complex with various transition metal ions were attempted, but we were successful in obtaining single-crystal of isostructural complexes of composition $[M_2(\mathbf{L3})Cl_4]\cdot 2H_2O$ {M = Co(II) (**1**) and Mn(II) (**2**)} in which **L3** behaved as bis-tridentate ligand.

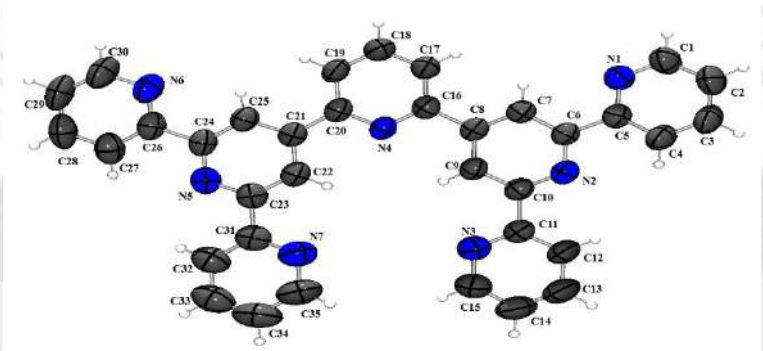

Figure 1. POV-Ray rendered ORTEP (50% probability) plot of **L3**.

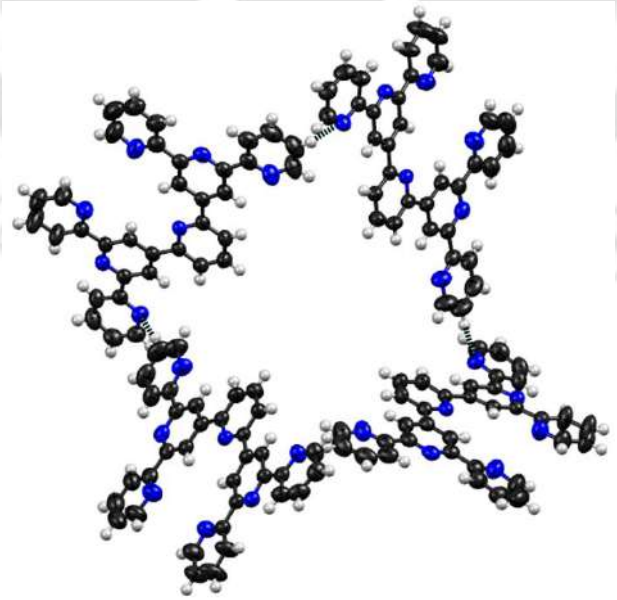

Figure 2. Tetrameric cyclic unit formed by C29–H29···N1 interaction in **L3** viewing down c-axis.

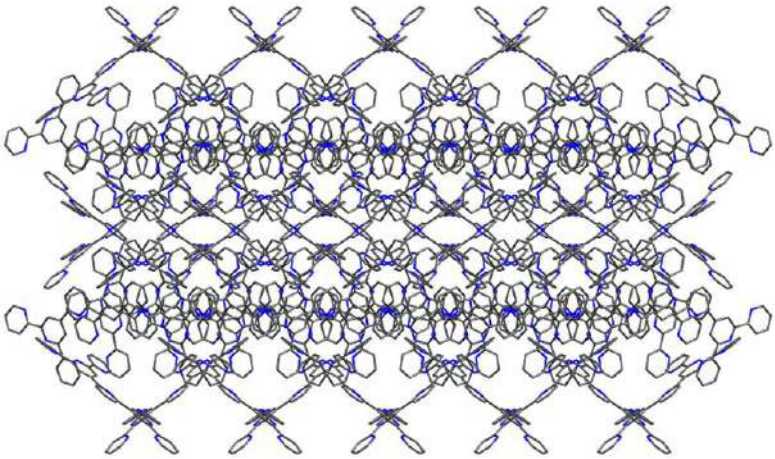

Figure 3. Packing diagram upon viewing down *b*-axis of **L3**.

2.3 Molecular structures of 1 and 2

Single crystals of **1** (green) and **2** (pale yellow) were obtained by slow diffusion of methanol solution of $MCl_2{\cdot}xH_2O$ {x = 6 (Co) and 4 Mn)} into the THF solution of **L3** in 2:1 ratio and the general reaction is shown in Scheme 2. In mass spectra, **1** and **2** showed peaks at *m/z* =763.9740 and *m/z* =758.2165 respectively (Figure 4 and 6) corresponding to the composition $[M_2(\mathbf{L3})Cl_3]^+$ having formulae $C_{35}H_{23}Cl_3Co_2N_7^+$ and $C_{35}H_{23}Cl_3Mn_2N_7^+$. The isotopic patterns of these peaks matched very well with the ones calculated using mMass software (Figure 5 and 7). Molecular structures of **1** and **2** were established using single crystal X-ray diffraction method and ORTEP diagrams have been shown in Figure 8 and 12.

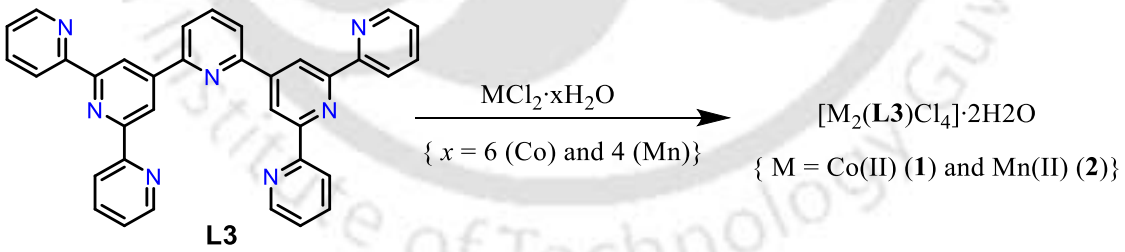

Scheme 2. Synthesis of complex **1** and **2**.

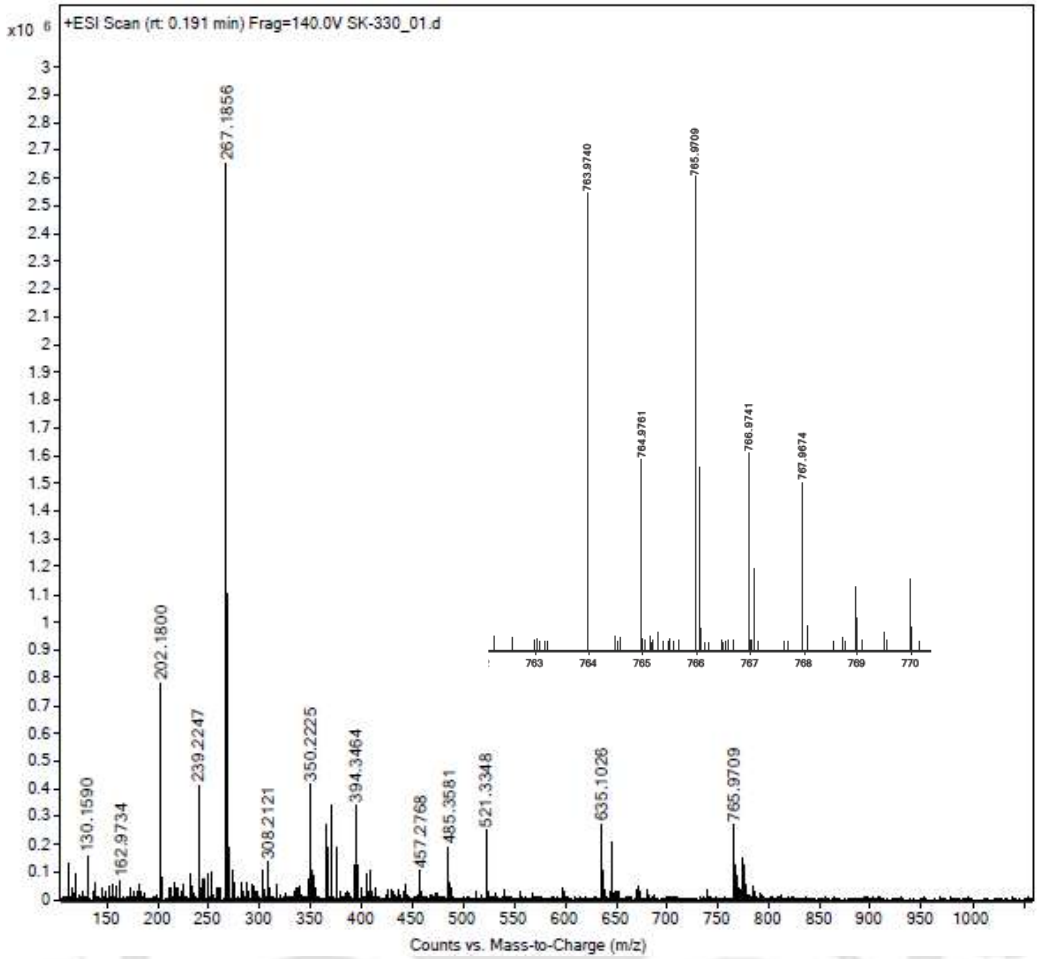

Figure 4. ESI-Mass spectrum of **1** and on set expansion of *m/z* = 763-770 region of mass spectrum of **1**.

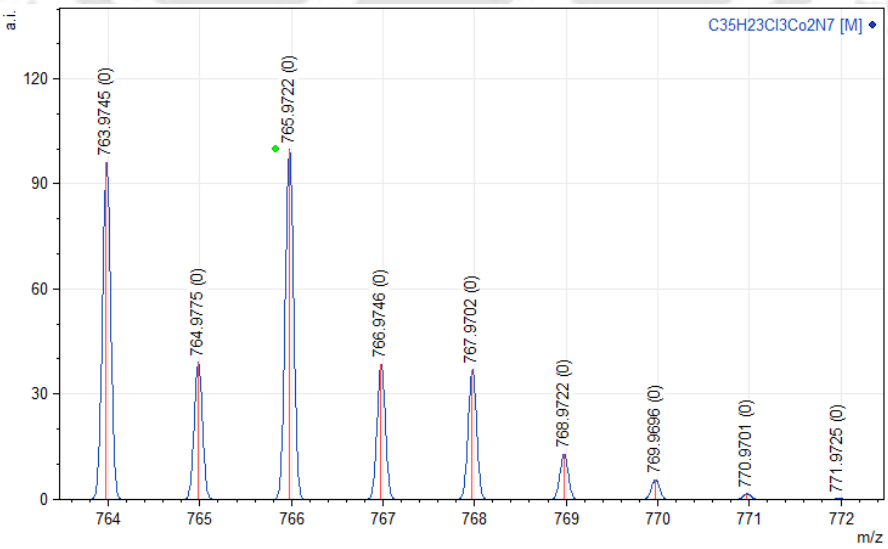

Figure 5. Isotopic pattern for the fragment in **1**, determined in mMass software.

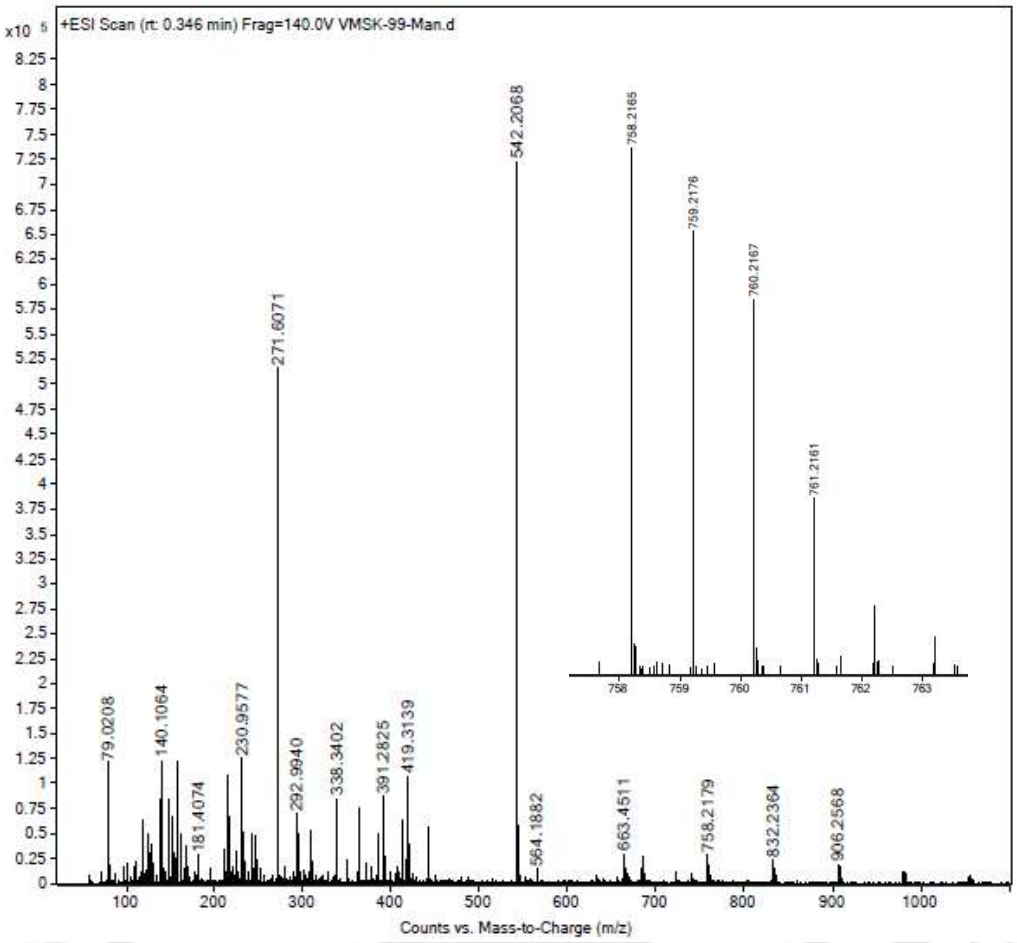

Figure 6. ESI-Mass spectrum of **2** and on set expansion of *m/z* = 758-763 region of mass spectrum of **2**.

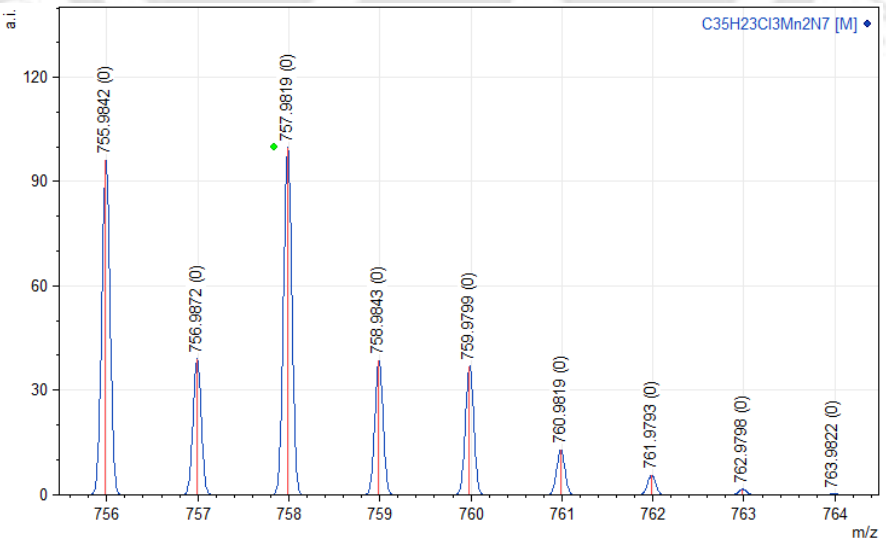

Figure 7. Isotopic pattern for the fragment in **2**, determined in mMass software.

Molecular structure of $[Co_2(\mathbf{L3})Cl_4]\cdot 2H_2O$ (**1**) and $[Mn_2(\mathbf{L3})Cl_4]\cdot 2H_2O$ (**2**) were determined and both crystallized in *P2₁* space group. The crystallographic data has been provided in Table

1 and they are isostructural and isomorphous in nature. The ligand **L3** has two pincer-type NNN arms connected by the central pyridine Ring-II, available to coordinate. Indeed the molecular structure contained two Co(II) or Mn(II) ions bound to two NNN arms by two five-membered chelate rings. Each of these metal metal centers in both complexes had pentacoordination (Figure 8 and 12), wherein remaining fourth and fifth coordination sites were occupied by two chloride ions. Also two water molecules were present in the lattice. The coordination geometry of each metal ion in both the complexes has been determined using distortion parameter (τ) utilizing Addison's method,[26] which is applicable for pentacoordinated system, $\tau = (\theta 1 - \theta 2)/60$, where $\theta 1$ and $\theta 2$ are the two largest angles in the coordination sphere. For a perfect square pyramidal geometry, τ value should be zero and for perfect trigonal bipyramidal geometry, it should be unity. In complex **1**, τ = 0.11 (for Co1) and 0.15 (for Co2) suggesting distorted square pyramidal geometry around both the Co(II) ions. Similarly, in complex **2**, τ = 0.08 (for Mn1) and 0.08 (for Mn2) suggested distorted square pyramidal geometry around both the Mn(II) ions.

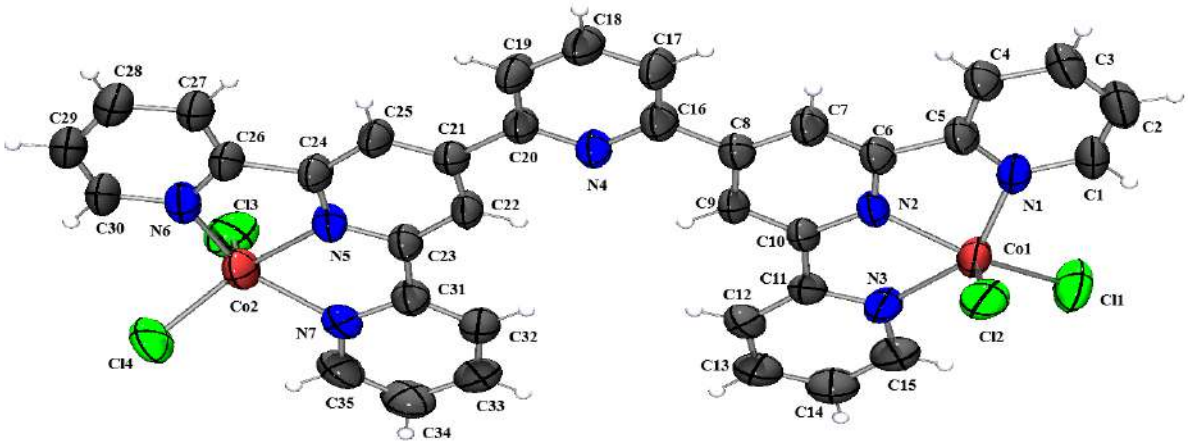

Figure 8. ORTEP diagram (50% probability) of complex **1**. Selected bond lengths (Å) and angles (°): Co1–N1 2.075(16), Co1–N2 2.061(13), Co1–N3 2.134(8), Co1–Cl1 2.271(6), Co1–Cl2 2.331(6), Co2–N5 2.047(14), Co2–N6 2.081(16), Co2–N7 2.141(17), Co2–Cl3 2.312(6), Co2–Cl4 2.270(6). Cl1–Co1–Cl2 112.5(2), N2–Co1–Cl1 152.7(5), N2–Co1–Cl2 94.8(4), N2–Co1–N1 74.6(5), N2–Co1–N3 75.6(5), N1–Co1–Cl1 100.7(5), N1–Co1–Cl2 94.7(5), N1–Co1–N3 145.6(5), N3–Co1–Cl1 97.9(3), N3–Co1–Cl2 104.5(4), Cl4–Co2–Cl3 111.1(2), N6–Co2–Cl3 100.2(5), N6–Co2–Cl4 96.2(5), N6–Co2–N7 150.9(6), N5–Co2–Cl3 107.4(5), N5–Co2–Cl4 141.4(5), N5–Co2–N6 75.8(6), N5–Co2–N7 76.6(6), N7–Co2–Cl3 96.6(5), N7–Co2–Cl4 99.7(4).

Various inter-molecular interactions found in **1** are mainly O–H···O, C–H···Cl, C–H···O and O–H···Cl interactions (Figure 9). Another weak interaction involved in complex **1** is π···π interaction (Figure10). Because of these interactions, a beautiful 3D packing of complex **1** on viewing down b-axis has been observed (Figure 11). Similar inter-molecular interactions including O–H···O, C–H···Cl, C–H···O and O–H···Cl (Figure 13) and π···π interactions (Figure 14) and packing diagram of complex **2** on viewing down b-axis have been shown in Figure 15.

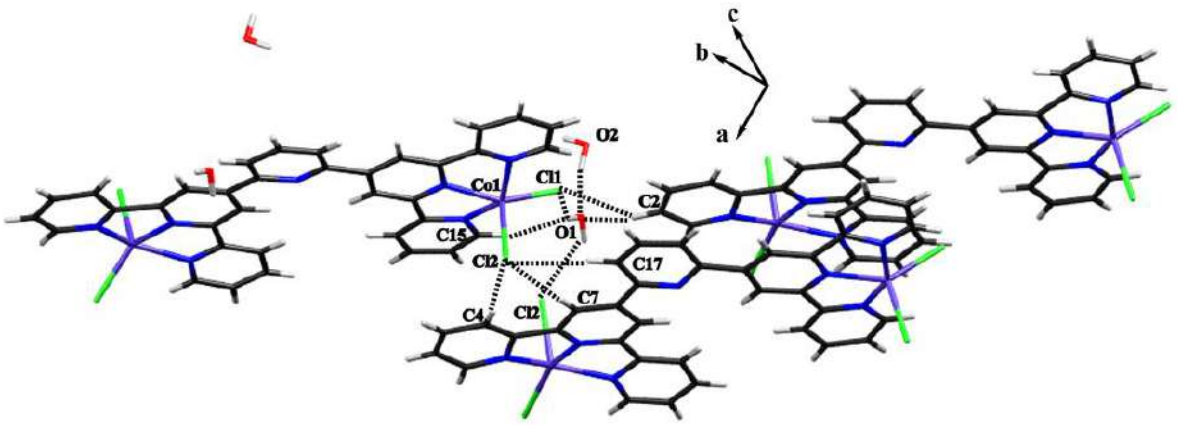

Figure 9. O–H···O, C–H···Cl, C–H···O and O–H···Cl interactions involved in complex **1**. O2···O1 2.56(6), C7···Cl2 3.78(2), C4···Cl2 3.60(2), C17···Cl2 3.71(2), C2···O1 3.47(4), Cl1···O1 3.46(4), C15···O1 3.85(4), C2···Cl1 3.58(2), Cl2···O1 3.38(4).

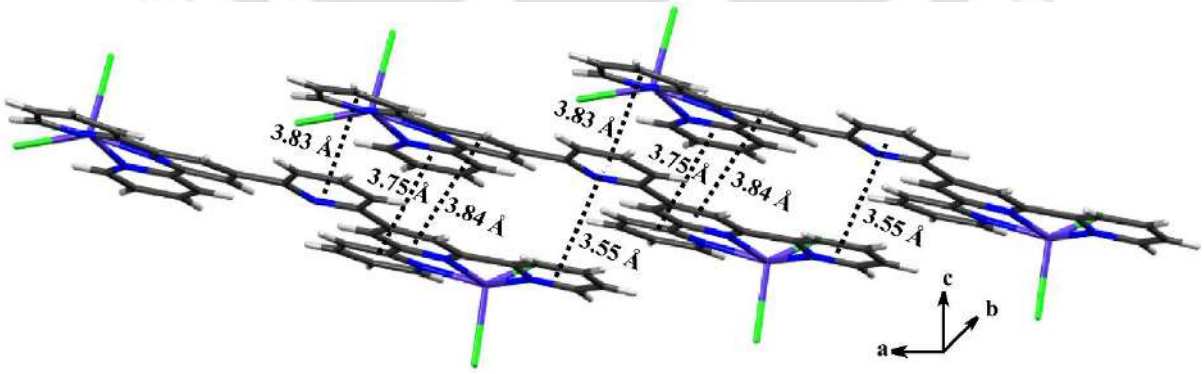

Figure 10. π···π interactions involved in complex **1**.

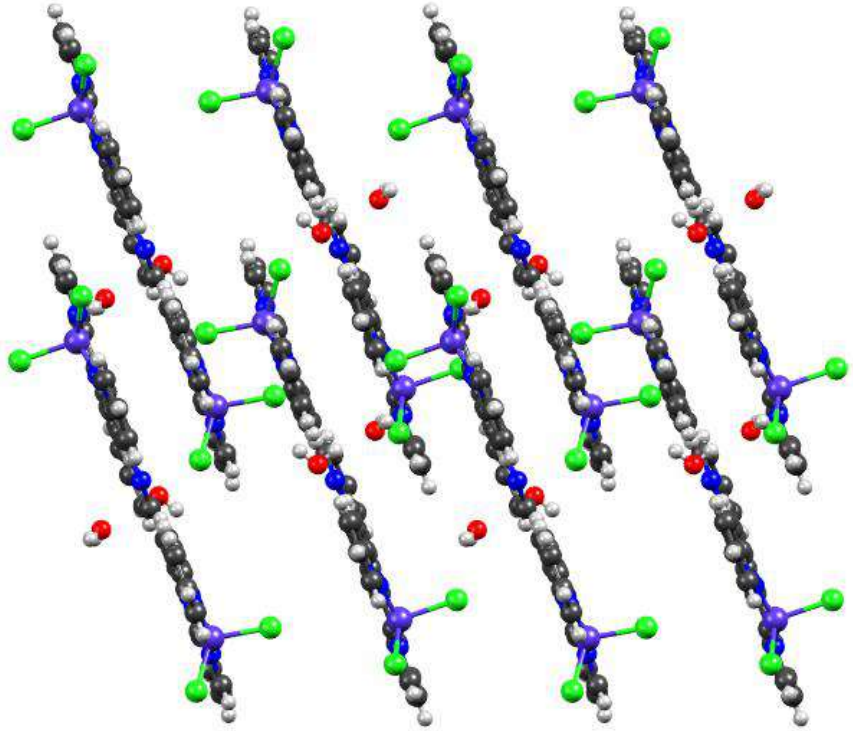

Figure 11. Packing diagram upon viewing down b-axis of complex **1**.

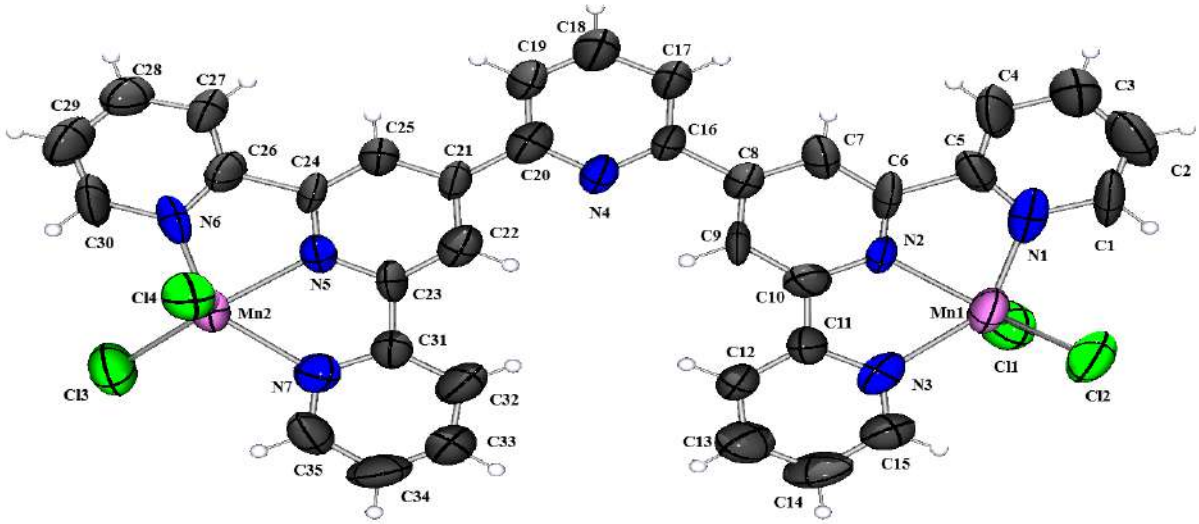

Figure 12. ORTEP diagram (50% probability) of complex **2**. Selected bond lengths (Å) and angles (°) Mn1–N1 2.199(18), Mn1–N2 2.165(12), Mn1–N3 2.265(18), Mn1–Cl1 2.355(6), Mn1–Cl2 2.327(6), Mn2–N5 2.194(13), Mn2–N6 2.137(17), Mn2–N7 2.252(14), Mn2–Cl3 2.346(6), Mn2–Cl4 2.367(6), Cl2–Mn1–Cl1 111.5(2), N2–Mn1–Cl2 138.1(4), N2–Mn1–Cl1 110.4(4), N2–Mn1–N3 72.3(6), N2–Mn1–N1 71.9(5), N3–Mn1–Cl2 101.6(4),

N3–Mn1–Cl1 99.9(4), N1–Mn1–Cl2 98.0(4), N1–Mn1–Cl1 101.8(4), N1–Mn1–N3 142.8(6), Cl3–Mn2–Cl4 115.5(2), N6–Mn2–Cl4 94.8(4), N6–Mn2–Cl3 102.4(4), N6–Mn2–N5 70.7(5), N6–Mn2–N7 140.2(5), N5–Mn2–Cl4 99.3(4), N5–Mn2–Cl3 145.1(4), N5–Mn2–N7 72.5(6), N7–Mn2–Cl4 105.7(4), N7–Mn2–Cl3 99.0(4).

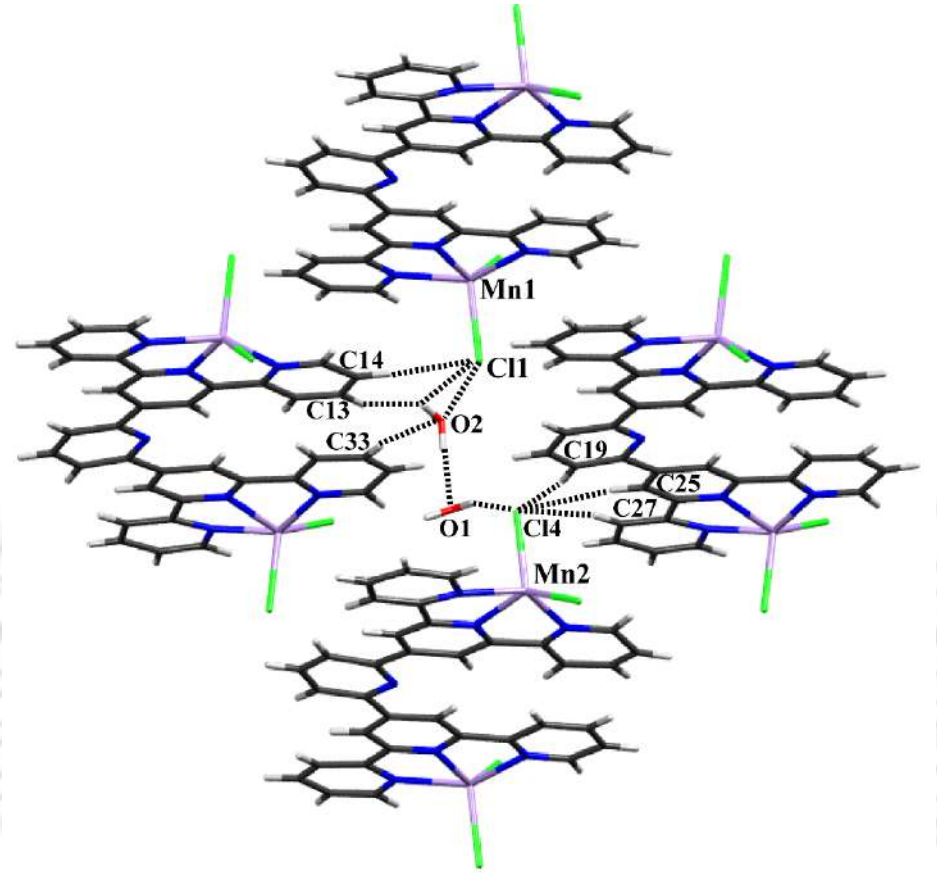

Figure 13. O–H···O, C–H···Cl, C–H···O and O–H···Cl interactions involved in complex **2** upon viewing down a-axis. Cl1···O2 3.22(3), C14···Cl1 3.66(2), C13···O2 3.70(3), C33···O2 3.32(3), O1···O2 2.86(4), Cl4···O1 3.36(3), C19···Cl4 3.66(2), C25···Cl4 3.81(2), C27···Cl4 3.59(2).

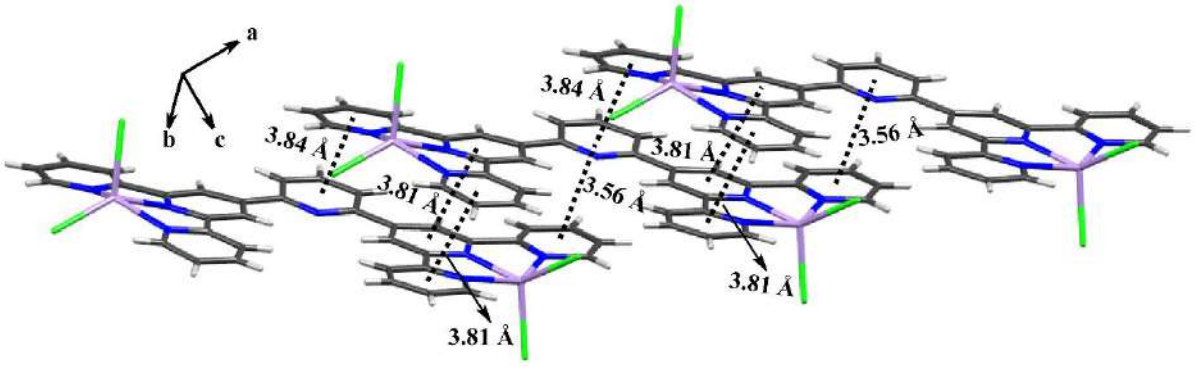

Figure 14. π···π interactions involved in complex **2**.

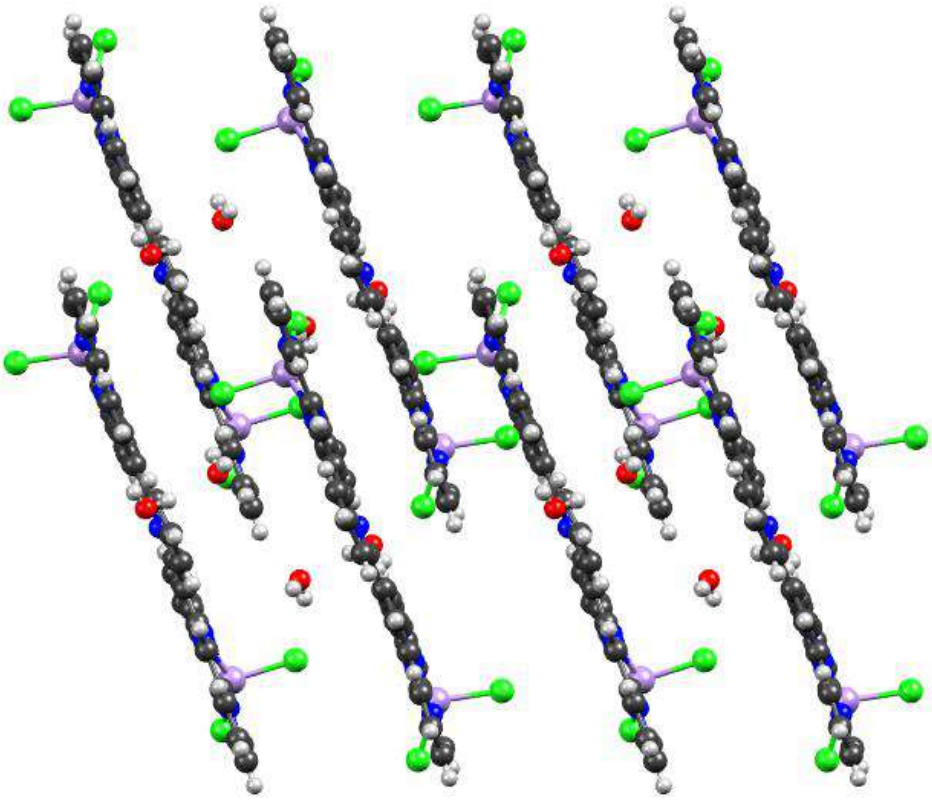

Figure 15. Packing diagram upon viewing down b-axis of complex **2**.

Table 1. Crystallographic data and refinement parameters

Entry	**L3**	**1**	**2**
Formula	$C_{35}H_{23}N_7$	$C_{35}H_{27}N_7O_2Co_2Cl_4$	$C_{35}H_{27}N_7O_2Mn_2Cl_4$
CCDC No.	2428965	2428966	2428967
Mol. wt.	541.60	837.29	829.31
Cryst.color, habit	colorless, block	green, needle	yellow, needle
T, K	297	295	295
Cryst. syst.	tetragonal	monoclinic	monoclinic
Space group	$I4_1/a$	$P2_1$	$P2_1$
a, Å	31.0994(9)	8.8512(8)	8.949(3)
b, Å	31.0994(9)	13.9603(12)	14.182(5)
c, Å	11.6070(5)	14.3857(13)	14.439(5)
α ,deg	90	90	90
β, deg	90	90.951(3)	91.155(11)
γ, deg	90	90	90
V, Å^3	11226.0(8)	1777.3(3)	1832.2(11)
Z	16	2	2
*D*calcd, g cm^{-3}	1.282	1.565	1.503
μ, mm^{-1}	0.079	1.278	1.023

GOF[a] on F^2	1.132	1.021	1.007
F(000)	4512.0	848.0	840.0
Reflection collected	132217	40556	17377
Unique reflections	5313	6275	6209
R_1[b], wR_2[c] $(I \geq 2\sigma(I))$	0.0616, 0.1615	0.0819, 0.2008	0.0853, 0.2073
R_1[b], wR_2[c] (all data)	0.1244, 0.2367	0.1689, 0.2637	0.2056, 0.2396

[a]GOF (Goodness-of-fit) = $[\sum[w(F_0^2 - F_c^2)^2] / M - N]^{1/2}$ (M =number of reflections, N = number of parameters refined). [b] $R_1 = \sum \| F_0 | - | Fc \| / \sum | F_0 |$. [c] $wR_2 = [\sum[w(F_0^2 - F_c^2)^2] / \sum[w(F_0^2)^2]]$.

3. Conclusion

A polypyridine ligand **L3** having two terpyridine (NNN) arms connected by a pyridine ring was synthesized and characterized using mass spectrometry, ^{1}H, ^{13}C NMR and IR spectroscopy. The molecular structure of **L3** was established using single crystal XRD measurement. Using **L3**, Co(II) and Mn(II) complexes were synthesized, characterized, molecular structures were confirmed using single crystal XRD. Their molecular structure contained two Co(II) or Mn(II) ions bound to two NNN arms by two five-membered chelate rings having pentacoordination with fourth and fifth coordination sites being occupied by two chloride ions. In **1** and **2**, Addison's τ values suggested a distorted square pyramidal geometry around the metal ions. Various molecular interactions in these metal complexes involved were also described.

4. Experimental Section

4.1 Synthesis

4.1.1 6',6'''-di(pyridin-2-yl)-2,2':4',2'':6'',4''':2''',2''''-quinquepyridine (**L3**)

2-Acetylpyridine (2 g, 16.5 mmol) and NaOH powder (0.67 g, 16.8 mmol) were mixed thoroughly till a gummy paste is formed. Then 2,6-pyridinedicarboxaldehyde (0.55 g, 4 mmol), PEG 300 (15 mL) and NH_4OAc (4 g, 52 mmol) were added, and heated at 100 °C for 7 h. The solution was allowed to cool to room temperature, water (20 mL) was added, precipitate was filtered and washed initially with plenty of water then ice-cold ethanol (10 mL). Yield: 1.13 g (51%); ^{1}H NMR (600 MHz, $CDCl_3$) δ 9.28 (s, 4H), 8.78 (d, *J* = 4.5 Hz, 4H), 8.70 (d, *J* = 7.9 Hz, 4H), 8.15 (d, *J* = 7.8 Hz, 2H), 8.01 (t, *J* = 7.8 Hz, 1H), 7.90 (t, *J* = 7.7 Hz, 4H), 7.38 (dd, *J* = 6.9, 5.2 Hz, 4H); ^{13}C NMR (150 MHz, $CDCl_3$) δ 156.4, 156.3, 155.3, 149.3, 148.6, 138.05, 137.0, 123.9, 121.6, 121.4, 119.0; IR (cm^{-1}) ATR mode: 3045(w), 1502(w), 1581(m), 1552(m), 1466(m), 1433(w), 1423(w), 1375(m), 1394(w), 1259(m), 990(m), 895(m), 788(s), 746(m),

717(m), 660(m), 639(m), 622(m), 602(m), 404(m). ESI-MS (+): *m*/*z* calcd. for (M + H^+) $C_{35}H_{24}N_7^+$ 542.2088, found 542.2090.

*4.1.2 [Co_2(**L3**)Cl_4] ·2H_2O (**1**)*

In a test-tube, a THF (2 mL) solution of **L3** (15 mg, 0.027 mmol) was layered firstly with MeOH (2 mL) and then with solution of $CoCl_2 \cdot 6H_2O$ (13 mg, 0.055 mmol) in MeOH (10 mL) and was kept undisturbed. Green needle shaped crystals suitable for single crystal XRD measurement were separated after 4-5 days. Yield: 13 mg (56 %); IR (cm^{-1}) ATR mode: 3400(br), 3068(w), 1646(w), 1614(m), 1604(m), 1571(m), 1566(m), 1474(m), 1439(w), 1418(m), 1250(m), 1164(w), 1049(w), 1024(m), 1012(m), 897(m), 817(m), 790(s), 727(m), 658(m), 614(w), 582(w), 409(w); ESI-MS (+): *m*/*z* calcd. for [M – Cl]$^+$ $C_{35}H_{24}N_7Cl_3Co_2^+$ 763.9740, found 763.9740.

*4.1.3 [Mn_2(**L3**)Cl_4] ·2H_2O (**2**)*

Light yellow crystals of **2** were obtained by adopting the same procedure using same molar ratio of **L3** and $MnCl_2 \cdot 4H_2O$. Yield: 11 mg (48%); IR (cm^{-1}) ATR mode: 3450(br), 3060(w), 1598(m), 1569(w), 1546(m), 1469(m), 1437(m), 1414(m), 1384(m), 1301(w), 1246(m), 1157(m), 1012(m), 901(m), 790(s), 745(m), 721(m), 658(m), 638(w), 605(m), 405(w); ESI-MS (+): *m*/*z* calcd. for [M – Cl]$^+$ $C_{35}H_{24}N_7Cl_3Mn_2^+$ 757.9819, found 758.2165.

References

[1] I. Eryazici, C. N. Moorefield, G. R. Newkome, *Chem. Rev.* **2008**, *108*, 1834–1895.

[2] B. Z. Momeni, S. Kazemzade Anari, J. Janczak, R. Fallahpour, *J. Inorg. Organomet. Polym. Mater*. **2022**, *32*, 2279–2297.

[3] S. Rajalakshmi, T. Weyhermüller, M. Dinesh, B. U. Nair, *J. Inorg. Biochem.* **2012**, *117*, 48–59.

[4] R. Indumathy, S. Radhika, M. Kanthimathi, T. Weyhermuller, B. Unni Nair, *J. Inorg. Biochem.* **2007**, *101*, 434–443.

[5] C. M. Che, C. Ho, T. C. Lau, *J. Chem. Soc. Dalt. Trans.* **1991**, 1901–1907.

[6] A. Wild, A. Winter, F. Schlütter, U. S. Schubert, *Chem. Soc. Rev.* **2011**, *40*, 1459–1511.

[7] G. R. Whittell, M. D. Hager, U. S. Schubert, I. Manners, *Nat. Mater.* **2011**, *10*, 176–188.

[8] C. L. Ho, W. Y. Wong, *Coord. Chem. Rev.* **2011**, *255*, 2469–2502.

[9] D. Saccone, C. Magistris, N. Barbero, P. Quagliotto, C. Barolo, G. Viscardi, *Materials* **2016**, *9*, 137.

[10] A. Winter, M. Gottschaldt, G. R. Newkome, U. S. Schubert, *Curr. Top. Med. Chem.* **2012**, *12*, 158–175.

[11] J. Limburg, J. S. Vrettos, L. M. Liable-Sands, A. L. Rhingold, R. H. Crabtree, G. W. Brudvig, *Chemtracts* **2000**, *13*, 326–332.

[12] J. J. Concepcion, J. W. Jurss, M. K. Brennaman, P. G. Hoertz, A. O. T. Patrocinio, N. Y. Murakami Iha, J. L. Templeton, T. J. Meyer, *Acc. Chem. Res.* **2009**, *42*, 1954–1965.

[13] R. Abhijnakrishna, K. Magesh, A. Ayushi, S. Velmathi, *Coord. Chem. Rev.* **2023**, *496*, 215380.

[14] S. Rau, D. Walther, J. G. Vos, *Dalt. Trans.* **2007**, 915–919.

[15] S. F. Kainat, M. B. Hawsawi, E. U. Mughal, N. Naeem, A. M. Almohyawi, H. M. Altass, E. M. Hussein, A. Sadiq, Z. Moussa, A. S. Abd-El-Aziz, S. A. Ahmed, *RSC Adv.* **2024**, *14*, 21464–21537.

[16] E. U. Mughal, M. Mirzaei, A. Sadiq, S. Fatima, A. Naseem, N. Naeem, N. Fatima, S. Kausar, A. A. Altaf, M. N. Zafar, B. A. Khan, *R. Soc. Open Sci.* **2020**, *7*, 201208.

[17] A. R. Guadalupe, D. A. Usifer, K. T. Potts, H. C. Hurrell, A. E. Mogstad, H. D. Abruña, *J. Am. Chem. Soc.* **1988**, *110*, 3462–3466.

[18] R. Franke, D. Selent, A. Börner, *Chem. Rev.* **2012**, *112*, 5675–5732.

[19] B. Heller, M. Hapke, *Chem. Soc. Rev.* **2007**, *36*, 1085–1094.

[20] H. Lebel, J. F. Marcoux, C. Molinaro, A. B. Charette, *Chem. Rev.* **2003**, *103*, 977–1050.

[21] A. Debuigne, R. Poli, C. Jérôme, R. Jérôme, C. Detrembleur, *Prog. Polym. Sci.* **2009**, *34*, 211–239.

[22] M. Garbe, K. Junge, M. Beller, *European J. Org. Chem.* **2017**, 4344–4362.

[23] R. Tagore, R. H. Crabtree, G. W. Brudvig, *Inorg. Chem.* **2008**, *47*, 1815–1823.

[24] H. Lim, P. Chohan, D. Moustafa, C. Sweet, B. Calalpa, P. Kaur, *ChemistrySelect* **2018**,

3, 9443–9447.

[25] C. B. Smith, C. L. Raston, A. N. Sobolev, *Green Chem.* **2005**, *7*, 650–654.

[26] A. W. Addison, T. N. Rao, J. Reedijk, J. V. Rijin, G. C. Verschoor, *J. Chem. Soc., Dalton Trans.* **1984**, 1349-1356.

Appendix:

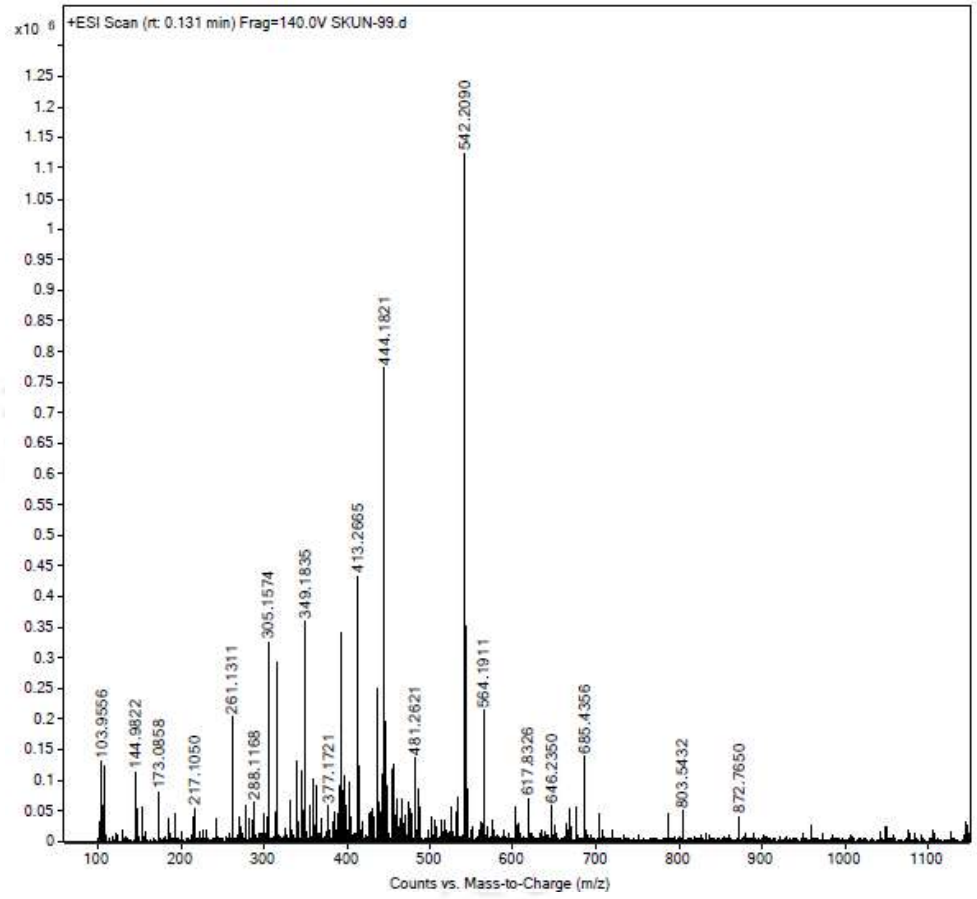

Figure A1. Mass spectrum of **L3**.

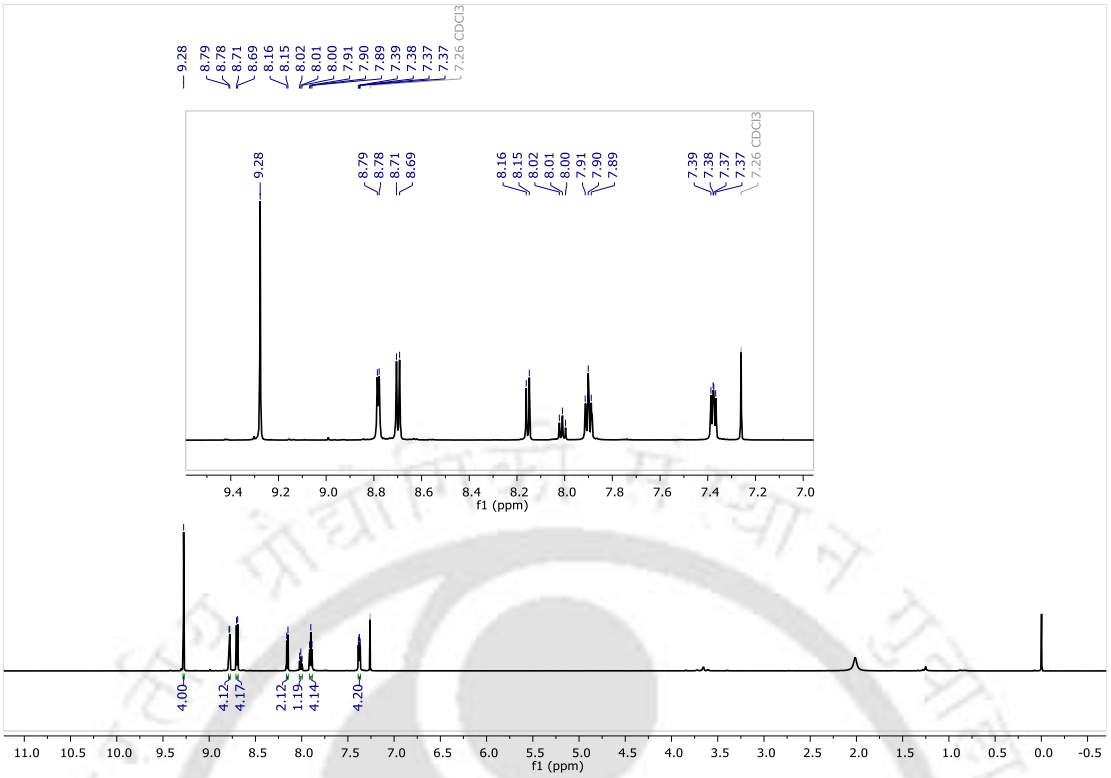

Figure A2. ^{1}H NMR spectrum of **L3**

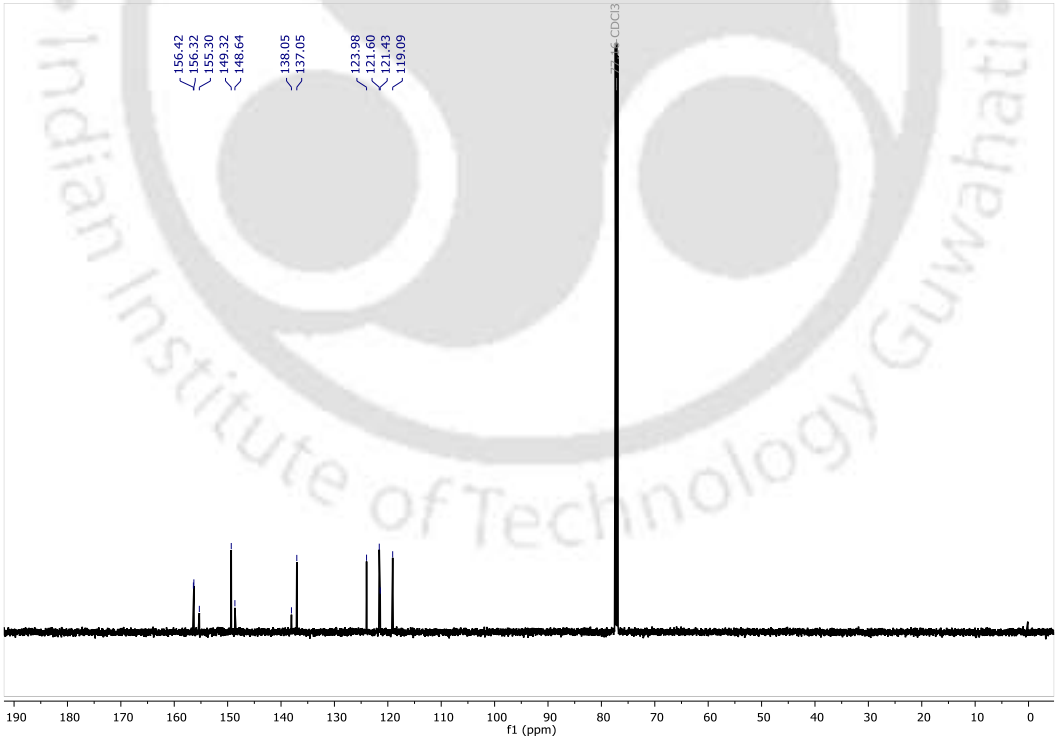

Figure A3. ^{13}C NMR spectrum of **L3**.

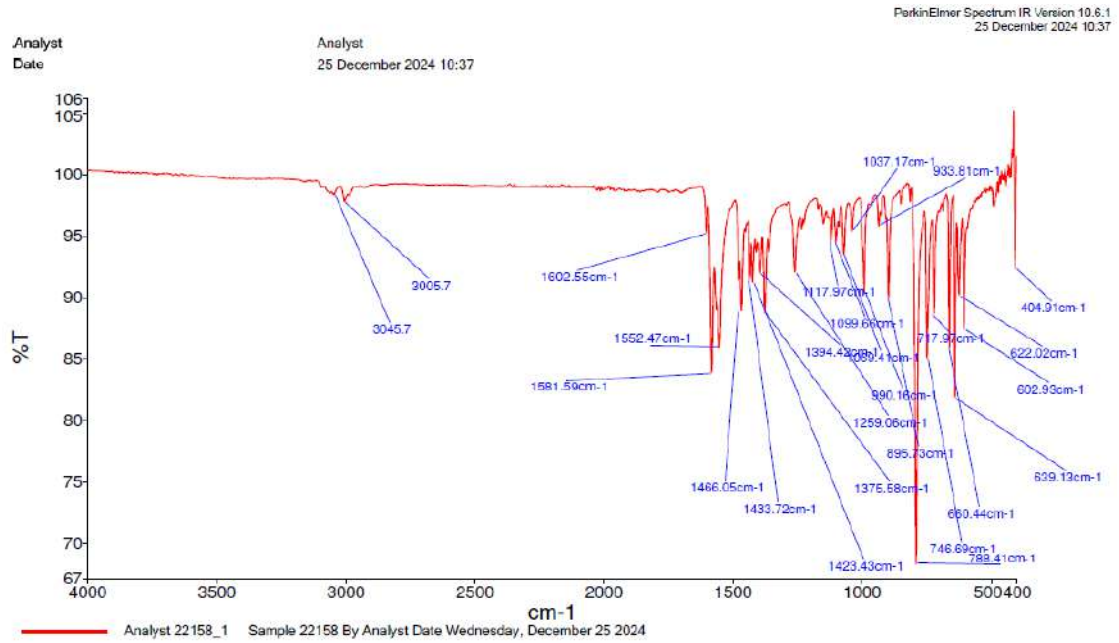

Figure A4. IR spectrum of **L3**.

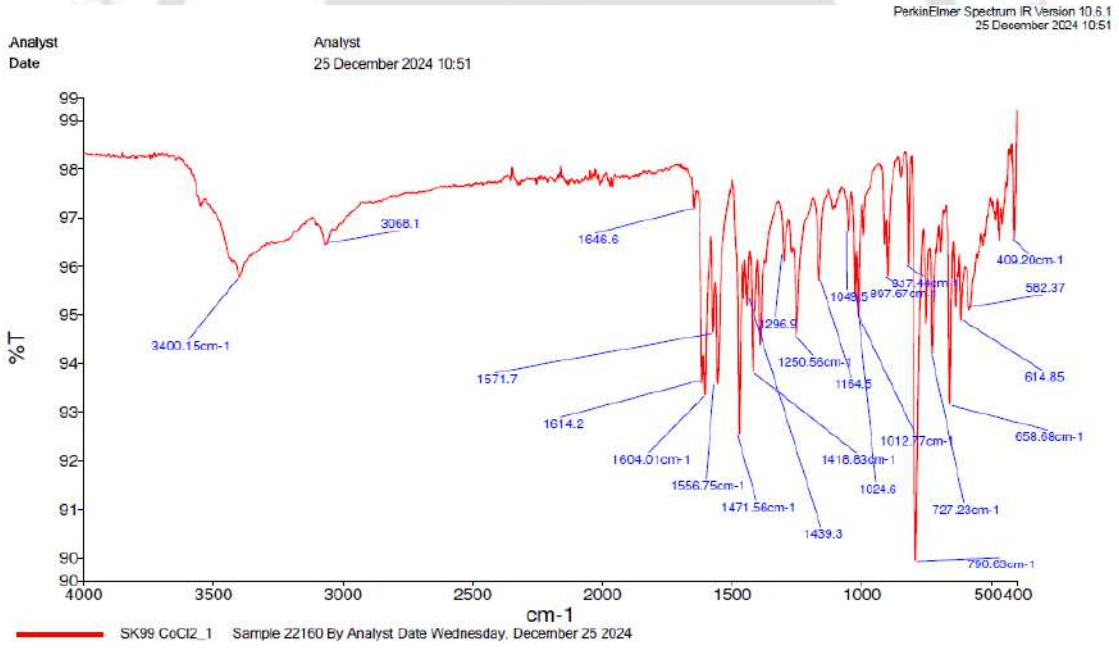

Figure A5. IR spectrum of **1**.

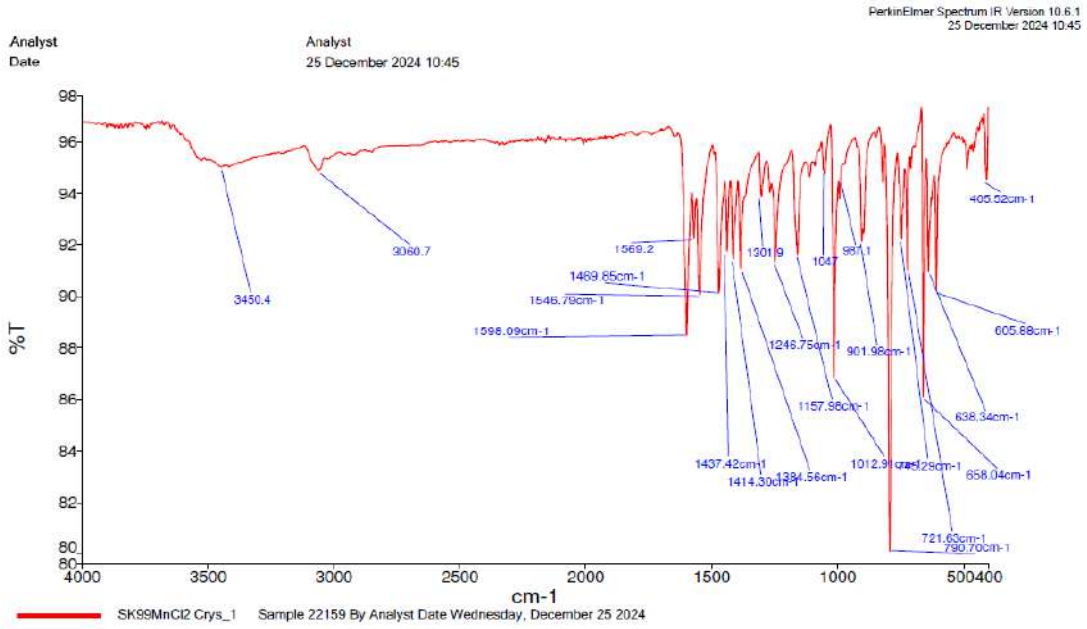

Figure A4. IR spectrum of **2**.

Chapter 5

De Novo Construction of Benzene Ring: Synthesis of 2,4,6-Trisubstituted Benzophenones Using NaH Promoted Cascade Reaction of Aryl Methyl Ketone and Aromatic Aldehyde*

Abstract

Benzannulation is one of the most important methods to construct the simplest aromatic ring *i.e.*, benzene ring. Various efforts to synthesize benzene derivatives were already made, but they generally require some transition metal species in stoichiometric or catalytic amount to carry out this transformation which contaminate with metal-based impurity. On the other hand, the reactant *i.e.*, alkyne used for these transformations is also quite expensive in nature. Keeping these facts in mind, a series of 2,4,6-trisubstituted benzophenones (*vis-à-vis* 1,2,4,6-tetrasubstituted benzenes) were synthesized under transition metal and solvent free conditions using simple chemicals aryl methyl ketones, aromatic aldehydes and sodium hydride. The beauty of this methodology is that 4 out of 6 σ and all 3 π bonds of benzene ring were generated within one reaction vessel. Using this methodology, 2,4,6-trisubstituted benzophenones bearing aromatic and heterocyclic groups can be readily accessed.

*This work has been published in

S. Kumar and V. Manivannan, *ChemistrySelect* **2025**, *10*, e202405611.

1. Introduction

Benzannulation is an important method for *de novo* construction of benzene ring having particular substitution pattern through cycloaddition or cyclization of acyclic building blocks.[1] This method enables access to many substituted benzene compounds which exhibit important properties including those used in various natural products, pharmaceuticals, agrochemicals optical and functional materials.[2] Importance of polysubstituted benzenes and their benzannulation syntheses using transition metal[3] as well as organo[4] catalyst has been a topic of interest. As many of the biologically active compounds and commercially available drugs contain at least one substituted benzene/phenyl ring, development of an efficient method for the synthesis of polysubstituted benzene has continuous attraction. Alternatively, polysubstitution in the benzene nucleus can be achieved by electrophilic and nucleophilic substitution reactions[5] and transition metal catalyzed cross coupling reactions.[6] The facile method is the benzannulation reactions involving cyclotrimerization of alkynes,[7] Diels-Alder,[8] Danheiser benzannulation,[9] Bergman cyclization[10] and Dötz reaction.[11] Since, many of these benzannulation reactions require stoichiometric or catalytic amount of transition metal ions that generate metal impurity thereby imposing the compulsion of purification. It may also be pertinent to note that some inorganic bases were used for benzannulation.[12] Another difficulty is the requirement of multistep preparation of starting material or some additives. Therefore, one-pot synthesis of polysubstituted benzenes under transition metal free benzannulation process using easily available chemicals is still in demand.

Recently, some tetrasubstituted benzene derivatives having 2-pyridyl substituent were synthesized using alkynyl ketones and 2-acetylpyridine in a Co(II) catalyzed reaction with 2,2'-bipyridine as ligand (Scheme 1).[13] A series of tetrasubstituted benzene (*m*-terphenyls) were also synthesized using vinyl sulfoxonium ylides and ynones.[4c] Another three-step synthesis of tetrasubstituted benzene was reported starting from 2,4,6-tribromobenzaldehyde, arylboronic acid and organolithium species, which also included the natural product selagibenzophenone A.[14]

In Chapter 4, synthesis of **L3** has been discussed which contains two terpyridine moieties linked by a central pyridine ring. The general procedure for the synthesis of terpyridine involves reaction of two molecules of 1-(pyridin-2-yl)ethan-1-one with one molecule of pyridine-2-carboxaldehyde in presence of base and ammonium acetate (as source of ammonia). Taking cue from this synthesis, in this Chapter, the synthesis of some 2,4,6-trisubstituted

benzophenones (*vis-à-vis* 1,2,4,6-tetrasubstituted benzenes) in a one-pot, transition metal free, sodium hydride mediated cascade reaction of aryl methyl ketones and aromatic aldehydes under solvent free condition has been described.

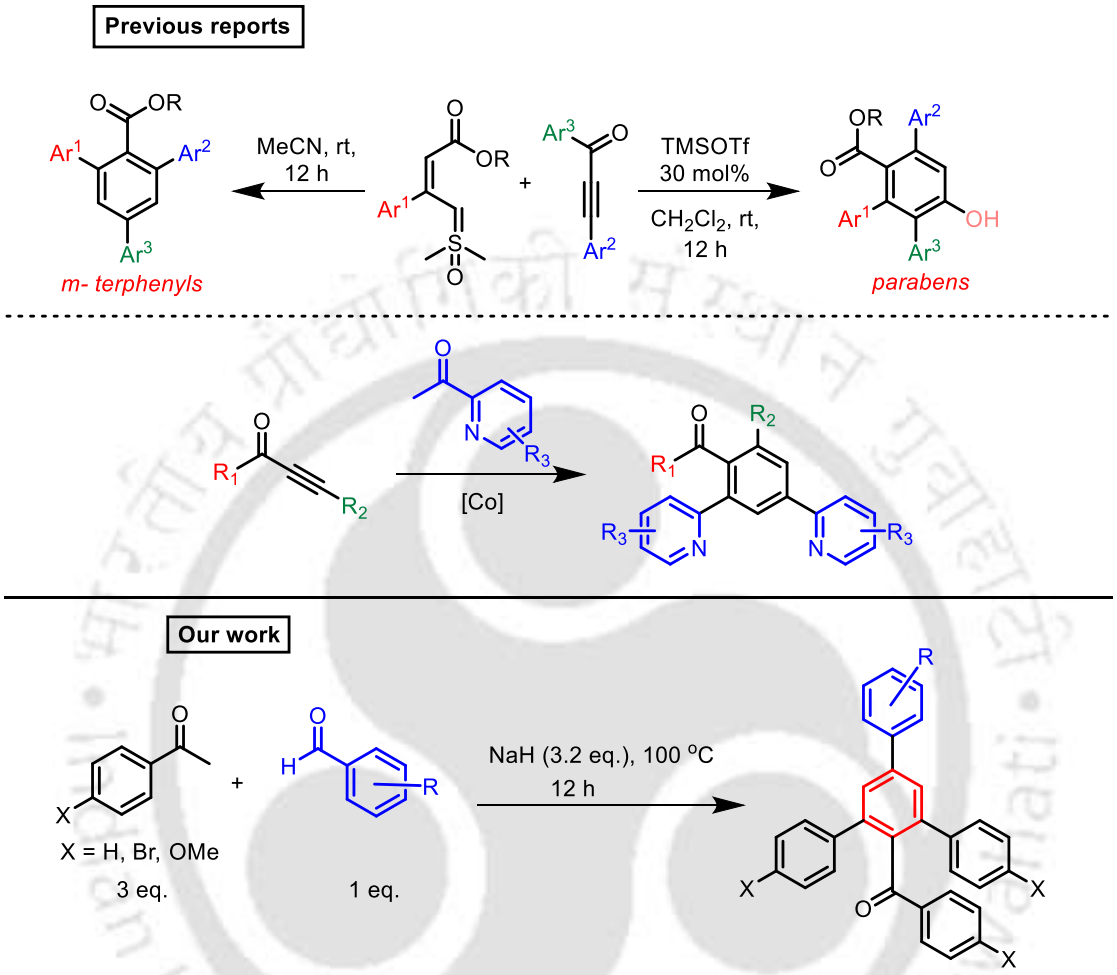

Scheme 1. Previous reports on synthesis of polysubstituted benzene and this work.

2. Results and discussion

Under neat conditions acetophenone was first treated with one molar equivalent of NaH (55-60% in mineral oil) at ambient conditions and typically both were stirred for ~20 min. Then the resultant gummy product was allowed to react at 100 °C for 12 h with one-third equivalent of benzaldehyde. From this solvent free reaction mixture after work up, 2,4,6-triphenylbenzophenone (**1a**), was isolated in good yields as white solid (Scheme 2). Thus aryl methyl ketone, NaH and aryl aldehyde when reacted in 3:3:1 ratio can yield a 2,4,6-trisubstituted benzophenones. To check the wider applicability of this procedure, acetophenone when reacted with o-tolualdehyde (**1b**), p-tolualdehyde (**1c**), 2-chlorobenzaldehyde (**1d**), 3-chlorobenzaldehyde (**1e**), 4-chlorobenzaldehyde (**1f**), 2-bromobenzaldehyde (**1g**), 3-

bromobenzaldehyde (**1h**), 4-bromobenzaldehyde (**1i**), 2-methoxybenzaldehyde (**1j**), 3-methoxybenzaldehyde (**1k**), 4-methoxybenzaldehyde (**1l**) and 1-pyrenecarboxaldehyde (**1v**), yielded respective 2,4,6-trisubstituted benzophenones in moderate to good yields. The methyl ketone, 4′-bromoacetophenone also reacted with aldehydes like 4-chlorobenzaldehyde (**1m**), 4-fluorobenzaldehyde (**1n**), 4-bromobenzaldehyde (**1o**), 2-methoxybenzaldehyde (**1p**) and 2-thiophenecarboxaldehyde (**1t**) while 4′-methoxyacetophenone with 4-methoxybenzaldehyde (**1q**), benzaldehyde (**1r**), 4-fluorobenzaldehyde (**1s**) and 2-acetylpyridine reacted with 2-pyridinecarboxaldehyde (**1u**), from these respective benzene compounds were isolated. The 3-methoxyacetophenone also reacted with benzaldehyde to give **1w** however, benzannulated product could not be isolated using *o*-substituted acetophenone.

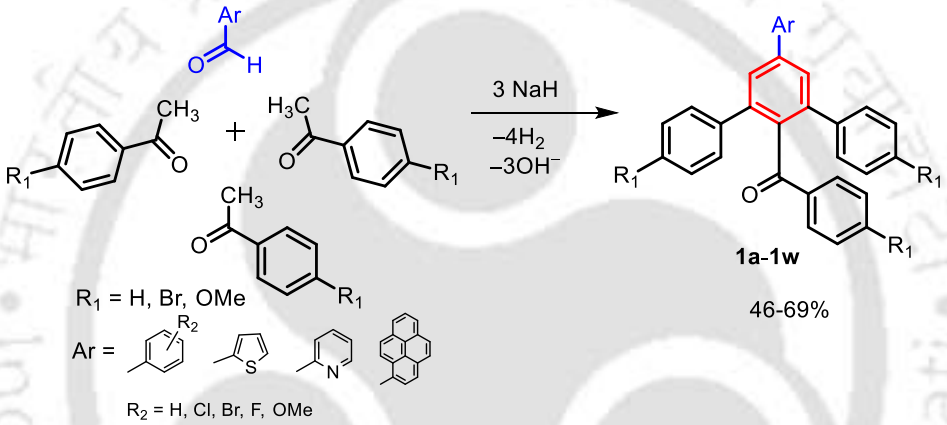

Scheme 2. Synthesis of **1a-1w**.

The annulated benzene product had three substituents arising from the aryl methyl ketone (two aromatic ring and one benzoyl ring) and one from the aldehyde. Out of the four substituents the aromatic ring arising from inclusion of the aldehyde group was found to be in para position with respect to the benzoyl ring. Two aromatic rings originating from three aryl methyl ketone were in two ortho positions with respect to benzoyl ring. Compounds **1a-1w** were characterized thoroughly using ^{1}H-, ^{13}C-NMR, mass and IR spectroscopy. In ^{1}H NMR spectra, the characteristic singlet peak for two protons of the annulated benzene ring appeared at δ = 7.67 ppm in **1a** and in all compounds it was found to appear in the range δ = 7.43-8.41. The characteristic signal for the carbonyl carbon of the benzoyl group in the ^{13}C NMR appeared at δ = 198.9 ppm in **1a** and was in the range 197.2-199.2 in other compounds.

Molecular structures of **1a**, **1b**, **1k**, **1m**, **1n** and **1t** were determined by single crystal X-ray diffraction method, which confirmed regioselectivity of substituents in the central benzene ring

formed by the benzannulation reaction. The plane formed by four aromatic rings linked to the central benzene ring (in **1a**) was twisted by the angles 33.9, 50.5, 59.5 and 73.1° wherein the highest angle was shown by the benzoyl ring. The C7–O1 distance was 1.218(2) Å, a representative diagram of **1a** and **1b** were displayed in Figure 1 and that of others in the supporting information file (Figure A3- A7).

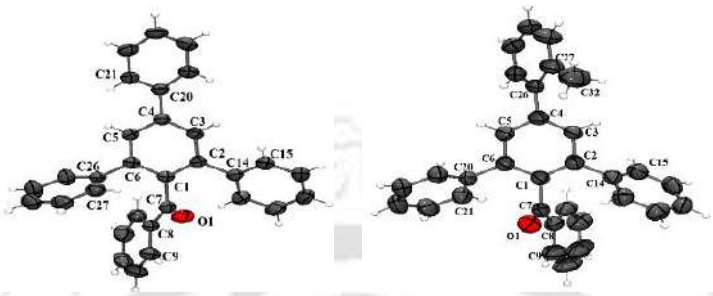

Figure 1. Pov Ray rendered ORTEP (50% probability) diagram of **1a** and **1b**.

The reaction condition was optimized using acetophenone and benzaldehyde under different conditions of base, temperature and solvent (Table 1). At 100 °C, only the chalcone and diketone were isolated when NaOH, KOH and KO*t*Bu was used as base but with Cs_2CO_3, Na_2CO_3 and K_2CO_3 no perceptible product was isolated. However, consistent with Le Chatelier-Braun principle, use of NaH produced 2-oxo-2-phenylethan-1-ide ion at 100 °C, since the hydrogen molecule formed escaped from the reaction mixture. So formed 2-oxo-2-phenylethan-1-ide ion produced **1a** readily upon adding benzaldehyde without requirement of solvents. In ethanol and methanol, the mixture of acetophenone, NaH and benzaldehyde did not yield any benzannulated product, while in toluene, DMF and DMSO, only 8-14% yield was obtained at 110-120 °C. Under neat condition, the best yield of **1a** was 66% at 100 °C and this condition was adopted for the synthesis of **1a**-**1w**. The conditions were not further optimized beyond this point.

Table 1: Optimization of reaction condition for the synthesis of 2,4,6-trisubstituted benzophenones.

Entry	Base	Solvent	Temp[^]	% Yield
1	NaOH	-	120	ND[#]
2	KOH	-	120	ND
3	KOtBu	-	120	ND
4	NaH[*]	EtOH	Reflux	ND
5	NaH	MeOH	Reflux	ND
6	NaH	Toluene	Reflux	8
7	NaH	DMF	120	14
8	NaH	DMSO	120	12
9	NaH	-	RT	ND
10	NaH	-	60	20
11	NaH	-	80	50
12	**NaH**	-	**100**	**66**
13	NaH	-	120	64
14	Cs_2CO_3	-	120	ND
15	K_2CO_3	-	120	ND
16	Na_2CO_3		120	ND

Condition: 4 mmol each of acetophenone and NaH, 1.33 mmol of benzaldehyde. [#]ND = Not Detected. [^] °C. [*]The purchased sodium hydride was of 55-60% in mineral oil and molar ratio was calculated using this strength. Caution: Sodium hydride may catch fire upon exposure to water/moisture.

Thus to check applicability of this methodology, a series of substrates were employed with five kinds of aryl methyl ketone and several aromatic aldehydes (Table 2). With acetophenone as the ketone, the reaction went smoothly with benzaldehyde bearing substituents –CH_3, –OMe

(electron donating), –Cl, –Br (electron withdrawing) in all three positions (*ortho*, *meta* and *para*) as well as polycyclic 1-pyrenecarboxaldehyde.

Table 2: Substrate scope.

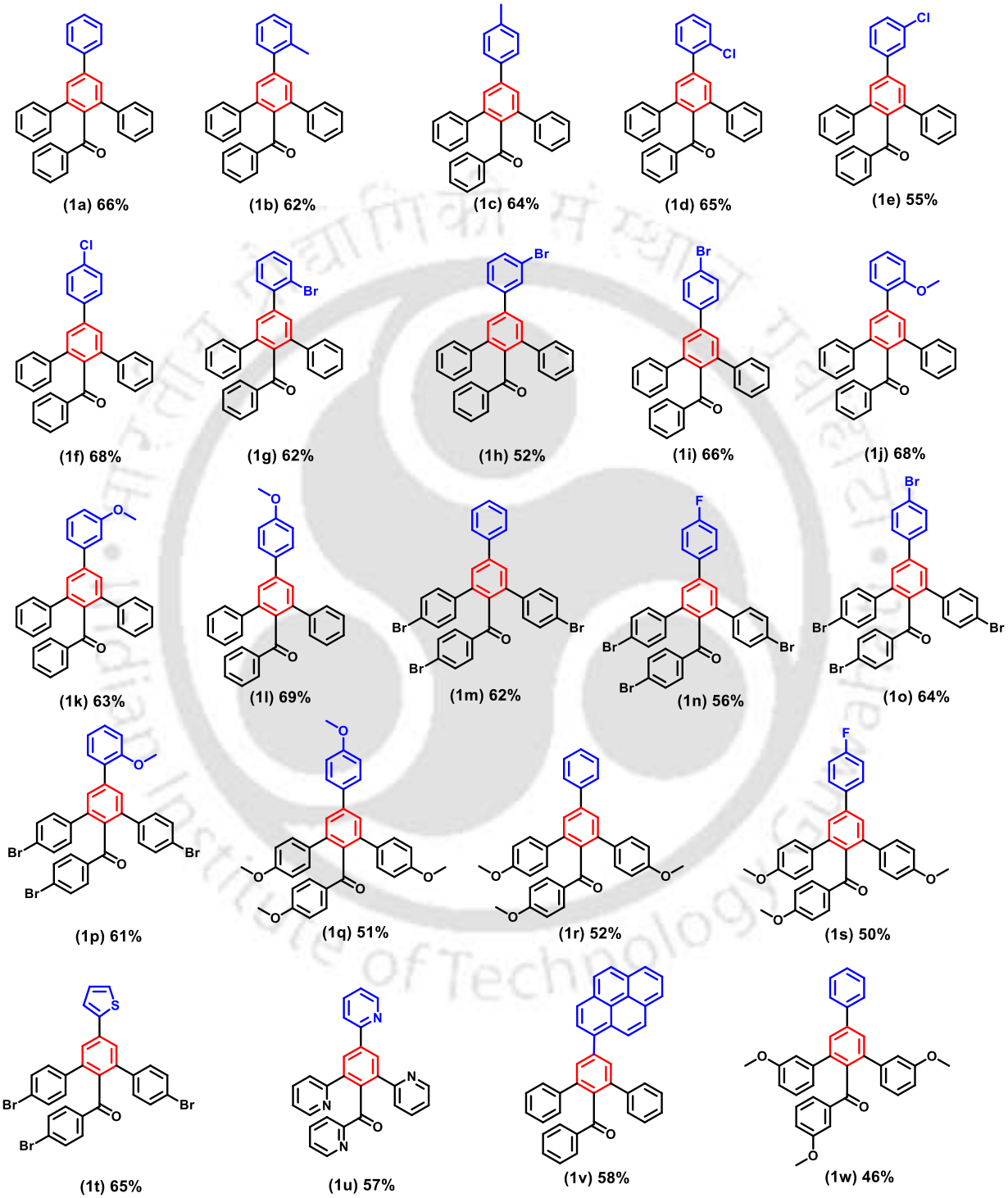

However, aldehydes having nitro group reacted violently at room temperature and desired product was not isolated even when the reaction was performed at 0°C, hence aldehyde

containing $–NO_2$ group were avoided. By using 4-hydroxyacetophenone and 4-aminoacetophenone desired product was not obtained even with excess of NaH.

The plausible mechanism has been proposed using acetophenone and benzaldehyde as the common substrate (Scheme 3). Acetophenone reacted readily with sodium hydride and liberated hydrogen gas to generate the carbanion (**I**). One-third equivalent of benzaldehyde added consumed one-third of the carbanion **I** and produced the chalcone (**II**). Thus formed **II** added another equivalent of **I** successively to generate anion (**III**), which upon protonation and tautomerization generated 1,3,5-triphenylpentane-1,5-dione (**IV**) first and then 3-hydroxy-1,3,5,7-tetraphenylheptane-1,7-dione (**V**).

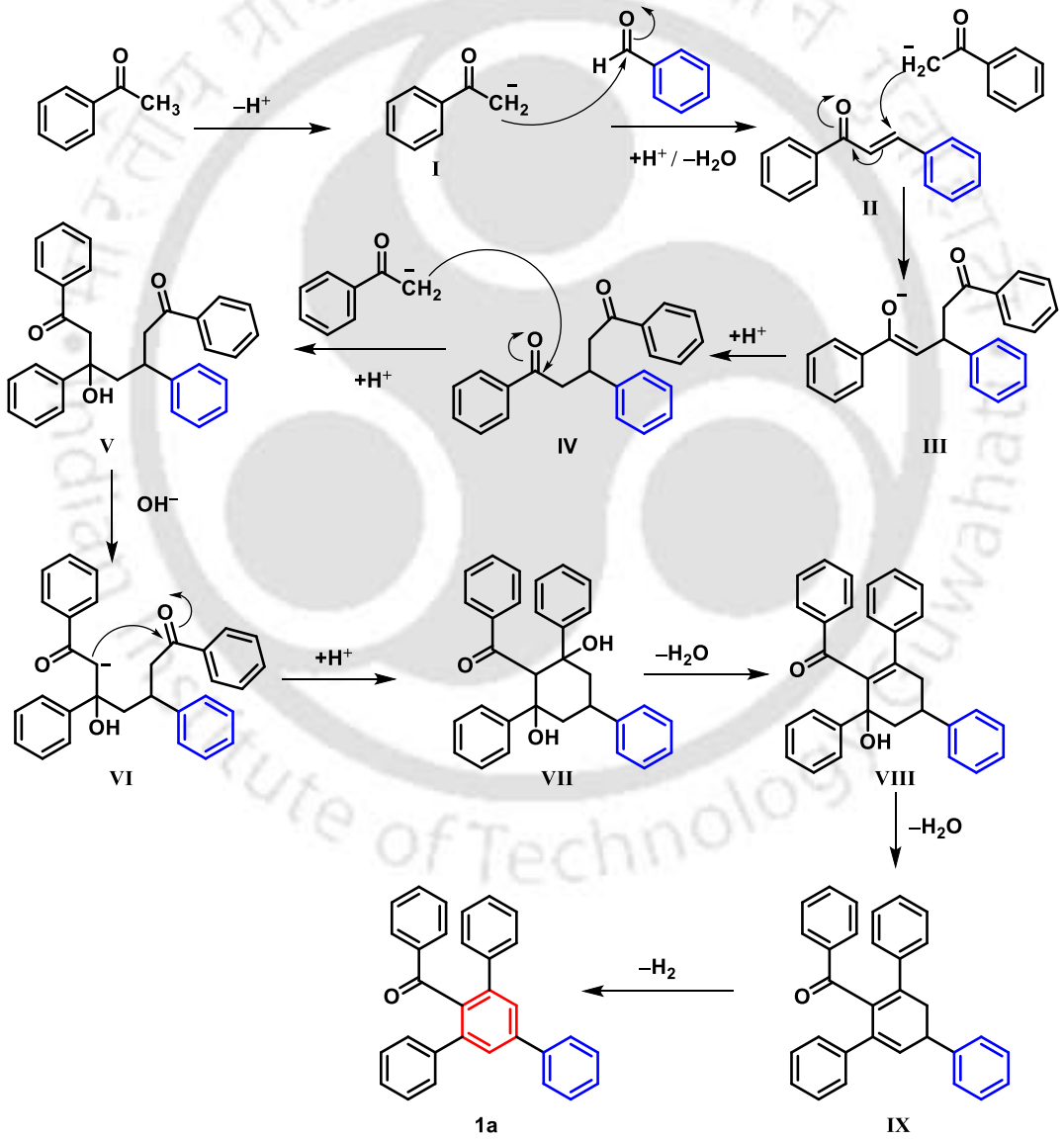

Scheme 3. Plausible mechanism for the formation of **1a**.

The intermediate **V** after losing proton formed 3-hydroxy-1,7-dioxo-1,3,5,7-tetraphenylheptan-2-ide ion (**VI**) which cyclized to the intermediate **VII**. Removal of one water molecule from **VII** led to formation of *α,β*-unsaturated ketone (**VIII**) which lost another water molecule to give conjugated diene (**IX**) and finally aromatization with the loss of a hydrogen molecule[15] yielded the final product **1a**. An aliquot of the reaction mixture was quenched after 1 h and the mass spectrum (Figure A1) of this sample contained peaks with *m*/*z* values corresponding to the intermediates **II** ($M + H^+$, found 209.0958, calcd. 209.0961) and **IV** ($M + H^+$, found 329.1527, calcd. 329.1537), as well as same values for **V** and **VII** ($M + H^+$, found 449.1291, calcd. 449.2111) since both have the same formula. The molecular structure of 1,5-diketone obtained from the reaction between 4'-bromoacetophenone and ferrocenecarboxaldehyde was also confirmed through single crystal XRD measurement of crystal. A representative diagram has been provided in the supporting information (Figure A2), but this diketone did not react further to yield the benzannulated product.

3. Conclusion

In summary, a neat one pot transition metal free NaH mediated reaction methodology was applied to synthesize a series of 2,4,6-trisubstituted benzophenones using aryl methyl ketones and aromatic aldehydes. Here 4 out of 6 σ and 3 π bonds of benzene ring formed in one reaction vessel. The reaction was regioselective in nature wherein the 1,2,4,6-tetrasubstituted benzene ring bear an aryl keto group at position 1 while aryl group at other three. The aryl groups at 2 and 6 positions originated from aryl methyl ketone and the one at 4 from the aldehydes. These compounds were characterized thoroughly by mass spectrometry, ^1H, ^{13}C NMR spectroscopy and regioselectivity was confirmed from determination of molecular structure of some of them using single crystal XRD method. This methodology provides a direct access to benzene derivatives which were usually synthesized by using various multistep cross coupling reactions. The reaction condition used here, is mild with respect to that of other benzannulation reactions. This reaction can be a new addition to benzannulation reactions to obtain 2,4,6-trisubstituted benzophenones bearing two or three different aromatic and heterocyclic substituents starting from a simple aryl methyl ketones and aromatic aldehydes.

4. Experimental section

4.1 General Procedure

*4.1.1 Phenyl(5'-phenyl-[1,1':3',1''-terphenyl]-4'-yl)methanone (**1a**):*

To acetophenone (0.50 g, 4.16 mmol) solid sodium hydride (0.18 g, 4.12 mmol) was added in small quantities and hydrogen gas started to bubble out. The colorless reaction mixture became brown after 20 to 30 min and hydrogen evolution ceased. Benzaldehyde (0.14 g, 1.32 mmol) was added slowly and the mixture was stirred with glass rod for 30 min. The brown solid mixture was heated at 100 °C for 12 h and then allowed to cool to room temperature. Ethanol (5 mL) was added to quench unreacted sodium hydride and stirred magnetically for 3 h. The white solid precipitated was filtered, washed with water, dried and subjected to column chromatography over silica gel, **1a** was eluted with 5% ethyl acetate in hexane. White solid (0.37 g, 66%). mp 166-168 °C; ^{1}H NMR (600 MHz, $CDCl_3$) δ 7.72 (d, J = 7.2 Hz, 2H), 7.67 (s, 2H), 7.56 (dd, J = 8.2, 1.1 Hz, 2H), 7.48 (t, J = 7.7 Hz, 2H), 7.41 (t, J = 7.4 Hz, 1H), 7.31 (d, J = 6.8 Hz, 4H), 7.23 – 7.17 (m, 9H); ^{13}C NMR (150 MHz, $CDCl_3$) δ 198.9, 142.0, 141.6, 140.4, 140.1, 138.4, 137.2, 132.8, 129.5, 129.3, 129.1, 128.2, 128.1, 128.1, 128.0, 127.5, 127.4; IR (cm^{-1}) ATR mode: 3056(w), 3028(w), 1666(s), 1594(m), 1494(m), 1445(m), 1310(w), 1264(s), 931(m), 888(m), 751(s), 695(s), 584(m), 522(m), 499(m). ESI-MS (+): *m*/*z* calcd. for (M + H^+) $C_{31}H_{23}O^+$ 411.1743, found 411.1723.

Same procedure was adopted to synthesize **1b** – **1l**, **1v** and **1w** by using same molar ratio of the reactants and for **1m** – **1p** and **1t**, 4'-bromoacetophenone and sodium hydride were heated together at 50 °C. In case of **1q**-**1s**, it was necessary to heat the mixture of 4'-methoxyacetophenone and sodium hydride for ~30 minute prior to addition of the aldehyde. In the case of **1u**, the temperature was kept at 0 °C during addition of sodium hydride to 2-acetylpyridine and then 2-pyridinecarboxaldehyde. The **1u** was eluted by using 40% ethylacetate in hexane.

4.2 Spectral information

The spectroscopic data are given below:

Phenyl(5'-(o-tolyl)-[1,1':3',1"-terphenyl]-2'-yl)methanone (**1b**): White solid (0.36 g, 62%). mp 212-214 °C, ^{1}H NMR (600 MHz, $CDCl_3$) δ 7.58 (d, J = 7.3 Hz, 2H), 7.43 (s, 2H), 7.38 (d, J = 8.2 Hz, 1H), 7.31 (m, 8H), 7.18 (m, 8H), 2.41 (s, 3H); ^{13}C NMR (150 MHz, $CDCl_3$) δ 199.1, 142.9, 140.8, 140.3, 138.3, 136.7, 135.5, 132.8, 130.7, 130.1, 129.9, 129.5, 129.3, 128.2, 128.1, 127.8, 127.4, 126.1, 20.8; IR (cm^{-1}) ATR mode: 3059(w), 3031(w), 1668(s), 1595(m),

1492(m), 1447(m), 1312(w), 1262(m), 929(m), 753(m), 728(w), 698(s), 524(w). ESI-MS (+): *m/z* calcd. for ($M+H^+$) $C_{35}H_{25}O^+$ 425.1900, found 425.1900.

Phenyl(5'-(p-tolyl)-[1,1':3',1''-terphenyl]-2'-yl)methanone (**1c**):White solid (0.37 g, 64%). mp 232-234 °C; ^{1}H NMR (600 MHz, $CDCl_3$) δ 7.66 (s, 2H), 7.62 (d, *J* = 8.1 Hz, 2H), 7.56 (d, *J* = 7.2 Hz, 2H), 7.33 – 7.28 (m, 7H), 7.23 – 7.16 (m, 8H), 2.42 (s, 3H); ^{13}C NMR (150 MHz, $CDCl_3$) δ 199.0, 141.9, 141.5, 140.4, 138.4, 138.0, 137.2, 136.9, 132.7, 129.8, 129.5, 129.3, 128.2, 128.1, 127.7, 127.4, 127.2, 21.3; IR (cm^{-1}) ATR mode: 2955(w), 2915(m), 2849(w), 1660(s), 1595(s), 1447(m), 1415(m), 1379(m), 1315(w), 1269(m), 928(m), 892(w), 827(m), 755(m), 698(s), 596(m), 502(m). ESI-MS (+): *m/z* calcd. for ($M+H^+$) $C_{32}H_{25}O^+$ 425.1900, found 425.1889.

(5'-(2-Chlorophenyl)-[1,1':3',1''-terphenyl]-2'-yl)(phenyl)methanone (**1d**): White solid (0.40 g, 65%); mp 217-219 °C; ^{1}H NMR (600 MHz, $CDCl_3$) δ 7.58 (dd, *J* = 8.3, 1.4 Hz, 2H), 7.55 (s, 2H), 7.52 (dd, *J* = 7.8, 1.5 Hz, 1H), 7.49 (dd, *J* = 7.4, 1.9 Hz, 1H), 7.39 – 7.32 (m, 3H), 7.31 (m, 4H), 7.22 – 7.16 (m, 8H); ^{13}C NMR (150 MHz, $CDCl_3$) δ 198.9, 140.8, 140.3, 140.2, 139.5, 138.3, 137.4, 132.9, 132.7, 131.6, 130.4, 130.3, 129.6, 129.4, 129.2, 128.2, 128.2, 127.5, 127.2; IR (cm^{-1}) ATR mode: 3059(w), 3028(w), 1668(s), 1597(m), 1493(m), 1478(m), 1447(m), 1396(w), 1263(s), 1147(w), 1076(w), 930(m), 893(w), 753(s), 698(s), 529(w). ESI-MS (+): *m/z* calcd. for ($M+H^+$) $C_{31}H_{22}ClO^+$ 445.1354 found 445.1366.

(5'-(3-Chlorophenyl)-[1,1':3',1''-terphenyl]-2'-yl)(phenyl)methanone (**1e**): white solid (0.34 g, 55%); mp 134-136 °C; ^{1}H NMR (600 MHz, $CDCl_3$) δ 7.70 (t, *J* = 1.9 Hz, 1H), 7.64 (s, 2H), 7.59 (dt, *J* = 7.6, 1.5 Hz, 1H), 7.55 (dd, *J* = 8.3, 1.4 Hz, 2H), 7.41 (t, *J* = 7.8 Hz, 1H), 7.38 (m, 1H), 7.33 (d, *J* = 7.4 Hz, 1H), 7.30 (m, 4H), 7.23 – 7.18 (m, 8H); ^{13}C NMR (150 MHz, $CDCl_3$) δ 198.7, 142.0, 141.8, 140.6, 140.1, 138.2, 137.8, 135.0, 132.9, 130.3, 129.5, 129.3, 128.3, 128.8, 128.0, 127.9, 127.6, 127.6, 125.6; IR (cm^{-1}) ATR mode: 2957(w), 2917(m), 2850(w), 1665(s), 1593(m), 1556(m), 1492(m), 1446(w), 1263(s), 1181(m), 1075(w), 930(s), 878(m), 861(m), 778(s), 758(s), 698(s), 645(m), 598(m), 556(m), 526(m). ESI-MS (+): *m/z* calcd. for ($M+H^+$) $C_{31}H_{22}ClO^+$ 445.1354 found 445.1363.

(5'-(4-Chlorophenyl)-[1,1':3',1''-terphenyl]-2'-yl)(phenyl)methanone (**1f**): White solid (0.42 g, 68%); mp 212-214 °C; ^{1}H NMR (600 MHz, $CDCl_3$) δ 7.65 (d, *J* = 8.4 Hz, 2H), 7.63 (s, 2H),

7.55 (d, J = 7.7 Hz, 2H), 7.45 (d, J = 8.4 Hz, 2H), 7.33 (d, J = 7.5 Hz, 1H), 7.30 (d, J = 7.3 Hz, 4H), 7.20 (m, 8H); ^{13}C NMR (150 MHz, $CDCl_3$) δ 198.8, 141.7, 140.8, 140.2, 138.6, 138.2, 137.5, 134.3, 132.9, 129.5, 129.3, 129.3, 128.7, 128.3, 128.2, 127.8, 127.6; IR (cm^{-1}) ATR mode: 1658(s), 1595(m), 1580(m), 1493(s), 1447(m), 1315(m), 1269(m), 1089(w), 1008(w), 927(m), 838(m), 781(m), 757(m), 698(s), 647(m), 589(w), 562(w), 502(w), 480(w). ESI-MS (+): *m/z* calcd. for ($M+H^+$) $C_{31}H_{22}ClO^+$ 445.1354 found 445.1367.

(5'-(2-Bromophenyl)-[1,1':3',1''-terphenyl]-2'-yl)(phenyl)methanone (**1g**): White solid(0.42 g, 62%); mp 235-237 °C; ^{1}H NMR (600 MHz, $CDCl_3$) δ 7.72 (dd, J = 8.0, 1.2 Hz, 1H), 7.57 (dd, J = 8.3, 1.3 Hz, 2H), 7.52 (s, 2H), 7.48 (dd, J = 7.6, 1.8 Hz, 1H), 7.40 (td, J = 7.5, 1.2 Hz, 1H), 7.35 – 7.32 (m, 1H), 7.31 (m, 4H), 7.24 (dd, J = 7.6, 1.7 Hz, 1H), 7.21 – 7.18 (m, 6H), 7.18 – 7.15 (m, 2H); ^{13}C NMR (150 MHz, $CDCl_3$) δ 198.9, 141.9, 141.6, 140.7, 140.1, 138.2, 137.4, 133.5, 132.9, 131.5, 130.3, 129.6, 129.4, 129.3, 128.2, 128.2, 127.7, 127.5, 122.6; IR (cm^{-1}) ATR mode: 3056(w), 3026(w), 1667(s), 1595(m), 1475(m), 1445(w), 1395(w), 1310(w), 1263(s), 1178(w), 1073(m), 1029(m), 929(m), 891(m), 781(m), 754(s), 696(s), 651(m), 617(m), 589(m), 559(m), 525(m), 444(w). ESI-MS (+): *m/z* calcd. for ($M+H^+$) $C_{31}H_{22}BrO^+$ 489.0849 found 489.0823

(5'-(3-Bromophenyl)-[1,1':3',1''-terphenyl]-2'-yl)(phenyl)methanone (**1h**): White solid (0.35 g, 52%). mp 156-158 °C; ^{1}H NMR (600 MHz, $CDCl_3$) δ 7.86 (t, J = 1.9 Hz, 1H), 7.63 (s, 2H), 7.56 – 7.52 (m, 3H), 7.36 (d, J = 7.9 Hz, 1H), 7.33 (d, J = 7.8 Hz, 1H), 7.31 – 7.29 (m, 4H), 7.24 – 7.17 (m, 9H); ^{13}C NMR (150 MHz, $CDCl_3$) δ 198.7, 142.3, 141.8, 140.5, 140.0, 138.2, 137.8, 132.9, 131.0, 130.6, 130.5, 129.5, 129.3, 128.3, 128.2, 127.9, 127.6, 126.0, 123.2; IR (cm^{-1}) ATR mode: 2956(w), 2917(m), 2850(w), 1666(s), 1592(m), 1493(m), 1447(w), 1379(m), 1311(m), 1262(s), 1178(w), 1148(w), 1074(w), 1027(m), 929(m), 877(w), 852(w), 755(m), 695(s), 644(m), 527(m). ESI-MS (+): *m/z* calcd. for ($M+H^+$) $C_{31}H_{22}BrO^+$ 489.0849 found 489.0813.

(5'-(4-Bromophenyl)-[1,1':3',1''-terphenyl]-2'-yl)(phenyl)methanone (**1i**): White solid; (0.45 g, 66%); mp 223-225 °C; ^{1}H NMR (600 MHz, $CDCl_3$) δ 7.62 (s, 2H), 7.59 (m, 4H), 7.54 (d, J = 8.3 Hz, 2H), 7.33 (d, J = 7.4 Hz, 1H), 7.30 (d, J = 6.7 Hz, 4H), 7.23 – 7.17 (m, 8H); ^{13}C NMR (150 MHz, $CDCl_3$) δ 198.8, 141.8, 140.8, 140.2, 139.0, 138.2, 137.6, 132.9, 132.2, 129.5,

129.3, 128.9, 128.3, 128.1, 127.8, 127.6, 122.5; IR (cm^{-1}) ATR mode: 2955(w), 2915(m), 2849(w), 1659(s), 1595(m), 1579(w), 1447(m), 1377(w), 1315(m), 1269(m), 1179(s), 1147(m), 1072(m), 1005(m), 927(m), 893(m), 828(m), 756(m), 698(s), 646(m), 588(m), 559(m), 522(m), 454(w). ESI-MS (+): *m/z* calcd. for ($M+H^+$) $C_{31}H_{22}BrO^+$ 489.0849 found 489.0839.

(5'-(2-Methoxyphenyl)-[1,1':3',1''-terphenyl]-2'-yl)(phenyl)methanone (**1j**): White solid; (0.42 g, 68%). mp 185- 187 °C; ^1H NMR (600 MHz, $CDCl_3$) δ 7.64 (s, 2H), 7.58 (dd, *J* = 8.2, 1.1 Hz, 2H), 7.46 (dd, *J* = 7.5, 1.7 Hz, 1H), 7.39 – 7.36 (m, 1H), 7.30 (m, 4H), 7.21 – 7.14 (m, 9H), 7.07 (td, *J* = 7.5, 0.9 Hz, 1H), 7.03 (d, *J* = 8.2 Hz, 1H), 3.86 (s, 3H); ^{13}C NMR (150 MHz, $CDCl_3$) δ 199.2, 156.7, 140.7, 140.6, 139.5, 138.4, 136.9, 132.7, 131.2, 130.5, 129.6, 129.4, 129.4, 128.2, 128.1, 127.3, 121.1, 111.4, 55.8; IR (cm^{-1}) ATR mode: 3059(w), 3026(w), 2934(w), 2833(w), 1667(s), 1597(s), 1557(s), 1493(m), 1412(m), 1264(m), 1247(m), 1178(w), 1119(m), 1024(m), 929(m), 753(s), 696(s), 589(w), 521(m). ESI-MS (+): *m/z* calcd. for ($M+H^+$) $C_{32}H_{25}O_2^+$ 441.1850 found 441.1838.

(5'-(3-Methoxyphenyl)-[1,1':3',1''-terphenyl]-2'-yl)(phenyl)methanone (**1k**): White solid (0.38 g, 63%). mp 144-146 °C; ^1H NMR (600 MHz, $CDCl_3$) δ 7.67 (s, 2H), 7.57 – 7.55 (m, 2H), 7.40 (t, *J* = 7.9 Hz, 1H), 7.34 – 7.30 (m, 6H), 7.23 – 7.17 (m, 9H), 6.96 (dd, *J* = 8.2, 1.9 Hz, 1H), 3.88 (s, 3H); ^{13}C NMR (150 MHz, $CDCl_3$) δ 198.9, 160.2, 141.9, 141.6, 141.6, 140.4, 138.3, 137.4, 132.8, 130.1, 129.5, 129.4, 128.3, 128.1, 128.0, 127.5, 119.9, 113.7, 112.9, 55.5; IR (cm^{-1}) ATR mode: 3049(w), 2955(w), 2916(m), 2848(w), 1661(s), 1593(s), 1493(m), 1449(m), 1386(m), 1311(m), 1265(s), 1212(m), 1144(w), 1030(m), 1000(m), 932(m), 890(m), 854(s), 779(s), 764(s), 701(s), 654(m), 606(m), 541(m), 524(m), 448(w). ESI-MS (+): *m/z* calcd. for ($M+H^+$) $C_{32}H_{25}O_2^+$ 441.1850 found 441.1832.

(5'-(4-Methoxyphenyl)-[1,1':3',1''-terphenyl]-2'-yl)(phenyl)methanone (**1l**): White solid (0.42 g, 69%). mp 211-213 °C; ^1H NMR (600 MHz, $CDCl_3$) δ 7.66 (d, *J* = 8.6 Hz, 2H), 7.63 (s, 2H), 7.55 (d, *J* = 7.8 Hz, 2H), 7.30 (d, *J* = 7.4 Hz, 5H), 7.19 (m, 8H), 7.01 (d, *J* = 8.5 Hz, 2H), 3.87 (s, 3H); ^{13}C NMR (150 MHz, $CDCl_3$) δ 199.0, 159.8, 141.6, 141.6, 140.5, 138.4, 136.6, 132.8, 132.6, 129.5, 129.3, 128.5, 128.2, 128.1, 127.5, 127.4, 114.52, 55.5; IR (cm^{-1}) ATR mode: 2954(m), 2916(m), 2871(w), 1659(s), 1595(s), 1513(s), 1447(m), 1270(m), 1238(s), 1181(m),

1029(m), 927(m), 838(s), 756(s), 696(s), 597(m), 551(m), 520(m), 419(w). ESI-MS (+): *m/z* calcd. for ($M+H^+$) $C_{32}H_{25}O_2^+$ 441.1850 found 441.1823.

(4-Bromophenyl)(4,4"-dibromo-5'-phenyl-[1,1':3',1"-terphenyl]-2'-yl)methanone (**1m**): White solid (0.34 g, 62%). mp 250-252 °C; ^{1}H NMR (400 MHz, $CDCl_3$) δ 7.69 (dd, *J* = 6.9, 1.6 Hz, 2H), 7.62 (s, 2H), 7.49 (m, 2H), 7.44 – 7.41 (m, 1H), 7.40 – 7.34 (m, 8H), 7.18 – 7.13 (m, 4H); ^{13}C NMR (150 MHz, $CDCl_3$) δ 197.5, 142.6, 140.3, 139.6, 138.8, 136.6, 136.3, 131.9, 131.6, 130.9, 129.2, 128.9, 128.8, 128.4, 128.2, 127.4, 122.3; IR (cm^{-1}) ATR mode: 2955(m), 2915(m), 2871(w), 2848(w), 1661(s), 1581(s), 1486(s), 1378(m), 1267(m), 1146(m), 1070(s), 1009(s), 926(s), 818(s), 765(s), 746(m), 697(s), 561(m), 524(m), 502(m), 468(m), 415(w). ESI-MS (+): *m/z* calcd. for ($M+H^+$) $C_{31}H_{20}Br_3O^+$ 646.9039 found 646.8975.

(4-Bromophenyl)(4,4"-dibromo-5'-(4-fluorophenyl)-[1,1':3',1"-terphenyl]-2'-yl)methanone (**1n**): White solid (0.31 g, 56%). mp 232-234 °C; ^{1}H NMR (600 MHz, $CDCl_3$) δ 7.65 (m, 2H), 7.57 (s, 2H), 7.40 – 7.36 (m, 8H), 7.18 (t, *J* = 8.7 Hz, 2H), 7.15 (d, *J* = 8.4 Hz, 4H); ^{13}C NMR (150 MHz, $CDCl_3$) δ 197.3, 163.1 (d, *J* = 248.2 Hz), 141.9, 140.4, 138.7, 136.6, 136.4, 135.7, 132.3, 131.9, 131.6, 130.8, 130.8, 129.0 (d, *J* = 8.1 Hz), 128.8, 127.9, 122.3, 116.2 (d, *J* = 21.6 Hz); IR (cm^{-1}) ATR mode: 2955(w), 2915(m), 2871(w), 2850(s), 1664(s), 1581(s), 1511(s), 1486(s), 1396(m), 1255(m), 1234(m), 1159(m), 1069(s), 1009(s), 926(m), 818(s), 779(m), 516(s), 466(m), 427(w). ESI-MS (+): *m/z* calcd. for ($M+H^+$) $C_{31}H_{19}Br_3FO^+$ 664.8945 found 664.8904.

(4-Bromophenyl)(4,4"-dibromo-5'-(4-bromophenyl)-[1,1':3',1"-terphenyl]-4'-yl)methanone (**1o**): White solid (0.39 g, 64%). mp 246-248 °C; ^{1}H NMR (600 MHz, $CDCl_3$) δ 7.62 (d, *J* = 8.6 Hz, 2H), 7.58 (s, 2H), 7.55 (d, *J* = 8.6 Hz, 2H), 7.39 – 7.35 (m, 8H), 7.14 (d, *J* = 8.5 Hz, 4H); ^{13}C NMR (150 MHz, $CDCl_3$) δ 197.2, 141.4, 140.5, 138.6, 138.5, 136.7, 136.5, 132.4, 131.9, 131.6, 130.9, 130.8, 128.9, 128.8, 127.9, 122.8, 122.4; IR (cm^{-1}) ATR mode: 2955(s), 2915(s), 2871(m), 2849(m), 1664(s), 1580(s), 1489(s), 1377(m), 1266(m), 1071(m), 1009(s), 925(m), 817(s), 778(m), 755(m), 687(m), 666(m), 506(s), 526(m), 439(w). ESI-MS (+): *m/z* calcd. for ($M+H^+$) $C_{31}H_{19}Br_4O^+$ 726.8123 found 726.8063.

(4-Bromophenyl)(4,4"-dibromo-5'-(2-methoxyphenyl)-[1,1':3',1"-terphenyl]-2'-yl)methanone (**1p**): White solid (0.34 g, 61%). mp 210-212 °C; ^{1}H NMR (600 MHz, $CDCl_3$) δ 7.60 (s, 2H), 7.42 (d, *J* = 8.4 Hz, 3H), 7.41 – 7.32 (m, 8H), 7.14 (d, *J* = 8.4 Hz, 4H), 7.07 (t, *J* = 7.4 Hz, 1H), 7.03 (d, *J* = 8.2 Hz, 1H), 3.86 (s, 3H); ^{13}C NMR (150 MHz, $CDCl_3$) δ 197.7, 156.6, 140.0, 139.4, 139.0, 136.7, 135.9, 131.8, 131.5, 131.0, 130.9, 130.9, 130.6, 129.7, 128.9, 128.6, 122.0, 121.2, 111.4, 55.8; IR (cm^{-1}) ATR mode: 3000(w), 2967(w), 2937(w), 2830(w), 1666(s), 1584(m), 1486(m), 1399(m), 1266(m), 1244(s), 1118(w), 1070(m), 1009(s), 926(s), 821(s), 746(s), 526(m), 472(w), 410(w). ESI-MS (+): *m/z* calcd. for ($M+H^+$) $C_{32}H_{22}Br_3O_2^+$ 676.9144 found 676.9124.

(4,4"-dimethoxy-5'-(4-methoxyphenyl)-[1,1':3',1"-terphenyl]-4'-yl)(4-methoxyphenyl)methanone (**1q**) : White solid (0.30g, 51%); mp 181-183 °C; ^{1}H NMR (400 MHz, $CDCl_3$) δ 7.64 (d, J = 8.8 Hz, 2H), 7.57 – 7.52 (m, 4H), 7.24 (d, J = 8.7 Hz, 4H), 7.00 (d, J = 8.8 Hz, 2H), 6.75 (d, J = 8.7 Hz, 4H), 6.67 (d, J = 8.9 Hz, 2H), 3.87 (s, 3H), 3.77 (s, 3H), 3.74 (s, 6H); ^{13}C NMR (100 MHz, CDCl3) δ 197.9, 163.2, 159.7, 158.9, 141.2, 140.8, 136.8, 133.1, 132.8, 131.9, 131.7, 130.4, 128.4, 127.2, 114.5, 113.7, 113.4, 55.5, 55.4, 55.3; IR (cm^{-1}) ATR mode: 3000(w), 2955(w), 2931(w), 2833(w), 1647(m), 1593(s), 1508(s), 1461(w), 1438(w), 1287(m), 1264(m), 1247(s), 1174(m), 921(m), 830(s), 789(m), 566(m). ESI-MS (+): *m/z* calcd. for ($M+H^+$) $C_{35}H_{31}O_5^+$ 531.2166 found 531.2142.

(4,4"-dimethoxy-5'-phenyl-[1,1':3',1"-terphenyl]-2'-yl)(4-methoxyphenyl)methanone (**1r**): White solid (0.29g, 52%); mp 114-116 °C;

^{1}H NMR (400 MHz, $CDCl_3$) δ 7.72 – 7.68 (m, 2H), 7.60 (s, 2H), 7.57 – 7.54 (m, 2H), 7.47 (td, *J* = 6.8, 1.5 Hz, 2H), 7.42 – 7.36 (m, 1H), 7.26 – 7.23 (m, 4H), 6.77 – 6.74 (m, 4H), 6.70 – 6.66 (m, 2H), 3.77 (s, 3H), 3.74 (s, 6H); ^{13}C NMR (100 MHz, $CDCl_3$) δ 197.8, 163.2, 158.9, 141.7, 140.9, 140.4, 137.4, 132.9, 131.9, 131.6, 130.4, 129.0, 127.9, 127.7, 127.4, 113.7, 113.5, 55.4, 55.3; IR (cm^{-1}) ATR mode: 2924(w), 2853(w), 2835(w), 1735(w), 1654(m), 1593(s), 1508(s), 1459(m), 1245(s), 1175(s), 1143(s), 1027(s), 928.85(m), 828(m), 765(m), 698(m), 569(w), 538(w). ESI-MS (+): *m/z* calcd. for ($M+H^+$) $C_{34}H_{29}O_4^+$ 501.2061 found 501.2048.

(5'-(4-fluorophenyl)-4,4"-dimethoxy-[1,1':3',1"-terphenyl]-2'-yl)(4-methoxyphenyl)methanone (**1s)**: White solid (0.28g, 50%); mp 163-165 °C; ^{1}H NMR (400 MHz, $CDCl_3$) δ 7.67 – 7.63 (m, 2H), 7.56 – 7.53 (m, 4H), 7.25 – 7.22 (m, 4H), 7.19 – 7.13 (m, 2H), 6.76 (d, *J* = 8.8 Hz, 4H), 6.68 (d, *J* = 8.9 Hz, 2H), 3.77 (s, 3H), 3.74 (s, 6H); ^{13}C NMR (150 MHz, Chloroform-*d*) δ 197.7, 162.9 (d, *J* = 247.1 Hz)., 159.0, 140.9, 140.7, 136.5, 137.5, 132.9, 131.9,131.6, 130.4, 128.9 (d, *J* = 8.1 Hz), 128.4, 127.5, 115.9 (d, *J* = 21.5 Hz)., 113.7, 113.5, 55.4, 55.3; IR (cm^{-1}) ATR mode: 2923(w), 2848(w), 1656(m), 1593(s), 1506(s), 1463(w), 1313(w), 1243(s), 1176(m), 1142(m), 1109(w), 1025(m), 928(m), 829(s), 790(m), 773(m), 729(w), 698(w), 568(w), 518(w). ESI-MS (+): *m/z* calcd. for ($M+H^+$) $C_{34}H_{28}FO_4^+$ 519.1967 found 519.1948.

(4-Bromophenyl)(4,4"-dibromo-5'-(thiophen-2-yl)-[1,1':3',1"-terphenyl]-2'-yl)methanone (**1t**): White solid (0.36 g, 65%). mp 215-217 °C; ^{1}H NMR (600 MHz, $CDCl_3$) δ 7.62 (s, 2H), 7.59 – 7.52 (m, 1H), 7.44 (d, *J* = 3.3 Hz, 1H), 7.37 (m, 8H), 7.14 (d, *J* = 7.6 Hz, 5H); ^{13}C NMR (150 MHz, $CDCl_3$) δ 197.2, 142.6, 140.5, 138.5, 136.6, 136.4, 135.8, 132.4, 131.9, 131.6, 130.8, 128.8, 128.5, 126.6, 126.4, 124.6, 122.4; IR (cm^{-1}) ATR mode: 1661(s), 1580(s), 1485(s), 1390(m), 1266(m), 1069(s), 1009(s), 924(m), 820(s), 778(m), 702(s), 554(m), 524(m), 467(m), 454(w), 419(w). ESI-MS (+): *m/z* calcd. for ($M+H^+$) $C_{29}H_{18}Br_3OS^+$ 652.8603 found 652.8534.

Pyridin-2-yl(2,4,6-tri(pyridin-2-yl)phenyl)methanone (**1u**): Brown solid (0.32 g, 57%). mp 223 -225 °C; ^{1}H NMR (600 MHz, $CDCl_3$) δ 8.74 (dd, *J* = 4.9, 0.9 Hz, 1H), 8.41 (s, 2H), 8.33 (dd, *J* = 4.8, 0.8 Hz, 1H), 8.28 (dd, *J* = 4.9, 0.9 Hz, 2H), 7.96 (d, *J* = 7.9 Hz, 1H), 7.91 (d, *J* = 7.9 Hz, 1H), 7.80 (td, *J* = 7.7, 1.8 Hz, 1H), 7.68 – 7.65 (m, 3H), 7.61 (td, *J* = 7.7, 1.8 Hz, 2H), 7.29 (m, 1H), 7.14 (m, 1H), 7.03 (m, 2H); ^{13}C NMR (150 MHz, $CDCl_3$) δ 197.4, 157.6, 156.30, 155.9, 149.9, 148.8, 148.6, 141.4, 140.2, 139.6, 137.0, 136.4, 136.3, 127.9, 125.3, 123.1, 122.8, 122.2, 121.9, 121.0; IR (cm^{-1}) ATR mode: 3074(w), 3049(w), 3008(w), 1677(s), 1584(s), 1471(s), 1439(m), 1233(m), 1155(m), 1092(m), 1049(w), 991(s), 900(m), 780(s), 759(s), 744(s), 695(s), 656(m), 618(m), 597(m), 562(m), 505(m), 407(m). ESI-MS (+): *m/z* calcd. for ($M+H^+$) $C_{27}H_{19}N_4O^+$ 415.1554 found 415.1573.

Phenyl(5'-(pyren-1-yl)-[1,1':3',1"-terphenyl]-2'-yl)methanone (**1v**): Yellow solid (0.43 g, 58%); mp 185-187 °C; ^{1}H NMR (600 MHz, $CDCl_3$) δ 8.38 (d, *J* = 8.8 Hz, 1H), 8.27 (d, *J* = 7.7 Hz, 1H), 8.22 (d, *J* = 7.5 Hz, 1H), 8.20 (d, *J* = 7.5 Hz, 1H), 8.12 (m, 4H), 8.03 (t, *J* = 7.6 Hz, 1H),

7.76 (s, 2H), 7.68 (d, *J* = 7.6 Hz, 2H), 7.39 (d, *J* = 7.6 Hz, 4H), 7.36 (d, *J* = 7.3 Hz, 1H), 7.22 (m, 8H); ^{13}C NMR (150 MHz, $CDCl_3$) δ 199.1, 142.3, 141.2, 140.2, 138.4, 137.2, 136.5, 132.9, 131.6, 131.5, 131.1, 131.0, 129.6, 129.4, 129.2, 128.6, 128.3, 128.2, 128.1, 127.9, 127.8, 127.6, 126.3, 125.5, 125.2, 125.2, 125.1, 125.0, 124.9; IR (cm^{-1}) ATR mode: 3036(w), 2955(w), 2916(w), 2845(w), 1666(s), 1594(s), 1492(m), 1446(m), 1310(w), 1260(m), 1148(w), 1028(w), 929(m), 845(s), 825(m), 781(m), 698(w), 563(w), 506(w). ESI-MS (+): *m*/*z* calcd. for ($M+H^+$) $C_{41}H_{27}O^+$ 535.2057 found 535.2062.

(3,3"-dimethoxy-5'-phenyl-[1,1':3',1"-terphenyl]-2'-yl)(3-methoxyphenyl)methanone(**1w**): Colorless liquid (0.25 g, 46%); ^{1}H NMR (400 MHz, $CDCl_3$) δ 7.71 (d, *J* = 7.0 Hz, 2H), 7.68 (s, 2H), 7.48 (t, *J* = 7.5 Hz, 2H), 7.41 (d, *J* = 7.3 Hz, 1H), 7.30 (t, *J* = 7.0 Hz, 1H), 7.22 (d, *J* = 7.6 Hz, 1H), 7.18 – 7.15 (m, 2H), 7.13 (d, *J* = 2.0 Hz, 1H), 7.11 (d, *J* = 2.1 Hz, 1H), 6.91 (s, 1H), 6.90 (s, 1H), 6.86 – 6.84 (m, 2H), 6.75 (dd, *J* = 2.6, 0.8 Hz, 1H), 6.74 – 6.72 (m, 1H), 3.72 (s, 3H), 3.65 (s, 6H); ^{13}C NMR (100 MHz, $CDCl_3$) δ 198.7, 159.4, 159.2, 142.0, 141.7, 141.3, 140.1, 139.7, 137.2, 129.3, 129.1, 129.1, 128.1, 127.9, 127.4, 122.9, 121.8, 119.7, 114.5, 113.8, 112.9, 55.5, 55.2; IR (cm^{-1}) ATR mode:3056(w), 2998(w), 2935(m), 1667(m), 1595(s), 1579(s), 1496(m), 1464(m), 1429(w), 1389(w), 1317(w), 1271(s), 1224(m), 1180(w), 1134(w), 1044(m), 977(w), 765(m), 740(m), 700(s). ESI-MS (+): *m*/*z* calcd. for ($M+H^+$) $C_{34}H_{29}O_4^+$ 501.2061 found 501.2074.

References:

[1] (a) P. Finkbeiner, K. Murai, M. Röpke, R. Sarpong, *J. Am. Chem. Soc.* **2017**, *139*, 11349–11352; (b) N. Asao, H. Aikawa, Y. Yamamoto, *J. Am. Chem. Soc.* **2004**, *126*, 7458–7459; (c) S. J. Hein, D. Lehnherr, W. R. Dichtel, *Chem. Sci.* **2017**, *8*, 5675–5681; (d) H. Arslan, F. J. Uribe-Romo, B. J. Smith, W. R. Dichtel, *Chem. Sci.* **2013**, *4*, 3973–3978; (e) M. Parameshwar, M. K. R. Singam, A. Nagireddy, J. B. Nanubolu, M. S. Reddy, *Chem. Commun.* **2020**, *56*, 13457–13460; (f) X. Xin, Y. Wang, W. Xu, Y. Lin, H. Duan, D. Dong, *Green Chem.* **2010**, *12*, 893–898.

[2] (a) Y. Izawa, D. Pun, S. S. Stahl, *Science* **2011**, *333*, 209–213; (b) Z. Xi, *J. Am. Chem. Soc.* **1998**, *120*, 1672–1680; (c) M. Shanmugasundaram, M. S. Wu, M. Jeganmohan, C. W. Huang, C. H. Cheng, *J. Org. Chem.* **2002**, *67*, 7724–7729; (d) W. A. L. Van Otterlo, C. B. De Koning, *Chem. Rev.* **2009**, *109*, 3743–3782; (e) D. Simoni, G. Giannini, M. Roberti, R. Rondanin, R. Baruchello, M. Rossi, G. Grisolia, F. P. Invidiata, S. Aiello, S.

Marino, S. Cavallini, A. Siniscalchi, N. Gebbia, L. Crosta, S. Grimaudo, V. Abbadessa, A. Di Cristina, M. Tolomeo, *J. Med. Chem.* **2005**, *48*, 4293–4299; (f) A. Kamal, M. Kashi Reddy, T. B. Shaik, Rajender, Y. V. V. Srikanth, V. Santhosh Reddy, G. Bharath Kumar, S. V. Kalivendi, *Eur. J. Med. Chem.* **2012**, *50*, 9–17; (g) G. Yu, J. Gao, J. C. Hummelen, F. Wudl, A. J. Heeger, *Science* **1995**, *270*, 1789–1791; (h) B. S. Udayakumar, G. B. Schuster, *J. Org. Chem.* **1992**, *57*, 348–352.

[3] (a) S. Saito, Y. Yamamoto, *Chem. Rev.* **2000**, *100*, 2901–2915; (b) T. Shibata, T. Fujimoto, K. Yokota, K. Takagi, *J. Am. Chem. Soc.* **2004**, *126*, 8382–8383; (c) D. H. Dethe, A. Uike, N. C. Beeralingappa, *Org. Lett.* **2024**, *26*, 2013–2017; (d) K. Tanaka, G. Nishida, A. Wada, K. Noguchi, *Angew. Chemie* **2004**, *116*, 6672–6674; (e) A. Gutnov, B. Heller, C. Fischer, H. J. Drexler, A. Spannenberg, B. Sundermann, C. Sundermann, *Angew. Chemie - Int. Ed.* **2004**, *43*, 3795–3797.

[4] (a) Q. Zhao, C. Peng, G. Zhan, B. Han, *RSC Adv.* **2020**, *10*, 40983–41003; (b) H. Wang, S. Li, X. Wu, T. Chen, W. Liu, X. Liu, H. Cao, *Org. Lett.* **2024**, *26*, 9648–9653 DOI 10.1021/acs.orglett.4c03299; (c) D. S. Davas, D. K. Gopalakrishnan, K. Bar, S. Kumar, T. Karmakar, J. Vaitla, *Org. Lett.* **2023**, *25*, 8992–8996; (d) S. He, J. Wang, J. Zheng, Q. Q. Luo, H. Leng, S. Zheng, C. Peng, B. Han, G. Zhan, *New J. Chem.* **2022**, *46*, 11617–11622; (e) P. Zhou, J. Y. Wang, T. S. Zhang, G. Li, W. J. Hao, S. J. Tu, B. Jiang, *Chem. Commun.* **2017**, *54*, 164–167; (f) K. B. Somai Magar, L. Xia, Y. R. Lee, *Chem. Commun.* **2015**, *51*, 8592–8595.

[5] (a) G. Illuminati, H. Gilman, *J. Am. Chem. Soc.* **1952**, *74*, 2896–2899; (b) W. J. Coates, A. McKillop, *J. Org. Chem.* **1990**, *55*, 5418–5420.

[6] (a) S. M. Bonesi, M. Fagnoni, A. Albini, *Angew. Chemie - Int. Ed.* **2008**, *47*, 10022–10025; (b) D. G. Yu, M. Yu, B. T. Guan, B. J. Li, Y. Zheng, Z. H. Wu, Z. J. Shi, *Org. Lett.* **2009**, *11*, 3374–3377; (c) J. L. Gustafson, D. Lim, K. T. Barrett, S. J. Miller, *Angew. Chemie - Int. Ed.* **2011**, *50*, 5125–5129; (d) F. Zhao, Y. F. Zhang, J. Wen, D. G. Yu, J. B. Wei, Z. Xi, Z. J. Shi, *Org. Lett.* **2013**, *15*, 3230–3233.

[7] (a) K. P. C. Vollhardt, *Angew. Chemie Int. Ed. English* **1984**, *23*, 539–556; (b) A. Takeda, A. Ohno, I. Kadota, *J. Am. Chem. Soc.* **1997**, *119*, 4547–4548; (c) S. Kotha, E. Brahmachary, K. Lahiri, *European J. Org. Chem.* **2005**, 4741–4767; (d) Y. Yamamoto, T. Arakawa, R. Ogawa, K. Itoh, *J. Am. Chem. Soc.* **2003**, *125*, 12143–12160.

[8] (a) T. R. Hoye, B. Baire, D. Niu, P. H. Willoughby, B. P. Woods, *Nature* **2012**, *490*, 208–211; (b) K. C. Nicolaou, S. A. Snyder, T. Montagnon, G. Vassilikogiannakis, *Angew. Chemie Int. Ed.* **2002**, *41*, 1668–1698.

[9] R. L. Danheiser, S. K. Gee, *J. Org. Chem.* **1984**, *49*, 1672–1674.

[10] C. J. Cramer, *J. Am. Chem. Soc.* **1998**, *120*, 6261–6269.

[11] H. Fischer, P. Hofmann, *Organometallics* **1999**, *18*, 2590–2592.

[12] (a) A. Diallo, Y. L. Zhao, H. Wang, S. S. Li, C. Q. Ren, Q. Liu, *Org. Lett.* **2012**, *14*, 5776–5779; (b) T. N. Poudel, Y. R. Lee, *Org. Lett.* **2015**, *17*, 2050–2053; (c) S. Nagahata, S. Takei, S. Ueno, *J. Org. Chem.* **2022**, *87*, 10377–10384; (d) T. N. Poudel, R. J. I. Tamargo, H. Cai, Y. R. Lee, *Asian J. Org. Chem.* **2018**, *7*, 985–1005.

[13] L. Yin, M. Xu, Y. Wang, H. Xie, Y. Yuan, C. Wang, Y. Jiang, *J. Org. Chem.* **2021**, *86*, 12158-12167.

[14] (a) D. Kunák, M. Mateus, L. Rycek, *European J. Org. Chem.* **2022**, *2022*, 1–5; (b) X. Liu, G. H. Tang, H. Z. Weng, J. S. Zhang, Y. K. Xu, S. Yin, *J. Asian Nat. Prod. Res.* **2018**, *20*, 1123–1128: (c) R. Lapinskaite, H. N. Atalay, Š. Malatinec, S. Donmez, Z. O. Cinar, P. F. Schwarz, A. F. Perhal, I. Císařová, L. Labanauskas, T. M. Karpiński, V. M. Dirsch, T. B. Tumer, L. Rycek, *ChemistrySelect* **2023**, *8*, e202204816.

[15] H. Meerwein, *Ber. Deut. Chem. Ges.*, **1944**, 77, 227-234 DOI 10.1002/cber.19440770316.

Appendix

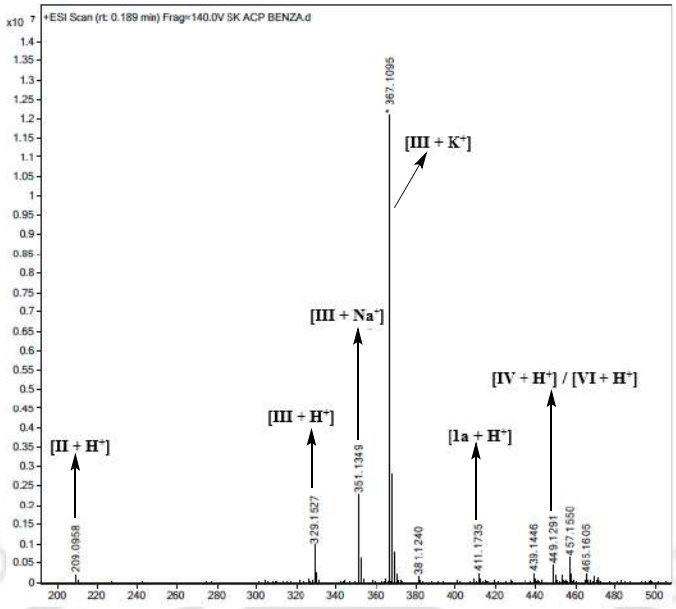

Figure A1. Mass spectrum of quenched reaction mixture of **1a**.

Figure A2. ORTEP diagram (50% probability) of ferrocene diketone.

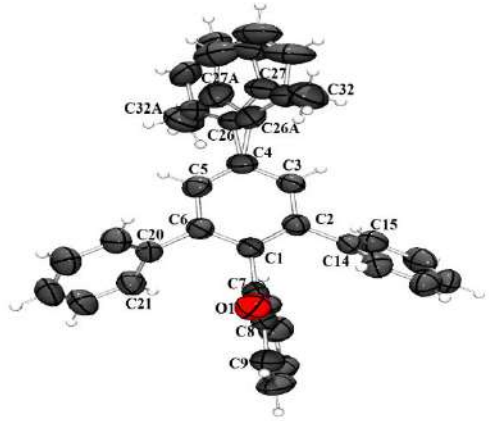

Figure A3. ORTEP diagram (50% probability) of **1b**. 2-Tolyl group was disordered here with occupancy 0.75 in part 1 and 0.25 in part 2.

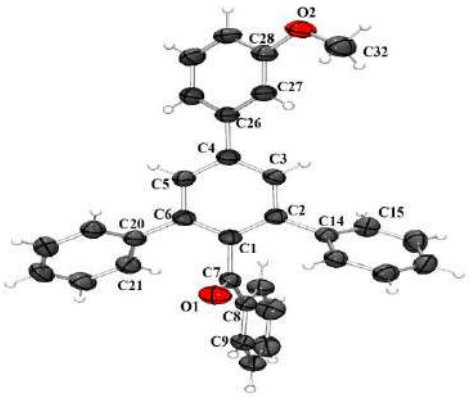

Figure A4. ORTEP diagram (50% probability) of **1k**.

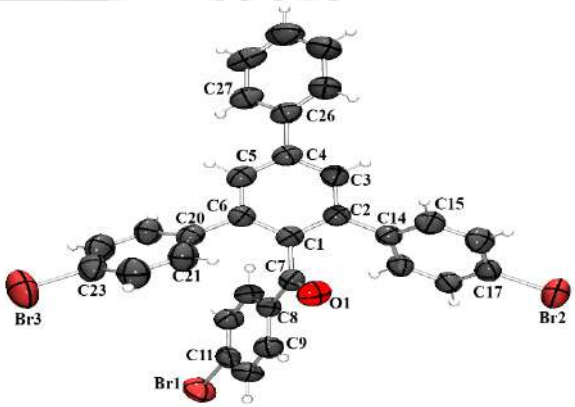

Figure A5. ORTEP diagram (50% probability) of **1m**.

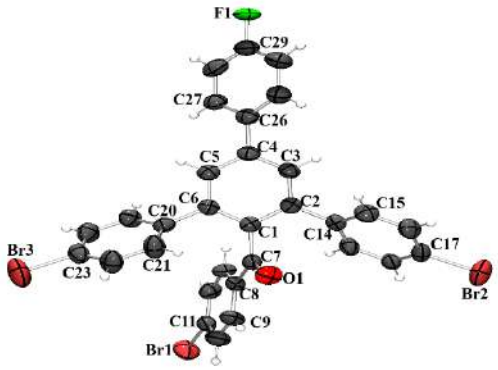

Figure A6. ORTEP diagram (50% probability) of **1n**.

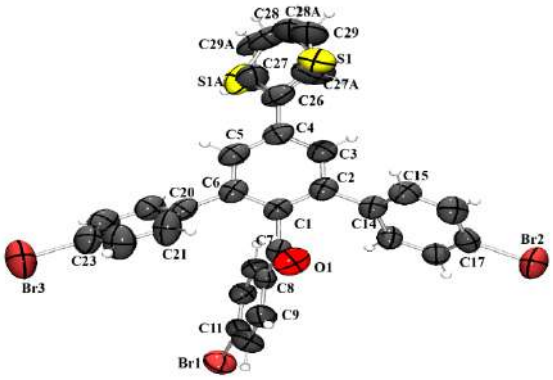

Figure A7. ORTEP diagram (50% probability) of **1t**. 2-Thiophene group was disordered here with occupancy of 0.60 in part 1 and 0.40 in part 2.

Table A1: Crystallographic data and refinement parameters

Entry	**1a**	**1b**
Formula	$C_{65}H_{51}O_2$	$C_{32}H_{24}O$
CCDC No.	2404353	2404354
Mol. wt.	864.05	424.51
Cryst.color, habit	Colorless, needle	Colorless, block
T, K	298	295
Cryst. syst.	Triclinic	monoclinic
Space group	P-1	C2/c
a, Å	10.9347(9)	20.589(7)
b, Å	12.2310(10)	10.146(3)
c, Å	18.5826(16)	24.465(8)
α ,deg	100.465(2)	90
β, deg	93.306(2)	110.932(9)
γ ,deg	92.699(2)	90
V, Å^3	2435.7(4)	4773(3)
Z	2	8
*D*calcd, g cm^{-3}	1.178	1.181
μ, mm^{-1}	0.069	0.070
GOF[a] on F^2	1.044	1.089
F(000)	914.0	1792.0
Reflection	53345	28036
Unique reflections	9911	4155
R_1[b], wR_2[c] (*I* ≥	0.0572, 0.1197	0.0839, 0.1815
R_1[b], wR_2[c] (all data)	0.0942, 0.1437	0.1244, 0.1991

[a]GOF (Goodness-of-fit) = $[\sum[w(F_0^2 - F_c^2)^2] / M - N]^{1/2}$ (M =number of reflections, N = number of parameters refined). [b] $R_1 = \sum \| F_0 | - | Fc \| / \sum | F_0 |$. [c]$wR_2 = [\sum[w(F_0^2 - F_c^2)^2] / \sum[w(F_0^2)^2]]$.

Table A2. Crystallographic data and refinement parameter.

Entry	Ferrocene diketone	**1k**	**1m**	**1n**	**1t**
Formula	$C_{27}H_{22}Br_2FeO_2$	$C_{32}H_{24}O_2$	$C_{62}H_{40}Br_6O_3$	$C_{31}H_{18}Br_3FO$	$C_{29}H_{19}Br_3O_2S$
CCDC No.	2404359	2404355	2404356	2404357	2404358
Mol. wt.	594.11	440.51	1312.40	665.18	671.23
Cryst.color, habit	Red, needle	Colorless, block	Colorless, needle	Colorless, block	Colorless, block
T, K	301	295	300	295	301
Cryst. syst.	Monoclinic	Triclinic	monoclinic	monoclinic	monoclinic
Space group	*P2₁/n*	*P-1*	*P2₁/n*	*P2₁/n*	*P2₁/n*
a, Å	5.7399(3)	8.2577(4)	6.6979(4)	6.6096(4)	6.6541(7)
b, Å	22.0772(11)	8.9317(4)	16.3506(9)	16.3765(10)	16.4813(17)
c, Å	18.4512(9)	17.4681(7)	23.8319(13	24.2811(16)	23.750(3)
α ,deg	90	81.2700(10)	90	90	90
β, deg	93.192(2)	80.7250(10)	96.587	96.556(2)	96.607
γ ,deg	90	70.0320(10)	90	90	90
V, Å^3	2334.5(2)	1188.56(9)	2592.7(3)	2611.1(3)	2587.3(5)
Z	4	2	2	4	4
*D*calcd, g cm^{-3}	1.690	1.231	1.681	1.692	1.723
μ, mm^{-1}	4.091	0.075	4.693	4.665	4.784
GOF[a] on F^2	1.106	1.044	1.094	1.052	1.084
F(000)	1184.0	464.0	1292.0	1304.0	1320.0
Reflection collected	54979	27222	61197	60261	61465
Unique reflections	4133	4138	4554	4615	4536
R_1[b], wR_2[c] *(I ≥ 2σ(I))*	0.0412, 0.0971	0.0394, 0.1006	0.0433, 0.1092	0.0461, 0.1051	0.0583, 0.1589
R_1[b], wR_2[c] (all data)	0.0697, 0.1207	0.0469, 0.1086	0.0827, 0.1353	0.0676, 0.1139	0.0819, 0.1720

[a]GOF (Goodness-of-fit) = $[\sum[w(F_0^2 - F_c^2)^2] / M - N]^{1/2}$ (M =number of reflections, N = number of parameters refined). [b] $R_1 = \sum \| F_0 | - | Fc \| / \sum | F_0 |$. [c]$wR_2 = [\sum[w(F_0^2 - F_c^2)^2] / \sum[w(F_0^2)^2]]$.

^{1}H, ^{13}C, Mass and IR Spectra of compounds 1a-1w

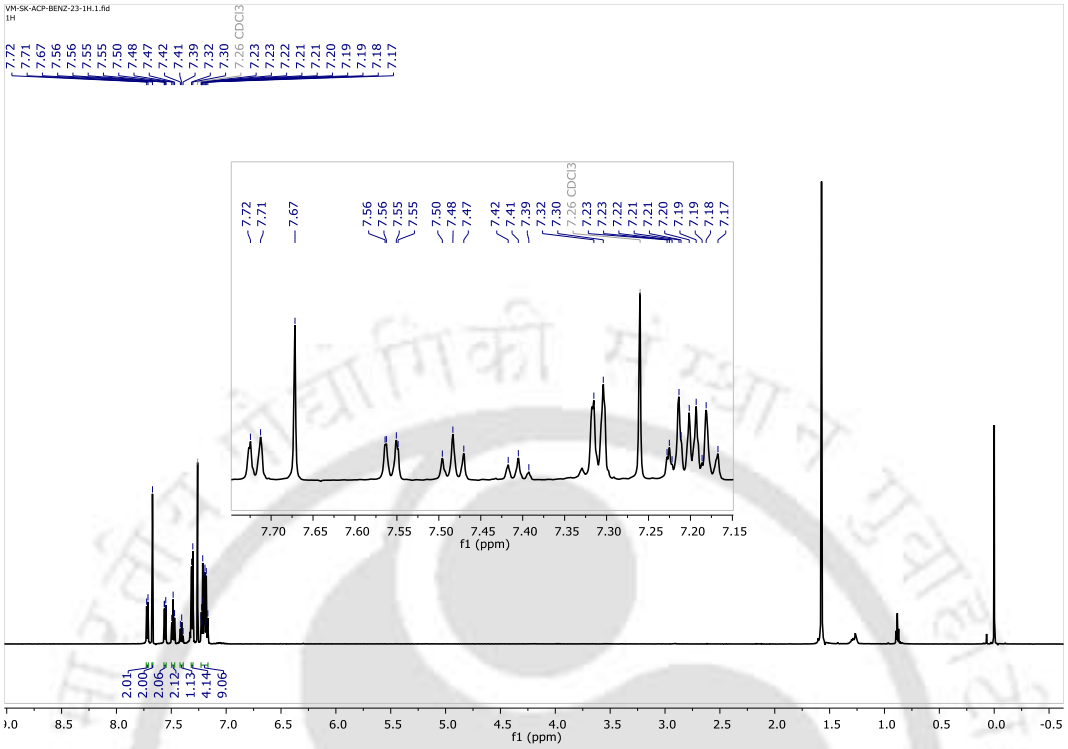

Figure A8. ^{1}H NMR spectrum of **1a**.

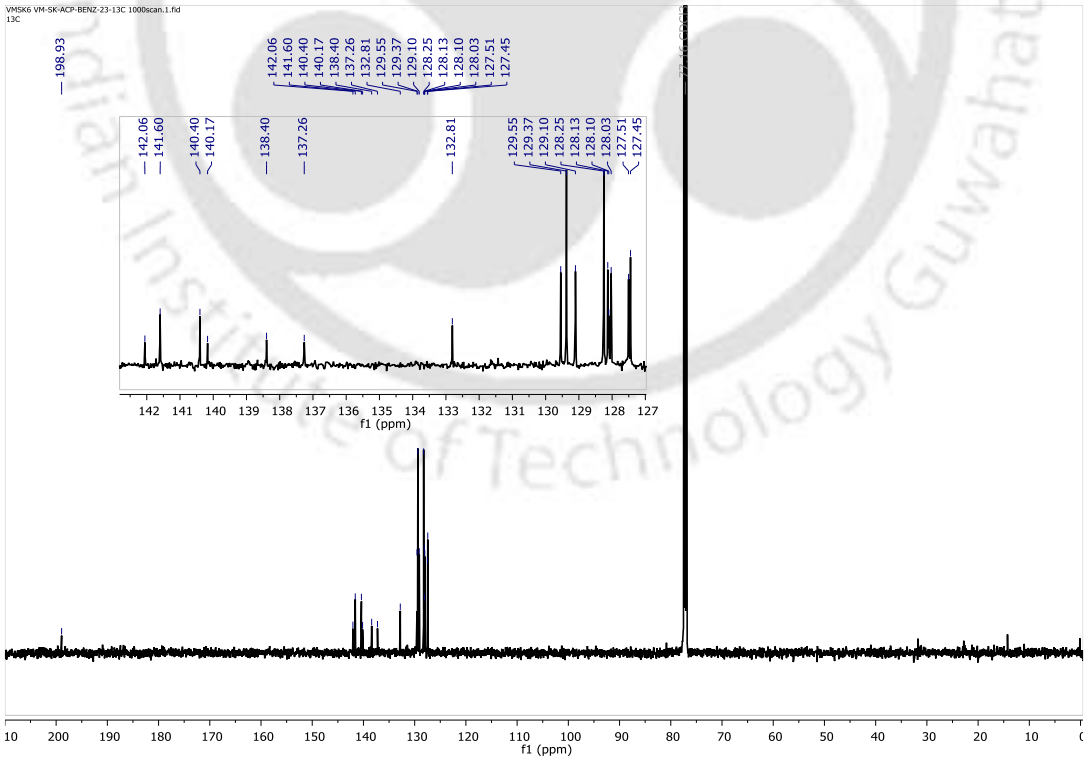

Figure A9. ^{13}C NMR spectrum of **1a**.

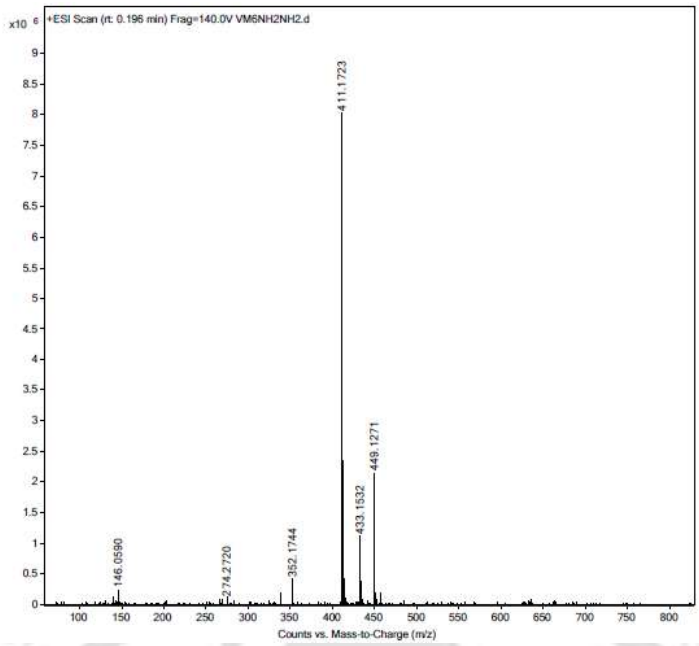

Figure A10. Mass spectrum of **1a**.

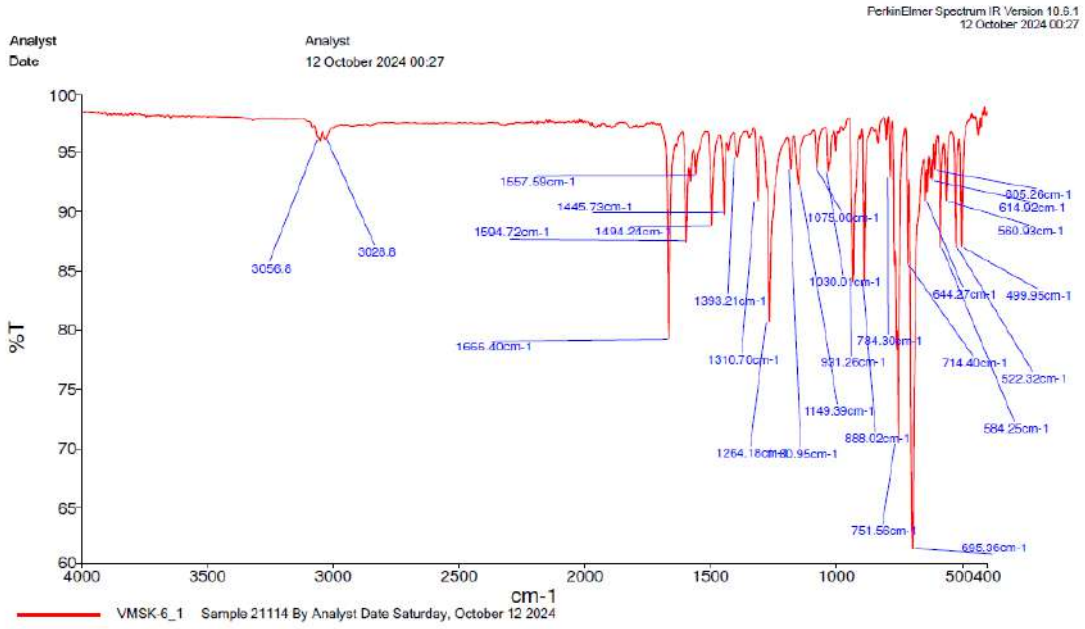

Figure A11. IR spectrum of **1a**

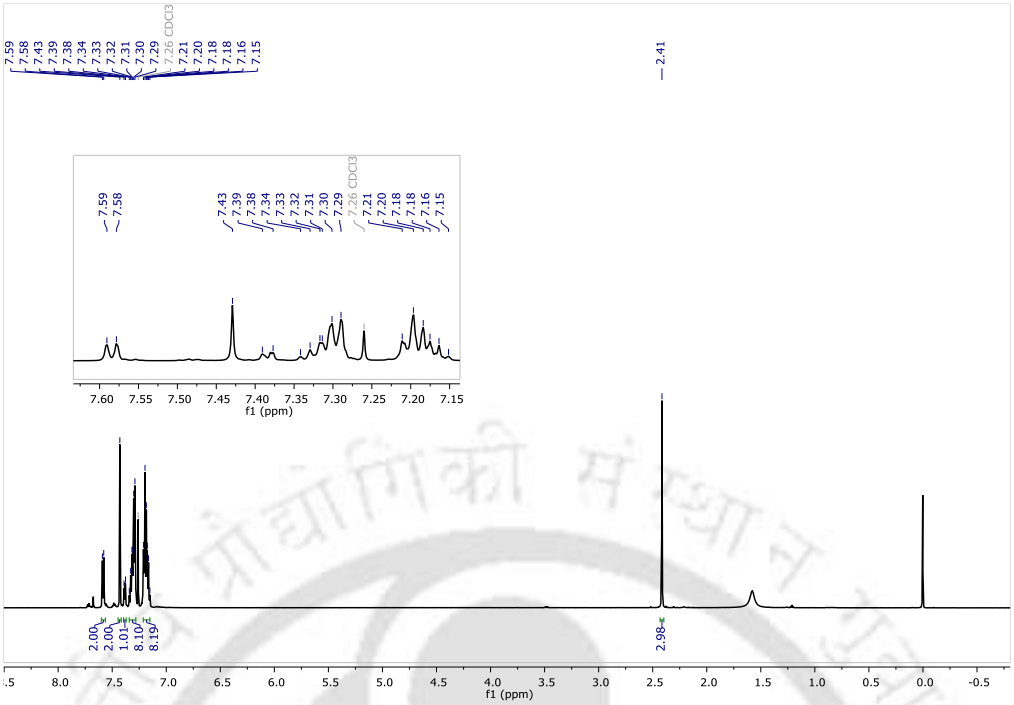

Figure A12. ^{1}H NMR spectrum of **1b**.

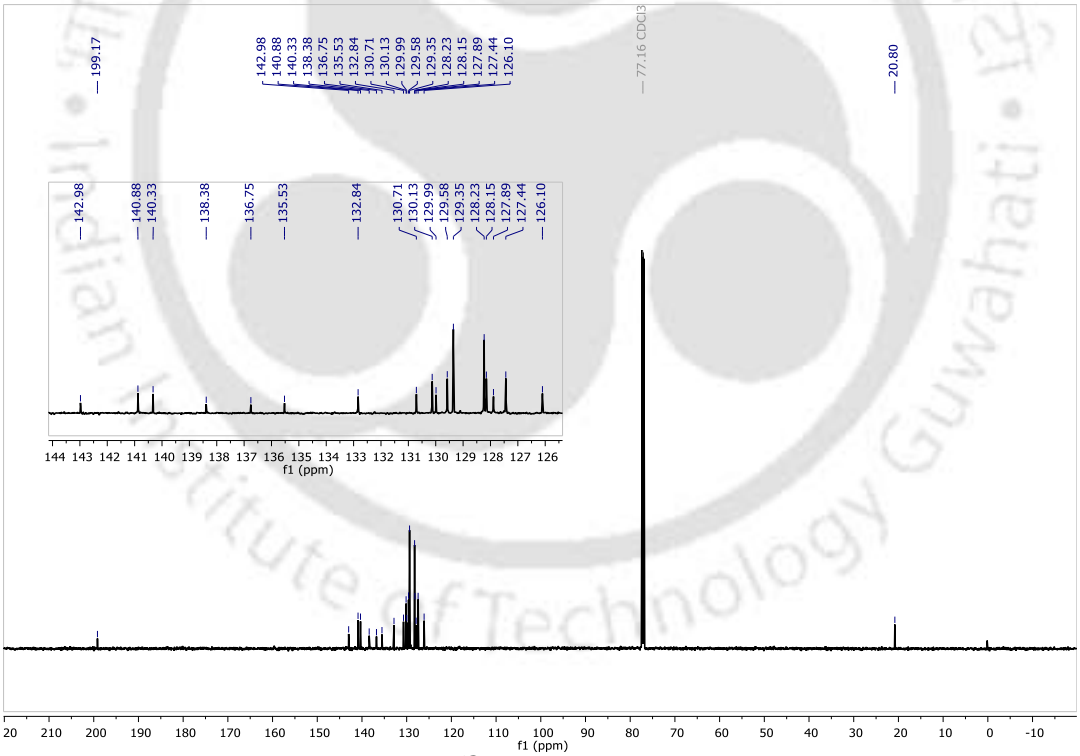

Figure A13. ^{13}C NMR spectrum of **1b**.

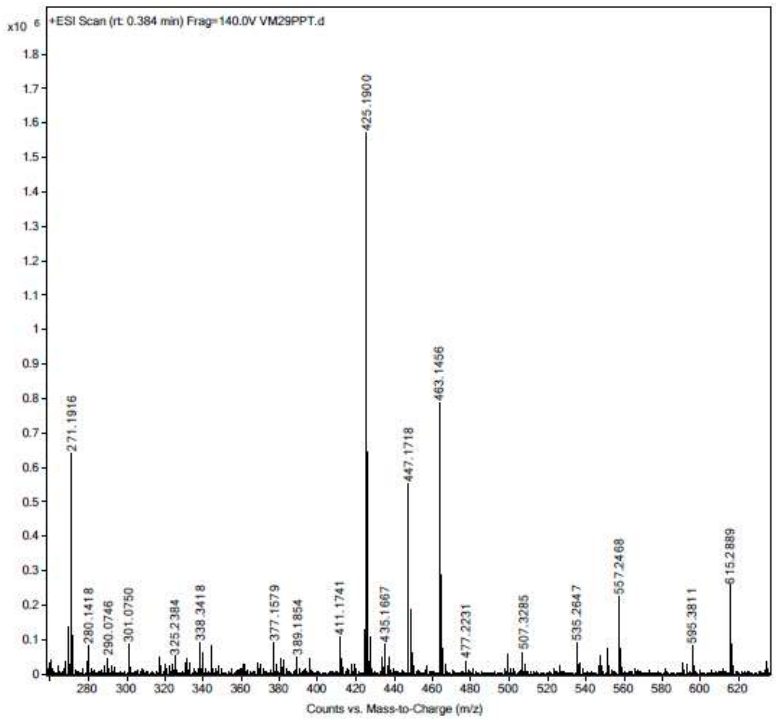

Figure A14. Mass spectrum of **1b**.

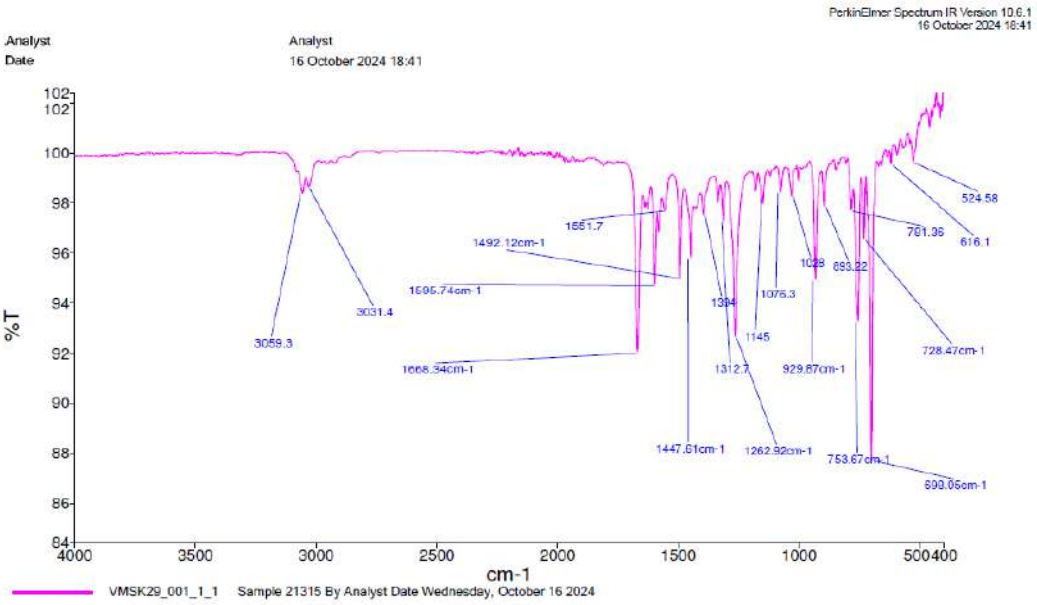

Figure A15. IR spectrum of **1b**

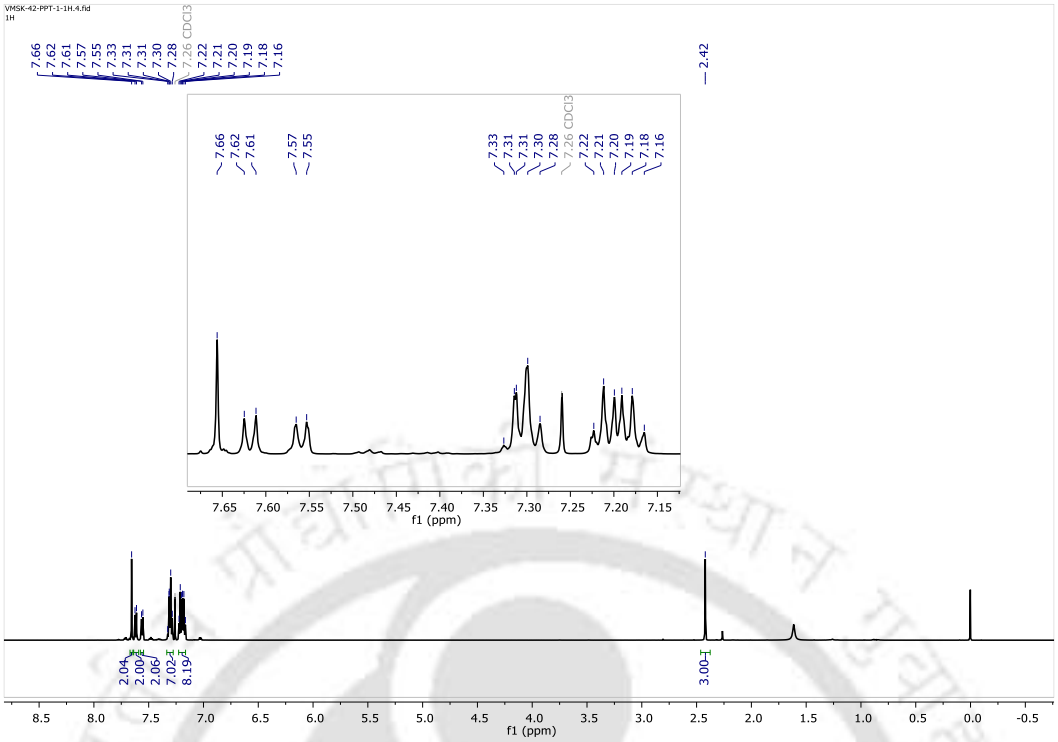

Figure A16. ^{1}H NMR spectrum of **1c**.

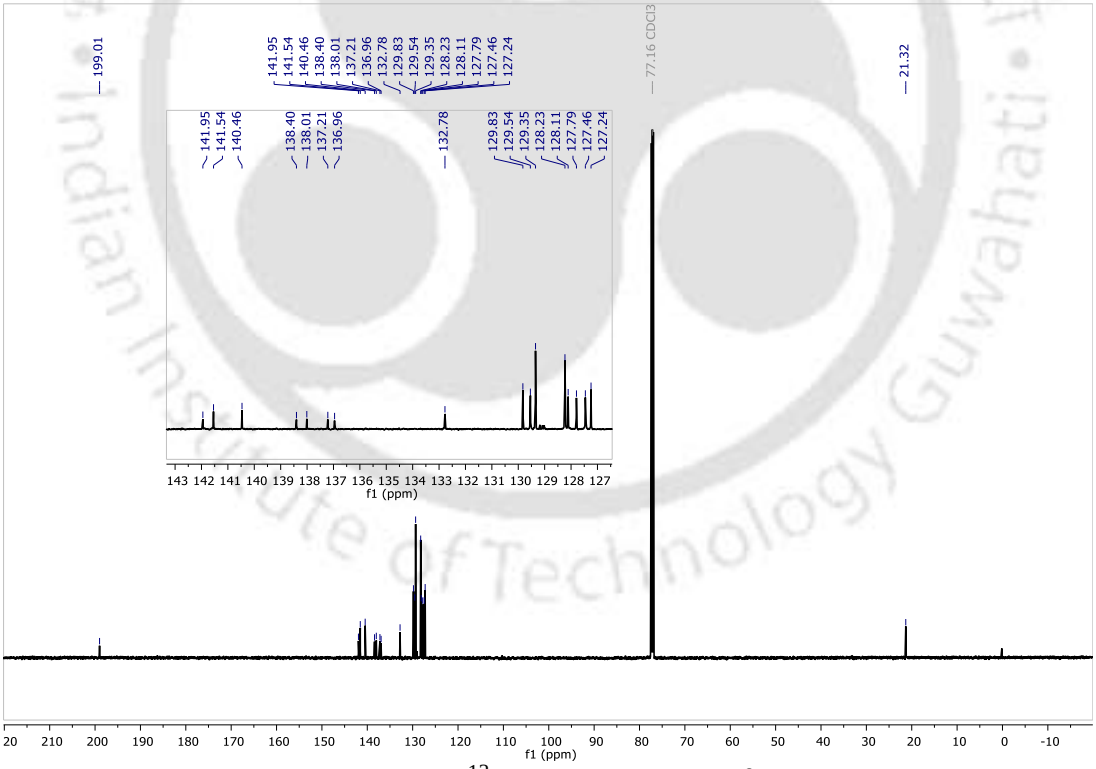

Figure A17. ^{13}C NMR spectrum of **1c**.

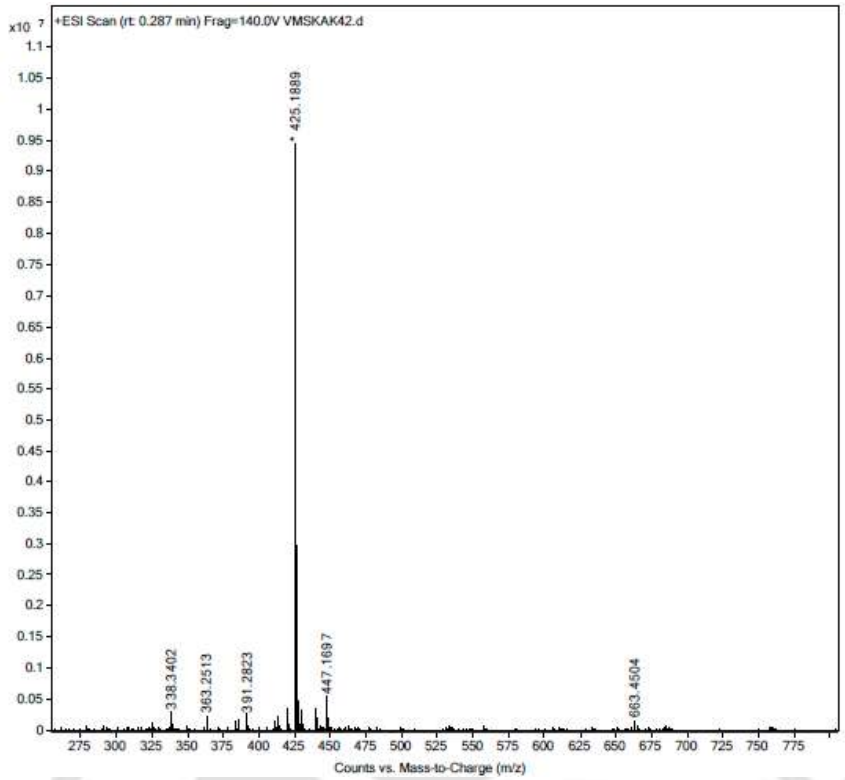

Figure A18. Mass spectrum of **1c**.

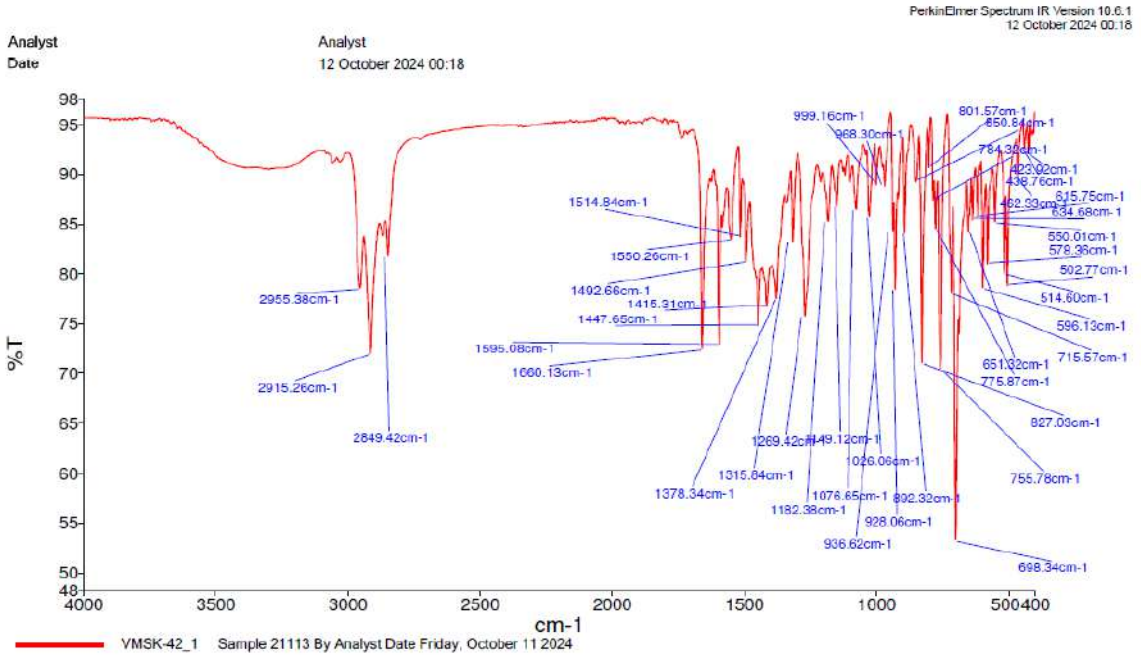

Figure A19. IR spectrum of **1c**

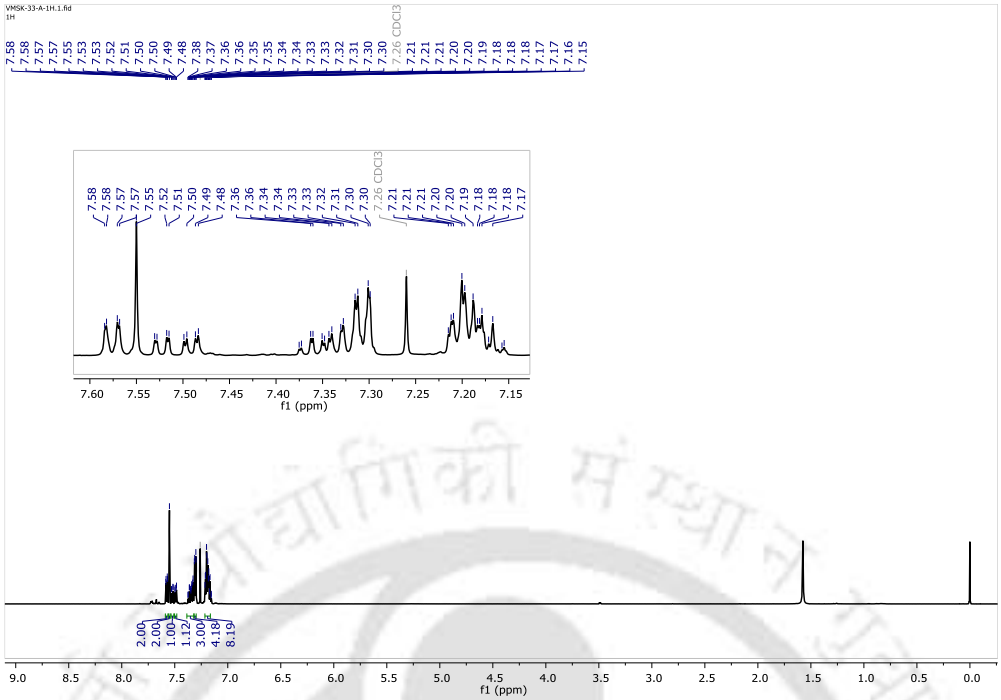

Figure A20. ^{1}H NMR spectrum of **1d**.

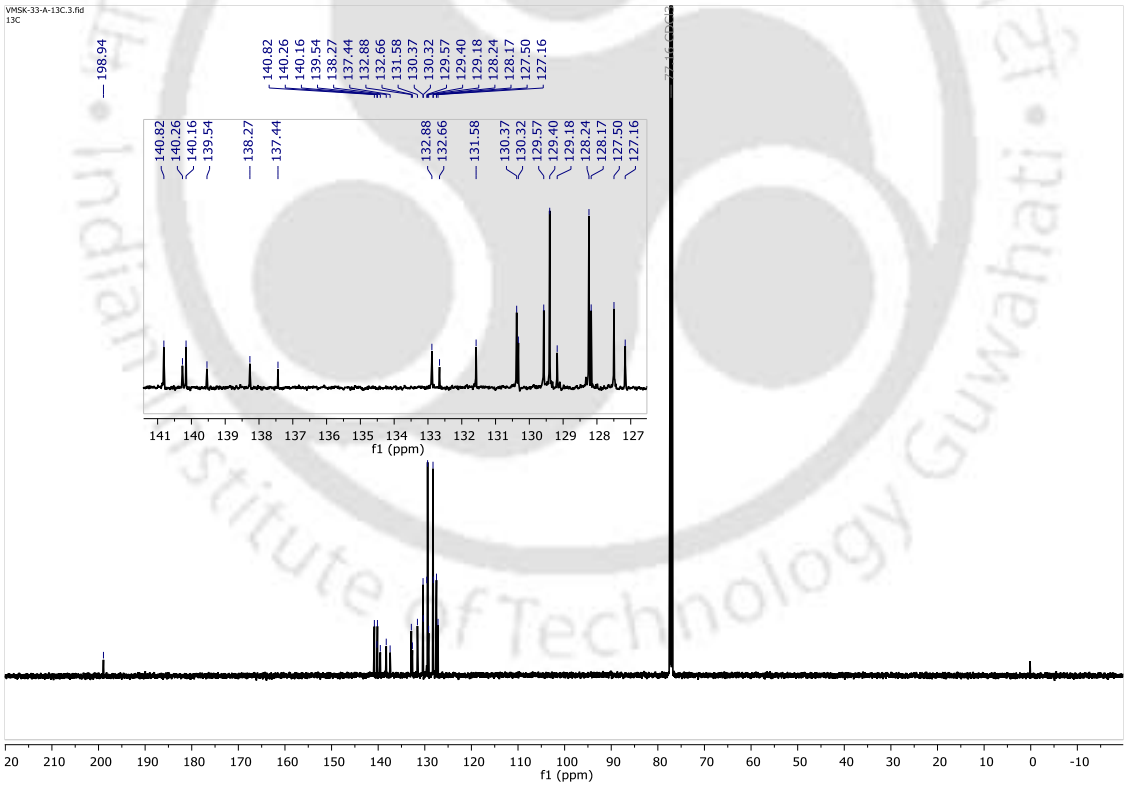

Figure A21. ^{13}C NMR spectrum of **1d**.

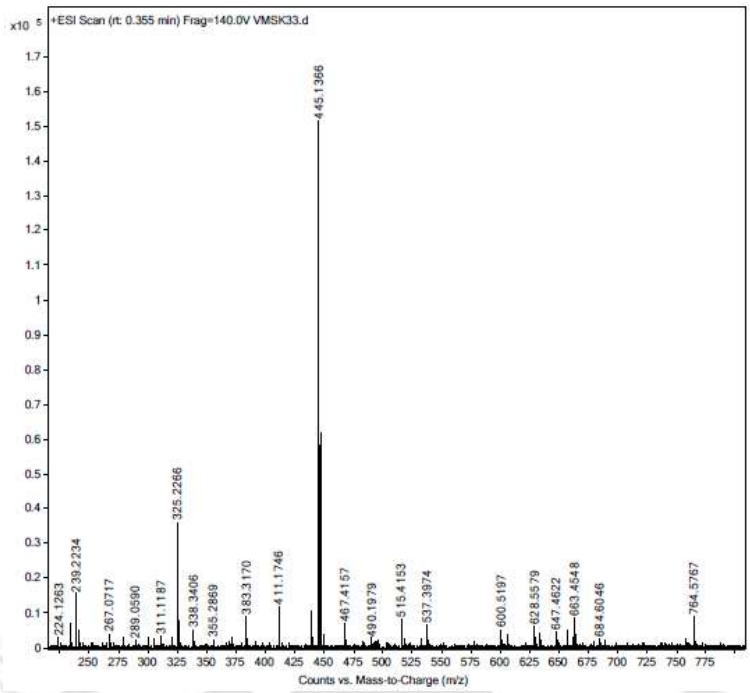

Figure A22. Mass spectrum of **1d**.

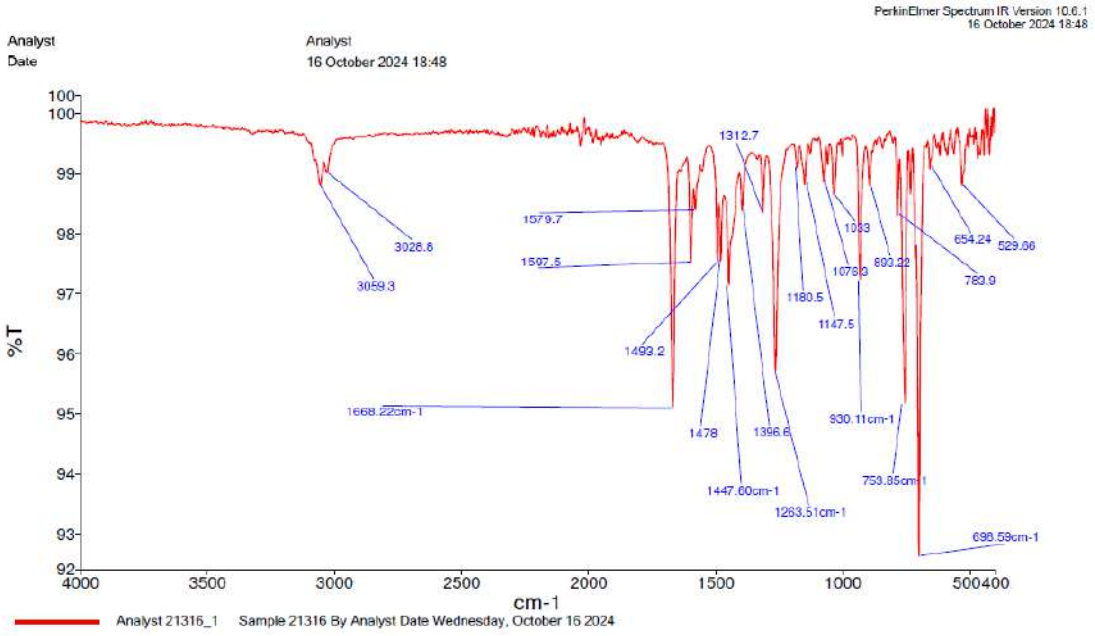

Figure A23. IR spectrum of **1d**

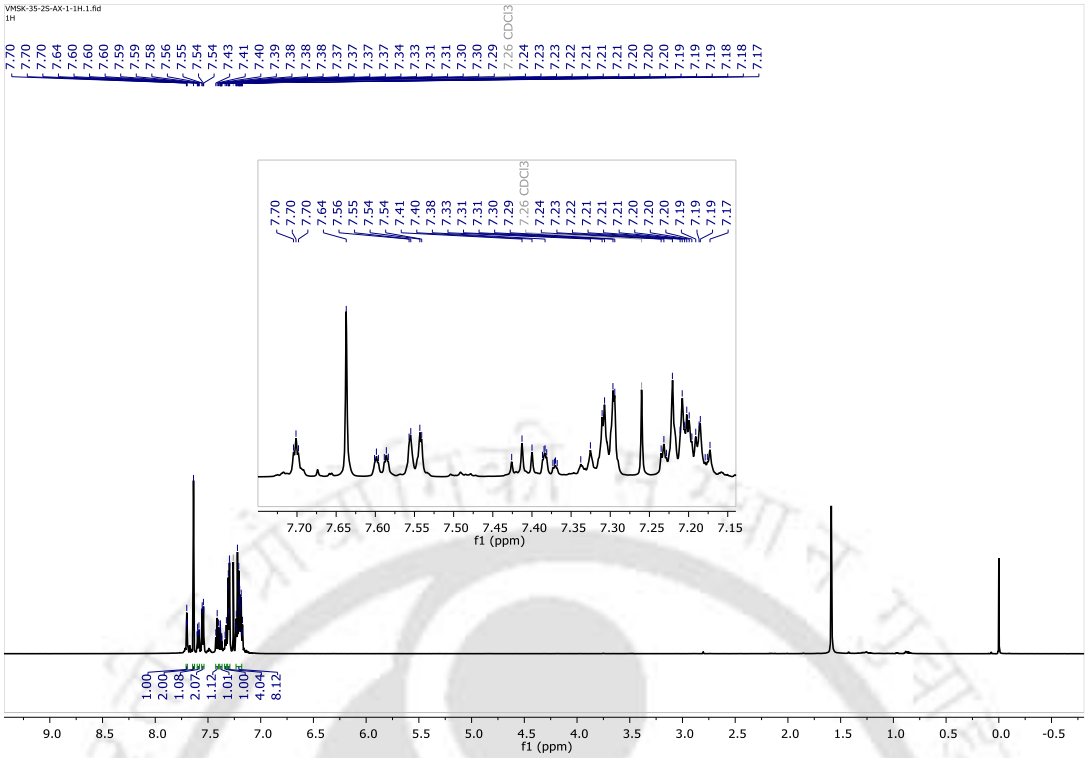

Figure A24. ^{1}H NMR spectrum of **1e**.

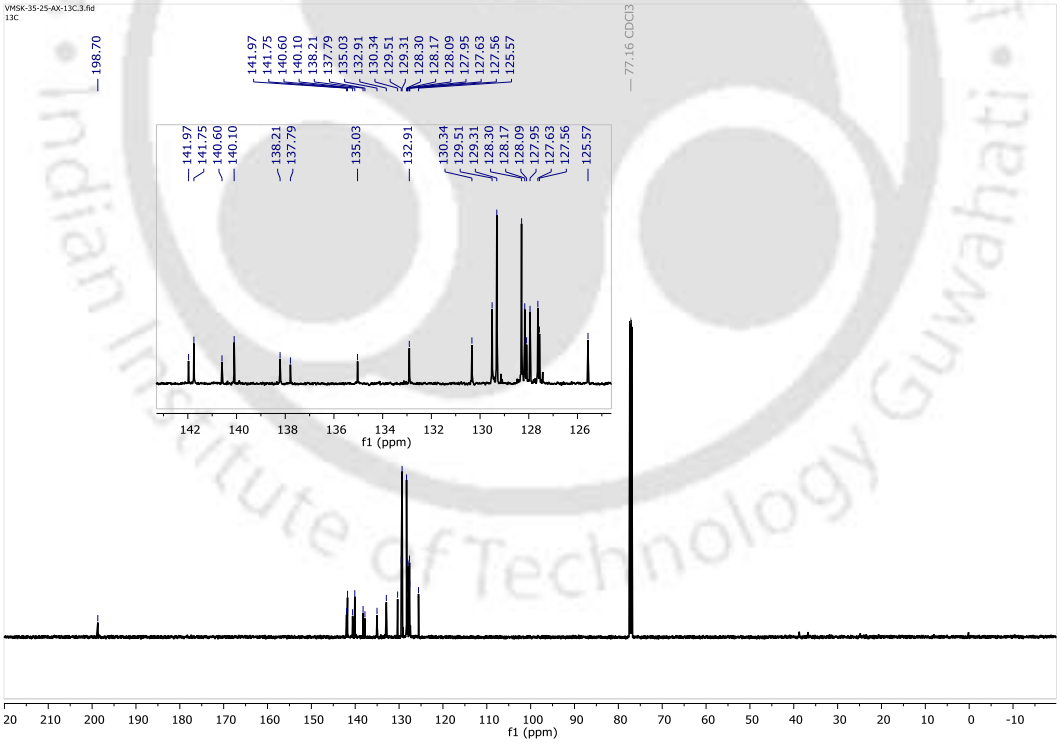

Figure A25. ^{13}C NMR spectrum of **1e**.

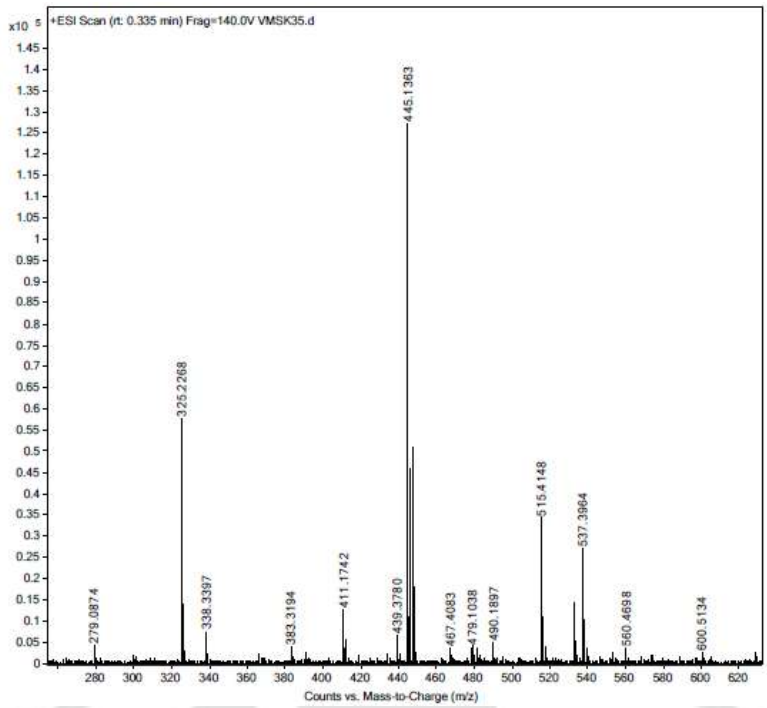

Figure A26. Mass spectrum of **1e**.

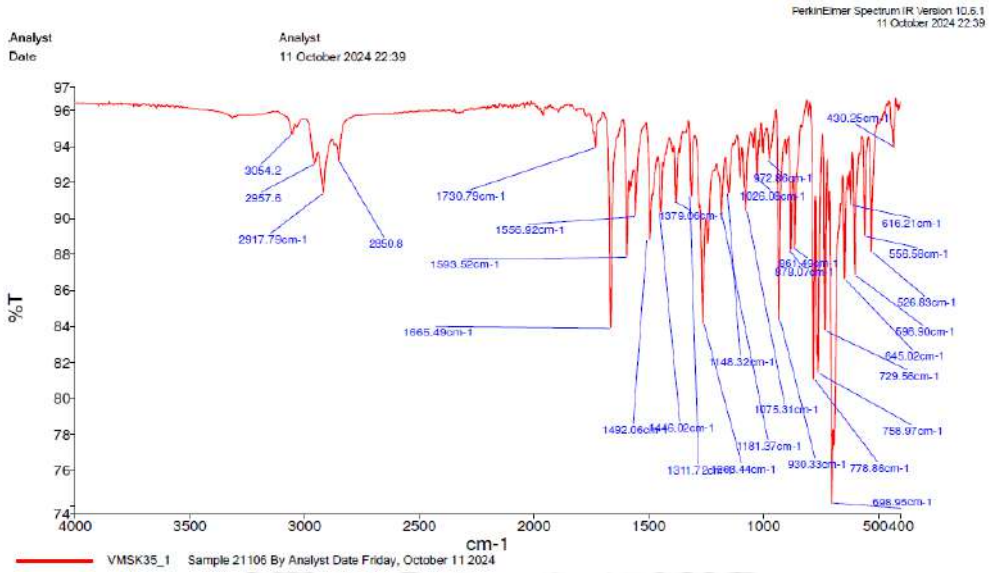

Figure A27. IR spectrum of **1e**

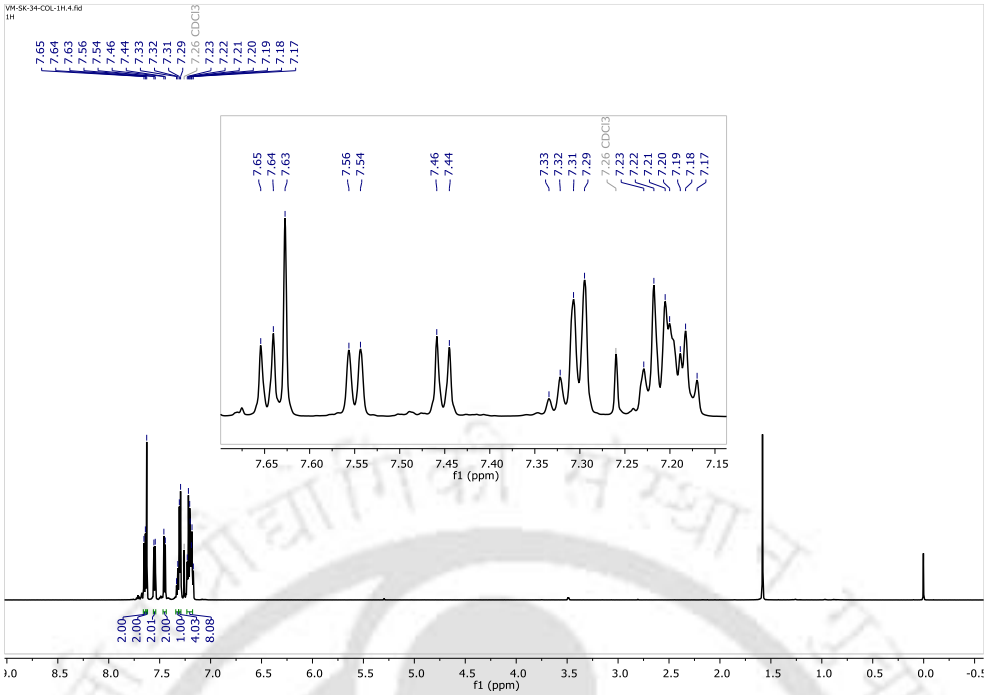

Figure A28. ^{1}H NMR spectrum of **1f**.

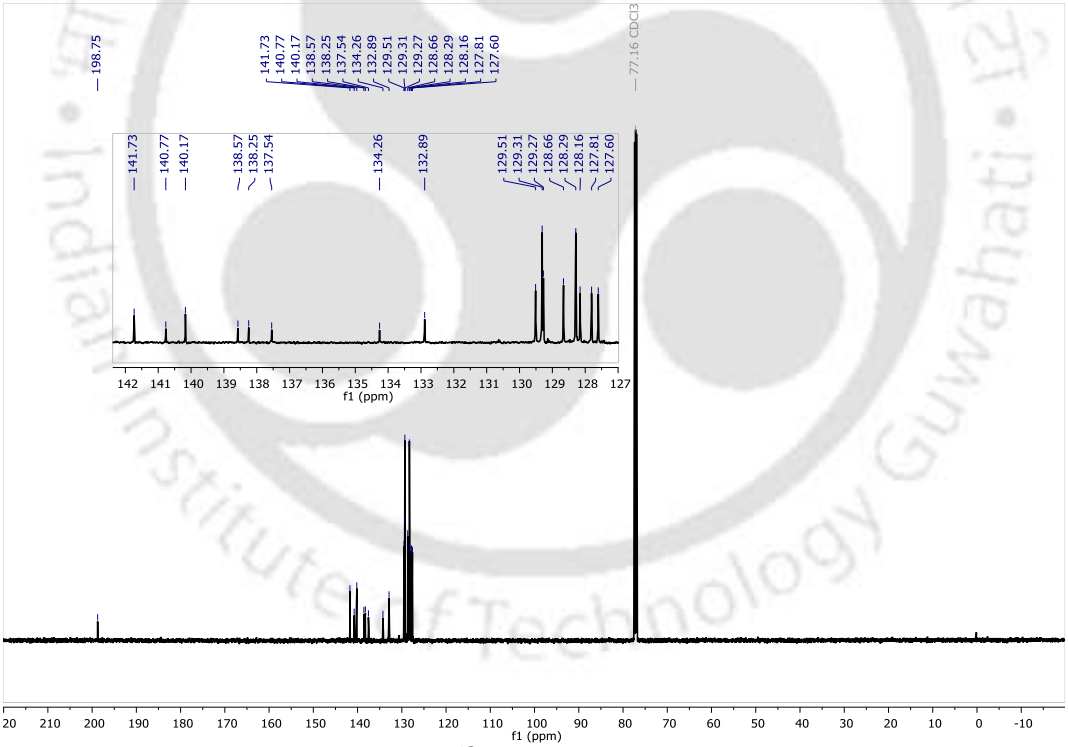

Figure A29. ^{13}C NMR spectrum of **1f**.

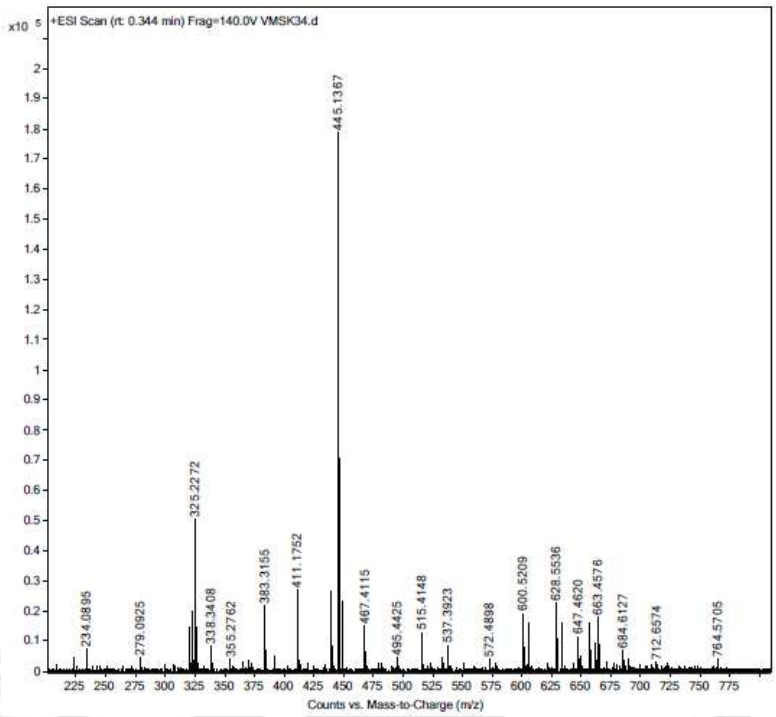

Figure A30. Mass spectrum of **1f**.

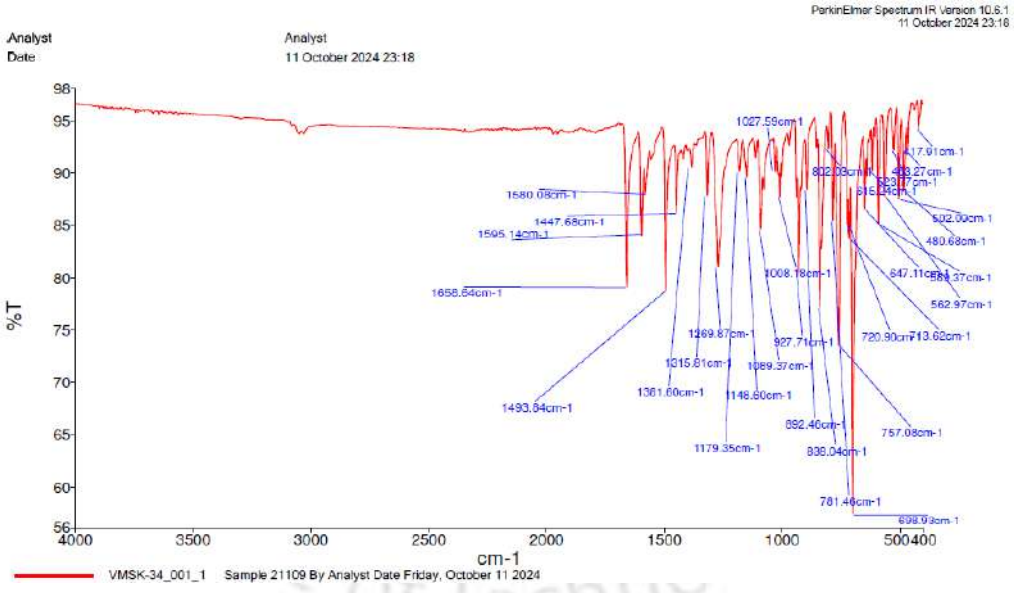

Figure A31. IR spectrum of **1f**.

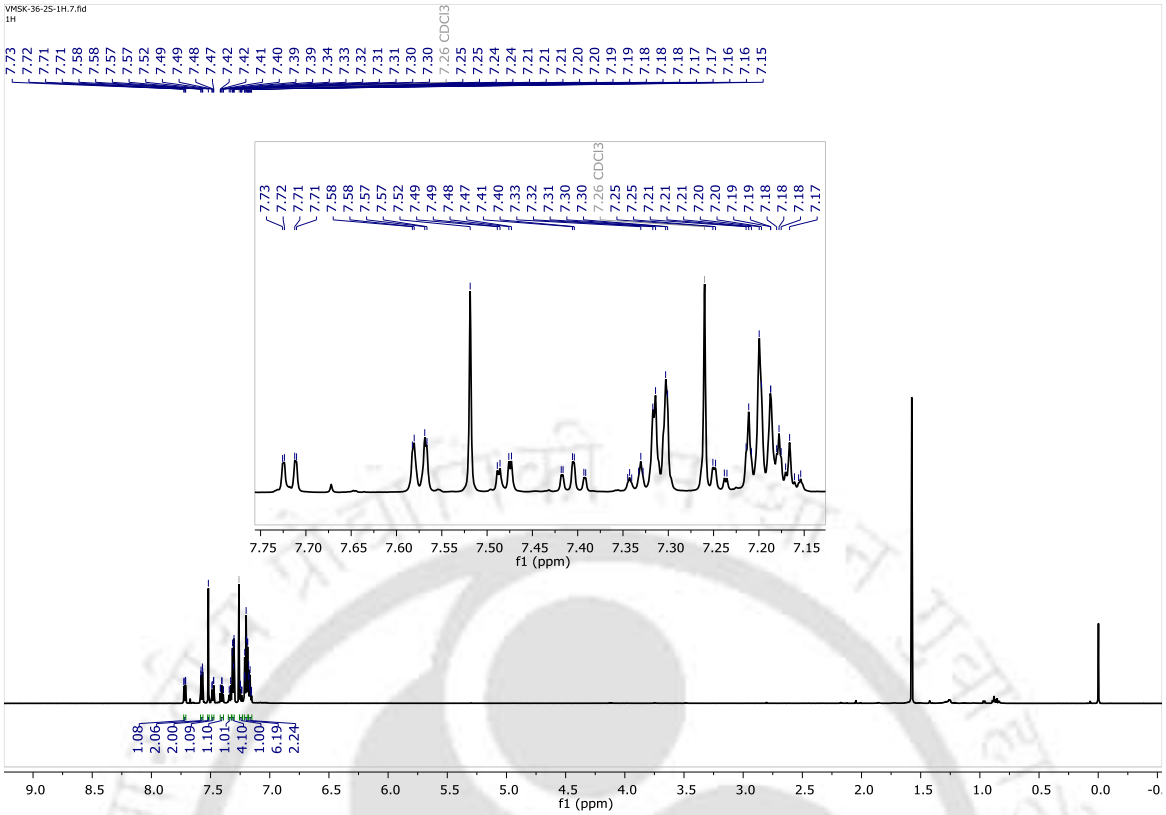

Figure A32. ^{1}H NMR spectrum of **1g**.

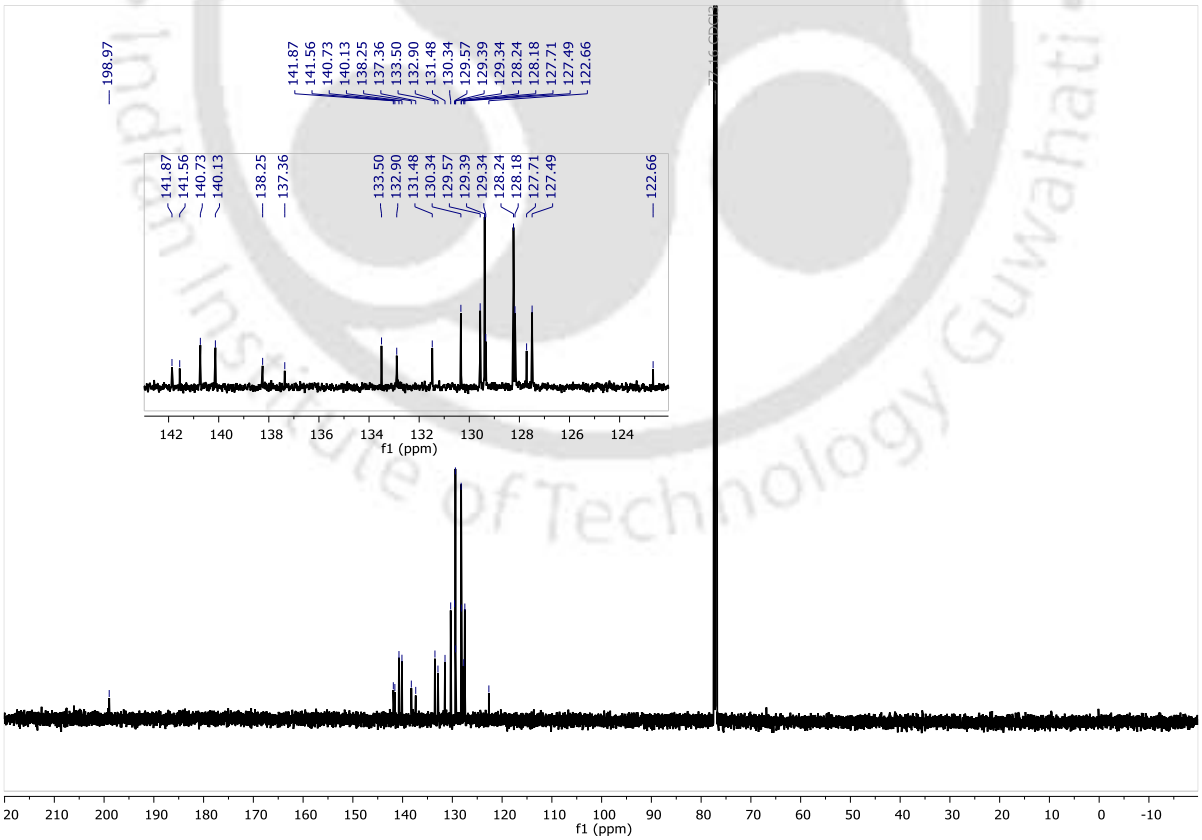

Figure A33. ^{13}C NMR spectrum of **1g**.

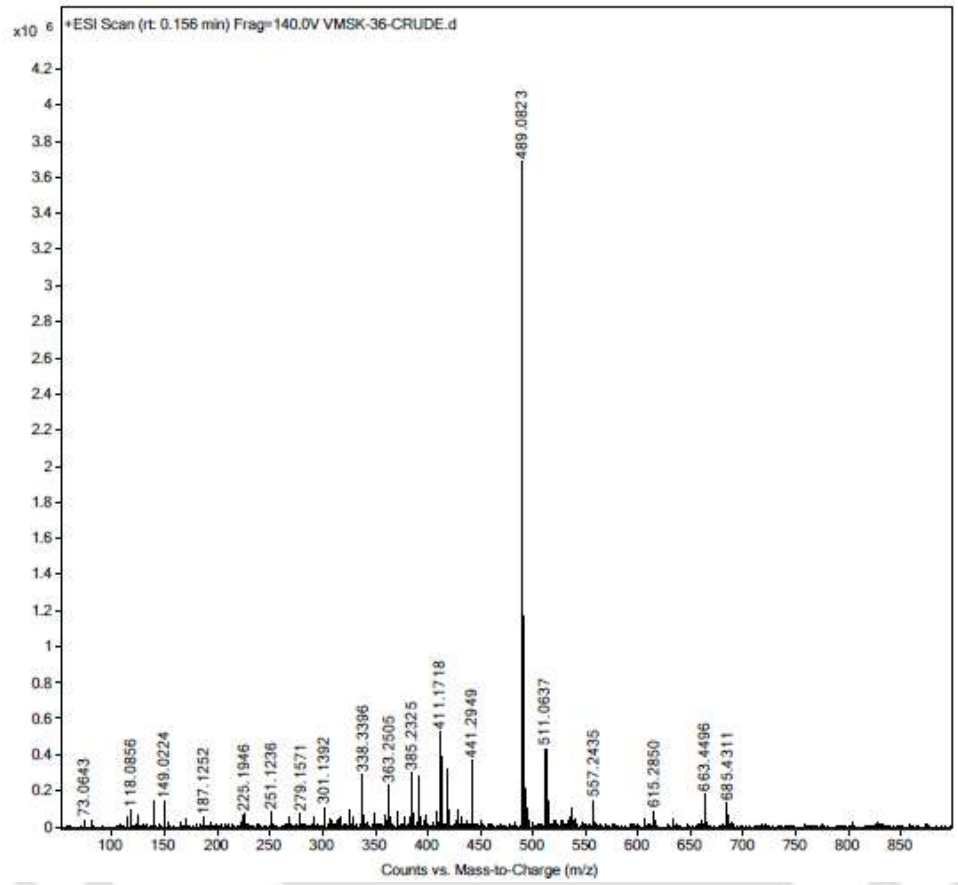

Figure A34. Mass spectrum of **1g**.

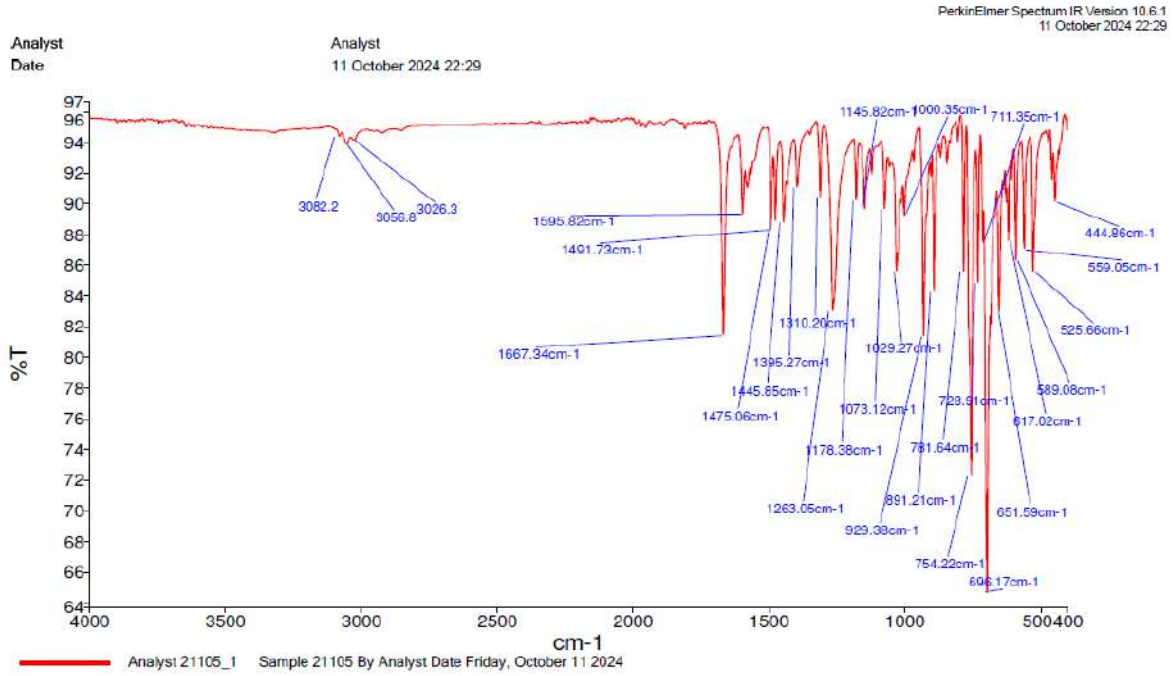

Figure A35. IR spectrum of **1g**.

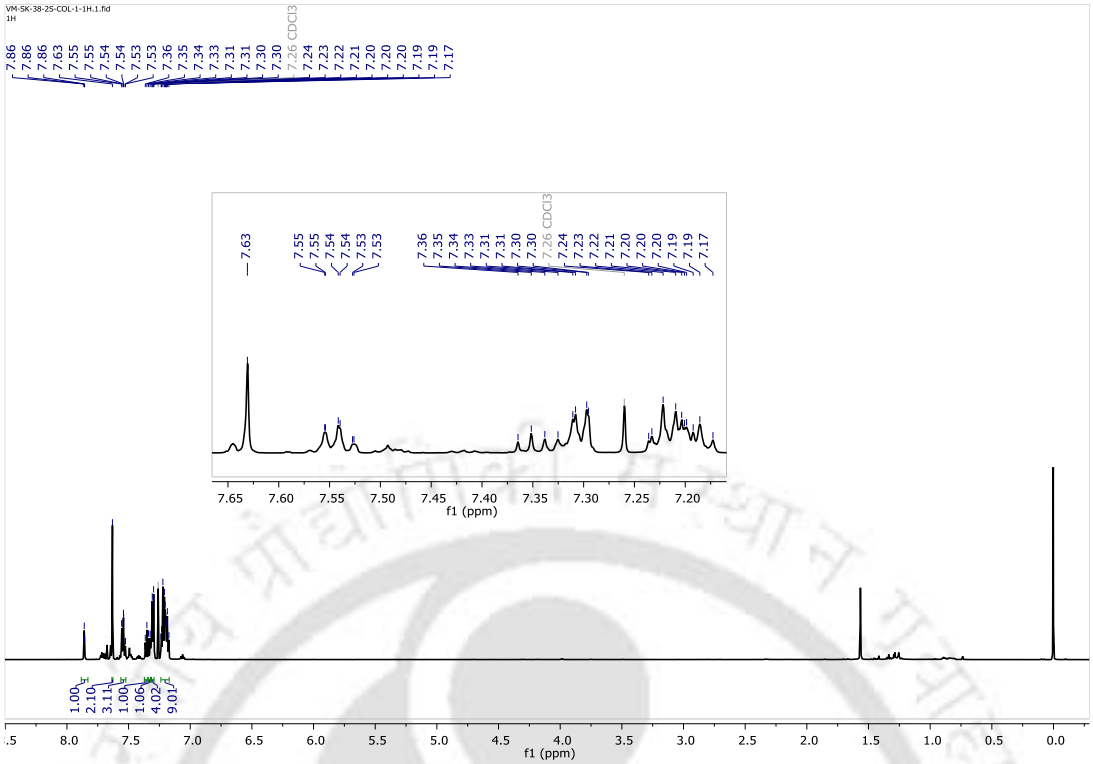

Figure A36. ^{1}H NMR spectrum of **1h**.

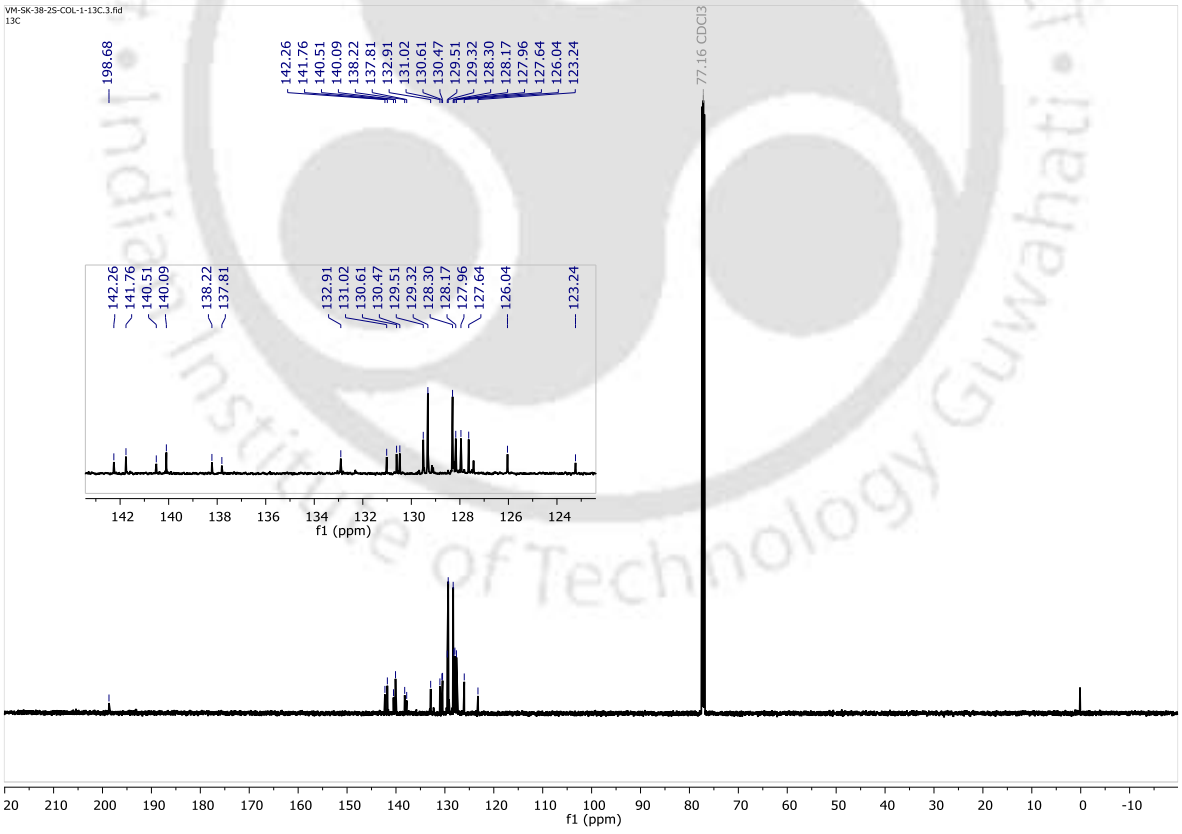

Figure A37. ^{13}C NMR spectrum of **1h**.

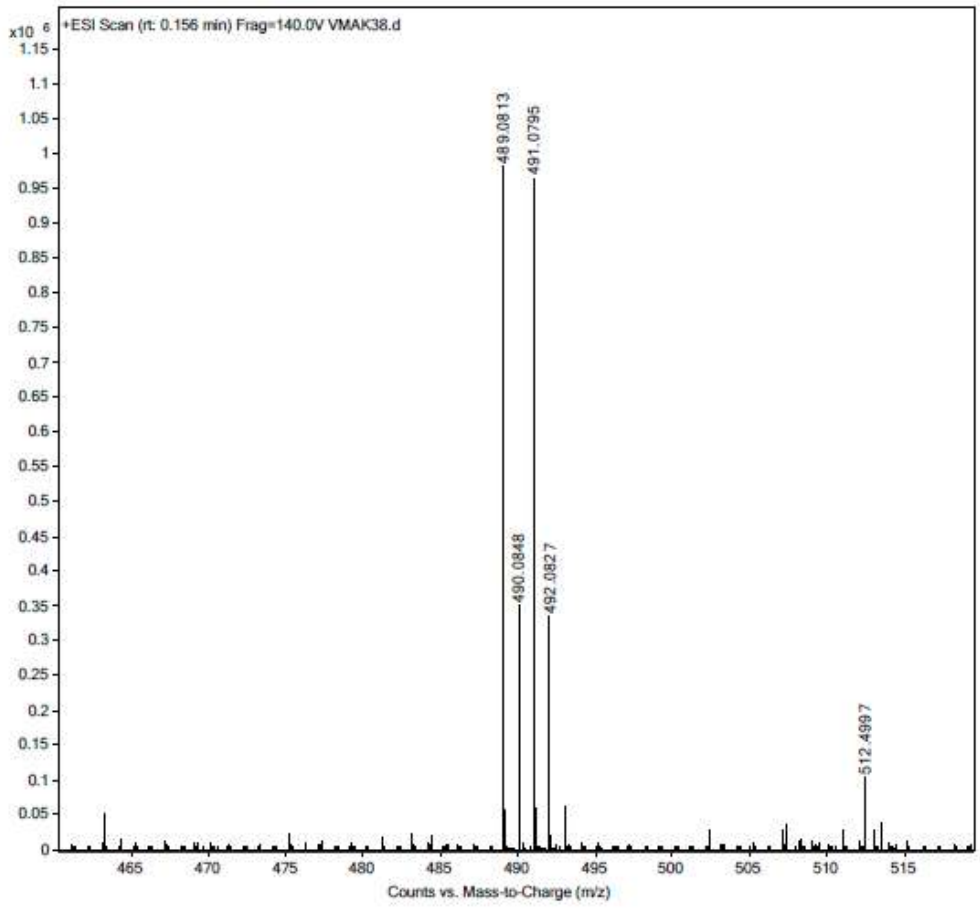

Figure A38. Mass spectrum of **1h**.

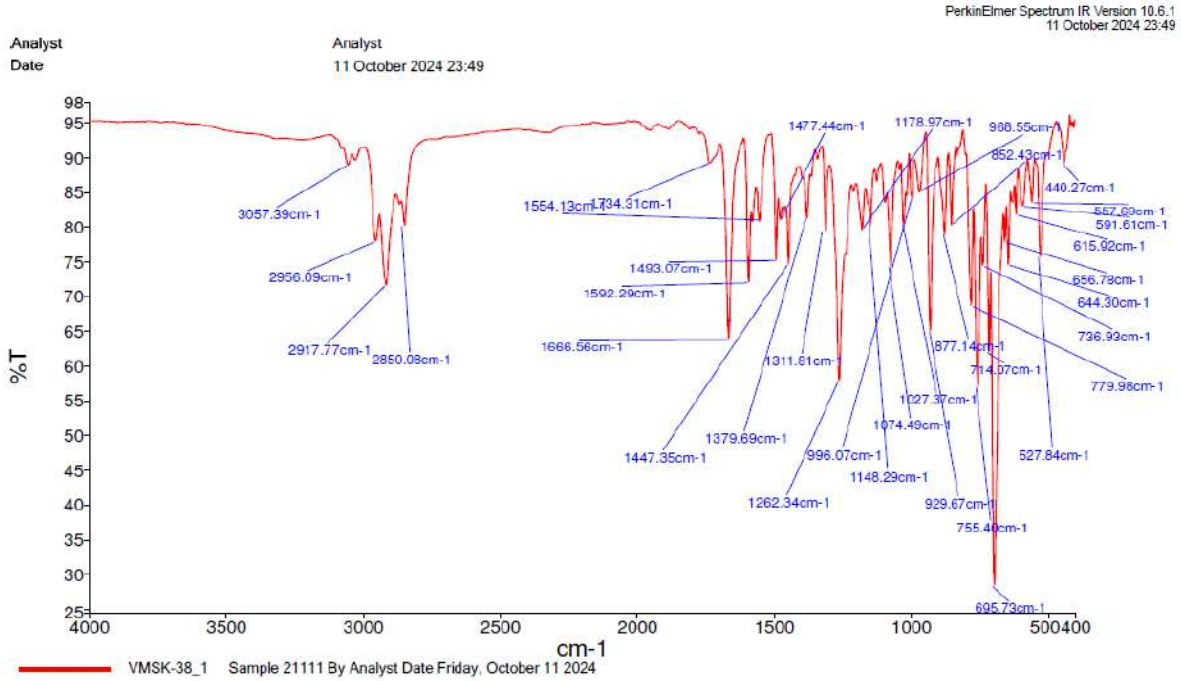

Figure A39. IR spectrum of **1h**.

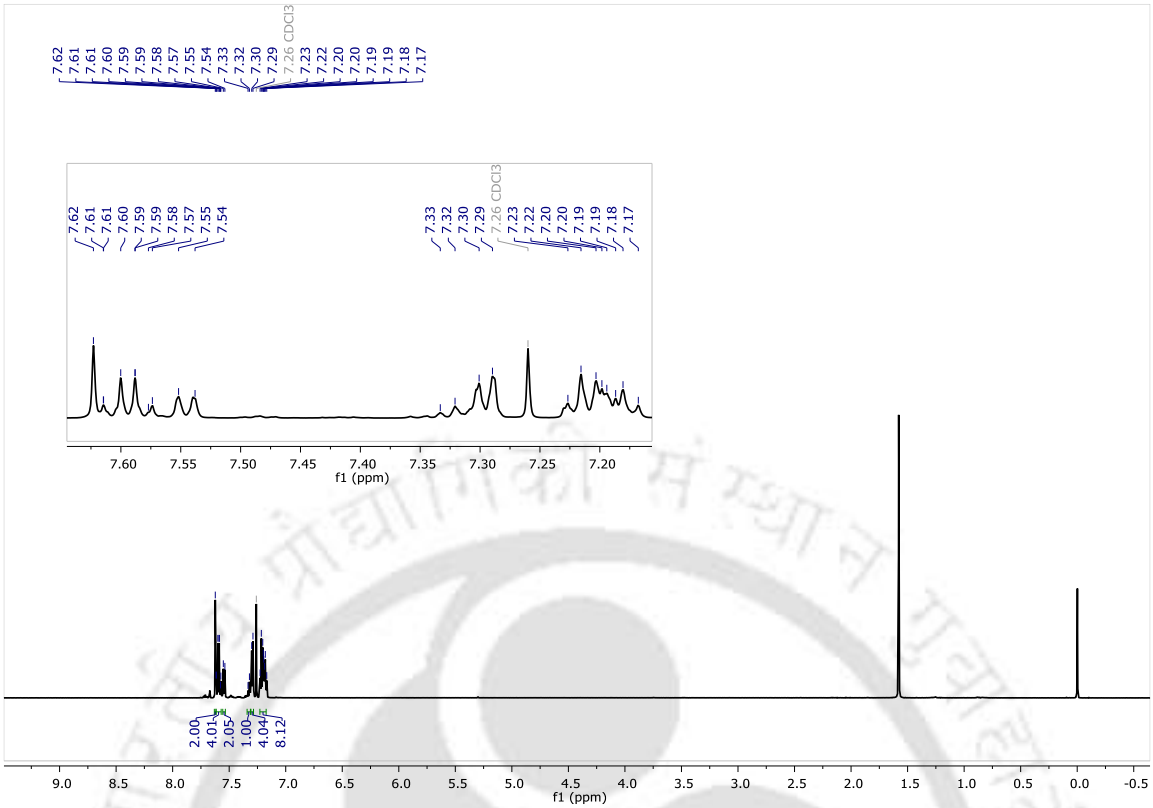

Figure A40. ^{1}H NMR spectrum of **1i**.

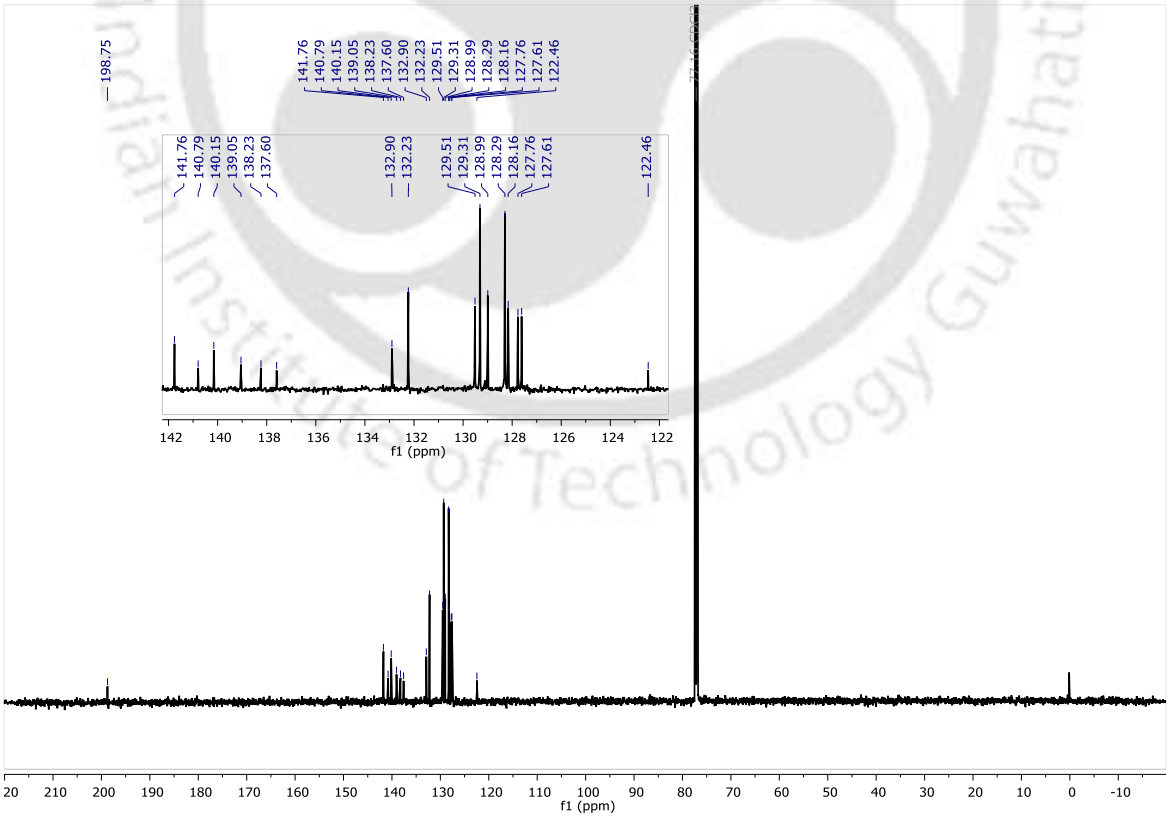

Figure A41. ^{13}C NMR spectrum of **1i**.

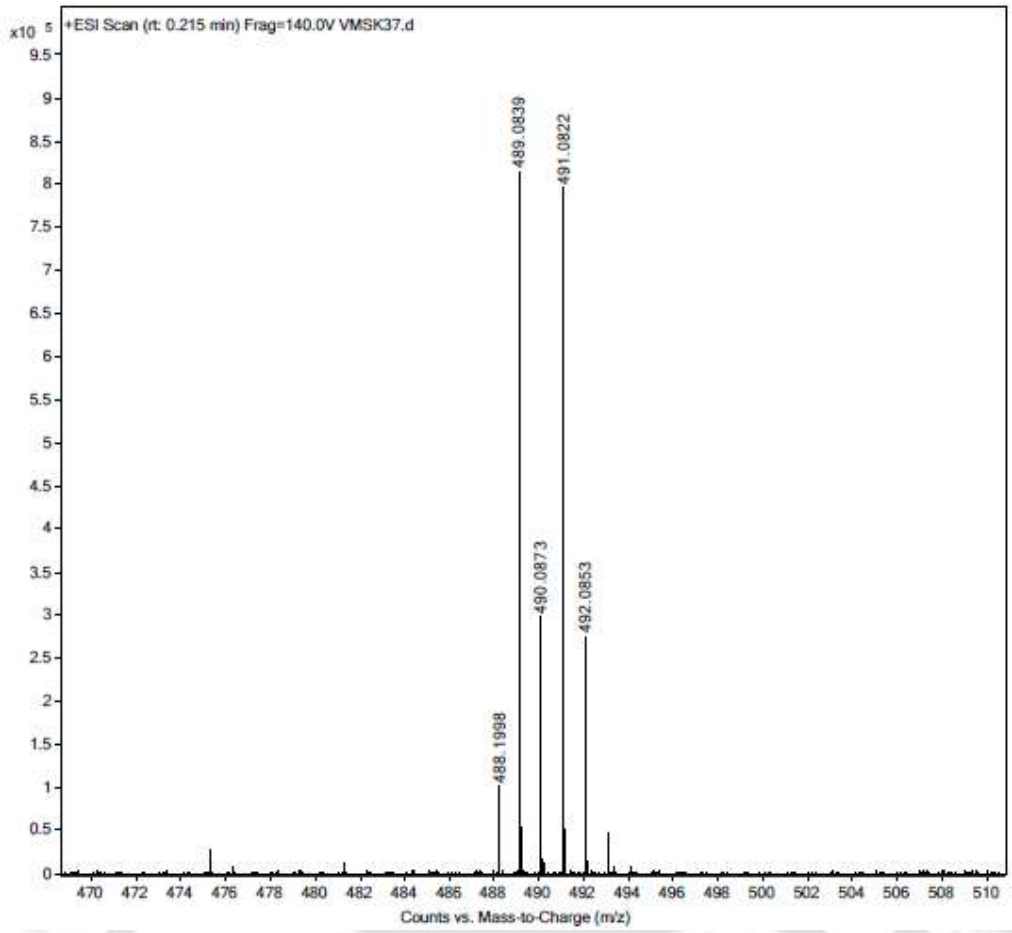

Figure A42. Mass spectrum of **1i**.

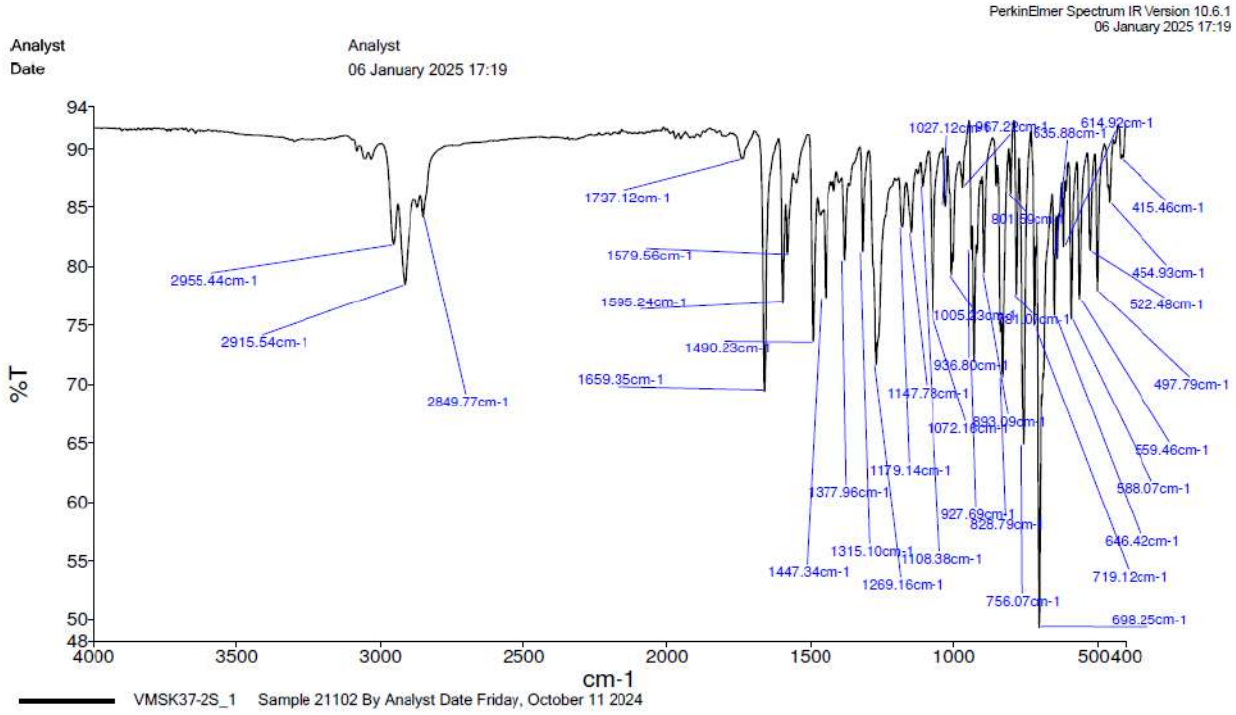

Figure A43. IR spectrum of **1i**.

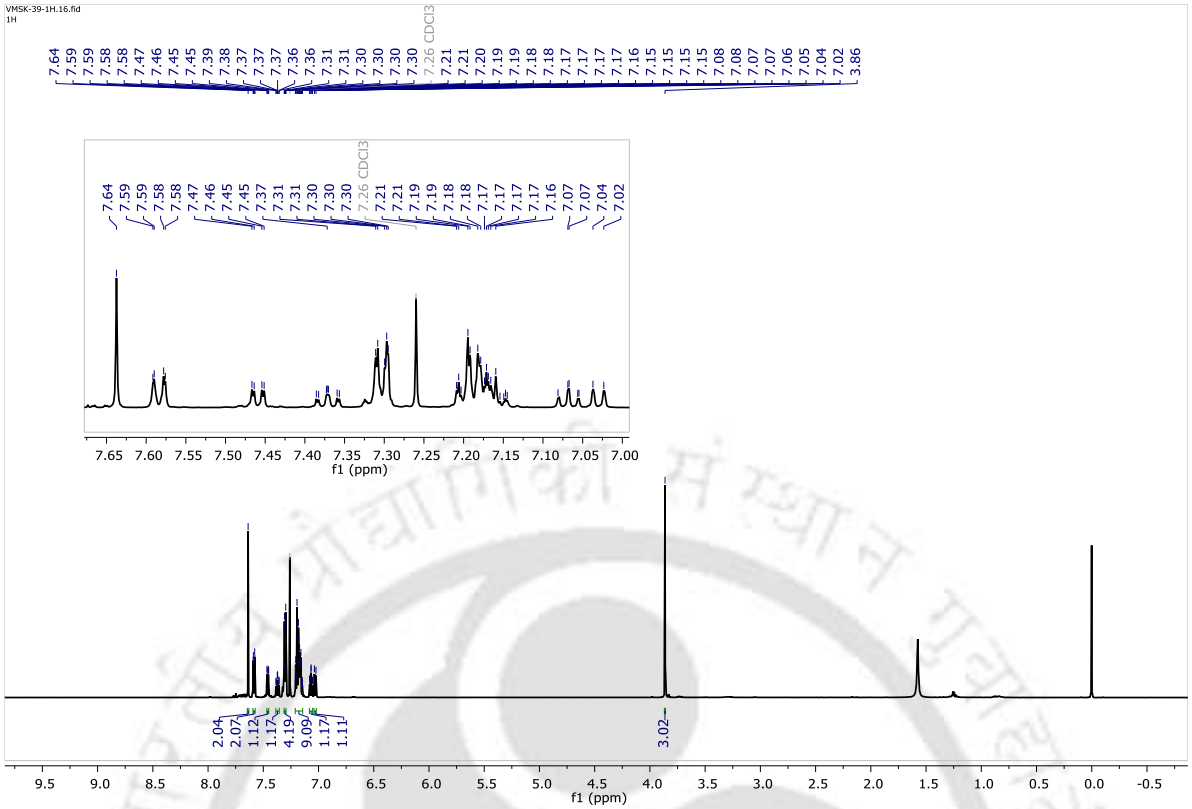

Figure A44. ^{1}H NMR spectrum of **1j**.

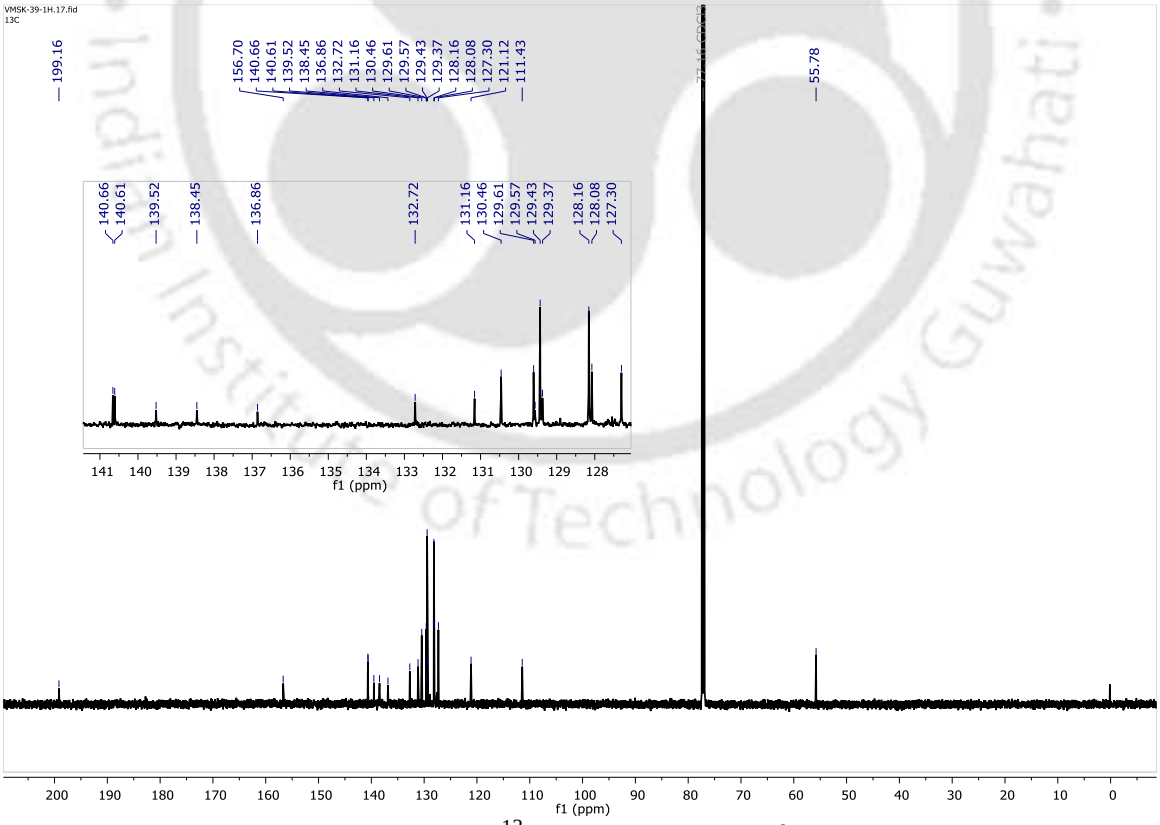

Figure A45. ^{13}C NMR spectrum of **1j**.

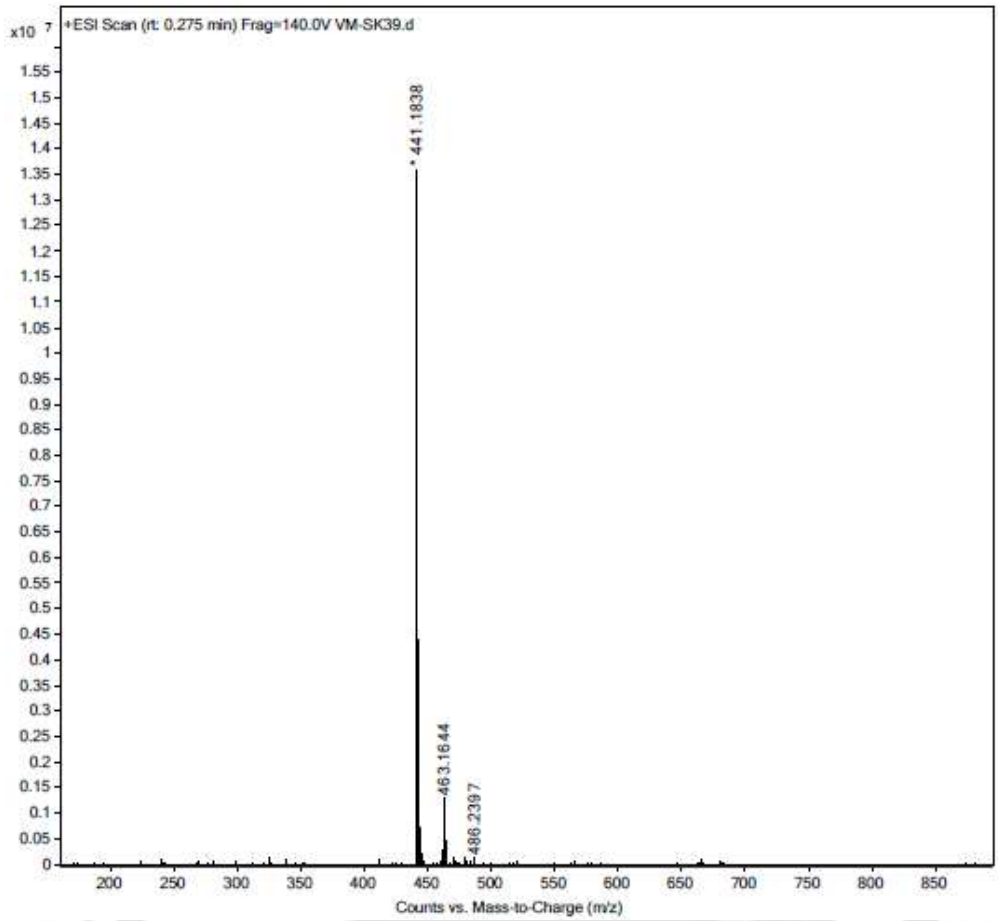

Figure A46. Mass spectrum of **1j**.

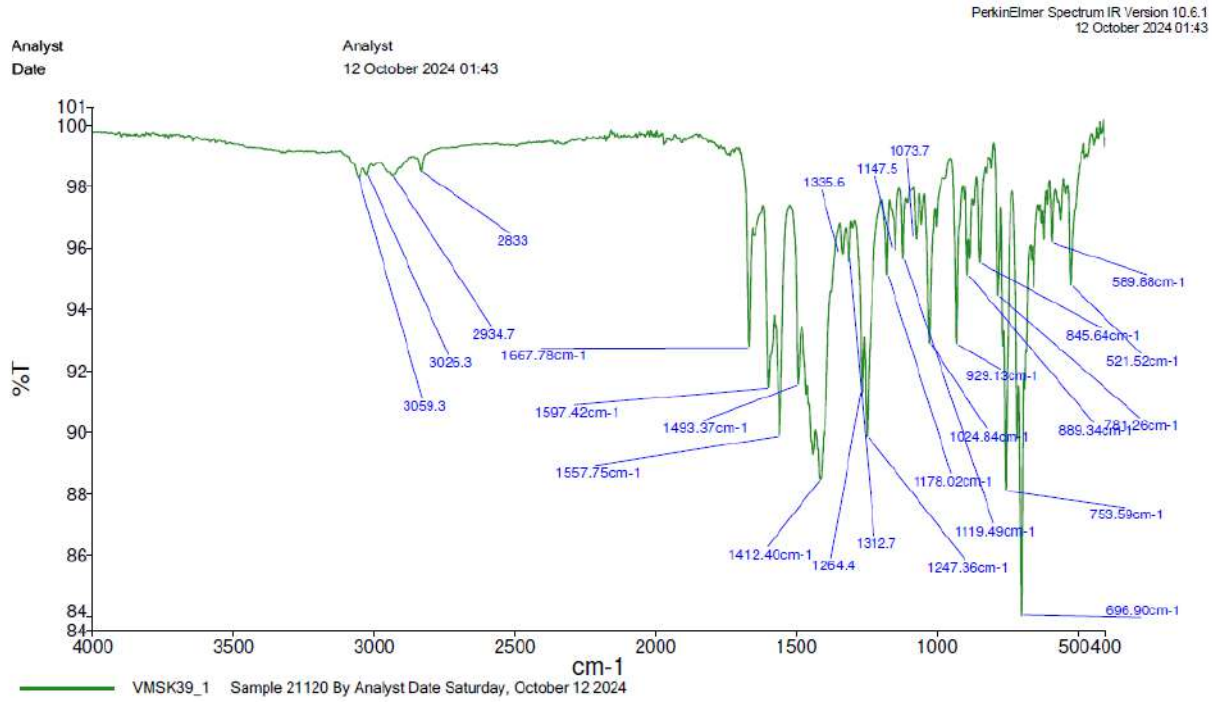

Figure A47. IR spectrum of **1j**.

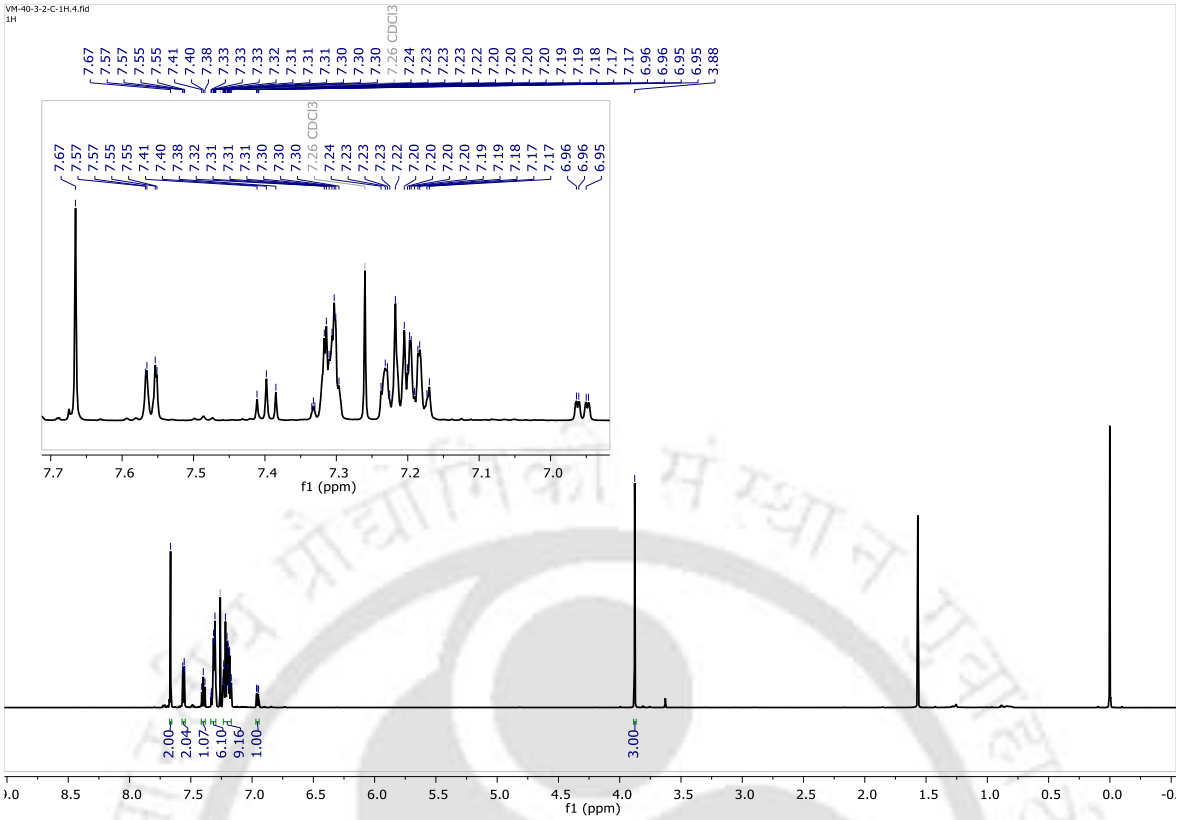

Figure A48. ^{1}H NMR spectrum of **1k**.

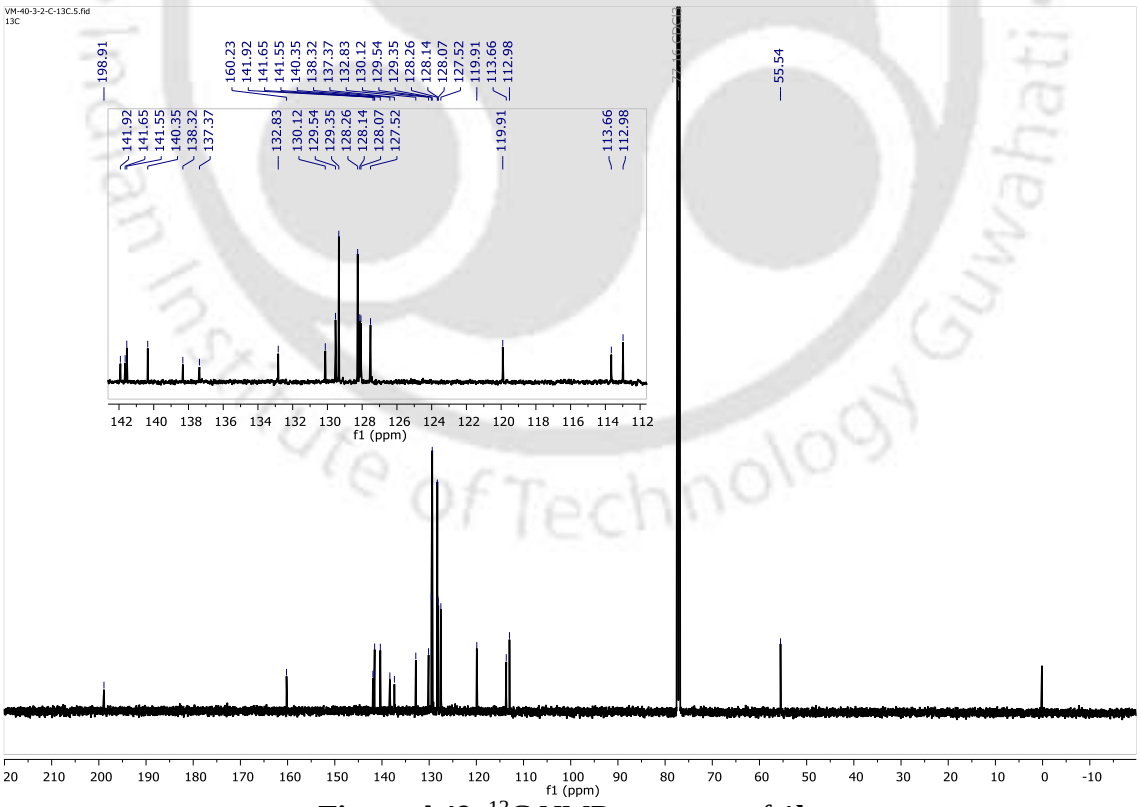

Figure A49. ^{13}C NMR spectrum of **1k**.

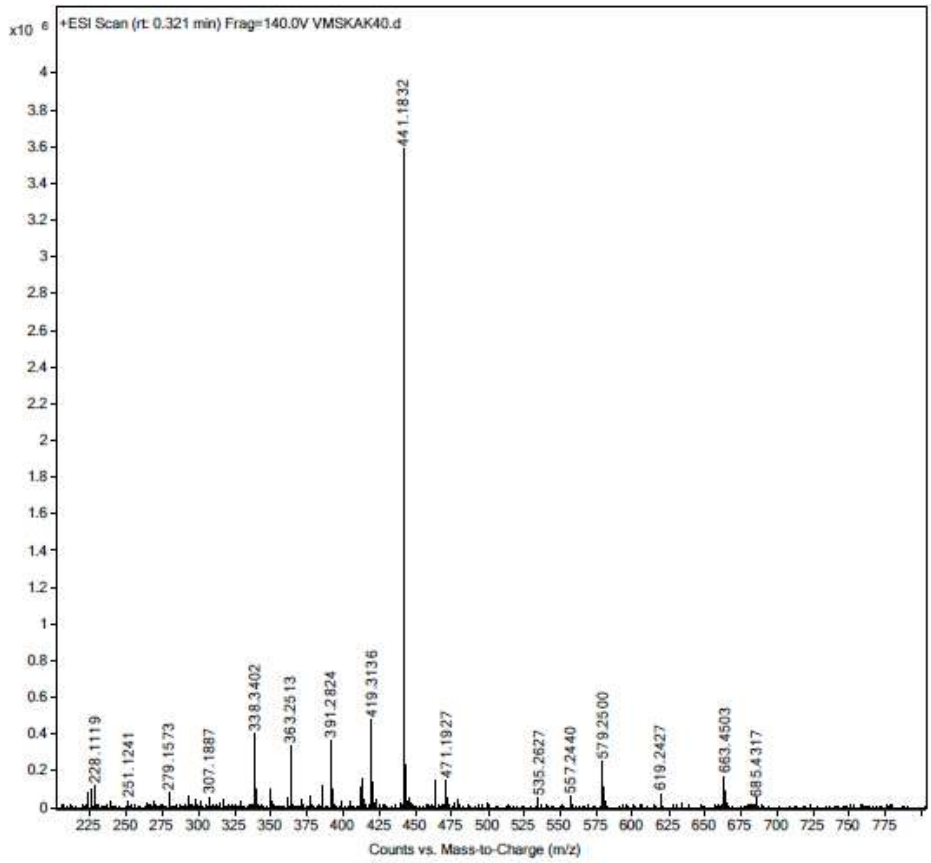

Figure A50. Mass spectrum of **1k**.

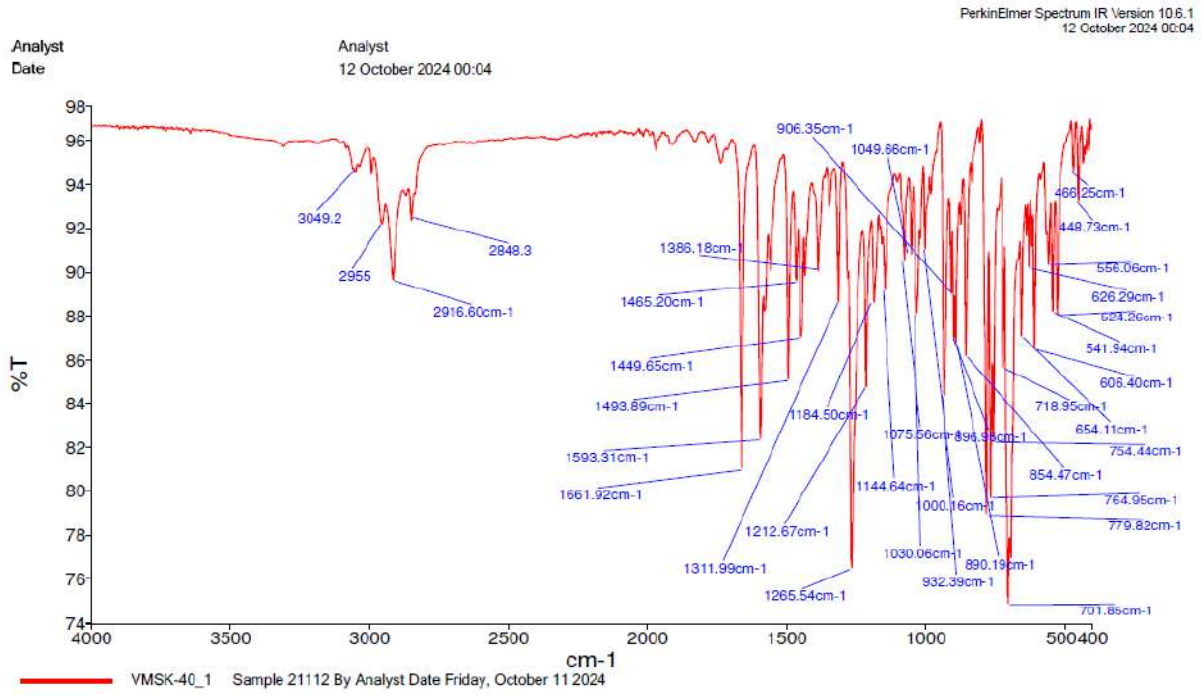

Figure A51. IR spectrum of **1k**.

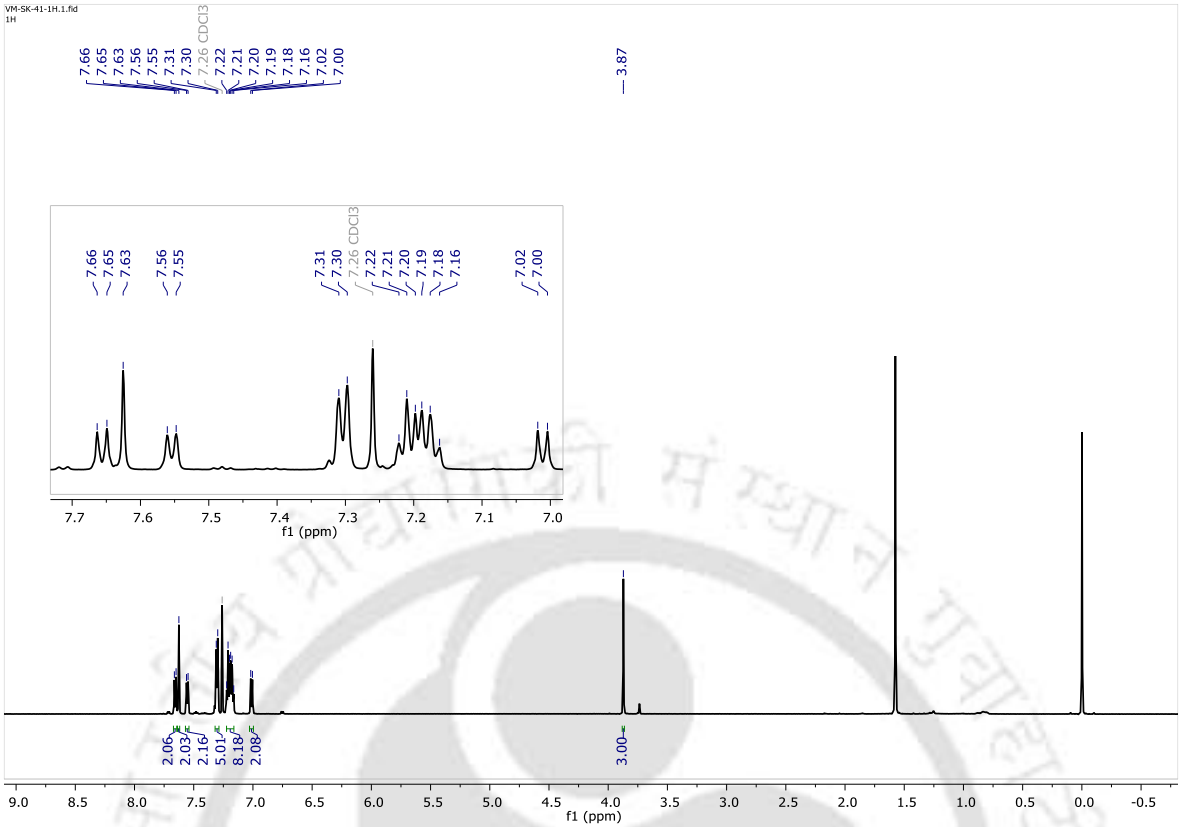

Figure A52. ^{1}H NMR spectrum of **1l**.

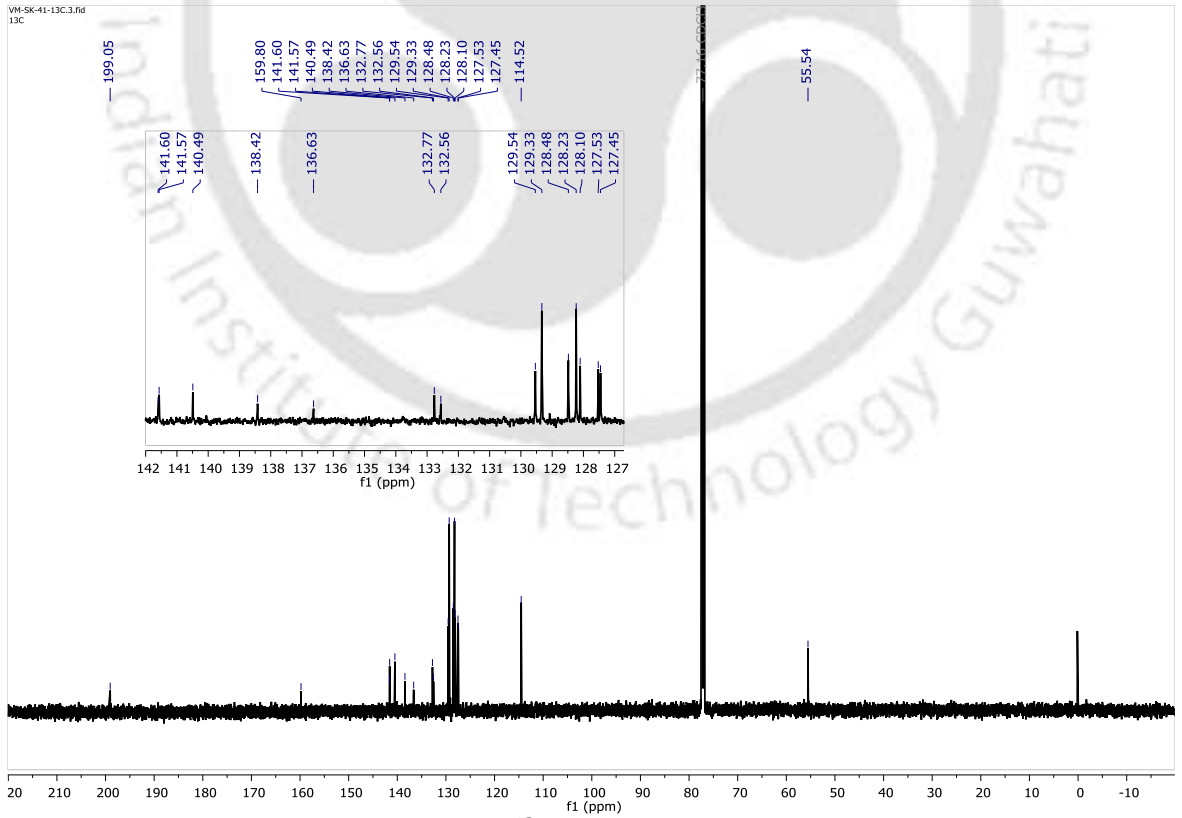

Figure A53. ^{13}C NMR spectrum of **1l**.

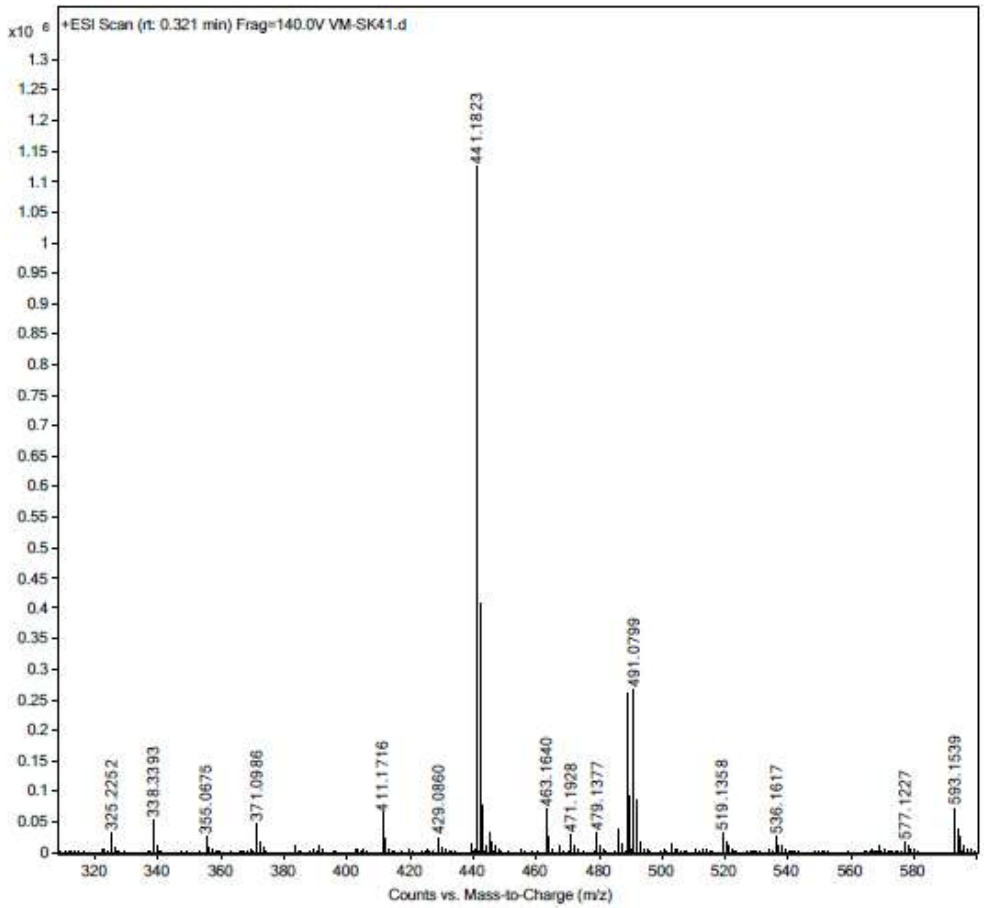

Figure A54. Mass spectrum of **1l**.

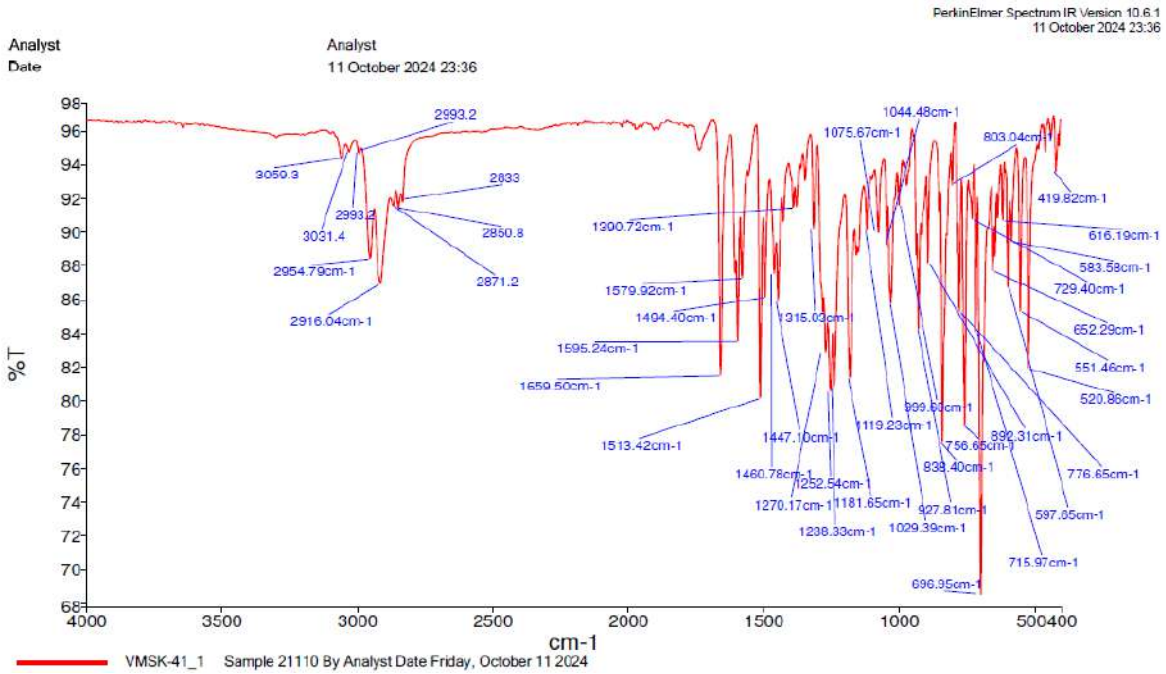

Figure A55. IR spectrum of **1l**.

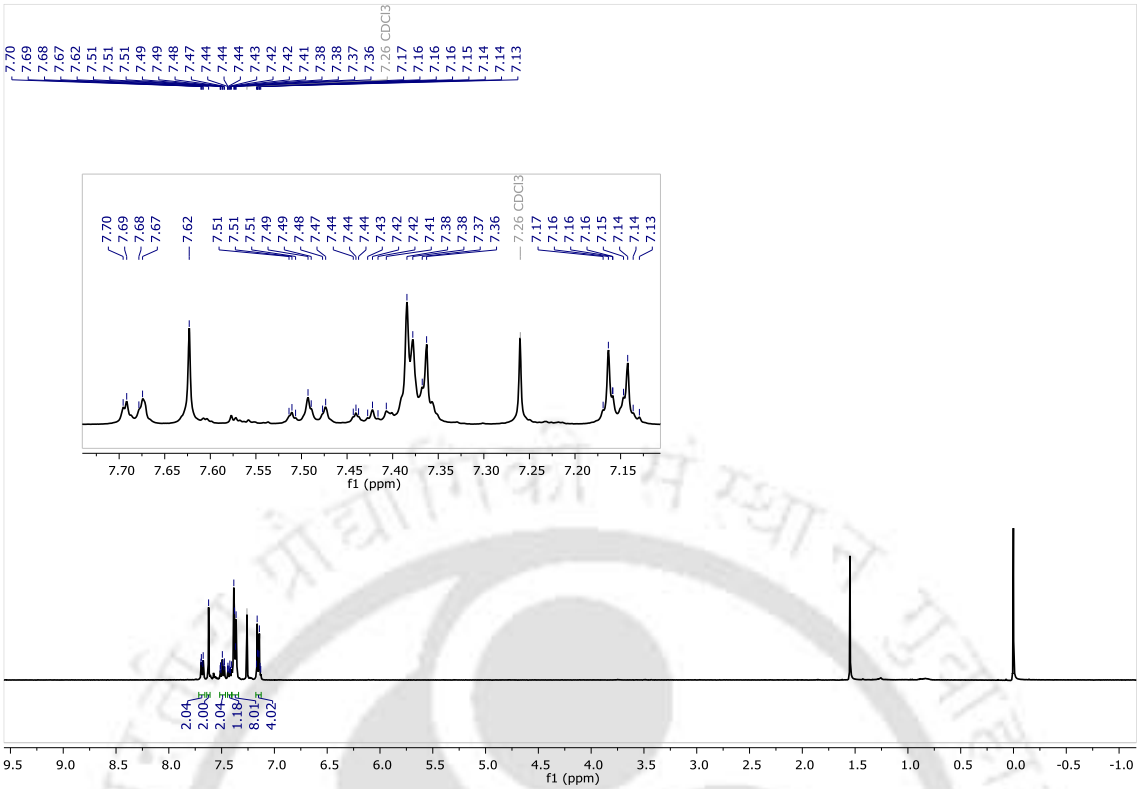

Figure A56. ^{1}H NMR spectrum of **1m**.

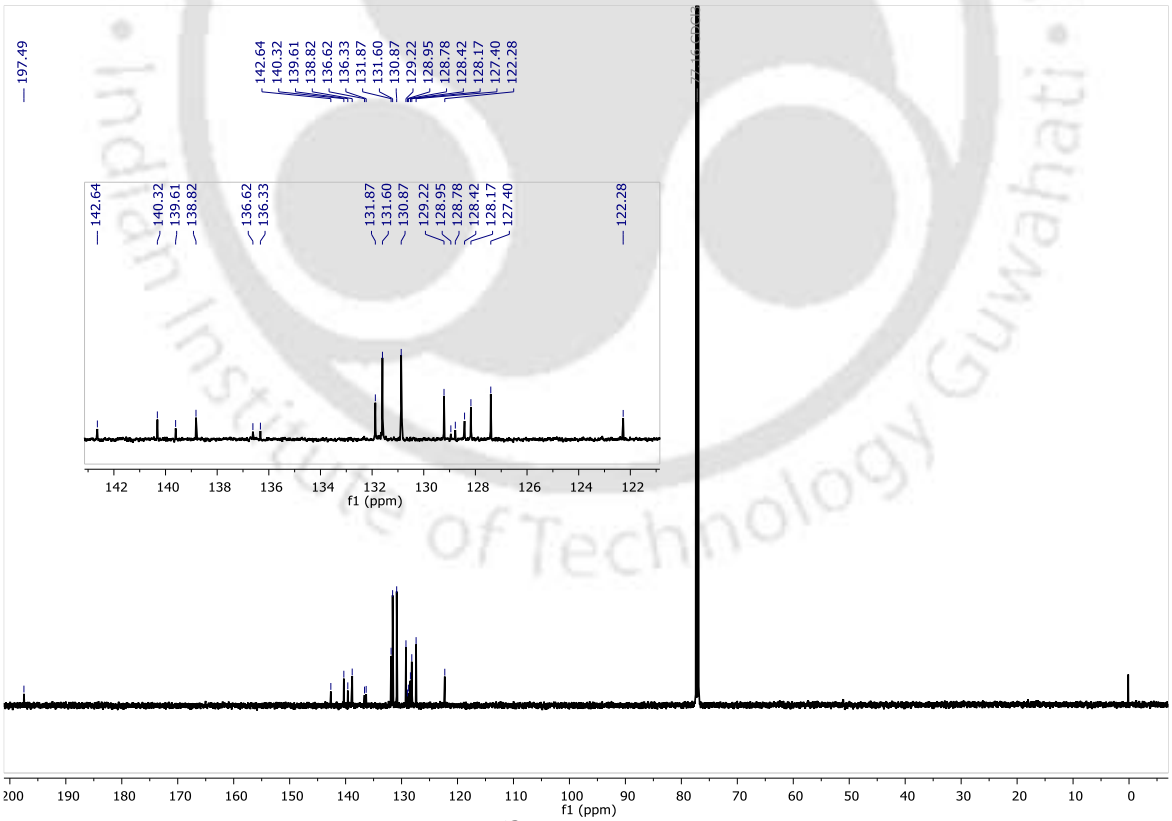

Figure A57. ^{13}C NMR spectrum of **1m**.

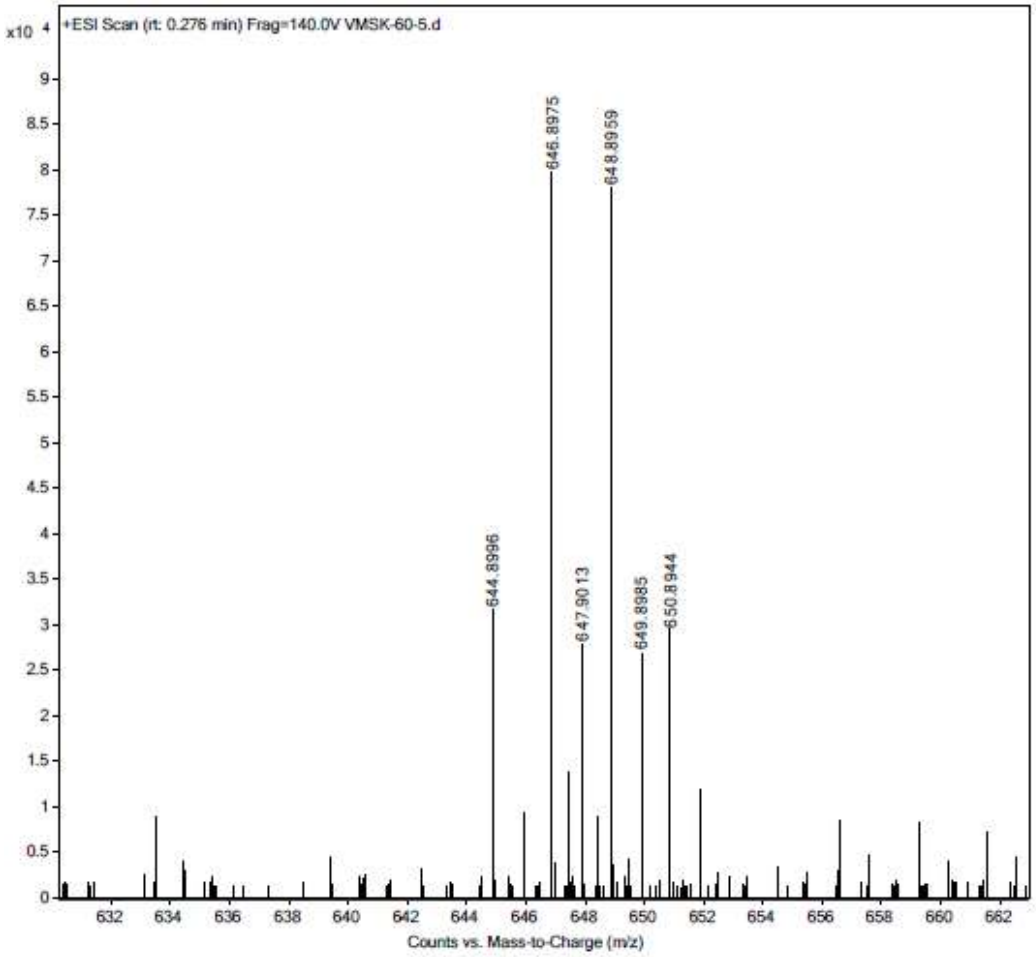

Figure A58. Mass spectrum of **1m**.

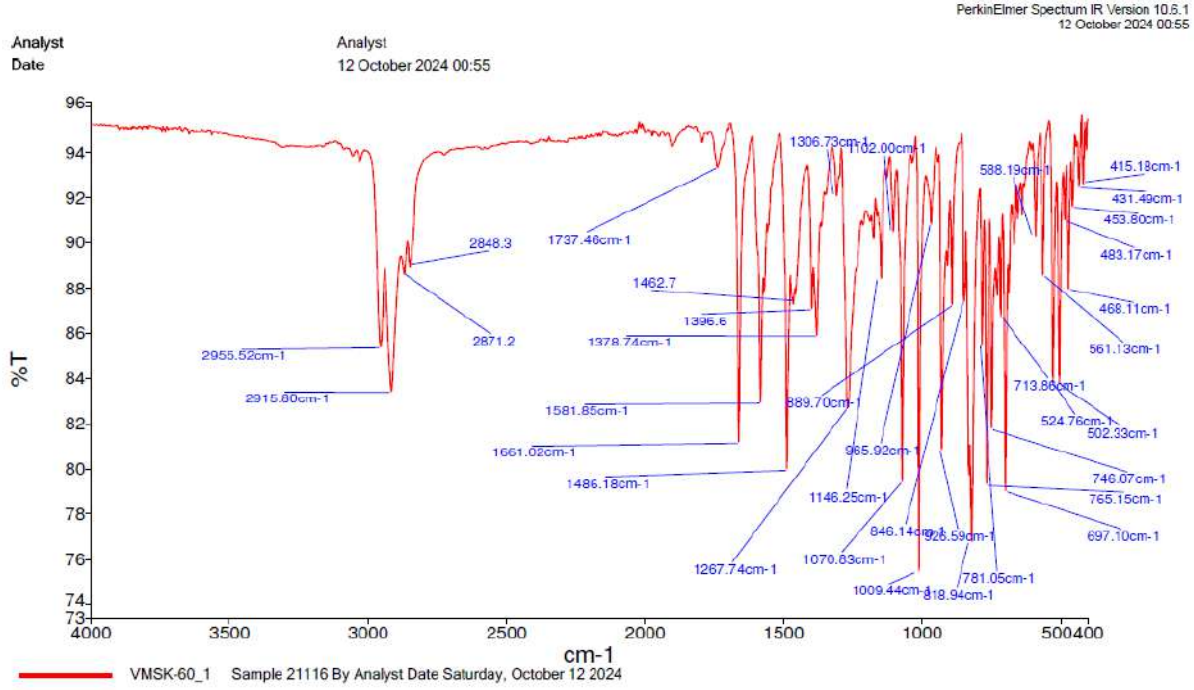

Figure A59. IR spectrum of **1m**.

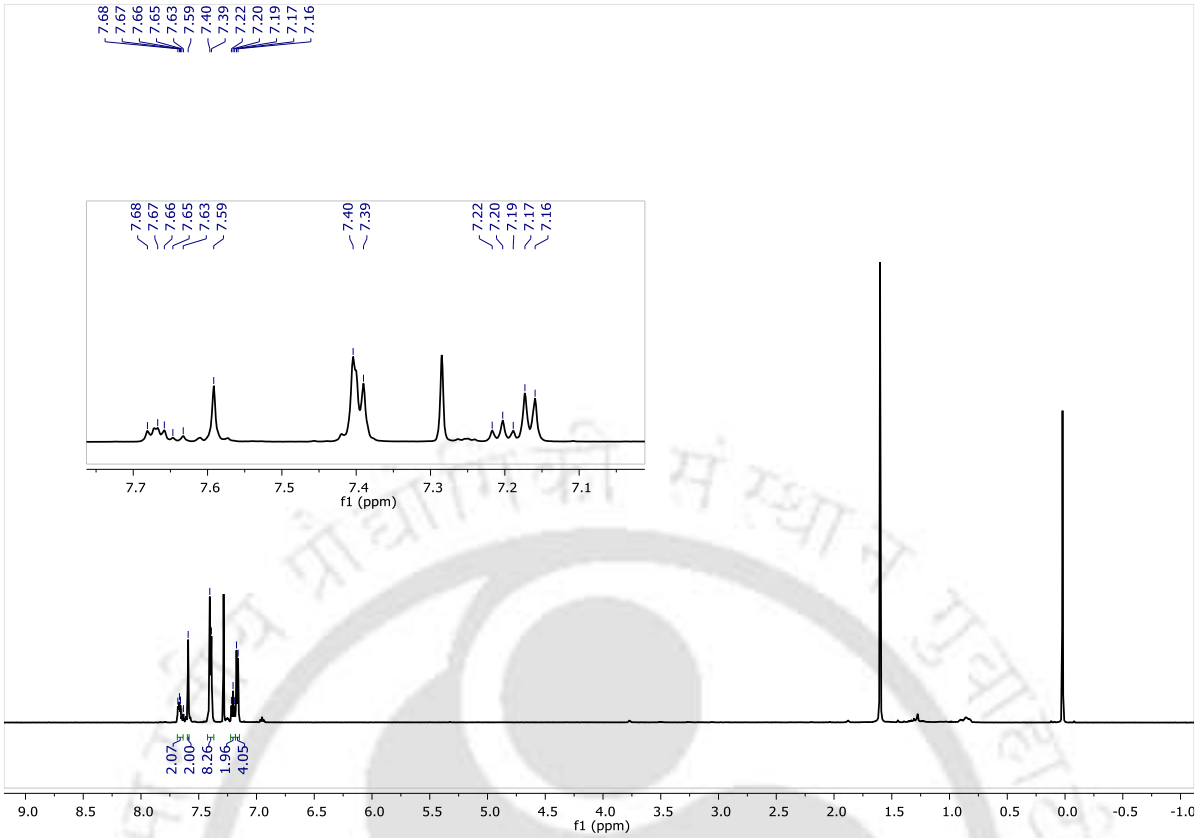

Figure A60. ^{1}H NMR spectrum of **1n**.

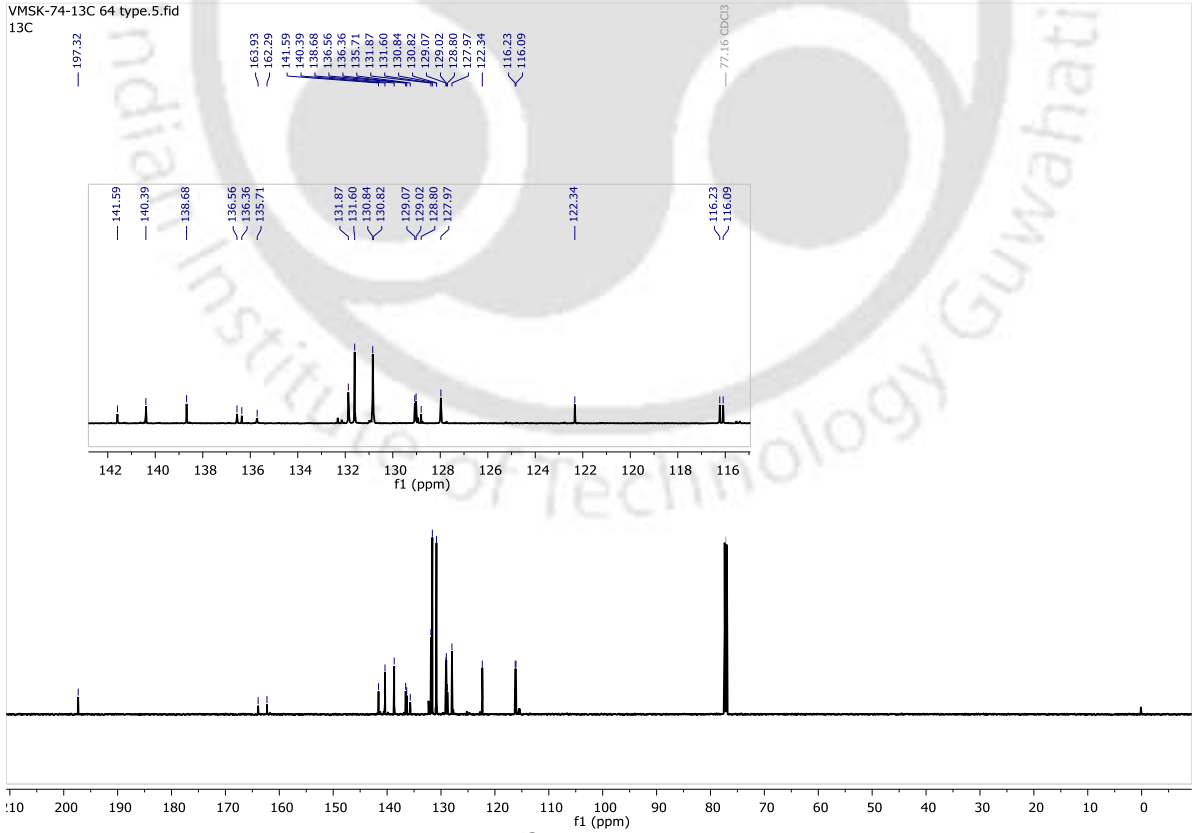

Figure A61. ^{13}C NMR spectrum of **1n**.

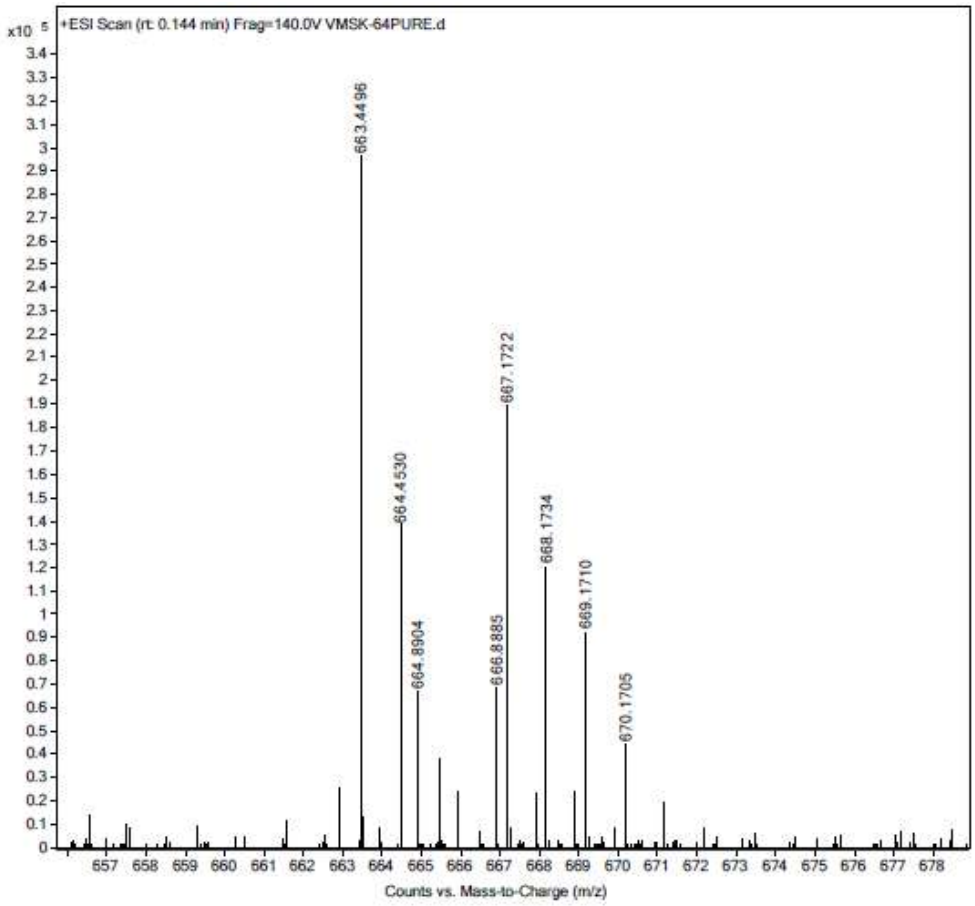

Figure A62. Mass spectrum of **1n**.

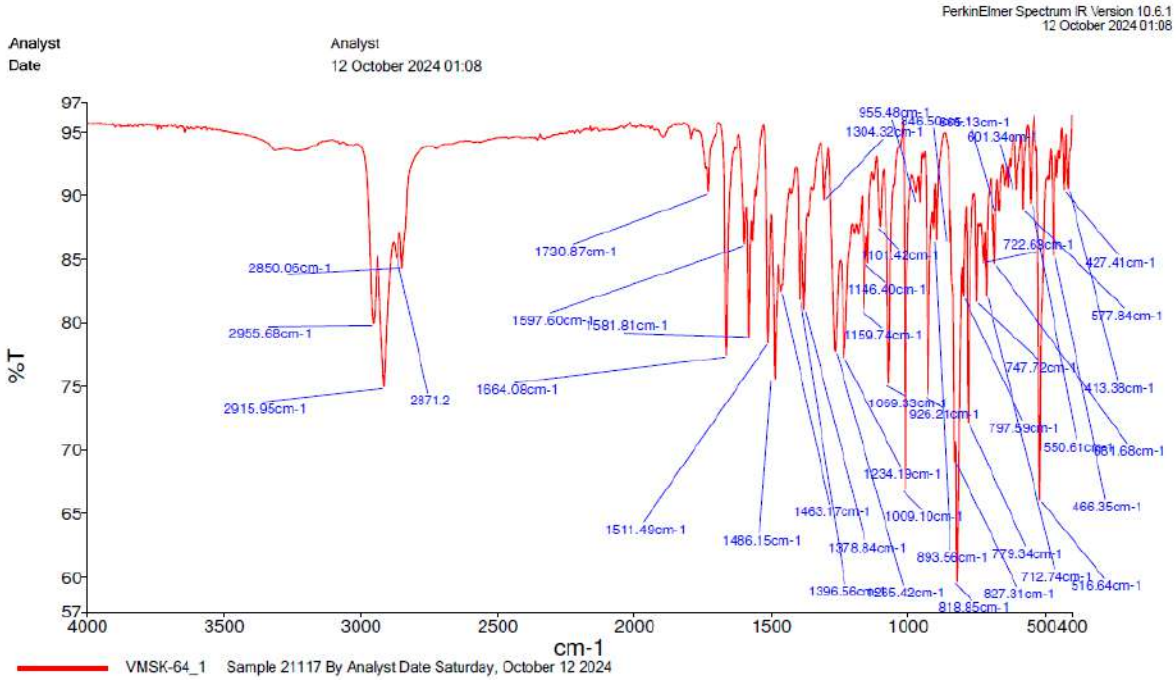

Figure A63. IR spectrum of **1n**.

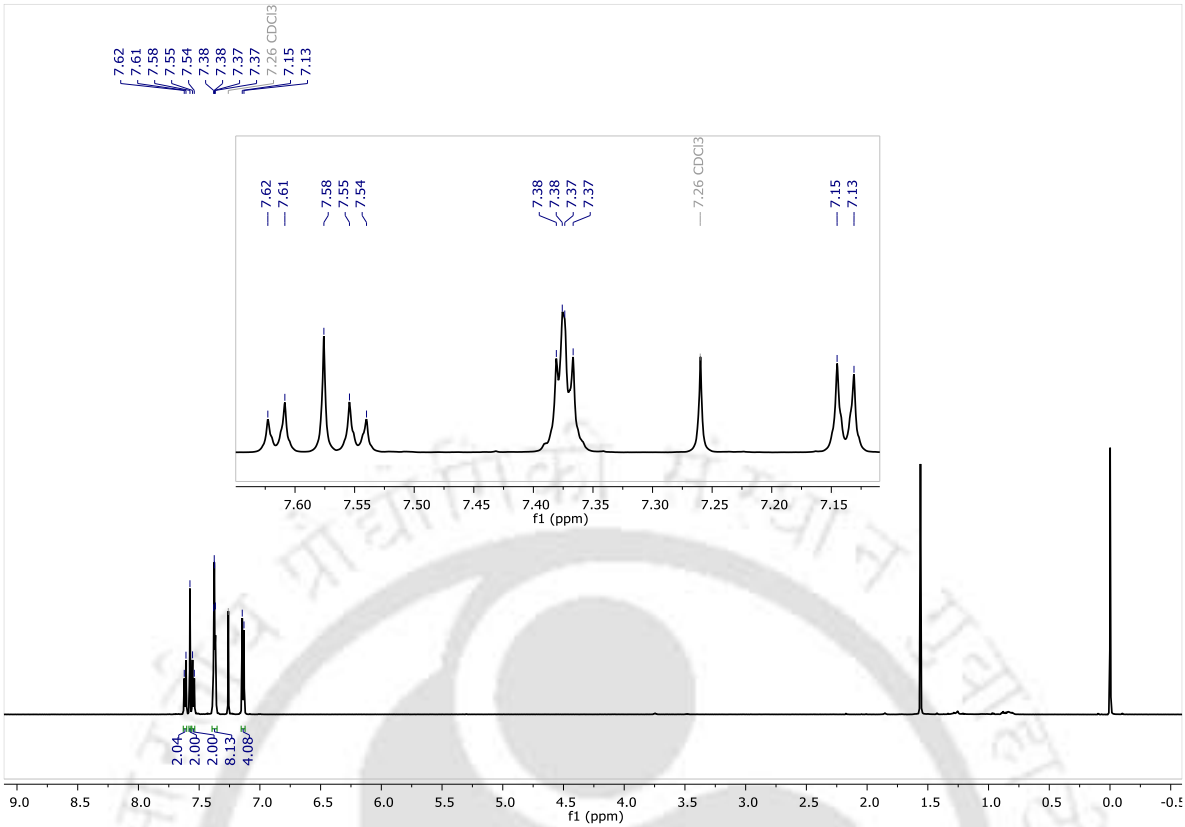

Figure A64. ^{1}H NMR spectrum of **1o**.

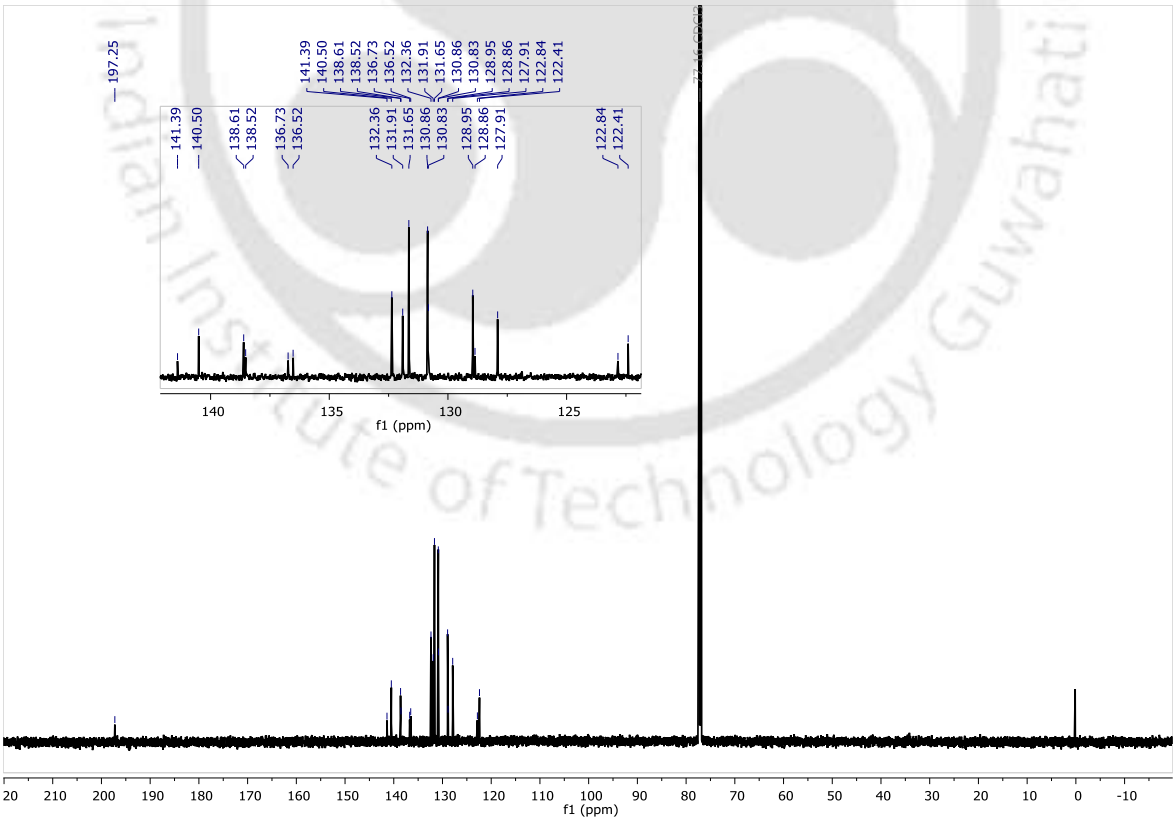

Figure A65. ^{13}C NMR spectrum of **1o**.

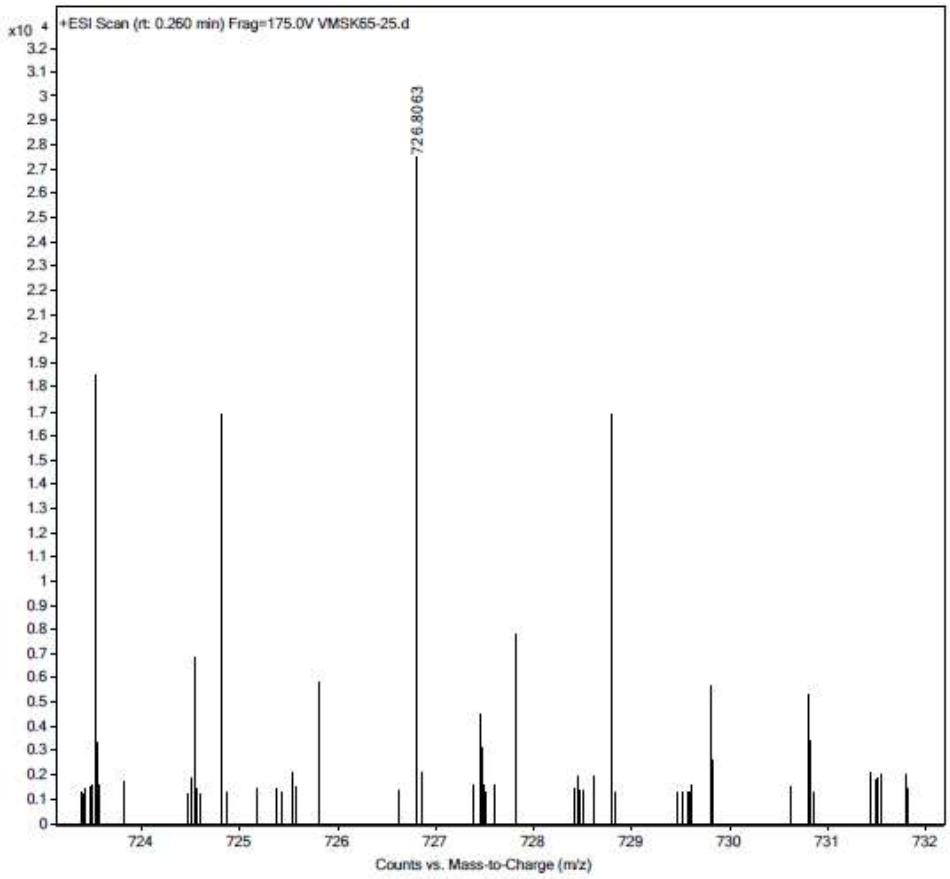

Figure A66. Mass spectrum of **1o**.

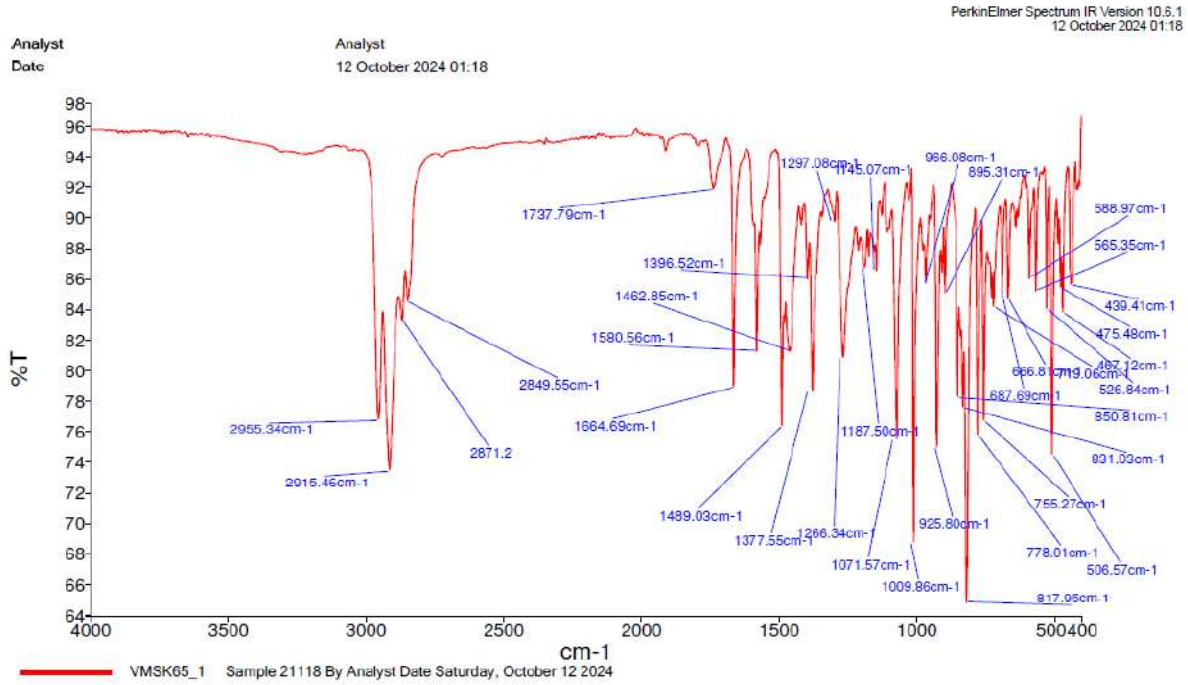

Figure A67. IR spectrum of **1o**.

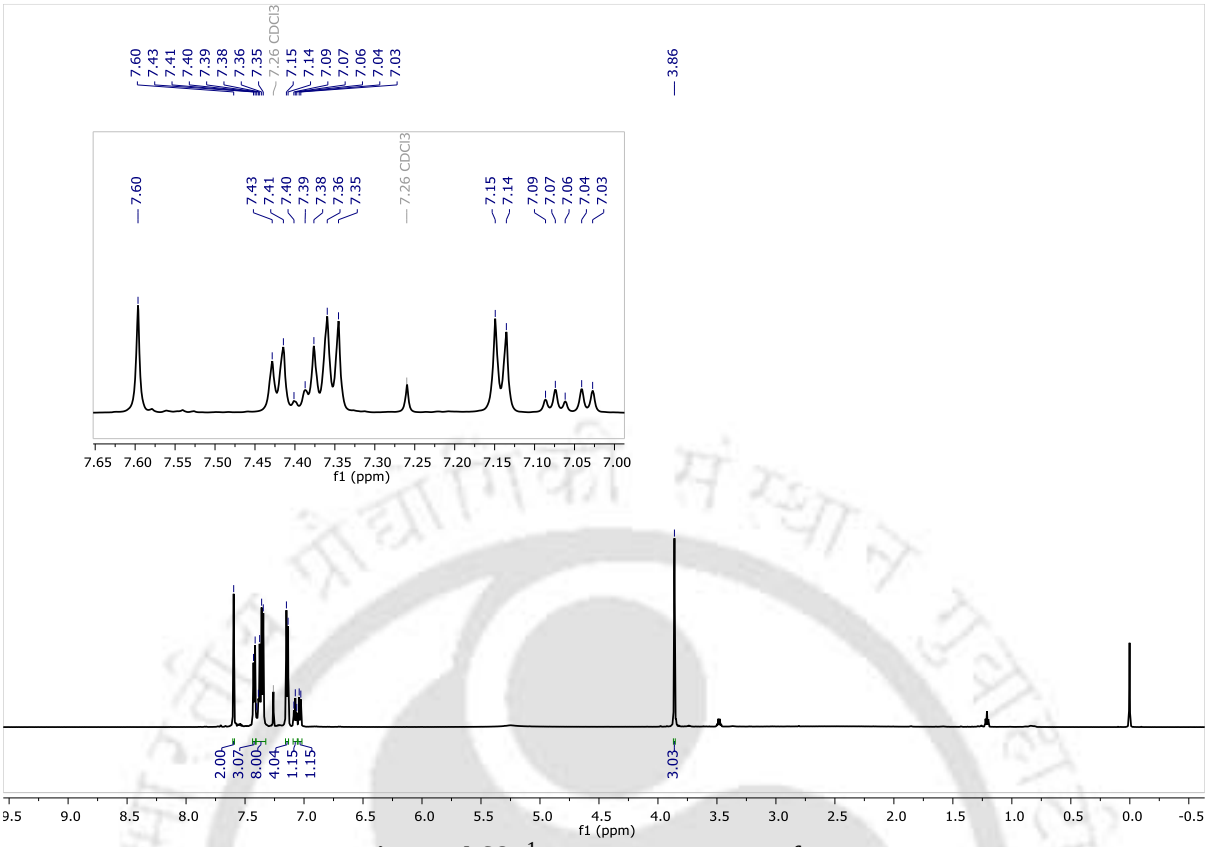

Figure A68. ^{1}H NMR spectrum of **1p**.

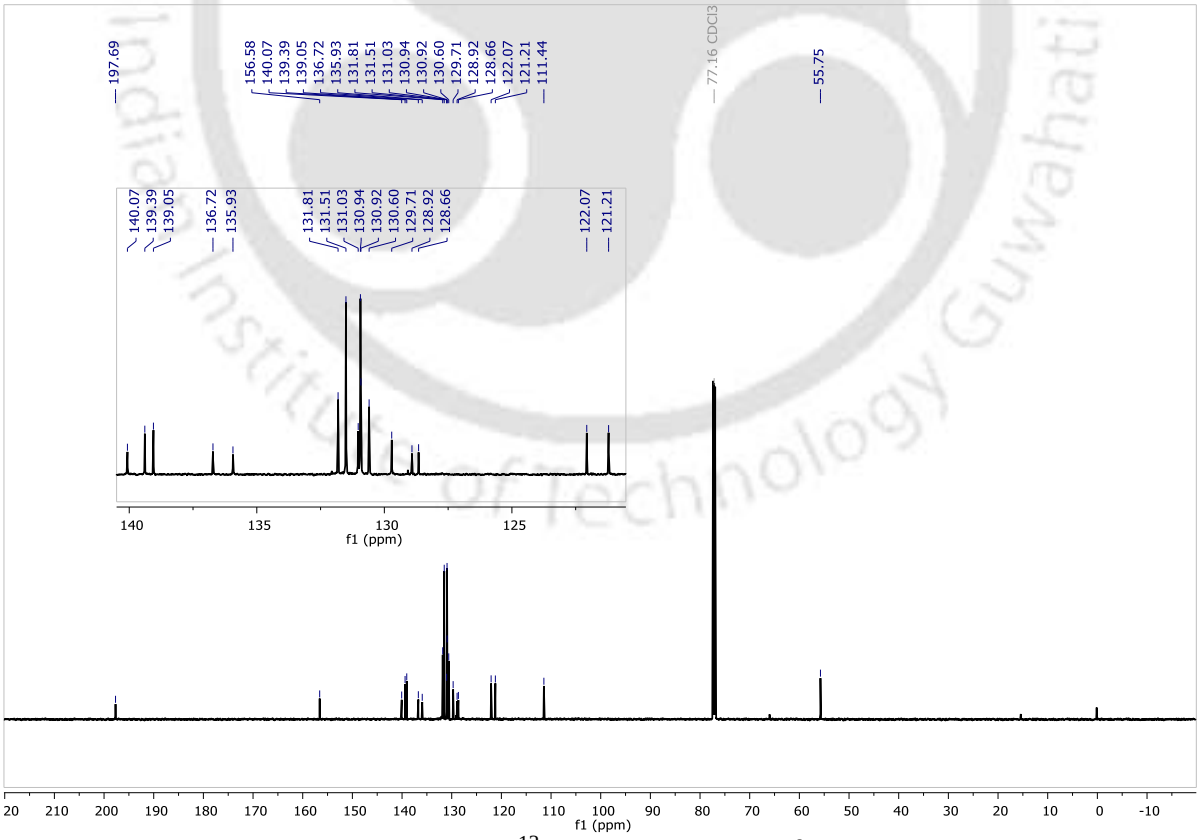

Figure A69. ^{13}C NMR spectrum of **1p**.

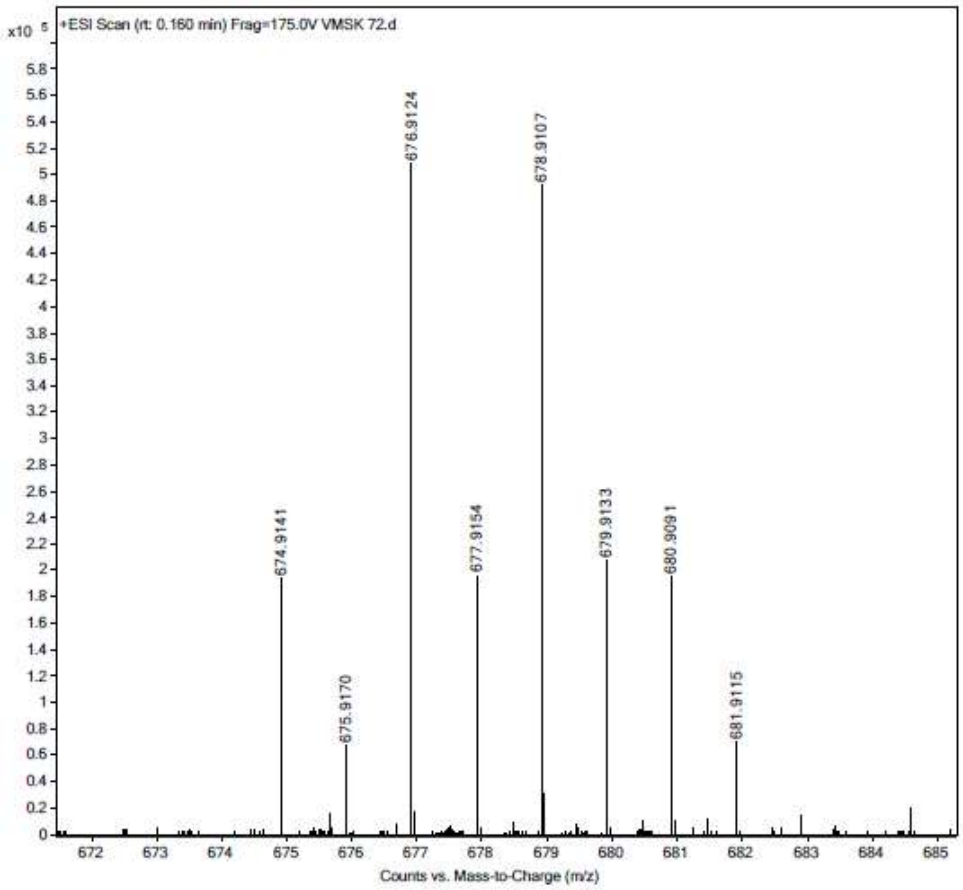

Figure A70. Mass spectrum of **1p**.

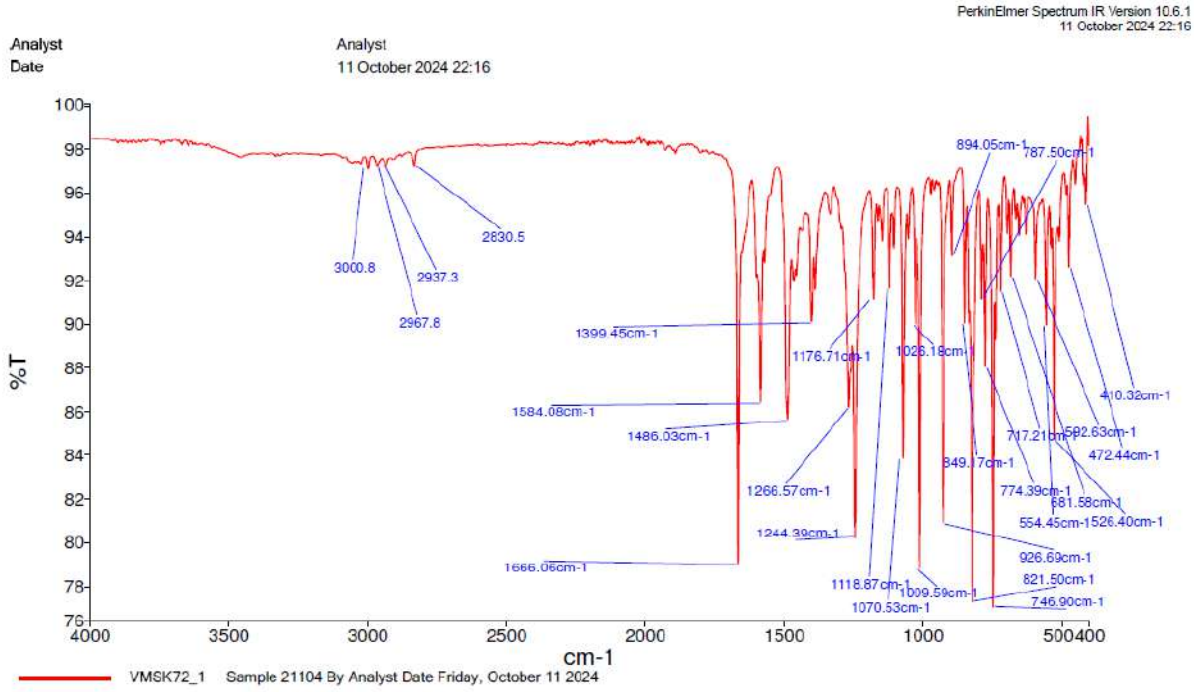

Figure A71. IR spectrum of **1p**.

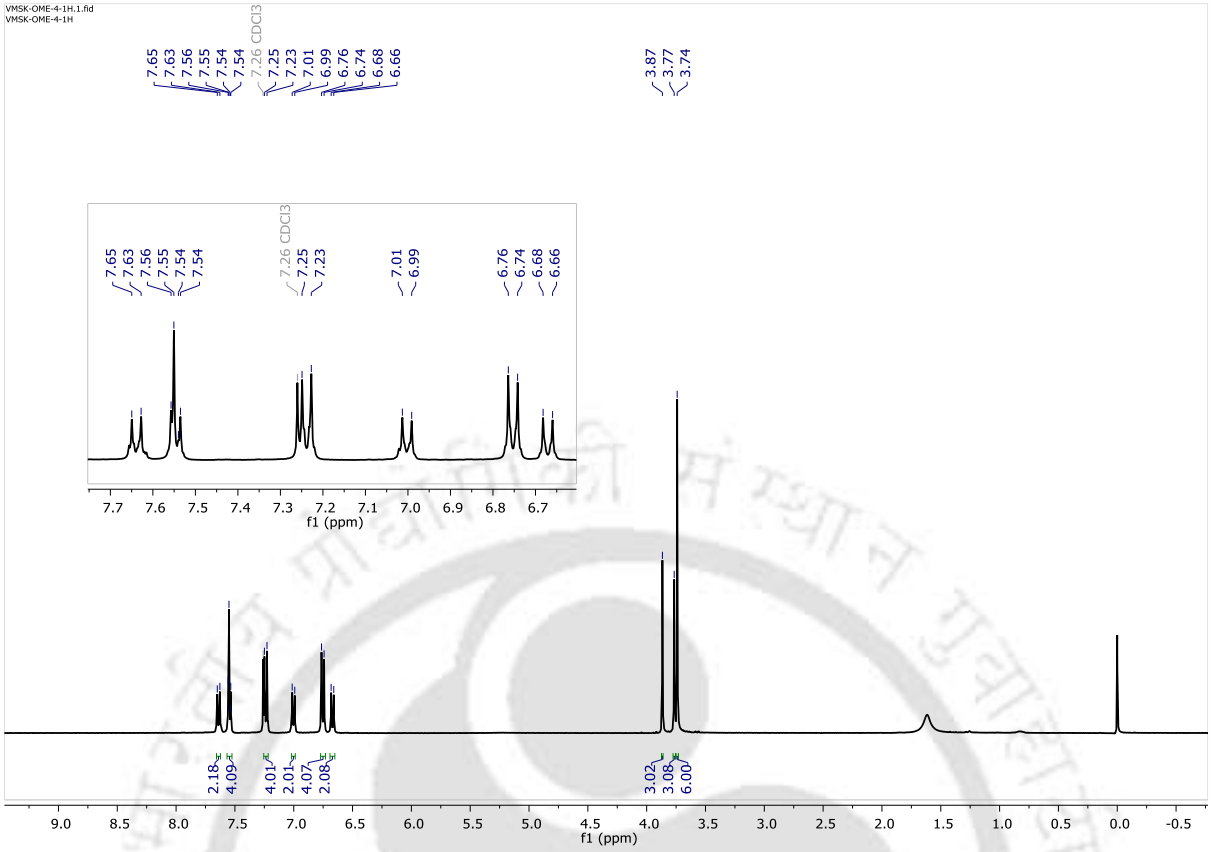

Figure A72. ^{1}H NMR spectrum of **1q**.

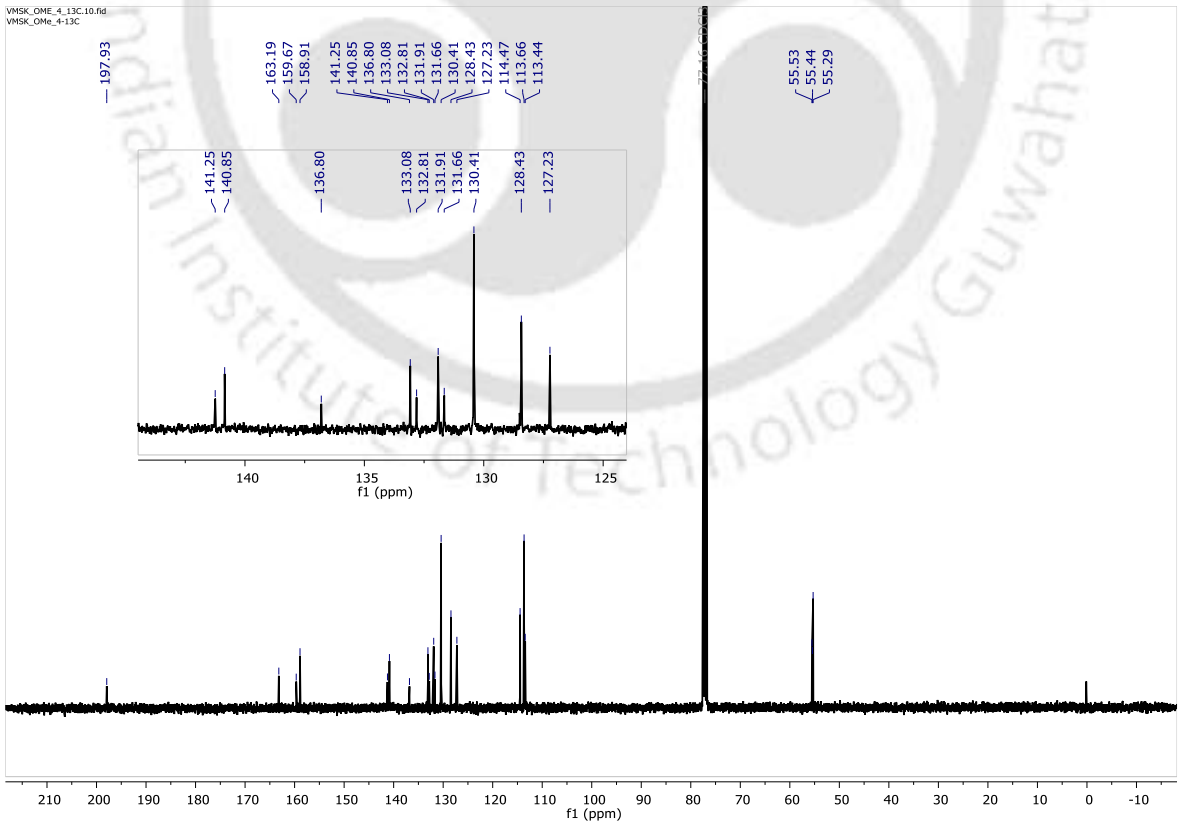

Figure A73. ^{13}C NMR spectrum of **1q**.

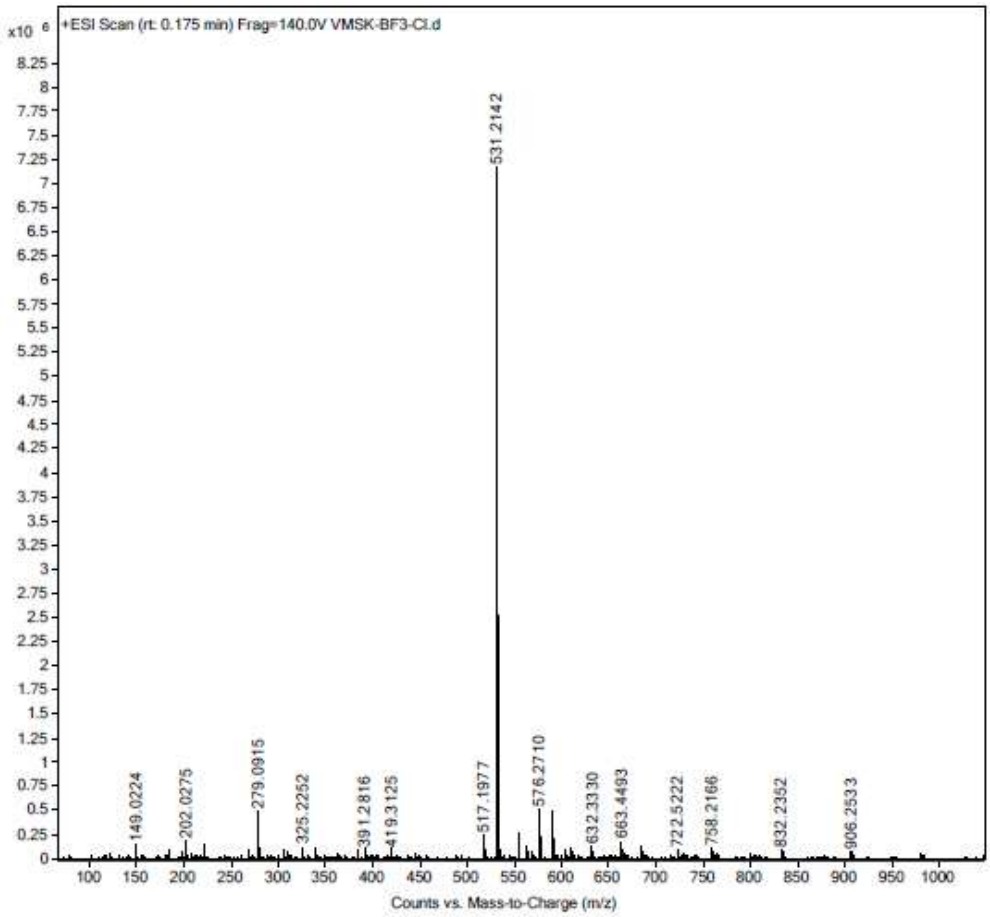

Figure A74. Mass spectrum of **1q**.

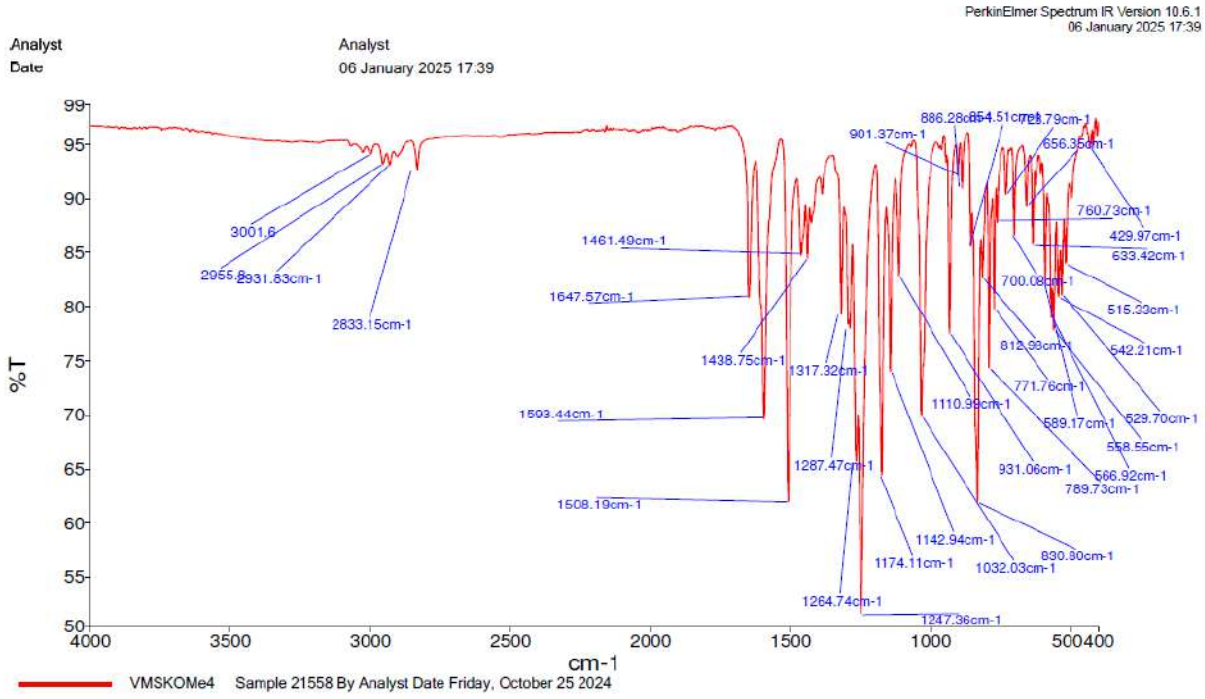

Figure A75. IR spectrum of **1q**.

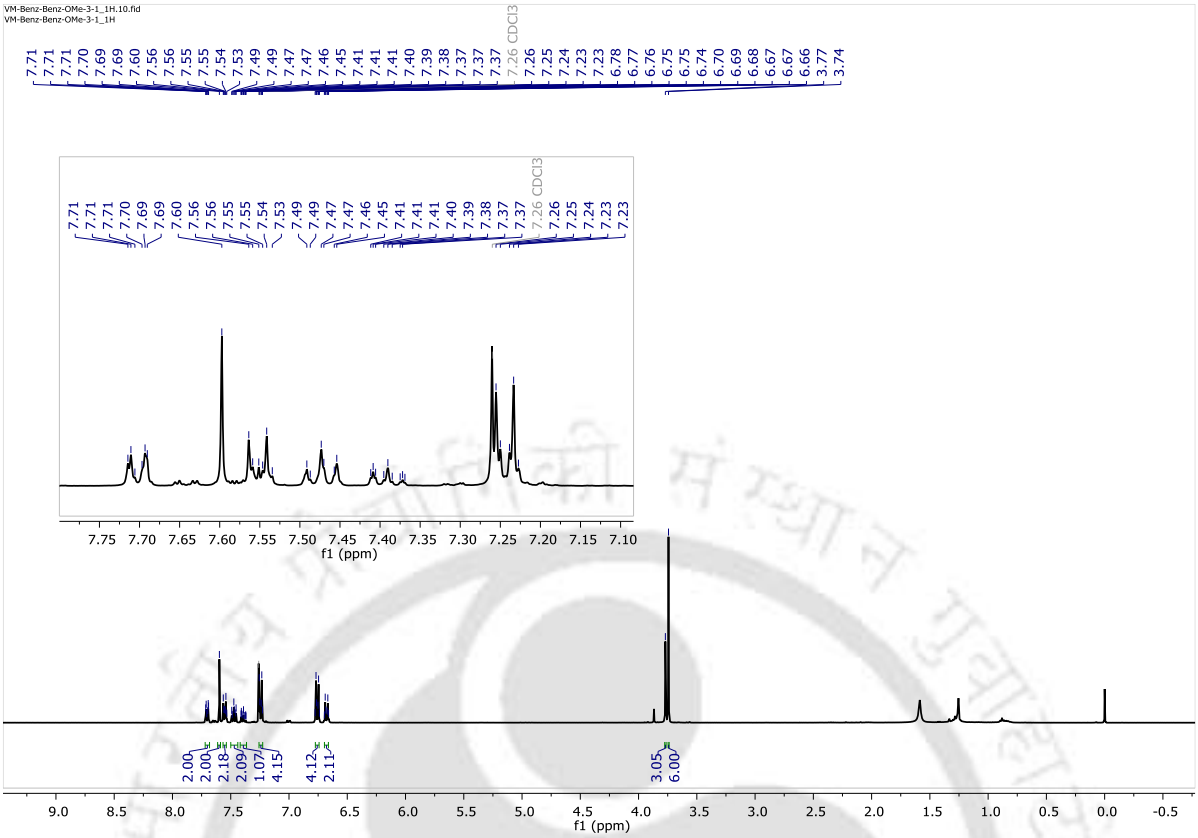

Figure A76. ^{1}H NMR spectrum of **1r**.

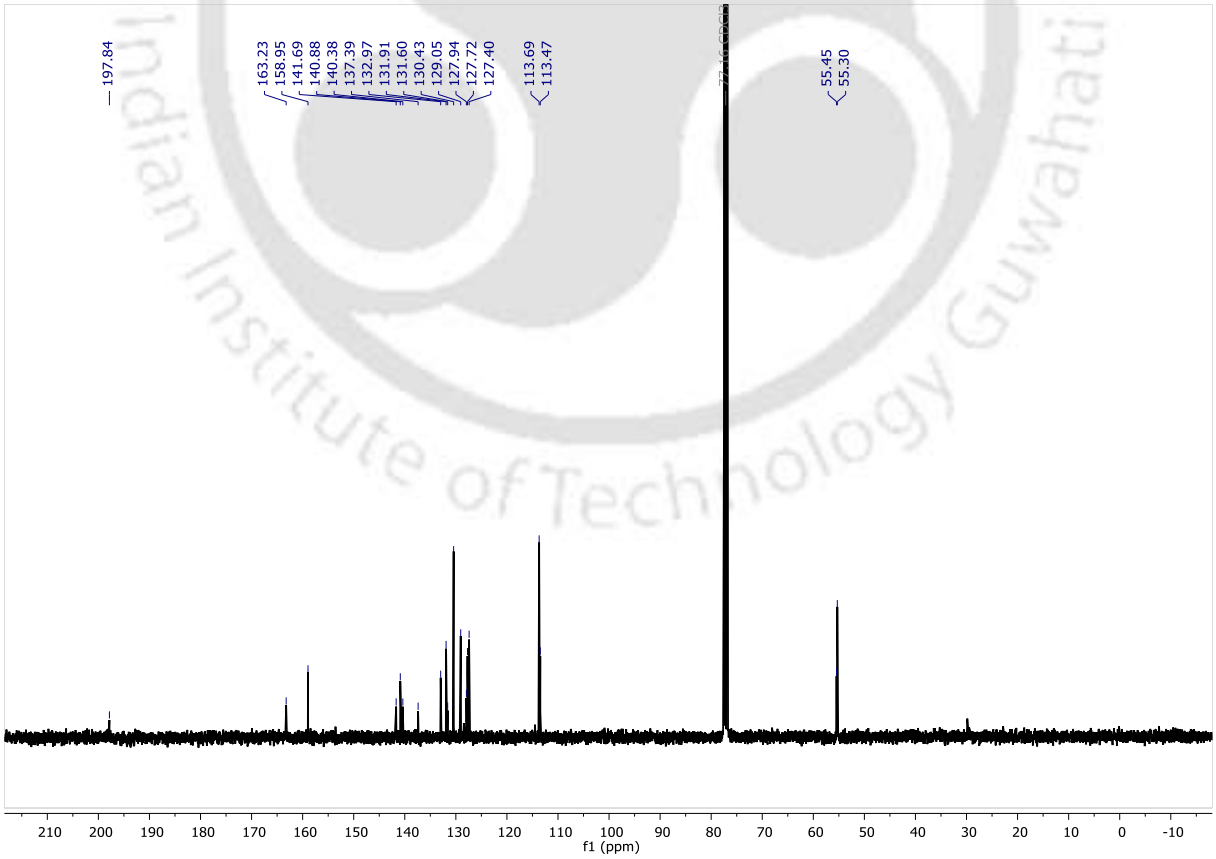

Figure A77. ^{13}C NMR spectrum of **1r**.

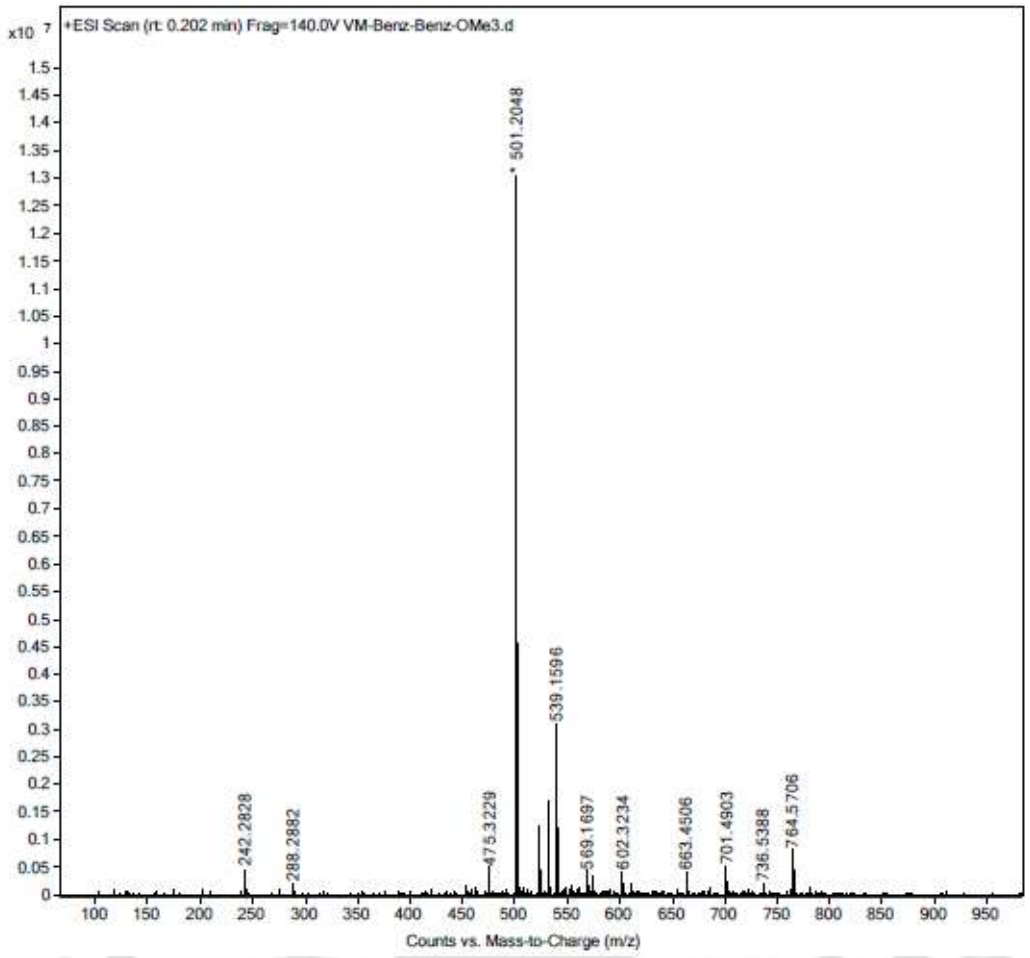

Figure A78. Mass spectrum of **1r**.

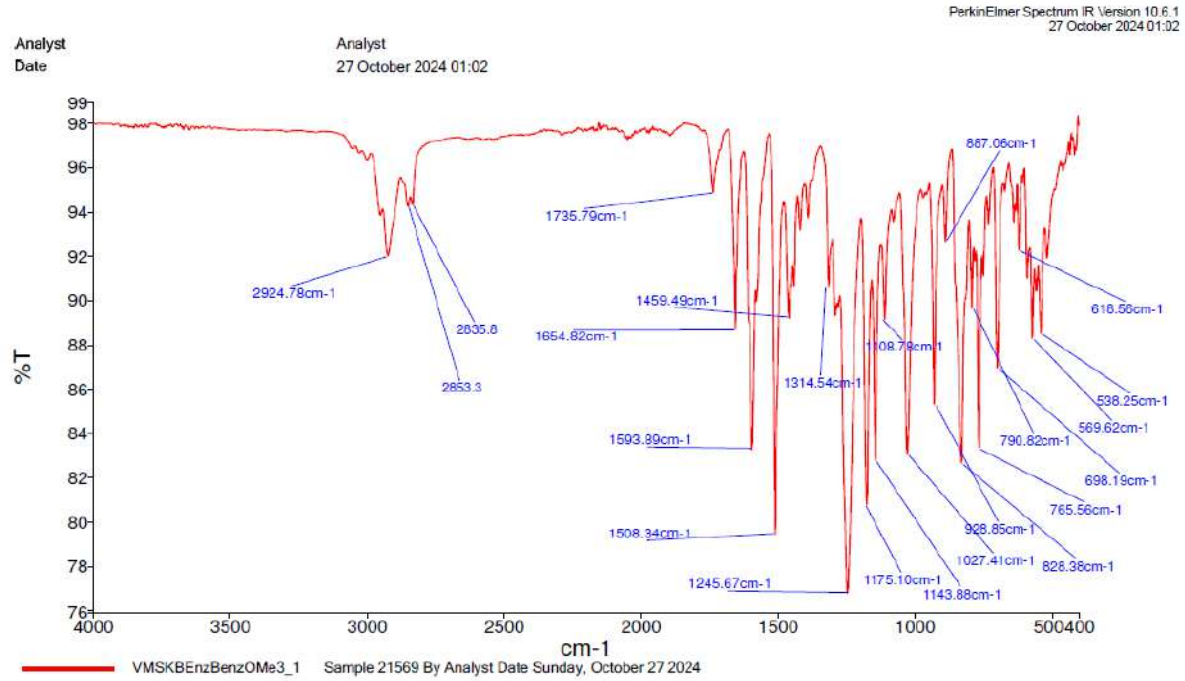

Figure A79. IR spectrum of **1r**.

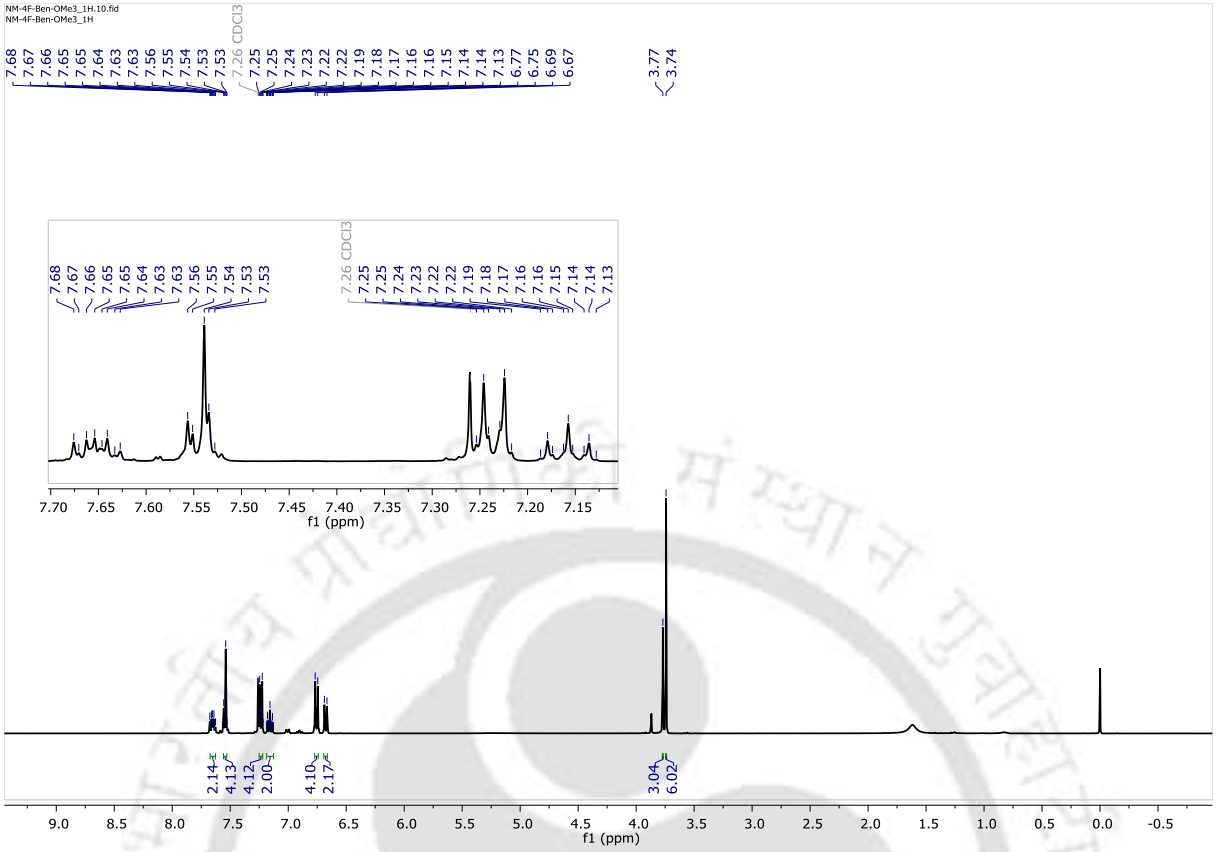

Figure A80. ^{1}H NMR spectrum of **1s**.

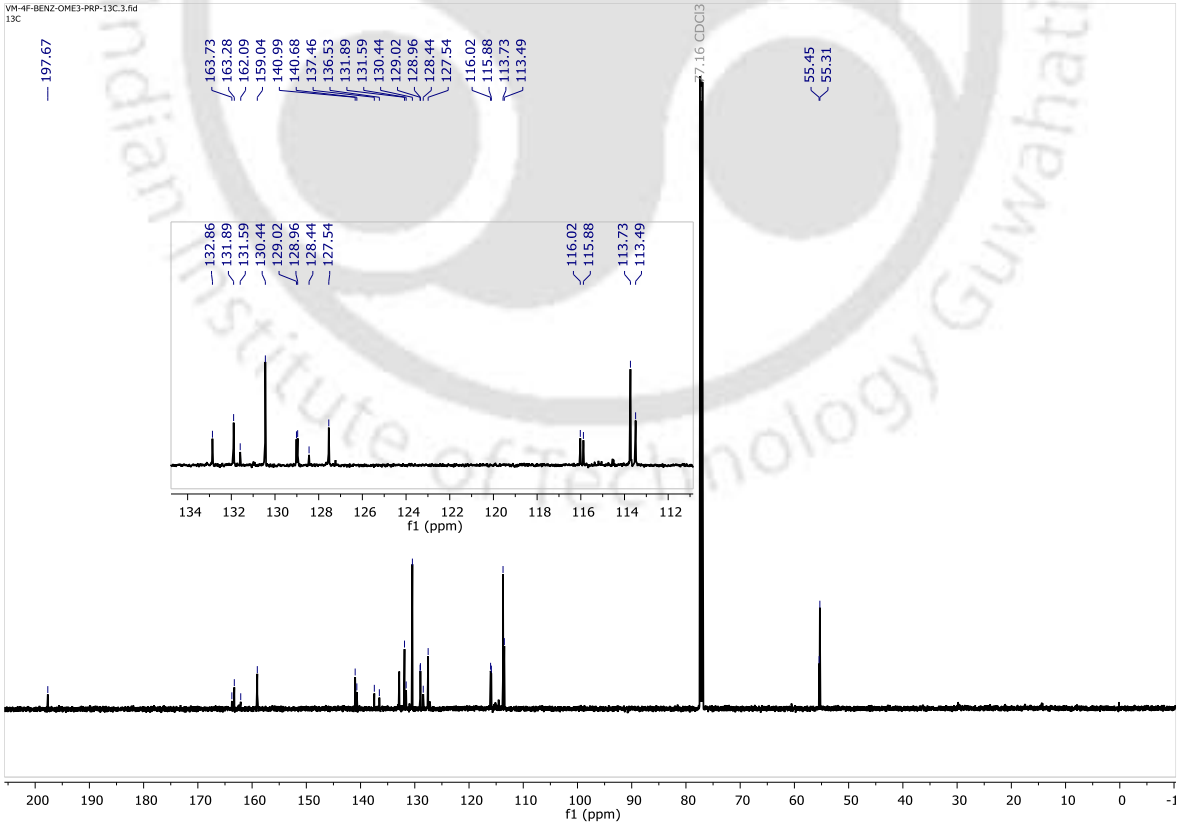

Figure A81. ^{13}C NMR spectrum of **1s**.

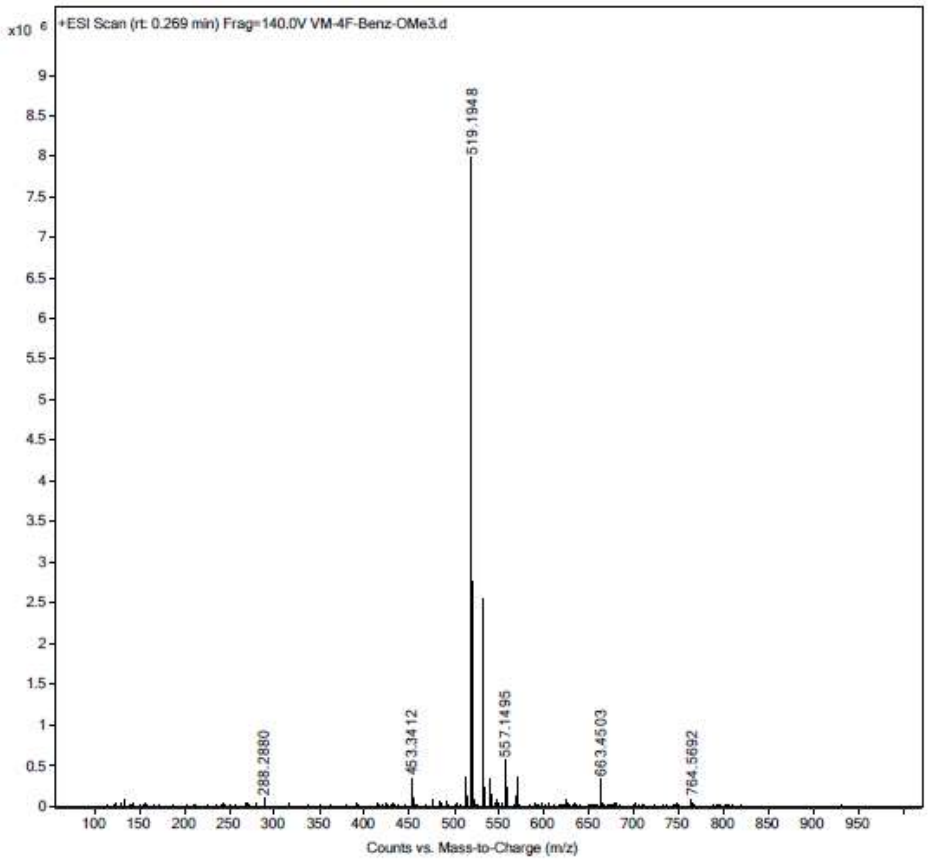

Figure A82. Mass spectrum of **1s**.

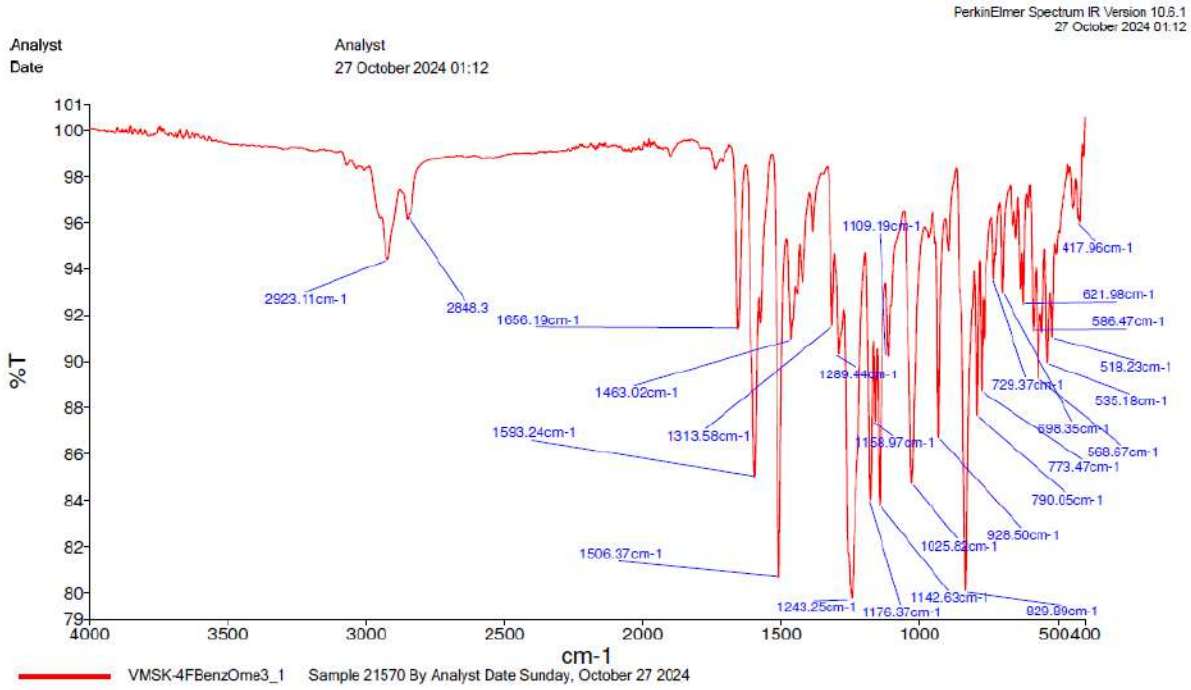

Figure A83. IR spectrum of **1s**.

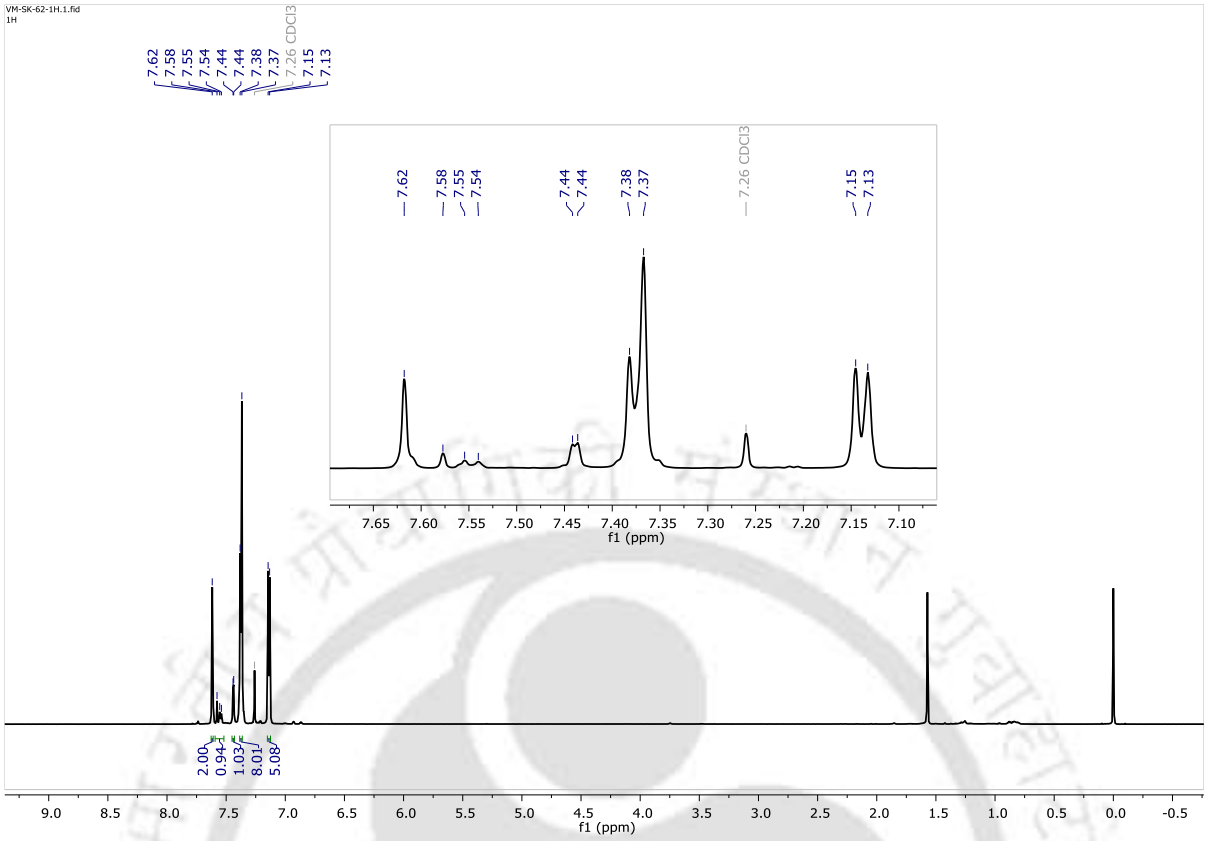

Figure A84. ^{1}H NMR spectrum of **1t**.

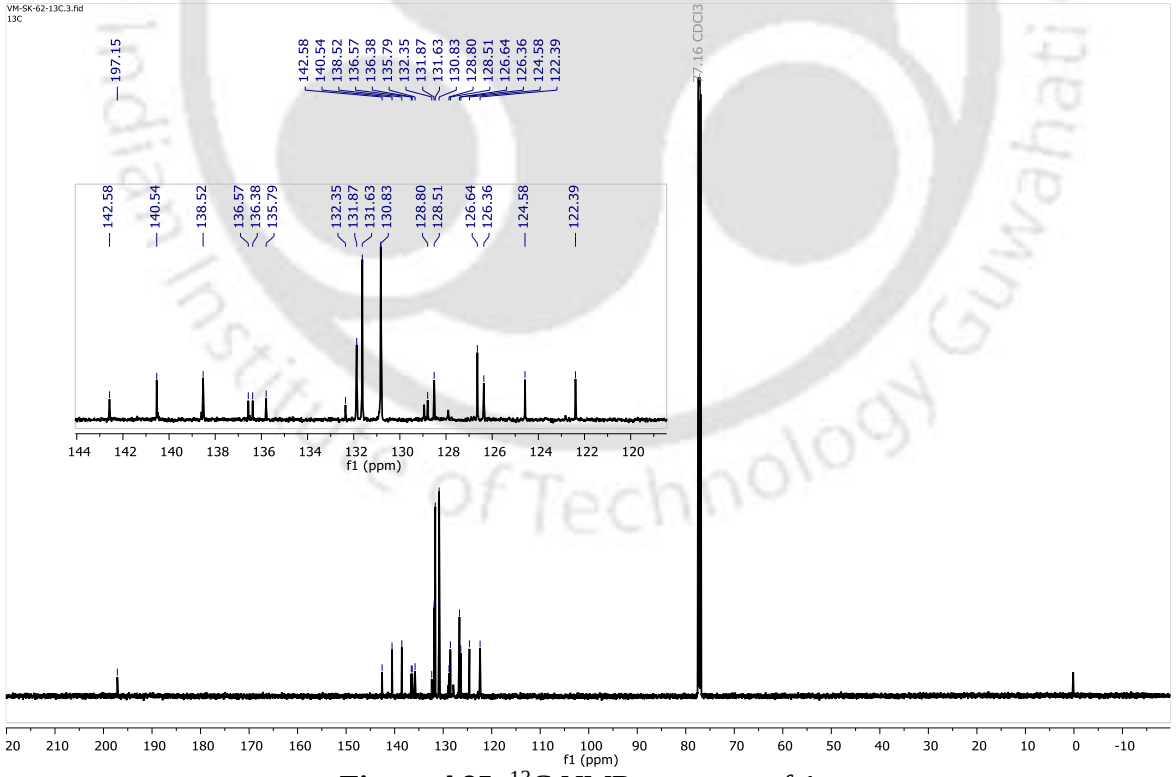

Figure A85. ^{13}C NMR spectrum of **1t**.

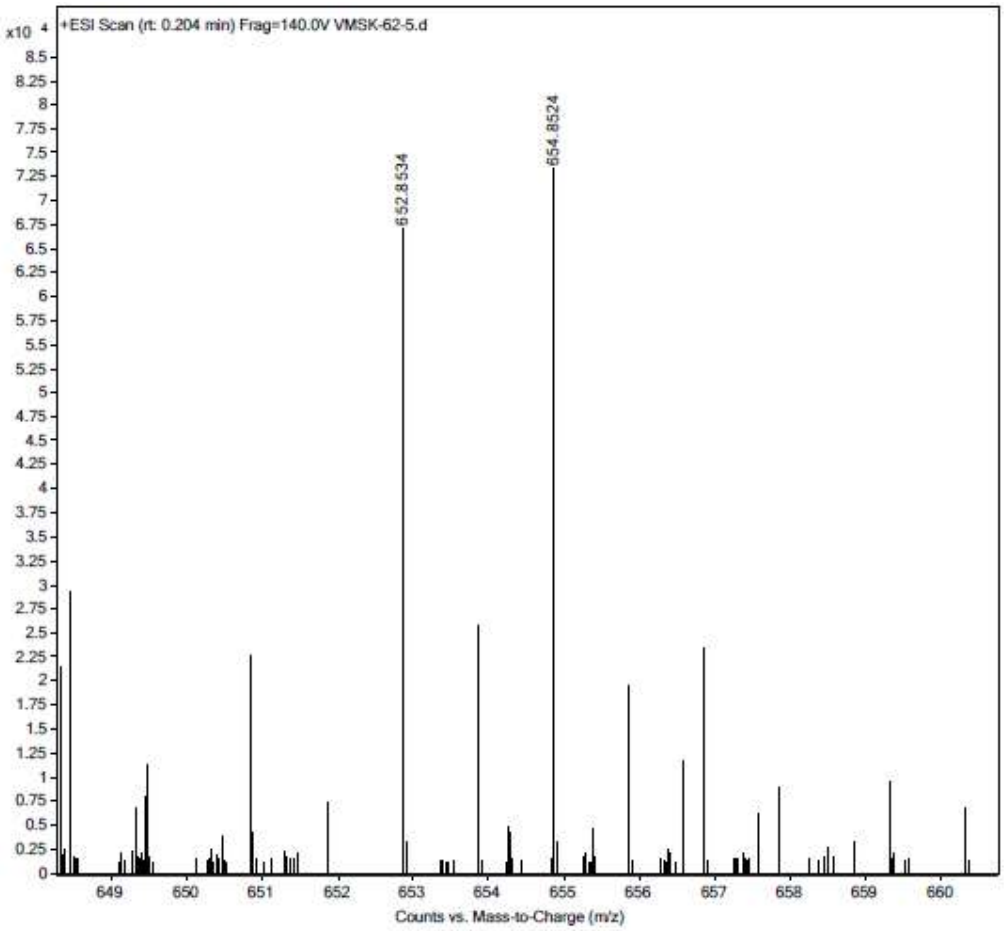

Figure A86. Mass spectrum of **1t**.

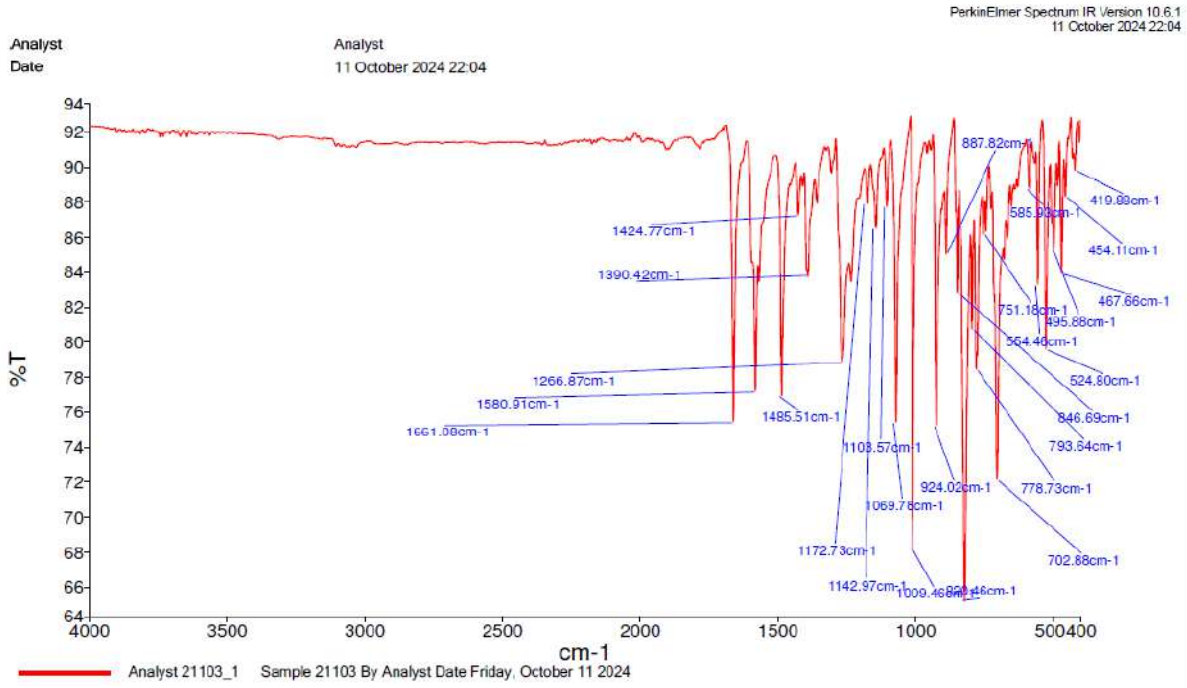

Figure A87. IR spectrum of **1t**.

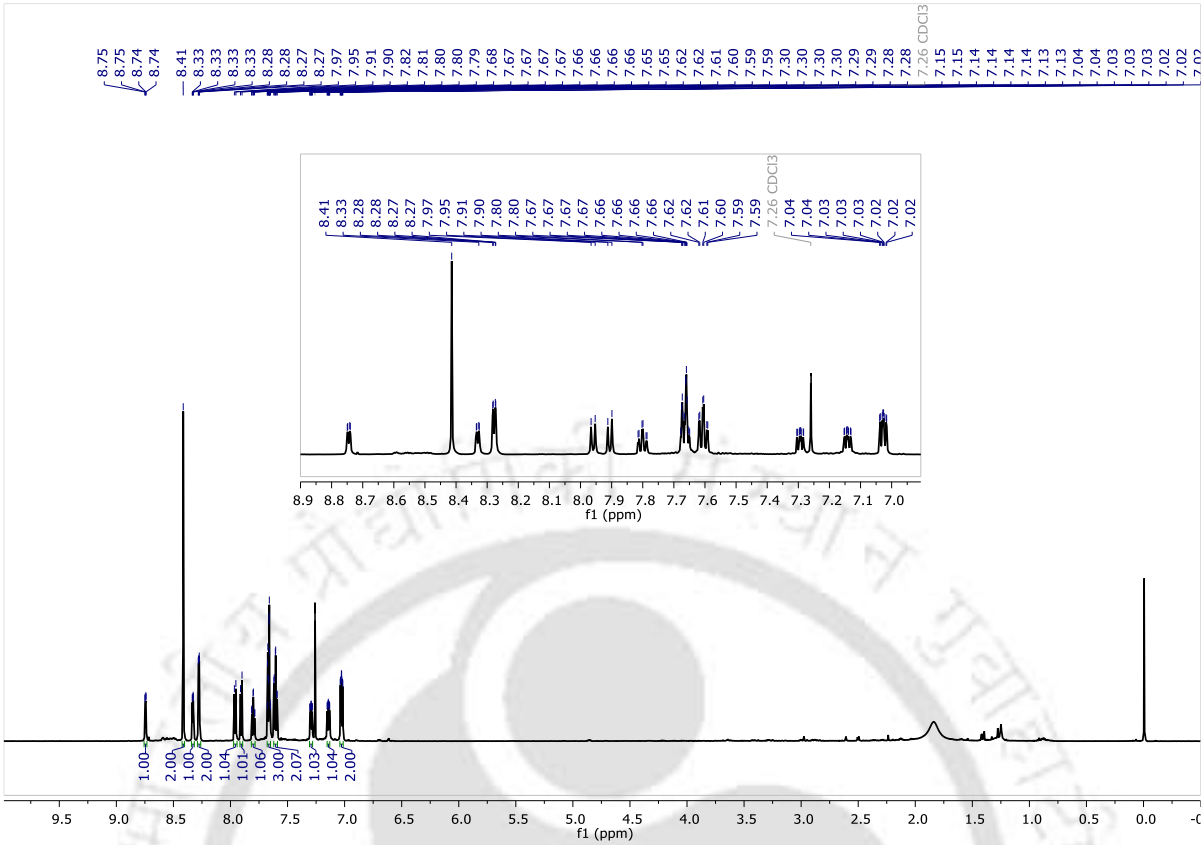

Figure A88. ^{1}H NMR spectrum of **1u**.

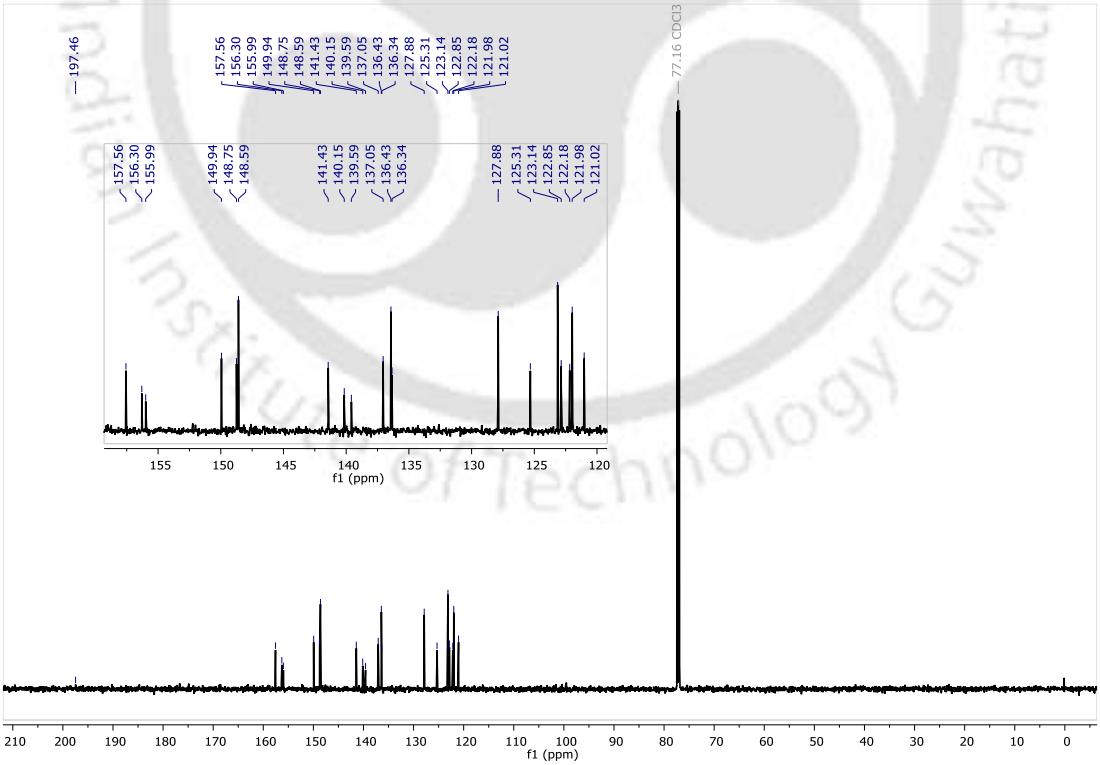

Figure A89. ^{13}C NMR spectrum of **1u**.

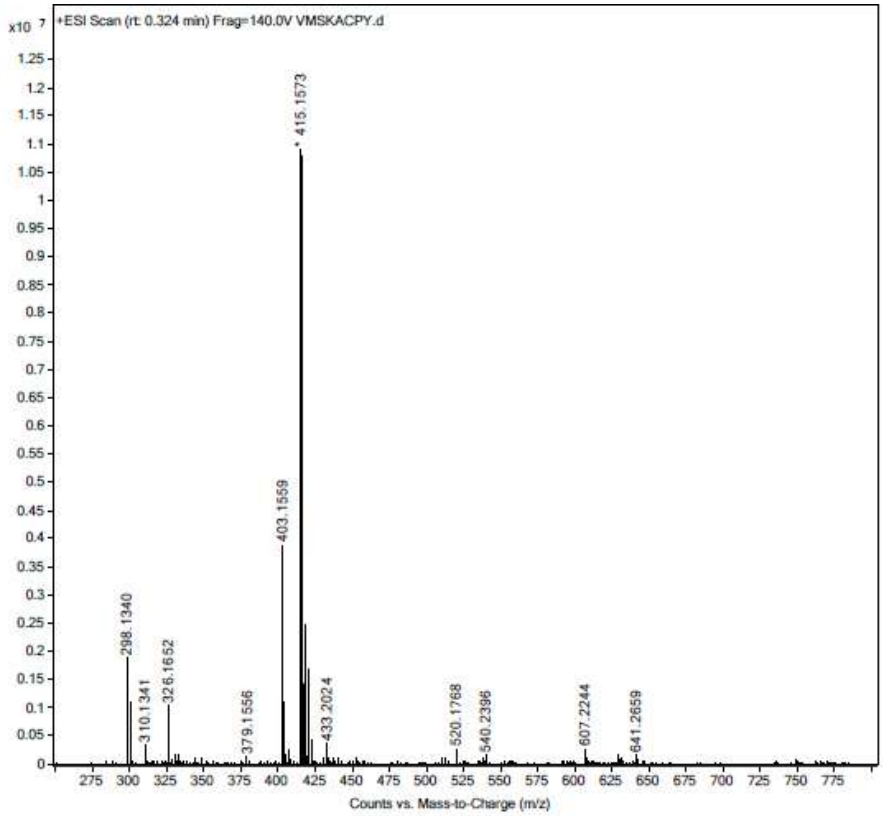

Figure A90. Mass spectrum of **1u**.

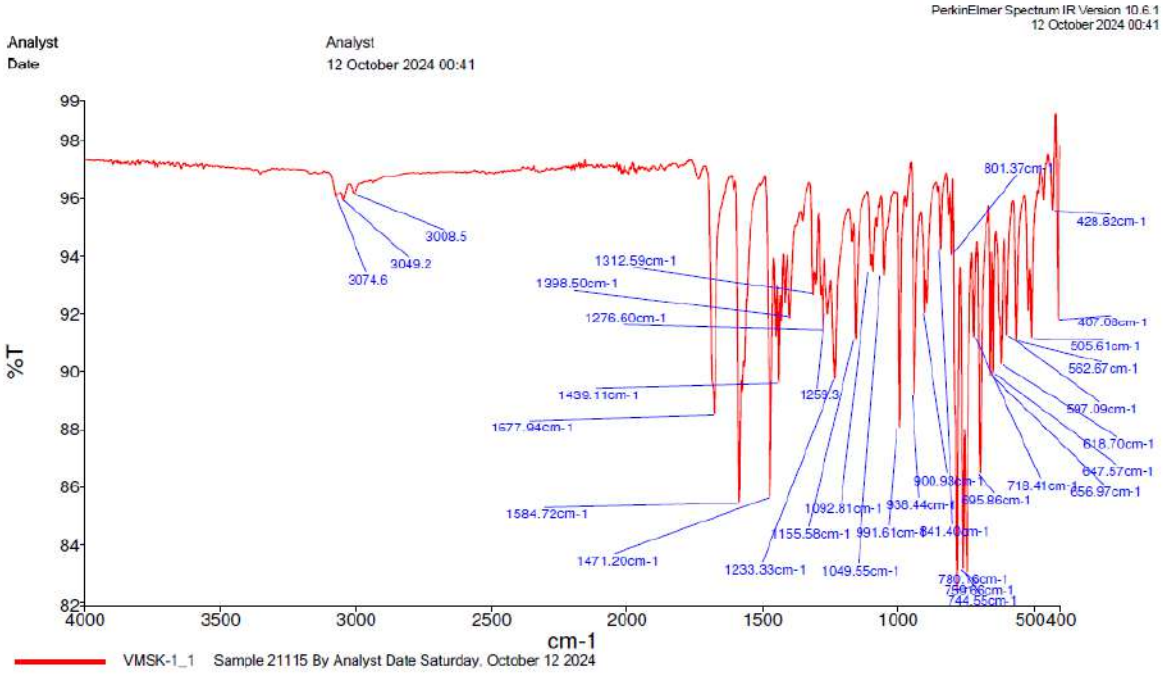

Figure A91. IR spectrum of **1u**.

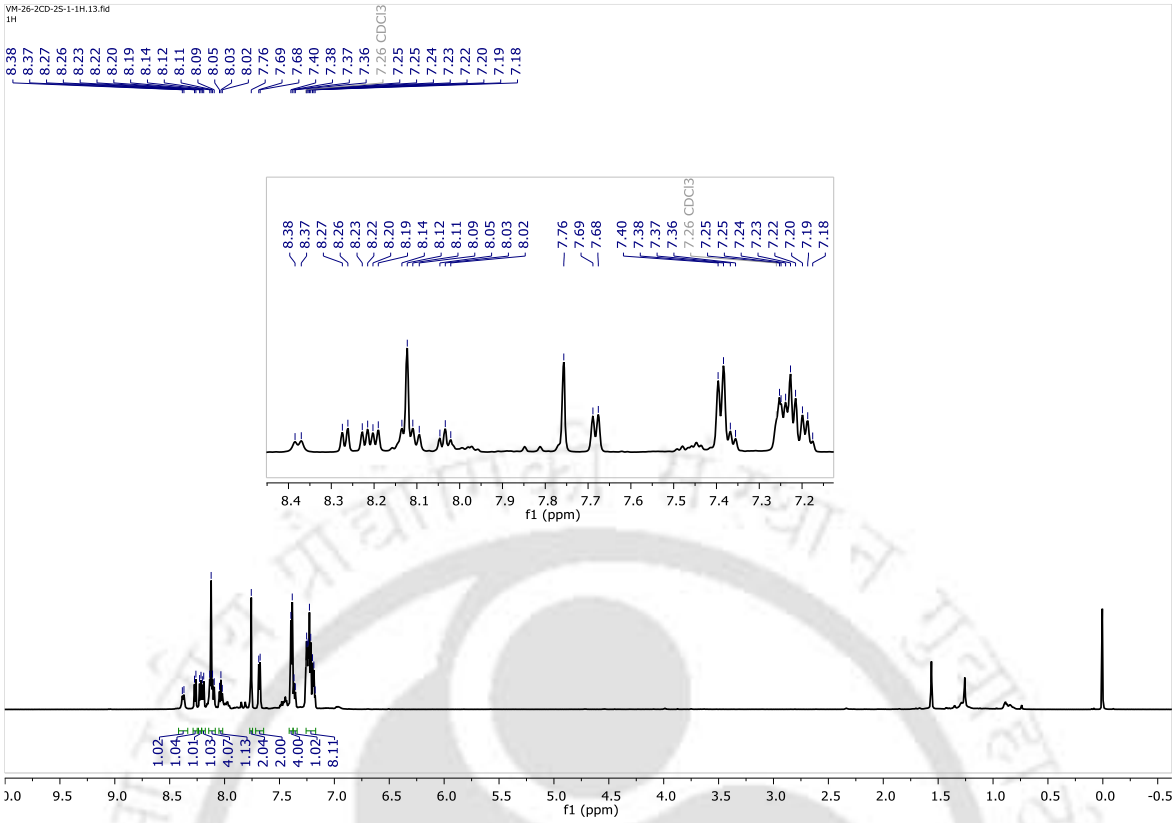

Figure A92. ^{1}H NMR spectrum of **1v**.

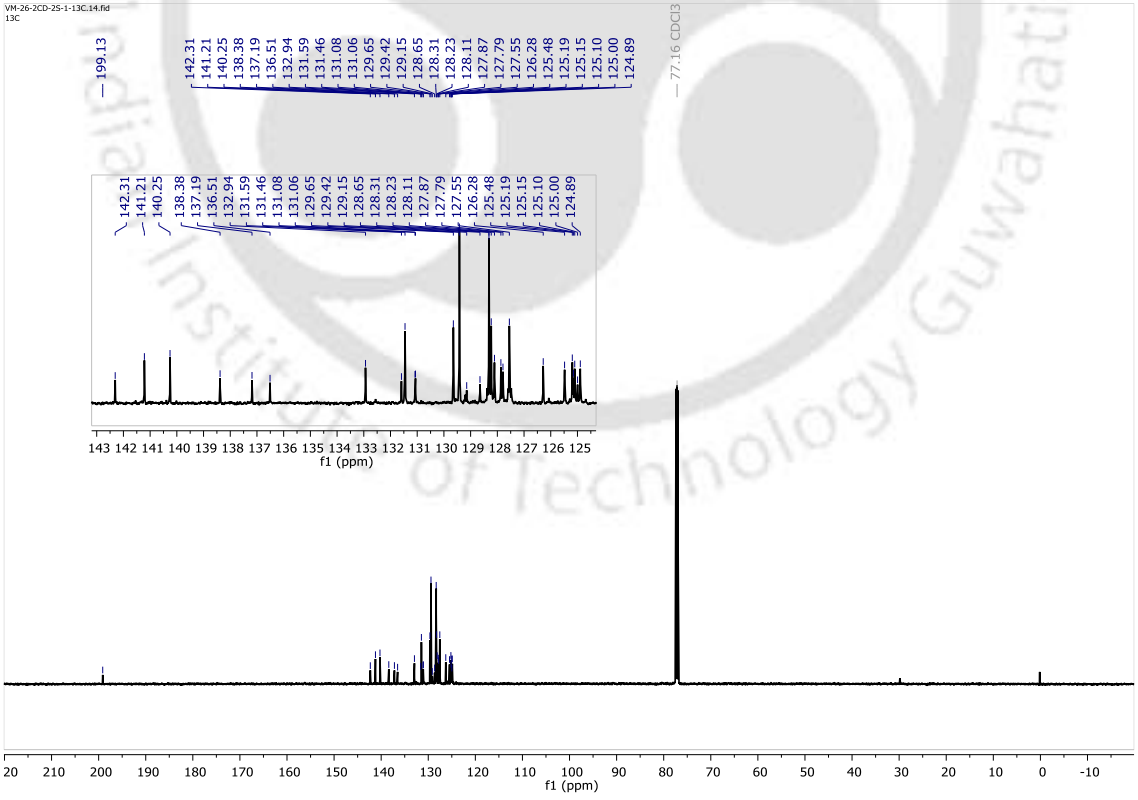

Figure A93. ^{13}C NMR spectrum of **1v**.

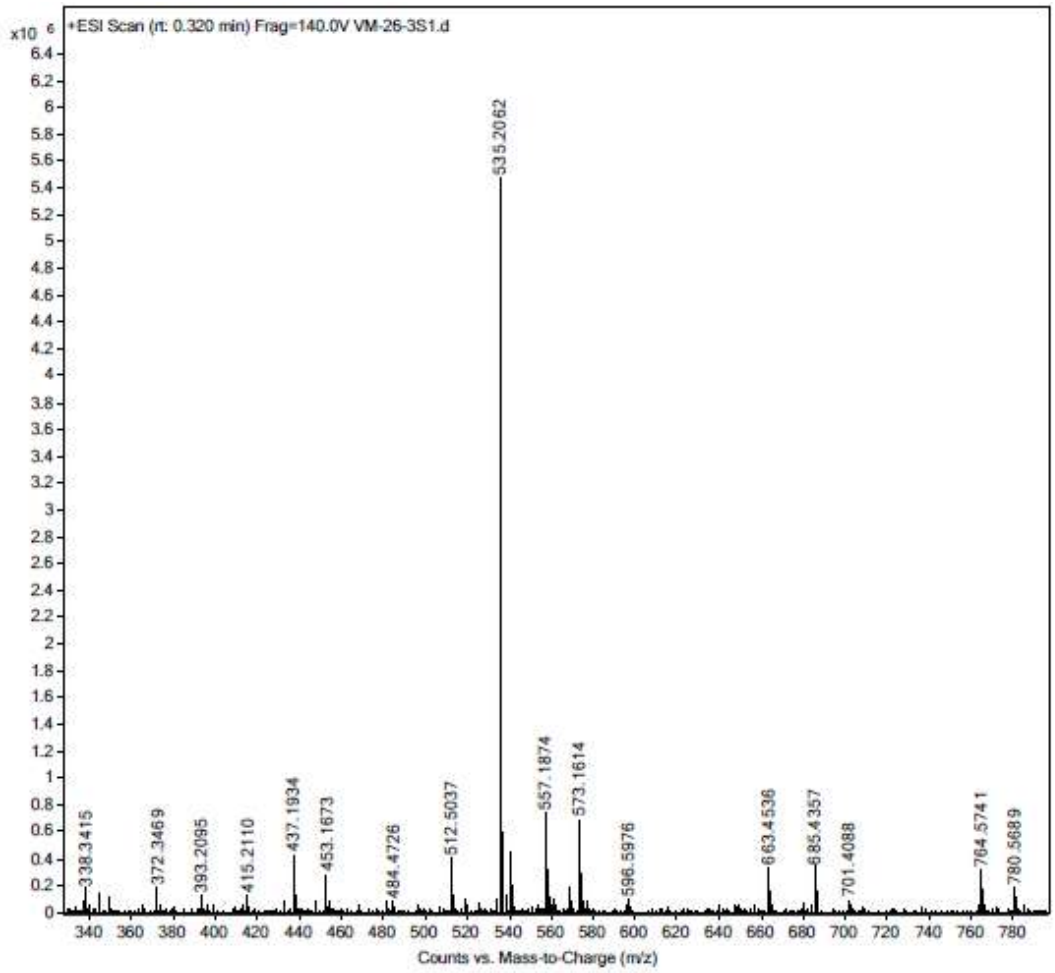

Figure A94. Mass spectrum of **1v**.

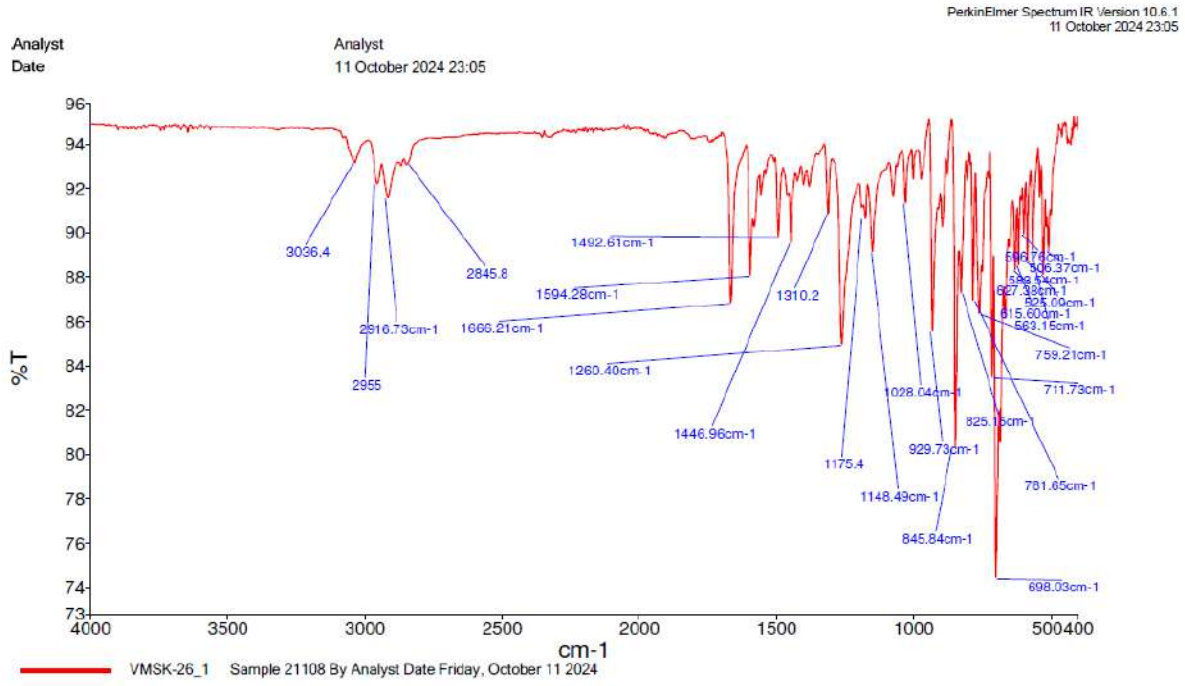

Figure A95. IR spectrum of **1v**.

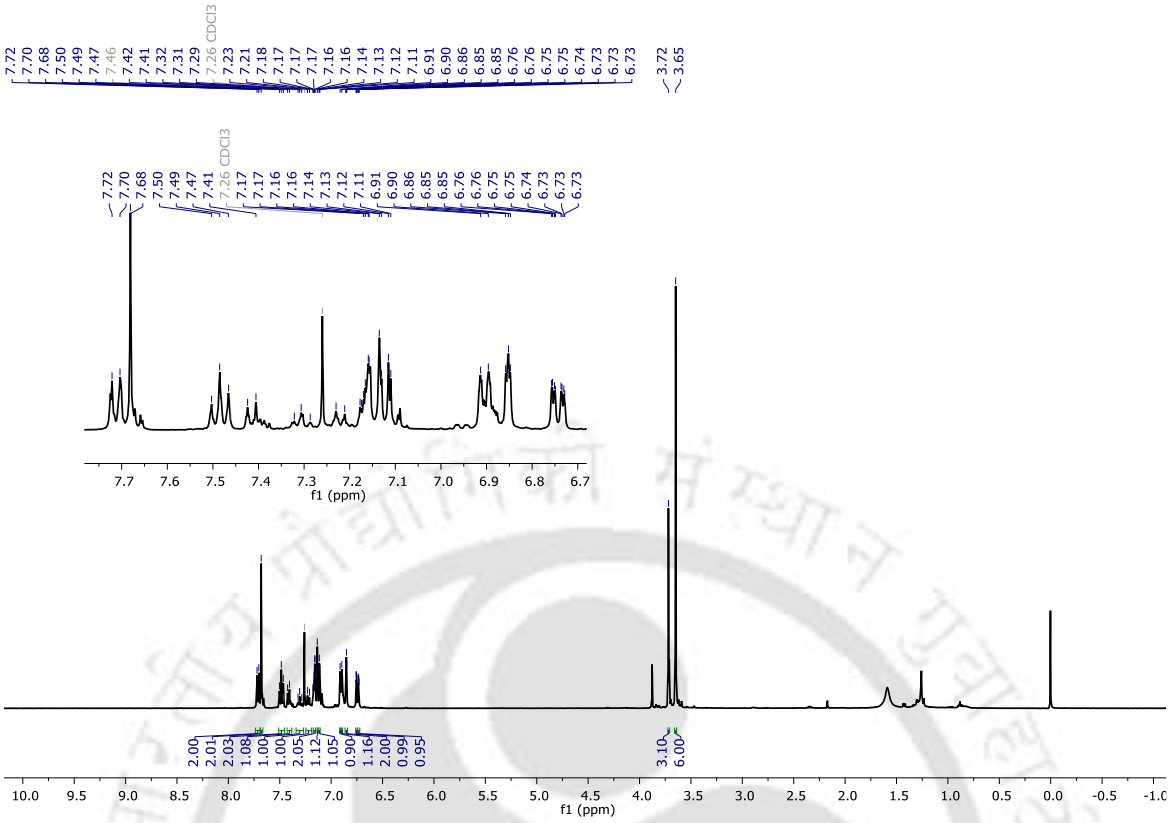

Figure A96. ^{1}H NMR spectrum of **1w**. Peaks (δ = 3.87, an impurity) due to grease and water (δ = 0.50-2.00) could not be removed.

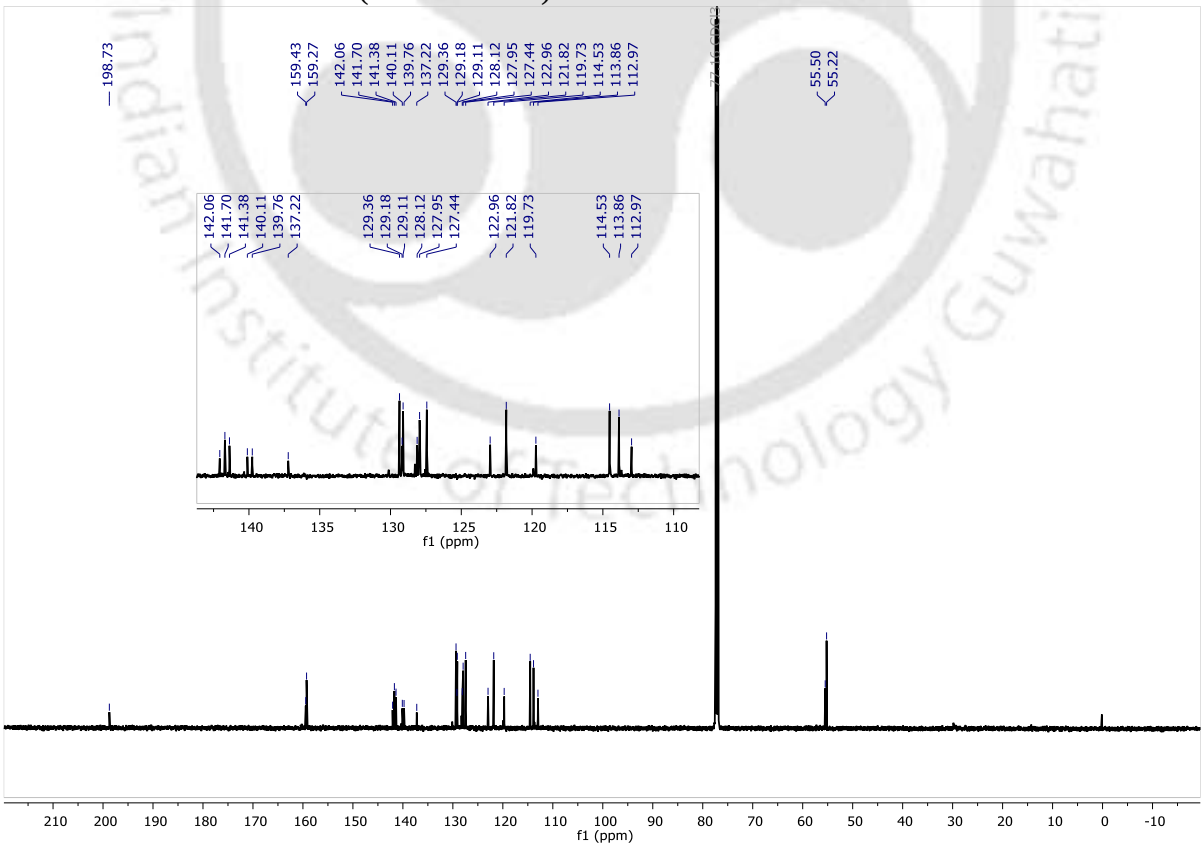

Figure A97. ^{13}C NMR spectrum of **1w**.

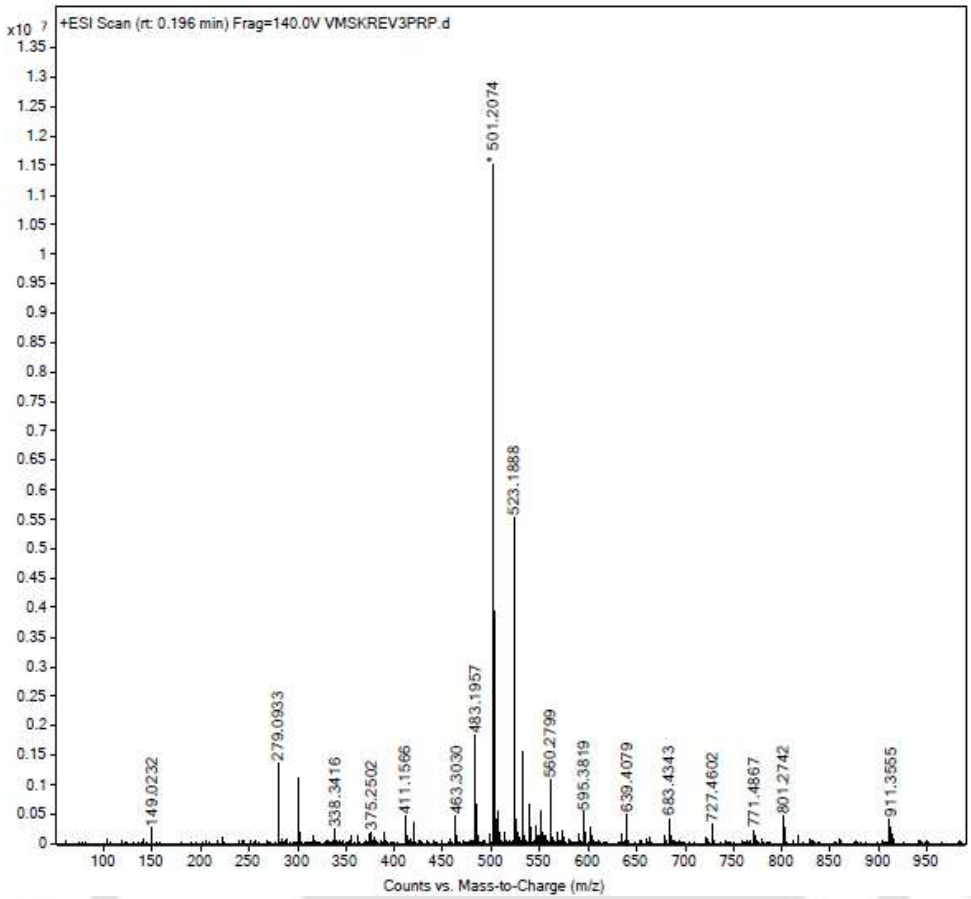

Figure A98. Mass spectrum of **1w**.

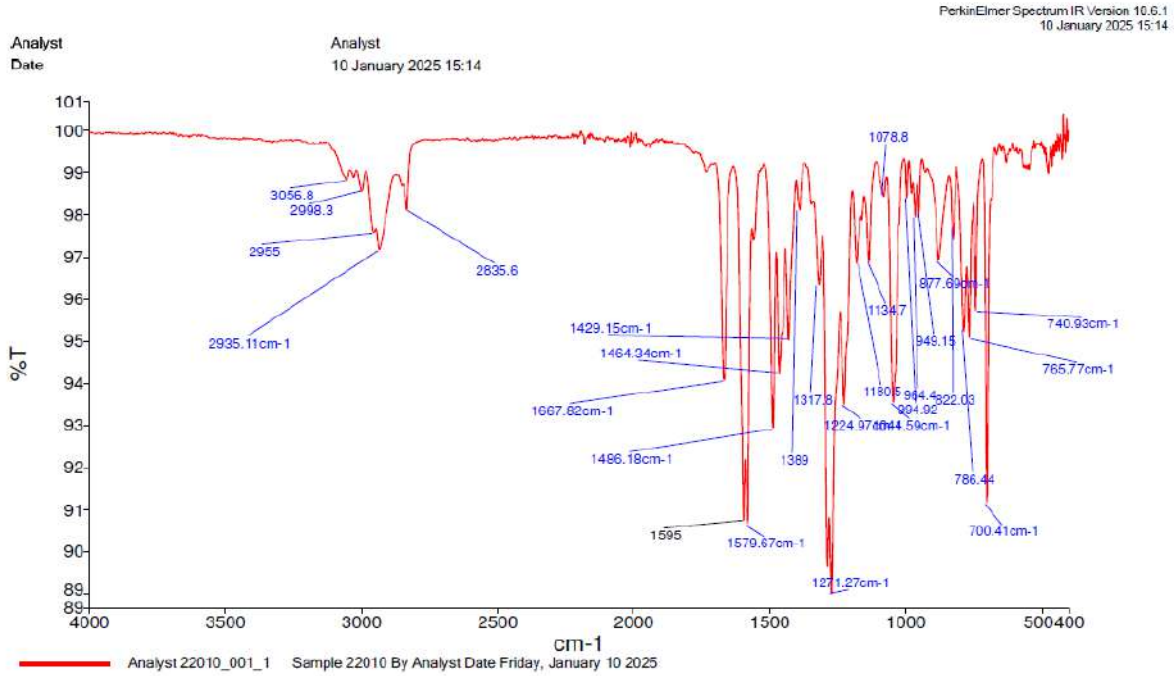

Figure A99. IR spectrum of **1w**.

Chapter 6

NaH Catalyzed Synthesis of Pentasubstituted Cyclohexanol from Aryl Methyl Ketone and Aromatic aldehyde

Abstract

A series of 1,2,3,4,5-pentasubstituted cyclohexanols was synthesized using 3:2 reaction mixture of aryl methyl ketone and aromatic aldehyde in presence of 20 mol% of NaH. These compounds are characterized by mass spectrometry, ^{1}H, ^{13}C- NMR and IR spectroscopy. This methodology adopts solvent free and aerobic conditions to obtain pentasubstituted cyclohexanols containing multiple stereocenters. Single crystal XRD method revealed the existence of enantiomeric pair and accordingly mechanism has been proposed for formation of both enantiomers.

1. Introduction

The carbocycle having six membered ring are commonly found in many natural products and biologically active compounds.[1] Substituted six membered carbocycles also serve as building block in synthetic organic chemistry.[2] As cyclohexane derivatives are the basic raw materials for the production of kerosene-based fuels, liquid crystal materials and coating agent, their synthesis has drawn a lot of attention.[3] Traditionally, cyclohexane derivatives were synthesized by hydrogenation of existing aromatic compounds having alkyl substituents obtained from Friedel-Craft reaction.[4] Cyclohexanol moieties are found in various drugs (Figure 1) like Ketamine (anesthetic), Tramadol (analgesic), Venlafaxine (antidepressant), Ambroxol (secretolytic agent).[5] Domino reactions i.e. reactions in which two or more chemical bond forming reaction takes place within one reaction vessel, are the most important one to synthesize cyclohexanol derivatives. These reactions are well within the requirement of green synthesis that rely on transformation required to have less number of steps, less waste production and increased atom economy.[6] Synthesis of 1,2,3,4,5-pentasubstituted cyclohexanols have been reported earlier[7] and a series were also synthesized by reacting acetophenone derivatives with various substituted benzaldehydes using KO*t*Bu (catalytic amount) in a domino reaction in DMSO[8a] and the one-pot asymmetric synthesis through a two-component reaction.[8b] In Chapter 5, synthesis of 2,4,6-trisubstituted benzophenones (*vis-à-vis* 1,2,4,6-tetrasubstituted benzenes) using NaH promoted cascade reaction of aryl methyl ketone and aromatic aldehyde in the ratio of 3:3:1 has been discussed. Incidentally, it was found that on changing this ratio of aryl methyl ketone and aromatic aldehyde to 3:2 and by using

NaH only in catalytic amount, 1,2,3,4,5-pentasubstituted cyclohexanols were obtained as major product, the details of which are discussed in this Chapter.

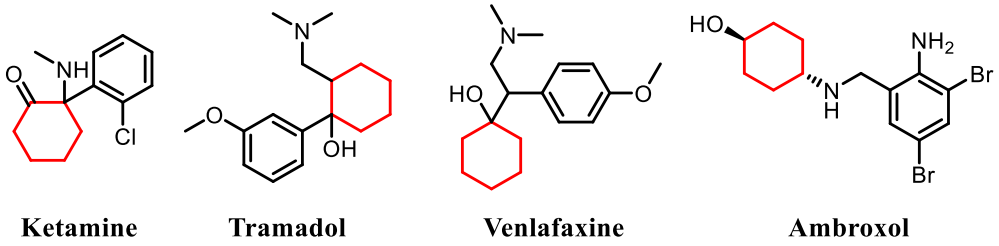

Figure 1. Some drugs that contain cyclohexane / cyclohexanol ring.

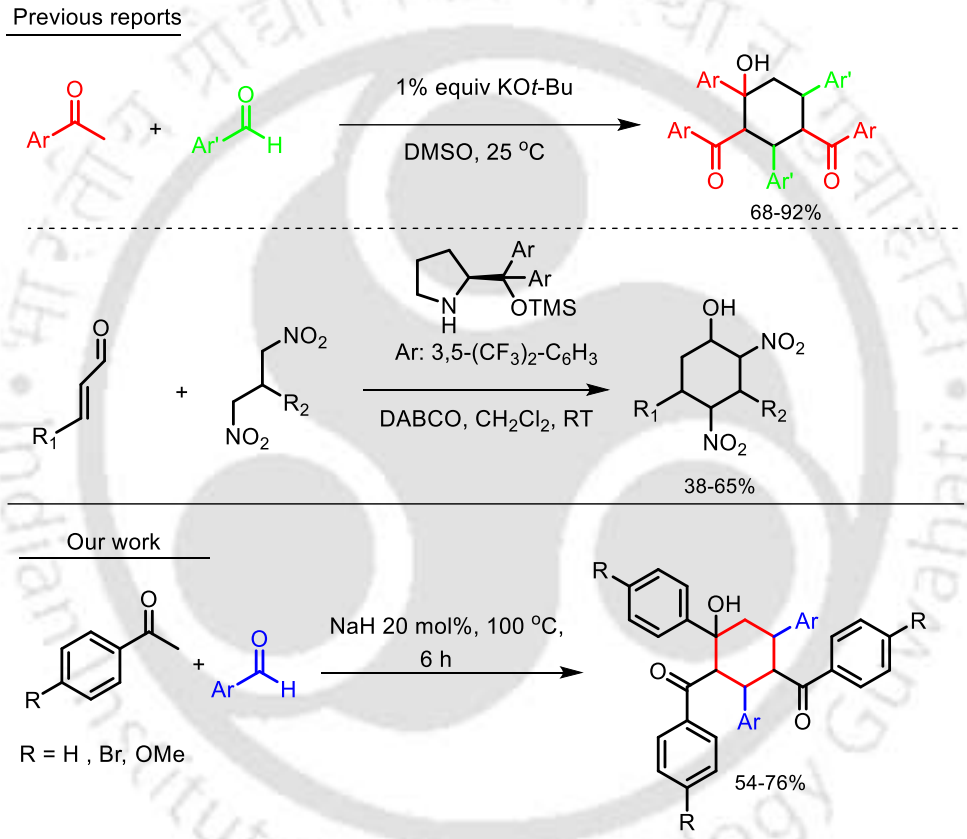

Scheme 1. Previous reports on synthesis of cyclohexanol derivatives and our work.

2. Results and Discussion

2.1 Synthesis

A neat 3:2 mixture of acetophenone and 4-pyridinecarboxaldehyde when heated at 100 °C for 6 h in presence of 20 mol% sodium hydride, yielded a gummy solid from which 1-phenyl-3,5-bis(4-pyridyl)-2,4-bis(benzoyl)cyclohexan-1-ol (**2a**) was isolated in good yield (Scheme 2). With acetophenone as the methyl ketone, reaction of benzaldehyde (**2b**), o-tolualdehyde (**2c**), p-tolualdehyde (**2d**), 4-methoxybenzaldehyde (**2e**), 4-fluorobenzaldehyde (**2f**), 4-

bromobenzaldehyde (**2g**) and 2-thiophenecarboxaldehyde (**2h**), yielded respective pentasubstituted cyclohexanol in moderate to good yields. The methylketone, 4′-bromoacetophenone also reacted with 4-methoxybenzaldehyde (**2i**), p-tolualdehyde (**2j**), benzaldehyde (**2k**), 4-fluorobenzaldehyde (**2l**), 4-chlorobenzaldehyde (**2m**), o-tolualdehyde (**2n**) and 3-methoxybenzaldehyde (**2o**), from which respective cyclohexanol compounds were isolated. The o-substituted acetophenone, 2′-chloroacetophenone reacted with o-toulaldehyde to give (**2p**). The 4′-methoxyacetophenone also reacted with o-tolualdehyde to give **2q**. Compounds **2a**-**2q** were characterized thoroughly using ^{1}H-, ^{13}C-NMR, mass, IR and single-crystal X-ray diffraction (**2b**) methods.

In ^{1}H NMR spectra, the characteristic peak for the –OH proton at C1 position (refer Figure 2 for numbering) of the cyclohexanol ring appeared as a singlet at δ = 5.31 ppm in **2a**, but in all other compounds as doublet in the region δ = 5.29 – 5.40 ppm due to weak coupling (J ~ 1.8 – 2.5 Hz) with C3 – H. The proton at C2 position was observed as doublet at δ = 4.50 ppm in **2b**. The protons at C3 and C4 positions were expected as triplets but got merged and appeared as multiplet at δ = 4.27-4.16 ppm. The proton at C5 position appeared as triplet of doublets at δ = 4.07 ppm because of coupling with two protons at C6 and then one at C4. The diastereotopic protons H_A at C6 positions appeared as triplet at δ = 2.56-2.50 ppm whereas the proton H_B appeared as doublet of doublets at δ = 2.26 ppm. The ^{13}C NMR spectrum of **2b** has two distinct peaks 207 and 203 ppm which suggested that two carbonyl carbons have different environments.

The molecular structure of **2b** was determined by single crystal X-ray diffraction method, which confirmed the regioselectivity of the substituents in the chair form of cyclohexanol ring. It is pertinent to note that crystal data, molecular compound **2b** crystallized in $P\bar{1}$ space group, in the asymmetric unit two molecules of **2b** along with one $CHCl_3$ were present and a schematic diagram of one of the molecules has been shown in (Figure 2) and both enantiomers has been shown in Figure A2. These two were mirror images and hence the crystal lattice consisted of 1:1 mixture of ((1*R*,2*S*,3*R*,4*S*,6*S*)-4-hydroxy-2,4,6-triphenylcyclohexane-1,3-diyl)bis(phenylmethanone) and ((1*S*,2*R*,3*S*,4*R*,6*R*)-4-hydroxy-2,4,6-triphenylcyclohexane-1,3-diyl)bis(phenylmethanone). The 1,2,3,4,5-pentasubstituted cyclohexanol had phenyl/4-bromophenyl at position C1, benzoyl/4-bromobenzoyl at positions C2 and C4 originating from the ketone while aryl group of the aldehyde occupied the position C3 and C5 (refer Figure 2 for numbering). The cyclohexan-1-ol existed in the chair conformation with –OH group

occupying the axial site at C1 and the bulky aryl group in the equatorial position. All other bulky groups in 2,3,4 and 5 positions were in the equatorial sites and the product formed thus had an equal proportion of racemic mixture. The hydrogen bonding interaction between the –OH group and the oxygen of the benzoyl group at the adjacent carbon is present and the non-bonded distances are O1···O2, 2.767(3) and O4···O5 2.704(3) Å. The crystal structure of **2b** matched with the details reported earlier by other group,[9] but the only relevant structural details of **2b** has been included here to support the synthetic methodology.

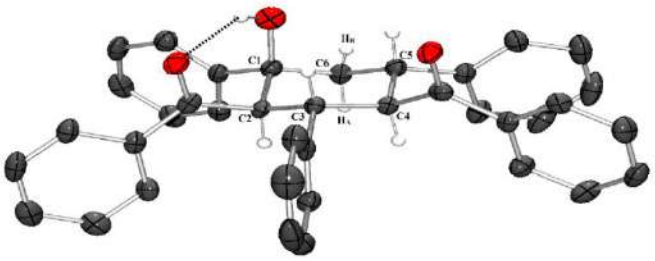

Figure 2. ORTEP diagram (50% Probability) of one of the enantiomers of **2b**. Hydrogen atoms of phenyl rings were omitted for clarity.

Table 1. Optimization of reaction condition of **2b**.

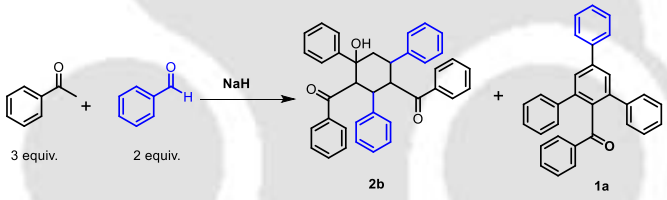

Entry	NaH* (equiv.)	Temp^	%Yield **2b**
1	1	RT	ND#
2	1	40	10
3	1	60	38
4	1	80	52
5	0.5	80	61
6	0.3	80	68
7	**0.2**	**100**	**74**
8	0.1	100	63

Condition: 4 mmol (3 eq.) of acetophenone and 2.93 mmol (2.2 eq.) of benzaldehyde. #ND = Not Detected. ^ °C.
*The purchased sodium hydride was of 55-60% in mineral oil and molar ratio was calculated using this strength.
Caution: Sodium hydride may catch fire upon exposure to water/moisture.

The reaction condition was optimized with acetophenone and benzaldehyde by varying temperature and mol % of NaH (with respect to acetophenone). Addition of 1 equivalent of NaH, did not yield the cyclohexanol (**2b**) at room temperature (Table 1). However, as the temperature was increased the yield of **2b** started to increase however along with 2,4,6-triphenylbenzophenone (**1a**, details of which were discussed in Chapter 5) as product mixture. Hence to isolate **2b** as exclusive product and to minimize the formation of **1a**, NaH loading was decreased and it was found that cyclohexanol **2b** was obtained exclusively with maximum yield when NaH was 20 mol%. This stoichiometric ratio of the reactants was adopted for the synthesis of all other cyclohexanols reported in this work. It is pertinent to note that synthesis of **2b** and some other cyclohexanols were reported earlier by other group as well,[7,8a] but the compounds **2a**, **2c**, **2l**, **2m**, **2n**, **2o**, **2p** and **2q** reported in this work are new compounds synthesised using this methodology.

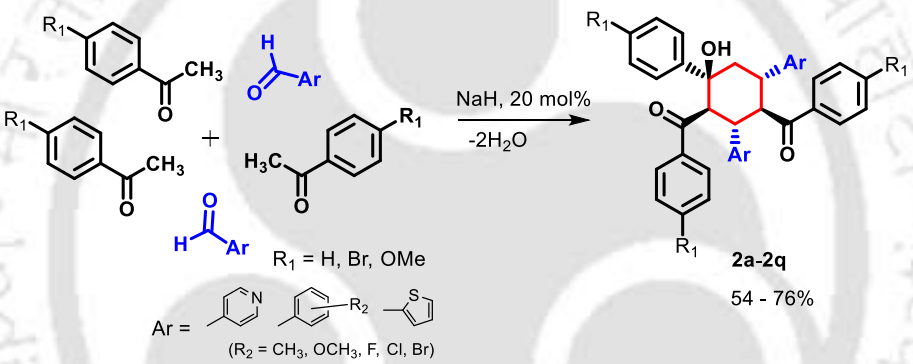

Scheme 2. Synthesis of 1,2,3,4,5-pentasubstituted cyclohexanols.

Table 2. Substrate scope.

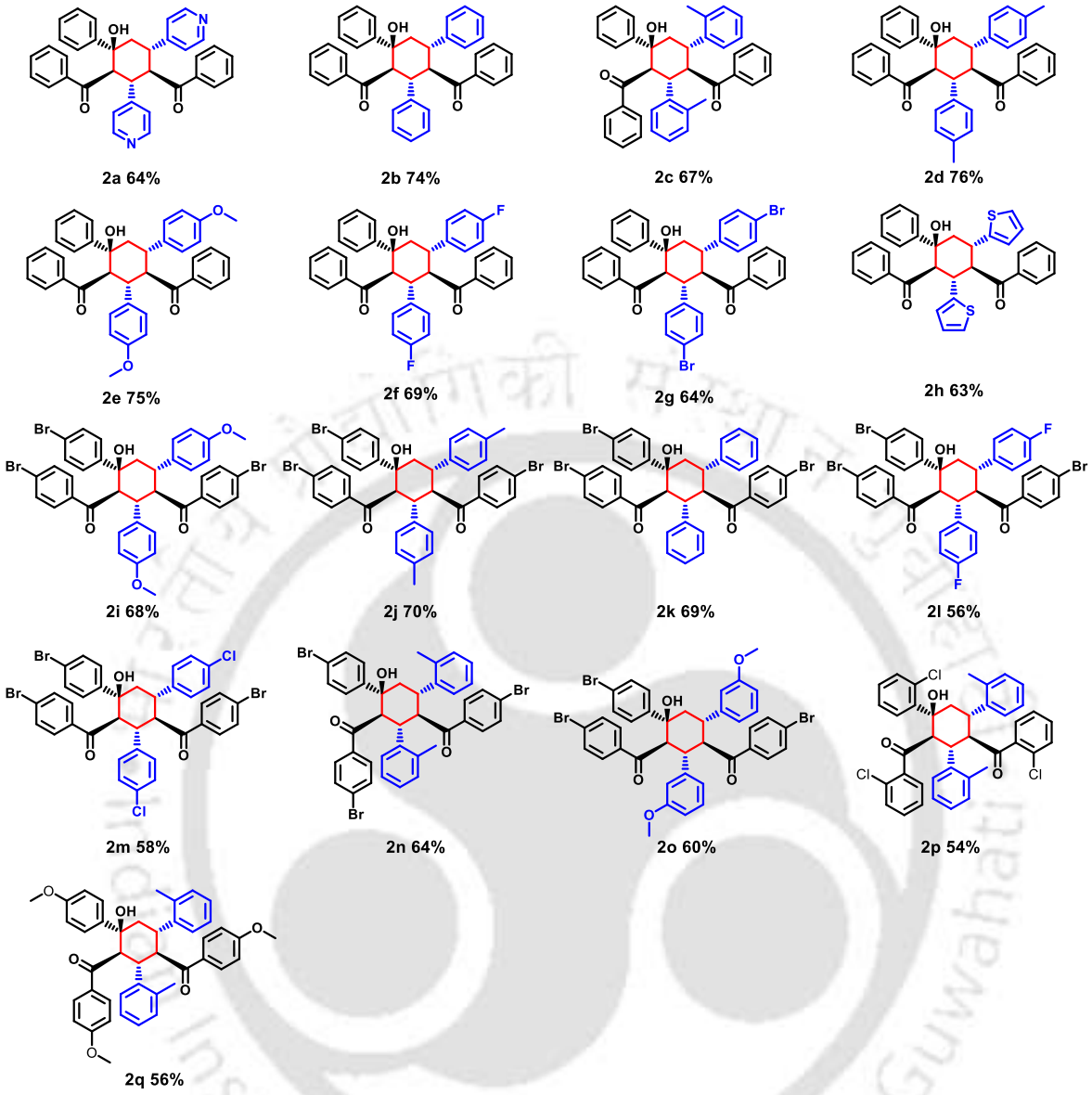

2.2 Mechanism

For mechanistic study, acetophenone and 4-pyridinecarboxaldehyde were chosen as reactants and ESI-MS (+) data were recorded to detect the intermediates, accordingly a plausible mechanism has been proposed (Scheme 3). Acetophenone in presence of catalytic amount of sodium hydride, deprotonated to carbanion **(I)** which readily reacted with 4-pyridinecarboxaldehyde to generate the anion which could have abstracted a proton from acetophenone to produce and chalcone (**II**) (*m/z* calculated for $C_{14}H_{12}NO^+$ 210.0914 ($M + H^+$); found 210.0900). A 1,4-attack on chalcone by **I** lead to formation of the anion **III** (*m/z* calculated for $C_{22}H_{20}NO_2^+$ 330.1489 ($M^- + 2H^+$); found 330.1482) which further can combine with **II** in two equivalent fashions to generate the two forms of anion **IV**. These two forms of

IV can undergo intramolecular aldol reaction to form racemic mixture of **2a**$^{-}$ from which **2a** formed after abstraction of proton from acetophenone which will regenerate **I**.

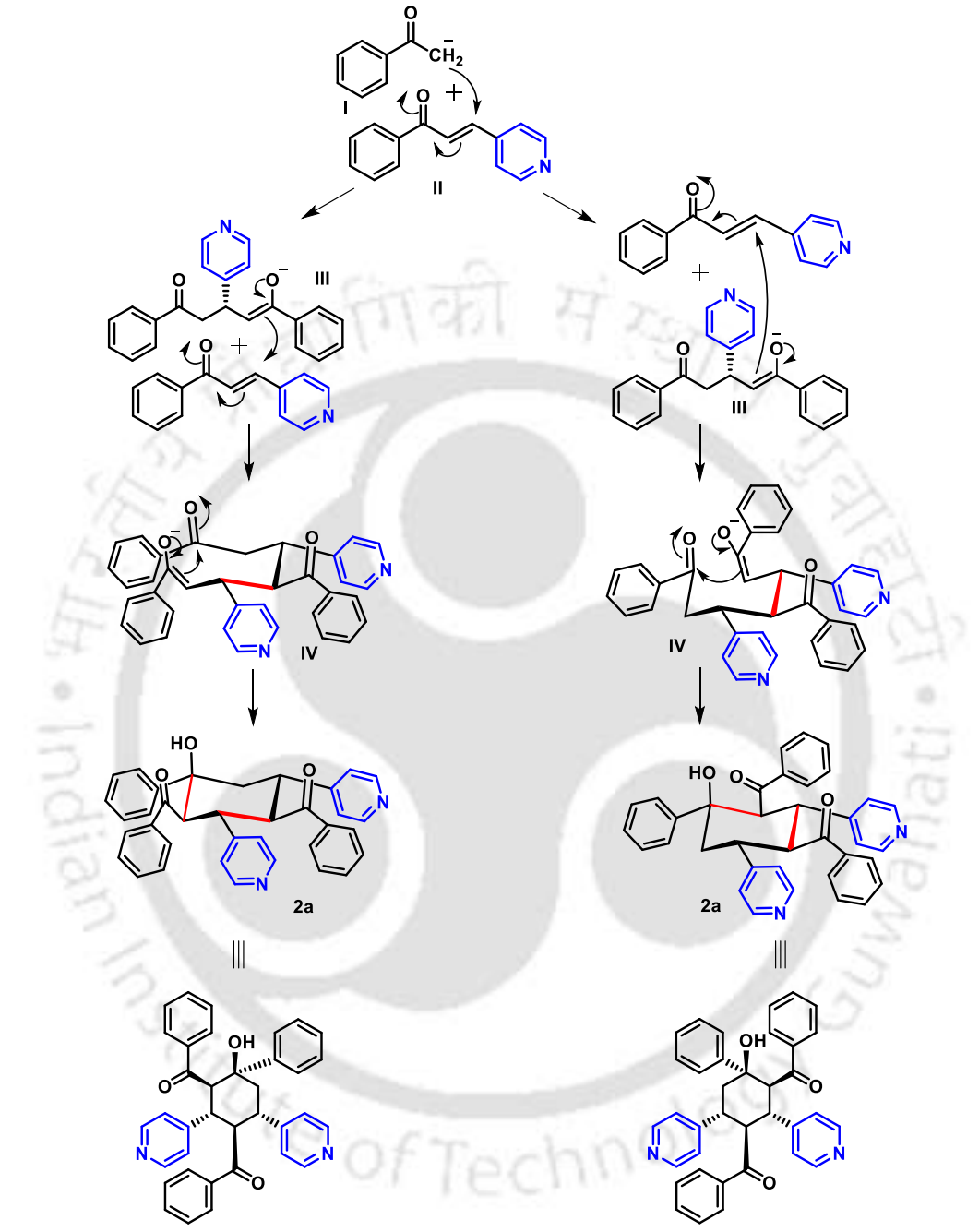

Scheme 3: Plausible mechanism for the formation of cyclohexanol **2a**.

3. Conclusion

Facile synthesis of a series of pentasubstituted cylohexanol was achieved in moderate to good yield by the reaction of aryl methyl ketone and aromatic aldehyde (3:2 ratio) using NaH (20 mol %) as base. These compounds are thoroughly characterized using ^{1}H, ^{13}C NMR spectroscopy, mass spectrometry and IR spectroscopy. These 1,2,3,4,5-pentasubstituted cyclohexanols had the positional pattern of phenyl/4-bromophenyl group at C1, benzoyl/4-bromobenzoyl at C2 and C4 all groups originating from the ketone, while aryl group of the aldehyde at C3 and C5. Determination of molecular structure of **2b** confirmed the pattern as well as that aryl and benzoyl groups occupied the equatorial sites of chair form of cyclohexane, while –OH occupied axial site.

4. Experimental Section

4.1 General Procedure

*4.1.1 Synthesis of **2a** to **2q***

4-Hydroxy-4-phenyl-2,6-di(pyridin-4-yl)cyclohexane-1,3-diyl)bis(phenylmethanone) (**2a**):

A mixture of acetophenone (0.50 g, 4.16 mmol), 4-pyridinecarboxaldehyde (0.32 g, 2.99 mmol) and solid sodium hydride (0.04 g, 20 mol%) was heated in air with stirring using a glass rod at 100 °C for 6 h and then allowed to cool to room temperature. Ethanol (15 mL) was added, stirred and the white solid precipitated was filtered, washed with ice-cold ethanol and dried. White solid (0.48 g, 64%). mp 262-264 °C; ^{1}H NMR (600 MHz, $CDCl_3$) δ 8.33 (d, *J* = 4.8 Hz, 2H), 8.07 (d, *J* = 4.9 Hz, 2H), 7.53 (d, *J* = 7.7 Hz, 2H), 7.31 (d, *J* = 7.9 Hz, 2H), 7.28 (d, *J* = 7.6 Hz, 3H), 7.22 (d, *J* = 7.4 Hz, 2H), 7.19 (d, *J* = 4.9 Hz, 2H), 7.12 – 7.02 (m, 8H), 5.31 (s, 1H), 4.50 – 4.47 (m, 1H), 4.21 – 4.16 (m, 2H), 4.09 – 4.04 (m, 1H), 2.50 (t, *J* = 13.3 Hz, 1H), 2.27 – 2.23 (m, 1H); ^{13}C NMR (150 MHz, $CDCl_3$) δ 205.9, 201.8, 150.7, 150.1, 149.8, 147.7, 145.0, 138.0, 137.7, 133.6, 133.2, 128.6, 128.3, 128.2, 127.9, 127.6, 127.5, 124.8, 123.4, 75.1, 55.7, 54.8, 47.6, 44.9, 42.8; IR (cm^{-1}) ATR mode: 3445(br), 3060(w), 3028(w), 1668(s), 1595(s), 1447(m), 1415(m), 1301(m), 1251(m), 1219(m), 1067(m), 1001(m), 972(m), 816(m), 784(m), 760(m), 694(s), 556(m), 539(m). ESI-MS (+): *m/z* calcd. for ($M + H^+$) $C_{36}H_{31}N_2O_3^+$ 539.2330 found 539.2350.

Same procedure was adopted to synthesize **2b** – **2q** by using same molar ratio of the reactant. The spectroscopic data are given below:

(4-hydroxy-2,4,6-triphenylcyclohexane-1,3-diyl)bis(phenylmethanone) (**2b**): White solid (0.55 g, 74%). mp 237-239 °C; ^{1}H NMR (600 MHz, $CDCl_3$); δ 7.56 (d, *J* = 7.4 Hz, 2H), 7.28 (d, *J* = 7.3 Hz, 2H), 7.26 – 7.23 (m, 4H), 7.23 – 7.11 (m, 6H), 7.10 (t, *J* = 7.7 Hz, 2H), 7.06 – 7.01 (m, 5H), 6.98 (t, *J* = 7.3 Hz, 1H), 6.83 (t, *J* = 7.8 Hz, 2H), 6.72 (t, *J* = 7.4 Hz, 1H), 5.40 (d, *J* = 2.4 Hz, 1H), 4.50 (d, *J* = 11.4 Hz, 1H), 4.27 – 4.16 (m, 2H), 4.07 (td, *J* = 12.5, 3.5 Hz, 1H), 2.56 – 2.50 (m, 1H), 2.26 (dd, *J* = 14.1, 3.6 Hz, 1H); ^{13}C NMR (150 MHz, $CDCl_3$) δ 207.3, 203.7, 146.0, 142.2, 139.1, 138.7, 138.2, 132.8, 131.9, 128.5, 128.3, 128.2, 128.1, 127.8, 127.8, 127.7, 127.5, 127.1, 127.0, 126.8, 124.9, 75.4, 56.9, 43.5; IR (cm^{-1}) ATR mode: 3482(br), 3064(w), 3028(w), 2922(w), 1666(s), 1641(s), 1595(m), 1578(m), 1493(m), 1448(s), 1344(m), 1252(m), 1219(m), 1182(w), 1065(m), 1001(m), 973(m), 752(m), 694(s), 681(s), 610(m), 539(m), 527(m). ESI-MS (+): *m/z* calcd. for (M + Na^+) $C_{38}H_{32}O_3Na^+$ 559.2244 found 559.2248

(4-Hydroxy-4-phenyl-2,6-di-o-tolylcyclohexane-1,3-diyl)bis(phenylmethanone) (**2c**): White solid (0.53 g, 67%). mp 242-244 °C; ^{1}H NMR (600 MHz, $CDCl_3$) δ 7.53 (d, *J* = 7.4 Hz, 2H), 7.47 (d, *J* = 7.7 Hz, 1H), 7.42 (d, *J* = 7.7 Hz, 1H), 7.28 (d, *J* = 7.5 Hz, 2H), 7.22 (dd, *J* = 18.5, 7.3 Hz, 3H), 7.19 – 7.15 (m, 3H), 7.03 (t, *J* = 7.6 Hz, 5H), 6.97 (t, *J* = 7.5 Hz, 1H), 6.94 (d, *J* = 7.3 Hz, 1H), 6.86 (t, *J* = 7.8 Hz, 1H), 6.72 (dd, *J* = 16.6, 7.7 Hz, 2H), 6.60 (t, *J* = 7.3 Hz, 1H), 5.39 (d, *J* = 2.5 Hz, 1H), 4.55 (t, *J* = 11.2 Hz, 1H), 4.47 (d, *J* = 11.6 Hz, 1H), 4.41 (td, *J* = 11.9, 3.2 Hz, 1H), 4.29 (t, *J* = 10.9 Hz, 1H), 2.39 (s, 3H), 2.37 (dd, *J* = 15.1, 3.2 Hz, 1H), 2.27 (s, 3H), 2.14 (dd, *J* = 14.2, 3.6 Hz, 1H); ^{13}C NMR (150 MHz, $CDCl_3$) δ 207.5, 203.9, 145.9, 140.6, 139.1, 138.3, 137.4, 136.8, 136.4, 132.7, 131.9, 130.7, 130.6, 128.3, 127.8, 127.7, 127.7, 127.4, 127.4, 127.1, 126.9, 126.5, 126.4, 125.8, 125.5, 124.9, 75.6, 57.3, 56.3, 46.5, 41.9, 37.8, 19.9; IR (cm^{-1}) ATR mode: 3492(br), 1665(s), 1651(m), 1596(w), 1491(m), 1447(m), 1377(m), 1254(m), 1214(m), 1065(m), 1002(m), 975(w), 955(w), 756(s), 694(s), 547(m), 455(m). ESI-MS (+): *m/z* calcd. for (M + Na^+) $C_{40}H_{36}O_3Na^+$ 587.2557 found 587.2564.

(4-Hydroxy-4-phenyl-2,6-di-p-tolylcyclohexane-1,3-diyl)bis(phenylmethanone) (**2d**): White solid (0.59 g, 76%). mp 253-255 °C; ^{1}H NMR (600 MHz, $CDCl_3$) δ 7.57 – 7.54 (m, 2H), 7.29 – 7.26 (m, 2H), 7.26 – 7.20 (m, 4H), 7.20 – 7.16 (m, 4H), 7.05 (q, *J* = 6.7, 6.0 Hz, 7H), 6.91 (d, *J* = 7.9 Hz, 2H), 6.64 (d, *J* = 8.1 Hz, 2H), 5.38 (d, *J* = 2.4 Hz, 1H), 4.49 (d, *J* = 11.4 Hz, 1H), 4.24 – 4.13 (m, 2H), 4.03 (td, *J* = 12.4, 3.5 Hz, 1H), 2.53 – 2.47 (m, 1H), 2.24 (dd, *J* = 14.1, 3.6 Hz, 1H), 2.14 (s, 3H), 1.93 (s, 3H); ^{13}C NMR (150 MHz, $CDCl_3$) δ 207.5, 203.9, 146.1, 139.2, 139.2, 138.3, 136.4, 136.2, 135.7, 132.6, 131.7, 129.1, 128.8, 128.2, 127.9, 127.9, 127.7, 127.6, 127.6, 127.0, 124.9, 75.5, 57.2, 57.1, 47.8, 46.2, 43.1, 20.9, 20.7; IR (cm^{-1}) ATR mode: 3497(br), 3024(w), 1667(s), 1637(m), 1595(m), 1578(w), 1514(m), 1447(m), 1348(w),

1255(m), 1220(m), 1069(m), 1001(m), 975(m), 807(m), 759(m), 708(m), 694(s), 682(m), 562(m), 535(m), 520(m). ESI-MS (+): *m*/*z* calcd. for ($M–H_2O + H^+$) $C_{40}H_{35}O_2^+$ 547.2632 found 547.2606.

(4-Hydroxy-2,6-bis(4-methoxyphenyl)-4-phenylcyclohexane-1,3-diyl)bis(phenylmethanone) (**2e**): White solid (0.62 g, 75%). mp 211-213 °C; ^{1}H NMR (600 MHz, $CDCl_3$) δ 7.56 (d, *J* = 7.8 Hz, 2H), 7.28 (d, *J* = 8.5 Hz, 3H), 7.26 – 7.14 (m, 7H), 7.07 (td, *J* = 7.9, 3.1 Hz, 7H), 6.65 (d, *J* = 8.6 Hz, 2H), 6.38 (d, *J* = 8.7 Hz, 2H), 5.38 (d, *J* = 2.2 Hz, 1H), 4.47 (d, *J* = 11.0 Hz, 1H), 4.16 (p, *J* = 11.0 Hz, 2H), 4.02 (t, *J* = 9.9 Hz, 1H), 3.64 (s, 3H), 3.48 (s, 3H), 2.51 – 2.45 (m, 1H), 2.23 (dd, *J* = 14.1, 3.5 Hz, 1H); ^{13}C NMR (150 MHz, $CDCl_3$) δ 207.5, 204.1, 158.3, 146.1, 139.2, 138.3, 134.4, 132.8, 131.9, 130.9, 129.0, 128.3, 127.8, 127.8, 127.7, 127.6, 127.1, 124.9, 113.9, 113.6, 75.5, 57.4, 57.1, 55.2, 55.1, 47.4, 46.2, 42.7; IR (cm^{-1}) ATR mode: 3423(br), 1666(s), 1640(s), 1611(m), 1596(w), 1579(w), 1446(m), 1249(s), 1220(m), 1177(m), 1032(m), 974(m), 825(m), 697(s), 537(s). ESI-MS (+): *m*/*z* calcd. for ($M–H_2O + H^+$) $C_{40}H_{35}O_4^+$ 579.2530 found 579.2501.

(2,6-Bis(4-fluorophenyl)-4-hydroxy-4-phenylcyclohexane-1,3-diyl)bis(phenylmethanone) (**2f**): White solid (0.55 g, 69%). mp 252-254 °C; ^{1}H NMR (600 MHz, $CDCl_3$) δ 7.56 (d, *J* = 7.5 Hz, 2H), 7.28 (t, *J* = 7.7 Hz, 5H), 7.26 (s, 1H), 7.25 – 7.20 (m, 4H), 7.14 – 7.06 (m, 7H), 6.80 (t, *J* = 8.6 Hz, 2H), 6.54 (t, *J* = 8.7 Hz, 2H), 5.38 (d, *J* = 2.3 Hz, 1H), 4.46 (d, *J* = 11.1 Hz, 1H), 4.17 (dt, *J* = 24.5, 11.0 Hz, 2H), 4.09 – 4.04 (m, 1H), 2.48 (m, 1H), 2.25 (dd, *J* = 14.1, 3.5 Hz, 1H); ^{13}C NMR (150 MHz, $CDCl_3$) δ 207.0, 203.4, 162.5, 162.4, 160.8, 160.8, 145.8, 138.8, 138.0, 137.8, 133.1, 132.4, 129.5, 128.4, 128.0, 127.9, 127.8, 127.5, 127.3, 124.8, 115.4, 115.3, 115.2, 115.0, 75.4, 57.1, 56.8, 47.5, 46.0, 42.8; IR (cm^{-1}) ATR mode: 3450(br), 1669(s), 1656(s), 1594(m), 1578(w), 1510(s), 1448(m), 1349(m), 1254(m), 1239(m), 1221(s), 831(s), 764(s), 711(m), 696(s), 537(m), 524(m), 478(w). ESI-MS (+): *m*/*z* calcd. for ($M–H_2O + H^+$) $C_{38}H_{29}F_2O_2^+$ 555.2131 found 555.2111.

(2,6-Bis(4-bromophenyl)-4-hydroxy-4-phenylcyclohexane-1,3-diyl)bis(phenylmethanone) (**2g**): White solid (0.62 g, 64%). mp 238-240 °C; ^{1}H NMR (600 MHz, $CDCl_3$) δ 7.52 (dd, *J* = 8.4, 1.3 Hz, 2H), 7.30 – 7.26 (m, 2H), 7.26 – 7.23 (m, 3H), 7.23 – 7.20 (m, 3H), 7.20 – 7.17 (m, 2H), 7.13 (d, *J* = 8.5 Hz, 2H), 7.12 – 6.98 (m, 7H), 6.96 – 6.94 (m, 2H), 5.31 (d, *J* = 2.4 Hz, 1H), 4.45 – 4.41 (m, 1H), 4.16 – 4.09 (m, 2H), 4.04 – 3.98 (m, 1H), 2.48 – 2.40 (m, 1H), 2.21 (dd, *J* = 14.1, 3.5 Hz, 1H); ^{13}C NMR (150 MHz, $CDCl_3$) δ 206.8, 203.0, 145.6, 141.0, 138.6, 138.0, 137.8, 133.2, 132.5, 131.6, 131.4, 129.8, 128.4, 128.1, 128.04, 127.8, 127.5,

127.4, 124.9, 121.0, 120.7, 75.4, 56.7, 56.5, 47.6, 45.8, 42.9; IR (cm^{-1}) ATR mode: 3423(br), 1668(s), 1631(m), 1596(m), 1487(m), 1447(w), 1408(w), 1257(m), 1073(m), 1009(s), 820(m), 806(m), 762(m), 694(s), 543(s), 526(m). ESI-MS (+): *m*/*z* calcd. for ($M–H_2O + H^+$) $C_{38}H_{29}Br_2O_2^+$ 677.0509 found 677.0468.

(4-Hydroxy-4-phenyl-2,6-di(thiophen-2-yl)cyclohexane-1,3-diyl)bis(phenylmethanone) (**2h**): White solid (0.48 g, 63%). mp 251-253 °C; ^{1}H NMR (600 MHz, $CDCl_3$) δ 7.52 (d, *J* = 7.4 Hz, 2H), 7.45 (d, *J* = 7.3 Hz, 2H), 7.36 (d, *J* = 7.3 Hz, 2H), 7.28 (t, *J* = 7.5 Hz, 2H), 7.18 (t, *J* = 7.8 Hz, 2H), 7.14 (t, *J* = 7.8 Hz, 2H), 7.09 (t, *J* = 7.8 Hz, 2H), 7.04 (t, *J* = 7.3 Hz, 1H), 6.93 (d, *J* = 4.9 Hz, 1H), 6.74 (d, *J* = 2.9 Hz, 1H), 6.66 (d, *J* = 5.0 Hz, 1H), 6.64 – 6.61 (m, 2H), 6.39 (dd, *J* = 5.0, 3.6 Hz, 1H), 5.29 (d, *J* = 2.5 Hz, 1H), 4.54 (t, *J* = 11.3 Hz, 1H), 4.43 (d, *J* = 11.7 Hz, 1H), 4.38 (td, *J* = 11.7, 3.8 Hz, 1H), 4.13 (t, *J* = 11.0 Hz, 1H), 2.48 (m, 1H), 2.39 (dd, *J* = 14.0, 3.8 Hz, 1H); ^{13}C NMR (150 MHz, $CDCl_3$) δ 206.8, 203.3, 145.6, 145.3, 142.2, 138.7, 137.9, 133.1, 132.3, 128.4, 128.0, 127.9, 127.8, 127.8, 127.3, 127.1, 126.7, 126.4, 125.7, 124.9, 124.0, 123.4, 75.4, 59.0, 57.8, 47.0, 43.4, 39.2; IR (cm^{-1}) ATR mode: 3368(br), 1667(s), 1634(s), 1594(m), 1578(m), 1446(w), 1407(m), 1253(m), 1065(m), 1001(m), 698(s), 681(m), 560(m), 527(m). ESI-MS (+): *m*/*z* calcd. for ($M–H_2O + H^+$) $C_{34}H_{29}O_2S_2^+$ 531.1447 found 531.1423.

(4-(4-Bromophenyl)-4-hydroxy-2,6-bis(4-methoxyphenyl)cyclohexane-1,3-diyl)bis((4-bromophenyl)methanone) (**2i**): White solid (0.47 g, 68%). mp 269-271 °C; ^{1}H NMR (600 MHz, $CDCl_3$) δ 7.40 (s, 2H), 7.31 (d, *J* = 8.6 Hz, 2H), 7.24 (d, *J* = 8.5 Hz, 2H), 7.20 (d, *J* = 8.5 Hz, 2H), 7.15 – 7.10 (m, 6H), 7.00 (s, 2H), 6.64 (d, *J* = 8.6 Hz, 2H), 6.40 (d, *J* = 8.8 Hz, 2H), 5.31 (d, J = 1.8 Hz, 1H), 4.32 (d, *J* = 10.9 Hz, 1H), 4.09 – 4.02 (m, 2H), 3.96 – 3.91 (m, 1H), 3.64 (s, 3H), 3.50 (s, 3H), 2.37 – 2.31 (m, 1H), 2.16 (dd, *J* = 14.1, 3.4 Hz, 1H); ^{13}C NMR (150 MHz, $CDCl_3$) δ 206.1, 202.8, 158.6, 145.1, 137.6, 136.5, 133.8, 131.5, 131.4, 131.1, 130.3, 129.3, 129.0, 128.9, 128.6, 127.2, 126.7, 121.3, 114.0, 113.9, 75.4, 57.2, 56.6, 55.3, 55.2, 47.3, 46.0, 42.6; IR (cm^{-1}) ATR mode: 3475(br), 1666(s), 1644(m), 1612(m), 1584(s), 1513(s), 1396(m), 1253(s), 1179(m), 1073(m), 1009(m), 975(m), 824(s), 753(m), 734(m), 550(m), 532(m), 457(w). ESI-MS (+): *m*/*z* calcd. for ($M–H_2O + H^+$) $C_{40}H_{32}Br_3O_4^+$ 814.9825 found 814.9825.

(4-(4-Bromophenyl)-4-hydroxy-2,6-di-p-tolylcyclohexane-1,3-diyl)bis((4-bromophenyl)methanone) (**2j**): White solid (0.47 g, 70%). mp 275-277 °C; ^{1}H NMR (600 MHz, $CDCl_3$) δ 7.38 (d, *J* = 8.6 Hz, 2H), 7.30 (d, *J* = 8.6 Hz, 2H), 7.23 (d, *J* = 8.6 Hz, 2H), 7.19 (d, *J* = 8.5 Hz, 2H), 7.13 – 7.08 (m, 6H), 7.00 – 6.93 (m, 2H), 6.90 (d, *J* = 7.8 Hz, 2H),

6.66 (d, *J* = 7.9 Hz, 2H), 5.30 (d, *J* = 2.0 Hz, 1H), 4.32 (d, *J* = 10.9 Hz, 1H), 4.10 – 4.03 (m, 2H), 3.93 (t, *J* = 11.2 Hz, 1H), 2.36 (t, *J* = 13.4 Hz, 1H), 2.18 (d, *J* = 3.5 Hz, 1H), 2.15 (s, 3H), 1.97 (s, 3H); ^{13}C NMR (150 MHz, $CDCl_3$) δ 205.9, 202.6, 145.0, 138.6, 137.5, 136.9, 136.6, 135.2, 131.4, 131.2, 130.9, 129.2, 129.0, 128.4, 127.7, 126.9, 126.6, 121.2, 75.2, 47.5, 45.8, 42.9, 20.9; IR (cm^{-1}) ATR mode: 3455(br), 1667(s), 1642(s), 1583(s), 1561(m), 1512(m), 1485(m), 1396(m), 1251(m), 1217(m), 1071(s), 1009(s), 845(m), 809(s), 537(m), 518(m), 437(w). ESI-MS (+): *m*/*z* calcd. for ($M–H_2O + H^+$) $C_{40}H_{32}Br_3O_2^+$ 782.9927 found 782.9908.

(4-(4-Bromophenyl)-4-hydroxy-2,6-diphenylcyclohexane-1,3-diyl)bis((4-bromophenyl)methanone) (**2k**): White solid (0.45 g, 69%). mp 235-237 °C; ^{1}H NMR (600 MHz, $CDCl_3$) δ 7.41 (d, *J* = 8.6 Hz, 2H), 7.32 (d, *J* = 8.6 Hz, 2H), 7.23 (t, *J* = 7.7 Hz, 4H), 7.18 – 7.07 (m, 10H), 7.01 (t, *J* = 7.3 Hz, 1H), 6.87 (t, *J* = 7.8 Hz, 2H), 6.79 (t, *J* = 7.4 Hz, 1H), 5.36 (d, *J* = 2.1 Hz, 1H), 4.40 – 4.35 (m, 1H), 4.17 – 4.11 (m, 2H), 4.04 – 3.98 (m, 1H), 2.46 – 2.39 (m, 1H), 2.22 (dd, *J* = 14.1, 3.5 Hz, 1H); ^{13}C NMR (150 MHz, $CDCl_3$) δ 205.9, 202.5, 145.0, 141.7, 138.3, 137.5, 136.5, 131.5, 131.4, 131.0, 129.3, 128.9, 128.7, 128.5, 127.9, 127.5, 127.3, 127.2, 126.7, 121.4, 75.3, 56.6, 56.3, 48.1, 45.7, 43.4; IR (cm^{-1}) ATR mode: 3415(br), 1666(s), 1651(s), 1585(s), 1564(m), 1485(m), 1396(m), 1250(m), 1217(m), 1071(s), 1009(s), 836(m), 699(s), 536(m). ESI-MS (+): *m*/*z* calcd. for ($M–H_2O + H^+$) $C_{38}H_{28}Br_3O_2^+$ 754.9614 found 754.9613.

(4-(4-Bromophenyl)-2,6-bis(4-fluorophenyl)-4-hydroxycyclohexane-1,3-diyl)bis((4-bromophenyl)methanone) (**2l**): White solid (0.38 g, 56%); mp 229-231; ^{1}H NMR (600 MHz, $CDCl_3$) δ 7.38 (t, *J* = 7.2 Hz, 2H), 7.33 (d, *J* = 8.6 Hz, 2H), 7.28 (s, 2H), 7.24 (d, *J* = 8.5 Hz, 2H), 7.18 (dd, *J* = 8.3, 5.4 Hz, 2H), 7.14 (d, *J* = 8.5 Hz, 2H), 7.11 (d, *J* = 8.4 Hz, 2H), 7.09 – 7.01 (m, 2H), 6.81 (t, *J* = 8.5 Hz, 2H), 6.58 (t, *J* = 8.5 Hz, 2H), 5.29 (d, *J* = 1.8 Hz, 1H), 4.32 (d, *J* = 11.6 Hz, 1H), 4.11 (t, *J* = 11.1 Hz, 1H), 4.05 – 3.96 (m, 2H), 2.35 (t, *J* = 12.2 Hz, 1H), 2.18 (dd, *J* = 14.1, 3.0 Hz, 1H); ^{13}C NMR (150 MHz, $CDCl_3$) δ 205.5, 202.0, 162.5, 160.9, 144.7, 137.3, 137.1, 136.3, 134.1, 131.6, 131.4, 129.4, 129.4, 129.2, 129.1, 128.9, 127.9, 126.6, 121.5, 115.7, 115.6, 115.5, 115.4, 75.2, 56.8, 56.3, 47.3, 45.8, 42.7; IR (cm^{-1}) ATR mode: 3490(br), 1665(s), 1647(m), 1607(m), 1584(s), 1510(s), 1486(m), 1397(m), 1236(s), 1073(s), 1009(s), 829(s), 762(m), 732(m), 539(m), 526(m). ESI-MS (+): *m*/*z* calcd. for ($M–H_2O + H^+$) $C_{38}H_{26}Br_3F_2O_2^+$ 790.9426 found 790.9413.

(4-(4-Bromophenyl)-2,6-bis(4-chlorophenyl)-4-hydroxycyclohexane-1,3-diyl)bis((4-bromophenyl)methanone) (**2m**): White solid (0.41 g, 58%). mp 234-236 °C; ^{1}H NMR (600

MHz, $CDCl_3$) δ 7.37 (d, *J* = 8.7 Hz, 2H), 7.32 (d, *J* = 8.7 Hz, 2H), 7.28 (d, *J* = 8.6 Hz, 2H), 7.24 (s, 2H), 7.16 – 7.08 (m, 8H), 7.07 – 6.96 (m, 2H), 6.86 (d, *J* = 8.7 Hz, 2H), 5.24 (d, *J* = 2.2 Hz, 1H), 4.31 (d, *J* = 11.5 Hz, 1H), 4.11 (t, *J* = 11.2 Hz, 1H), 4.03 (t, *J* = 10.9 Hz, 1H), 3.97 (td, *J* = 11.7, 3.1 Hz, 1H), 2.37 – 2.31 (m, 1H), 2.17 (dd, *J* = 14.0, 3.3 Hz, 1H); ^{13}C NMR (150 MHz, $CDCl_3$) δ 205.3, 201.7, 144.6, 140.0, 137.0, 136.8, 136.2, 133.4, 132.9, 131.6, 131.6, 131.5, 129.2, 129.2, 128.9, 128.8, 128.7, 128.0, 126.6, 121.6, 75.2, 56.3, 56.1, 47.4, 45.7, 42.8; IR (cm^{-1}) ATR mode: 3459(br), 1665(s), 1642(s), 1583(s), 1563(m), 1487(m), 1396(m), 1252(m), 1215(m), 1073(s), 1009(s), 844(m), 817(s), 761(m), 535(m), 517(m). ESI-MS (+): *m*/*z* calcd. for ($M–H_2O + H^+$) $C_{38}H_{26}Br_3Cl_2O_2^+$ 822.8835 found 822.8821.

(4-(4-Bromophenyl)-4-hydroxy-2,6-di-o-tolylcyclohexane-1,3-diyl)bis((4-bromophenyl)methanone) (**2n**): White solid (0.43 g, 64%); mp 210-212 °C; ^{1}H NMR (600 MHz, $CDCl_3$) δ 7.43 (d, *J* = 7.8 Hz, 1H), 7.38 (d, *J* = 8.7 Hz, 2H), 7.36 (d, *J* = 7.7 Hz, 1H), 7.31 (d, *J* = 8.7 Hz, 2H), 7.23 (d, *J* = 8.6 Hz, 2H), 7.17 (d, *J* = 8.6 Hz, 2H), 7.13 (dd, *J* = 8.6, 2.0 Hz, 4H), 7.00 (t, *J* = 7.5 Hz, 1H), 6.94 (d, *J* = 7.2 Hz, 1H), 6.90 (t, *J* = 7.2 Hz, 1H), 6.79 (t, *J* = 7.4 Hz, 1H), 6.72 (d, *J* = 7.3 Hz, 1H), 6.67 (t, *J* = 7.2 Hz, 1H), 5.33 (d, *J* = 2.3 Hz, 1H), 4.49 (t, *J* = 11.2 Hz, 1H), 4.35 (t, *J* = 10.2 Hz, 2H), 4.19 (t, *J* = 11.0 Hz, 1H), 3.49 (d, *J* = 4.1 Hz, 1H), 2.35 (s, 3H), 2.21 (s, 3H), 2.09 (dd, *J* = 14.2, 3.5 Hz, 1H); ^{13}C NMR (150 MHz, $CDCl_3$) δ 205.9, 202.6, 145.0, 140.0, 137.5, 136.9, 136.8, 136.5, 136.4, 131.5, 131.4, 131.1, 130.9, 130.9, 129.2, 128.9, 128.6, 127.3, 127.2, 127.1, 126.7, 126.2, 125.9, 125.8, 75.4, 56.7, 56.2, 46.4, 41.9, 37.7, 19.8; IR (cm^{-1}) ATR mode: 3435(br), 1668(s), 1641(s), 1583(s), 1563(m), 1485(m), 1396(m), 1254(m), 1211(m), 1071(s), 1007(s), 838(m), 753(s), 731(s), 545(m), 459(m). ESI-MS (+): *m*/*z* calcd. for ($M–H_2O + H^+$) $C_{40}H_{32}Br_3O_2^+$ 782.9927 found 782.9928.

(4-(4-Bromophenyl)-4-hydroxy-2,6-bis(3-methoxyphenyl)cyclohexane-1,3-diyl)bis((4-bromophenyl)methanone) (**2o**): White solid (0.42 g, 60%); mp 218-220 °C; ^{1}H NMR (600 MHz, $CDCl_3$) δ 7.39 (d, *J* = 8.6 Hz, 2H), 7.32 (d, *J* = 8.6 Hz, 2H), 7.24 (d, *J* = 8.6 Hz, 2H), 7.21 (d, *J* = 8.6 Hz, 2H), 7.17 – 7.14 (m, 4H), 7.03 (t, *J* = 7.9 Hz, 1H), 6.80 (dd, *J* = 18.3, 7.9 Hz, 2H), 6.74 (s, 1H), 6.73 – 6.56 (m, 2H), 6.56 – 6.53 (m, 1H), 6.33 – 6.30 (m, 1H), 5.34 (d, *J* = 2.1 Hz, 1H), 4.32 (d, *J* = 11.0 Hz, 1H), 4.08 (p, *J* = 11.0 Hz, 2H), 3.97 – 3.91 (m, 1H), 3.67 (s, 3H), 3.54 (s, 3H), 2.40 – 2.32 (m, 1H), 2.20 (dd, *J* = 14.1, 3.5 Hz, 1H); ^{13}C NMR (150 MHz, $CDCl_3$) δ 205.8, 202.3, 159.7, 159.5, 145.0, 143.3, 139.9, 137.6, 136.6, 131.5, 131.4, 131.1, 129.7, 129.6, 129.3, 129.1, 128.6, 127.3, 126.7, 121.4, 120.2, 114.2, 112.3, 75.3, 56.3, 55.3,

48.0, 45.8, 43.5; IR (cm^{-1}) ATR mode: 3391(br), 2916(w), 2835(w), 1672(s), 1648(s), 1584(s), 1484(m), 1395(m), 1251(s), 1213(m), 1156(m), 1071(s), 1009(s), 830(m), 701(m), 551(m), 499(m), 450(m). ESI-MS (+): *m*/*z* calcd. for ($M–H_2O + H^+$) $C_{40}H_{32}Br_3O_4^+$ 814.9825 found 814.9838.

(4-(2-chlorophenyl)-4-hydroxy-2,6-di-o-tolylcyclohexane-1,3-diyl)bis((2-chlorophenyl)methanone) (**2p**) White solid (0.39 g, 54%); mp 240-242 °C; ^1H NMR (600 MHz, $CDCl_3$) δ 7.90 (dd, *J* = 8.0, 1.3 Hz, 1H), 7.46 (d, *J* = 7.7 Hz, 1H), 7.36 (dd, *J* = 7.3, 1.9 Hz, 1H), 7.27 (d, *J* = 6.8 Hz, 1H), 7.20 (t, *J* = 7.2 Hz, 1H), 7.11 – 7.01 (m, 6H), 7.01 – 6.98 (m, 2H), 6.96 – 6.93 (m, 2H), 6.90 (m, 3H), 6.86 (t, *J* = 7.4 Hz, 1H), 6.79 (t, *J* = 7.3 Hz, 1H), 5.35 (d, *J* = 11.6 Hz, 1H), 5.18 (d, *J* = 2.6 Hz, 1H), 4.57 (t, *J* = 11.0 Hz, 1H), 4.33 – 4.23 (m, 2H), 3.19 – 3.13 (m, 1H), 2.46 (s, 3H), 2.45 (s, 3H), 1.87 (dd, *J* = 14.4, 3.7 Hz, 1H); ^{13}C NMR (150 MHz, $CDCl_3$) δ 206.1, 202.9, 141.7, 140.0, 138.4, 137.9, 137.4, 136.7, 132.3, 132.1, 132.1, 131.7, 131.2, 131.1, 131.0, 130.9, 130.7, 129.9, 129.8, 129.3, 129.0, 128.9, 127.8, 127.5, 127.1, 126.7, 126.4, 125.8, 125.7, 125.5, 125.4, 75.8, 58.7, 55.5, 42.3, 41.1, 38.1, 20.5, 20.1; IR (cm^{-1}) ATR mode: 3442(br), 1688(m), 1654(m), 1588(m), 1491(w), 1469(m), 1434(m), 1339(w), 1268(m), 1248(s), 1192(w), 1077(m), 976(m), 943(w), 758(s), 732(s), 704(m), 650(m), 558(m), 464(m), 426(w). ESI-MS (+): *m*/*z* calcd. for ($M–H_2O + H^+$) $C_{40}H_{32}Cl_3O_2^+$ 649.1463 found 649.1443.

(4-hydroxy-4-(4-methoxyphenyl)-2,6-di-o-tolylcyclohexane-1,3-diyl)bis((4-methoxyphenyl)methanone) (**2q**) White solid (0.40 g, 56%); mp 156-158 °C; ^1H NMR (500 MHz, $CDCl_3$) δ 7.48 (d, *J* = 7.9 Hz, 1H), 7.42 (t, *J* = 7.8 Hz, 3H), 7.35 (m, 4H), 6.99 (t, *J* = 7.7 Hz, 1H), 6.92 (d, *J* = 7.6 Hz, 1H), 6.86 (t, *J* = 7.5 Hz, 1H), 6.77 (t, *J* = 7.7 Hz, 1H), 6.68 (t, *J* = 6.8 Hz, 3H), 6.59 (t, *J* = 7.5 Hz, 1H), 6.53 (m, 4H), 5.55 (s, 1H), 4.52 (t, *J* = 11.2 Hz, 1H), 4.37 (d, *J* = 11.6 Hz, 2H), 4.22 (t, *J* = 11.0 Hz, 1H), 3.70 (s, 3H), 3.68 (s, 3H), 3.66 (s, 3H), 2.37 (s, 3H), 2.30 (t, *J* = 13.3 Hz, 1H), 2.24 (s, 3H), 2.08 (dd, *J* = 14.1, 3.2 Hz, 1H); ^{13}C NMR (125 MHz, $CDCl_3$) δ 205.2, 201.7, 163.2, 162.5, 158.3, 140.9, 138.5, 137.7, 136.7, 136.4, 131.9, 131.0, 130.6, 130.5, 130.4, 129.9, 127.3, 126.6, 126.3, 126.2, 126.1, 125.7, 125.4, 113.5, 113.0, 112.8, 75.2, 66.0, 56.4, 55.4, 55.3, 55.2, 46.9, 41.9, 37.7, 19.8, 15.4; IR (cm^{-1}) ATR mode: 3442(br), 1658(m), 1633(w), 1592(s), 1513(m), 1464(m), 1391(w), 1344(w), 1313(w), 1293(w), 1276(m), 1255(s), 1171(s), 1077(w), 1033(m), 974(w), 833(s), 762(s), 689(w), 638(w), 608(w), 554(s), 518(w), 457(w). ESI-MS (+): *m*/*z* calcd. for ($M–H_2O + H^+$) $C_{43}H_{41}O_5^+$ 637.2949 found 637.2912.

References

[1] (a) H. D. Orloff, *Chem. Rev.* **1954**, *54*, 347–447. (b) H. X. Ding, K. K.C. Liu, S. M. Sakya, A. C. Flick, C. J. O'Donnell, *Bioorg. Med. Chem.* **2013**, *21*, 2795–2825.

[2] (a) M. A. Varner, R. B. Grossman, *Tetrahedron* **1999**, *55*, 13867–13886. (b) L.Yu, Q. Yang, P. Li, **2014**, 7499–7504.

[3] (a) G. Moos, M. Emondts, A. Bordet, W. Leitner, *Angew. Chemie - Int. Ed.* **2020**, *59*, 11977–11983. (b) E. Liu, Z. S. Jin, F. F. Jian, *Russ. J. Org. Chem.* **2023**, *59*, 196–201.

[4] (a) H. Miyamura, A. Suzuki, T. Yasukawa, S. Kobayashi, *J. Am. Chem. Soc.* **2018**, *140*, 11325–11334. (b) B. Léger, A. Denicourt-Nowicki, H. Olivier-Bourbigou, A. Roucoux, *Inorg. Chem.* **2008**, *47*, 9090–9096.

[5] N. Attal, D. Bouhassira, L. Colvin, *Br. J. Anaesth.* **2023**, *131*, 79–92.

[6] (a) L. F. Tietze, *Chem. Rev.* **1996**, *96*, 115–136. (b) J.C. Wasilke, S. J. Obrey, R. T. Baker, G. C. Bazan, *Chem. Rev.* **2005**, *105*, 1001–1020. (c) C. J. Chapman, C. G. Frost, *Synthesis (Stuttg).* **2007**, *1*, 1–21. (d) K. C. Nicolaou, T. Montagnon, S. A. Snyder, *Chem. Commun.* **2003**, *3*, 551–564. (e) K. C. Nicolaou, D. J. Edmonds, P. G. Bulger, *Angew. Chemie - Int. Ed.* **2006**, *45*, 7134–7186.

[7] (a) B. K. Vasilyev, N. P. Bagrina, V. I. Vysotskii, *Acta Cryst.* **1990**. *46*, 2265-2267. (b) J. Zhang, Q. He, Y. Wang, *Acta Cryst.* **2007**, E63, o4652. (c) X. Luo, Z. Shan, *Tetrahedron lett.* **2006**, *47*, 5623–5627. (d) Z. Shan, X. Hu, L. Hu, X Peng, *Helv. Chim. Acta* **2009**, *92*, 1102–1111. (e) P. N. Patel, A. Chadha, *Tetrahedron* **2018**, *74*, 204–216. (f) J. Zhang, L. Y. Shi, L. P. Ding, Y. Liu, H. Liang, P. F. Tu, L. Li, Q. Y. Zhang, *Phytochemistry* **2021**, *192*, 112960.

[8] (a) H. Gezegen, M. Ceylan, *Synth. Commun.* **2015**, *45*, 2344–2349. (b) E. Reyes, H. Jiang, A. Milelli, P. Elsner, R. G. Hazell, K. A. Jørgensen, *Angew. Chem.* **2007**, *119*, 9362–9365.

[9] M. E. Minyaev, D. M. Roitershtein, I. E. Nifant'ev, I. V Ananyev, T. V Minyaeva, T. A. Mikhaylyev, *Acta Cryst*. **2015**, *71*, 491–498.

Appendix

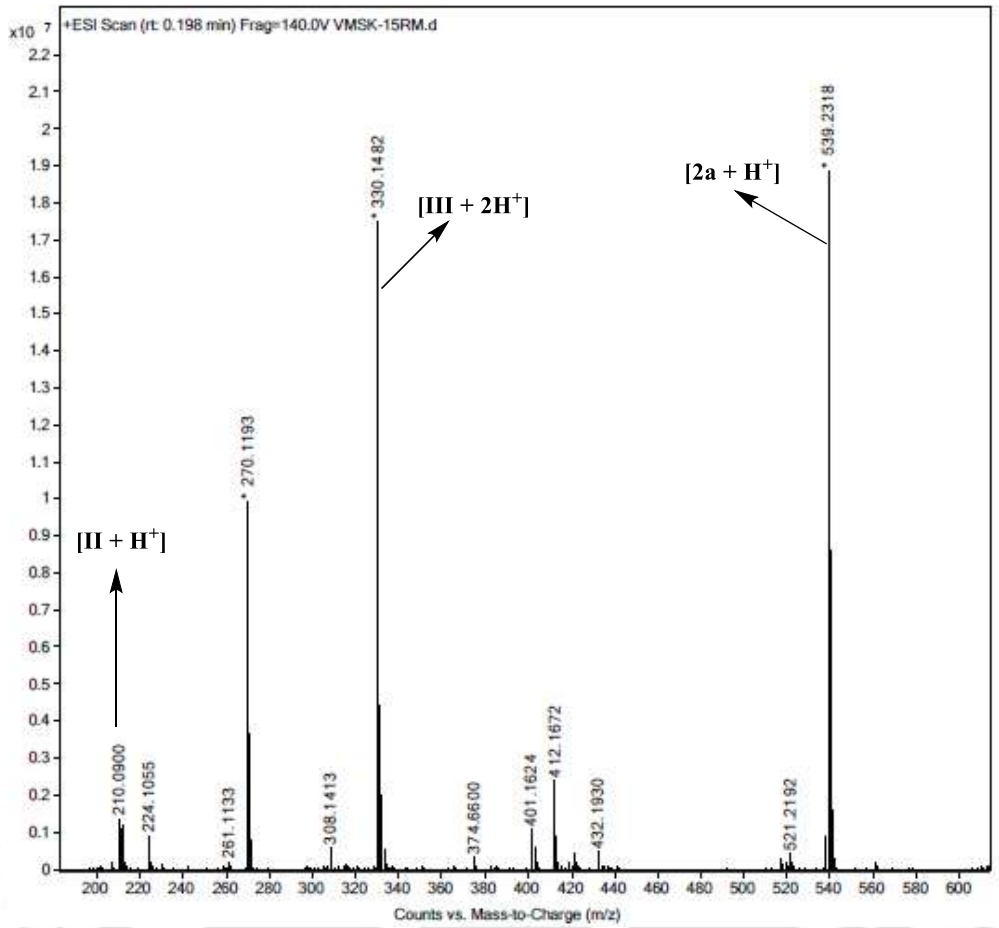

Figure A1. Mass spectrum of quenched reaction mixture of **2a**.

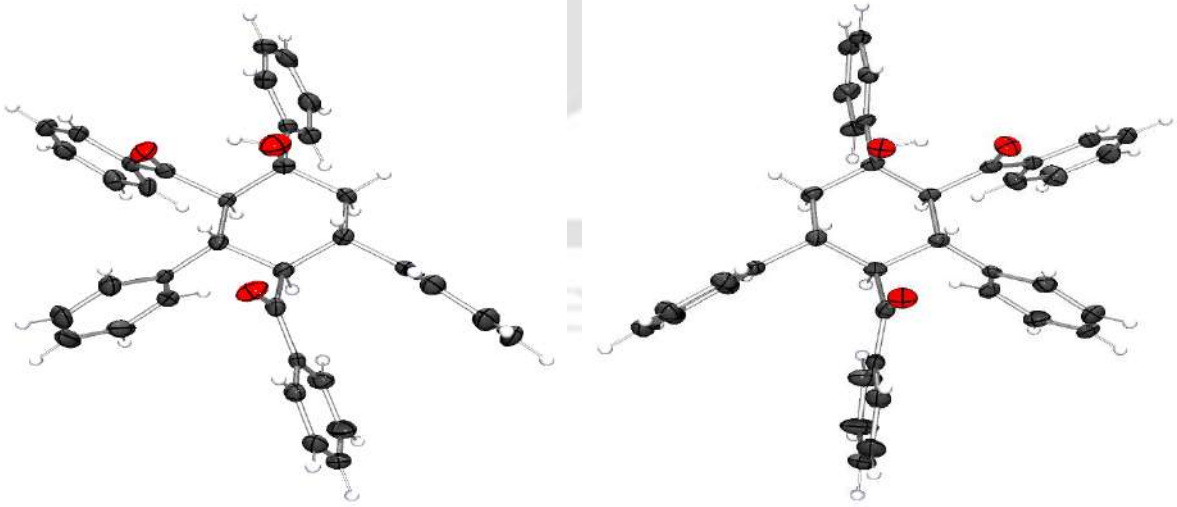

Figure A2. ORTEP diagram (50% probability) of enantiomeric pair **2b**.

Table S1: Crystallographic data and refinement parameters

Entry	**2b**
Formula	$C_{77}H_{65}Cl_3O_6$
Mol. wt.	1192.64
Cryst.color, habit	Colorless, block
T, K	130
Cryst. syst.	Triclinic
Space group	*P-1*
a, Å	12.317(2)
b, Å	12.430(2)
c, Å	20.484(4)
α ,deg	94.706(7)
β, deg	97.277(6)
γ ,deg	101.085(7)
V, Å^3	3034.6(9)
Z	2
*D*calcd, g cm^{-3}	1.305
μ, mm^{-1}	0.208
GOF[a] on F^2	1.093
F(000)	1252.0
Reflection collected	71603
Unique reflections	10728
R_1[b], wR_2[c] $(I \geq 2\sigma(I))$	0.0551, 0.1434
R_1[b], wR_2[c] (all data)	0.0884, 0.1546

[a]GOF (Goodness-of-fit) = $[\sum[w(F_0^2 - F_c^2)^2] / M - N]^{1/2}$ (M =number of reflections, N = number of parameters refined). [b] $R_1 = \sum \| F_0 | - | Fc \| / \sum | F_0 |$. [c]$wR_2 = [\sum[w(F_0^2 - F_c^2)^2] / \sum[w(F_0^2)^2]]$.

Spectral information

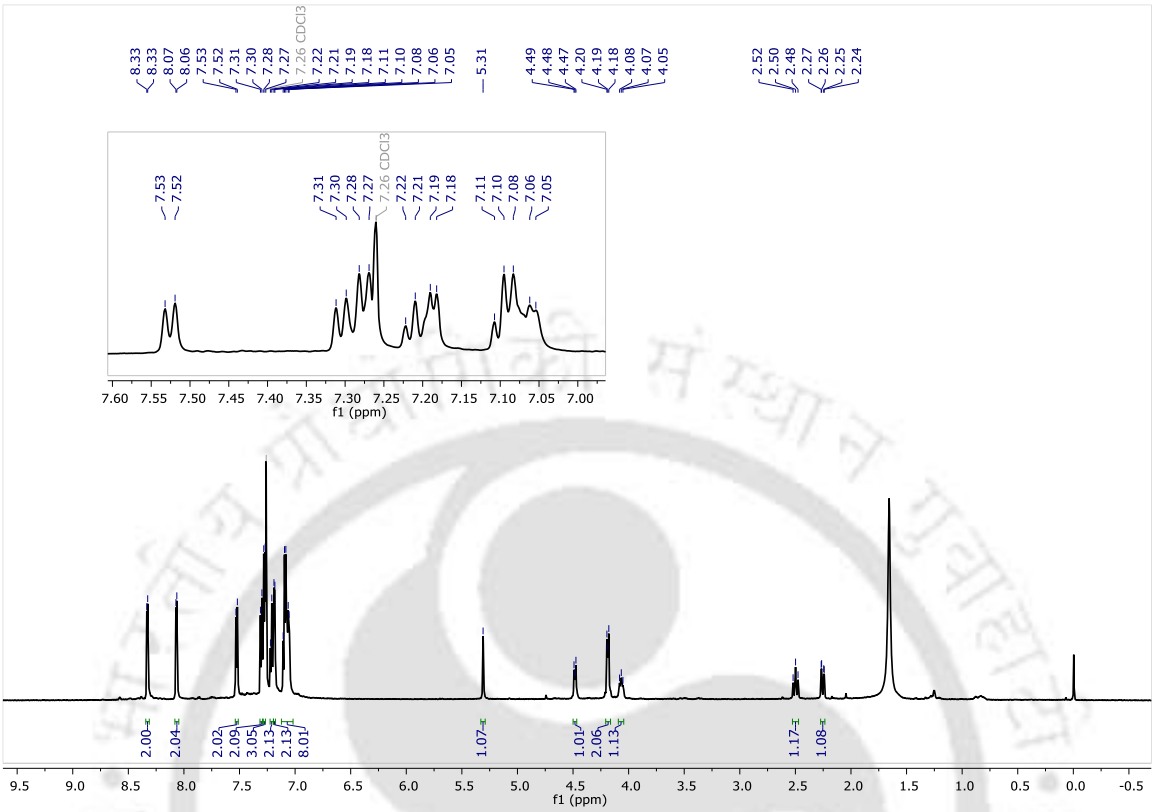

Figure A3. ^{1}H NMR spectrum of **2a**.

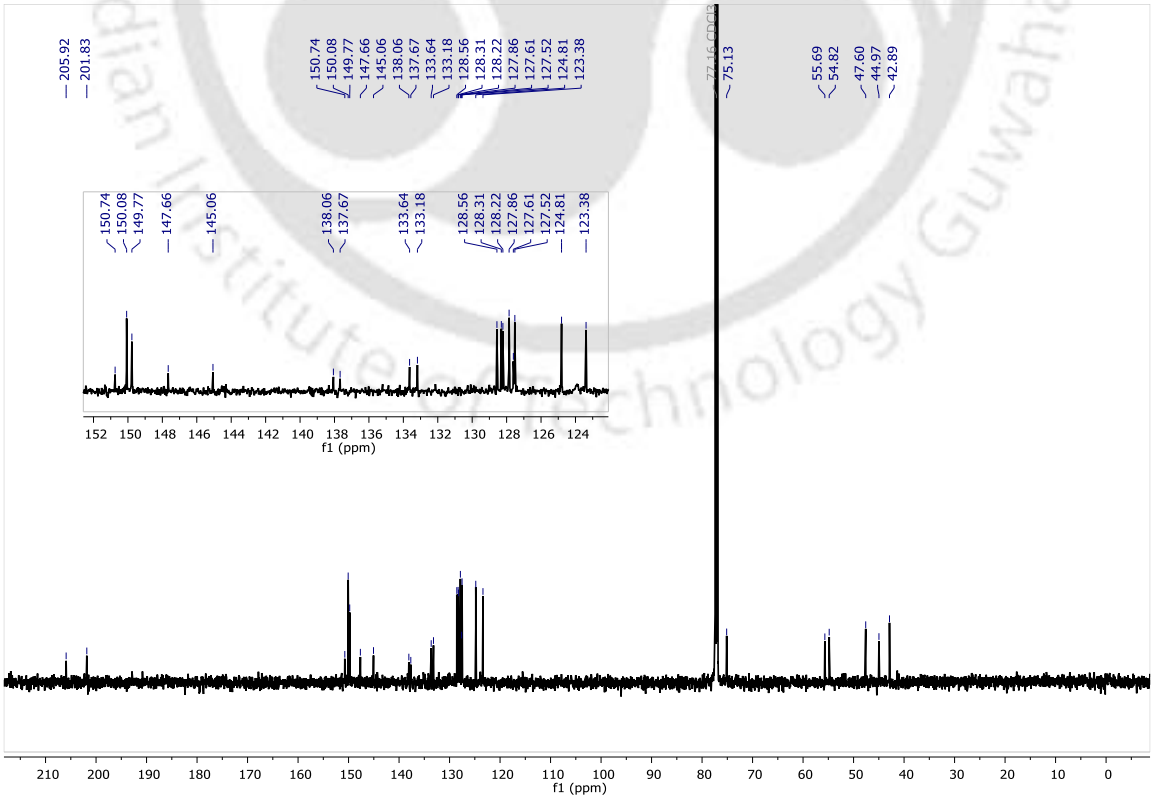

Figure A4. ^{13}C NMR spectrum of **2a**.

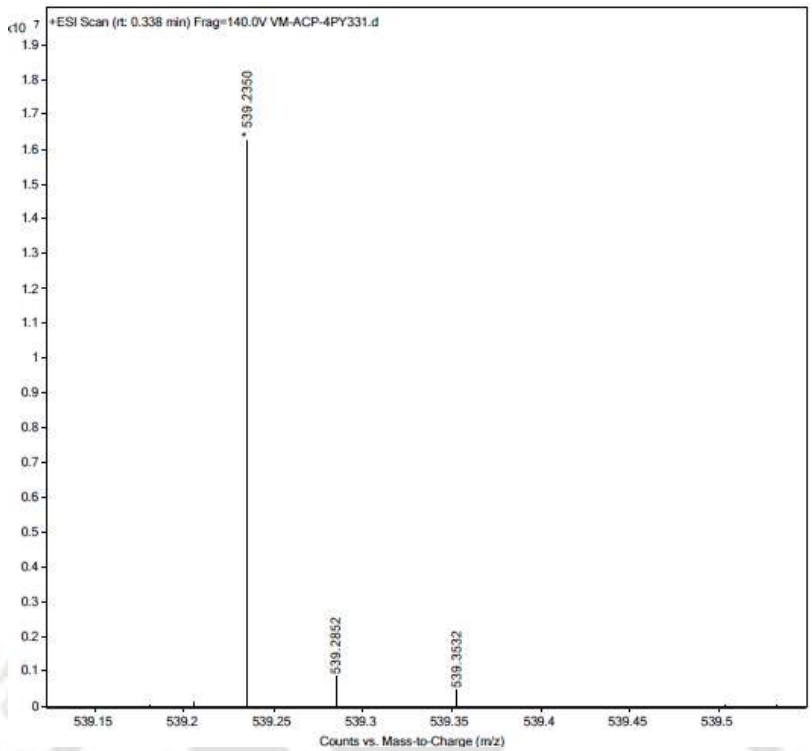

Figure A5. Mass spectrum of **2a**.

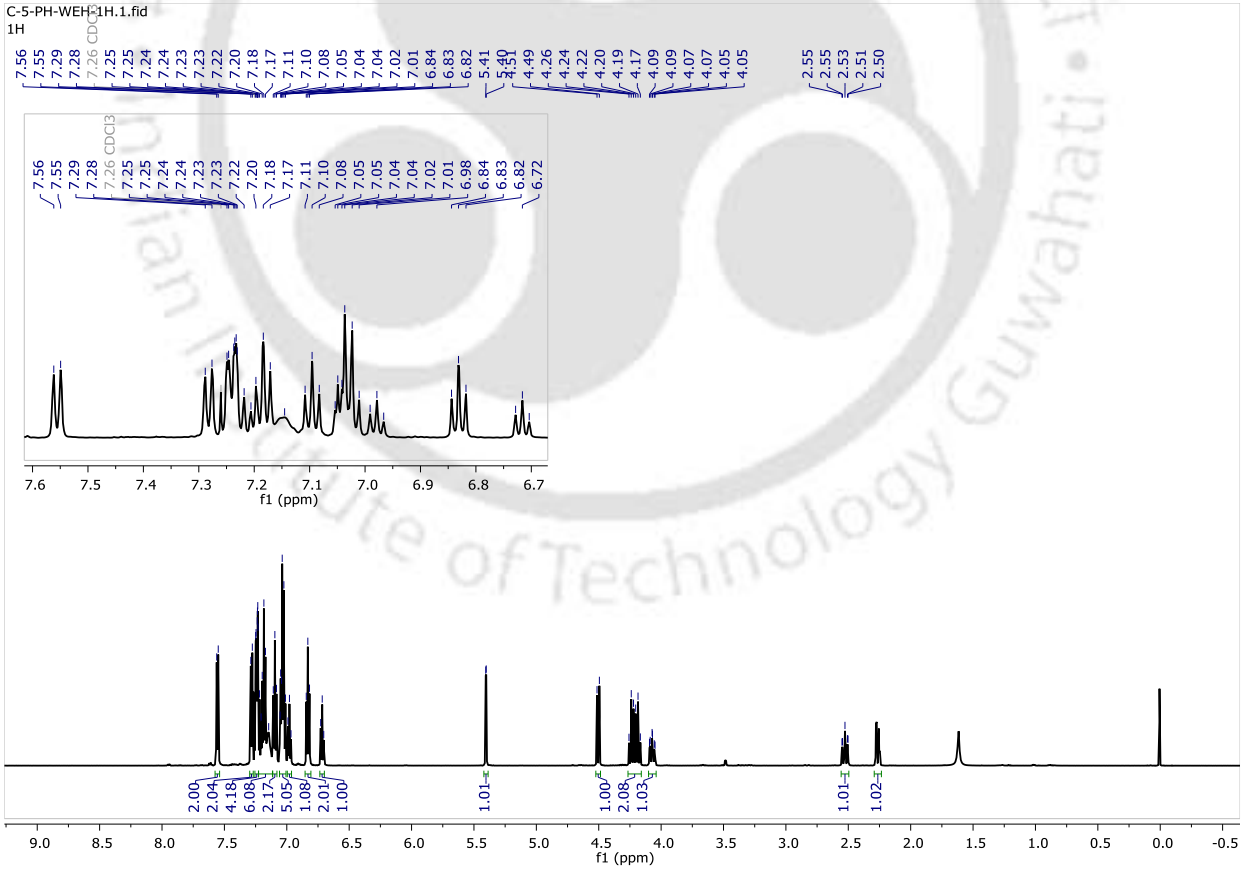

Figure A6. ^{1}H NMR spectrum of **2b**.

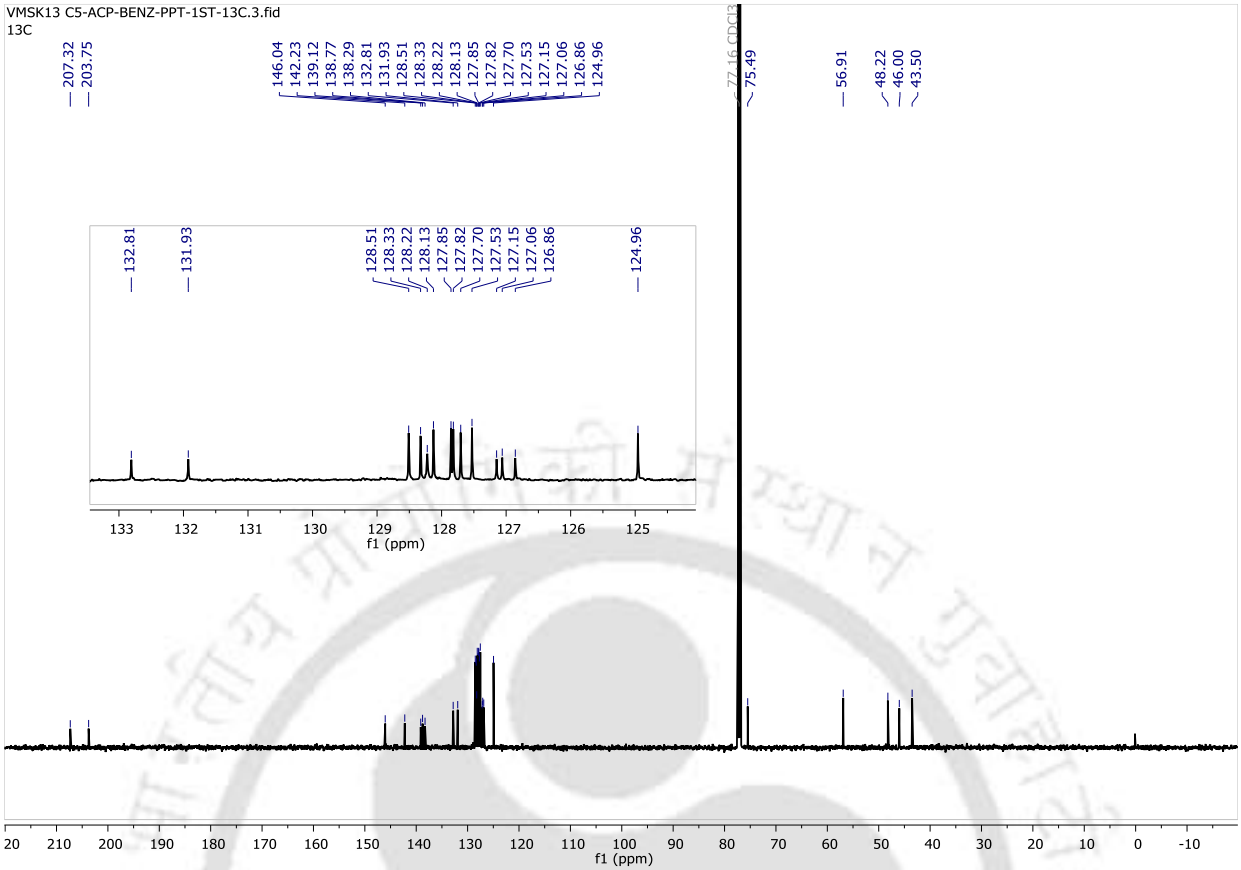

Figure A7. ^{13}C NMR spectrum of **2b**.

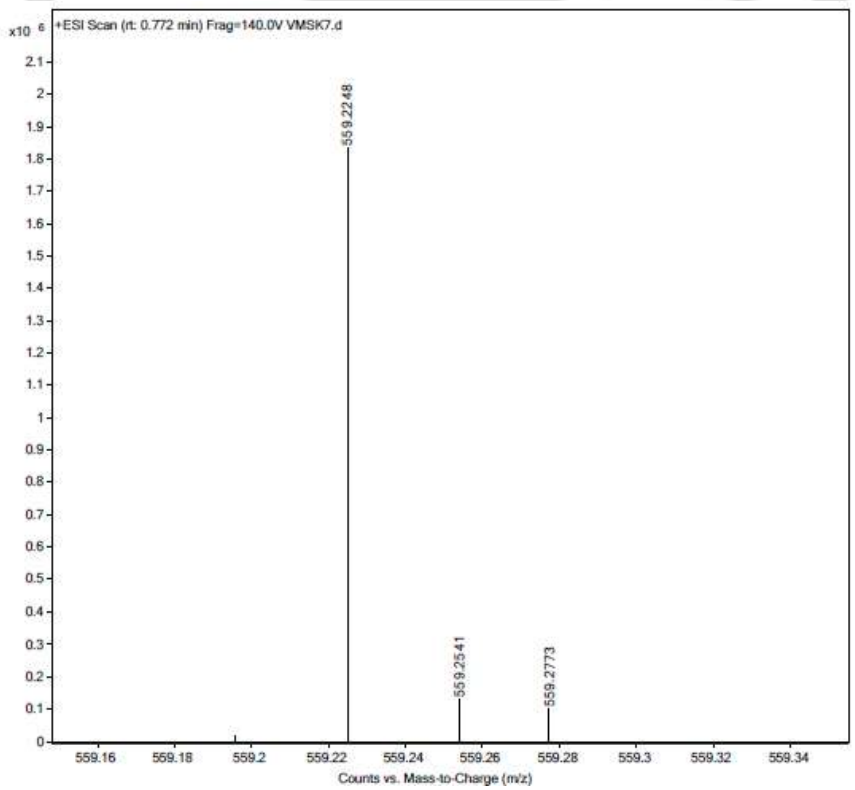

Figure A8. Mass spectrum of **2b**.

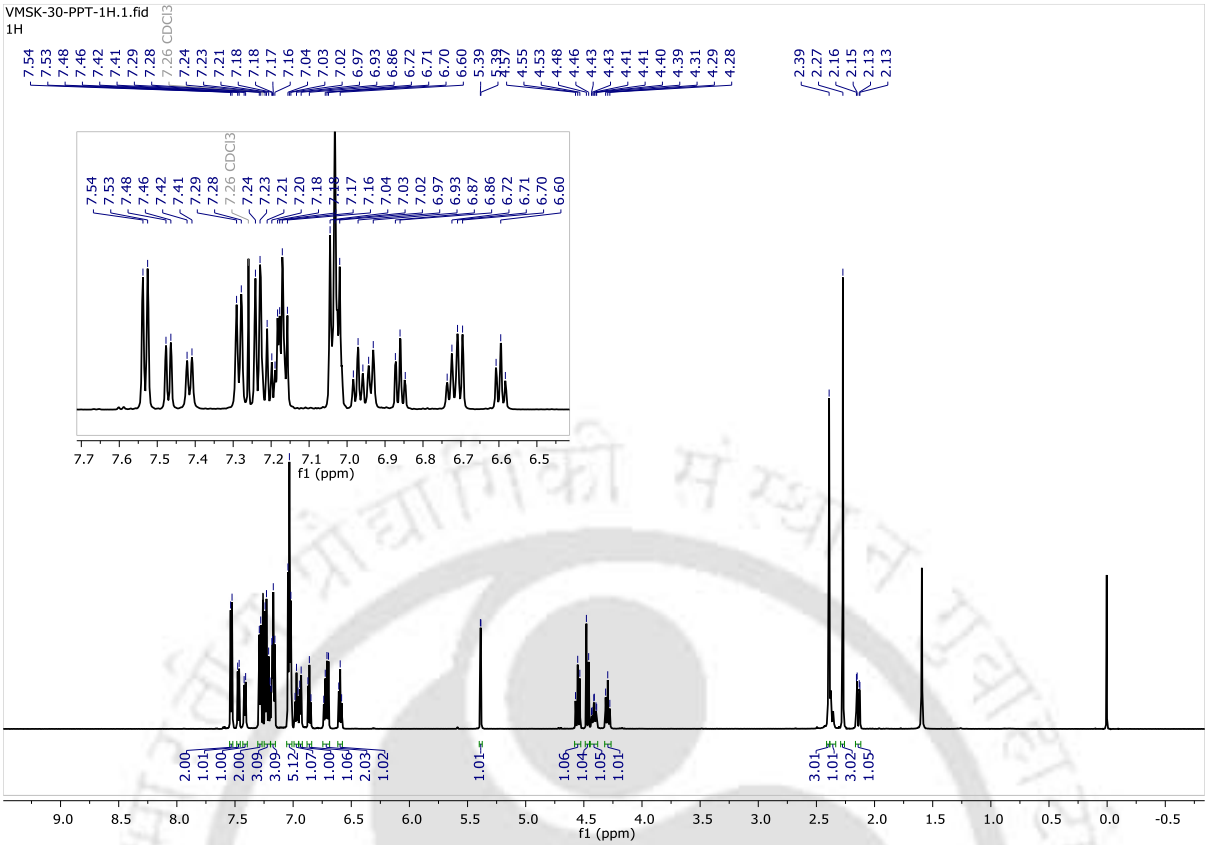

Figure A9. ^{1}H NMR spectrum of **2c**.

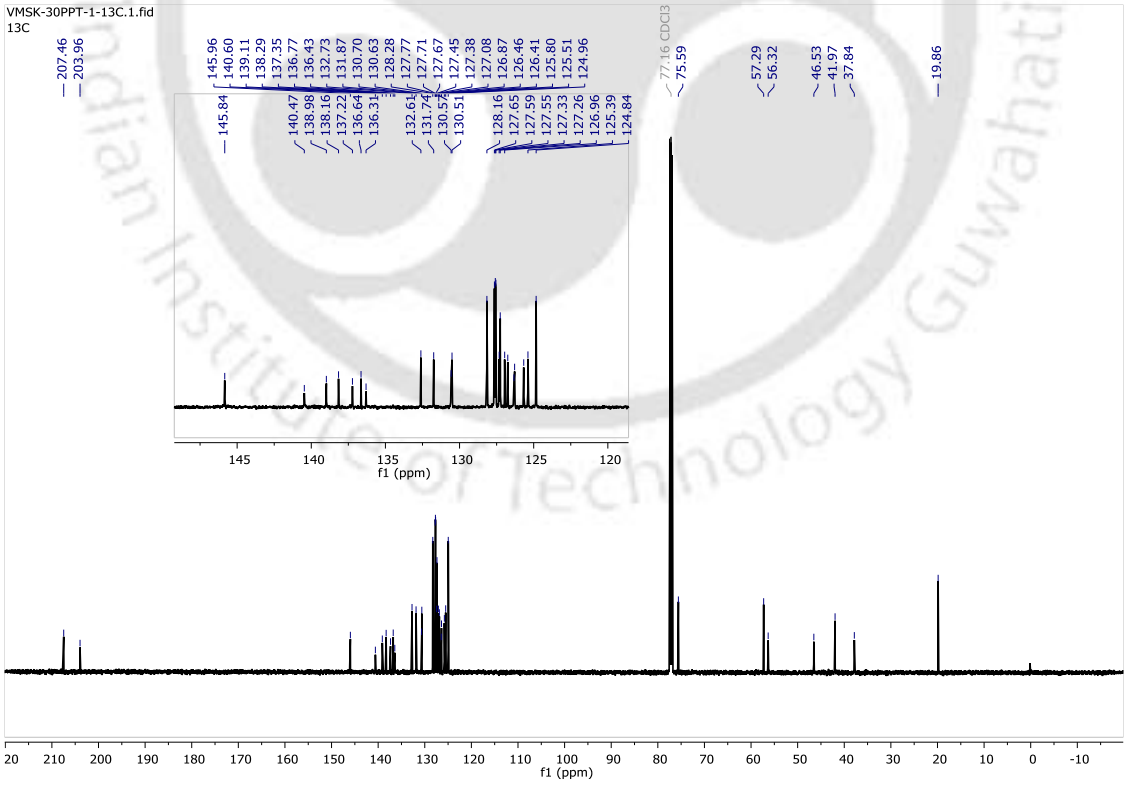

Figure A10. ^{13}C NMR spectrum of **2c**.

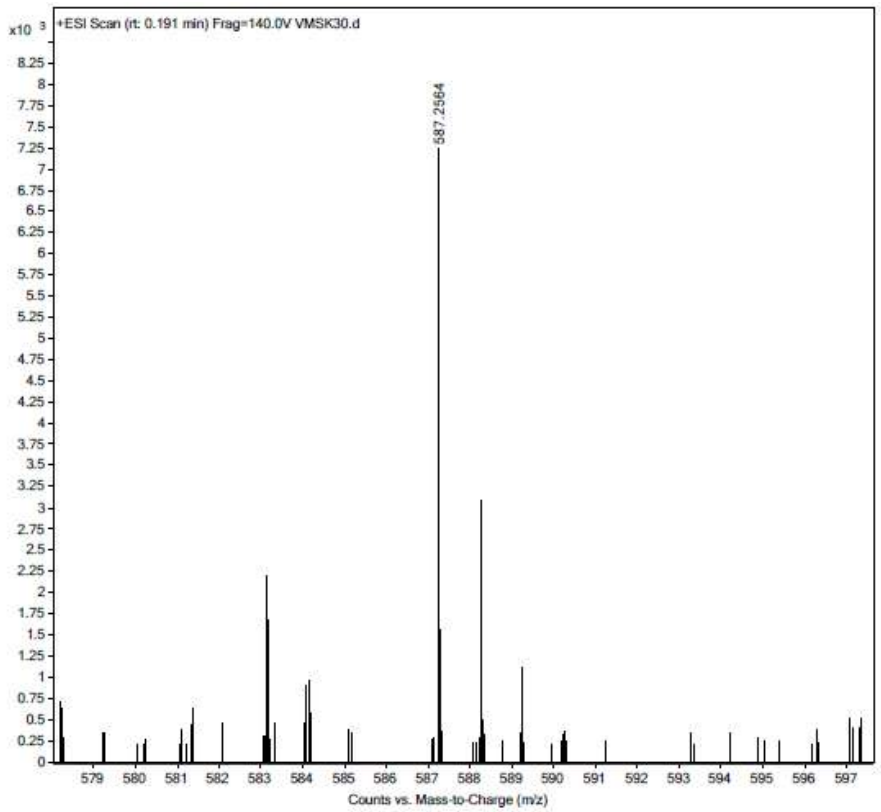

Figure A11. Mass spectrum of **2c**.

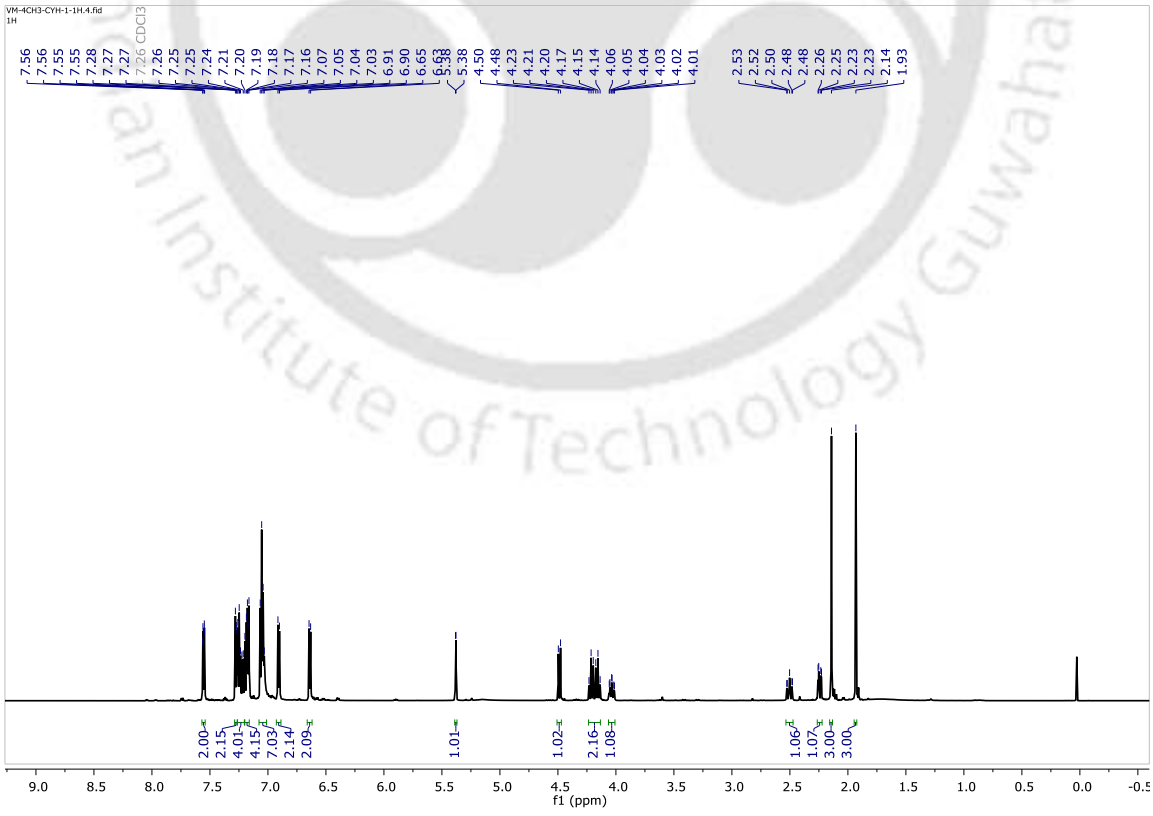

Figure A12. ^{1}H NMR spectrum of **2d**.

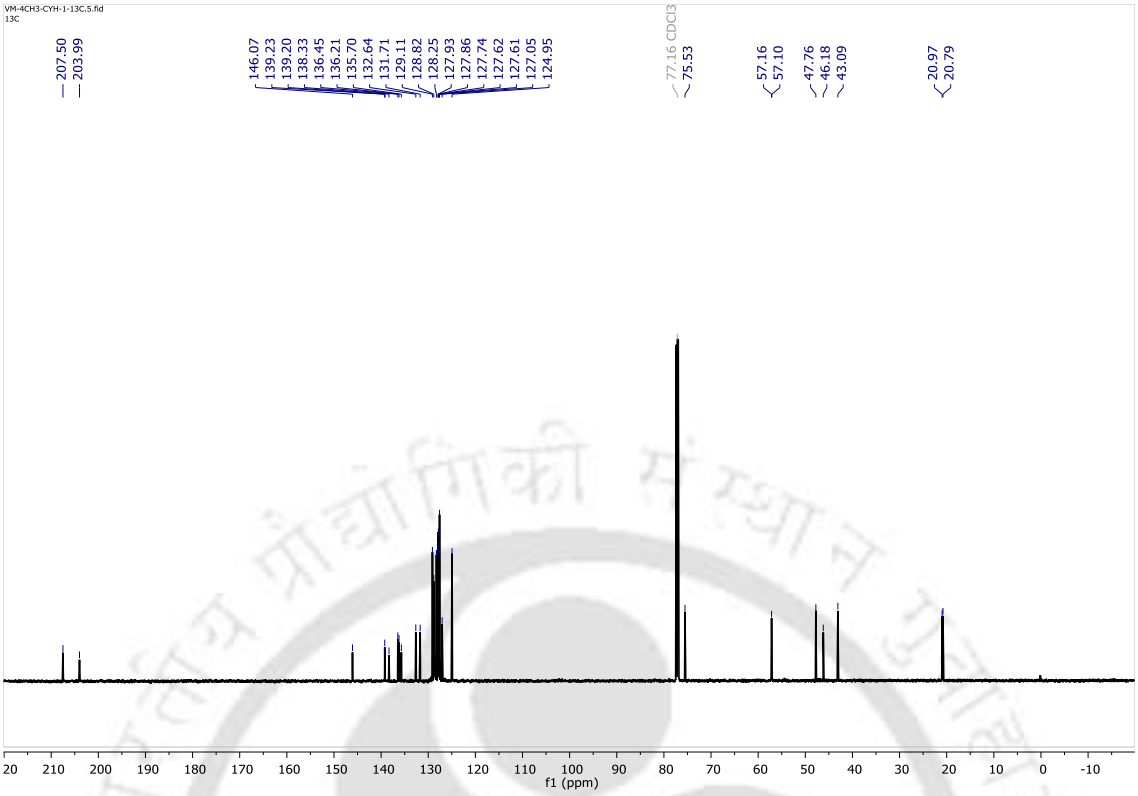

Figure A13. ^{13}C NMR spectrum of **2d**.

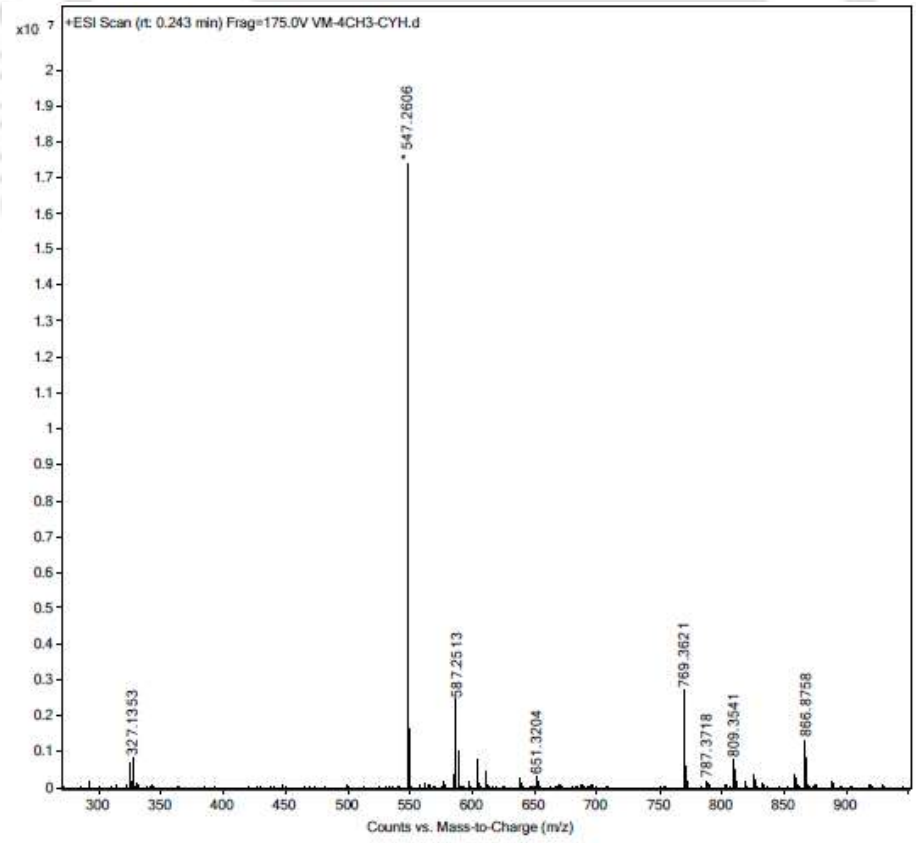

Figure A14. Mass spectrum of **2d**.

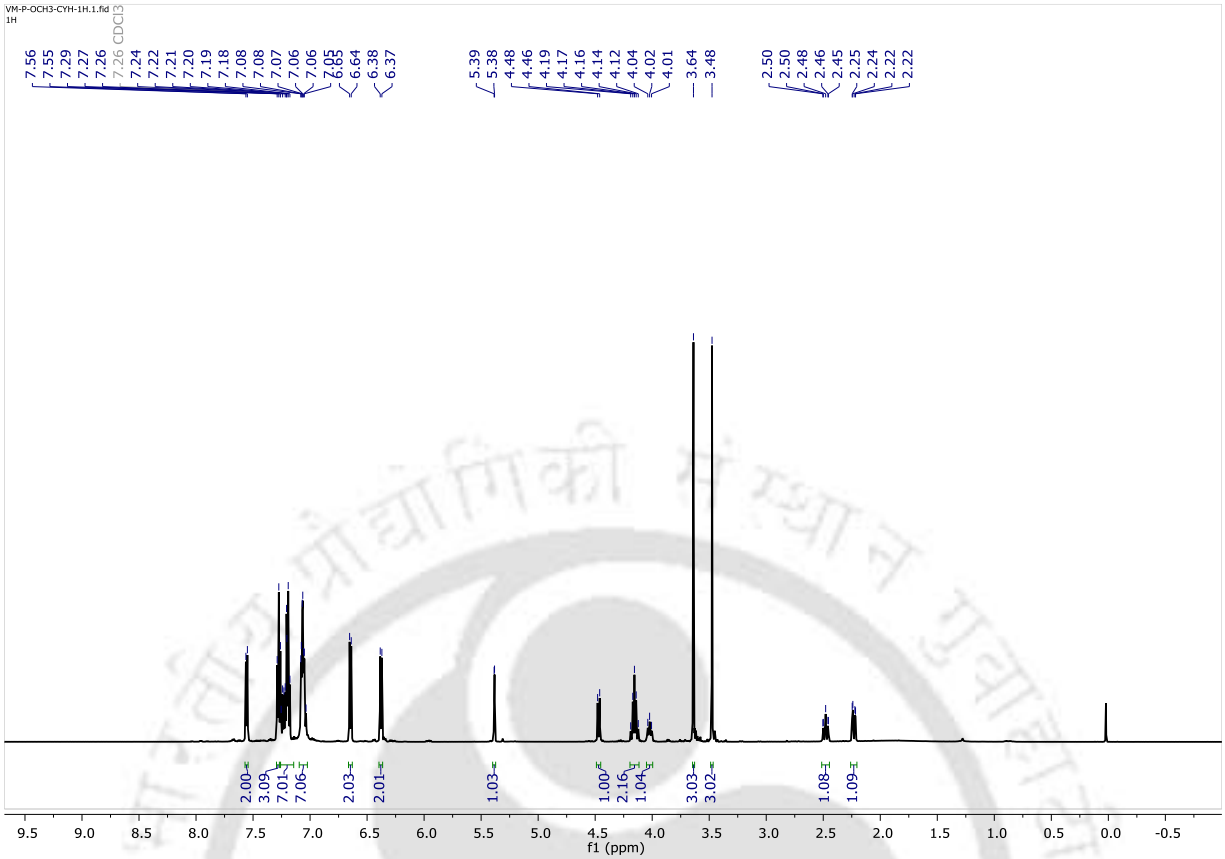

Figure A15. ^{1}H NMR spectrum of **2e**.

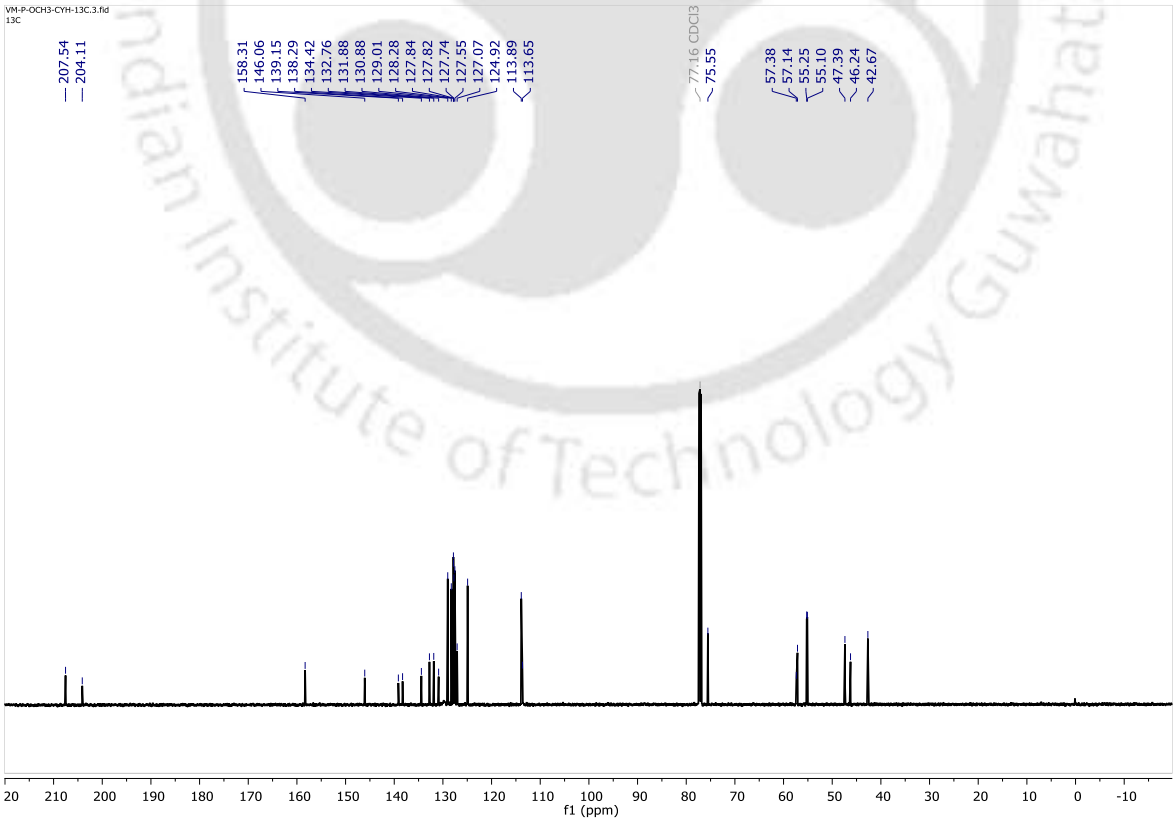

Figure A16. ^{13}C NMR spectrum of **2e**.

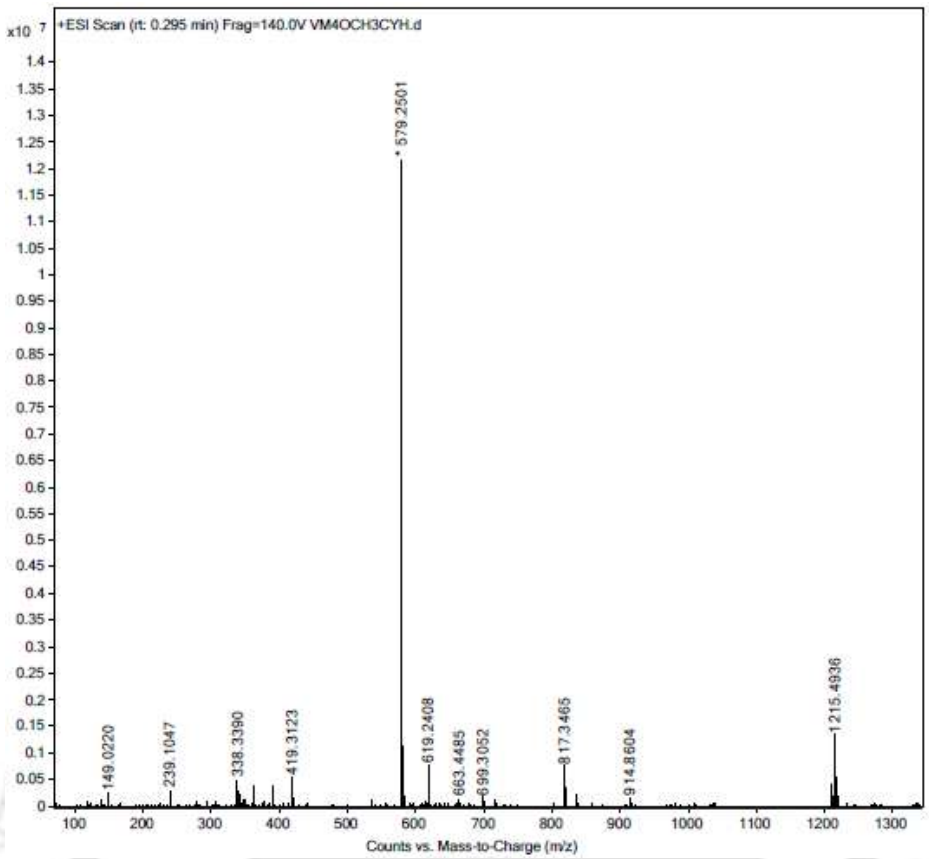

Figure A17. Mass spectrum of **2e**.

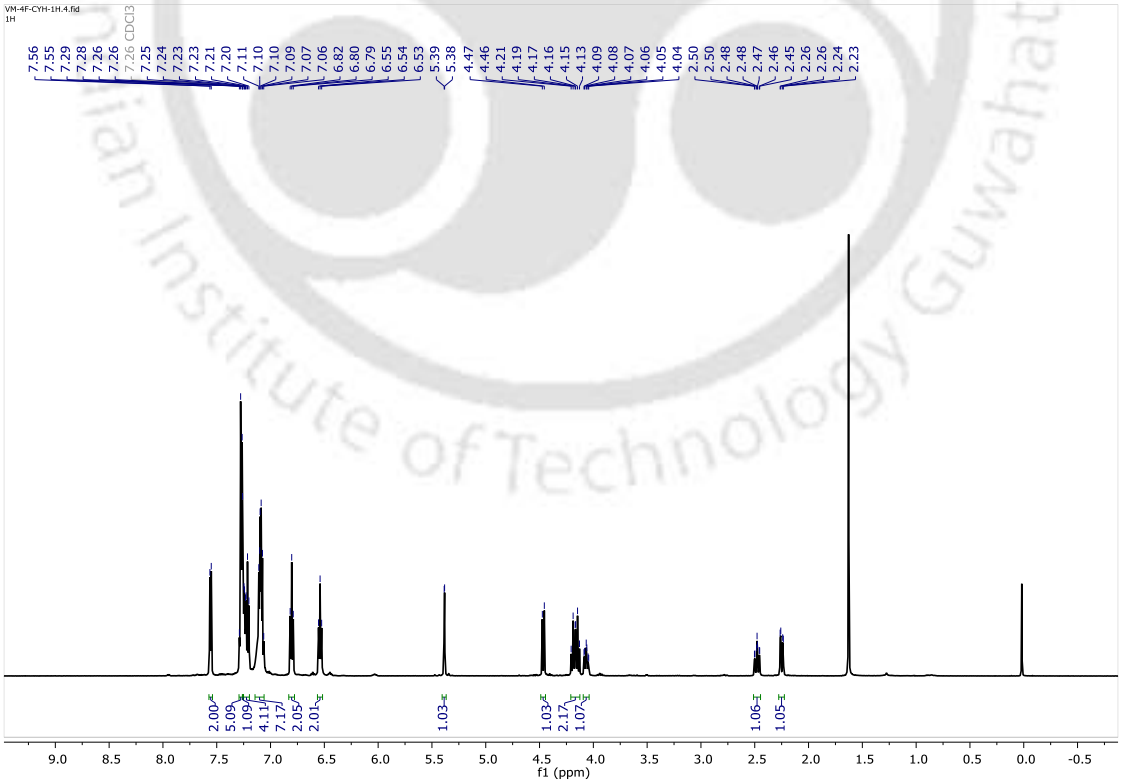

Figure A18. ^{1}H NMR spectrum of **2f**.

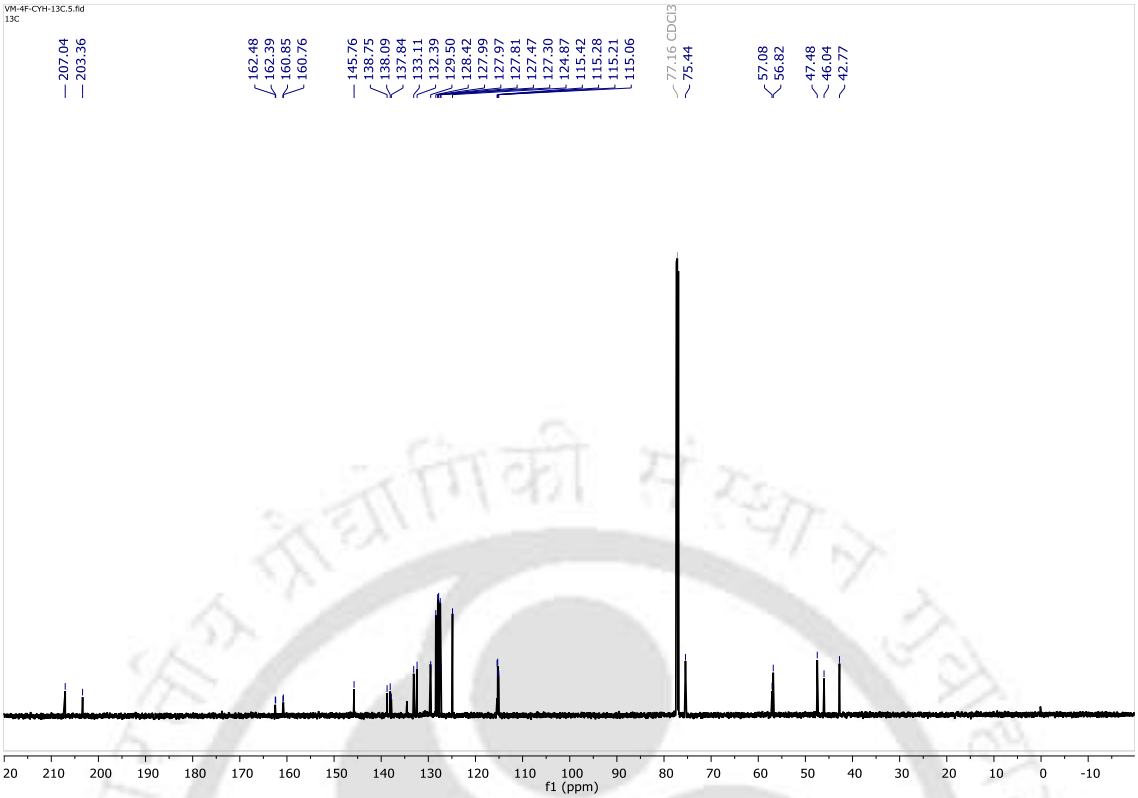

Figure A19. ^{13}C NMR spectrum of **2f**.

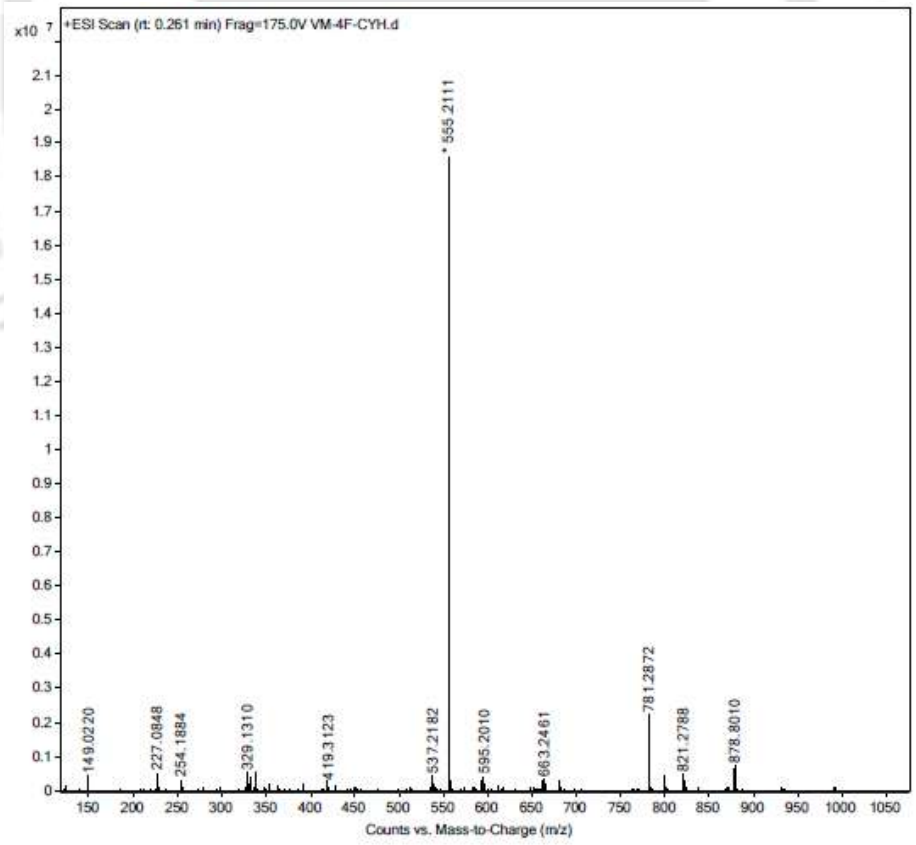

Figure A20. Mass spectrum of **2f**.

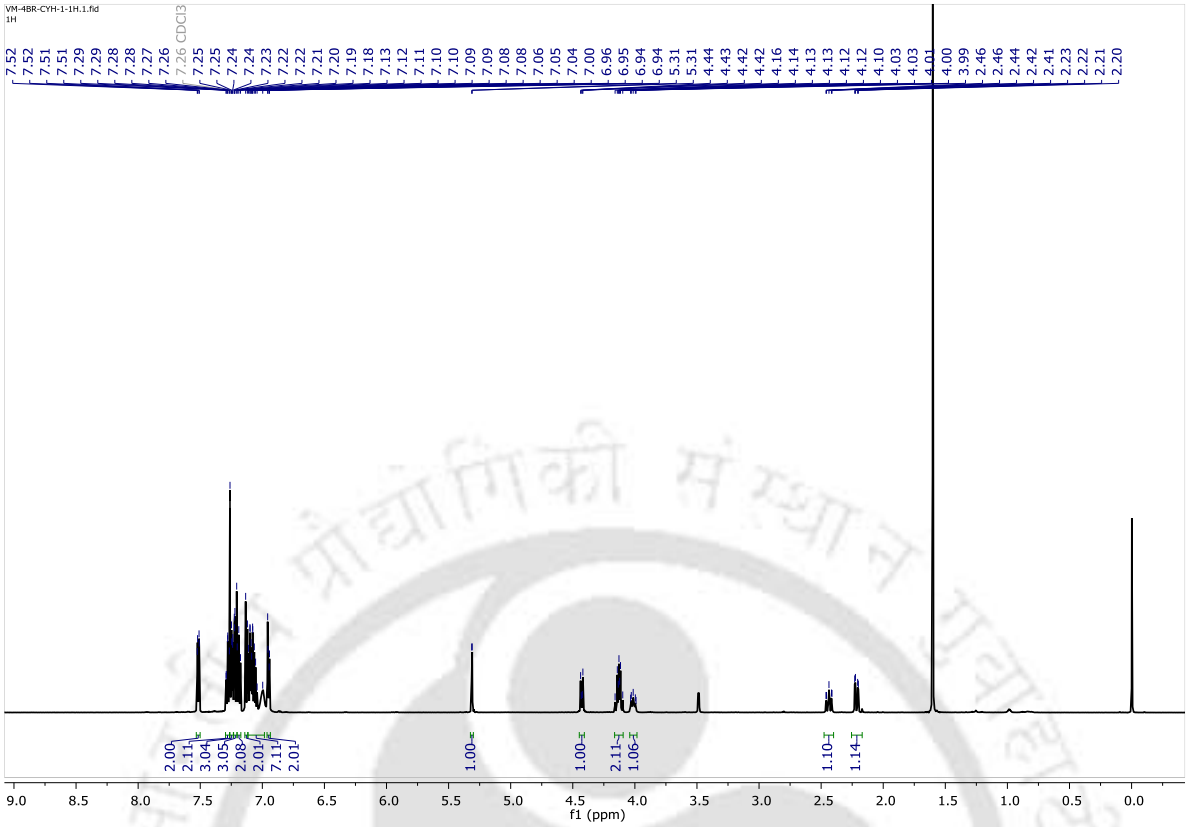

Figure A21. ^{1}H NMR spectrum of **2g**.

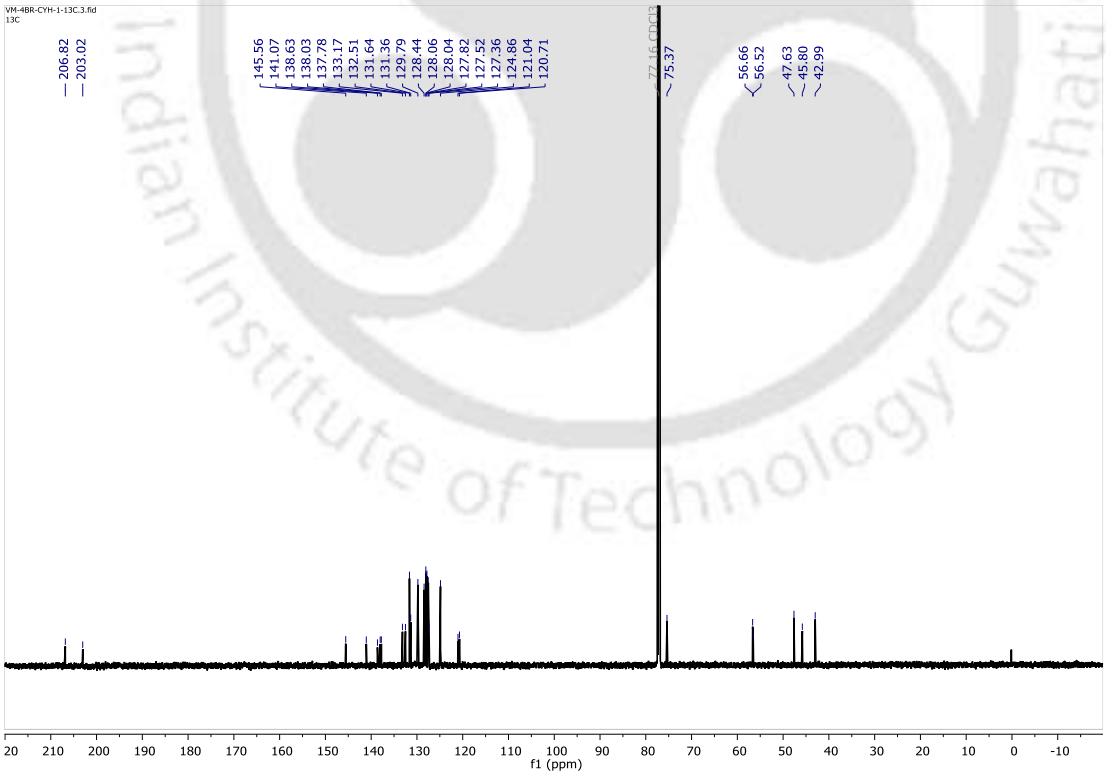

Figure A22. ^{13}C NMR spectrum of **2g**.

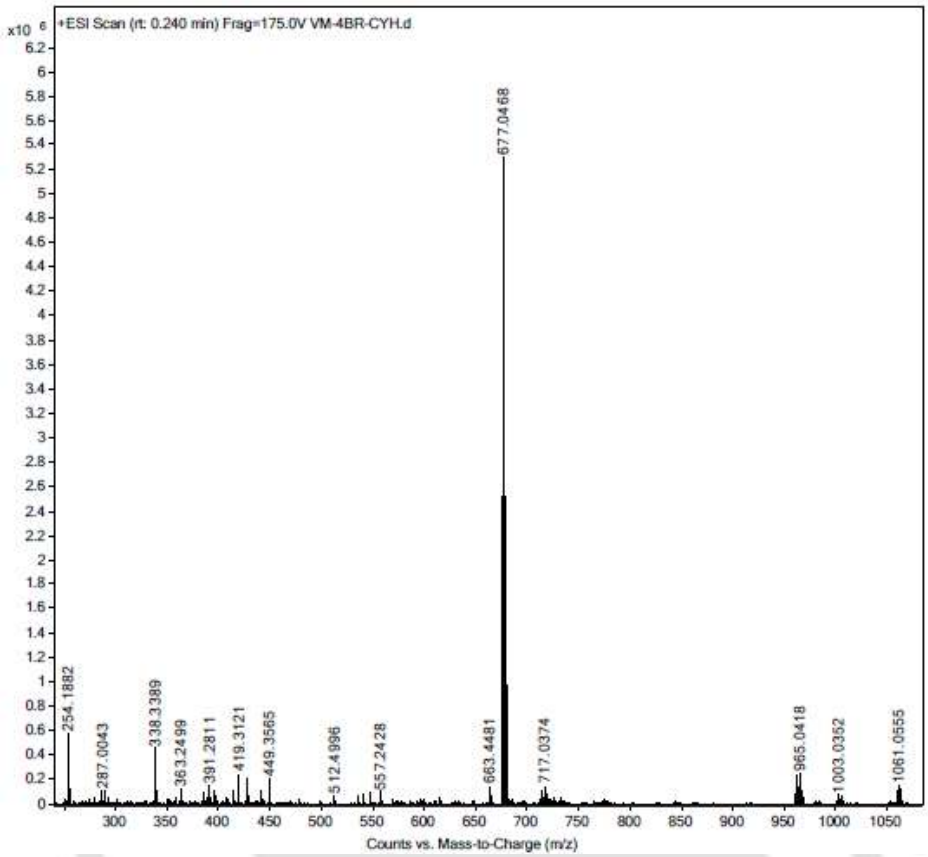

Figure A23. Mass spectrum of **2g**.

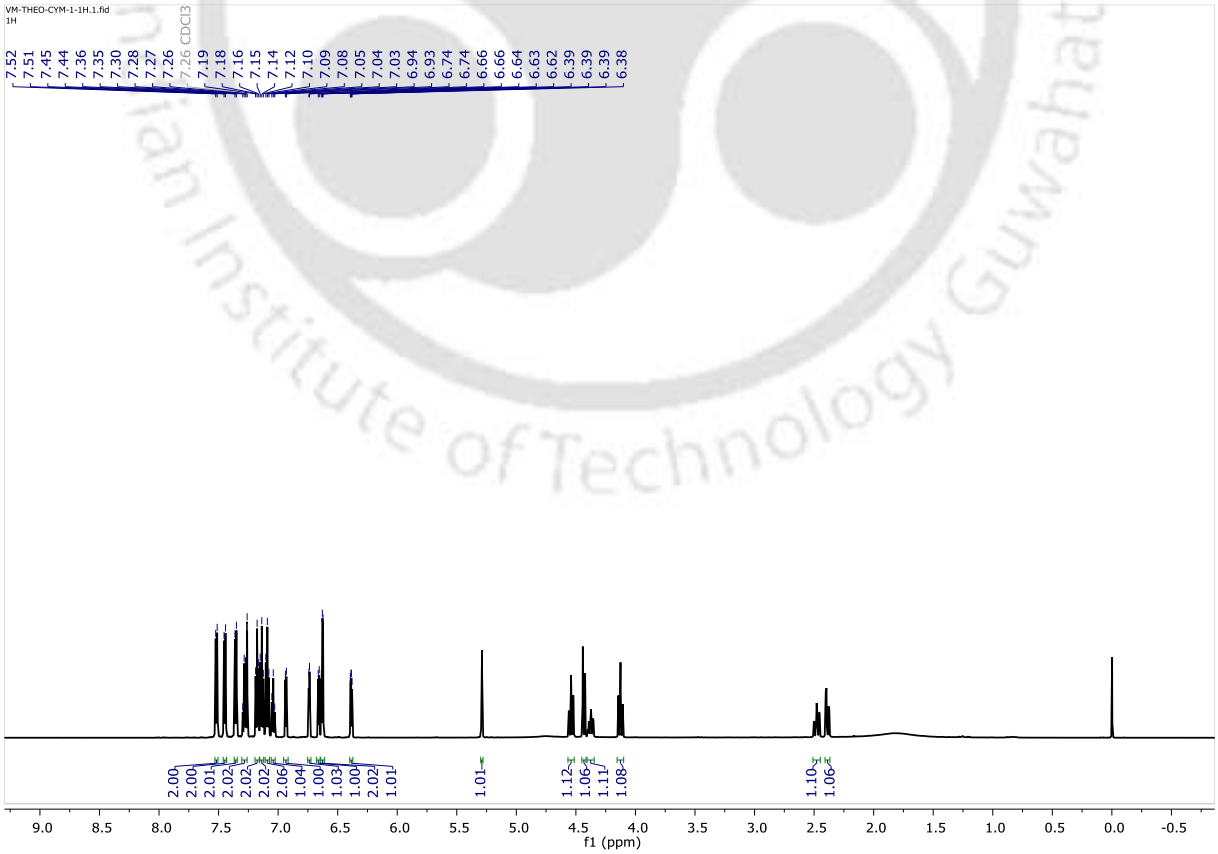

Figure A24. ^{1}H NMR spectrum of **2h**.

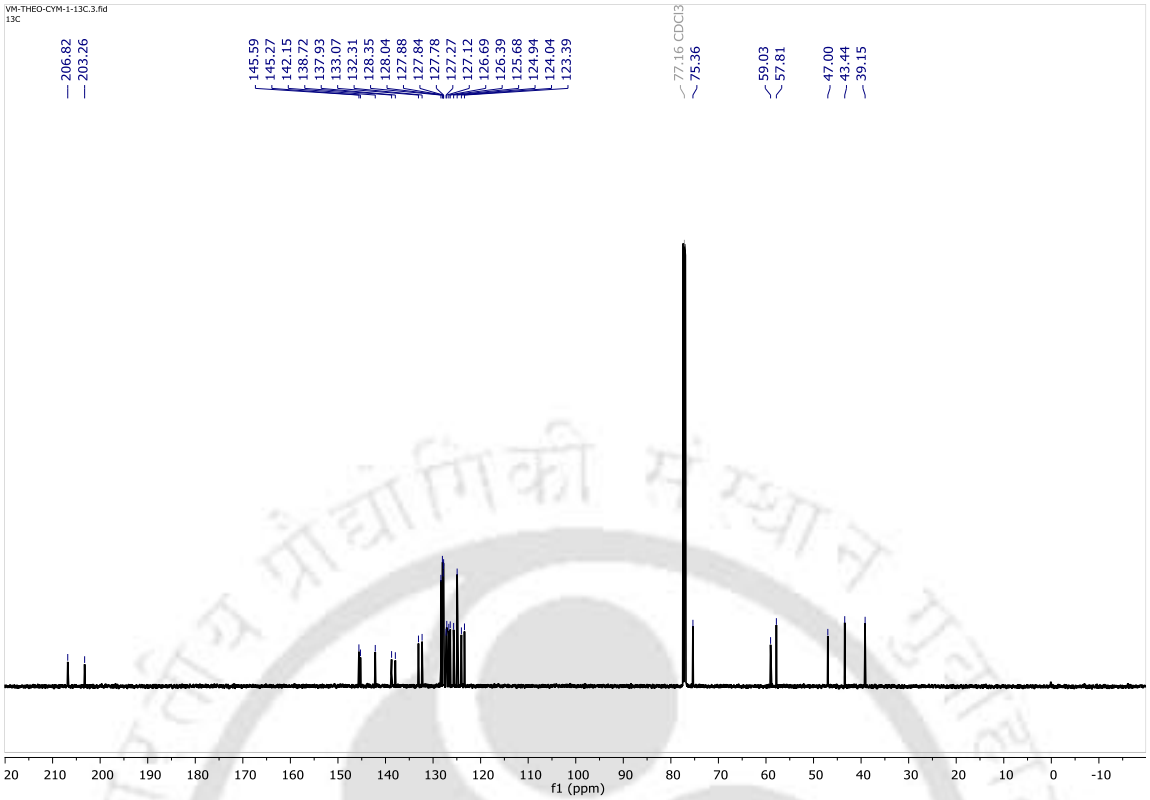

Figure A25. ^{13}C NMR spectrum of **2h**.

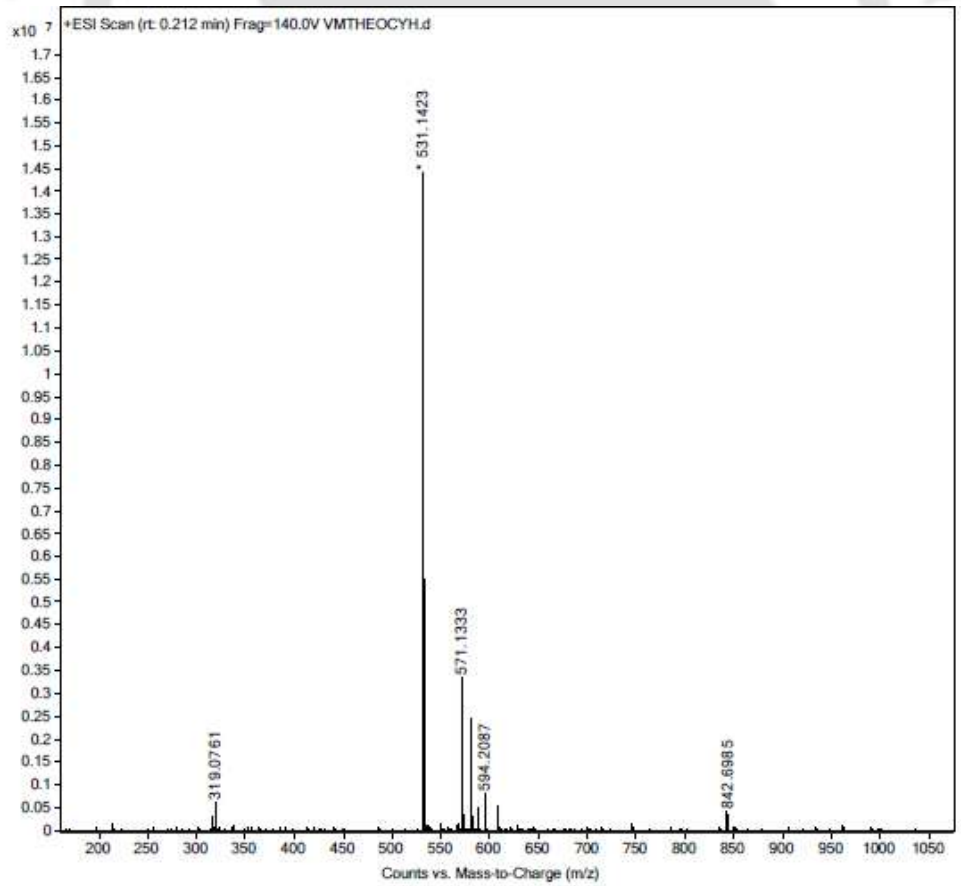

Figure A26. Mass spectrum of **2h**.

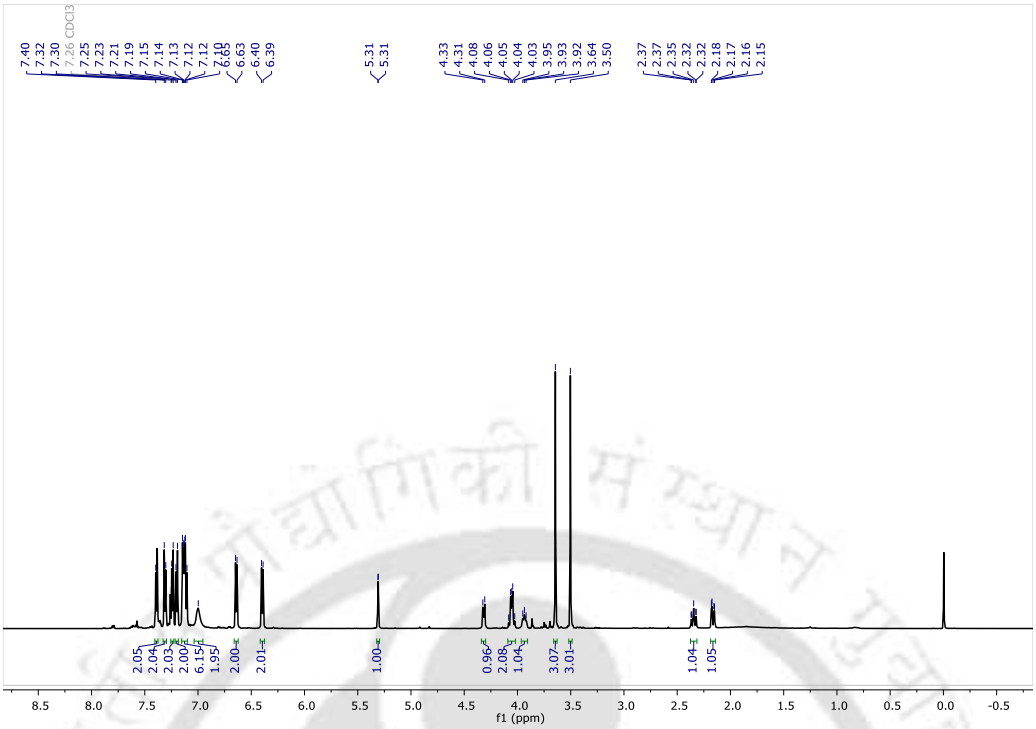

Figure A27. ^{1}H NMR spectrum of **2i**.

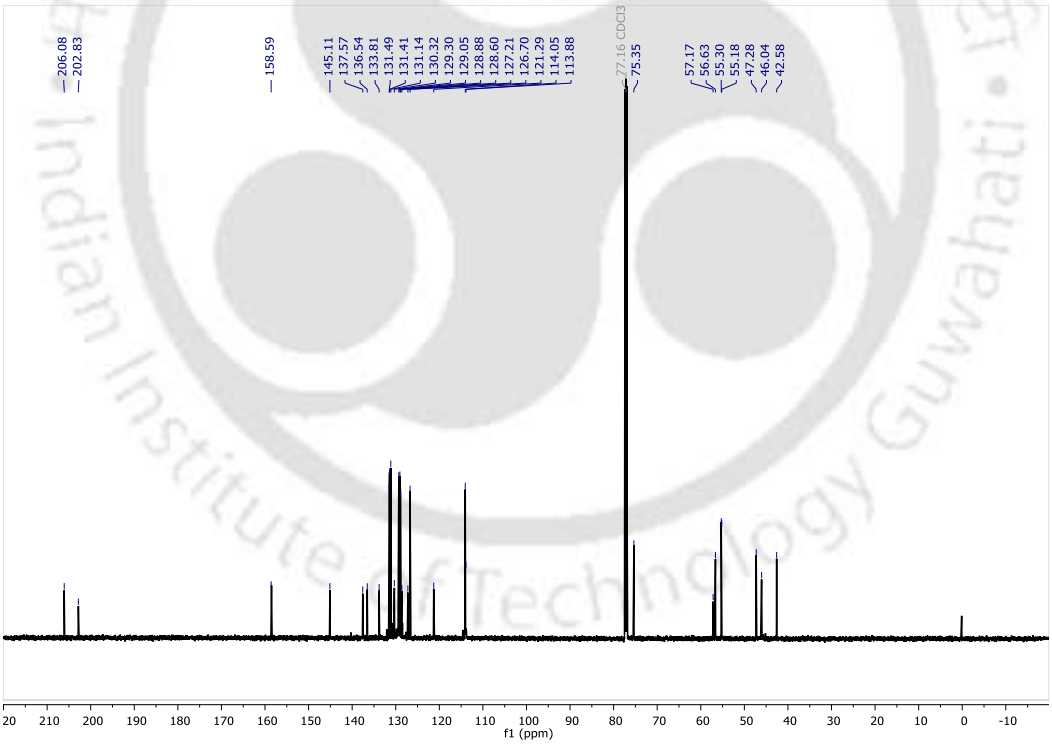

Figure A28. ^{13}C NMR spectrum of **2i**.

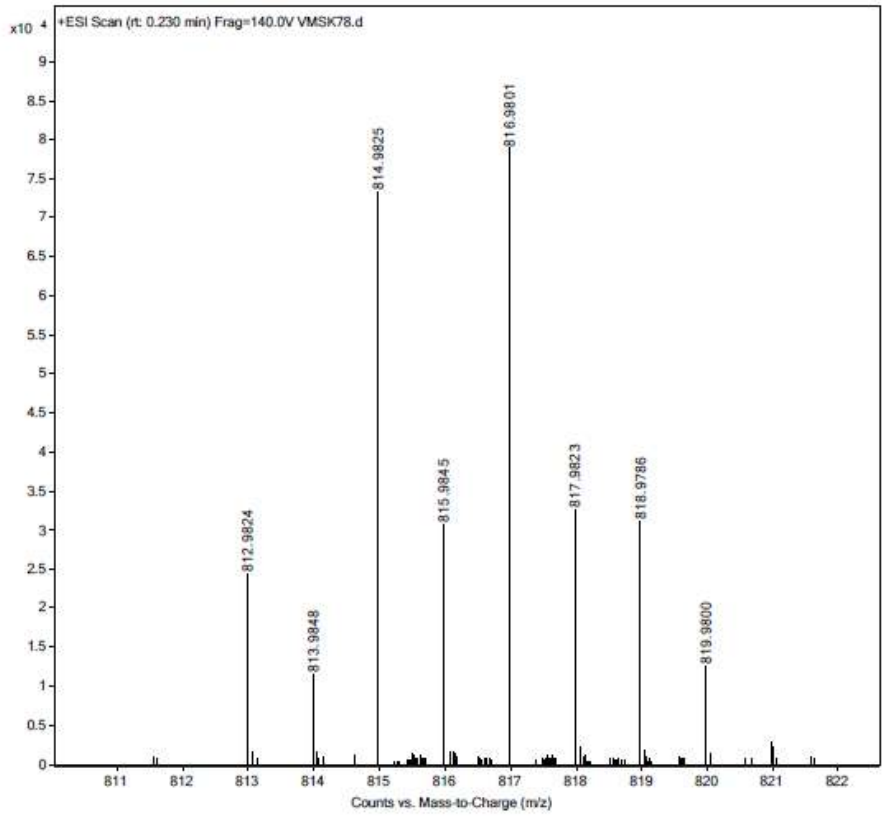

Figure A29. Mass spectrum of **2i**.

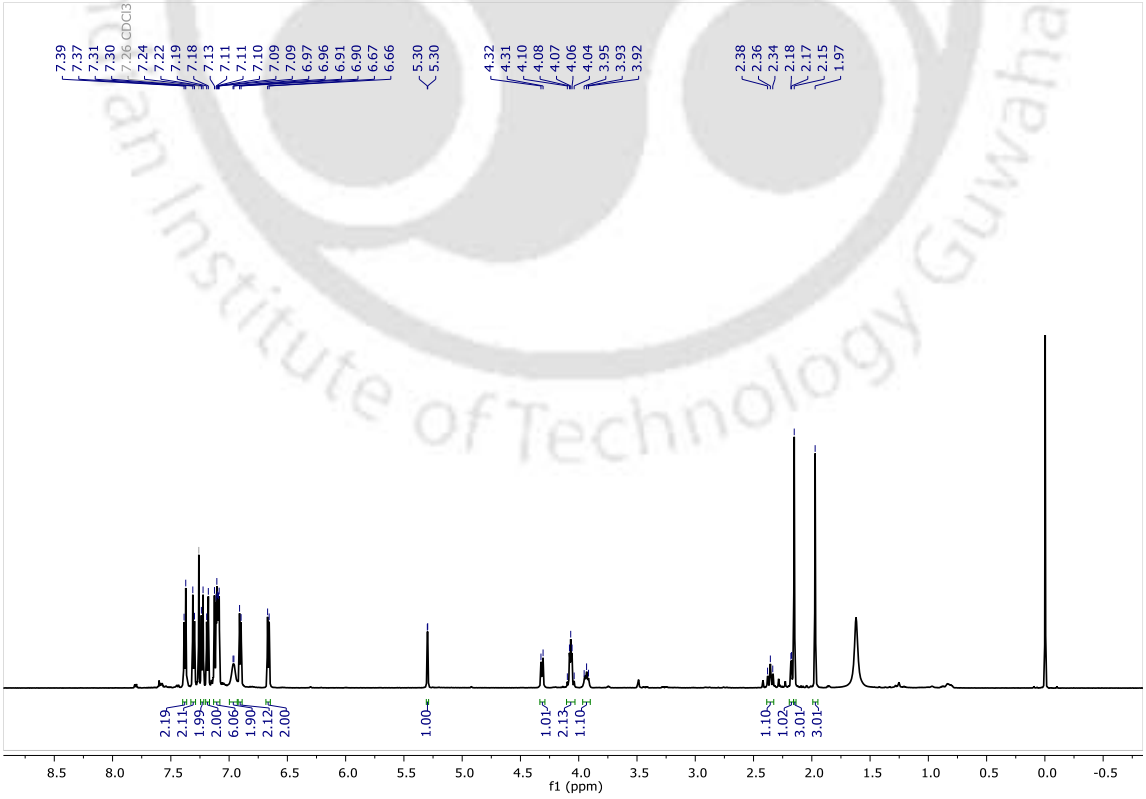

Figure A30. ^{1}H NMR spectrum of **2j**.

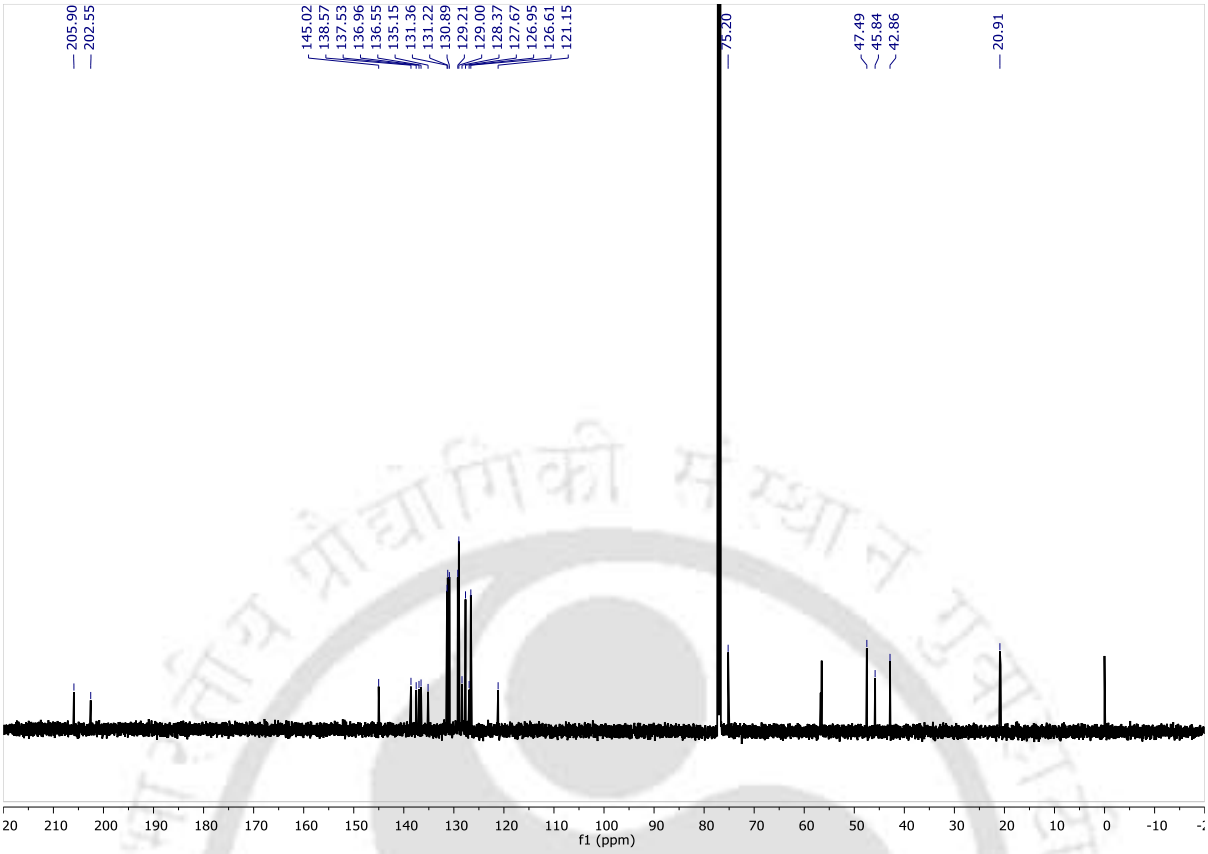

Figure A31. ^{13}C NMR spectrum of **2j**.

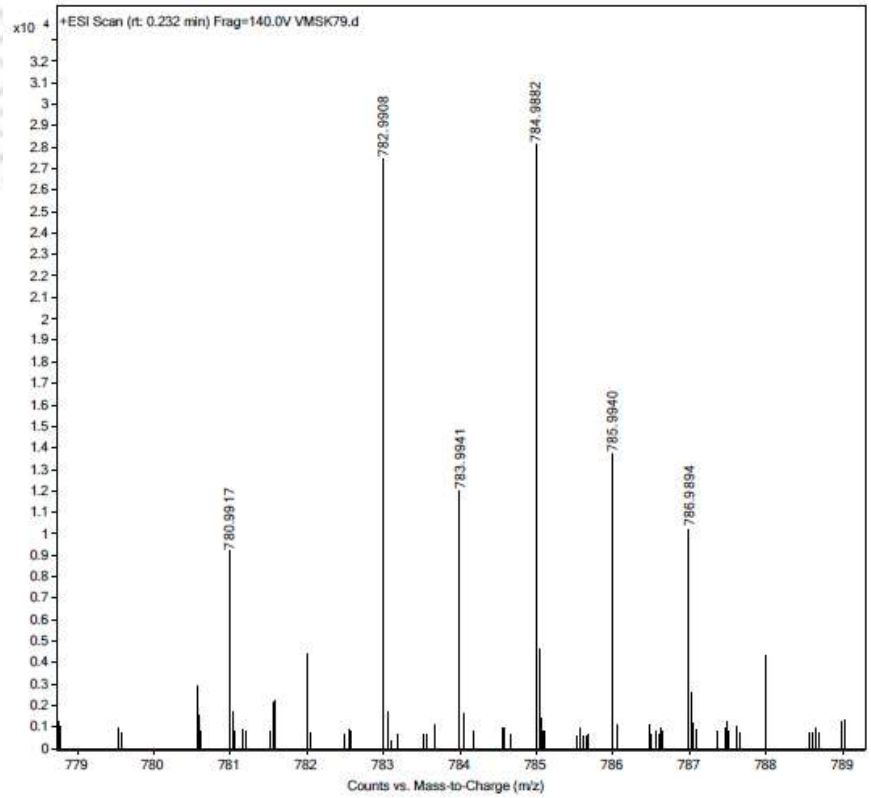

Figure A32. Mass spectrum of **2j**.

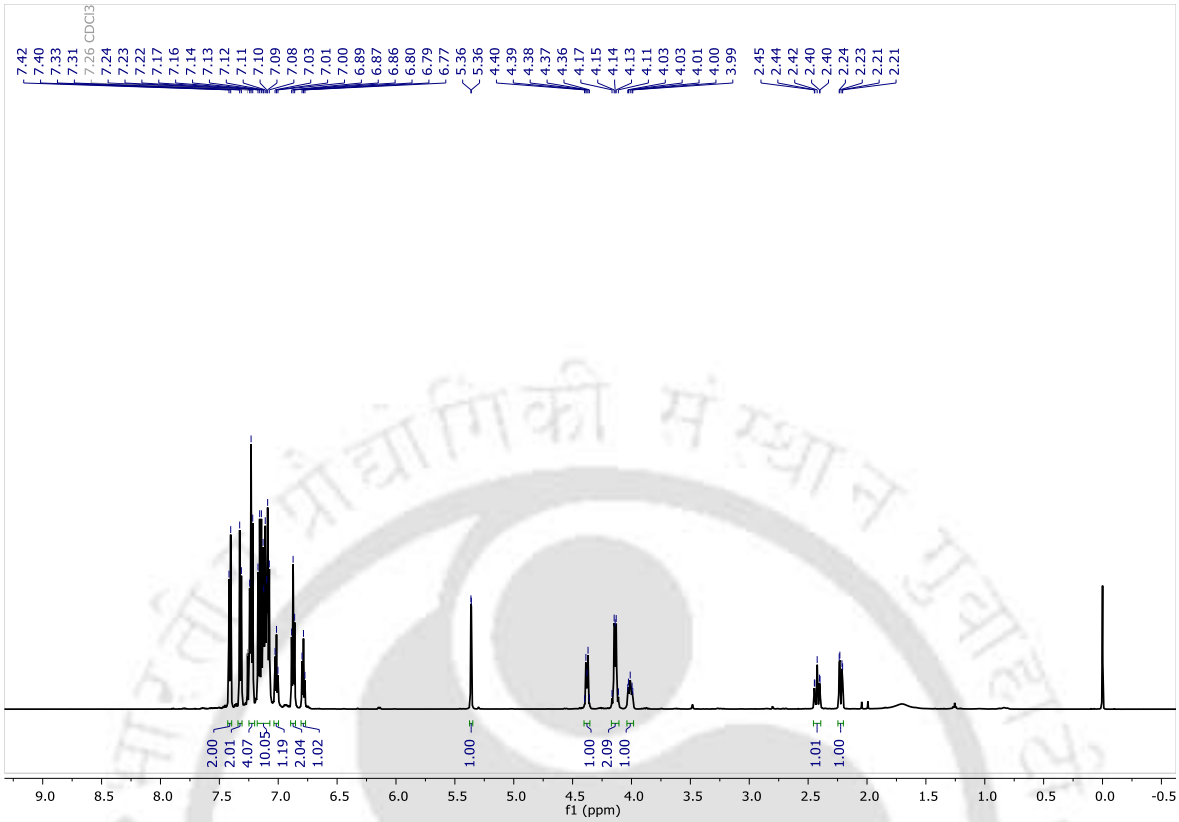

Figure A33. ^{1}H NMR spectrum of **2k**.

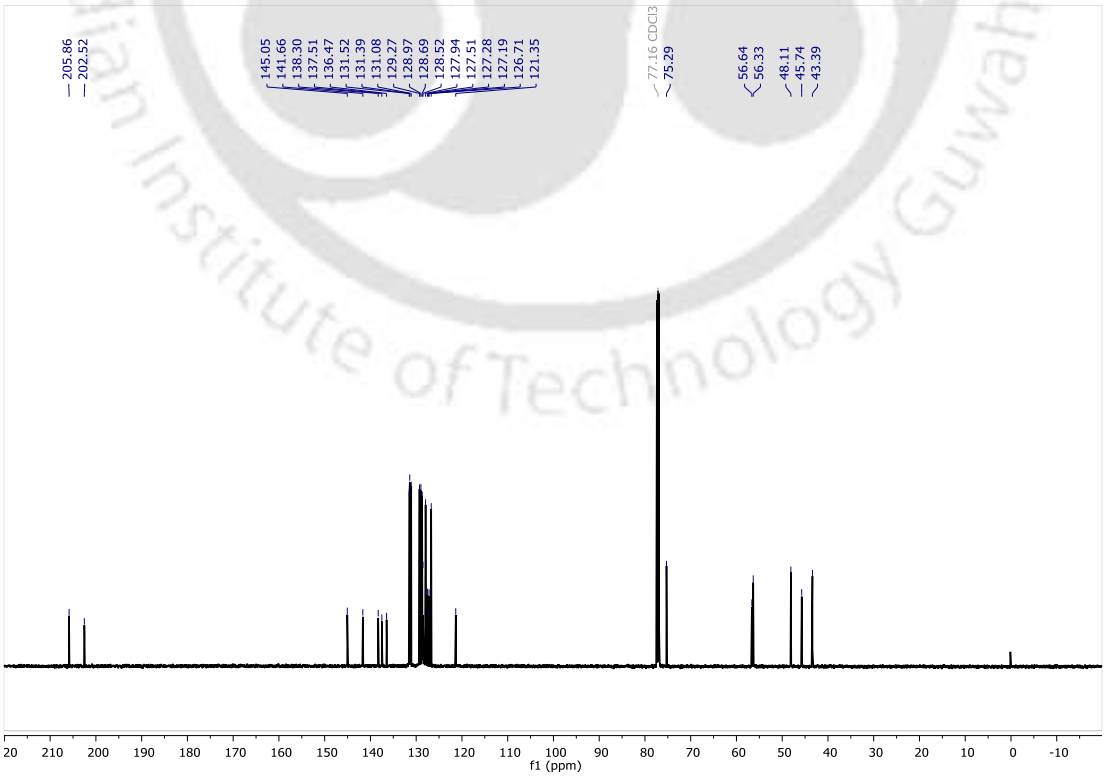

Figure A34. ^{13}C NMR spectrum of **2k**.

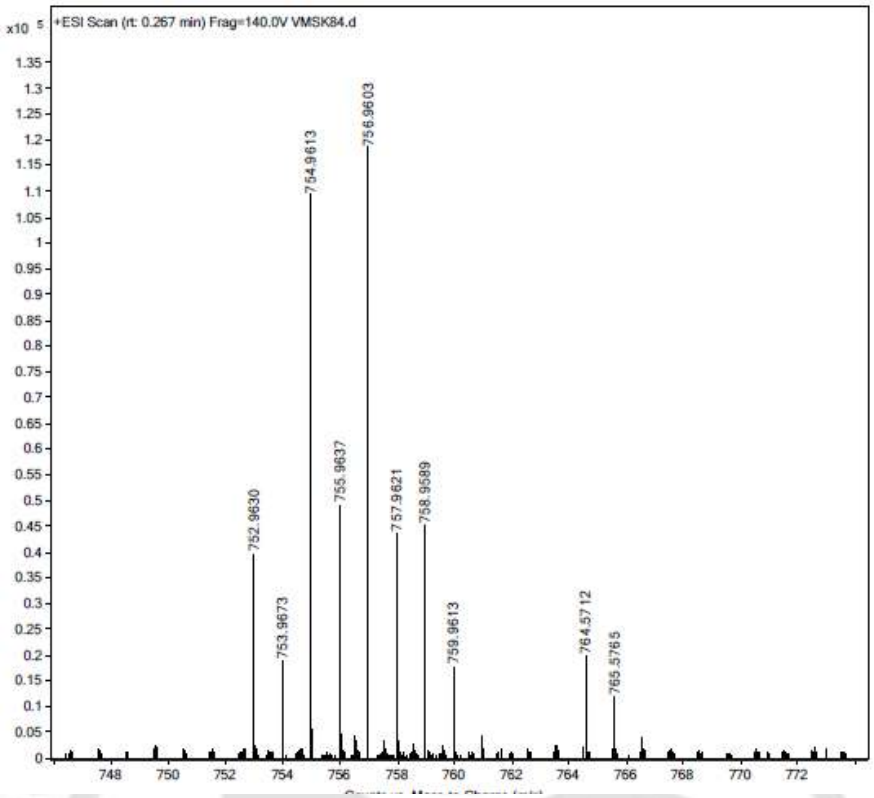

Figure A35. Mass spectrum of **2k**.

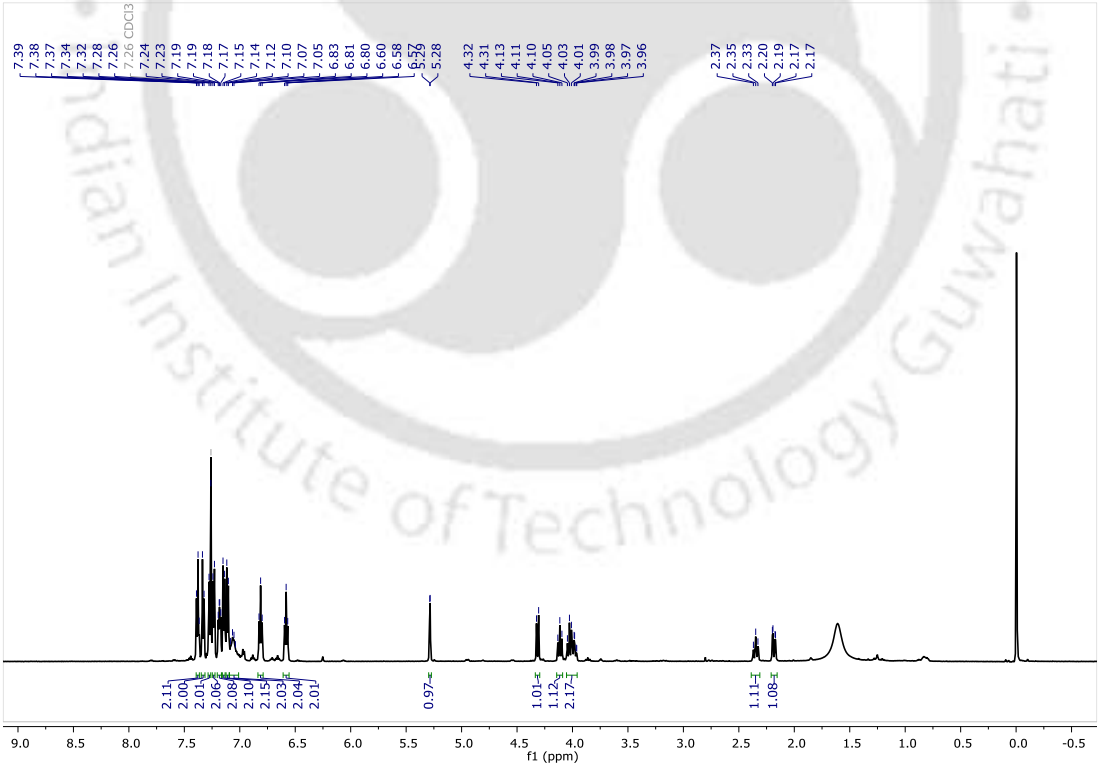

Figure A36. ^{1}H NMR spectrum of **2l**.

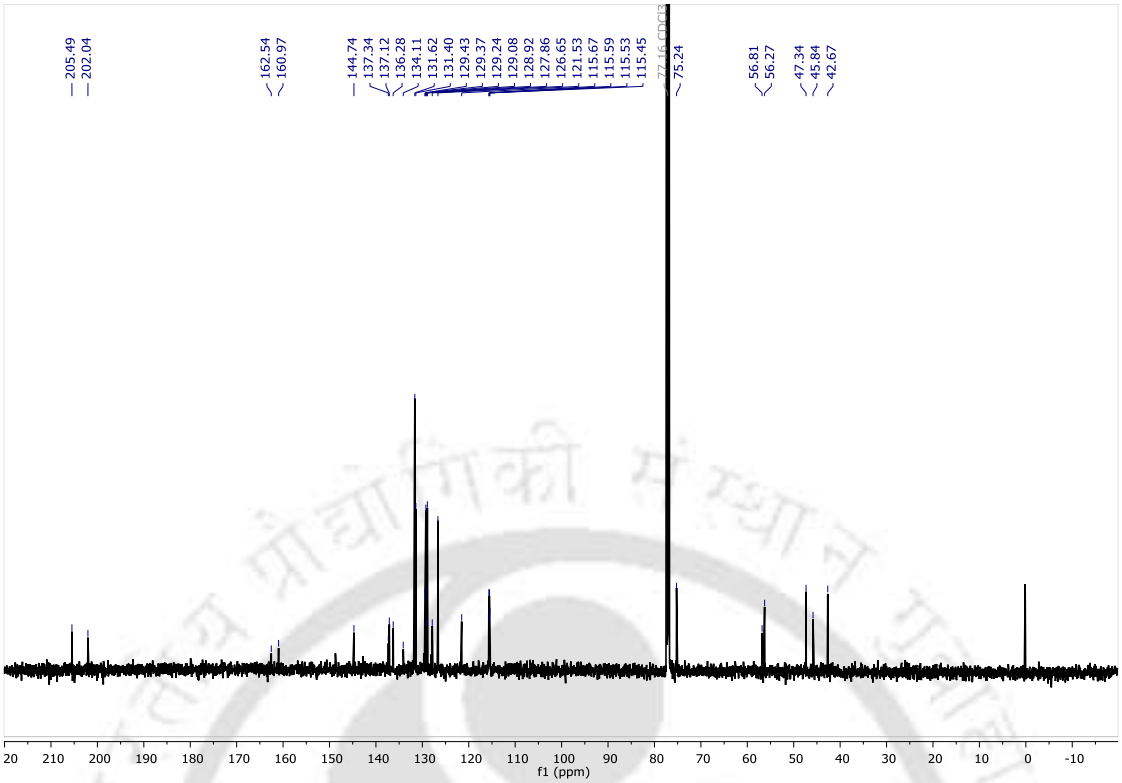

Figure A37. ^{13}C NMR spectrum of **2l**.

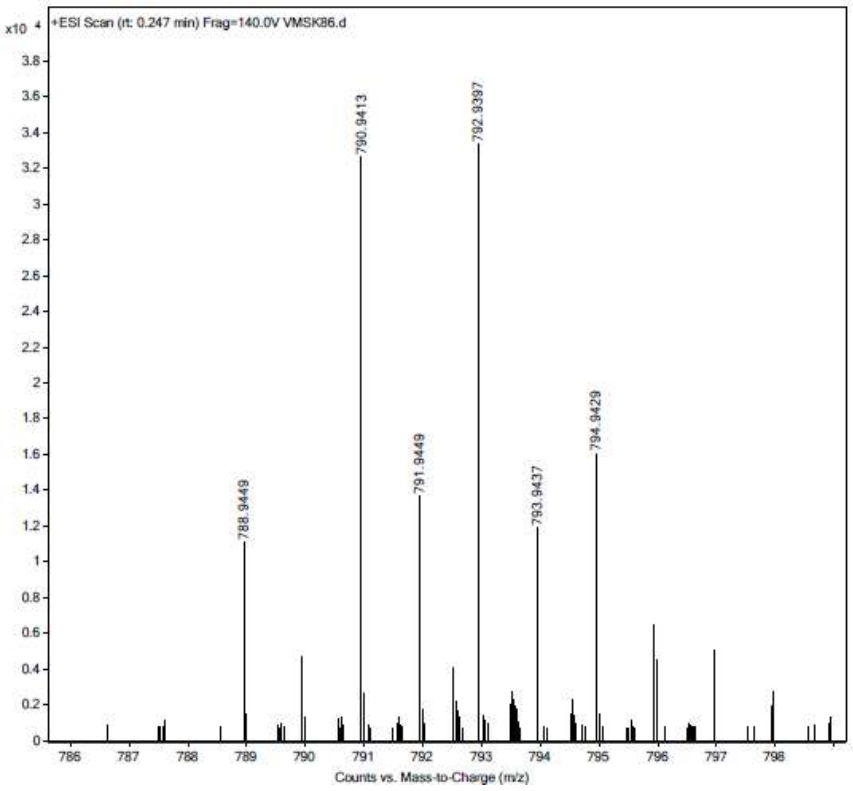

Figure A38. Mass spectrum of **2l**.

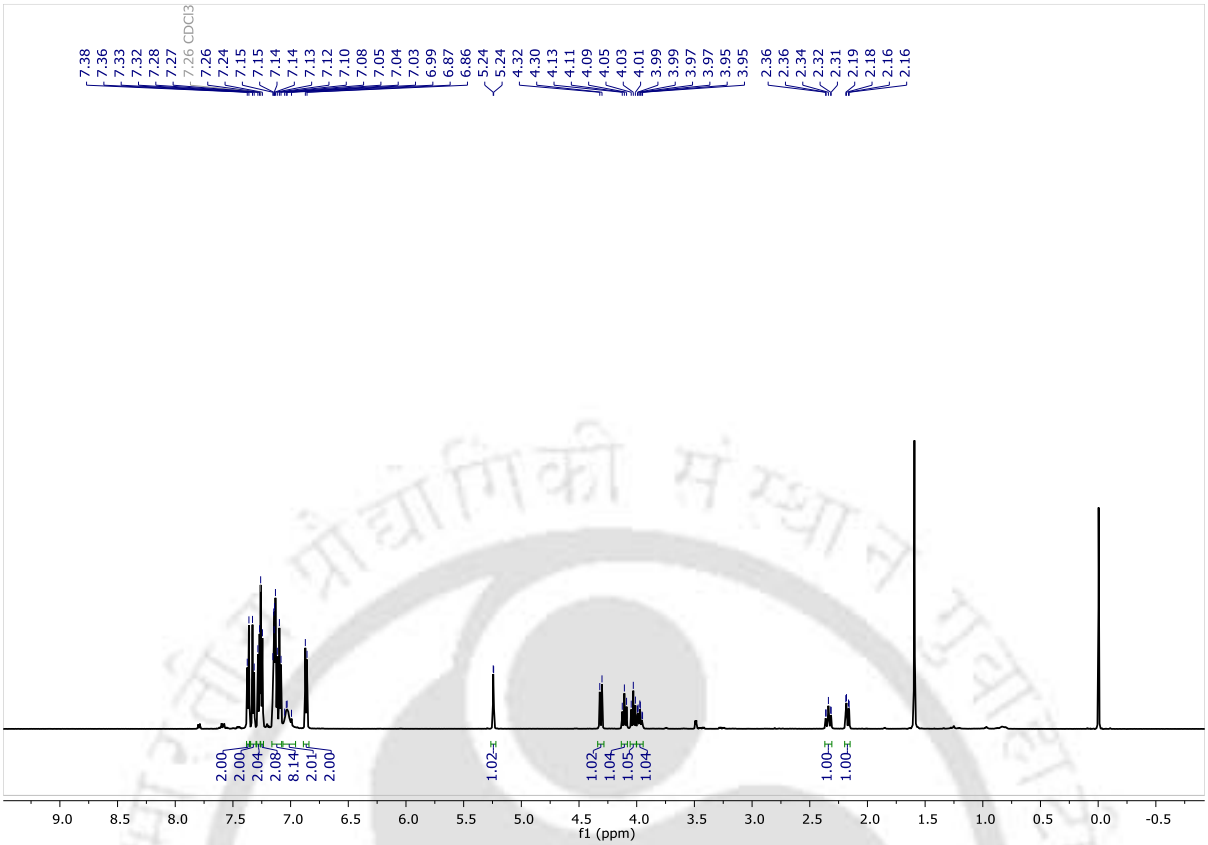

Figure A39. ^{1}H NMR spectrum of **2m**.

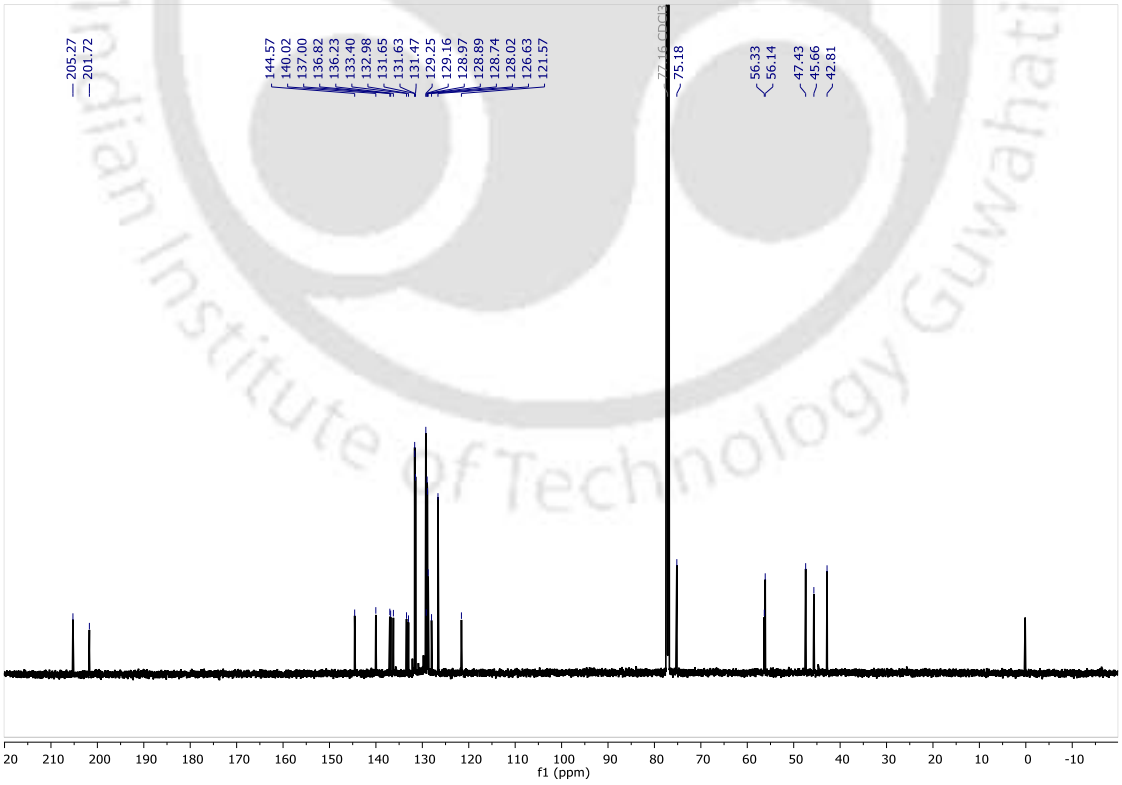

Figure A40. ^{13}C NMR spectrum of **2m**.

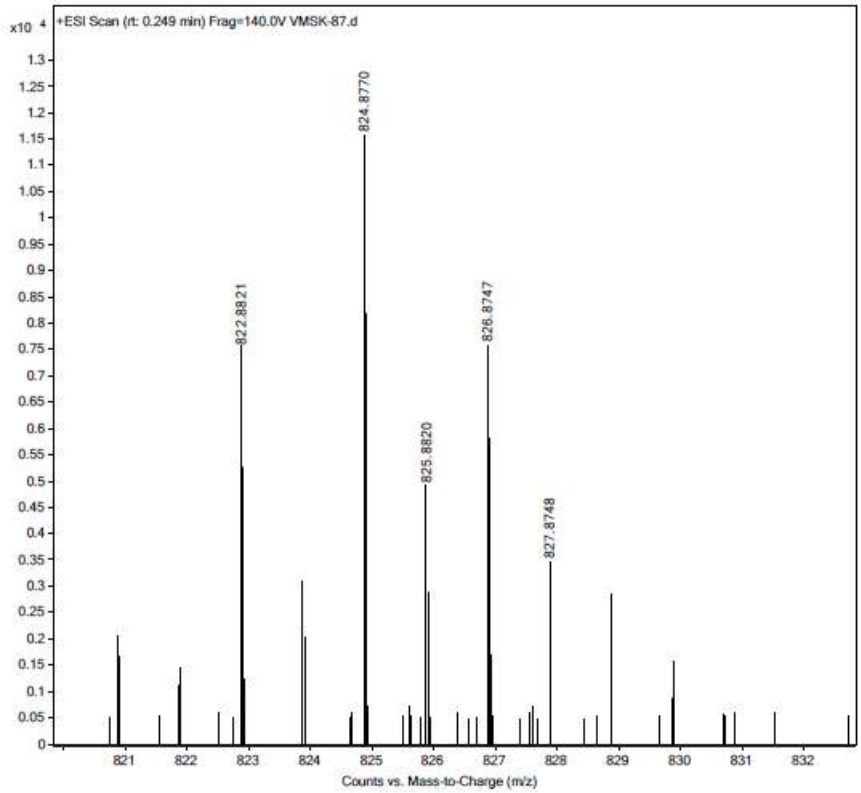

Figure A41. Mass spectrum of **2m**.

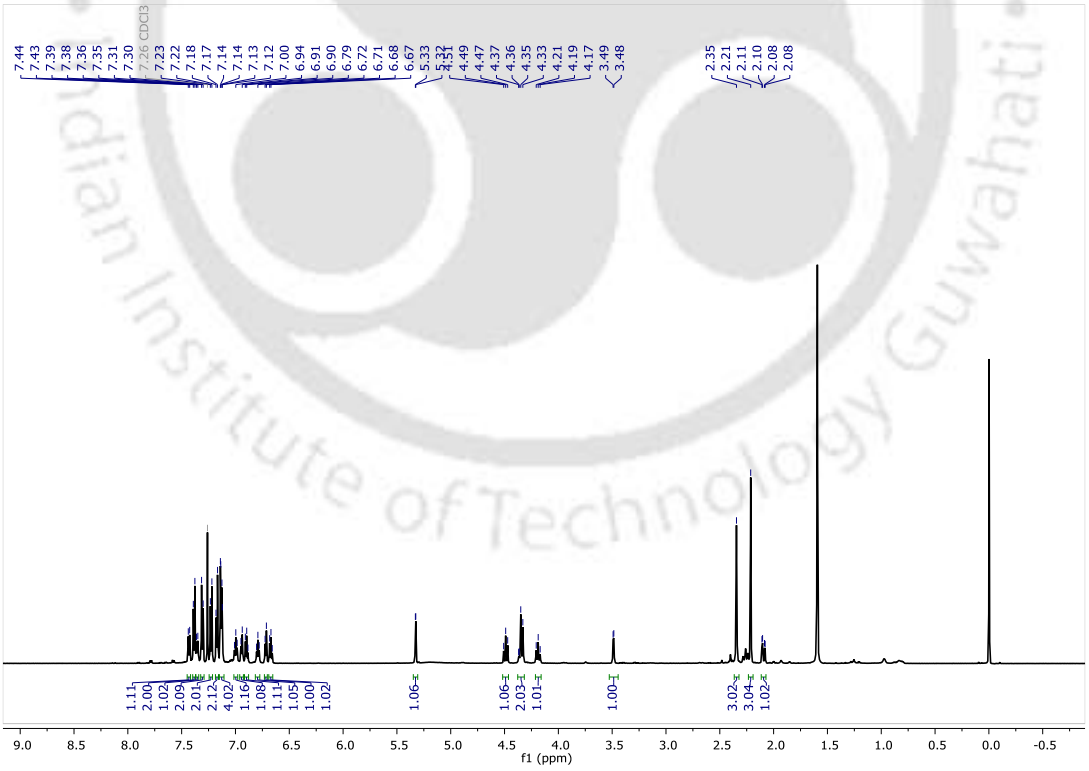

Figure A42. ^{1}H NMR spectrum of **2n**.

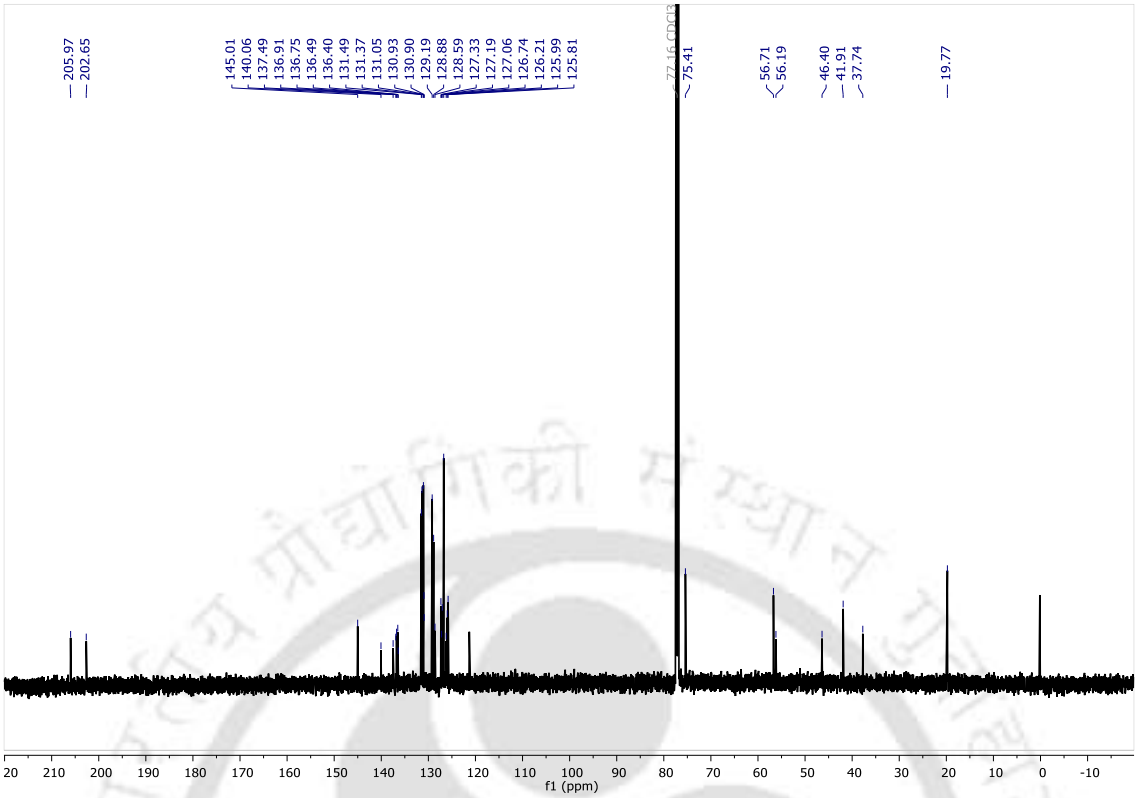

Figure A43. ^{13}C NMR spectrum of **2n**.

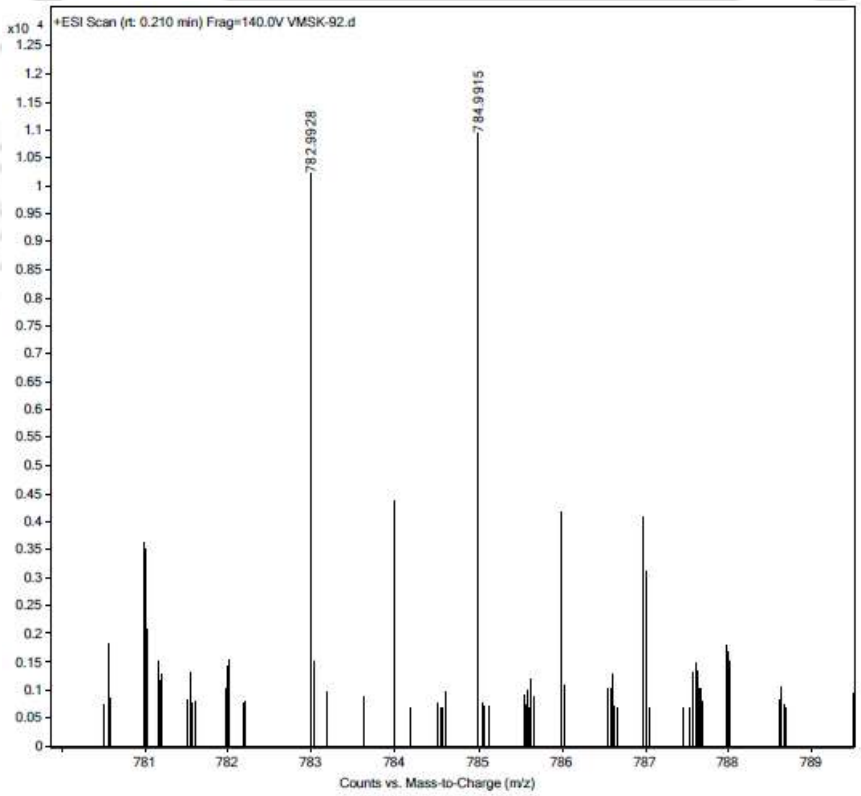

Figure A44. Mass spectrum of **2n**.

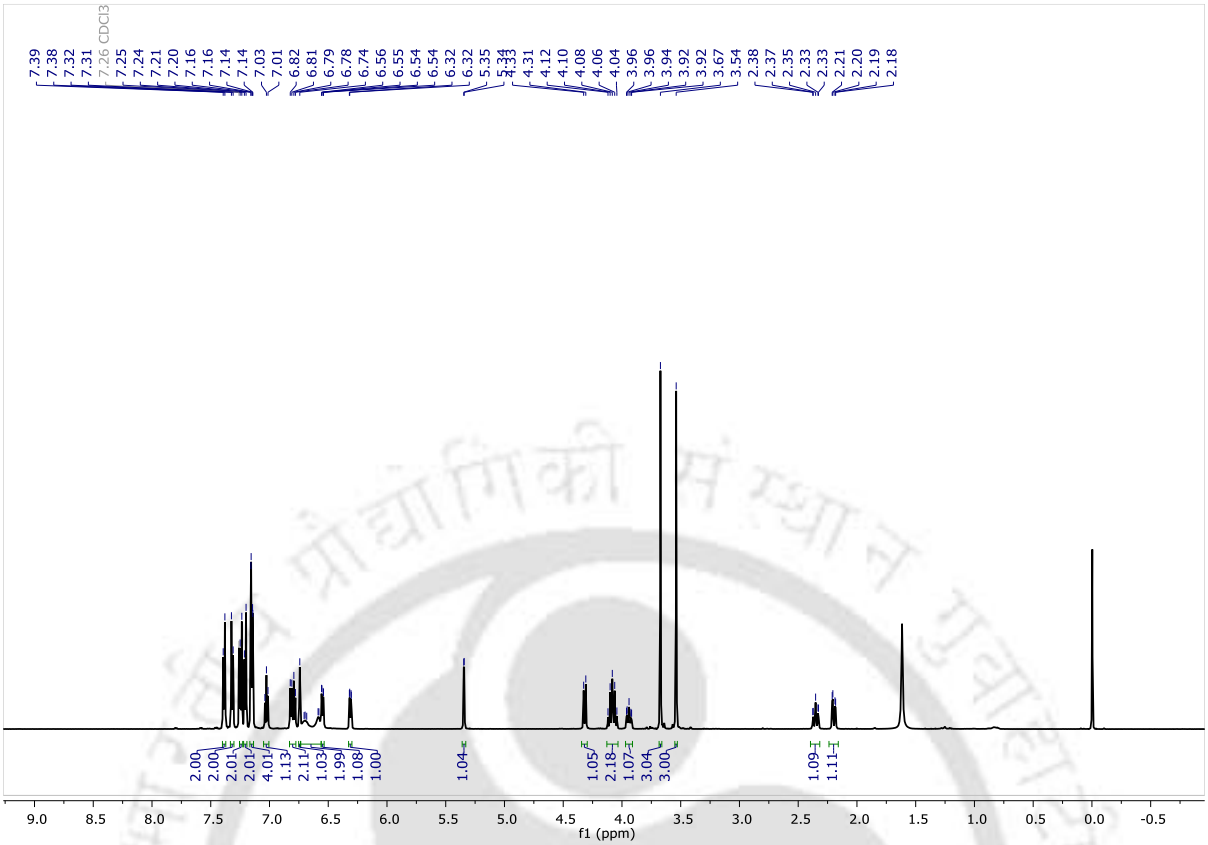

Figure A45. ^{1}H NMR spectrum of **2o**.

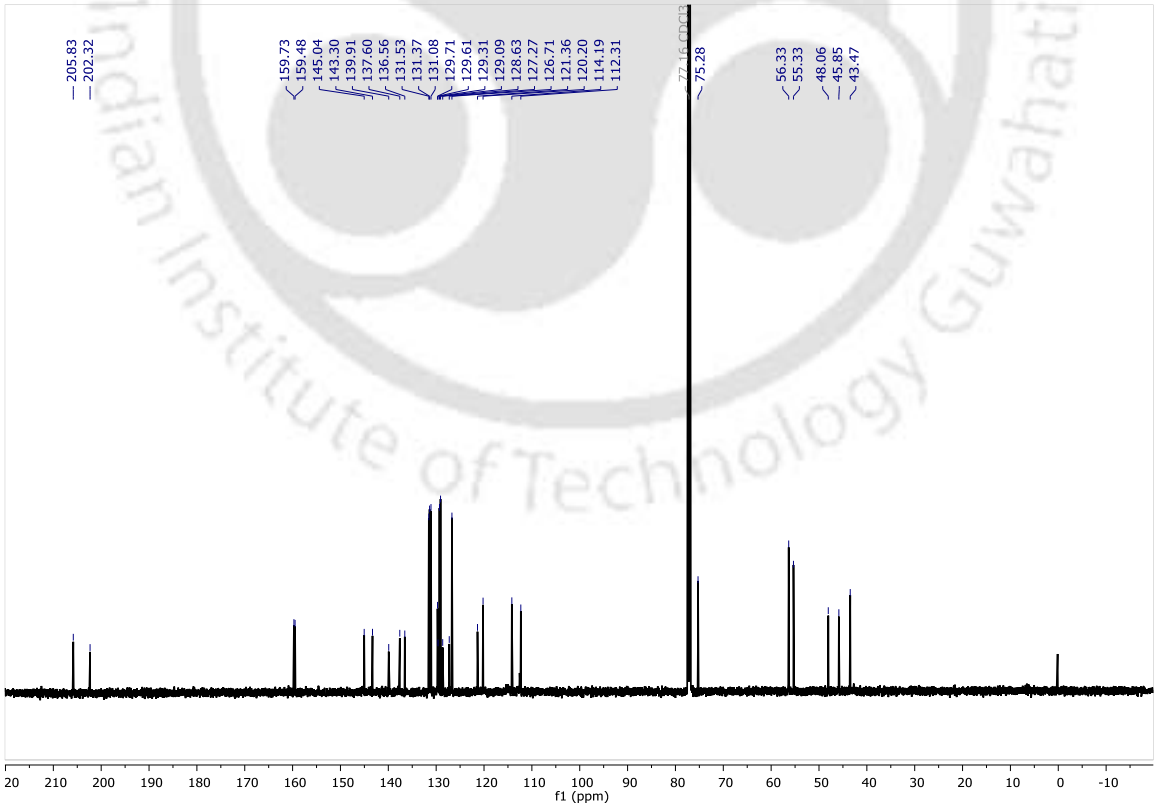

Figure A46. ^{13}C NMR spectrum of **2o**.

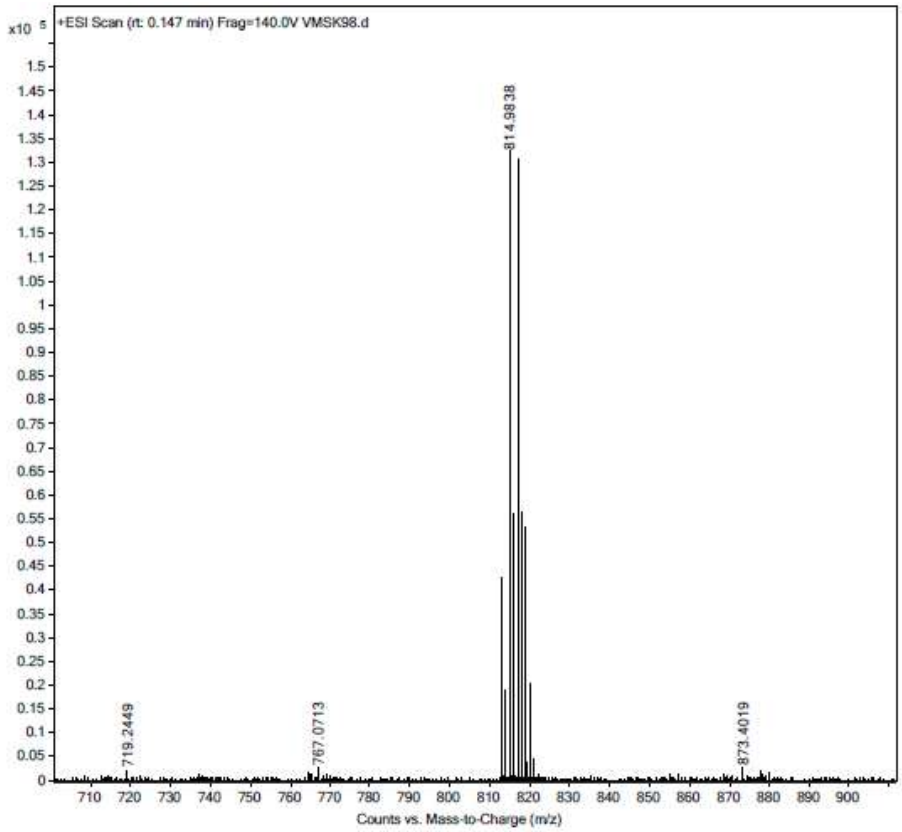

Figure A47. Mass spectrum of **2o**.

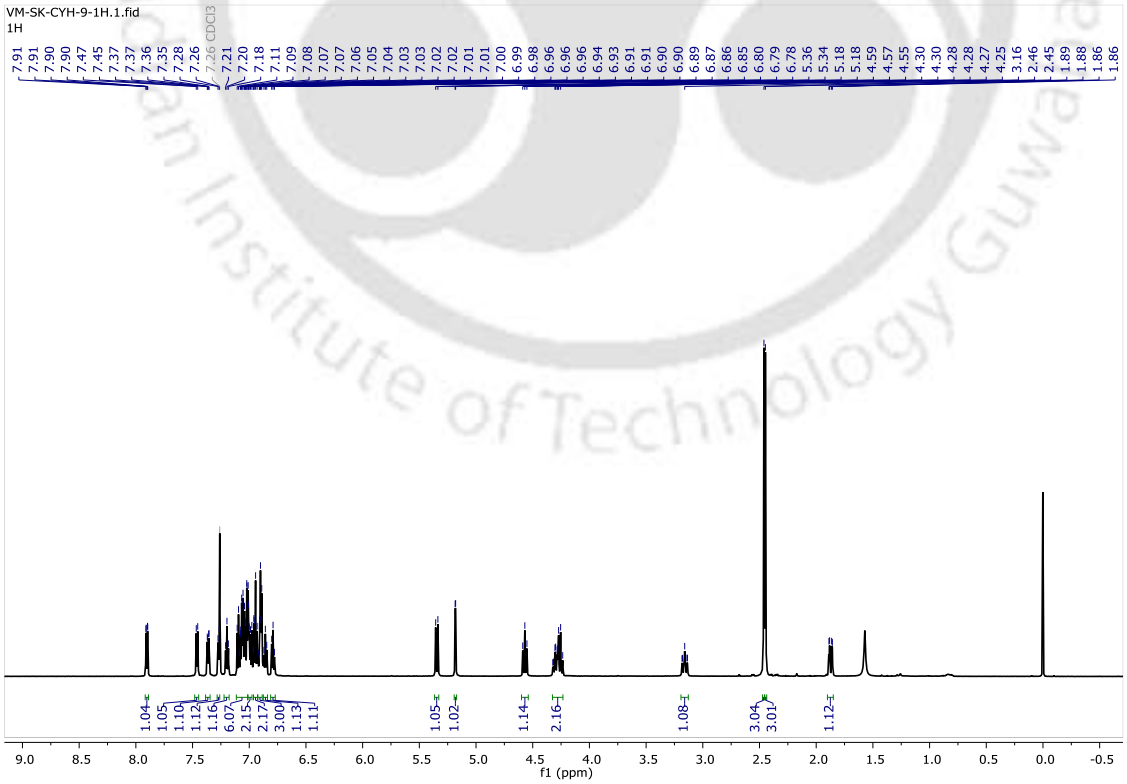

Figure A48. ^{1}H NMR spectrum of **2p**.

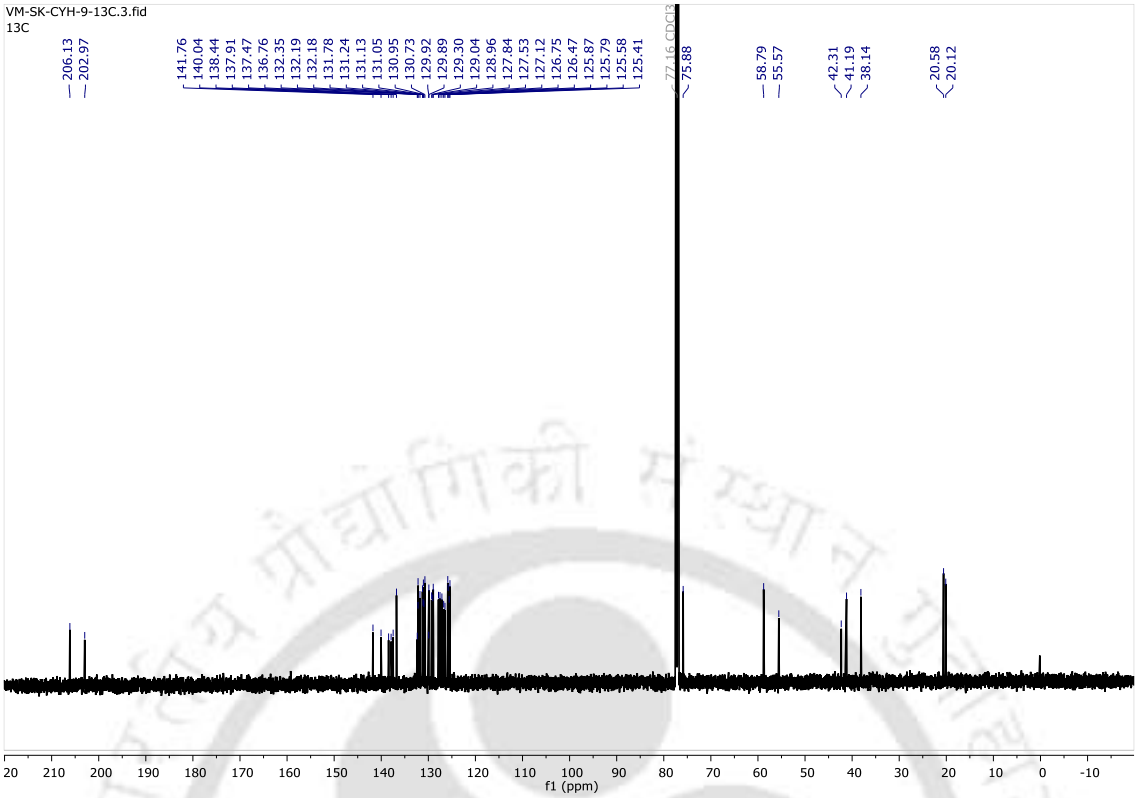

Figure A49. ^{13}C NMR spectrum of **2p**.

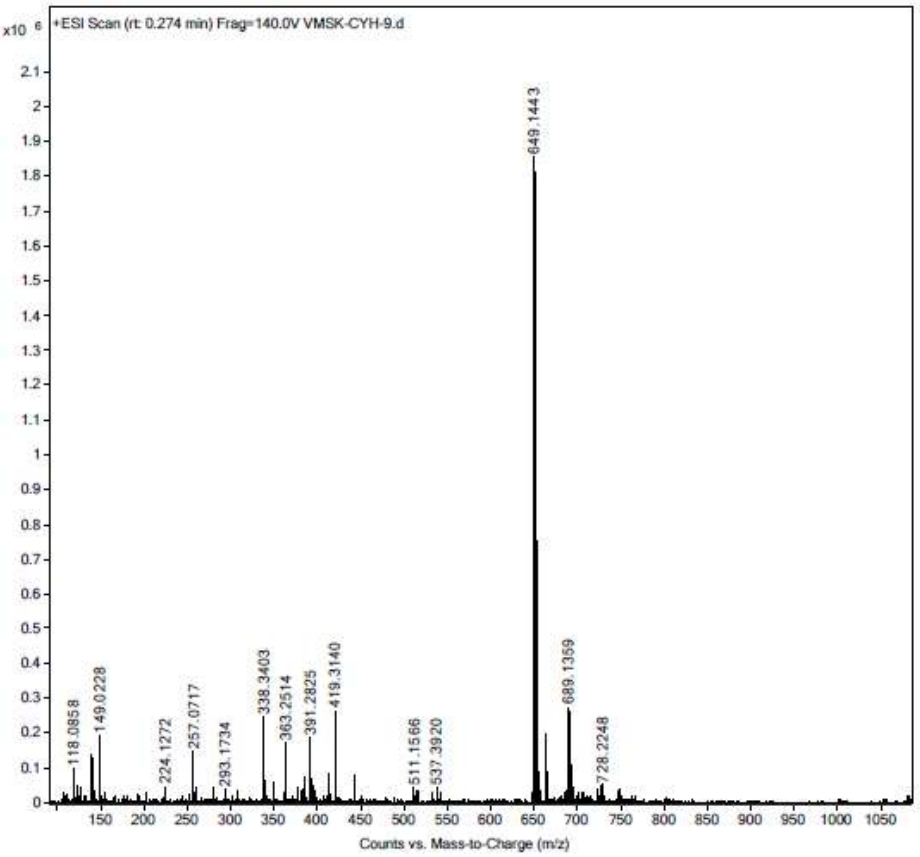

Figure A50. Mass spectrum of **2p**.

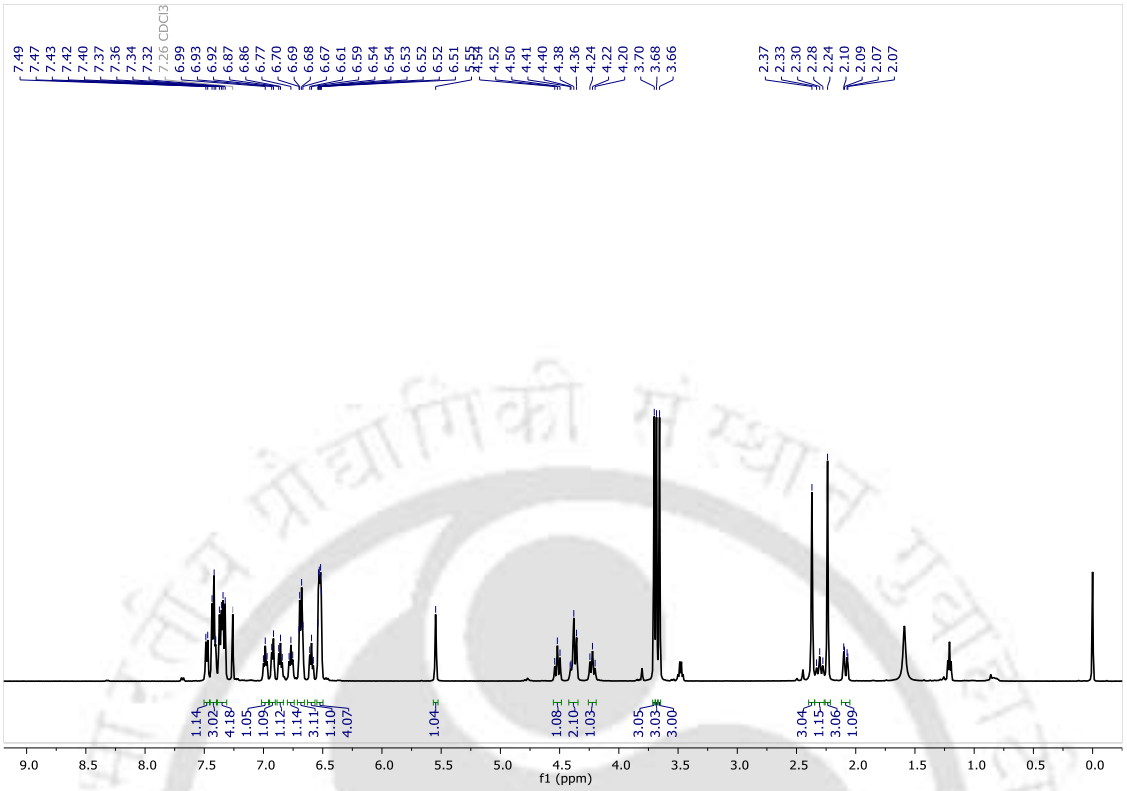

Figure A51. ^{1}H NMR spectrum of **2q**.

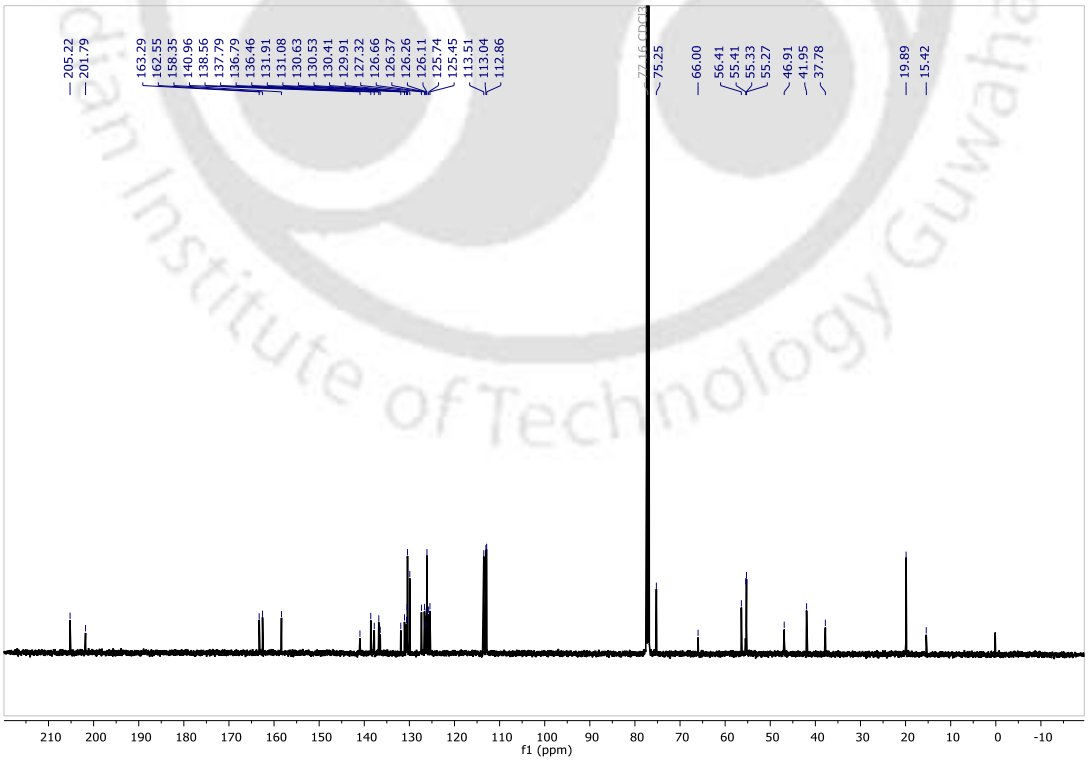

Figure A52. ^{13}C NMR spectrum of **2q**.

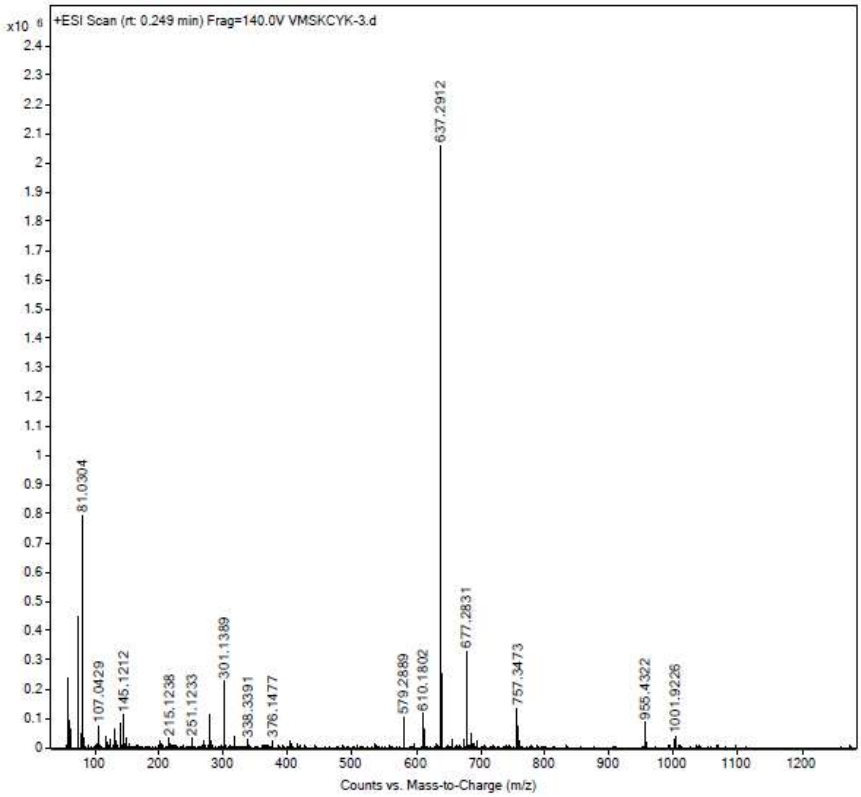

Figure A53. Mass spectrum of **2q**.

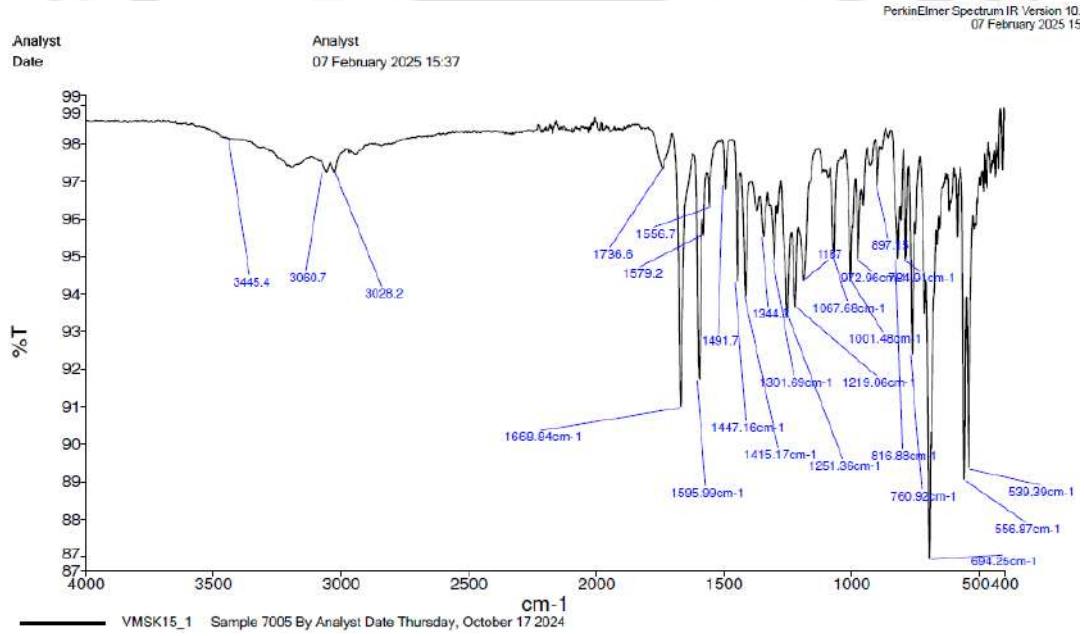

Figure A54. IR spectrum of **2a**.

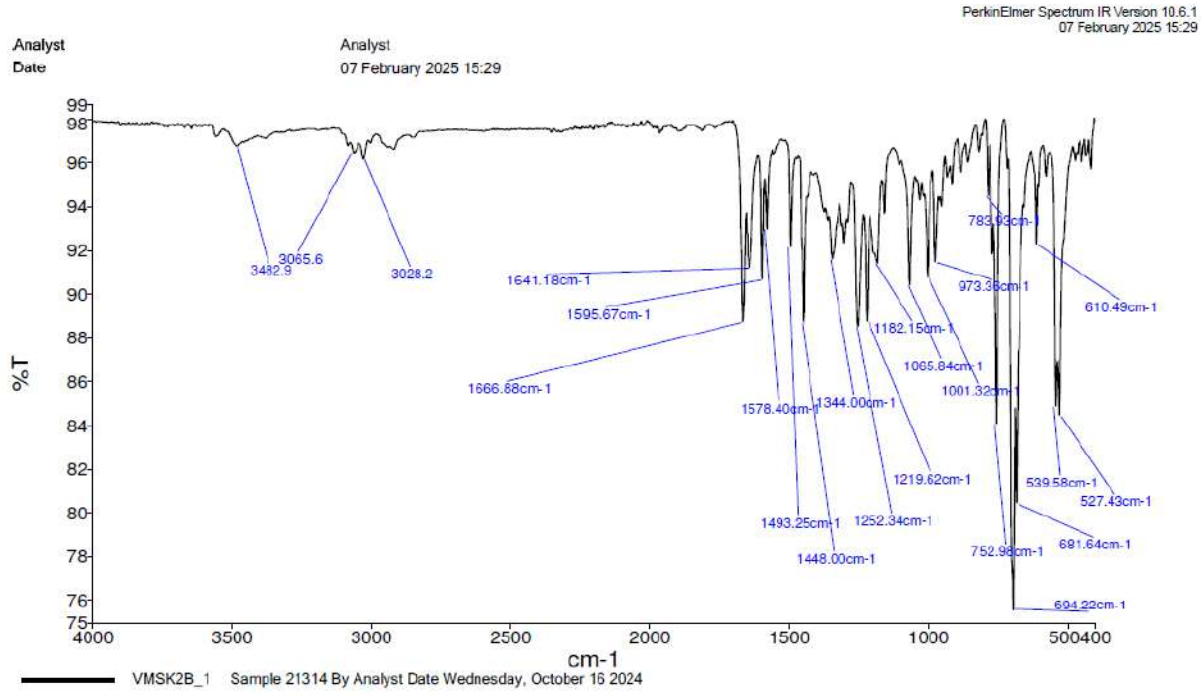

Figure A55. IR spectrum of **2b**.

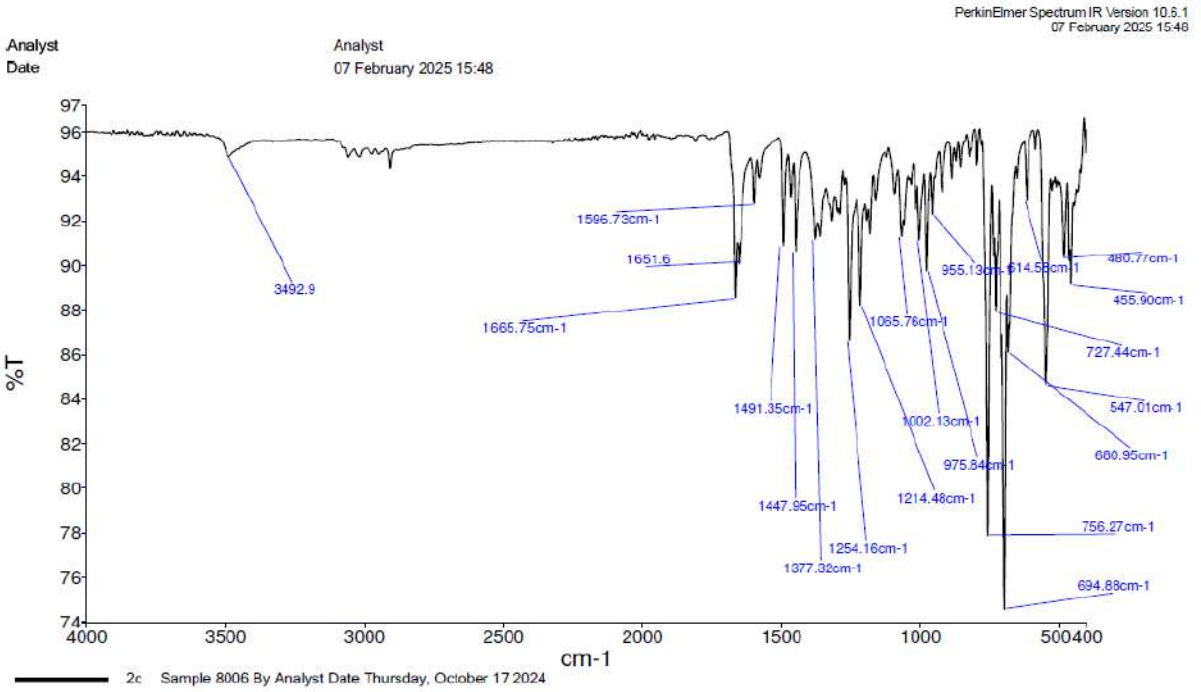

Figure A56. IR spectrum of **2c**.

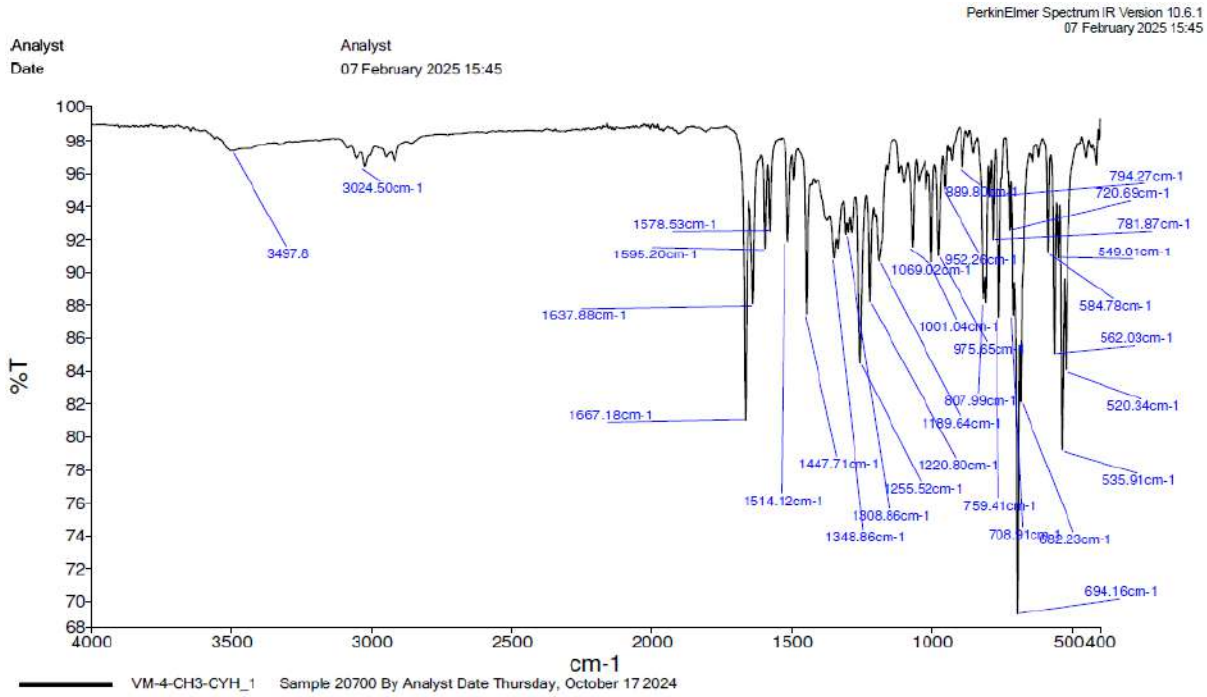

Figure A57. IR spectrum of **2d**.

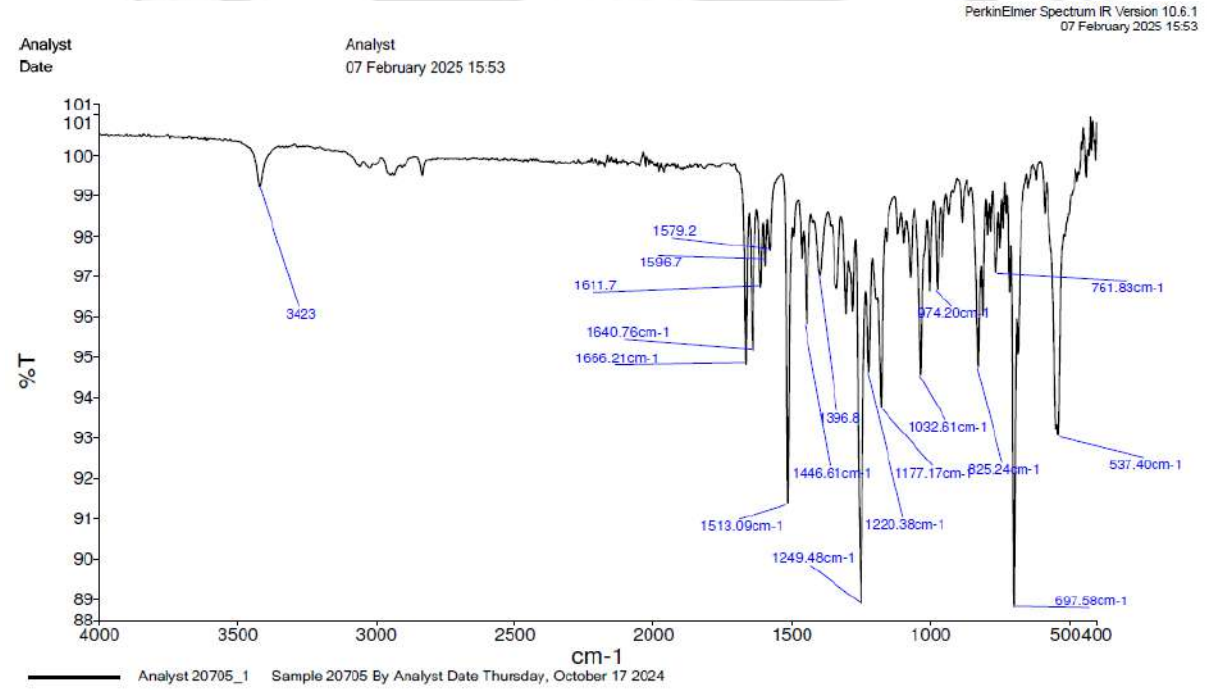

Figure A58. IR spectrum of **2e**.

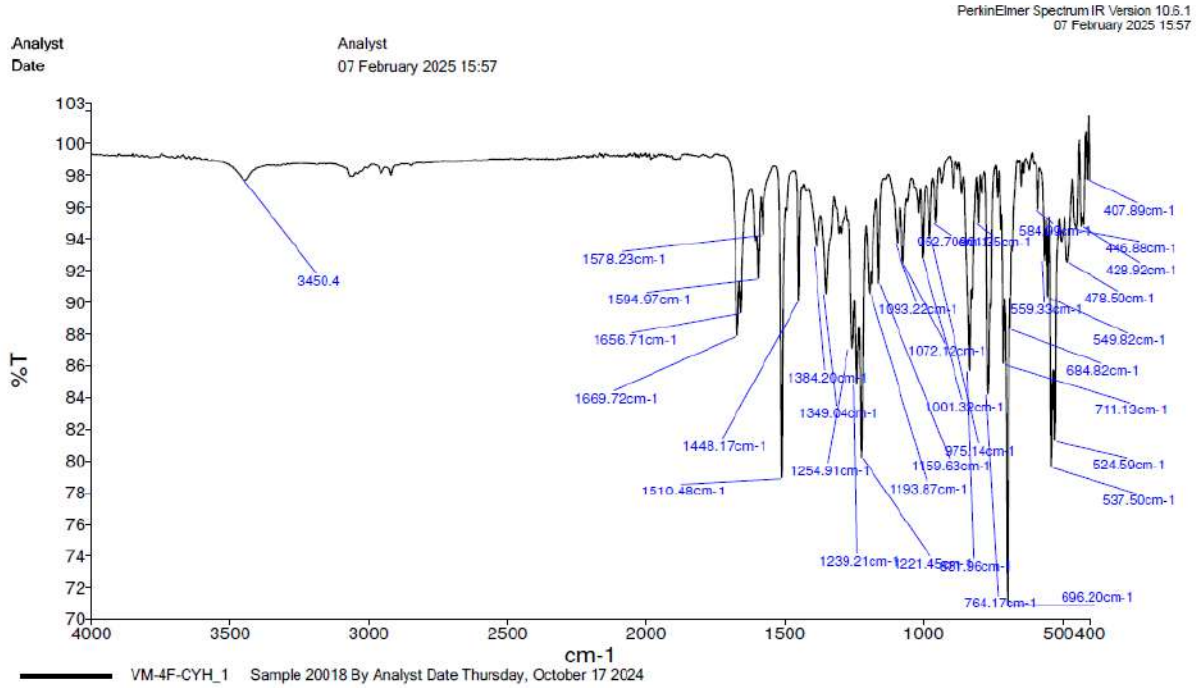

Figure A59. IR spectrum of **2f**.

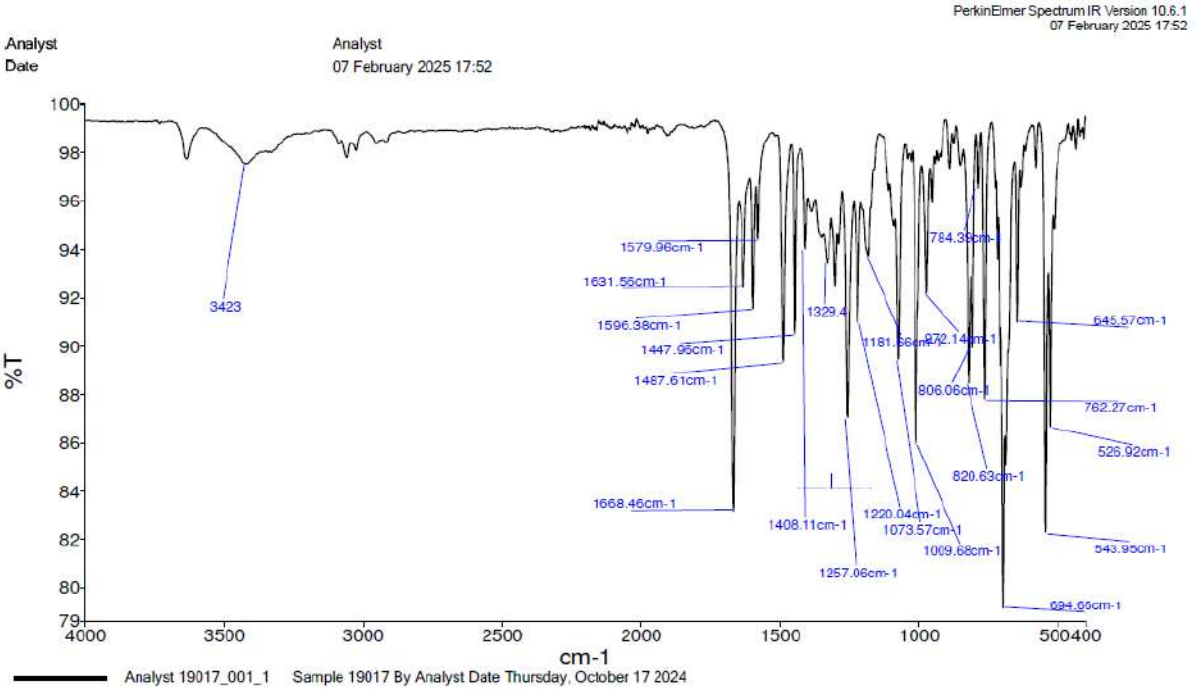

Figure A60. IR spectrum of **2g**.

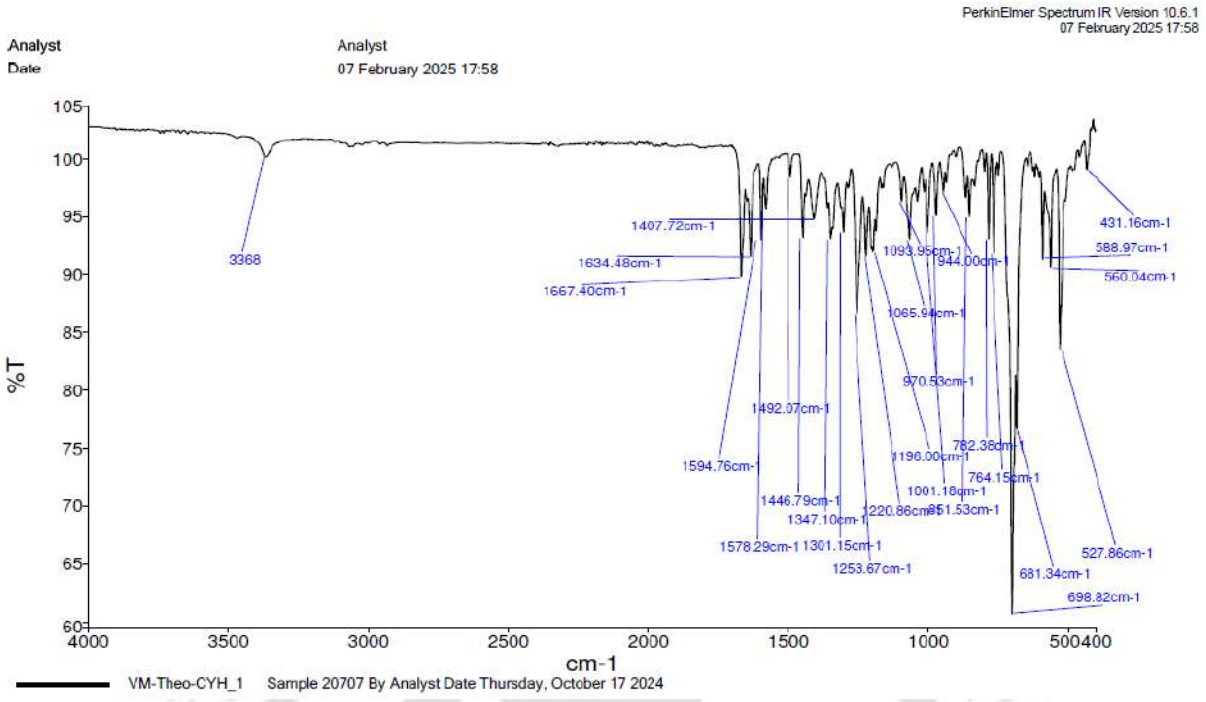

Figure A61. IR spectrum of **2h**.

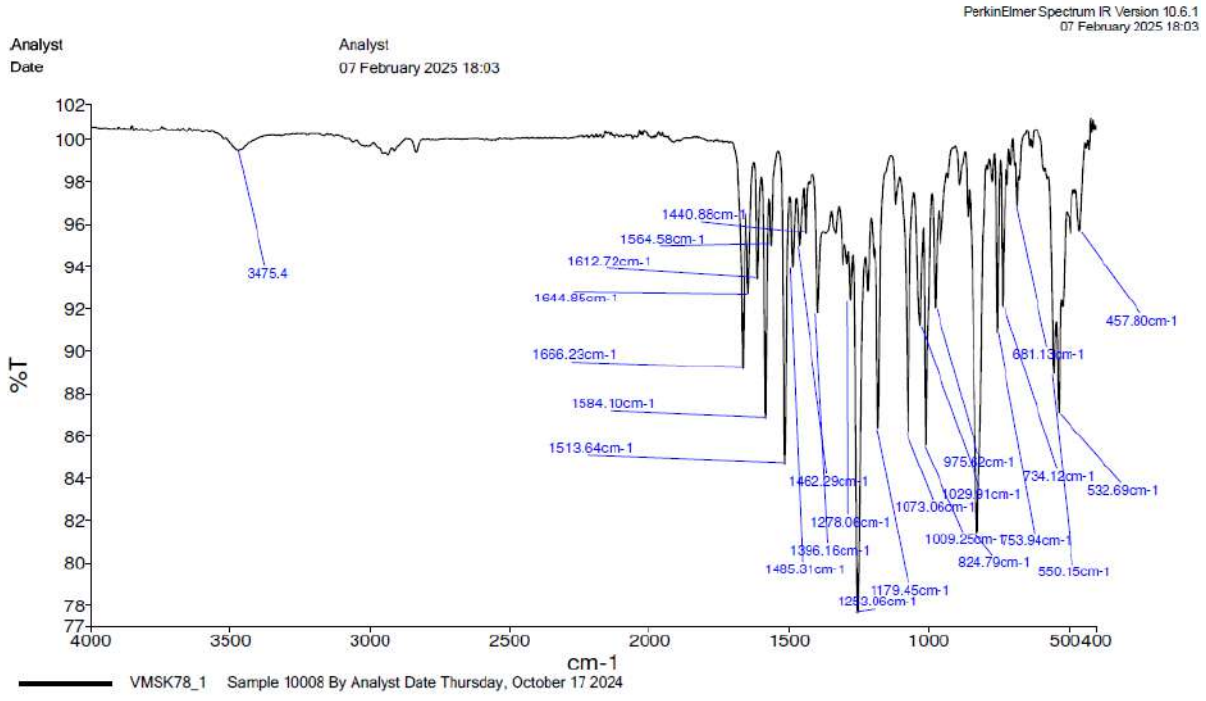

Figure A62. IR spectrum of **2i**.

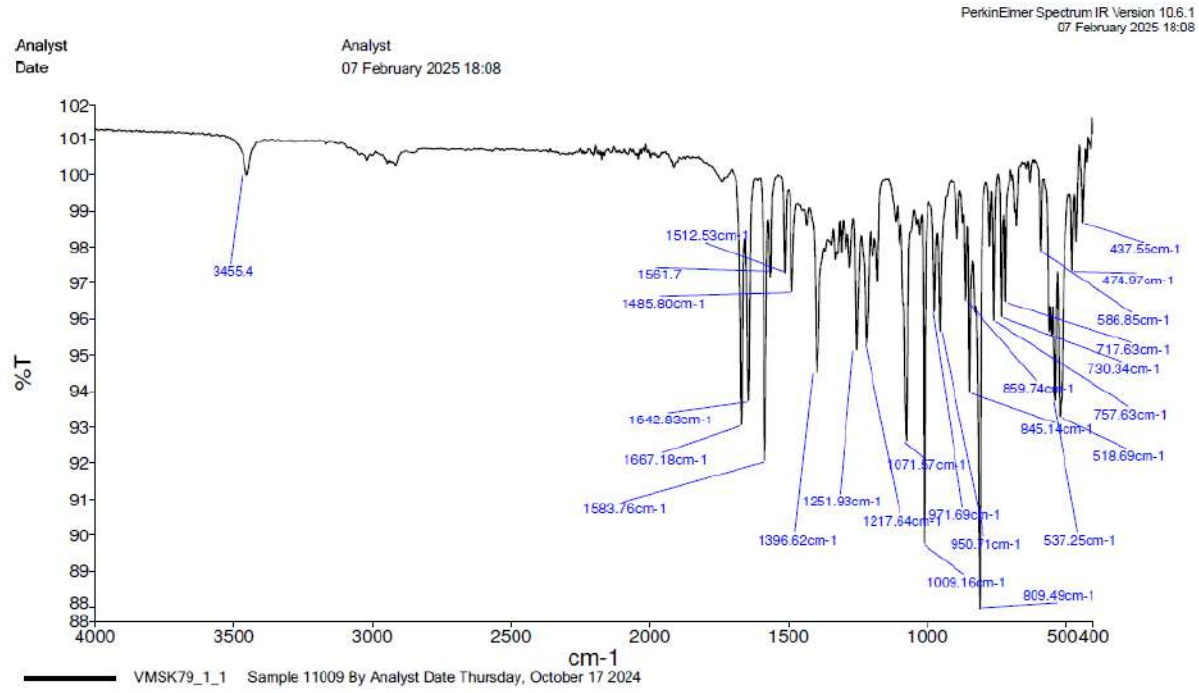

Figure A63. IR spectrum of **2j**.

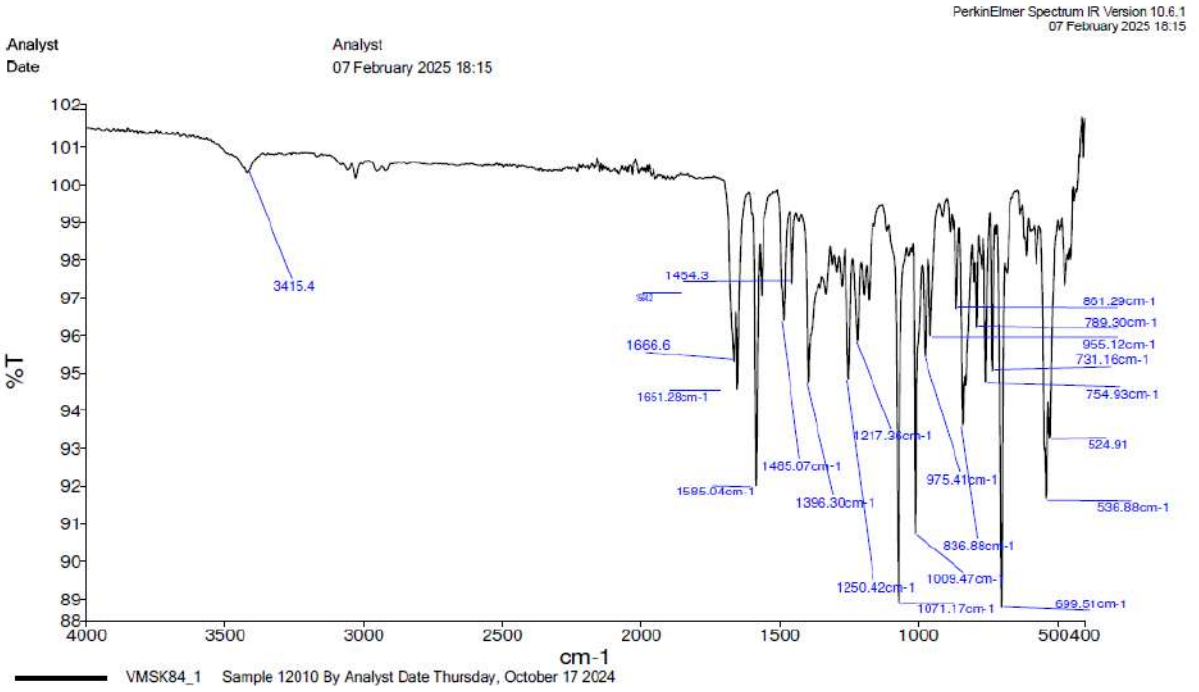

Figure A64. IR spectrum of **2k**.

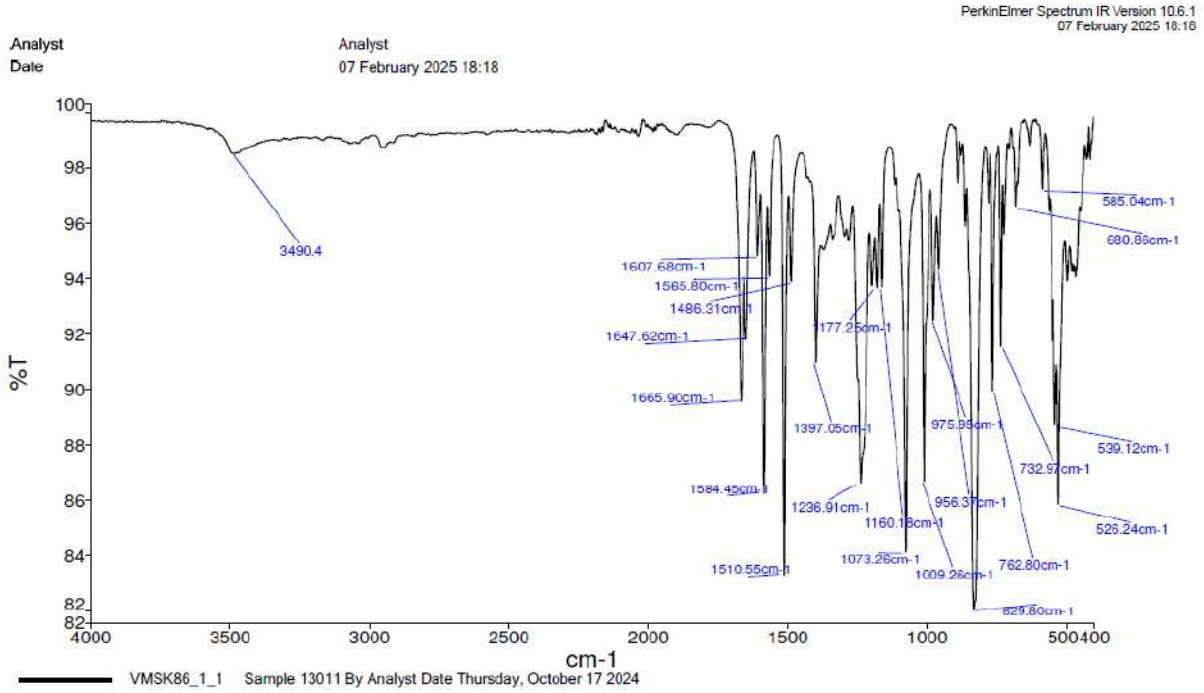

Figure A65. IR spectrum of **2l**.

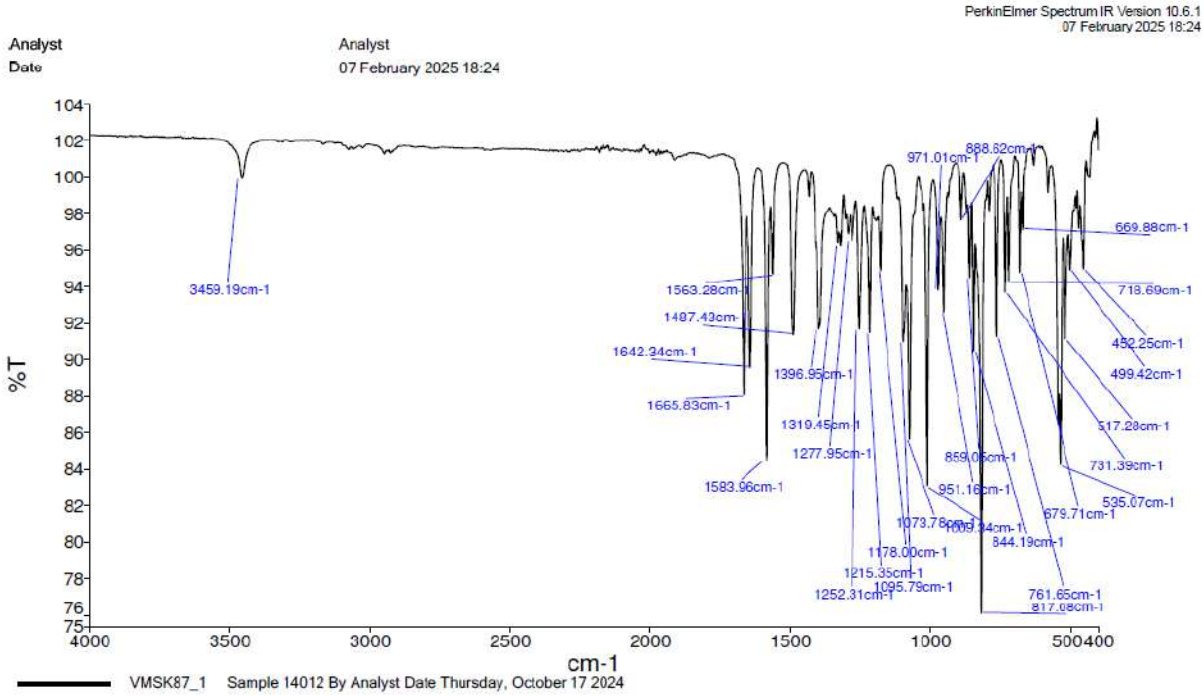

Figure A66. IR spectrum of **2m**.

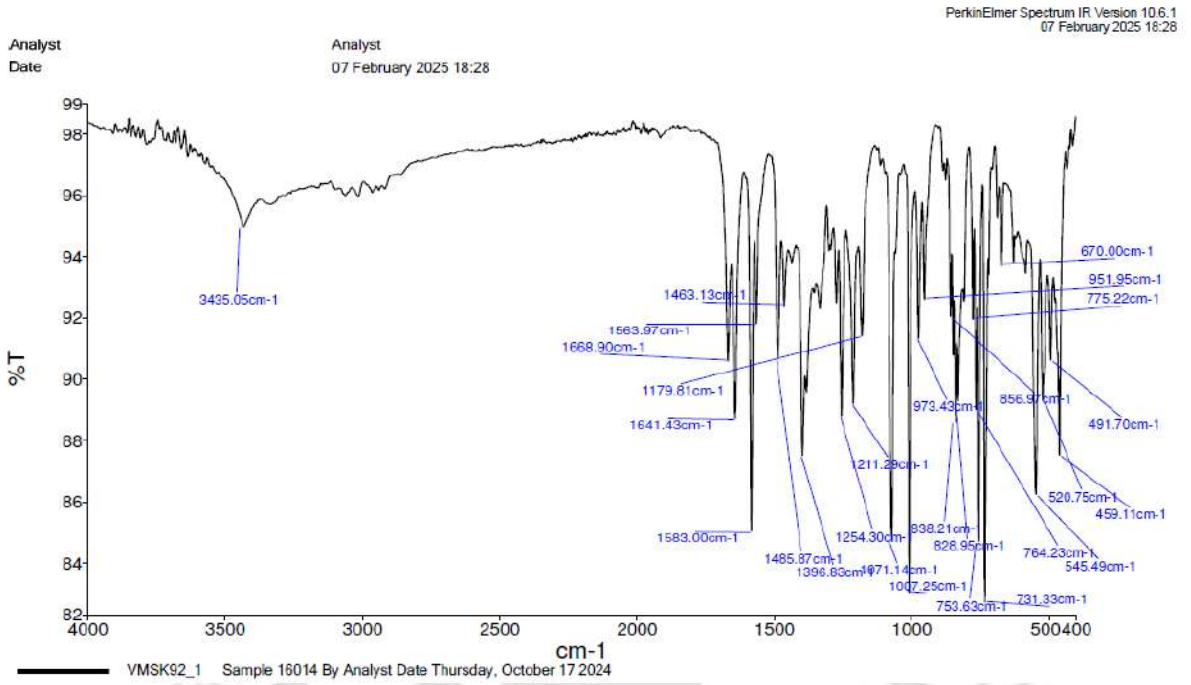

Figure A67. IR spectrum of **2n**.

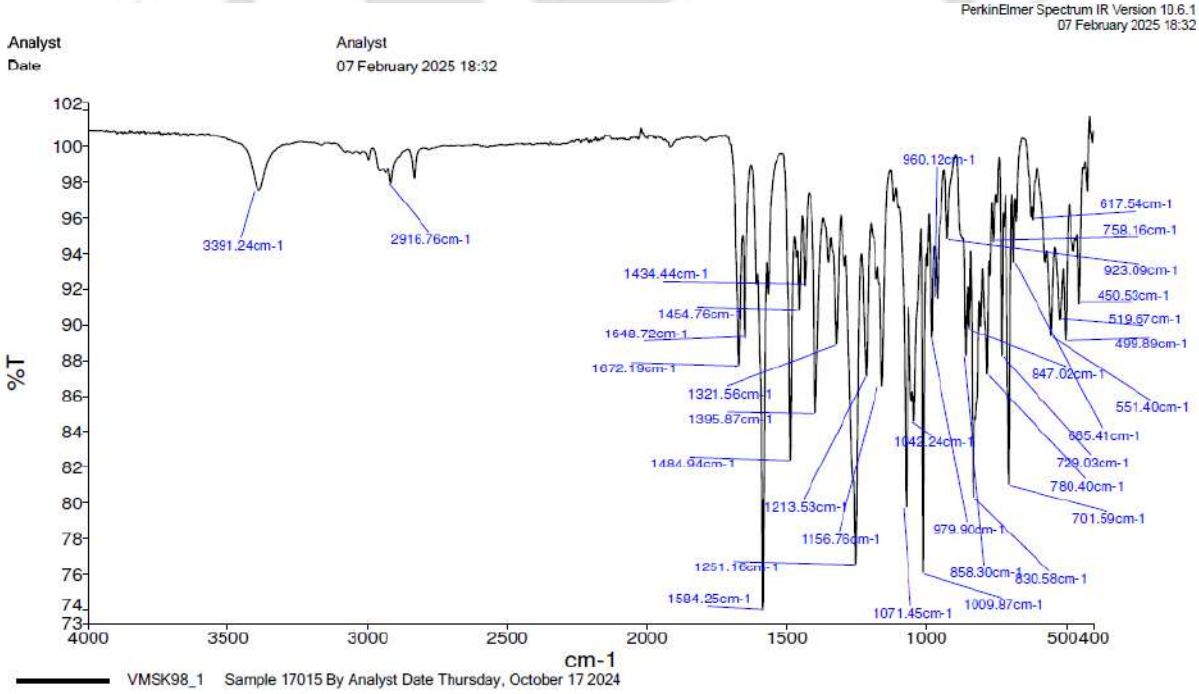

Figure A68. IR spectrum of **2o**.

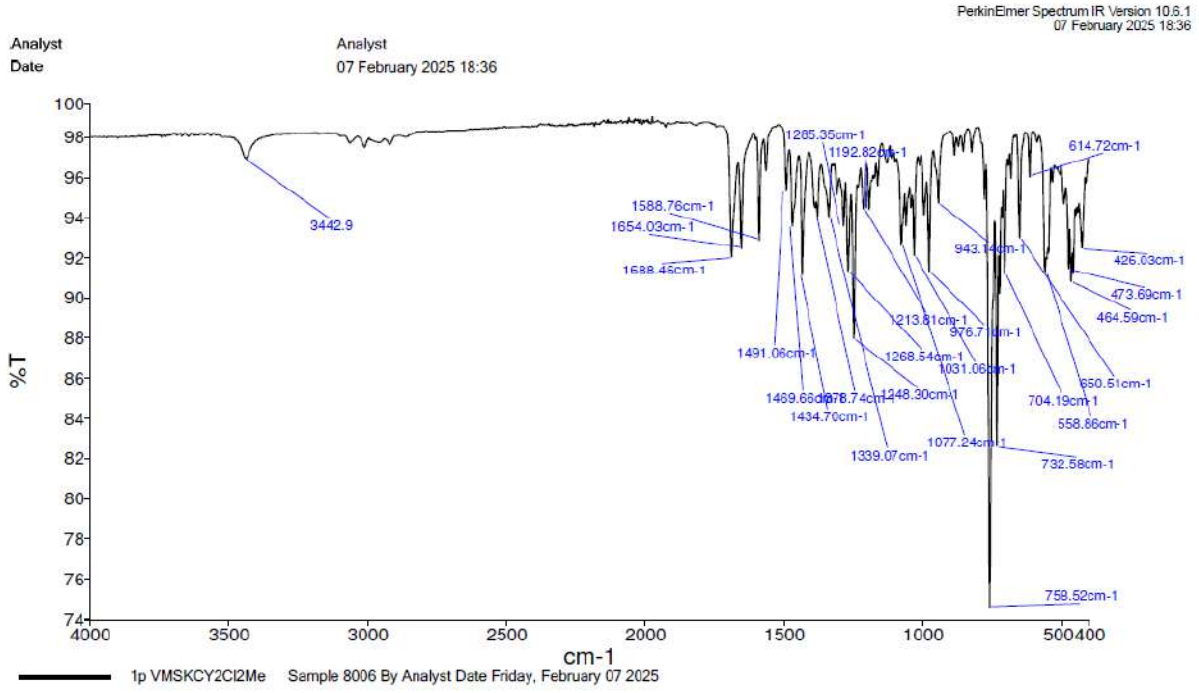

Figure A69. IR spectrum of **2p**.

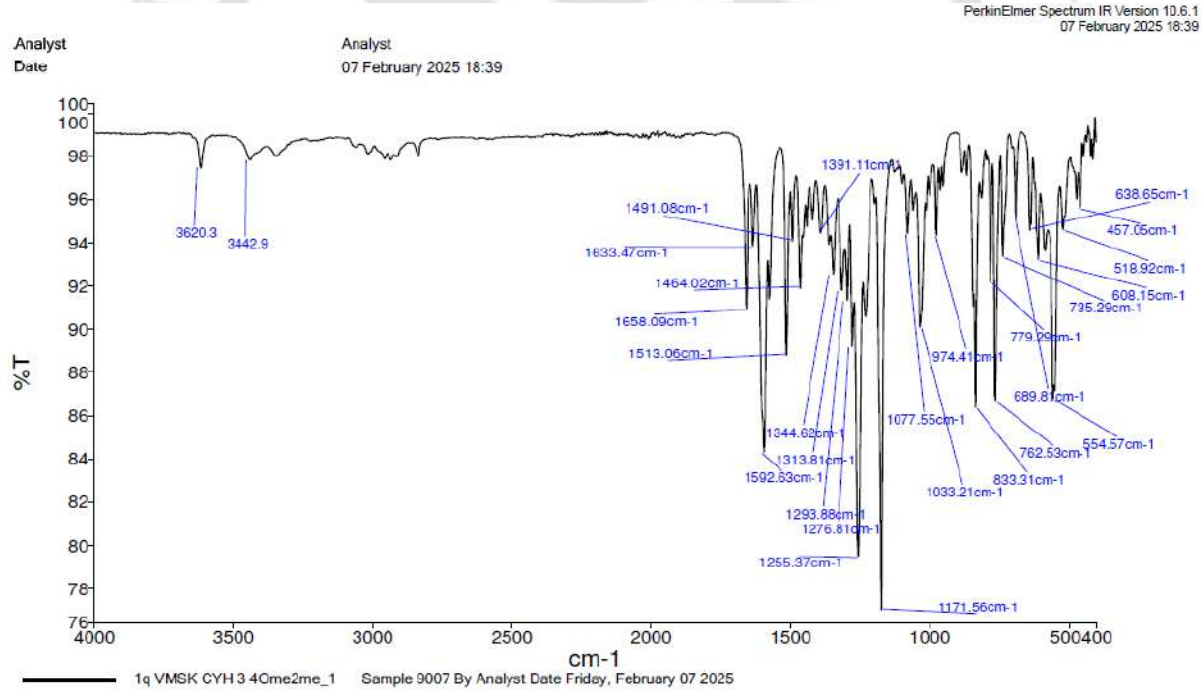

Figure A70. IR spectrum of **2q**.

Thesis Summary:

This dissertation includes six chapters out of which Chapter 1 contains introduction about fluorescence detection of metal ions, sensing mechanism with examples and recent progress on fluorescent detection of Zn^{2+}, Cu^{2+} and Pd^{2+} ions. Furthermore, various recent reports on synthesis of substituted benzenes using benzannulation reactions have also been discussed. Materials and methods used have also been described in this chapter. Chapter 2 deals with the synthesis and characterization of a probe 3,3'-((-(5-(tert-butyl)-2-hydroxy-1,3-phenylene)bis(methaneylylidene))bis(hydrazin-1-yl-2-ylidene))bis(quinoxalin-2(1H)-one) (**LH**) and the probe was utilized in selective "*turn on*" fluorescent detection of Zn^{2+} ion over various metal ions and anions. The structure of complex obtained from the reaction of 2:1 mixture of $ZnCl_2$ and **LH** has been established using single crystal XRD method. In Chapter 3, synthesis and characterization of a probe 1-(imidazo[5,1-*a*]isoquinolin-3-yl)naphthalen-2-ol (**L2H**) has been described. The probe has potential to detect Cu^{2+} and Pd^{2+} ions in fluorescent *turn off* fashion over various metal ions and anions. Chapter 4 deals with synthesis and characterization of a polypyridine ligand **L3** has been described. Using **L3**, two new metal complexes of metal chlorides (cobalt(II) and manganese(II)) were synthesized. Molecular structures of **L3**, $[M_2(\mathbf{L3})Cl_4]\cdot 2H_2O$ {M = Co(II) (**1**) and Mn(II) (**2**)} were established using single crystal XRD method. The intermolecular interactions involve has also been described. In Chapter 5, *de novo* construction of benzene ring from 3:1 mixture of aryl methyl ketone and aldehyde using NaH has been discussed. With this methodology, various tetrasubstituted benzenes were synthesized. The reaction was regioselective in nature which was confirmed by single crystal XRD method. Chapter 6 describes the facile synthesis of a series of pentasubstituted cyclohexanol achieved in moderate to good yield by the reaction of aryl methyl ketone and aromatic aldehyde (3:2 ratio) using NaH (20 mol %) as base. Some new and reported cyclohexanols were synthesized using this methodology.

Future Perspective:

In Chapter 2 and 3, N,O-donor probes were utilized in fluorescent detection of Zn^{2+}, Cu^{2+} and Pd^{2+} ions. Various probes which contain N,N and N,S-donor atoms would have potential to detect toxic metal ions. In Chapter 4, two metal complexes of Co(II) and Mn(II) ions were synthesized using a polypyridine ligand, which contains two terpyridine arms and from various reports, it was found that metal terpyridine complexes have excellent catalytic activity. So these complexes will be utilized in various organic transformations. Chapter 5

and 6 deal with synthesis of substituted benzenes and cyclohexanols, may be useful synthons as well as metal ion sensing ability and biological activity of these compounds may be evaluated.

List of Publications

From Thesis:

1. S. Kumar, S. Mahata and V. Manivannan, *J. Photochem. Photobiol. A: Chem.* **2024**, *450*, 115436.
2. S. Kumar, H. Phogat and V. Manivannan, *Luminescence* **2025**, *40*, e70104.
3. S. Kumar and V. Manivannan, *ChemistrySelect* **2025**, *10*, e202405611.

From other:

1. S. Mahata, S. Kumar, S. Dey, B. B. Mandal, V. Manivannan, *Inorganica Chim. Acta* **2022**, *535*, 120876.